41st Lunar and Planetary Science Conference
Program of Technical Sessions

Sponsored by
Lunar and Planetary Institute
NASA Johnson Space Center

Lunar and Planetary Institute

FORTY-FIRST LUNAR AND PLANETARY SCIENCE CONFERENCE

Program of Technical Sessions

March 1–5, 2010

The Woodlands Waterway Marriott Hotel and Convention Center
The Woodlands, Texas

Sponsored by
Lunar and Planetary Institute
NASA Johnson Space Center
Northrup Grumman Aerospace Systems

Conference Co-Chairs
Stephen Mackwell, Lunar and Planetary Institute
Eileen Stansbery, NASA Johnson Space Center

Program Committee

Paul Abell, *NASA Johnson Space Center*
Carlton Allen, *NASA Johnson Space Center*
Robert Anderson, *Jet Propulsion Laboratory*
Mary Sue Bell, *Jacobs Engineering*
Michael Bland, *Washington University*
Jacob Bleacher, *NASA Goddard Space Flight Center*
Debra Buczkowski, *Johns Hopkins University Applied Physics Laboratory*
Nathalie Cabrol, *NASA Ames Research Center/SETI*
Nancy Chabot, *Johns Hopkins University Applied Physics Laboratory*
J. Bradley Dalton, *Jet Propulsion Laboratory*
David Draper, *NASA Johnson Space Center*
Denton Ebel, *American Museum of Natural History*
Justin Filiberto, *Rice University*
Christine Floss, *Washington University*
Herbert Frey, *NASA Goddard Space Flight Center*
Jon Friedrich, *Fordham University*
Gerald Galgana, *Lunar and Planetary Institute*
Martha Gilmore, *Wesleyan University*
Lori Glaze, *NASA Goddard Space Flight Center*
Cyrena Goodrich, *Planetary Science Institute*
Rose Hayward, *U.S. Geological Survey*
Peter Isaacson, *Brown University*
Motoo Ito, *NASA Johnson Space Center*
Noam Izenberg, *Johns Hopkins University Applied Physics Laboratory*
Elizabeth Jensen, *ACS Consulting/ Multi-Mirror Telescope Observatory*
Walter Kiefer, *Lunar and Planetary Institute*
Noriko Kita, *University of Wisconsin/Madison*
Rachel Klima, *Johns Hopkins University Applied Physics Laboratory*
Alexander Krot, *University of Hawaii*
Frank Kyte, *University of California, Los Angeles*
Nicholas Lang, *Mercyhurst College*
Jeremie Lasue, *Lunar and Planetary Institute*
Kevin Lewis, *Princeton University*
James Lyons, *University of California, Los Angeles*
Glenn MacPherson, *Smithsonian Institution*
Rhiannon Mayne, *Texas Christian University*
Thomas McCord, *Bear Fight Center*
Harry Y. McSween Jr., *University of Tennessee*
Scott Messenger, *NASA Johnson Space Center*
Bradley Meyer, *Clemson University*
David Mittlefehldt, *NASA Johnson Space Center*
Julianne Moses, *Lunar and Planetary Institute*
Lan-Anh Nguyen, *Jacobs Engineering*
Eldar Noe Dobrea, *California Institute of Technology*
Noah Petro, *NASA Goddard Space Flight Center*
Jeffrey Plescia, *Johns Hopkins University Applied Physics Laboratory*
Andrew Shaner, *Lunar and Planetary Institute*
Tomasz Stepinski, *Lunar and Planetary Institute*
Timothy Titus, *U.S. Geological Survey*
Stefanie Tompkins, *Defense Advanced Research Projects Agency*
Tomo Usui, *NASA Johnson Space Center*
Faith Vilas, *University of Arizona/ Multi-Mirror Telescope Observatory*
Michael Weisberg, *Kingsborough College/ CUNY*
Axel Wittmann, *Lunar and Planetary Institute*
Ryan Zeigler, *Washington University*
James Zimbelman, *Smithsonian Institution*

Woodlands Waterway Convention Center Map

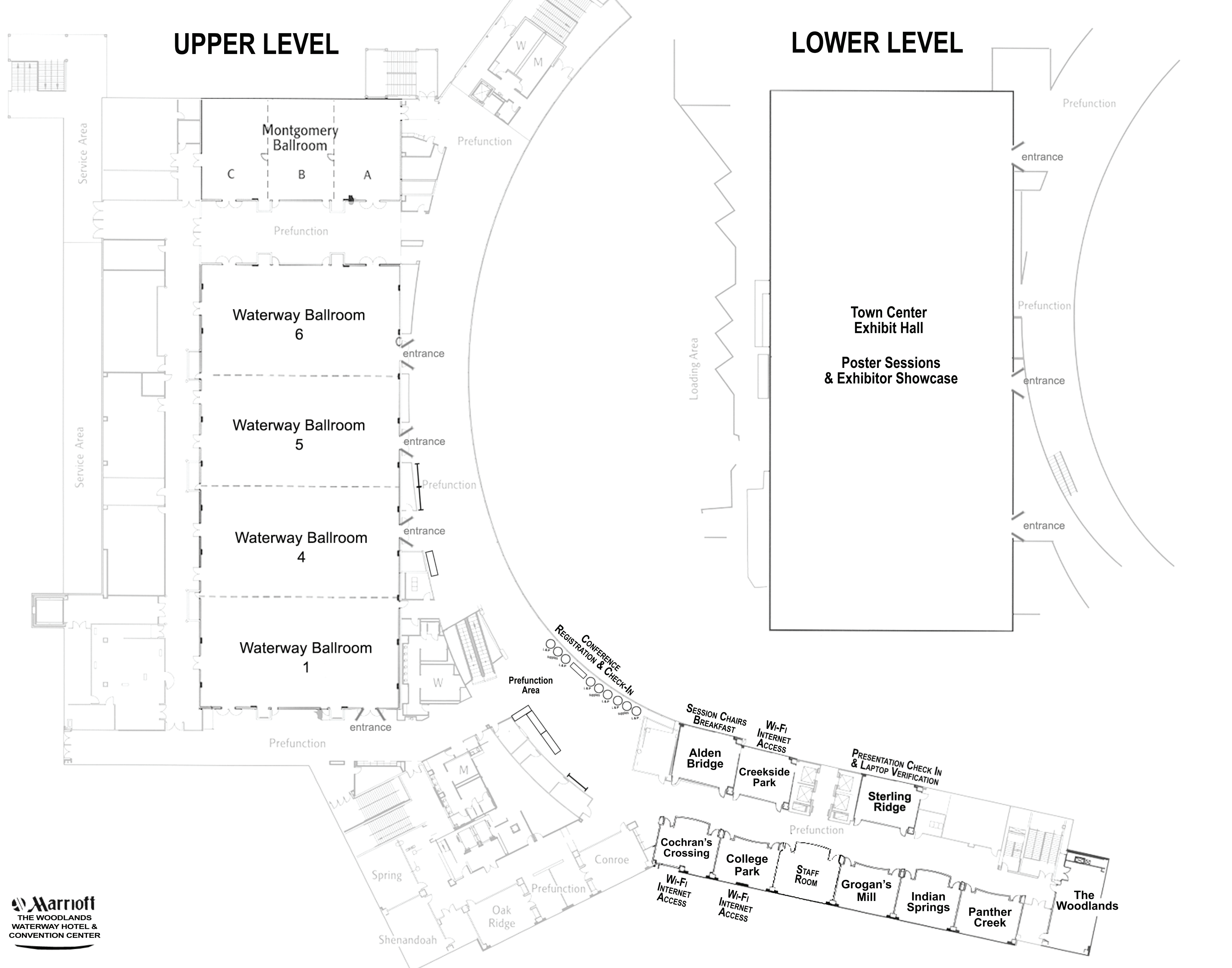

LIST OF EXHIBITORS

Boeing Company

7700 Boston Boulevard
Springfield VA 22153 USA
Attn: Lisa Mercado
Phone: 703-270-6787
E-mail: lisa.mercado@boeing.com

Boeing is the world˙s leading aerospace company and largest and most versatile manufacturer of commercial and military aircraft. Boeing designs and manufactures aircraft, electronic and defense systems, missiles, satellites and advanced communication systems. Boeing also is a major service provider to NASA for the space shuttle and International Space Station.

Cambridge University Press

32 Avenue of the Americas
New York NY 10013-2473 USA
Attn: James Murphy
Phone: 212-924-3900 x5074
E-mail: jmurphy@cambridge.org

Cambridge˙s publishing in books and journals combines state-of-the-art content with the highest standards of scholarship, writing and production. Visit our stand to browse new titles, available at a 20% discount, and to pick up sample issues of our journals. Visit our website to see everything we do: www.cambridge.org/us/.

Center for Lunar Science and Exploration

3600 Bay Area Boulevard
Houston TX 77058-1113 USA
Attn: Julie Tygielski
Phone: 281-486-2122
E-mail: tygielski@lpi.usra.edu

The Lunar and Planetary Institute (LPI) and the Johnson Space Center (JSC) have a long and successful history of collaborative research and exploration activities that began with the Apollo program. The LPI and JSC have harnessed that heritage to build the new Center for Lunar Science and Exploration to better support our nation's new lunar science and exploration activities.

Copernicus Meetings & Publications

Copernicus GmbH
Bahnhofsallee 1e
Goettingen
Lower Saxony 37081 Germany
Attn: Nadine Deisel
Phone: +49 551 900339-50
E-mail: nadine.deisel@copernicus.org

Serving Sciences since 1988! Copernicus.org aims to promote the sciences by organizing meetings, conferences and exhibitions; publishing peer-reviewed journals, in particular open access; supporting associations, societies and organizations in the fulfilment of their tasks and in their relation amongst each other; archiving data and information for public usage; and developing appropriate software solutions for achieving these aims.

EHS-Publishing

Ernest H Stegeman Publishing
P.O. Box 330
Eureka CA 95502 USA
Attn: Ernest H. Stegeman
Phone: 707-822-1597
E-mail: info@ehs-publishing.com

Self-published independent geologic research. Current research focused on Hudson Bay centered astrobleme.

Lockheed Martin

P. O. Box 179
Mail Stop S8110
Denver CO 80201 USA
Attn: Melissa Croswhite
Phone: 303-971-9646
E-mail: melissa.croswhite@lmco.com

Expanding our knowledge and understanding of the universe is a challenging endeavor that Lockheed Martin has been actively engaged in for nearly five decades. We have developed and deployed numerous spacecraft and products supporting our understanding of Earth and Planetary Science, Heliophysics, and Astrophysics. We˙re accountable to one standard: 100% Mission Success. We understand the risks and will not shy away from the hard challenges associated with this mission.

Lunar and Planetary Institute

3600 Bay Area Boulevard
Houston TX 77058-1113 USA
Attn: Julie Tygielski
Phone: 281-486-2122
E-mail: tygielski@lpi.usra.edu

The Lunar and Planetary Institute is a research institute that provides support services to NASA and the planetary science community, and conducts planetary science research under the leadership of staff scientists, visiting researchers, and postdoctoral fellows.

NASA

NASA Goddard Space Flight Center
Greenbelt MD 20771, USA
Attn: Winnie Humberson
Phone: 301 614-5560
E-mail: Winnie.H.Humberson@nasa.gov

NASA˙s Science Mission Directorate (SMD) carries out the scientific exploration of the Earth, Moon, Mars, and beyond. SMD engages the Nation˙s science community around the world to answer fundamental questions requiring the view from and into space. The Vision for Space Exploration is fostering a renaissance in lunar science, as the return of humans to the Moon both requires and enables greater scientific understanding of Earth˙s natural satellite.

NASA Ames Planetary Content Team

NASA Ames Research Center
Mail Stop 269-3
Moffett Field CA 94035 USA
Attn: Mike Lundy
Phone: 408-315-2509
E-mail: mike.lundy@nasa.gov

The Moon and Mars in Google Earth were developed through a collaboration between Google and the Planetary Content Team at the NASA Ames Research Center. The Planetary Content Team develops software that makes it easier for scientists and engineers to publish and access Earth and planetary imagery and data via the Internet.

NASA Lunar Science Institute

NASA Ames Research Center
Mail Stop 17-1
Moffett Field CA 94087 USA
Attn: Doris Daou
Phone: 650-604-2021
E-mail: Doris.Daou-1@nasa.gov

The NLSI brings together leading lunar scientists from around the world to further NASA lunar science and exploration.

PDS Geosciences Node

Washington University
Campus Box 1169
1 Brookings Drive
St. Louis MO 63130 USA
Attn: Dan Scholes
Phone: 314-935-8555
E-mail: scholes@wunder.wustl.edu

The Geosciences Node of NASA˙s Planetary Data System (PDS) archives and distributes data related to the study of the surfaces and interiors of terrestrial planetary bodies. We work with NASA missions to help them generate well-documented, permanent data archives. We provide data to NASA-sponsored researchers upon request, make data available using Analyst˙s Notebooks and Orbital Data Explorers, and provide expert assistance in using the data.

PDS Imaging Node

U.S. Geological Survey
2255 N. Gemini Drive
Flagstaff AZ 86001 USA
Attn: Patricia A. Garcia
Phone: 928-556-7246
E-mail: pgarcia@usgs.gov

The Imaging Node of the NASA Planetary Data System (PDS) maintains and distributes archives of large planetary image data collections acquired from NASA˙s flight projects with the primary goal of enabling the science community to perform image processing and analysis on the data. The Node provides direct access to the digital image archives via ftp transfer and a variety of websites. The Node also provides digital image processing tools and the expertise and guidance necessary to understand the image collections. Visit the PDS Imaging Node at http://pds-imaging.jpl.nasa.gov.

Southwest Research Institute

1050 Walnut Street, Suite 300
Boulder CO 80302, USA
Attn: William F. Bottke
Phone: 303-546-9670
E-mail: bottke@boulder.swri.edu

Southwest Research Institute, based in San Antonio, Texas, is an independent, nonprofit, applied engineering and physical science research and development organization. SwRI-Boulder˙s Department of Space Studies conducts observational, theoretical, and experimental research over a wide range of solar system and astrophysical topics. SwRI-Boulder˙s Department of Space Operations oversees science operations for several missions and conducts engineering and instrument development work.

Springer

233 Spring St.
Sixth Floor
New York NY 10013, USA
Attn: Maury Solomon
Phone: 212-460-1594
E-mail: maury.solomon@springer.com

Knowledge, information, and quality — these are the three things that shape Springer Science + Business Media's business activities. We develop, manage, and disseminate knowledge — through books, journals, and the Internet. We work with the world's best academics and authors in long-standing loyal partnerships based on mutual trust and we are always open to new input.

The National Academies/ Space Studies Board

500 5th Street NW
Washington DC 20001 USA
Attn: Celeste Naylor
Phone: 202-334-1886
E-mail: cnaylor@nas.edu

The Space Studies Board serves as the focus of the interests and responsibilities in space research within the National Academies. It provides an independent, authoritative forum for information and advice on all aspects of space science and applications. It oversees advisory studies (principally, the decadal surveys), facilitates international research coordination, and promotes communications on space science and science policy between the research community, the federal government, and the interested public.

The University of Arizona Press

355 S. Euclid, Suite 130
Tucson AZ 85719 USA
Attn: Arin Cumming
Phone: 520-621-4913
E-mail: acumming@uapress.arizona.edu

The University of Arizona Press is celebrating 50 years as a nonprofit publisher of scholarly and regional books. Under the guidance of General Editor Richard P. Binzel, The University of Arizona Space Science Series publishes state-of-the-art research across the space sciences. Recent titles in the series include *The Solar System Beyond Neptune* (2008), edited by M. A. Barucci, H. Boehnhardt, D. P. Cruikshank, and A. Morbidelli with assistance from Renée Dotson, and *Europa* (2009), edited by Robert T. Pappalardo, William B. McKinnon, and Krishan K. Khurana with assistance from Renée Dotson.

USGS Astrogeology Science Center

2255 N. Gemini Drive
Flagstaff AZ 86001 USA
Attn: Patricia A. Garcia
Phone: 928-556-7246
E-mail: pgarcia@usgs.gov

The United States Geological Survey˙s Astrogeology Science Center (USGS-ASC), located in Flagstaff, Arizona, provides support to the planetary community with unique in-house and on-line resources and tools to help researchers accomplish their science objectives. The USGS-ASC conducts innovative research and develops state-of-the-art software and techniques that advance the fields of planetary cartography, geoscience, and remote sensing. The USGS-ASC establishes mapping and data archive standards and distributes data and products using modern technology.

Wiley-Blackwell

350 Main Street
Malden MA 02148 USA
Attn: Taryn Goggin
Phone: 781-388-8361
E-mail: tgoggin@wiley.com

Wiley-Blackwell is the international scientific, technical, medical, and scholarly publishing business of John Wiley & Sons, with strengths in every major academic and professional field and partnerships with many of the world's leading societies. Wiley-Blackwell publishes over 1400 peer-reviewed journals as well as 1500+ new books annually in print and online, as well as databases, major reference works, and laboratory protocols. For more information, please visit www.wileyblackwell.com or www.interscience.wiley.com.

Guide to Technical Sessions and Activities

Tuesday Evening, March 2, 7:00 p.m.

Wednesday Morning, March 3, 8:30 a.m.

Friday Morning, March 5, 8:30 a.m.

Friday Afternoon, March 5, 1:30 p.m.

Print-Only Presentations

**** Denotes speaker***

PARENT CLOUD AND SOLAR NEBULA
Monday, 8:30 a.m. Waterway Ballroom 1

Chairs: **Subrata Chakraborty and Richard Carlson**

8:30 a.m. Smith R. L. * Pontoppidan K. M. Young E. D. Morris M. R.
Observations of High $^{12}CO/^{13}CO$ Toward Protostars and Implications for the Origin of the $^{12}C/^{13}C$ Ratio in the Solar System **[#2254]**
We present high $^{12}CO/^{13}CO$ abundance ratios toward several YSOs in Rho Ophiuchus. Our results may be revealing an evolutionary trend from diffuse cloud to YSO, which would impact GCE models used to explain solar system and ISM $^{12}C/^{13}C$ discrepancies.

8:45 a.m. Young E. D. * Pontoppidan K. M. Smith R. L. Morris M. R. Gounelle M.
The Oxygen Isotopic Case for Supernova Enrichment of the Solar System Birth Environment **[#1550]**
New oxygen isotope ratios for young stellar objects establish the disparity between solar system and galactic $^{18}O/^{17}O$. We present evidence that the best explanation for this disparity is enrichment of the solar birth environment by exploding B stars.

9:00 a.m. Throop H. B. *
Formation of Jupiter's Atmosphere from a Supernova-Contaminated Molecular Cloud **[#1409]**
Jupiter's heavy element enrichment may have come from late injection of SN debris into the Sun's birth molecular cloud.

9:15 a.m. Dominguez G. *
A Heterogeneous Chemical Origin for ^{16}O Enriched and ^{16}O Depleted Reservoirs in the Early Solar System **[#1992]**
I propose that the ^{16}O-rich and ^{16}O-poor reservoirs present in the early solar system were produced by heterogeneous chemical reactions that produce H_2O on the surface of interstellar dust grains in dense molecular clouds.

9:30 a.m. Liffman K. *
Particle Formation and ^{16}O Enrichment from the Inner Rim of the Solar Nebula. **[#1135]**
The Jet Flow Model is used to deduce an evolutionary track on the oxygen three-isotope diagram. In terms of age, the model predicts that ordinary chondrite chondrules > enstatite chondrules > carbonaceous chondrite chondrules.

9:45 a.m. Chakraborty S. * Davis R. Ahmed M. Jackson T. L. Thiemens M. H.
Wavelength Dependent Oxygen Isotopic Fractionation in the VUV Photodissociation of CO: An Early Solar System Perspective **[#2077]**
In this abstract we present new data on wavelength dependent oxygen isotopic fractionation in CO photolysis. The direct relevance of this data set for the oxygen isotopic composition of the solar system is discussed.

10:00 a.m. Lyons J. R. * Stark G. Heays A. N.
Asessment of CO Photodissociation Experiments by Model Simulations and Spectroscopic Measurements **[#2651]**
Model simulations of CO photodissociation experiments demonstrate strong self-shielding, but also show a dependence on the residence time of the gas in the photocell.

10:15 a.m. Yokoyama T. * Alexander C. M. O'D. Walker R. J.
Osmium Isotope Anomalies in Acid Residues from Enstatite Chondrites **[#1568]**
Acid residues from type 3–4 enstatite chondrites are enriched in Os isotopes produced by s-process, suggesting the preferential preservation of s-process-enriched phases under reducing conditions in the early solar system.

10:30 a.m. Papanastassiou D. A. * Chen J. H. Dauphas N.
Anomalous ^{53}Cr and ^{54}Cr and Nearly Normal Ni in Differential Dissolution Steps of Murchison **[#2068]**
Acid leachates of Murchison confirm the presence of large ^{54}Cr and ^{53}Cr effects, but significantly smaller than in the bulk acid residues of Murchison. Ni isotopes on the first leachate are normal, while the second leachate shows resolved Ni anomalies.

10:45 a.m. de Leuw S. Papanastassiou D. A. Wasson J. T. *
Chromium Isotopes in Chondrites and the Heterogeneous Accretion of the Solar Nebula **[#2703]**
There are different $\varepsilon^{54}Cr$ values in CC, EC and OC; the ^{54}Cr anomaly is a nuclear effect. Cr isotopes were not homogenized in the nebula or in the parental molecular cloud. CAIs cannot form by evaporation of chondritic materials.

11:00 a.m. Carlson R. W. * Qin L. Alexander C. M. O'D.
Ba, Nd and Sm Isotope Anomalies in Murchison Leaches: Distinct Carriers of s- and r-Process Nucleosynthetic Components **[#2415]**
Isotopic anomalies in Ba, Nd and Sm in Murchison leaches indicate variable mixes of s- and r-process contributions. $^{142}Nd/^{144}Nd$ is sensitive to such variability, but the data do not support a nucleosynthetic origin for chondrite-Earth differences.

11:15 a.m. Huang S. * Farkas J. Jacobsen S. B.
Non-Mass Dependent Ca Isotopic Composition in the Inner Solar System Objects **[#1379]**
We report non-mass dependent Ca isotopic compositions of samples from Earth, Moon, Vesta, chondrites, and Allende CAIs.

11:30 a.m. Nagahara H. * Ozawa K.
Condensation and Its Inference on Cosmochemical Fractionation **[#1748]**
Kinetic condensation calculation with heterogeneous nucleation explains the cosmochemical fractionations in chondrites and inner planets. Carbonaceous chondrites were formed in more slowly cooled gas than ordinary chondrites.

11:45 a.m. Boss A. P. * Keiser S. A.
Increased Short-lived Radioisotope Injection Efficiencies for Presolar Cloud Collapse Triggered by a Supernova or AGB Star Shock Wave **[#1090]**
New models of simultaneous triggered collapse and injection show that injection efficiencies and dilution factors can be increased by factors greater than 10 and 100, respectively, bringing them into agreement with inferred SLRI abundances.

MARTIAN ALTERATION PROCESSES: IN THE LABORATORY, FROM ORBIT, AND IN SITU
Monday, 8:30 a.m. Waterway Ballroom 4

Chairs: **Albert Yen and Debra Buczkowski**

8:30 a.m. Kraft M. D. * Rogers A. D. Fergason R. L. Michalski J. R. Sharp T. G.
Spectral and Geomorphic Evidence for Chemical Weathering in the Icy Plains of Acidalia Planitia, Mars **[#2600]**
Known compositional differences in high-silica materials of Acidalia Planitia are explored in detail with THEMIS data. They are closely correlated to periglacial features, suggesting aqueous alteration in icy soil environments in northern Acidalia.

8:45 a.m. Arvidson R. E. * Athena Science Team
Recent Scientific Results from Spirit's Observations of Sulfate Sands on the Side of Scamander Crater, Columbia Hills, Mars **[#1247]**
Spirit has observed sulfate enriched material at Scamander crater that is interpreted to have formed via aqueous processes associated with early volcanism and later redistributed in association with orbitally-induced climate change.

9:00 a.m. McGlynn I. O. * McSween H. Y. Fedo C. M. Rogers A. D.
Indications of Water-limited Alteration from Martian Soil Mineralogy **[#2166]**
The physical and chemical weathering of basaltic soils is characterized through the evaluation of mineralogical changes, regional differences, and the timing and mechanisms of alteration, in sediments at Gusev Crater and Meridiani Planum.

9:15 a.m. Yen A. S. * Clark B. C. Ming D. W. Mittlefehldt D. W. Gellert R. Morris R. V.
Chemical Alteration on Mars Indicated by the Iron-Manganese Ratio **[#2546]**
The iron-manganese ratio can be used to establish the extent of aqueous weathering in samples analyzed by the Mars Exploration Rovers.

9:30 a.m. Wendt L. * Gross C. Kneissl T. Sowe M. Combe J.-P. LeDeit L. McGuire P. C. Neukum G.
Sulfates and Iron Oxides in Ophir Chasma, Mars **[#1699]**
We identified sulfates, including jarosite, and iron oxides in Ophir Chasma around and within Ophir Mensa, based on OMEGA and CRISM data. This suggests sulfate formation both before or during ILD deposition and after their erosion.

9:45 a.m. Kounaves S. P. * Hecht M. H. Kapit J. Quinn R. C. Catling D. C. Clark B. C. Ming D. W. Gospodinova K. Hredzak P. McElhoney K. Shusterman J.
Confirmation of Soluble Sulfate at the Phoenix Landing Site: Implications for Martian Geochemistry and Habitability **[#2199]**
The Wet Chemistry Lab on the Phoenix Mars Lander has identified soluble sulfate in the soil, allowing for better accounting of soluble salts and indicating that under past conditions, a ratio of liquid water to soil > a few percent by mass could have led to habitable brines.

10:00 a.m. Milliken R. E. * Bish D. L. Bristow T. Mustard J. F.
The Case for Mixed-layered Clays on Mars **[#2030]**
We discuss the importance of mixed-layered clays in constraining crustal fluid circulation and heat flow, as well as the possibility that previously reported smectite clays may in fact be mixed-layered clays.

10:15 a.m. Noe Dobrea E. Z. * Swayze G.
Acid Pedogenesis on Mars? Evidence for Top-Down Alteration on Mars from CRISM and HiRISE Data **[#2620]**
We present evidence that suggests that at least some parts of Mars underwent a period of acid pedogenic alteration.

10:30 a.m. Flahaut J. * Clenet H. Mustard J. F. Quantin C. Allemand P.
Phyllosillicates and Low Calcium Pyroxene-rich Noachian Crust Exposures in the Walls of Valles Marineris, Mars **[#1524]**
The walls of Valles Marineris present the most well-exposed cross-sections through the martian crust. The present survey investigates this geologic record with CRISM and HiRISE data, revealing some very interesting mafic and hydrated mineralogies.

10:45 a.m. Lee C. B. * Park S. J.
Phyllosilicate Bearing Deposits at Mawrth Vallis: Stratigraphy and Possible Formation Processes **[#2138]**
This paper suggests that both weathering and hydrothermal alteration processes contribute to the stratigraphic development of phyllosillicates at Mawrth Vallis region.

11:00 a.m. Buczkowski D. L. * Seelos K. D. Murchie S. Seelos F. Malaret E. Hash C. CRISM Team
Extensive Phyllosilicate-bearing Layer Exposed by Valley Systems in Northwest Noachis Terra **[#1458]**
Evidence for a widespread phyllosilicate-bearing layer has been identified in a distinct region in northwest Noachis Terra.

11:15 a.m. Velbel M. A. * Stopar J. D. Taylor G. J. Vicenzi E. P.
Aqueous Alteration of Olivine in Mars Meteorite MIL 03346: Corrosion Textures and Redistribution of Elements in Alteration Products **[#2223]**
Textural observations help distinguish terrestrial from pre-terrestrial aqueous alteration of olivine and associated alteration products in Mars meteorite MIL 03346.

11:30 a.m. Grotzinger J. P. *
Mars Science Laboratory, Preservation Potential of Biosignatures and Environmental Records, and the Attributes of Promising Landing Sites **[#2726]**
MSL will investigate a site that shows clear evidence for ancient aqueous processes based on orbital data and undertake the search for past and present habitable environments.

PLANETARY DIFFERENTIATION THROUGHOUT THE SOLAR SYSTEM
Monday, 8:30 a.m. Waterway Ballroom 5

Chairs: Jie Li and Wim van Westrenen

8:30 a.m. Barr A. C. * Canup R. M.
Origin of the Ganymede/Callisto Dichotomy by Impacts During an Outer Solar System Late Heavy Bombardment **[#1158]**
We show that the Ganymede/Callisto dichotomy arises as a natural result of dynamical sculpting of the outer solar system. Hypervelocity impacts occurring during an outer solar system late heavy bombardment trigger runaway differentiation in Ganymede, but not Callisto.

8:45 a.m. Li J. * Chen B. Hsieh W.-P. Trinkle D. Cahill D. G.
From Thermal Conductivity of Compressed Water Ices to Ganymede-Callisto Dichotomy and Callisto's Internal Ocean **[#1776]**
New measurements show doubling of water ice's thermal conductivity upon transformation from VI to VII under pressure. Highly conductive ice VII may shed light on thermal evolution and chemical differentiation of large icy moons.

9:00 a.m. Watson H. C. * Roberts J. J.
Permeability and Connectivity of Core Forming Melts: Quantitative Constraints from 3-D Imaging and Electrical Conductivity **[#2399]**
We experimentally determine the permeability and connectivity of up to 10 vol% sulfide melt in an olivine matrix using the complementary methods of X-ray microtomography and electrical conductivity.

9:15 a.m. Rubie D. C. * Frost D. J. Nimmo F. O'Brien D. P. Mann U. Palme H.
Accretion of Volatile Elements to the Earth and Moon **[#1134]**
Based on the results of high-pressure liquid-metal – liquid-silicate partitioning experiments, the volatile elements Mn, Ga, Na, Zn and In were accreted to the Earth towards the end of accretion but before core formation was complete.

9:30 a.m. Righter K. *
Conditions of Core Formation in the Early Earth: Single Stage or Heterogeneous Accretion? **[#2301]**
Combination of new and literature data for metal-silicate partition coefficients for siderophile elements (Ni, Co, Mo, W, P, Ga, Cu, Mn, V, Cr, Pd) show that Earth's mantle equilibrated with core forming Fe metal at 32–42 GPa and 2500–2700 K.

9:45 a.m. Burkemper L. K. * Agee C. B.
The Effect of Pressure and Temperature on Molybdenum Solubility in Silicate Melts **[#1376]**
Molybdenum solubility in peridotite and basaltic melts over a range of pressures and temperatures was investigated and implications for core formation are presented.

10:00 a.m. Hill E. Domanik K. Drake M. J. *
Metal/Silicate Partitioning of the Moderately Siderophile Elements: The Effect of Temperature and C Concentration **[#1519]**
Increasing T in a magma ocean would result in reduced metal/silicate partitioning for Mo, W and V, simultaneously, the C-concentration in the metal may determine the presence or absence of V in the metal-melt.

10:15 a.m. Rai N. * Walter M. J. Hawkesworth C. J.
Metal Silicate Partitioning of Siderophile Elements and Core Formation in Planets **[#1624]**
We investigate whether the silicate Earth's abundance of siderophile elements can be reconciled with single stage metal-silicate equilibrium.

10:30 a.m. Chabot N. L. * McDonough W. F. Saslow S. A. Draper D. S. Jones J. H. Agee C. B.
Examining the Effect of Pressure on Solid Metal/Liquid Metal Partitioning Behavior **[#1398]**
We present results from experiments in the Fe-S system at 9 GPa that show that pressure affects the solid metal/liquid metal partitioning behavior of many trace elements in this system.

10:45 a.m. Médard E. * Schmidt M. W. Wähle M. Keller N. S. Günther D.
Pt in Silicate Melts: Centrifuging Nanonuggets to Decipher Core Formation Processes **[#2639]**
We describe a series of experiments to constrain the nature and the formation mechanisms of nanonuggets, and develop new techniques for accurate determination of partition coefficients for the highly siderophile elements.

11:00 a.m. Nebel O. van Westrenen W. * Vroon P. Z. Raith M. M.
Storing Earth's Missing Niobium in the Terrestrial Counterpart of Evolved Lunar Magma Ocean Melts **[#1814]**
High-precision Nb-Ta data for Fe-rich rocks associated with a terrestrial anorthosite resemble lunar KREEP, with superchondritic Nb/Ta ratios and elevated Nb contents. Early deep mantle storage of such rocks can readily explain Earth's Nb deficit.

11:15 a.m. Sio K. * Dauphas N. Roskosz M.
Can Core Formation in Planetesimals Fractionate Iron Isotopes? Clues from a Study of Metal-Silicate Assemblages in Disko Basalt, Greenland **[#1467]**
Iron isotopes are found to be fractionated in terrestrial metal-silicate assemblages in Disko basalts. Measurements are compared to theoretical predictions of Polyakov and Mineev (2000). Discussions involved kinetic and equilibrium fractionation.

11:30 a.m. Weiss B. P. * Carporzen L. Elkins-Tanton L. T. Shuster D. L. Ebel D. S. Gattacceca J. Zuber M. T. Chen J. H. Papanastassiou D. A. Binzel R. P. Rumble D. Irving A. J.
A Partially Differentiated Body for CV Chondrites? **[#1688]**
Magnetic analyses suggest the CV chondrite parent body was partially differentiated. We are testing this hypothesis with new magnetic studies, analyses of possibly cogenetic achondrites, and by searching for partially differentiated asteroids.

11:45 a.m. Yang J. * Goldstein J. I. Scott E. R. D.
Meteorite and Theoretical Constraints on the Crystallization of Asteroidal Cores: Inside-Out or Outside-In? **[#1557]**
This research shows why some metallic core of asteroids crystallized inside-out and others outside-in and meteorite evidence is given.

SPECIAL SESSION: A NEW MOON: LUNAR RECONNAISSANCE ORBITER RESULTS
Monday, 8:30 a.m. Waterway Ballroom 6

Chairs: Jeff Plescia and Mike Wargo

8:30 a.m. Vondrak R. * Keller J. Chin G. Garvin J.
The Lunar Reconnaissance Orbiter at the Midpoint of the Exploration Mission **[#1660]**
The Lunar Reconnaissance Orbiter (LRO) was launched on June 18, 2009 and arrived at the Moon five days later. This presentation updates the status and recent results from the LRO Exploration Mission, as well as the plans for the Science Mission.

8:55 a.m. Spence H. E. * CRaTER Science Team
Lunar Cosmic Ray Albedo Measurements Using the Cosmic Ray Telescope for the Effects of Radiation on the Lunar Reconnaissance Orbiter **[#2659]**
CRaTER measurement capabilities provide new insights on the spatial and temporal variability of the GCR populations and their interactions with the lunar surface.

9:20 a.m. Gladstone G. R. *
Initial Results from the Lyman Alpha Mapping Project (LAMP) Instrument on the Lunar Reconnaissance Orbiter (LRO) Mission **[#2277]**
LAMP is a far-ultraviolet (FUV) imaging spectrograph on NASA's LRO mission. LAMP will map the Moon at FUV wavelengths, allowing new studies of the microphysical and reflectance properties of the regolith. Preliminary mapping and LCROSS support results are presented.

9:45 a.m. Mitrofanov I. * Boynton W. Chin G. Golovin D. Evans L. Harshman K. Garvin J. Kozyrev A. Litvak M. McClanahan T. Malakhov A. Milikh G. Mokrousov M. Nandikotkur G. Nuzhdin I. Sanin A. Starr R. Sagdeev R. Shevchenko V. Shvetsov V. Tretyakov V. Trombka J. Varennikov A. Vostrukhin A.
LEND Experiment Onboard LRO: Testing Local Areas with High Concentrations of Hydrogen at the Lunar Poles **[#2250]**
The LEND measurements of lunar neutron emission allow us to test local areas with high concentration of hydrogen at lunar poles and to compare two models of the nature of the hydrogen reach area.

10:10 a.m. Robinson M. S. * Eliason E. M. Hiesinger H. Jolliff B. L. McEwen A. S. Malin M. C. Ravine M. A. Thomas P. C. Turtle E. P. Bowman-Cisneros E. LROC Team
Lunar Reconnaissance Orbiter Camera: First Results **[#1874]**
Overview of LROC data collection to date, with summary of early exploration and science results.

10:35 a.m. Bussey D. B. J. * Spudis P. D. Butler B. Carter L. M. Gillis-Davis J. J. Heggy E. Kirk R. Neish C. Nozette S. Patterson G. W. Robinson M. S. Raney R. K. Thompson T. Thomson B. J. Ustinov E.
Initial Results from Mini-RF: A Synthetic Aperture Radar on Lunar Reconnaissance Orbiter **[#2319]**
Mini-RF is a lightweight Synthetic Aperture Radar instrument orbiting the Moon aboard Lunar Reconnaissance Orbiter. It is acquiring high-quality data in both S and X bands in support of the LRO mission goals.

11:00 a.m. Smith D. E. * Zuber M. T. Neumann G. A. Lemoine F. G. Mazarico E. Torrence M. H. Duxbury T. H. Head J. III Aharonson O. LOLA Science and Instrument Team
LOLA Observations of the Moon **[#1993]**
The LOLA instrument on LRO has been operating since July 2009 and acquired significant altimetric data of the Moon.

11:25 a.m. Paige D. A. * Greenhagen B. T. Vasavada A. R. Allen C. Bandfield J. L. Bowles N. E. Calcutt S. B. DeJong E. M. Elphic R. C. Foote E. J. Foote M. C. Donaldson Hanna K. L. McCleese D. J. Ghent R. R. Glotch T. D. Hayne P. O. Lucey P. G. Murray B. C. Schofield J. T. Siegler M. A. Snook K. Soderblom L. A. Song E. . Taylor F. W. Thomas I. R. Wyatt M. B.
Diviner Lunar Radiometer Experiment: Early Mapping Mission Results **[#2267]**
Diviner's growing dataset is revealing the extreme nature of the lunar thermal environment and its diurnal and seasonal variability, as well as aspects of the Moon's composition and the nature of the lunar polar cold traps.

PLENARY SESSION: MASURSKY LECTURE AND DWORNIK AWARD PRESENTATIONS
Monday, 1:30 p.m. Waterway Ballroom 4

Chairs: **Stephen Mackwell and Eileen Stansbery**

Presentation of the 2009 GSA Stephen E. Dwornik U.S. Citizen Student Award Winners

Best Graduate Oral Presentation:
Brendan Hermalyn, Brown University, *"Early-Stage Ejecta Velocity Distribution"*
Best Undergraduate Oral Presentation:
Paul Richardson, University of Washington, "*The Relationship Between Lava Fans and Tubes on Olympus Mons in the Tharsis Region, Mars"*
Best Graduate Poster Presentation:
Michael Krawczynsky, Massachusetts Institute of Technology, *"Titanium Oxidation State and Coordination in the Lunar High-Titanium Glass Source Mantle"*

Best Undergraduate Poster Presentation:
Mairi Litherland, Rice University, *"Effects of Planetary Radius on Lithospheric Stresses and Magma Ascent on the Terrestrial Planets"*
Honorable Mention (Oral):
Mark Salvatore, Brown University, *"Assessing the Mineralogy of Acidalia Planitia, Mars, Using Near-Infrared Orbital Spectroscopy"*
Honorable Mention (Oral):
Kaylan Burleigh, University of Arizona, *"Small Impacts Trigger Dust Landslides on Mars"*

Presentation of the 2010 LPI Career Development Award Winners

Masursky Lecture
Masursky Lecture by Dr. Ronald Greeley
Shifting Sands: Planetary Atmosphere-Surface Interactions

FORMATION OF FIRST SOLAR SYSTEM SOLIDS
Monday, 2:30 p.m. Waterway Ballroom 1

Chairs: **Steven Simon and Julie Paque**

1:30 p.m. Nagashima K. * Krot A. N. Huss G. R. Yurimoto H.
Micron Scale Oxygen Isotope Heterogeneity in Anorthite of A Forsterite-bearing Type B CAI E60 from Efremovka **[#2255]**
Oxygen isotope imaging with UH Cameca ims 1280+SCAPS isotope microscope of a Fo-B CAI E60 from Efremovka revealed complex distributions of O-isotopes in anorthite supporting isotopic exchange with ^{16}O-poor gas during remelting and recrystallization.

1:45 p.m. Mendybaev R. A. * Richter F. M. Spicuzza M. J. Valley J. W. Davis A. M.
Oxygen Isotope Fractionation During Evaporation of Mg- and Si-rich CMAS-Liquids in Vacuum **[#2725]**
We report oxygen isotope data for the residues produced by evaporation of Mg- and Si-rich CMAS-liquids. The results on oxygen together with Mg- and Si-isotopes in the experimental run products are used to estimate the isotopic compositions of natural FUN CAIs.

2:00 p.m. Simon S. B. * Sutton S. R. Grossman L.
Ti-XANES Analyses of Spinel in Coarse-grained Refractory Inclusions from Allende **[#1459]**
The valence of Ti in spinel in each of the major types of coarse-grained refractory inclusions is reported. Ti^{3+} is found in most spinels, and there is a relationship between the Ti valence of a spinel grain and its petrographic setting.

2:15 p.m. Dyl K. A. * Young E. D.
A Reaction Space for Wark-Lovering Rim Formation in an Oxidizing Solar Nebula **[#2388]**
We explore reaction space for CAI interior pyroxene in a chondritic, oxidizing solar nebula. This results in pyroxene compositions found in Wark-Lovering rims.

2:30 p.m. Paque J. M. * Sutton S. R. Burnett D. S. Beckett J. R. Simon S. B.
An Intimate Mix of Highly Oxidizing and Highly Reducing Environments: Relict Spinel Determined by XANES in a Partially Melted Allende Ca-Al-Rich Inclusion **[#1391]**
Ti and V valence in spinels from a Type B1 CAI and an experimental sample run under reducing conditions were determined by X-ray absorption near edge spectroscopy (XANES). The Ti^{4+}-rich cores of spinels are not in equilibrium with the host mineral.

2:45 p.m. Bullock E. S. * Richter F. M. Kita N. T. Davis A. M.
Mg Isotope Fractionation in Melilite Within an Allende Type B2 CAI **[#2500]**
Differences between Type B1 and Type B2 CAIs are explored in terms of their petrography and Mg isotopic composition.

3:00 p.m. Bermingham K. R. * Mezger K.
Ba Isotope Abundances in Equilibrated Meteorites and CAIs **[#1735]**
We report on the Ba isotope abundances in eleven bulk meteorite and CAI samples. Our data indicates that bulk meteorite samples are isotopically indistinguishable from terrestrial standards and that some CAIs possess an excess in ^{135}Ba of ~ ½ ε unit.

3:15 p.m. Ciesla F. J. * Yang L.
The Dynamics and Ages of Refractory Objects in the Solar Nebula **[#1081]**
The evolution of the solar nebula favors the survival of refractory objects formed during t <50,000 years of solar system formation over those formed at later times. This explains the brief formation interval of CAIs inferred from ^{26}Al studies.

3:30 p.m. Desch S. J. * Morris M. A. Connolly H. C. Jr.
A Critical Examination of the X Wind Model for the Formation of Chondrules and CAIs **[#2200]**
We critically examine the "X wind model" for chondrule and CAI formation and radionuclide production. We identify internal inconsistencies and predictions at odds with observations that lead us to reject it.

EXPERIMENTAL CONSTRAINTS ON MARTIAN ALTERATION PROCESSES
Monday, 2:30 p.m. Waterway Ballroom 4

Chairs: **Adrian Brearley and Harry McSween**

2:30 p.m. Maturilli A. * Helbert J. D'Amore M.
Dehydration of Phyllosilicates Under Low Temperatures: An Application to Mars **[#1299]**
Experiment on dehydration of standard martian soil analogue (phyllosilicate) was conducted at low temperatures, typical of daily Mars. Spectra shows the trend of water loss with temperature increase and time.

2:45 p.m. Morris R. V. * Ming D. W. Golden D. C. Graff T. G. Achilles C. N.
Evidence for Interlayer Collapse of Nontronite on Mars from Laboratory Visible and Near-IR Reflectance Spectra **[#2156]**
The low relative intensity of H_2O bands compared to $(Fe^{3+})2OH$ bands and the absence of well-defined Fe^{3+} bands for martian nontronite are evidence for loss of interlayer H_2O if not interlayer collapse in response to arid environmental conditions.

3:00 p.m. Che C. * Glotch T.
The Effect of High Temperatures on the Emission and VNIR Reflectance Spectra of Phyllosilicates and Zeolites **[#1513]**
In this study, we will report emissivity and visible and near-IR (VNIR) reflectance spectra of 14 phyllosilicates, 2 zeolites, and their heating products in order to provide laboratory data for martian exploration.

3:15 p.m. Zahrai S. K. * Elwood Madden M. E. Madden A. S. Miller M. A. Rimstidt J. D.
Jarosite Dissolution Rates and Lifetimes Under Mars-Analog Conditions **[#1411]**
Jarosite particle lifetimes have been determined based on laboratory dissolution rate experiments. Calculations suggest that even under low temperature, high salinity conditions, Meridiani Planum was wet for geologically short periods of time.

3:30 p.m. Madden A. S. Elwood Madden M. E. * Hamilton V. E.
Formation of Mars Analog Crystalline Hematite from Nanophase Hematite Under Low Temperature Aqueous Conditions **[#1528]**
We demonstrate that freeze-thaw cycles and/or cryodesiccation can produce crystallographically oriented coarse crystalline hematite from hematite nanoparticles, similar to the nanophase iron oxide commonly observed on Mars.

3:45 p.m. Wang Alian. * Ling Z. C. Freeman J. J.
Stability Fields and Phase Transition Pathways of Ferric Sulfates in 50°C to 5°C Temperature Range **[#2303]**
We report the results from a set of 150 experiments on stability fields and phase transition pathways of five hydrated ferric sulfates at three temperatures and ten relative humidity levels.

4:00 p.m. Chevrier V. * Dehouck E. Gaudin A. Mangold N. Mathe P. E. Rochette P.
Experimental Verification of the "Burns" Hypothesis for the Formation of Meridiani Planum Sediments Through Weathering of Sulfide-rich Deposits **[#2440]**
Four-year-long experiments in CO_2 + (H_2O or H_2O + H_2O_2) atmospheres show that oxidative weathering of pyrrhotite and primary silicate (olivine, pyroxene) mixtures reproduces the mineralogical assemblages observed in the Meridiani Planum deposits.

4:15 p.m. Adcock C. T. Hausrath E. M.
Kinetic Studies of Phosphate Containing Minerals and Implications for Mars **[#2177]**
Aqueous alteration on Mars is important for understanding the climate history and potential for life. Dissolution studies of phosphate-bearing minerals may help interpret observations from meteorites, remote sensing, and rover analyses from Mars.

4:30 p.m. Jänchen J. * Feyh N. Möhlmann D. T. F.
The Hydration and Dehydration Properties of Hygroscopic Chlorides and Biofilms Under Martian Environmental Conditions **[#1244]**
We show results of the hydration and dehydration of chlorides recently identified in deposits on the martian surface and of biofilms to improve the understanding of exobiological aspects on Mars for future missions such as MSL and ExoMars/MicrOmega.

VENUS
Monday, 2:30 p.m. Waterway Ballroom 5

Chairs: **Sue Smrekar and Gerald Galgana**

2:30 p.m. Basilevsky A. T. * Shalygin E. V. Titov D. V. Markiewicz W. J. Scholten F. Roatsch Th. Fiethe B. Osterloh B. Michalik H. Kreslavsky M. A. Moroz L. V.
Geologic Analysis of the Surface Thermal Emission Images Taken by the VMC Camera, Venus Express **[#1133]**
Analysis of Venus Monitoring Camera 1-µm images and surface emission modeling showed apparent emissivity at Chimon-mana tessera and shows that Tuulikki volcano is higher than that of the adjacent plains; Maat Mons did not show any signature of ongoing volcanism.

2:45 p.m. Bondarenko N. V. *
Integrated Study of the Venus Surface with Magellan Data: An Opportunity to Search for Surficial Deposits and Warm Lava Flows **[#1579]**
Magellan data were used to show that the combination of radiometry and scatterometry can be useful for detection of volcanic flows on Venus surface with temperature excess at shallow depth and the presence of extended crater-related deposits not seen in SAR images.

3:00 p.m. Russell C. T. * Strangeway R. J. Wei H. Y. Zhang T. L.
Venus Lightning: What We Have Learned from the Venus Express Fluxgate Magnetometer **[#1215]**
The Venus Express magnetometer sees short (tens of milliseconds) pulses of EM waves in the Venus ionosphere as predicted by the lightning model for the PVO electric pulses. These waves are stronger than similar terrestrial signals produced by lightning.

3:15 p.m. James P. B. * Zuber M. T. Phillips R. J.
Geoid to Topography Ratios on Venus and Implications for Crustal Thickness **[#2663]**
Using gravity and topography data from the Magellan mission, we develop a crustal thickness map of Venus. We also calculate geoid to topography ratios in order to identify regions of dynamic support.

3:30 p.m. Smrekar S. E. * Stofan E. R. Martin P. Hoogenboom T. Buck W. R.
Models of Hecate Chasma, Venus and Implications for Active (?) Extension **[#1422]**
A simple uniform extension model applied to Hecate Chasma provides a good fit to rift style and width for an extensional velocity of ~0.1 cm/yr. The transition between narrow and wide rifts occurs at a similar width (~125 km) as for rifts on Earth.

3:45 p.m. Galgana G. A. * Grosfils E. B. McGovern P. J.
Radial Dike Formation on Venus from Upper Lithosphere Magma Chambers: Insights from Models of Uplift, Flexure and Magmatism **[#1777]**
This research explains the coupled effects of magma chamber pressurization and flexure-causing lithosphere uplift on magma reservoir failure, radial dike formation, and magma ascent on Venus.

4:00 p.m. Clegg S. M. * Barefield J. E. Wiens R. C. Sharma S. K. Misra A. K. Tucker J. Dyar M. D. Lambert J. Smrekar S. Treiman A.
Venus Geochemical Analysis by Remote Laser-induced Breakdown Spectroscopy (LIBS) **[#1631]**
This paper focuses on development of the LIBS technique to extract chemical composition and facilitate mineral/rock identification from LIBS spectra acquired under Venus-like conditions. Samples for these experiments were chosen to be geochemically-likely on Venus.

4:15 p.m. Herrick R. R. * Stahlke D. L. Sharpton V. L.
A New Data Set for Venus: Stereo-derived Topography for 20% of the Planet at Km-Scale Horizontal Resolution **[#1622]**
We have processed the Magellan same-side stereo data to produce topography with km-scale horizontal resolution. We will be describing the processing and showing examples of the data.

4:30 p.m. Hensley S. * Shaffer S.
Repeat Pass Radar Observations of Venus from the Magellan Radar System **[#2369]**
A demonstration of radar interferometric observation of Venus using Magellan S-band SAR data with a temporal baselines of 243 days is presented.

SPECIAL SESSION: WATER IN THE SOLAR SYSTEM: INCORPORATION INTO PRIMITIVE BODIES AND EVOLUTION
Monday, 2:30 p.m. Waterway Ballroom 6

Chairs: Lysa Chizmadia and Maria Teresa Capria

2:30 p.m. Dyar M. D. * Hibbitts C. A. Orlando T. M.
Mechanisms for Incorporation of Hydrogen in and on Terrestrial Planetary Surfaces **[#2116]**
Mechanisms for incorporation of hydrogen on terrestrial planetary surfaces are considered, including endogenic (juvenile) H in the interiors of planetary materials, bulk H on the surface, and results of exogenic alterations of surfaces.

2:45 p.m. Stimpfl M. Muralidharan K. * de Leeuw N. H. Runge K. Deymier P. A. Drake M. J.
Atomistic Simulations of Adsorption of Water onto Forsterite and Fayalite Planar Surfaces: Implication for the Origin of Water in the Inner Solar System **[#2493]**
Using atomistic and electronic structure calculations, it is shown that adsorption is a significant source of terrestrial planetary water.

3:00 p.m. Hoffman E. J. * Stewart E. J. Jr. Abreu N. M.
Hydration of Synthetic Mg-Silicates: A Temperature Study **[#2681]**
Synthetic Mg-silicate dust, humidified at temperatures around 20°C, produces XRD peaks differing from those of the raw material.

3:15 p.m. Chizmadia L. J. * Lebrón-Rivera S. A.
Temperature and pH Changes Associated with the Hydration of Amorphous Silicate Smokes **[#2536]**
The hydration of Fe-Si smokes results in acidic pH levels and negligible change in temperature. When mixed with Mg-Si smokes, pH becomes alkaline and temperature increases slightly. Water-rock ratio is a minor variable relative to composition.

3:30 p.m. Hibbitts C. A. * Dyar M. D. Orlando T. M. Grieves G. Moriaty D. Poston M. Johnson A.
Thermal Stability of Water and Hydroxyl on Airless Bodies **[#2417]**
This paper focuses on distinguishing between molecular water (H_2O) and hydroxyl (OH-) on the illuminated Moon and discusses their thermal stabilities, possible abundances, and mobilities.

3:45 p.m. Ostrowski D. R. * Sears D. W. G. Lacy C. H. S. Gietzen K. M.
Heating Experiments on Phyllosilicates-Evaporite Mixtures: Implications for the Surface Composition of C Asteroids **[#1235]**
Phyllosilicate-evaporite mixtures have been heated to various temperatures. The resulting samples have had their infrared spectra analyzed and compared to that of C asteroids to examine implications for the surface of the C asteroid complex.

4:00 p.m. Beck P. * Quirico E. Montes-Hernandez G. Bonal L. Bollard J. Orthous-Daunay F-R. Howard K. Schmitt B. Brissaud O.
Hydrous Mineralogy of CM and CI Chondrites from Infrared Spectroscopy and Their Relationship with Low Albedo Asteroids **[#1586]**
We report on NIR measurements of 9 CM and 3 CI chondrites. We reveal a spectral evolution among CM. We also show that high-T spectra are required to have a valid comparison with low albedo asteroids.

4:15 p.m. Kammer J. A. Sparks D. W. Tice M. M.
Molecular Hydrogen Evolution in Small Icy Planetesimals **[#2690]**
We evaluate the availability of hydrogen to potential biospheres in subsurface oceans of icy planetesimals in the early solar system. Much of the hydrogen produced is lost due to the rapidity of serpentinization and the low solubility of hydrogen.

4:30 p.m. Capria M. T. * Marchi S. De Sanctis M. C. Coradini A.
The Activity of Main Belt Comets **[#1207]**
Main belt comets are active objects orbiting in the main belt. We estimate the average time of formation of a crater and apply a model to investigate the dependence of activity on mantle thickness and how long the activity can last.

RADIONUCLIDES AND EARLY SOLAR SYSTEM CHRONOLOGY
Tuesday, 8:30 a.m. Waterway Ballroom 1

Chairs: **Harold C. Connolly Jr. and Ming-Chang Liu**

8:30 a.m. Amelin Y. * Kaltenbach A. Iizuka T. Stirling C. H. Ireland T. R. Petaev M. Jacobsen S. B.
Importance of Uranium Isotope Variations for Chronology of the Solar System's First Solids **[#1648]**
We report combined U-Pb age for Allende CAI SJ101, and U isotopic composition of that CAI and Allende chondrules and bulk meteorite. The CAI-chondrule formation time interval is revised considering the difference in U isotope composition.

8:45 a.m. Brennecka G. A. * Wadhwa M. Janney P. E. Anbar A. D.
Towards Reconciling Early Solar System Chronometers: The 238U/235U Ratios of Chondrites and D'Orbigny Pyroxenes **[#2117]**
A new 238U/235U ratio for the pyroxene fraction of the D'Orbigny angrite adjusts the previously reported Pb-Pb age of –0.6±0.3 Ma. This adjustment affects all short-lived chronometers anchored to D'Orbigny and reconciles some discrepancies in early solar system materials.

9:00 a.m. Chakrabarti R. * Jacobsen S. B.
The Isotopic Composition of Magnesium in the Inner Solar System **[#1415]**
We have accurately determined the Mg isotopic composition of the bulk silicate Earth, chondrites, Mars, Moon and pallasites and show that the Earth is chondritic in Mg isotopes; the stable Mg isotopic composition of inner solar system is homogeneous.

9:15 a.m. Makide K. * Nagashima K. Krot A. N. Huss G. R.
Variations of Initial Abundance of ^{26}Al Among the Micron-sized ^{16}O-rich, Solar Corundum Grains from Ordinary and Carbonaceous Chondrite **[#2283]**
Magnesium isotopic compositions measured in µm-sized ^{16}O-rich, solar corundum grains from UOCs and unmetamorphosed CCs revealed lack of resolvable 26Mg excess in 43% of them, suggesting heterogeneous distribution of ^{26}Al in the early solar system.

9:30 a.m. Connolly H. C. Jr. * Young E. D. Huss G. R. Nagashima K. Beckett J. R. McCoy T. J.
To Be or Not To Be Canonical, What's New? The Search for the Initial ^{26}Al Abundance of the Solar System **[#1933]**
We report on our confirmation by SIMS analyses of the initial ^{26}Al/^{27}Al data by LA-MC-ICMPS of Young et al. (2005) for Leoville 144A. The major question we explore is how the initial ^{26}Al/^{27}Al of inclusions became disturbed.

9:45 a.m. Kita N. T. * Ushikubo T. Davis A. M. Knight K. B. Mendybaev R. A. Richter F. M. Fournelle J. H.
Initial ^{26}Al Abundance in a Type B CAI: Remelting of Pre-Existing Refractory Solid **[#2154]**
High precision SIMS internal isochron of Leoville 3535-1 type B1 CAI indicates that it melted 30–40 k.y. after the formation of first solids in the solar system from refractory precursor solids and possibly it melted multiple times.

10:00 a.m. MacPherson G. J. * Kita N. T. Ushikubo T. Bullock E. S. Davis A. M.
High-Precision ^{26}Al/^{27}Al Isochron Microchronology of the Earliest Solar System **[#2356]**
High precision SIMS Mg-isotopic measurements of 6 diverse Vigarano CAIs yield values for initial ^{26}Al/^{27}Al that resolvably differ, with primitive CAIs consistently near 5.2×10^{-5} but melted CAIs extending over a range $4.2–5.2 \times 10^{-5}$.

10:15 a.m. Davis A. M. * Kita N. T. Ushikubo T. MacPherson G. J. Bullock E. S. Knight K. B.
Magnesium Isotopic Evolution of CAIs **[#2496]**
Mg isotopic evolution of CAIs is used to infer the timing of Mg/Al fractionation of CAIs, which, for most melted CAIs, occurred earlier than melting. New CAI data are consistent with uniform $^{26}Al/^{27}Al$ and initial Mg isotopic composition in the solar system.

10:30 a.m. Krot A. N. * Nagashima K. Hutcheon I. D. Ishii H. A. Jacobsen B. Yin Q.-Z. Davis A. M. Simon S. B.
Mineralogy, Petrography, Oxygen and Magnesium Isotopic Compositions and Formation Age of Grossular-bearing Assemblages in the Allende CAIs **[#1406]**
Large excesses of 26Mg corresponding to the canonical $^{26}Al/^{27}Al$ in grossular veins crosscutting åkermanite-poor melilite mantles in Type B1 CAIs ratio were inherited from melilite and do not require early formation of grossular in the solar nebula.

10:45 a.m. Matzel J. E. P. * Jacobsen B. Hutcheon I. D. Krot A. N. Nagashima K. Yin Q.-Z. Ramon E. C. Weber P. K. Wasserburg G. J.
Distribution and Origin of 36Cl in Allende CAIs **[#2631]**
We present ^{36}Cl-^{36}S isotope data from wadalite and sodalite in Allende CAIs to investigate the origin and distribution of ^{36}Cl in early solar system materials.

11:00 a.m. Liu M.-C. * Nittler L. R. Alexander C. M. O'D. Lee T.
Boron Isotopic Compositions in CM Hibonites: A NanoSIMS Approach **[#1277]**
We developed a technique to analyze the ^{10}Be-^{10}B short-lived system in hibonite grains extracted from the Murchison meteorite.

11:15 a.m. Ito M. * Messenger S.
Fe-Ni Systematics in Fe-rich Olivine and Enstatite Chondules in Semarkona Chondrite Utilizing a NanoSIMS 50L Ion Microprobe **[#1724]**
We report results of Ni isotopic measurements in Fe-rich olivine and Fe-rich enstatite chondrules in Semarkona ordinary chondrite utilizing the JSC NanoSIMS 50L ion microprobe, and calculated the inferred $^{60}Fe/^{56}Fe$ of $(6.2 \pm 2.2) \times 10^{-7}$.

11:30 a.m. Steele R. C. J. * Elliott T. Coath C. D. Regelous M. Russell S. S.
Correlated Neutron Rich Ni Isotope Anomalies in Chondritic and Iron Meteorites **[#1984]**
Correlated $\varepsilon^{62}Ni$ and $\varepsilon^{64}Ni$ in bulk chondritic and iron meteorites suggests a variable contribution from a type Ia supernova component in the early solar system.

TERRESTRIAL PLANET CRYOSPHERES: ICE TABLES, GLACIERS, AND PERIGLACIAL LANDFORMS
Tuesday, 8:30 a.m. Waterway Ballroom 4

Chairs: Stephen Clifford and Douglas Kowalewski

8:30 a.m. Grimm R. E. * Painter S. L.
The Secular Loss of Groundwater on Mars **[#1329]**
The instability of ice at low latitudes on Mars also leads to massive groundwater evaporation. If loss has been retarded by lateral heterogeneity, the mid-latitude northern plains may be the last, best hope for accessible groundwater.

8:45 a.m. Clifford S. M. * Lasue J.
The Evolution and Fate of Groundwater on Mars: The Influence of Modeling Assumptions and Consistency of Predictions with Observational Constraints **[#2739]**
Two models of the hydrologic evolution of Mars are compared to identify the basis for their differing conclusions regarding the survival and distribution of present-day groundwater.

9:00 a.m. Plaut J. J. * Holt J. W. Head J. W. III Gim Y. Choudhary P. Baker D. M. Kress A. SHARAD Team
Thick Ice Deposits in Deuteronilus Mensae, Mars: Regional Distribution from Radar Sounding **[#2454]**
Radar sounding data from SHARAD on MRO are used to map the distribution of mid-latitude ice in the Deuteronilus Mensae region of Mars. Ice is widespread in the region, with thicknesses up to 1 km.

9:15 a.m. Kadish S. J. * Head J. W.
Impacts into Ice-rich Deposits on Mars: Excess Ejecta Craters, Perched Craters, and Pedestal Craters **[#1017]**
We compare formation mechanisms based on impacts into ice-rich material for excess ejecta craters, perched craters, and pedestal craters. We offer evidence for a genetic relationship based on their topography, morphology, and geographic distribution.

9:30 a.m. Byrne S. * Banks M. E. Dundas C. M. Mattson S. Russell P. S. Herkenhoff K. E. McEwen A. S.
North Polar Ice Accumulation Modeled from Impact Crater Statistics **[#1697]**
The population statistics and morphological evolution of 100 newly-discovered impact craters in the north polar ice cap of Mars are modeled to relate current climate to polar surface mass balance.

9:45 a.m. Kreslavsky M. A. * Head J. W. Maine A. Gray H. Asphaug E.
North-South Asymmetry in Degradation Raters of Small Impact Craters at High Latitudes on Mars: Implications for Recent Climate Change **[#2560]**
Density of small (5–50 m) impact craters on patterned ground at high latitudes is much lower in the N than in the S. This is explained by climate-precession-driven deposition of icy mantles ~1 ka ago in the N and ~20 ka ago in the S.

10:00 a.m. Séjourné A. * Costard F. Gargani J. Soare R. J. Marmo C.
The Polygon Junction Pits as an Evidence of a Particularly Ice-rich Area in Utopia Planitia **[#2113]**
The western part of Utopia Planitia contains different periglacial landforms. With HiRISE imagery we show that the polygon junction pits have a geographic distribution coinciding with an ice-rich unit and a thermokarst morphological evolution.

10:15 a.m. Hauber E. * Reiss D. Ulrich M. Krohn K. Preusker F. Trauthan F. Zanetti M. Hiesinger H. van Gasselt S. Jaumann R. Johansson L. Johnsson A. Olvmo M.
Debris Flow Fans and Permafrost Landforms on Svalbard (Norway): Terrestrial Analogues for Martian Mid-Latitude Periglacial Landscapes **[#1922]**
Young water- and ice-related landforms on Mars show a latitude-dependent distribution and bear a record of the recent climatic past. Morphological analogues from Svalbard help to develop evolutionary scenarios of martian permafrost environments.

10:30 a.m. Kowalewski D. E. * Morgan G. A. Marchant D. R. Head J. W. III
Influence of Textural and Topographic Variability on Sublimation of Buried Ice: Implications for Near Surface Ice Stability in Antarctica and Mars **[#2511]**
Our vapor diffusion modeling suggests surface textures, topography, and the presence of salt layers demonstrably alter sublimation rates in the McMurdo Dry Valleys and offer insight into similar environments in the hyper-arid cold climate of Mars.

10:45 a.m. Marchant D. R. * Mackay S. L. Head J. W. III Kowalewski D. E.
Documenting Microclimate Variation and the Distribution of Englacial Debris in Mullins Glacier, Antarctica: Implications for the Origin, Flow, and Modification of LDA and LVF on Mars **[#2601]**
Our results suggest that variations in both englacial-debris concentration and local environmental conditions impart first-order changes in the surface morphology of Mullins Glacier. Results can be applied toward understanding the distribution of debris in LDA and LVF.

11:00 a.m. Baker D. M. H. * Head J. W. Marchant D. R.
Plains and Transitional Textures Adjacent to Lobate Debris Aprons in Deuteronilus Mensae, Mars **[#1378]**
Analyses suggest that glacial ice in the northern mid-latitudes of Mars was more extensive in the recent past. Plains units and textures surrounding lobate debris aprons in Deuteronilus Mensae are examined in search of former glacial maxima.

11:15 a.m. Mège D. * Bourgeois O.
Destabilization of Valles Marineris Wallslopes by Retreat of Ancient Glaciers **[#1713]**
Deep-seated gravitational spreading of most Valles Marineris inter-chasma basement ridges strongly argues in favor of a minimum of 1 km of glacial infill, probably during the Hesperian.

11:30 a.m. Vincendon M. * Mustard J. Forget F. Kreslavsky M. Spiga A. Murchie S. Bibring J.-P.
Discovery of Buried Perennial Ice at Low Latitudes on Mars **[#1249]**
We show that the observed stability of seasonal CO_2 ice at low to mid-latitudes on Mars requires a high thermal inertia subsurface that can only be water ice. Ice is inferred in the southern hemisphere down to 25° latitude on pole facing slopes.

GROUND TRUTH GALORE: TERRESTRIAL IMPACT CRATERS
Tuesday, 8:30 a.m. Waterway Ballroom 5

Chairs: Axel Wittmann and Horton Newsom

8:30 a.m. Ormö J. * Sturkell E. Lepinette A.
Geological and Numerical Evidence for a Crater Bound Sedimentary Impact Breccia Lining the Basement Crater at the Lockne Impact Structure **[#1420]**
Drill core data combined with numerical simulation show that some more plastic parts of the 80 m sediments that covered the basement at the 7.5 km diameter marine-target Lockne impact remained inside the crater cavity before onset of water resurge.

8:45 a.m. Bron K. A. *
Tookoonooka Impact Sedimentation: Evidence for Resurge Cyclicity within the Crater Fill **[#2034]**
The buried Tookoonooka complex impact structure in Australia has been interpreted as being the product of a marine impact event. Evidence of a marine impact resurge sequence capped with post-impact debris flow deposits in the crater fill is presented.

9:00 a.m. Watson J. S. Gilmour I. * Jolley D. W. Kelley S. P. Gilmour M. A. Gurov E. P.
Molecular Parameters of Post Impact Cooling in the Boltysh Impact Structure **[#2296]**
Molecular parameters of thermal maturity combined with palynology and carbon isotope stratigraphy indicates post impact thermal processes in the Boltysh crater were short-lived.

9:15 a.m. King D. T. Jr. * Ormo J. Harris R. S. Petruny L. W. Markin J. K.
New Core-Hole Drilling at Wetumpka Impact structure, Alabama — Preliminary Results **[#1424]**
We present preliminary interpretations from each of the four new core holes drilled during 2009 into the marine-target, Late Cretaceous, Wetumkpa impact structure, Alabama.

9:30 a.m. Kalleson E. * Dypvik H. Riis F.
The Ritland Impact Structure, Western Norway **[#1326]**
The Ritland impact structure is 2.5 km in diameter and 350 m deep. Based on the geological setting, an age between 500 and 600 Ma is proposed for the impact. Impactites include brecciated basement and minor amounts of a melt-rich unit.

9:45 a.m. Biren M. B. * Spray J. G.
Shock Veins in the Central Uplift of the Manicouagan Impact Structure **[#2314]**
We report our investigations of target rocks located in the central uplift of the Manicouagan impact structure of Quebec. Thin white veins there appear to be shock derived features similar to shock veins observed in lunar and martian meteorites.

10:00 a.m. O'Connell-Cooper C. D. * Spray J. G.
Geochemistry of the Manicouagan Impact Melt Sheet **[#1755]**
Acquisition in 2006 by the University of New Brunswick's Planetary and Space Science Centre (PASSC) of ~18 km of core has shed new light on the extent and nature of the Manicouagan impact structure, Quebec.

10:15 a.m. Ukstins Peate I. * Kloberdanz C. Peate D. W. Chung Wan L. Cabrol N. Grin E. Piatek J. Chong G.
Non-Modal Melting of Target Rocks to Produce Impactite at Monturaqui Crater, Chile **[#2089]**
Monturaqui (Chile) is a small young impact with five melt rock compositions: (1) bulk melt of plag. + quartz, (2) bulk melt of ignimbrite target rock, and (3) multi-component melts with iron-rich impactor, non-modal biotite melt, and target rock.

10:30 a.m. Osinski G. R. * Sukara R. Grieve R. A. F.
"Suevites" of the Popigai Impact Structure, Russia: (Mis)understood? **[#2171]**
"Suevites" are a poorly understood product of meteorite impacts. Here, we present new data on "suevites" from the Popigai structure. These impactites do not conform to the original definition of suevite (cf. "suevites" at the Ries and Rochechouart structures).

10:45 a.m. Poelchau M. H. * Kenkmann T.
Feather Features: Microstructural Deformation in the Low-Shock Pressure Regime **[#1987]**
Feather features, a recently discovered planar microstructure in shocked quartz, are analyzed in natural and experimentally shocked samples. They are proposed as a diagnostic low-shock pressure indicator.

11:00 a.m. Buchner E. * Schmieder M. Schwarz W. H. Trieloff M. Jourdan F. Wartho J.-A. van Soest M. C. Hodges K. V. Pösges G.
A New Look at the Ries-Steinheim Event **[#2151]**
$^{40}Ar/^{39}Ar$ dating of monomineralic K-feldspar melt yielded an age of ~14.4 Ma for the Ries crater, S Germany. Isotopic dating of newly recovered impact melt lithologies from the nearby Steinheim Basin is attempted.

11:15 a.m. Jourdan F. * Moynier F. Koeberl C.
First $^{40}Ar/^{39}Ar$ Age of the Lonar Crater: A ~0.65 Ma Impact Event? **[#1661]**
We obtained a statistically robust global $^{40}Ar/^{39}Ar$ isochron age at 656 ± 81 ka (MSWD = 1.29; P = 0.12), dating the Lonar impact event. This age is based on the combination of five isochrons and strongly contrasts with a previous age estimate of ~52 ka.

11:30 a.m. Wartho J-A. * van Soest M. C. Cooper F. J. Hodges K. V. Spray J. G. Schmieder M. Buchner E. Bezys R. K. Reimold W. U.
Updated (U-Th)/He Zircon Ages for the Lake Saint Martin Impact Structure (Manitoba, Canada) and Implications for the Late Triassic Multiple Impact Theory **[#1930]**
New (U-Th)/He zircon ages from a Lake Saint Martin impact melt sample yield a Late Triassic age of 213.3 ± 3.0 Ma (2σ), which suggests that the Lake Saint Martin impact structure may be a candidate for the hypothesized ~214 Ma multiple impact chain.

SPECIAL SESSION: A NEW MOON: LCROSS, CHANDRAYAAN, AND CHANG'E-1 RESULTS
Tuesday, 8:30 a.m. Waterway Ballroom 6

Chairs: **Alian Wang and Jennifer Heldmann**

8:30 a.m. Colaprete A. * Ennico K. Wooden D. Shirley M. Heldmann J. Marshall W. Sollitt L. Asphaug E. Korycansky D. Schultz P. Hermalyn B. Galal K. Bart G. D. Goldstein D. Summy D.
Water and More: An Overview of LCROSS Impact Results **[#2335]**
This talk reviews the current results from the LCROSS impact as observed by the instrument suite on the LCROSS Shepherding Spacecraft.

8:45 a.m. Heldmann J. L. * Colaprete T. Ennico K. Shirley M. Wooden D. Science Team LCROSS.
Lunar Crater Observation and Sensing Satellite (LCROSS) Mission: Results from the Visible Camera and UV/Visible Spectrometer Aboard the Shepherding Spacecraft **[#1015]**
This paper will report on science results from the visible camera and UV-visible spectrometer aboard the LCROSS shepherding spacecraft.

9:00 a.m. Wooden D. H. * Colaprete A. Ennico K. Shirley M. H. Heldmann J. L. LCROSS Science Team
Lunar Crater Observation and Sensing Satellite (LCROSS) Mission: Results from the Nadir Near-Infrared Spectrometer Aboard the Shepherding Spacecraft **[#2025]**
The nadir-viewing Near-Infrared Spectrometer (1.17–2.45 µm) on the LCROSS Shepherding Spacecraft observed 4 min of the impact plume/curtain from the Centaur impact inside Cabeus Crater. We present identifications of water and other absorption bands.

9:15 a.m. Hong P. K. * Sugita S. Okamura N. Sekine Y. Terada H. Takatoh N. Hayano Y. Fuse T. Kawakita H. Wooden D. H. Young E. F. Lucey P. G. Furusho R. Watanabe J. Haruyama J. Nakamura R. Kurosawa K. Hamura T. Kadono T.
Hot Bands Observation of Water in Ejecta Plume of LCROSS Impact Using the Subaru Telescope **[#1939]**
We observed infrared spectra of LCROSS impacts using the Subaru telescope to find H_2O hot band emission lines. Although there was no clear sign of H_2O line detected, the upper limit of H_2O mass is much lower than pre-impact predictions.

9:30 a.m. Hayne P. O. * Greenhagen B. T. Paige D. A. Foote M. C. Siegler M. A.
Diviner Observations of the LCROSS Impact **[#2484]**
With its synoptic-scale view of the LCROSS impact site from orbit, combined with excellent sensitivity across a broad range of temperatures, Diviner provides an important set of constraints on the impact process and subsequent evolution.

9:45 a.m. Schultz P. H. * Hermalyn B. Colaprete A. Ennico K. Shirley M. LCROSS Team
Interpreting the LCROSS-EDUS Impact **[#2503]**
The LCROSS-EDUS impact excavated material from beneath a permanently shadowed region of the Moon. Here we discuss the results in the context of the impact with implications for the nature and source of buried volatiles.

10:00 a.m. Okamura N. * Sugita S. Hong P. K. Kawakita H. Sekine Y. Terada H. Takatoh N. Hayano Y. Fuse T. Wooden D. H. Young E. F. Lucey P. G. Furusho R. Watanabe J. Haruyama J. Nakamura R. Kurosawa K. Hamura T. Kadono T.
The Estimate of the Amount of Ejecta in LCROSS Mission **[#1821]**
Using the Subaru telescope, we observed LCROSS impacts. Although no clear signal of ejecta plume has been detected, an upper limit for the ejecta mass beyond 2.5 km of height is 1000 kg, only 1/20 of a pre-impact theoretical estimate.

10:15 a.m. Goswami J. N. *
An Overview of the Chandrayaan-1 Mission **[#1591]**
An overview of the Chandrayaan-1 mission, including performance of the eleven payloads, their lunar coverage and examples of salient results from the mission are presented. Chandrayaan-1 mission made important discoveries that provide new insights on lunar evolution.

10:30 a.m. Huang Q. * Ping J. S. Wieczorek M. A. Yan J. G. Su X. L.
Improved Global Lunar Topographic Model by Chang'E-1 Laser Altimetry Data **[#1265]**
The improved global lunar topographic model, a 360th degree and order spherical harmonic expansion of the lunar shape, is designated as Chang'E-1 Lunar Topography Model s01 (CLTM-s01).

10:45 a.m. Jiang J. S. * Wang Z. Z. Zhang X. H. Zhang D. H. Wu J. Li Y. Lei L. Q. Zhang W. G. Cui H. Y. Guo W. Li D. H. Dong X. L. Liu H. G.
China Probe CE-1 Unveils the World First Moon-Globe Microwave Emission Map — The Microwave Moon: Some Exploration Results of Change'E-1 Microwave Sounder **[#1125]**
With the data obtained by the China probe Chang'E-1 Lunar Microwave Sounder (CELMS), China has created a Moon globe microwave brightness temperature distribution map, and some new conclusions were drawn from it, which will make the Moon closer to its true nature.

11:00 a.m. Ling Z. C. * Zhang J. Zhang W. X. Liu J. J. Zhang G. L. Liu B. Liu J. Z.
Preliminary Results of Mapping Iron Abundance from Chang'e-1 IIM Data **[#2061]**
We present a preliminary study to map FeO from Chang'e-1 Imaging Interferometer (IIM) data. As shown by our studies in comparison with Clementine UVVIS results, IIM data exhibit the potential to extract FeO abundance distributions on Moon surface.

11:15 a.m. Wu Y. Z. * Tang Z. S.
Mapping the Absorption Center of the Lunar Minerals: Preliminary Results from CE-1 IIM Data **[#1216]**
We showed our experience in the use of Chang'E-1 IIM data. We produced the global map of the stagnation point of the Moon with IIM data. This global map can contribute to the lunar research and has some potential to be explored.

11:30 a.m. Zhu M. H. Mr. * Chang J. Dr. Ma T. Dr. Xu A. A. Dr.
Chang'E-1 Gamma-Ray Spectrometer and Its Preliminary Radioactive Results **[#1046]**
This abstract describes the preliminary radioactive results on the lunar surface from Chang'E-1 gamma-ray spectrometer.

UREILITIC ASTEROIDS: INSIGHTS FROM ALMAHATA SITTA
Tuesday, 1:30 p.m. Waterway Ballroom 1

Chairs: **Jason Herrin and Scott Sandford**

1:30 p.m. Herrin J. S. * Ito M. Zolensky M. E. Mittlefehldt D. W. Jenniskens P. M. Shaddad M. H.
Thermal History and Fragmentation of Ureilitic Asteroids; Insights from the Almahata Sitta Fall **[#1095]**
We detail the thermal history of recovered fragments of asteroid 2008 TC3 (the Almahata Sitta ureilite) and compare the size of fragments within TC3 to those initially dislodged from the ureilite parent body.

1:45 p.m. Welten K. C. * Meier M. M. M. Caffee M. W. Nishiizumi K. Wieler R. Jenniskens P. Shaddad M. H.
High Porosity and Cosmic-Ray Exposure Age of Asteroid 2008 TC3 Derived from Cosmogenic Nuclides **[#2256]**
Cosmogenic radionuclides in the Almahata Sitta ureilite, combined with measured size of 28 m^3, indicate that asteroid 2008 TC3 had a density of 1.5 g/cm^3 and a porosity of 55%. Cosmogenic noble gas concentrations indicate a cosmic-ray exposure age of 15 Myr.

2:00 p.m. Mikouchi T. * Zolensky M. Takeda H. Hagiya K. Ohsumi K. Satake W. Kurihara T. Jenniskens P. Shaddad M. H.
Mineralogy of Pyroxene and Olivine in the Almahata Sitta Ureilite **[#2344]**
Two Almahata Sitta samples (7 and 3-1) analyzed are two unique members of ureilites with possible genetical relationship on the same parent body. All low-Ca pyroxenes have a pigeonite crystal structure, suggesting the formation at high temperature.

2:15 p.m. Rumble D. * Zolensky M. E. Friedrich J. M. Jenniskens P. Shaddad M. H.
Oxygen Isotope Composition of Almahata Sitta **[#1245]**
It is demonstrated that a single asteroidal body, asteroid 2008 TC3, contained clasts representative of all known ureilite monomict and polymict ureilites in their oxygen isotope compositions.

2:30 p.m. Qin L. * Rumble D. Alexander C. M. O'D. Carlson R. W. Jenniskens P. Shaddad M. H.
Chromium Isotopic Composition of Almahata Sitta **[#1910]**
The $\varepsilon^{54}Cr$ values of Almahata Sitta samples are similar to that of HEDs. This suggests that they are derived from a parent body that is different from that of known carbonaceous chondrites. No correlation was found between $\delta^{54}Cr$ and $\delta^{17}O$.

2:45 p.m. Sandford S. A. * Milam S. N. Nuevo M. Jenniskens P. Shaddad M. H.
Infrared Spectroscopy of Samples from Multiple Stones from the Almahata Sitta Meteorite **[#1229]**
The infrared spectra of samples from 26 different stones from the Almahata Sitta meteorite strewn field will be presented.

VESTA AND DAWN
Tuesday, 3:15 p.m. Waterway Ballroom 1

Chairs: Carol Raymond and Rhiannon Mayne

3:15 p.m. Raymond C. A. * Russell C. T. Dawn Science Team
Exploring Asteroid 4 Vesta with the Dawn Mission **[#2155]**
Dawn reaches Vesta in August 2011. Science observations planned during the one-year stay using cameras, visible/infrared and gamma ray/neutron spectrometers, and radiometric tracking are discussed in the context of the mission's science goals.

3:30 p.m. Nugent C. R. * Margot J. L. Russell C. T. Nolan M. C. Magri C. Giorgini J. D.
SHAPE Modeling of (4) Vesta for Dawn Mission Support and SHAPE Inversion Validation **[#2637]**
This work supports the Dawn mission by using SHAPE software to invert radar images, light curves, and optical images of Vesta to generate a 3-D model of an asteroid as well as characterize its spin state.

3:45 p.m. Reddy V. * Gaffey M. J. Kelley M. S. Nathues A. Li J.-Y. Yarbrough R.
Rotationally-resolved Compositional Study of Asteroid (4) Vesta's Southern Hemisphere: Implications for the DAWN Mission **[#1373]**
We present results from the first rotationally-resolved spectroscopy of Vesta's Southern Hemisphere including the South Pole Crater. Existence of olivine in this crater will be explored.

4:00 p.m. Jutzi M. * Asphaug E.
Impacts on Vesta **[#2129]**
We present three-dimensional SPH simulations of impacts on asteroid 4 Vesta using a new model to simulate the granular flow of post-impact regolith.

4:15 p.m. Schmidt B. E. * Moore W. B.
Giant Impacts Can Drive Asteroid Dynamics: Lessons for Vesta **[#2700]**
We present the result of geophysical modeling of Vesta to determine its interior state prior to impact and the subsequent surface deformation and rotational and thermal evolution of the asteroid.

4:30 p.m. Bills B. G. * Nimmo F.
Are the Spin Poles of Ceres and Vesta Fully Damped? **[#2604]**
We examine the possibility, and implications, of fully damped spin poles for Ceres and Vesta. Their spin poles are close to estimates of damped states. If confirmed, damped spin poles would yield estimates of moments of inertia.

MARS POLAR PROCESSES: SEASONAL ICE AND POLAR LAYERED DEPOSITS
Tuesday, 1:30 p.m. Waterway Ballroom 4

Chairs: **Timothy Titus and Candice Hansen**

1:30 p.m. Hansen C. J. * Portyankina G. Thomas N. Byrne S. McEwen A.
HiRISE Images of Spring on Mars **[#2029]**
Spring on Mars is a time of active change at latitudes covered by seasonal CO_2 ice. HiRISE on MRO has imaged two southern and one northern spring seasons. We compare phenomena in the south to the north and investigate interannual variability.

1:45 p.m. Portyankina G. * Thomas N. Hansen C. Aye K.-M.
Cracks in Seasonal Semi-Translucent Ice Layer in Martian Polar Areas **[#2671]**
We report observations of cracks in translucent ice layer in martian polar areas, both south and north. We argue in favour of them being fracture cracks.

2:00 p.m. Russell P. S. * Byrne S. Hansen C. J.
Active Mass Wasting of Ice Layers and Seasonal CO_2 Frost in the North Polar Region of Mars **[#2667]**
We discuss new findings relating to two dramatic forms of recently discovered mass-wasting in the north polar region: block-wise failure of NPLD and basal-unit scarps as rockfalls and rockslides, and actively observed CO_2 frost-dust falls and avalanches at steep NPLD scarps.

2:15 p.m. Smith I. B. * Holt J. W. Mohrig D. Kim W.
Quantitative Radar Stratigraphy of the Uppermost North Polar Layered Deposits, Mars, and Processes Controlling Spiral Trough Migration **[#2431]**
We quantitatively look at radar stratigraphy within the northern polar layered deposits to map accumulation patterns and learn about the processes governing spiral trough migration.

2:30 p.m. Holt J. W. * Byrne S. Fishbaugh K. Christian S. Putzig N. E. Phillips R. J. Tanaka K.
Chasma Boreale, Mars: A Product of Non-Uniform Polar Accumulation Influenced by Basal Topography **[#2547]**
The mapping of radar unconformities within Planum Boreum, Mars reveals episodes of deposition and erosion leading to non-uniform accumulation of the NPLD and the early creation of Chasma Boreale, Gemina Lingula, and a now-buried, major chasma.

2:45 p.m. Guallini L. * Rossi A. P. Marinangeli L.
"Unconformity-Bounded" Units on Mars SPLD (Promethei Lingula): A First Step Towards Formal Stratigraphic Classification? **[#1721]**
Preliminary SPLD stratigraphy (Promethei Lingula) has been defined using "Unconformity-Bounded" units. The unconformities allow us to correlate sections regionally. At present we hypothesize two depositional cycles divided by one erosional event.

PLANETARY AEOLIAN PROCESSES: DUNES, DUST, AND DEVILS
Tuesday, 3:15 p.m. Waterway Ballroom 4

Chairs: Jani Radebaugh and Matt Golombek

3:15 p.m. Radebaugh J. * Lorenz R. D. Lancaster N. Savage C. J. Wall S. D. Stofan E. R. Lunine J. I. Kirk R. L. Le Gall A.
Winds and Sand Transport Patterns on Titan from Dune Interactions with Topography **[#2513]**
Dunes on Titan interact with topographic obstacles, leading to features like those seen in the Namib and Saharan deserts. These results are correlated with studies of wind directions from dune morphologies, not with current GCM model wind directions.

3:30 p.m. Edgar L. A. * Grotzinger J. P. Hayes A. G. Squyres S. Bell J. III
Large-Scale Eolian Bedforms and Stratigraphic Architecture at Victoria Crater, Meridiani Planum, Mars **[#2626]**
Victoria Crater exposes cliffs up to ~15 m high, revealing thick bedsets (3–7 m) of large-scale cross-bedding, interpreted as fossil eolian dunes.

3:45 p.m. Michaels T. I. * Fenton L. K.
Characterizing the Sensitivity of Daytime Turbulent Activity and Aeolian Erosion Potential on Mars with the MRAMS LES **[#1955]**
Daily aeolian erosion potential is preliminarily characterized for two landing sites on Mars (VL1 and Phoenix), using a turbulence-resolving model.

4:00 p.m. Chojnacki M. * Burr D. M. Moersch J.
Recent Dune Changes at Endeavour Crater, Meridiani Planum, Mars, from Orbital Observations **[#2326]**
Here we present orbit-based evidence that aeolian bedforms in Endeavour crater, Meridiani Planum, Mars, have been active (erosion) in the span of the past decade. Also we suggest these modest dunes are not in equilibrium with their environment.

4:15 p.m. Silvestro S. * Fenton L. K. Vaz D . A.
Ripple Migration and Small Modifications of Active Dark Dunes in Nili Patera (Mars) **[#1820]**
We present the first evidence of widespread ripple migration on Mars detected from orbit. The movement of the ripples, together with other morphological changes, indicates that sand saltation can occur on Mars in present-day atmospheric conditions.

4:30 p.m. Golombek M. * Robinson K. McEwen A. Bridges N. Ivanov B. Tornabene L. Sullivan R.
Constraints on Ripple Migration at Meridiani Planum from Observations of Fresh Craters by Opportunity and HiRISE **[#2373]**
The most recent phase of ripple migration at Meridiani Planum from Opportunity observations of a fresh crater cluster and HiRISE observations of fresh rayed craters occurred between ~100 ka and ~300 ka.

IMPACT MODELS, EXPERIMENTS, AND IMPACT DEPOSITS
Tuesday, 1:30 p.m. Waterway Ballroom 5

Chairs: **Gareth Collins and Kieren Howard**

1:30 p.m. Fritz J. * Wünnemann K. Reimold W. U. Hornemann U.
Shocking Cool Quartz **[#1341]**
We present results of shock recovery experiments on quartz targets pre-cooled with liquid nitrogen, and show that the shock deformation effects in quartz are dominated by pressure and not temperature.

1:45 p.m. Price M. C. * Burchell M. J. Miljkovic K. Kearsley A. T. Cole M. J.
Shock Synthesis of Organics from Simple Ice Mixtures? **[#1830]**
Preliminary results from a programme of impact experiments on simple ice mixtures (CO_2, NH_3 and H_2O) give a tantalising suggestion of the successful shock synthesis of complex organics — including glycine.

2:00 p.m. Kraus R. G. * Stewart S. T.
Impact Induced Melting and Vaporization on Icy Planetary Bodies **[#2693]**
Using hydrocode simulations we calculate the volume of ice that is melted and vaporized for a wide range of impact conditions and derive scaling laws as a function of initial temperature, projectile size, impact velocity, and impact angle.

2:15 p.m. Elder C. M. * Bray V. J. Melosh H. J.
Central Pit Formation in Ganymede Craters via Melt Drainage **[#2519]**
We investigate the hypothesis that central pits in craters on Ganymede can form by impact melt draining into fractures beneath the crater and compare the predicted drainage volume to the volume of observed central pits.

2:30 p.m. Stickle A. M. * Schultz P. H.
Comparing Experimental and Numerical Results for Subsurface Failure Following Oblique Impacts into Planar Targets **[#2598]**
Comparison of experimental results and CTH codes of subsurface failure under oblique impacts to identify distinct markers for the style of target damage and to better interpret styles of failure in terrestrial and planetary craters at broader scales.

2:45 p.m. Jahn A. * Riller U.
The Deep Structure of a Collapsed Central Uplift — Insights in the Development of the Vredefort Dome, South Africa **[#2311]**
We constructed a three-dimensional structural model for the overturned upper parts of the Vredefort Central Uplift. From the orientation and truncation relationships of sedimentary rocks and major dislocations a succession ofmovements through the modification phase was deduced.

3:00 p.m. Tong C. H. * Lana C. Marangoni Y. R. Elis V. R.
Resistivity Tomography of the Araguainha Impact Structure: Constraints on Melt and Breccia Emplacement **[#1783]**
We discuss the novel application of resistivity tomography to imaging the shallow subsurface of the central uplift of the Araguainha impact structure for understanding melt and breccia emplacement during an impact event (Tong et al., Geology, 2010).

3:15 p.m. Wünnemann K. * Lynett P. Weiss R.
The Impact-induced Tsunami Hazard — Insight from Numerical Modeling of the Eltanin Event **[#2220]**
We present numerical models to simulate the Eltanin impact and assess the hazardous potential of generated tsunami waves. We combine hydrocode modeling with wave propagation models to quantify wave generation and decay as a function of distance from point of impact.

3:30 p.m. Pierazzo E. * Garcia R. Kinnison D. Marsh D.
Quantifying the Perturbation of Atmospheric Chemistry from Medium-sized Asteroid Impacts in the Ocean **[#2445]**
We used a whole atmosphere general circulation model with interactive chemistry to investigate the perturbation of atmospheric chemistry in oceanic impacts of 500-m and 1-km asteroids.

3:45 p.m. Kyte F. T. * Omura C. Snead C. McKeegan K. D. Gersonde R.
Trace Elements in Refractory Eltanin Impact Spherules **[#2619]**
Spherules from the Eltanin impact can have refractory compositions that reflect distillation and/or condensation processes in the impact plume. We examine this effect with new electron and ion microprobe analyses of major and trace elements.

4:00 p.m. Deutsch A. * Schulte P.
Carbonates in the Proximal Ejecta Deposits of the K/T Chicxulub Impact Crater **[#1596]**
We show that the carbonate spherules in the Chicxulub-related K/T ejecta deposits have a primary origin as impact melt droplets — they are neither a diagenetic nor an alteration product of silicic impact melt spherules.

4:15 p.m. Simonson B. M. * Hassler S. W. Beukes N. J. Sumner D. Y.
Large Impacts Around the Archean-Proterozoic Boundary: An Update **[#2386]**
At least four large impacts generated spherule-rich layers in Australia and/or South Africa within 140 million years around the A-P boundary. They differ from Phanerozoic ejecta layers, e.g., in target and impactor compositions.

4:30 p.m. Lowe D. R. Byerly G. R. *
Did LHB End Not with a Bang but a Whimper? The Geologic Evidence **[#2563]**
We present evidence for three new major impacts from our geologic studies of the 3.55 to 3.25 Ga Barberton greenstone belt, increasing the number of major impacts to seven.

SPECIAL SESSION: WATER IN THE SOLAR SYSTEM: MOON
Tuesday, 1:30 p.m. Waterway Ballroom 6

Chairs: **Francis McCubbin and Richard Elphic**

1:30 p.m. Clark R. * Pieters C. M. Green R. O. Boardman J. Buratti B. J. Head J. W. III Isaacson P. J. Livo K. E. McCord T. B. Nettles J. W. Petro N. E. Sunshine J. M. Taylor L. A.
Water and Hydroxyl on the Moon as Seen by the Moon Mineralogy Mapper (M^3) **[#2302]**
A new water+hydroxyl map was constructed using M^3 data which shows that the water and hydroxyl detected by M^3 is more extensive than first reported and in better agreement with the VIMS and Deep Impact results.

1:45 p.m. McCord T. B. * Taylor L. A. Orlando T. M. Pieters C. M. Combe J.-Ph. Kramer G. Sunshine J. M. Head J. W. Mustard J. F.
Origin of OH/Water on the Lunar Surface Detected by the Moon Mineralogy Mapper **[#1860]**
We present characteristics of the M^3 3-µm OH/H_2O spectral feature across the observed Moon and explore solar-wind induced surface chemistry as the source.

2:00 p.m. Farrell W. M. * Killen R. M. Delory G. T. NLSI-DREAM Team
The Case of Reactive Surface Geochemistry at the Moon **[#2228]**
There is a mounting body of evidence suggesting that there are active geochemical processes occurring at the lunar surface.

2:15 p.m. Hurley D. *
Surficial OH/H_2O on the Moon: Modeling Delivery, Redistribution, and Loss **[#1844]**
We model the solar wind interaction with the lunar regolith to understand the observations of OH on the lunar surface and what they imply for the migration of water to the lunar poles.

2:30 p.m. Burke D. * Dukes C. A. Famá M. Kim J. Shi J. Baragiola R. A.
Negligible Contribution of Solar Wind Protons to Surficial Lunar Water: Laboratory Studies **[#2567]**
We performed a series of laboratory simulations irradiating lunar simulants with low and high energy protons and examined the results of infrared reflectance absorption spectroscopy (IRAS) for signs of the O-H absorption band for water.

2:45 p.m. Zent A. P. * Ichimura A. I. McCord T. B. Taylor L. A.
Production of OH/H_2O in Lunar Samples via Proton Bombardment **[#2665]**
We report on a laboratory simulation of solar-wind lunar implantation, and demonstrate that we are able to dehydrate/dehydroxylate lunar samples, expose them to moderately energetic H plasma, and detect the presence of newly formed OH/H_2O.

3:00 p.m. Elphic R. C. * Paige D. A. Siegler M. A. Vasavada A. R. Eke V. R. Teodoro L. F. A. Lawrence D. J.
South Pole Hydrogen Distribution for Present Lunar Conditions: Implications for Past Impacts **[#2732]**
We compare the inferred hydrogen distribution at the Moon's south pole to what might be expected after deposition from a large, volatile-rich impact, as the deposits evolve with time under model temperatures.

3:15 p.m. Mazarico E. * LOLA Science Team
Illumination of the Lunar Poles From Lunar Orbiter Laser Altimeter (LOLA) Topographic Data **[#1828]**
LOLA data enable precise modeling of polar illumination conditions over timescales relevant to mission planning. At 10 m above the surface, an area near the South Pole offers 95% average illumination, and continuous sunlight ~200 days in most years.

3:30 p.m. Greenwood J. P. * Itoh S. Sakamoto N. Taylor L. A. Warren P. H. Yurimoto H.
Water in Apollo Rock Samples and the D/H of Lunar Apatite **[#2439]**
Hydrogen isotopes of lunar water in apatite are measured in Apollo rock samples for the first time. The Moon has a unique D/H.

3:45 p.m. McCubbin F. M. * Steele A. Nekvasil H. Schnieders A. Rose T. Fries M. Carpenter P. K. Jolliff B. L.
Detection of Structurally Bound Hydroxyl in Apatite from Apollo Mare Basalt 15058,128 Using TOF-SIMS **[#2468]**
Using TOF-SIMS, we have shown that hydroxyl is present within apatite in lunar mare basalt 15058,128. This is the first find of water in a lunar magmatic mineral, and this result holds important implications for the water content of the lunar interior.

4:00 p.m. Liu Y. * Boyce J. W. Rossman G. R. Guan Y. Eiler J. Taylor L. A.
Water in Lunar Mare Basalt: Confirmation from Apatite in Lunar Basalt 14053 **[#2647]**
We present direct analyses of H (presumably OH) in apatite through ion microprobe measurements of apatite in Apollo 14 basalt 14053 (1640 ± 180 ppm H_2O by weight), with implications to water in the primary melt.

4:15 p.m. Elkins-Tanton L. T. *
Water in the Lunar Mantle: Results from Magma Ocean Modeling **[#1451]**
Modeling lunar magma ocean solidification including a small amount of initial water produces predictions for the locations and quantities of water that should be found in the lunar interior, and which would have been degassed and possibly interacted with the lunar surface.

4:30 p.m. Grieves G. * Hibbitts C. A. Dyar M. D. Orlando T. M. Poston M. Johnson A.
Mobility and Subsurface Redistribution of Volatiles Through Regolith Materials **[#2552]**
Increasing evidence supports the notion that water is present on the Moon. We report here on development of models to assess the mobility of volatiles such as hydrogen (as H_2O and OH) on grain surfaces within the top meter of a regolith.

MERCURY AFTER MESSENGER'S THIRD FLYBY
Tuesday, 1:30 p.m. Montgomery Ballroom

Chairs: **Sean C. Solomon and Noam Izenberg**

1:30 p.m. Solomon S. C. * McNutt R. L. Jr. Anderson B. J. Blewett D. T. Evans L. G. Gold R. E. Krimigis S. M. Murchie S. L. Nittler L. R. Phillips R. J. Prockter L. M. Slavin J. A. Zuber M. T. MESSENGER Team
MESSENGER's Three Flybys of Mercury: An Emerging View of the Innermost Planet **[#1343]**
MESSENGER's three Mercury flybys revealed a planet with a rich geological history and interactions among solar wind, magnetosphere, internal field, and surface that are stronger and operate on shorter timescales than for any other solar system body.

1:45 p.m. Vervack R. J. Jr. * McClintock W. E. Bradley E. T. Burger M. H. Killen R. M. Sprague A. L. Mouawad N. Izenberg N. R. Kochte M. C. Lankton M. R.
MESSENGER Observations of Mercury's Exosphere: Where Do We Stand After Three Flybys? **[#2329]**
The three MESSENGER flybys have revealed never before seen details of Mercury's exosphere. Observations of sodium, calcium (both neutral and ionized), and magnesium show interesting and as yet unexplained spatial distributions about the planet.

2:00 p.m. Lawrence D. J. * Feldman W. C. Goldsten J. O. McCoy T. J. Blewett D. T. Boynton W. V. Evans L. G. Nittler L. R. Rhodes E. A. Solomon S. C.
Measurements of Neutron Absorbing Elements on Mercury from the Three MESSENGER Flybys **[#1465]**
With MESSENGER neutron data, we find that Mercury's surface composition is similar in neutron absorption to a Luna 16 soil. These data cannot be matched by prior models of Mercury surface composition, which have low abundances of Fe, Ti, Gd, and Sm.

2:15 p.m. Perry M. E. * Kahan D. S. Ernst C. M. Solomon S. C. Zuber M. T. Smith D. E. Phillips R. J. Oberst J. Asmar S. W.
Mercury Radii from MESSENGER Flyby Occultations **[#2188]**
During flybys 1 and 3, MESSENGER's RF transmissions were occulted by Mercury. The occultation times provide estimates of the planet radius at the surface location of the grazing ray with uncertainties of 100 m to 300 m.

2:30 p.m. Barnouin O. S. * Zuber M. T. Oberst J. Preusker F. Smith D. E. Neumann G. A. Solomon S. C. Hauck S. A. Phillips R. J. Head J. W. III Prockter L. M. Robinson M. S.
The Morphology of Craters on Mercury: Results from the MESSENGER Flybys **[#1243]**
Altimetry and imaging from the MESSENGER spacecraft were used for investigations of the relationship between depth and diameter for impact craters on Mercury.

2:45 p.m. Prockter L. M. * Ernst C. M. Denevi B. W. Chapman C. R. Solomon S. C. Blewett D. T. Head J. W. III Cremonese G. Marchi S. Massironi M. Merline W. J.
Evidence for Young Volcanism on Mercury from MESSENGER's Third Flyby **[#1931]**
During MESSENGER's third flyby of Mercury, a new basin was imaged which contains comparatively young smooth plains that show evidence of flow and extensional deformation. Nearby is the largest candidate explosive volcanic feature seen on Mercury.

3:00 p.m. Martellato E. Massironi M. * Cremonese G. Marchi S. Ferrari S. Prockter L. M.
Age Determination of Raditladi and Rembrandt Basins and Related Geological Units **[#2148]**
Mercury surface has revealed new interesting features during the three fly-bys of the MESSENGER spacecraft. Among these, we analyzed Raditladi and Rembrandt basins with age determination and geological purposes.

3:15 p.m. Blair D. M. * Freed A. M. Melosh H. J. Solomon S. C. Prockter L. M. Watters T. R. Zuber M. T. Phillips R. J.
Testing Mechanisms for the Formation of a Ring of Graben in Central Raditladi Basin, Mercury **[#1762]**
We use finite element models to test a number of possible scenarios to explain the formation of a ring of circumferentially oriented graben near the center of the Raditladi basin on Mercury.

3:30 p.m. Ritzer J. A. * Hauck S. A. II Barnouin O. S. Solomon S. C. Watters T. R.
Mechanical Structure of Mercury's Lithosphere from MESSENGER Observations of Lobate Scarps **[#2122]**
Lobate scarps detected by the MESSENGER spacecraft are the main expression of contraction at Mercury. We model these scarps using a finite element analysis to constrain their geometry to gain a better understanding of lithospheric structure.

3:45 p.m. De Sanctis M. C. * Capaccioni F. Filacchione G. Ammanito E.
Classification of MESSENGER MASCS Data **[#1198]**
We applied classification method to MASCS data to obtain mineralogical maps of Mercury surface, giving indication of the different mineralogy and maturity of the soil present on the Hermean surface.

4:00 p.m. Helbert J. * D'Amore M. Maturilli A. Izenberg N. R. Holsclaw G. M. Head J. W. Solomon S. C.
Combining High-Temperature Spectroscopy and Principal Component Analysis to Understand Mercury Surface Spectra from MESSENGER **[#1496]**
For the first time we a PCA approach for the MESSENGER spectral data with new spectral data obtained in the Planetary Emissivity Laboratory (PEL) at the Deutsches Zentrum für Luft- und Raumfahrt (DLR) in Berlin.

4:15 p.m. Zuber M. T. * Smith D. E. Phillips R. J. Solomon S. C. Neumann G. A. Lemoine F. G. Peale S. J. Margot j.-L. Hauck S. A. II Head J. W. Johnson C. L. Purucker M. E. Oberst J. Farmer G. T. Lu J. Sun Y. Toksöz M. N. Barnouin O. S. Perry M. E. Srinivasan D. K. Torrence M. H.
Emerging Perspectives on Mercury's Internal Structure from MESSENGER Flyby Observations and Geophysical Modeling **[#1832]**
Study of the current internal structure of Mercury from MESSENGER geophysical observations and past plausible internal structures from modeling provide constraints on Mercury's internal dynamics over time that can be linked to the surface record.

4:30 p.m. Hauck S. A. II * Solomon S. C. Peale S. J. Margot J.-L. Phillips R. J. Smith D. E. Zuber M. T.
Constraints on the Internal Structure of Mercury After Three MESSENGER Flybys **[#2107]**
Gravity results from MESSENGER's three flybys of Mercury have provided improved constraints on the internal structure of the planet. We investigate the implications of these new results for Mercury's internal density structure.

POSTER SESSION I
Tuesday, 7:00 p.m.   Town Center Exhibit Area

PARENT CLOUD AND PROTOPLANETARY DISK PROCESSES

Yang L.   Ciesla F. J.
The Effects of Disk Building on the Chemical Evolution of the Solar Nebula **[#1461]**
We investigate the dynamical evolution of the solar nebula while it accretes material from its parent molecular cloud. We explore the implications for the chemistry, isotopic homogeneity and the preservation of early-formed solids in the nebula.

Hughes A. L. H.   Armitage P. J.
Particle Concentration in an Evolving Disk: Implications for Early Accretion and Planetesimal Formation **[#1847]**
We model the radial drift and turbulent diffusion of particles in a one-dimensional viscously evolving and accreting gas disk to examine the potential for possibilities for dust-to-gas concentration above cosmic.

Wada K.   Tanaka H.   Suyama T.   Kimura H.   Yamamoto T.
Collisional Growth Possibility of Dust Aggregates: A Bouncing Problem **[#1717]**
We carry out numerical simulations of collisions of aggregates with various coordination numbers to investigate the bouncing conditions and collosional growth possibility of dust in protoplanetary disks.

Eöry M.   Futó P.   Gucsik A.
Microstructural Evolution of the Fractal Dust Aggregates **[#1023]**
According to fractal dimension calculations, sticking and compaction may occur in case of low velocity collision of fractal dust aggregates due to energy dissipation and interdigitation.

Curtis S. A.   Clark P. E.   Minetto F.   Nuth J.   Marshall J.
SPARKLED: Dust Removal Tool and Implications for Solar System Formation **[#1254]**
We have had the first successful tests for a low power, lightweight electrostatically-based tool to remove dust in the airlock environment and, in the process, demonstrated plasma/dust interactions with implications for solar system formation.

Perry J.   Matthews L. S.   Hyde T. W.
Dipole-Dipole Interactions of Charged-Magnetic Grains **[#2580]**
The interaction between dust grains is an important process in planetesimal formation. This work considers the effects that electrostatic and magnetic forces, alone or in combination, can have on the coagulation of dust in various environments.

Wilson T. L.
Modelling Cosmic-Ray Effects in the Protosolar Disk **[#1018]**
The dynamic effects of cosmic rays during the evolution of protosolar disks and the origin of the solar system are addressed. Three computational categories are discussed: plasma transport codes, solar modulation codes, and Monte Carlo codes.

Boney E. T. D.   Lyons J. R.   Marcus R. A.
Self-Shielding of the E(1)-X(0) Band of CO in a Hot Solar Nebular **[#1999]**
CO self-shielding at the X-point of the early nebula has been put forth as a possible mechanism to explain the slope-1 oxygen 3-isotope plot observed in CAIs. We are testing this hypothesis in multiple X-point geometries.

RADIONUCLIDES AND EARLY SOLAR SYSTEM CHRONOLOGY

Young E. D.   Shahar A.
Inverting Silicon and Magnesium Isotope Ratio Data for the Evaporation Histories and Primordial Elemental Compositions of CAIs **[#1551]**
We describe a Monte Carlo method for inverting Si and Mg isotope ratios of igneous CAIs for timescales of evaporation, primordial compositions, and PH2 attending evaporation.

Sanders I. S.
The Meltdown Era: A Time for Making Ancient Iron Cores and Younger Chondrules **[#2376]**
Clear new evidence that planetesimals had melted before chondrules were made flies in the face of conventional wisdom, but is entirely consistent with ^{26}Al induced meltdown.

Bricker G. E.   Caffee M. W.
Solar Wind Implantation Model for the Incorporation of ^{10}Be in Calcium Aluminum Inclusions **[#2380]**
We propose a model for the incorporation of ^{10}Be within CAIs in primitive carbonaceous meteorites. We calculate the content of solar wind implanted ^{10}Be of $\sim 1.5 \times 10^{12}$ ^{10}Be g^{-1} in CAIs.

Gounelle M.   Chaussidon M.
The Boron Isotopic Composition of Isheyevo (CH/CB) Calcium-, Aluminium-rich Inclusions **[#1674]**
We report Be-B systematics in CAIs from the chondrite Isheyevo (CH/CB). The inferred ^{10}Be/^{9}Be ratio might be significantly higher than the one in CV3 chondrites.

Tang H.   Dauphas N.
High Precision Nickel Isotopic Analyses of Meteorites **[#1773]**
A new procedure for nickel separation was developed for high precision analysis by MC-ICPMS. Chondritic and iron meteorites were studied for past presence and heterogeneity level of ^{60}Fe in the solar nebula.

Ouellette N.   Gounelle M.   Hennebelle P.
Abundance of Iron-60 in Molecular Clouds **[#1676]**
A new model to explain the abundance of Iron-60 in the early solar system is described. This model used supernova shocks to trigger the rapid formation of the presolar molecular cloud. Computer simulations test this model.

Huss G. R.   Tachibana S.   Nagashima K.   Telus M.
Development of Multi-Collection Ni Isotopic Analysis of Ferromagnesian Silicates in the Ion Microprobe **[#1567]**
We describe a new multi-collection protocol to measure the ^{60}Fe-60Ni system with a Cameca ims 1280. Although interferences are still a problem, we believe this can be solved leading to much more precise measurements. Some new data will be reported.

Teng F.-Z.   Ke S.   Marty B.   Dauphas N.   Huang S.   Pourmand A.
The Magnesium Isotopic Composition of the Earth and Chondrites **[#2019]**
A comprehensive study of over 200 global oceanic basalts, olivine grains, peridotites, and 38 chondrites from all groups suggests that the Earth and chondrites have similar and homogenous Mg isotopic composition.

ISOTOPES AND REEs

Dauphas N.   Remusat L.   Chen J. H.   Stodolna J.   Roskosz M.   Guan Y.   Eiler J. M.   Papanastassiou D. A.
A Coordinated Search for the Carrier of ^{54}Cr Anomalies in Meteorites **[#1073]**
We present a coordinated search for the carrier of ^{54}Cr anomalies in residues from Orgueil and Murchison. In bulk, those residues display the highest ^{54}Cr-excesses ever reported in solid residues of meteorites.

Chen J. H. Papanastassiou D. A. Dauphas N.
Anomalous Cr-54 and Cr-53 in Bulk Acid Residues from Orgueil and Murchison **[#2005]**
Bulk residues from leaching of Orgueil and Murchison contain large $^{54}Cr/^{52}Cr$ effects, which are, hence, not restricted only to leachates. Large Cr-54 effects are thus a characteristic of bulk residues and potentially not so elusive.

Moynier F. Simon J. I. Podosek F. Brannon J. DePaolo D. J.
Ca Isotope Anomalies in Orgueil Leachates and Implications for the Carrier Phases of Ca and Cr Anomalies **[#1181]**
In this work we measured the relative isotopic abundances of ^{40}Ca, ^{42}Ca, ^{43}Ca, ^{44}Ca, ^{46}Ca, and ^{48}Ca from Ca separated from leachates from Orgueil in which ^{54}Cr anomalies were already measured to search for possible collateral effects.

Burkhardt C. Kleine T. Oberli F. Bourdon B.
The Molybdenum Isotopic Composition of Meteoritic Metals: Evidence for Planetary Scale Isotope Heterogeneity of the Solar Nebula **[#2131]**
We report new Mo isotopic data for iron meteorites and metals from chondrites and an angrite. Our data reveal a large-scale isotopic heterogeneity among planetary bodies. Genetic relations between planetary objects and constraints on nebula processes may be inferred.

LABORATORY INSTRUMENTS AND SAMPLES

Zhang J. J. Dauphas N. Davis A. M.
A New Chemical Separation Method for MC-ICPMS Measurement of Titanium Isotopic Compositions in Natural Materials **[#2170]**
We have developed a new approach to separate titanium from silicate matrices with TODGA and AG1-X8 ion exchange resins. Preliminary titanium isotope results for two geostandards are reported.

Nakamura N. Nyquist L. E. Reese Y. Shih C.-Y. Fujitani T. Okano O.
Stable Chlorine Isotope Study; Application to Early Solar System Materials **[#2233]**
In order to clarify the stable chlorine isotope features of early solar sytem materials, we have initiated TIMS technique applicable for analysis of small planetary materials at NASA JSC. We report the current status of chlorine isotope analysis at JSC.

Strashnov I. Blagburn D. J. Gilmour J. D.
RISK: A Resonance Ionization Mass Spectrometer for Krypton **[#1708]**
A resonance ionization mass spectrometer for krypton (RISK) has been developed. Atoms are released by a step-heating and ionized by pulsed tunable lasers. The sensitivity below 1000 atoms is demonstrated by detecting 81 Kr in noncumulate eucrite Stannern.

Pourmand A. Dauphas N. Ireland T.
A Novel Technique for Accurate Analysis of Lanthanides, Sc and Y in Meteorites: Towards a Reevaluation of Cosmic Abundances **[#2544]**
A novel sample digestion and MC-ICP-MS technique is proposed for accurate analysis of rare Earth elements (REE). REE concentrations are determined in a group of meteorites to help re-examine the cosmochemical behavior of lanthanides in meteorites.

Stephan T. Davis A. M. Pellin M. J. Savina M. R. Veryovkin I. V.
CHILI — The Chicago Instrument for Laser Ionization — A Progress Report **[#2321]**
CHILI, a new RIMS instrument with ~10 nm lateral resolution and 40–50% useful yield, is under construction at the University of Chicago. It will be applied to the analysis of samples from the Stardust mission and may be able to date presolar dust.

Anderson R. C. Beegle L. W. Fleeming II G. M.
Understanding the Effects of Triboelectric Charging on Cross Sample Contamination in the Mars Science Laboratory Sample Handling System **[#2003]**
Accurate analysis requires that materials analyzed by *in situ* instruments represent the initial material prior to its collection and delivery. Here we will discuss the role of adhesion (electrostatic) within the MSL sample handling system.

Andreev G. Dominguez G. Gainsforth Z. Westphal A. J. Basov D. Thiemens M. H.
Scanning Scattering Near-Field Infrared Microscopy: A New Tool for the Mapping of Functional Groups at the Ten Nanometer Scale **[#2265]**
A novel infrared spectral mapping instrument has been developed offering the ability characterize the functional group composition of returned samples with ten nanometer spatial resolutions with minimal or no sample alteration.

Nakashima D. Ushikubo T. Kita N. T. Valley J. W.
Development of Multiple Hole Disk for Isotope Analysis of Tiny Samples Using Ion Microprobe **[#2309]**
We developed a multiple hole disk for stable isotope analysis of tiny samples using ion microprobe. Potential analytical biases derived from surface shape of the disk are 1‰ or less, and the disk is applicable to tiny particle analysis.

Stojic A. N. Brenker F. E.
Argon Ion Slicing (ArIS): A Murchison Close Up and Its Implications for TEM Sample Preparation in Earth and Planetary Sciences **[#1765]**
We report the successful preparation of an electron transparent area >40,000 µm2 from the Murchison meteorite. We obtained this enormously large TEM foil by using the refined argon ion slicing (ArIS) technique.

McCausland P. J. A. Brown P. G. Holdsworth D. W.
Rapid, Reliable Acquisition of Meteorite Volumes and Internal Features by Laboratory X-Ray Micro-CT Scanning **[#2584]**
X-ray Micro-CT imaging is a benchtop lab technique that can be used to obtain meteorite volume, surface area and the dimensions of objects of interest within the meteorite.

Ohno S. Namiki N. Ishibashi K. Kobayashi M. Arai T. Senshu H. Wada K. Yamagishi A. Miyamoto H. Komatsu G. Matsui T.
Development of Mars Environment Simulation Chamber at Planetary Exploration Research Center, Chiba Institute of Technology **[#1754]**
A new Mars environment simulation chamber is being developed in the PERC/Chitech in Japan. The aim of its development is to reproduce the surface conditions of Mars and to contribute the instrumental development and martian science.

Sobron P. Wang A.
A Planetary Environment and Analysis Chamber Equipped with Multiple Spectroscopic Sensors **[#1994]**
A Planetary Environment and Analysis Chamber (PEACH) has been developed at Washington University in St. Louis, in order to conduct co-registered spectroscopic measurements on geological samples under planetary relevant environmental conditions.

Edmunson J. Betts W. Rickman D. McLemore C. Fikes J. Stoeser D. Wilson S. Schrader C.
NASA Lunar Regolith Simulant Program **[#1786]**
This abstract is an introduction to the NASA Exploration Technology Development Program's lunar regolith simulant team at Marshall Space Flight Center, the U.S. Geological Survey, and Glenn Research Center. Requests for simulant are also addressed.

Allen C. Sellar G. Nuñez J. I. Winterhalter D. Farmer J.
Lunar Reference Suite to Support Instrument Development and Testing **[#1457]**
Instruments are being developed for possible use on lunar robotic landers, for lunar field work, and for analyses at a lunar outpost. JSC Curation will support such instrument testing by providing lunar sample "ground truth".

Nuñez J. I. Farmer J. D. Sellar R. G. Allen C. C.
The Multispectral Microscopic Imager: Integrating Microimaging with Spectroscopy for the In-Situ Exploration of the Moon **[#1581]**
The MMI combines microscopic imaging with VIS-NIR spectroscopy to provide *in situ* mineralogy within a microtextural framework for the exploration of the Moon. We present our latest results of analysis of a suite of Apollo samples with the MMI.

Nissinboim A. Ebel D. S. Harlow G. E. Boesenberg J. S. Sherman K. M. Lewis E. R. Brusentsova T. N. Peale R.. E. Lisse C. M. Hibbitts C. A.
The American Museum of Natural History Mineral Library for Spectroscopic Standards **[#2518]**
Minerals from the AMNH collections are highly characterized (crystal XRD, EMPA), powdered <2 µm, reanalyzed (SEM, powder XRD), and transmission IR spectra analyzed for Herschel PACS. Library minerals will also serve reflectance spectra needs.

FORMATION OF FIRST SOLAR SYSTEM SOLIDS

Allen M. K. Connolly H. C. Jr. Dunn S. R. Beckett J. R. Hill D. H.
Analyses of Atypical Type A Refractory Inclusion from Allende: The Eye of Horus **[#1963]**
We have characterized a compound type A inclusion from Allende, the Eye of Horus, and show its complex formation history.

Ivanova M. A. Lorenz C. A. Korochantseva E. V. MacPherson G. J.
Petrological Investigations of CAIs from Efremovka and NWA 3118 CV3 Chondrites **[#1670]**
Several new big CAIs were extracted from the Efremovka and NWA 3118 CV3 chondrites to analyze petrology, chemistry and isotopic compositions. Here we report preliminary results on mineralogy, petrology and bulk chemistry of two CAIs, of Type B1 and of Type A.

Sweeney Smith S. A. Connolly H. C. Jr. Ma C. Rossman G. R. Beckett J. R. Ebel D. S. Schrader D. L.
Initial Analysis of a Refractory Inclusion Rich in $CaAl_2O_4$ from NWA 1934: Cracked Egg **[#1877]**
We report on our characterization of a 4 mm refractory inclusion rich in $CaAl_2O_4$ from NWA 1934 named Cracked Egg with rims of grossite, spinel + hibonite, and melilite + spinel surrounding a core rich in $CaAl_2O_4$ (with minor melilite and perovskite).

Sweeney Smith S. A. Jr. Connolly H. C. Jr Young E. D. Huss G. R. Nagashima K. Beckett J. R. Hill D. H.
Characterization of an Atypical Type B2 CAI from Allende, Burnt Toast: Evidence for a Complex Thermal History as Constrained by Petrology and Inferred Initial ^{26}Al Abundance **[#1911]**
We report on out petrographic and isotopic characterization of an atypical type B CAI with an internal rim of fassaite with a model age of 4.5 10^{-5}, but a melilite core of essential 0.

Petaev M. I. Nagashima K. Krot A. N. Jacobsen S. B.
Oxygen Isotopic Compositions of the Allende FoB CAI SJ101 **[#1818]**
O-isotopic data confirm that the origin of precursors of SJ101 and their melting occurred in a relatively closed system in an ^{16}O-rich region of the solar nebula.

Wakaki S. Itoh S. Tanaka T. Yurimoto H.
Petrology, Rare Earth Element Composition and Oxygen Isotopic Composition of a Compound CAI-Chondrule Inclusion from Allende **[#2057]**
A compound CAI-chondrule inclusion from Allende represents a mixture of partially melted CAI and chondrule materials that have underwent multiple heating processes under nebula gases with different ^{16}O enrichments.

Chen H. W. Chen J. C. Lee T. Shen J. J.
Calcium Isotopic Anomalies in the Allende CAIs and the Angrite Angra dos Reis **[#2088]**
Both negative ^{48}Ca and 50Ti anomalies of the Angrite Angra dos Reis was identified in this study, and the result supported previous study of correlated negative ^{54}Cr and ^{50}Ti anomalies in achondrites.

Yoshitake M.   Yurimoto H.
Oxygen and Magnesium Isotopic Compositions of Minerals In/Around Wark-lovering Rim of Type B2 CAI from Vigarano **[#1545]**
Most coarse-grained CAIs have Wark-Lovering rim (WL rim). We report O-isotopic and Mg-isotopic compositions of WL rim and melilite adjacent to WL rim. These results indicate that condensation is probably dominant for the WL rim formation.

Simon J. I.   Hutcheon I. D.   Simon S. B.   Matzel J.   Ramon E. C.   DePaolo D. J.
A Record of Solar System Scale Variation in Oxygen Isotopes at the Microscale: Cosmochemical Origins of CAIs and Their Wark-lovering Rims **[#1540]**
We measured O isotope variations in Allende CAI A37 and its surrounding rim, using the NanoSIMS. At the µm scale, both the CAI and rim exhibit significant variation in $\Delta^{17}O$ that encompasses the range observed for all solids in the solar system.

Ito M.   Messenger S.   Keller L. P.   Rahman Z. U.   Ross D. K.   Nakamura-Messenger K.
FIB-NanoSIMS-TEM Coordinated Study of a Wark-lovering Rim in a Vigarano Type A CAI **[#1177]**
We present preliminary results of O isotopic and elemental images by NanoSIMS and mineralogical analysis by FE-SEM of a FIB section of a WL rim in the Vigarano reduced CV3 chondrite in order to understand of nature of a WL rim.

Ma C.   Beckett J. R.   Rossman G. R.
Grossmanite, Davisite, and Kushiroite: Three Newly-approved Diopside-Group Clinopyroxenes in CAIs **[#1494]**
Grossmanite, davisite and kushiroite are newly-approved Ca-clinopyroxenes. We outline here procedures by which EMP analysis of a Ca-clinopyroxene can be assigned the correct name and illustrate the usage with examples of the new minerals from CAIs.

UREILITES

Karczemska A.   Jakubowski T.
Raman Imaging of Ureilitic Diamonds **[#1639]**
We performed Raman Imaging of diamonds from three ureilitic samples. Results show the coexistence of several diamond types based on the various observed shift positions in the studied ureilites.

Ash R. D.   Goodrich C. A.   Van Orman J. A.   McDonough W. F.
Petrography and Siderophile Geochemistry of Metal and Sulphide in Ureilites **[#1302]**
We have measured highly siderophile elements in sulphides and metals in well characterised olivine-low Ca pyroxene ureilites with a range of petrogenetic characteristics. Metals are the dominant carriers of PGEs, but Pd may be affected by sulphides.

Ross A. J.   Downes H.   Smith C. L.   Jones A. P.
DaG 1047: A Polymict Ureilite Containing Exotic Clasts Including a Chondrite **[#2361]**
We present EPMA data for the polymict ureilite DaG 1047. This meteorite contains multiple exotic clasts not found in monomict ureilites such as feldspars, Si-bearing metals (suessite) and a chondritic clast containing well-preserved chondrules.

Goodrich C. A.
Late Orthopyroxene + Metal Assemblages in Ureilites, Brachinites, and Other Olivine-rich Achondrites **[#1091]**
Fine-grained assemblages of orthopyroxene + metal in some brachinites and related olivine-rich achondrites may have formed by late reduction, similar to ureilites.

Warren P. H.
Ureilites: Pigeonite Thermometry and the Unimportance of Pressure-buffered Smelting During Evolution as Asteroidal Mantle Restites **[#1530]**
Ureilite equilibration T derived from pigeonite composition shows a strong (+) correlation with olivine Fo. Combinations of T and Fo implicit in combinations of P and Fo proposed for P-buffered smelting match real ureilite data very poorly.

Bischoff A. Horstmann M. Laubenstein M. Haberer S.
Asteroid 2008 TC3 — Almahata Sitta: Not Only a Ureilitic Meteorite, but a Breccia Containing Many Different Achondritic and Chondritic Lithologies **[#1763]**
Meteorite Almahata Sitta has been classified as a polymict ureilite. We have studied more than 30 fragments from the strewn field and found that Almahata Sitta is a complex mixture of ureilitic and chondritic lithologies.

Horstmann M. Bischoff A.
Characterization of Spectacular Lithologies from the Almahata Sitta Breccia **[#1784]**
Meteorite Almahata Sitta has been classified as a polymict ureilite, but it contains a huge number of spectacular fragments of different ureilitic and chondritic lithologies.

Zolensky M. E. Herrin J. Mikouchi T. Satake W. Kurihara T. Sandford S. A. Milam S. N. Hagiya K. Ohsumi K. Friedrich J. M. Jenniskens P. Shaddad M. H. Le L. Robinson G. A.
Olivine in Almahata Sitta — Curiouser and Curiouser **[#2306]**
Description of olivine in the Almahata Sitta urilite.

Hoffmann V. H. Hochleitner R. Torii M. Funaki M. Mikouchi T. Almahata Sitta Consortium
Magnetism and Mineralogy of Almahata Sitta **[#2120]**
The aims of our investigations are unrevealing Almahata Sitta's (AS) magnetic signature, phase composition and mineralogy (main focus on the opaques) and getting new insights to the ureilite parent body magnetism (2008TC3 belongs to F-type asteroids).

Ott U. Herrmann S. Jenniskens P. M. Shaddad M.
A Noble Gas Study of Two Stones from the Almahata Sitta Meteorite **[#1195]**
Noble gases analyzed in two stones from the Almahata Sitta polymict ureilite indicate a cosmic ray exposure age of ~12.5 Ma. No evidence is seen for implanted solar wind, while heavy primordial noble gases show a typical ureilite pattern.

Hiroi T. Jenniskens P. M. Bishop J. L. Shatir T.
Reflectance Spectroscopy of Almahata Sitta Meteorite Samples from Asteroid 2008 TC3 **[#1148]**
As a preliminary study, the visible-NIR reflectance spectra of chip and powder samples of select stones of Almataha Sitta meteorite have been measured to provide insights into the surface and internal compositions and possibly the surface physical properties of 2008 TC_3.

ACHONDRITES

Senshu H. Usui T.
Numerical Consideration for the Themal Evolution and Physical Constraints of GRAs' Parent Body **[#1587]**
Numerical simulations on thermal evolution of possible parent body of GRA06128/9 with wide variety of parameters are carried out. We could seek out locations which satisfy all of the constraints given from analytical study.

Fernandes V. A. S. M. Shearer C. K.
^{40}Ar-^{39}Ar Ages of Metamorphism Preserved in the Achondrite GRA 06129 **[#1008]**
^{40}Ar-^{39}Ar analyses on achondrite GRA 06129 suggest two main episodes of metamorphism: 1) at 4.460± 0.028 Ga when likely the granoblastic texture formed, and 2) at ≤2.673±0.038 Ga possibly related to the low-temperature alteration.

Delaney J. S.
Oxygen in HEDs: Signatures of Multiple Planetoids or Accretionary Stratigraphy in a Planetary Open System? **[#1397]**
Oxygen isotopes of HEDs may reflect open system accretion rather than multiple parent bodies.

Righter M. Lapen T. J.
Petrology, Mineralogy and Mineral Chemistry of Antarctic Monomict Eucrites CMS 04049 and QUE 97053 **[#2629]**
We report petrology and mineral chemistry data including trace element abundances in minerals of two monomict eucrites, CMS 04049 and QUE 97053 to understand igneous and post-crystallization history of eucrite.

McFerrin B. Worsham E. A. McSween H. Y. Taylor L. A.
Petrology of Two New Eucrites from North West Africa **[#2381]**
Newly discovered monomict and polymict eucrite breccias from North West Africa help define igneous processes on the HED parent body.

Mittlefehldt D. W. Herrin J. S. Mertzman S. A. Mertzman K. R.
Petrology and Composition of HED Polymict Breccias **[#2655]**
We present the results of our petrology and compositional studies of howardites and polymict eucrites.

Boesenberg J. S.
A Petrological and Chemical Study of the Winterhaven Howardite **[#1787]**
Winterhaven is new howardite. The petrogenesis of this sample is considered using the Ti/(Ti+Cr) and Fe/(Fe+Mg) ratios.

Beck A. W. McSween H. Y. Jr
Connections Between Dunite MIL 03443 and the Diogenite Meteorites **[#1104]**
Similarities in mineral chemistries and textures in MIL 03443 (anomalous dunite) to olivine-bearing diogenites further supports the grouping of MIL 03443 with the HEDs.

Cordier C. Folco L. Taylor S.
Origin of Differentiated Cosmic Spherules: Insights from Trace Element Geochemistry **[#1132]**
Based on trace element composition of five differentiated cosmic spherules, we propose key trace elements that allow identification of differentiated compositions and discrimination between martian and vestoid origin.

Towner M. C. Duffy C. M. Bland P. A. Spurný P. Abel R. L.
The Bulk Properties of Bunburra Rockhole: Results of Micro-CT Scan Analysis **[#1758]**
Bunburra Rockhole is an anomalous basaltic achondrite, delivered from an Aten-type orbit. Here we use micro-CT analysis to determine material properties. Distribution of cracks may constrain fragmentation behaviour as it entered the atmosphere.

Benedix G. K. Bland P. A. Howard K. T. Spurny P. Bevan A. W. R.
The Mineralogy and Petrology of Bunburra Rockhole **[#1438]**
We describe Bunburra Rockhole, the first recovered meteorite from the Desert Fireball Network. It is an anomalous basaltic achondrite and this abstract will explore aspects of its mineralogy and petrology.

Bouvier A. Wadhwa M.
Pb-Pb Isotope Dating of the Unique Basaltic Achondrite NWA 2976 **[#1489]**
We report an absolute Pb-Pb age for the basaltic achondrite NWA 2976 of 4563.81 ± 0.19 Ma. This age is concordant with the Al-Mg model ages anchored to the Al-Mg and Pb-Pb systematics of the D'Orbigny angrite and NWA 2364-B1 CAI.

Bunch T. E. Rumble D. III Wittke J. H. Irving A. J. Sipiera P. P. Gregory D. A.
Northwest Africa 5782: A Complex, Polymict Acapulcoite + Lodranite Breccia Containing HEDOD Clasts **[#1281]**
This meteorite represents the first direct evidence for derivation of acapulcoites and lodranites from a common parent body, which evidently underwent at least partial differentiation.

Shirai N.   Humayun M.
Initial Tungsten Isotopic Compositions for Angrites Obtained from Phosphates **[#2642]**
Initial isotopic compositions of W from angrites are obtained by new method from W-bearing phosphates.

Sanborn M. E.   Wadhwa M.
Rare Earth Element Geochemistry of Quenched Angrites Northwest Africa 1296 and Northwest Africa 1670 **[#1490]**
We report rare earth element abundances in the quenched angrites NWA 1296 and NWA 1670. Implications are presented for the petrogenetic history of these two angrites and their relationship to other quenched angrites.

IRON AND STONY IRON METEORITES

Garvie L. A. J.   Bell D. R.   Buseck P. R.
Petrography and Geochemistry of a 30-Centimeter Pyroxenite Nodule from the Bondoc Mesosiderite **[#1386]**
The Bondoc mesosiderite contains one large pyroxenite nodule, which we suggest is an intact fragment of the mafic crust from a differentiated parent body.

Tarduno J. A.   Cottrell R. D.   Hopkins J.   Erickson A.
The Paleomagnetic Record of Pallasite Meteorites **[#2150]**
We present paleointensity data from olivine containing magnetic inclusions from main group pallasite meteorites that suggest magnetization in strong magnetic fields, and discuss the implications for pallasite parent body evolution.

Lauretta D. S.
Trace Element Distributions in the Fukang Pallasite **[#1462]**
We present the first results from our new laser-ablation ICP-MS facility. Trace-element abundances have been measured in metal, olivine, sulfide, and phosphide phases in the Fukang pallasite. The results provide insight into the origin and thermal history of this meteorite.

Walker R. J.   Yokoyama T.   Herzog G.   Cook D. L.
Osmium Isotopic Heterogeneities in Iron Meteorites and Pallasites **[#1324]**
Osmium isotope ratios in iron meteorites from five groups show variable modification by long-term cosmic ray exposure. There is no evidence for nucleosynthetic anomalies in Os in the five groups, or the Eagle Station pallasite.

Fukami Y.   Kimura J.   Irisawa K.   Yokoyama T.   Hirata T.
Mass-Dependent Fractionation of Tungsten Isotopes in IIIAB Iron Meteorites and Main-Group Pallasites **[#1649]**
The W stable isotope compositions in IIIAB irons and metallic phases of PMG were precisely determined. The results suggest the possibility that W stable isotopes in IIIAB irons fractionate during fractional crystallization of metallic core.

Blichert-Toft J.   Moynier F.   Lee C.-T.   Albarede F.
Radiogenic Pb in Muonionalusta Troilite and the Old Age of the IVA Asteroid **[#1127]**
We present Pb-Pb data on troilite from Muonionalusta (IVA). The data reveal highly radiogenic Pb giving a ^{207}Pb*/^{206}Pb* age of 4.5651±0.0005 Ga (range of 4.563–4.567 Ga), implying that the IVA parent body formed within 3±2 Ma of planetary accretion.

Varela M. E.   Kurat G.   Zinner E.   Brandstätter F.
The Tucson Ungrouped Iron Meteorite: A Step in Deciphering Its Enigmatic Origin **[#1316]**
Tucson seems to be the result of co-precipitation of metal and silicates from the solar nebula gas and precipitation of metal before silicates in accordance with theoretical condensation calculations for high-pressure solar nebula gas [*Ebel 2006*].

Defouilloy C.   Duhamel R.   Robert F.   Clog M.
The Isotopic D/H Ratio of Iron Meteorites **[#1340]**
The D/H ratio of iron meteorites has been measured with a IMS 3f to document the idea that irons are samples from the core of differentiated bodies. Measurements on four irons show an absolute D/H ratio between 131×10^{-6} and 154×10^{-6}.

EDUCATION AND PUBLIC OUTREACH: METEORITES

Singletary S. J.
Increasing the Participation of Minority Students in Earth/Environmental/Space Science: Classification of Unknown Meteorites Using the Electron Microprobe **[#1859]**
The classification of unknown meteorites is used as a vehicle to train minority students to use the electron microprobe and to inspire them to pursue advanced degrees in Earth/Environmental/Space Science.

Mayne R. G.   Moss T.
The Oscar E. Monnig Meteorite Collection and Museum **[#1162]**
An overview of the Oscar E. Monnig Meteorite Collection and Gallery and associated public outreach efforts.

Anand M.   Kelley S. P.   Tindle A. G.   Whalley P. C.
Virtual Microscope for Extra-Terrestrial Samples: A New Tool for Public Engagement in Planetary Sciences **[#2409]**
We would like to describe a new outreach project that we have piloted at the Open University which involves developing a web-based virtual microscope for extraterrestrial rock samples.

Hines R.   Taylor W.   Minitti M. E.   Wadhwa M.
Bringing Outer Space into the Classroom: Loanable Space Science Modules from the Center for Meteorite Studies and Mars Education Program at Arizona State University **[#2617]**
The Center for Meteorite Studies (CMS) and Mars Education Program at Arizona State University have developed loanable teaching modules designed to provide high-quality educational materials to local educators and students.

PLANETARY DIFFERENTIATION THROUGHOUT THE SOLAR SYSTEM

King C.   Righter K.   Danielson L.   Pando K.   Lee C.
Determining the Metal/Silicate Partition Coefficient of Germanium: Implications for Core and Mantle Differentiation **[#1257]**
Ge is a moderately siderophile element that was studied systematically at high temperatures using a piston cylinder apparatus. Evidence observed finds extremely high T is not necessary, therefore suggesting a shallow ocean.

Duncan M. S.   Agee C. B.
High Pressure Experiments on Carbonated Peridotite with Applications to the Mantle **[#1488]**
The sink/float method was used to determine the partial molar volume of CO_2, which can be used to calculate the density of carbonated partial melts. This can be applied to magma mobility in the mantle and planetary differentiation scenarios with CO_2.

Ardia P.   Hirschmann M. M.
Preliminary Investigations of Methane Solubility at Reduced Condition in a Haplobasaltic Liquid, with Applications to Magma Oceans **[#1347]**
We report small solubilities (~0.2 wt.%) of CH_4 from experiments in basaltic liquid at 1.5-2.5 GPa. We conclude that CH_4 is the principal dissolved species of C in magma oceans and discuss consequences for C outgassing to protoatmospheres.

Jones J. H.
Variations on a Theme by Longhi: I. An Analysis of the Thermodynamic Underpinning of Fe, Mn, and Ni Partitioning into Olivine **[#1338]**
The magic of D vs. D(Mg) regressions for olivine/liquid partitioning explained (i.e., Jones thinks he's gotten it right this time).

Hayden L. A. Van Orman J. A. McDonough W. F. Ash R. D. Goodrich C. A.
Trace Element Partitioning in the Fe-S-C System **[#1520]**
New data in the Fe-S-C system show that partition coefficients between immiscible C- and S-rich liquids are high at high T, suggesting that strong fractionations are possible in C-saturated systems if there is a mechanism for separating the liquids.

Shofner G. A. Danielson L. Righter K. Campbell A. J.
High Pressure/Temperature Metal Silicate Partitioning of Tungsten **[#2612]**
High P-T experiments examined DW in peridotite, three of which (P 18–26 GPa, T 2200C) show DW essentially constant in this P range, consistent with predictions. Core formation models predict P as high 50 GPa, so DW is still poorly constrained to this P.

Hill E. Huss G. R. Domanik K. Drake M. J.
Subsolidus Metal — Olivine Trace Element Partitioning **[#1493]**
Metal – olivine subsolidus diffusion experiments provide diffusion rates and trace-element diffusion profiles that allow us to study the cooling rates of mesosiderites and calculate subsolidus distribution coefficients .

Danielson L. R. Righter K. Newville M. Sutton S. Pando K.
Molybdenum Valence in Basaltic Silicate Melts **[#1946]**
XANES analyses of molybdenum were performed on basaltic glass run products experiments conducted at varying P, T, and fO_2. The transition from Mo^{6+} to Mo^{4+} occurs around IW, only Mo^{4+} remains at IW-1 and below, conditions relevant to core formation.

Tsuno K. Frost D. J. Rubie D. C.
Effect of Silicon on the Partitioning of Oxygen Between Liquid Iron Metal and Silicate Liquid **[#2041]**
We have investigated metal-silicate reaction experiments, showing that the presence of Si dissolved in liquid Fe has a large effect in reducing the concentration of oxygen, and partitioning of Si into liquid Fe-alloy increases with temperature and decreases with pressure.

Kletetschka G. Zila V. Wasilewski P. T.
Magnetic Effects of Allende and Bjurbole Chondrules Moving from Space to Terrestrial Environments **[#1273]**
Temperature has a strong effect on the stability of meteorite magnetization. When natural magnetization is significantly different below the room temperature, caution should be exercised when reaching for conclusions, about the parent body formation.

Monteux J. Jellinek M. Johnson C. L.
Why Might Planets and Moons Have Early Dynamos? **[#1375]**
We address whether processes governing core formation through Fe-segregation from large impacts might lead to dynamo action. We show that the accretion conditions determine whether or not a planet or a moon can have an early magnetic field.

Citron R. I. Barr A. C. Canup R. M.
Formation and Early Evolution of an Undifferentiated Titan **[#1270]**
We show that Titan can accrete undifferentiated in a gas starved disk, even with modest amounts of ammonia mixed in with its ice, and that Titan can remain partially differentiated after an outer solar system late heavy bombardment.

Grocholski B. Shim S.-H. Prakapenka V. B.
The Mantle Convection in the Super-Earths; Implications from High-Pressure Experiments on Silicate Analogs **[#1515]**
Our study on mantle silicate analog material shows that Super-Earths may have whole mantle convection.

COSMIC-RAY EXPOSURE DATING

Welten K. C.   Caffee M. W.   Leclerc M. D.   Jull A. J. T.   Metzler K.   Franke L.   Ott U.
Evidence for Recent Near-Catastrophic Collision on Large Chondritic Meteoroid, Northwest Africa 869 **[#2611]**
Cosmogenic nuclides in six fragments of the NWA 869 L-chondrite shower show evidence of a recent near-catastrophic collision, thus exposing previously buried samples close to the surface of the meteoroid.

Ott U.   Herrmann S.   Haack H.   Grau T.
Noble Gases in Two Meteorites that Fell in Denmark and Slovenia in 2009 **[#1196]**
From noble gas analyes we obtain for CM2 Maribo and an as yet unapproved stone (ordinary chondrite) that fell in Slovenia in April 2009 CRE ages of ~1 and ~ 4 Ma. Ne and Xe isotopes in Maribo indicate the presence of presolar diamond and SiC.

Cosarinsky M.   Calmonte U.   Hofmann B.   Leya I.
Noble Gas Data on Ureilites from the Lybian, Omani, and Moroccan Deserts **[#1770]**
Here we report noble gas data on ureilites from hot deserts. He and Ne are mostly cosmogenic, with a few exceptions, whereas Ar is mostly primordial in composition. Cosmic-ray exposure ages are in the range of 3–27 Myr.

Schulz T.   Upadhyay D.
Neutron Capture Induced Sm Isotope Anomalies in Metal-shielded and -unshielded Silicates **[#1738]**
In this study we evaluate the effect of meteoroid bulk chemical composition on neutron-capture by isotopes of Sm using bulk-silicate separates of non-magmatic iron meteorites, mesosiderites and stony meteorites.

Fink D.   Klein J.   Middleton R.   Albrecht A.   Ma P.   Herzog G. F.   Bogard D. D.   Nyquist L. E.   Shih C.-Y.   Reese Y.   Garrison D. H.   Masarik J.   Reedy R. C.   Rugel G.   Faestermann T.   Korschinek G.
Cosmogenic Samarium-150 and Calcium-41 in Norton County **[#1354]**
We have inferred thermal neutron fluences in Norton County from (1) Sm isotope data and (2) ^{41}Ca activities coupled with a cosmic-ray exposure age of 115 Ma. The fluences disagree, suggesting that the exposure history of Norton County was not simple.

Qin L.   Dauphas N.   Horan M. F.   Carlson R. W.   Alexander C. M. O'D.   Leya I.   Masarik J.
Cosmogenic Stable Isotope Effects on Tungsten, Osmium and Chromium in the Carbo Iron Meteorite **[#2517]**
Osmium isotopic variations in Carbo can be best explained by neutron capture. They are also correlated with $\varepsilon^{182}W$ variations, which suggests that they can be used as neutron dose monitor. Cr isotope variations may reflect the heterogeneity in Fe/Cr.

MAIN BELT: SOURCES AND SINKS

Ivanov A. B.   Thomas N.
Reconstruction of a Digital Elevation Model for Phobos from HIRISE Data **[#1923]**
We report on a preliminary study to derive a digital elevation model of Phobos based on HIRISE stereo pair data.

Palomba E.   D'Amore M.   Zinzi A.   D'Aversa E.   Maturilli A.   Helbert J.
Revisiting the Thermal Infrared Spectral Observations of Phobos **[#1899]**
Here we re-analyse Phobos TIR spectra taken by the TES instrument. We use a multi-planckian approach and a statistical analysis to retrieve Phobos emissivities that are compared with laboratory emissivities and TIR observations of other asteroids.

Lim L. F.   Emery J. P.   Moskovitz N. A.
Mid-IR Spectra of HED Meteorites and Synthetic Pyroxenes: Reststrahlen Features (9–12 µm) **[#2001]**
We discuss the 9–12 µm Reststrahlen features in the spectra of diogenites and eucrites and place them in the context of a suite of well-characterized synthetic pyroxenes (Klima et al., 2005).

Li J.-Y.   Naidu S.   McFadden L. A.
HST NICMOS Mapping of Asteroid 4 Vesta **[#2149]**
We took the archived HST NICMOS images to generate the reflectance maps of Vesta in the 1–2.4 µm range.

Jensen E. A.   Vilas F.   Sykes M. V.
Searching for Satellites of Vesta **[#2556]**
Twenty-four arcminutes of the sky around Vesta is investigated for the presence of satellites.

Reddy V.   Cloutis E. A.   Gaffey M. J.   Galád A.   Pravec P.   Harris A. W.   Nathues A.   Sanchez J. A.
Compositional Investigation of (5404) Uemura: The Largest Fast-Rotating Monolith **[#1227]**
Rotational state of an asteroid gives insights into internal structure. Photometry of (5404) Uemura revealed it is the fastest rotating large MBA (>1 km) with a period P = 1.72 h. Here we present its compositional analysis.

Fieber-Beyer S. K.   Gaffey M. J.
Near-Infrared Spectroscopy of 3:1 Kirkwood Gap Asteroids 908 Buda and 1772 Gagarin **[#1853]**
This research explores possible links between two asteroids located near the 3:1 resonance, 908 Buda and 1772 Gagarin, and potential meteorite analogs in the terrestrial collections.

Rivkin A. S.   Sunshine J. M.   Blewett D. T.   Hurley D. M.   Hibbitts C. A.
Lunar Water, Asteroidal Observations: Implications and Opportunity **[#1088]**
The discovery of lunar water/OH has implications for other inner solar system bodies. We will discuss implications of the lunar findings for asteroidal interpretations and vice versa, and suggest future work to move our general understanding forward.

Noll K. S.   Benecchi S. D.
Component Sizes in Small-Body Multiples: A Clue to Formation? **[#2330]**
The pattern of component size and separation in the nine known small-body multiples may provide constraints on the modes of formation for multiples and binaries in the various small body populations.

Yoshida F.   Yagi M.   Komiyama Y.   Nakata F.   Furusawa H.   Ohno T.   Okamura S.   Nakamura T.
Slitless Spectroscopy of Small Solar System Bodies on a Dark Cloud Curtain **[#1290]**
We performed slitless spectroscopy of small bodies with Subaru Telescope + Suprime-Cam attached grism filters using a dark cloud as a curtain for avoiding contamination from background stars. Spectra of 50 objects with R < 23 mag will be on the poster.

SMALL BODY MISSIONS

Nathues A.   Reddy V.   Schaeff S.   Wiegand A.   Michelsen R.   Sanchez J. A.   Boehnhardt H.
Ground-based Mineralogical Characterization of low Δv ASTEX Mission Targets **[#1047]**
ASTEX is an *in situ* exploration mission study to two near-Earth asteroids for which we have identified target candidates. Since many of the potential targets are without compositional information we have started a spectral survey.

Murdoch N.   Rozitis B.   Michel P.   Losert W.   de Lophem T-L.   Green S. F.
AstEx Microgravity Experiment: Simulating Asteroid Regoliths **[#1715]**
This experiment aims to characterise the response of granular material to rotational shear forces in a microgravity environment in order to help design an asteroid sampling mechanism and interpret the fascinating geology found on asteroids.

Mainzer A. K.   Masiero J.   Bauer J. M.   Grav T.   Cutri R.   McMillan R.   Walker R.   Wright E. L.   WISE Team
WISE Solar System Research – Clearer Views of the Darkest Objects **[#2505]**
The WISE mission will be capable of performing a vast array of solar system observations. WISE will observe and detect thousands of main-belt asteroids and hundreds of near-Earth objects, providing IR-derived diameters and albedos for many of these bodies.

Grav T.   Bauer J. M.   Dailey J.   Mainzer A. K.   Cutri R.   Masiero J.   McMillan R.   Walker R.   Wright E. L.
WISE Preliminary Detection Statistics of Minor Planets **[#2320]**
We present the preliminary detection statistics of moving objects from the first two months of WISE scan operations discuss such topics as survey efficiency, pipeline reliability and orbit determination accuracy.

Bauer J. M.   Grav T.   Dailey J.   Myers J.   Mainzer A. K.   Masiero J.   Cutri R.   McMillan R.   Jedicke R.   Denneau L.   Walker R.   Wright E. L.   WISE Team
The WISE Moving Object Pipeline Subsystem — Design and Implementation **[#2466]**
WISE will detect a large number of solar system bodies, a large fraction of which have been previously unknown. We describe the design and implementation of the moving object detection subsystem for the spacecraft imaging data.

Masiero J.   Mainzer A.   Grav T.   Delbó M.   Mueller M.   WISE Team
The WISE Survey of the Albedo Distribution of Main Belt Asteroids **[#1283]**
Using date from the Wide-field Infrared Survey Explorer (WISE) we investigate the albedo distribution across the main belt of asteroids. When complete WISE will measure albedos and diameters for ~100,000 asteroids.

Bauer J. M.   Grav T.   Mainzer A. K.   Masiero J.   Cutri R.   Dailey J.   McMillan R.   Walker R.   Wright E. L.   WISE Team
WISE and the Outer Solar System — Searching for Objects in "The Back Forty" (AU) **[#2418]**
The vast majority of objects observed by the WISE mission will be in the inner solar system. However, several larger solar system objects beyond 5 AU will also be imaged. We will present an overview of outer solar system object observations to date.

Tricarico P.   Sykes M. V.
The Dynamics of Dawn at Vesta **[#2289]**
The Dawn Discovery mission will encounter a challenging dynamical environment at its first rendezvous target, Vesta, in 2011. It will be subject to significant perturbations and even trapping as it operates at and moves between its survey orbits.

Burbine T. H,.   Buchanan P. C.
Determining Constraints on Crustal Formation Processes on Vesta Using Data from the Dawn Mission **[#1843]**
We will discuss how we can possibly determine constraints on the mechanisms for forming Vesta's crust using Dawn reflectance spectra.

IMPACT EJECTA AND OTHER DEPOSITS

Newsom H. E.   Salge T.   Nelson M. J.   Spilde M. N.
Discovery of Andradite Garnet and Evidence for High Temperature Hydrothermal Processes (>300°C) in the Lower Yaxcopoil-1 Impact-Melt Breccias **[#1751]**
Andradite garnet discovered in the matrix of the lower breccia units of the Yax-1 core in the Chicxulub impact provides evidence of an early high temperature hydrothermal system (>300°C), with a fluid that became more oxidizing with time.

Newsom H. E.   Misra S.   Wright S. P.   Muttik N.
Contrasting Alteration and Enrichment of Mobile Elements During Weathering of Basaltic Ejecta and Ancient Soils at Lonar Crater, India **[#2210]**
Alteration of impacted basalt has led to mobilization and enrichment of proximal and distal ejecta in alkali elements. In contrast, the underlying ancient paleosol materials are depleted and are the residual product of weathering over a longer time.

Adolph L.   Deutsch A.
Trace Element Analysis of Impact Glass Spherules of the El'gygytgyn Crater, Siberia **[#2421]**
Seven small glass spheres from a terrace deposit outside the crater have been analysed by LA-ICP-MS for 31 trace elements.

Adolph L.   Deutsch A.
Impact Glasses of the Lake Bosumtwi Impact Structure, Ghana: Ivory Coast Tektites, Microtektites, Fallback Particles and Suevite Glass — Similarities and Differences **[#2106]**
We present EMP and LA-ICP-MS data for a variety of fresh glass samples from the Bosumtwi impact structure, and the relevance of these data for the origin of the glass.

Howard K. T.   Bailey M. J.   Bland P. A.   Cressey G.   Howard L. E.   Jeynes C.   Stolojand V.   Verchovsky S.
Spherical Carbonaceous Inclusions in (Darwin) Impact Glass and Co-Genetic Mineral (SiO_2 + TiO_2) Growth Under Impact Conditions **[#1603]**
We have discovered spherical carbonaceous inclusions in Darwin glass associated with co-genetic crystalline SiO_2 and TiO_2. This is the first example of carbonaceous melt and co-genetic mineral growth in an ejected impact glass or tektite.

Engrand C.   Narcisi B.   Petit J.-R.   Dobrică E.   Duprat J.
Oxygen Isotopes of EPICA — Dome C Extraterrestrial Dust Layers: Constraints on the Nature of the Impactors **[#1981]**
The oxygen isotopic compositions of the two extraterrestrial dust layers recorded in EPICA-Dome C ice core suggest a production by two distinct impacts, one of them possibly being by a comet.

van Ginneken M.   Folco L.   Perchiazzi N.   Rochette P.   Bland P. A.
Meteoritic Ablation Debris from the Transantarctic Mountains: Evidence for a Tunguska-like Impact over Antarctica **[#1321]**
Meteorite Ablation Spheres were found in Antarctica. They are likely paired with particles from two coeval dust layers from Dome F and Dome C ice cores. Continental scale distribution of the MAS can be explained by a Tunguska-like impact event.

Petaev M. I.   Nagashima K.   Krot A. N.   Chakrabarti R.   Jacobsen S. B.   Becker L.   Basu A. R.
Terrestrial and Extraterrestrial Mafic Silicates from the P-T Boundary Claystone Breccia of Graphite Peak, Antarctica: Evidence from Oxygen Isotopes and Mineral Chemistry **[#1808]**
The O isotopes and mineral chemistry confirm the presence of terrestrial and extraterrrestrial forsterites and enstattites in the P-T boundary claystone breccia from Graphite Peak, Antarctica.

Heck P. R.   Schmitz B.   Meier M. M. M.   Wieler R.
Fossil Meteorites in Ordovician Sediments from Sweden are not Redistributed Meteorites from a Single Fall **[#1001]**
We present independent lines of evidence showing that the fossil meteorites found in Ordovician sediments from Sweden have been delivered to Earth over several million years, and hereby dismiss a recent claim that the meteorites originated in a single fall.

Piatek J. L.   Ukstins Peate I.   Cabrol N. A.   Grin E. A.   Chong G.
Monturaqui Crater (Atacama Desert, Chile) as a Mars Analog: Exploring the Impact Spherule Hypothesis for Meridiani **[#2236]**
Monturaqui is a young terrestrial impact in the Atacama Desert. The impact affected volcanic rocks and created a vesicular impactite that contains iron oxide spherules, representing a potential analog for "blueberries" in Meridiani Planum, Mars.

IMPACTITE PETROLOGY AND AGES

Ormö J.   King D. T. Jr.   Harris R. S.   Petruny L. W.   Markin J. K.
Sediment-laden Flow of Mooreville Chalk Within the Interior of Wetumpka Marine Target Impact Structure, Alabama: Evidence for a Shallow Water Resurge **[#1430]**
A mudflow deposit with sporadic shocked mineral grains indicates that the impact occurred in very shallow water. This makes Wetumpka a uniquely well preserved example of impacts in near-shore environment.

Dypvik H.   Claeys P.   Deutsch A.   Kyte F. T.   Matsui T.   Smelror M.
Drilling the Late Jurassic Mjølnir Impact Crater in the Barents Sea **[#1086]**
The proposal suggests drilling of five core holes around the Mjølnir structure in the Barents Sea (Norway). The study includes ejecta formation/distribution, and sediment disturbance due to seismic and shock waves, or erosion by displaced water.

Malone L.   Boonsue S.   Spray J.   Wittmann A.
Zircon-Reidite Relations in Breccias from the Chesapeake Bay Impact Structure **[#2286]**
The natural high pressure polymorph of ZrSiO4 exhibits distinct zonations in shock stage III (45–60 GPa, 900°–1500°C) materials. A decomposition front at the rim still contains reidite, which raises questions about the durability of reidite-zircon.

Bartosova K.   Koeberl C.   Gier S.   Horton J. W. Jr.   Mader D.   Dypvik H.
Gravelly Sand Interval of the Eyreville Drill Core, Chesapeake Bay Impact Structure, USA **[#1734]**
Results of detailed investigations of the gravelly sand interval (1371–1397 m depth) of the Eyreville drill core including macro- and microscopic observations, modal point counting, X-ray diffraction analyses, and geochemical analyses are presented.

Jaret S. J.   Chakrabarti R.   Jacobsen S. B.   Patev M.   Kalleson E.   Dypvik H.
Re-Examination of Gardnos Impactites **[#2359]**
This study is a geochemical and petrologic study of impact melts and breccias from the Gardnos Impact Structure. Here we present initial results and proposal for futher detailed isotope geochemistry studies.

Anders D.   Kring D. A.   Holzheid A.
Carbonate-rich Material Associated with Meteor Crater Impact Melt Particles **[#1799]**
Carbonate coatings were recently found around some of Meteor Crater silicate melt particles. The origin is unclear. To evaluate the origin of the observed carbonate rinds, the chemical compositions and textures of three particles with carbonate coatings were investigated.

Muttik N.   Kirsimäe K.   Somelar P.   Vennemann T. W.
Alteration of Suevitic Impactites at the Ries Crater, Germany: Stable Isotope Composition of Smectite Minerals and Fluid Temperatures **[#1468]**
This study represents $\delta^{18}O$ and δD analyses of smectite minerals in crater fill and surficial suevite from the Ries crater, Germany to elucidate the origin and temperature of the fluids responsible for alteration of impact glass and primary silicates.

Mohr-Westheide T.   Reimold W. U.   Gibson R. L.   Mader D.   Koeberl C.
Genesis of Pseudotachylitic Breccias from the Vredefort Dome, South Africa: New Microchemical and Petrographic Findings **[#1796]**
We discuss the results of new mineralogical and chemical analyses of mafic and felsic pseudotachylitic breccias from the core and collar of the Vredefort Dome, South Africa, highlighting mineralogical controls on melt composition.

Misra S.   Newsom H. E.
Geochemistry and Petrology of Maskelynite in NWA1195 Shergottites and Its Comparison with Maskelynite from Lonar Crater, India **[#1806]**
The absence of fractures and the smooth texture of NWA1195 maskelynite suggest its evolution by rapid chilling of a liquid feldspar melt, compared to the highly fractured Lonar maskelynite, which is characteristic of diaplectic plagioclase glass.

Ferrière L.   Osinski G. R.
Shatter Cones and Associated Shock-induced Microdeformations in Minerals — New Investigations and Implications for Their Formation **[#1392]**
We report on preliminary results of a study of shatter cones from several impact structures, combining field and macroscopic observations with microscopic properties of minerals, to infer the course of events that result in their formation.

Ferrière L.   Raiskila S.   Osinski G. R.   Pesonen L. J.   Lehtinen M.
The Keurusselkä Structure (Finland) — Impact Origin Confirmed by Universal-Stage Characterization of Planar Deformation Features in Quartz Grains **[#1072]**
We report on the discovery and characterization, using universal-stage, of planar fractures and planar deformation features in quartz and plagioclase grains. Our investigations substantiate a meteorite impact origin for the Keurusselkä structure.

Schmieder M.   Buchner E.   Jourdan F.   Schwarz W. H.   Trieloff M.   van Soest M. C.   Wartho J.-A.
Hodges K. V.   Moilanen J.   Hietala S.   Öhman T.
Updating the Finnish Impact Cratering Record **[#2036]**
New isotopic age data are presented for the Keurusselkä, Paasselkä, Suvasvesi South, and Karikkoselkä impact structures, Finland.

Schmieder M.   Buchner E.
Possible Iron Meteoritic Contamination in Impact Melt Particles from the Steinheim Basin (Baden-Württemberg, Germany) **[#2103]**
High Ni and Co contents and Ni/Co and Ni/Cr ratios in Fe-sulfides within the suevitic Steinheim (Germany) impact breccia suggest an iron meteorite as the Steinheim impactor.

Cooper F. J.   van Soest M. C.   Wartho J-A.   Hodges K. V.   Buchner E.   Schmieder M.   Koeberl C.
(U-Th)/He Dating of the Nördlinger Ries Impact Structure, Germany **[#2243]**
New (U-Th)/He zircon data for the Nördlinger Ries impact structure give a mean age of 13.60 ± 0.58 Ma (2σ). This is slightly younger than but within error of the most recent Ar/Ar age of ~14.4 Ma.

Buchner E.   Schmieder M.   Schwarz W. H.   Trieloff M.   Hopp J.   Spray J. G.
Dating the Charlevoix Impact Structure (Québec, Canada) — A Tough Nut to Crack in $^{40}Ar/^{39}Ar$ Geochronology **[#2017]**
$^{40}Ar/^{39}Ar$ step-heating analysis of an impact melt rock from the Charlevoix impact structure (Québec) suggests an Early Devonian minimum age for the impact.

Jourdan F.   Schmieder M.   Buchner E.
The Lake Saint Martin Impact and the Problem of Isotopic Dating on Altered Impact Melt Rocks **[#1654]**
We undertook a $^{40}Ar/^{39}Ar$ high-resolution step-heating experiment on the St Martin impact melt rock. This provides a strictly minimum age of >>210 Ma for the impact and warns for the interpretation of low- to medium-temperature isotopic data.

Ukstins Peate I.   van Soest M. C.   Wartho J.-A.   Cabrol N.   Grin E.   Piatek J.   Piatek J.   Chong G.
A Novel Application of (U-Th)/He Geochronology to Constrain the Age of Small, Young Meteorite Impact Craters: A Case Study of the Monturaqui Crater, Chile **[#2161]**
We report a (U-Th)/He apatite and zircon single crystal age of 663 ± 90 ka for Monturaqui impact structure (Chile), which acts as an ultimate test of the applicability of the (U-Th)/He technique for dating very small, young impact structures.

IMPACT EXPERIMENTS

Kurosawa K.   Sugita S.   Kadono T.   Shigemori K.   Hironaka Y.   Ozaki N.   Shiroshita A.   Cho Y.   Sakaiya T.   Fujioka S.   Tachibana S.   Vinci T.   Kodama R.   Matsui T.
Roles of Shock-induced Ionization due to >10 km/s Impacts on Evolution of Silicate Vapor Clouds **[#1785]**
We conducted shock-induced silicate vaporization experiments and carried out *in situ* time-resolved spectroscopic observation. We found that electrons works as an energy reservoir in energy partitioning during hypervelocity impacts.

Daly T.   Call S.   Austin D. E.
Electrospray Charging of Quartz Microparticles for Studies of High-Velocity Micrometeorite Impact Chemistry **[#2270]**
We are developing an instrument that introduces innovative capabilities to the laboratory study of hypervelocity microparticle impacts, including capabilities for directly characterizing the chemical speciation that occurs during these events.

Carmona J. A.   Cook M.   Schmoke J.   Laufer R.   Matthews L. S.   Hyde T. W.
Low-Velocity Impacts on PVDF Targets Using a Light Gas Gun **[#2232]**
PVDF was tested for its piezoelectric capabilities along with the advantages of ruggedness, ease of large area sensor construction, high counting rate capability, and space reliability, which makes it an ideal space debris sensor.

Simcox T. B.   Wall D. R. I.   Burchell M. J.
Hypervelocity Impact Experiments on Low Temperature Sand:Ice Targets **[#1357]**
Laboratory hypervelocity impacts on sand:ice mixtures are reported using JSC Mars simulant. High water content and low sand grain size result in wide shallow craters. At low temperatures the crater diameter is unchanged but depth decreases slightly.

Ernst C. M.   Barnouin O. S.   Schultz P. H.
High-Speed Imaging of the Impact Flash: Observations of Source Location and Transient Crater Growth **[#1381]**
Experimental impacts into non-volatile, particulate targets produce long-duration impact flashes dominated by hot thermal sources. High-speed photometry and imaging reveal the source location and transient crater growth through time.

Hermalyn B.   Schultz P. H.   Heineck J. T.
Early-Stage Coupling for Oblique Impacts in Granular Material **[#2565]**
Early-time impact processes affect the emplacement of distal ejecta and play an important role at planetary scales, especially for oblique impacts. This experimental study examines the ejecta dynamics for oblique impacts through a novel imaging technique.

Weirich J. R.   Isachsen C. E.   Johnson J. R.   Swindle T. D.
Argon Diffusion in Pyroxene and Albite **[#2137]**
Shock greatly raises the diffusivity of albite, and also explains why meteorites often have low activation energies. Unshocked pyroxene cannot explain the high temperature release of argon in meteorites, though shocked pyroxene is a possibility.

Kimberley J.   Ramesh K. T.   Barnouin O. S.   Ernst C. M.
Dynamic Strength Measurements of L5 Chondrite MacAlpine Hills 88118 **[#2588]**
Quasistatic and dynamic compression experiments are performed on meteoritic material. Significant rate effects are observed in the failure strength and elastic modulus.

Domke I.   Deutsch A.   Hecht L.   Kenkmann T.
MEMIN Project: The Search for Suitable Projectile Material in Meso-Scale Hypervelocity Cratering Experiments **[#1605]**
We report textural and geochemical data (EMP, LA-ICP-MS) for different types of steel and the iron meteorites Arispe (IC) and Campo del Cielo (IAB) that are evaluated as projectile materials in hypervelocity cratering experiments .

Craig M. A.   Flemming R. L.   Osinski G. R.   Cloutis E. A.
UV-VIS-NIR Reflectance Spectra of Intimate Mixtures of Synthetic CaCO3 and Amorphous SiO_2: 0.35–2.5 µm; Implications for the Spectral Identification of Shocked Assemblages on Mars **[#2110]**
A comparison of the spectroscopic features generated in shock metamorphosed and melted/recrystallized carbonates from the Haughton impact structure with spectroscopic features in an intimate mixture suite of synthetic calcite and amorphous silica.

Gavin P.   Chevrier V.   Ninagawa K.   Gucsik A.   Hasegawa S.
Experimental Investigation into the Effects of Meteoritic Impacts on the Spectral Properties of Phyllosilicates on Mars **[#1890]**
Analysis of shock pressures and temperatures reached during impact experiments, as well as XRD and NIR spectral analysis, help determine whether phyllosilicates found in association with impact craters on Mars were preexisting or were formed during the impact.

Okamoto C.   Arakawa M.   Hasegawa S.
Impact Fragmentation of Iron Meteorite Parent Bodies: Implications for Energy Fraction of Iron Core in Collisional Disruption **[#2679]**
We conducted impact experiments on core-mantle targets with metal cores covered with porous mantles in order to study the collisional disruption of iron meteorite parent bodies.

IMPACTS MODELING

Mehta M.   Renno N. O.   Sengupta A.   Pokora M.
Cratering on Planetary Bodies Due to Spacecraft Landings **[#2350]**
Erosion and plume impingement pressure characteristic curves provide insight into the cratering physics due to spacecraft landings and possible evidence for brines on Mars.

Chappelow J. E.   Golombek M. P.
Can Mars' Current Atmosphere Land Block Island Sized Meteorites? **[#2351]**
Given the recent discovery of three more iron meteorites on Mars, the question arises: Can Mars' current atmosphere decelerate them sufficiently or is a denser one required? And if it can, how does this happen?

Lunine J.   Artemieva N.   Tobie G.
Impact Cratering on Titan: Hydrocarbons Versus Water **[#1537]**
The lack of ethane at Titan's surface is shown to be consistent with impact breaching of Titan's crust through most of its history.

Bray V. J.   Collins G. S.   Morgan J. V.   Melosh H. J.
Development of a Hydrocode Strength Model for Large Impacts in Pure Water Ice **[#2430]**
We present a material strength model for simulating impacts into ice, comparing results to observational data from Ganymede. Results from this work have future applications for investigation of central pit formation and Europa's crustal thickness.

Artemieva N.   Shuvalov V.
Tunguska Explosion — Final Remarks **[#1268]**
We present distal effects related to the Tunguska explosion in 1908 (white nights in Europe, in particular) and discuss the possibility of finding Tunguska-related cosmic material.

Pierazzo E.   Collins G. S.   Holsapple K. A.   Housen K. R.   Korycanksy D. G.   Plesko C. S.
Price M. C.   Wünnemann K.
Impact Hydrocode Benchmark and Validation Project: Impacts Into Cohesionless Soil **[#2048]**
We present initial results of validation tests of a polyethylene cylinder impacting a cohesionless soil (dry sand) at 1G and 464G (where G is Earth's gravity).

Collins G. S.   Melosh H. J.   Wilson C. R.   Wünnemann K.
Improvements to the Epsilon-Alpha Porosity Model for Impact Simulations **[#2033]**
We have modified the epsilon-alpha porosity model to improve the treatment of highly porous materials and include dilatancy in planetary-scale impact simulations. We describe model developments and present validation results.

Anderson J. L. B.   Burleson T.   Cintala M. J.
Target and Projectile: Material Effects on Crater Excavation and Growth **[#2084]**
Three suites of impact crater experiments are compared using ejection-speed and crater-size scaling. Implications for the deformation style of the projectile (ductile or brittle) and the grain size of the target material are discussed.

Watters W. A.
The Concave Planform of Transient Impact Craters in Fractured Targets **[#2684]**
Transient impact craters forming in targets that have aligned fractures can sometimes have a concave planform. We estimate the planform hinge trace at Endurance Crater (Meridiani Planum), and propose a physical model that illustrates the origin of the concave shape.

Zucker R. V.   Stewart S. T.
Fault Weakening and Shear Localization During Crater Collapse **[#2460]**
We present a model of temperature- and pressure-dependent strain-weakening along faults during crater collapse.

Stewart S. T.
Toward an Impact Basin Formation Scaling Law **[#2722]**
The impact energies required to form the largest impact scars on planets remains an unsolved problem. In this work, I present a method of constraining the size of the transient cavity for impact basins.

Billingham L.   Collins G. S.   Nevard S. A.   Wünnemann K.
Transient Crater Scaling for Giant Impacts **[#1996]**
We use the iSALE hydrocode to test crater scaling relations for giant impacts. Our parameter study explores the influence of both target curvature and temperature profile on the diameter and volume of transient craters.

Head J. W. III
The Transition from Complex Craters to Multi-Ringed Basins on Terrestrial Planetary Bodies: The Scale-Dependent Role of the Expanding Melt Cavity and Progressive Interaction with the Displaced Zone **[#1029]**
The "nested melt-cavity" model combines main components of the cratering process (transient cavity, displaced zone, melt cavity) and provides a basis for understanding the characteristics of the transition from complex craters to multi-ringed basins.

Roberts J. H.
Heating of the Martian Interior Due to Giant Impacts: Revisited **[#2049]**
Heating from giant impacts has been suggested as a possible cause for the cessation of the martian dynamo. Core heat flow heterogeneity and shock heating models are revisited to better understand how impacts can affect the thermal evolution of Mars.

IMPACT CRATERS REMOTE SENSING AND STRUCTURAL GEOLOGY

Thomas N. Stelter R. Ivanov A. Bridges N. T. Herkenhoff K. E. McEwen A. S.
Spectral Heterogeneity on Phobos and Deimos: HiRISE Observations and Comparisons to Mars Pathfinder Results **[#2595]**
The Mars Reconnaissance Orbiter's High Resolution Imaging Science Experiment has been used to observe Phobos and Deimos at special scales of ~6 and 20 m/px, respectively, providing, for the first time, high-resolution colour images of the satellites.

Boyce J. M. Barnouin-Jha O.
The Relationship of Layered (Fluidized) Ejecta Run-out Distance to Rampart Width: Implications to the Properties of Ejecta **[#2327]**
Ejecta of DLE craters behaves differently than of MLE and SLE craters independent of planet. This difference in behavior may be due to a rheology effect produced by differences in such factors as the fraction of fines or water in the ejecta of each type crater.

Wintzer A. E. Barlow N. G.
Sinuosity of Martian Layered Ejecta Blankets **[#1066]**
We are conducting a survey of craters with layered ejecta blankets on Mars to determine if their lobateness varies with latitude, diameter, and ejecta type. We report here our preliminary results for the northern equatorial region of Mars.

Vijayan S. Vani K. Sanjeevi S.
Characterising The Ejecta Spectra of Lonar Crater, India in Hyperion Image — Implications for Lunar Studies **[#1541]**
Spectral separability analysis for Lonar crater ejecta using the Hyperion hyperspectral image.

Monegato G. Massironi M. Martellato E.
The Ring Structure of Wembo-Nyama (Eastern Kasai, R.D. Congo): A Possible Impact Crater in Central Africa **[#1601]**
The structure of Wembo-Nyama (Eastern Kasai, R.D. Congo) is a new ringstructure found in Central Africa. We discuss the possibility of an impact origin, considering its geomorphological characteristics and the geology of the area.

Thompson L. M. Spray J. G. Whitehead J.
Re-Assessment of Large Terrestrial Impact Structures: Rim and Maximum Damage Diameters **[#2712]**
We re-assess and revise the final rim diameters (collapsed transient cavities) and maximum damage diameters of Earth's largest impact structures.

Kenkmann T. Vasconcelos M. Crósta A. P. Reimold W. U.
Serra da Cangalha, Tocantins, Brazil: Insights to the Structure of a Complex Impact Crater with an Overturned Central Uplift **[#1237]**
Results of a field study are presented. The 5.8-km central uplift shows sign of gravitational instability that resulted from the target's rheological stratification with clays in the center. Preexisting joint systems controlled crater modification.

Vasconcelos M. A. R. Góes A. M. Crósta A. P. Kenkmann T. Reimold W. U.
Serra da Cangalha Impact Structure, Parnaíba Basin, Northeastern Brazil: Target Characterization and Stratigraphic Estimates of Uplift **[#1868]**
The stratigraphic information provided by two boreholes out of the Serra da Cangalha impact structure was used for comparison with the deformed sedimentary strata within SdC to estimate the amount of uplift at the center of the crater.

Daly R. G.   Kattenhorn S. A.
Deformation Styles at Upheaval Dome, Utah Imply Both Meteorite Impact and Subsequent Salt Diapirism **[#1969]**
Upheaval Dome's ambiguous origin, either as a salt diapir or a meteorite impact, has been debated for the last 75 years. We propose two methods of deformation present at the dome: meteorite impact and subsequent salt diapirism.

Wright S. P.   Tegtmeier E. L.   Newsom H. E.
Diversity of Breccias Associated with the Santa Fe Impact Structure **[#1286]**
Early mapping efforts of Proterozoic rocks surrounding recently discovered shattercones have turned up at least three distinctive breccias. One with a matrix that appears to be recrystallized granite might be an impact breccia.

EDUCATION AND PUBLIC OUTREACH: IMPACTS

Croft S. K.   Pierazzo E.   Canizo T.   Lebofsky L. A.   Palmero Rodriguez J. A.
The Explorer's Guide to Impact Craters: An Interactive Website and Rock Kit for Outreach and Professional Development Workshops for Elementary and Middle School Science Teachers **[#1460]**
Description of a website, rock kit, and workshop designed to educate elementary and middle school teachers about impact craters.

LUNAR METEORITES

Gyollai I.   Gucsik A.   Nagy Sz.   Fürj J.   Bérczi Sz.   Szekrényes Zs.   Veres M.
Petrographic and Mid-Infrared Spectroscopy Study of Shocked Feldspar in Asuka-881757 Lunar Gabbro Meteorite Sample **[#1602]**
In Asuka-881757 lunar meteorite we measured by mid-infrared spectroscopy (reflectance mode) shocked feldspars with: (1) undulatory extinction, (2) undulatory extinction with isotropic patches, (3) isotropy, lath-shaped feldspars (maskelynite).

Isaacson P. J.   Liu Y.   Patchen A. D.   Pieters C. M.   Taylor L. A.
Spectroscopy of Lunar Meteorites as Constraints for Ground Truth: Expanded Sample Collection Diversity **[#1927]**
We present new integrated mineralogy/petrography/spectroscopy results for a suite of lunar meteorite samples. These results will be needed to apply these samples as ground truth and to determine their geologic context through remote sensing.

Takeda H.   Kobayashi S.   Yamaguchi A.   Otsuki M.   Ohtake M.   Haruyama J.   Morota T.   Karouji Y.   Hasebe N.   Nakamura R.   Ogawa Y.   Matsunaga T.
Olivine Fragments in Dhofar 307 Lunar Meteorite and Surface Materials of the Farside Large Basins **[#1572]**
Based on mineralogy of clasts derived from spinel troctolite and very low Th contents of Dhofar 307, we found that Dirichlet-Jackson basin in the lowest-Th region found by the GRS onboard Kaguya, is a good candidate where the breccia was developed.

Basilevsky A. T.   Neukum G.   Nyquist L.
Lunar Meteorites: What They Tell Us About the Spatial and Temporal Distribution of Mare Basalts **[#1214]**
An analysis of data from the Lunar Meteorite Compendium shows that a significant fraction of lunar meteorite source craters are less than hundreds of meters in diameter; cryptomaria are abundant in the highlands; and the meteorite mare basalt ages fill the gaps in the Apollo/Luna basalt age distribution.

Robinson K. L.   Treiman A. H.
Mare Basalt Fragments in Lunar Highlands Meteorites: Connecting Measured Ti Abundances with Orbital Remote Sensing **[#1788]**
We retrieved Ti contents of parent magmas for seven basalt clasts in highlands meteorites. The magmas are VLT and low-Ti basalts. A histogram of their Ti contents is similar to that from global remote sensing, and not like that of the Apollo mare basalts.

Gibson K. E. Jolliff B. L. Zeigler R. A. Korotev R. L.
Testing Petrogenetic Relationships of the Lunar NWA 773 Meteorite Clan with Nickel and Cobalt in Olivine **[#2593]**
This study tests the apparent petrogenetic relationship between volcanic and cumulate lithologies in the lunar NWA 773 meteorite clan by using bulk compositions and high precision electron microprobe analyses of Ni and Co in olivine.

Zhang A. C. Taylor L. A. Hsu W. B. Floss C. Li X. H. Liu Y.
Petrogenesis of Lunar Meteorite Northwestern Africa 2977: Rare Earth Element Geochemistry and Baddeleyite Pb/Pb Dating **[#1052]**
This abstract reports REE geochemistry of minerals in NWA 2977 and precise baddeleyite Pb/Pb dating.

Kuehner S. M. Irving A. J. Gellissen M. Korotev R. L.
Petrology and Composition of Lunar Troctolitic Granulite Northwest Africa 5744: A Unique Recrystallized, Magnesian Crustal Sample **[#1552]**
We describe the petrologic, major and trace element characteristics of a highly recrystallized granulitic breccia formed from a magnesian troctolitic protolith in the ancient lunar crust.

Korotev R. L. Zeigler R. A. Jolliff B. L.
New Geochemical Constraints on Pairing of the Dhofar 961 Clan of Lunar Meteorites **[#2126]**
New data support the hypothesis that the unusual and heterogeneous Dhofar 925, 960, and 961 lunar meteorite stones are paired.

Joy K. H. Crawford I. A. Snape J. F.
Lunar Meteorite Miller Range 07006: Petrography and VLT Basalt Clast Inventory **[#1793]**
MIL 07006 is a feldspathic, basalt bearing, regolith breccia lunar meteorite likely paired to Yamato-791197. We discuss the petrography and crystallization history of several very low-Ti basalt clasts.

LUNAR PETROLOGY AND GEOCHEMISTRY

Meyer C.
Lunar Sample Compendium **[#1016]**
The Lunar Sample Compendium is a succinct summary of what has been learned from the study of Apollo and Luna samples of the Moon.

Carpenter P. K. Zeigler R. A. Jolliff B. L.
Advances in Defocused-Beam Electron-Probe Microanalysis **[#2656]**
Advances in defocused-beam electron-probe microanalysis are presented, with an Excel VBA algorithm which uses a polynomial alpha factor correction algorithm coupled with a catanorm procedure to correct DBA data.

O'Sullivan K. M. Neal C. R.
Petrogenesis of Apollo 12 Basalts 12031 and 12038 **[#2307]**
We report crystal size distributions along with major and minor element abundances to model the petrogenesis of these rocks.

Singer K. I. Riches A. J. V. Patchen A. Liu Y. Taylor L. A.
Insights into the Petrogenesis of Apollo 17 High-Ti Mare Basalts **[#2694]**
We report petrographic and mineralogical results of a detailed study of several Apollo 17 samples to complement recent Fe and O isotopic studies.

Liu Y. Spicuzza M. J. Valley J. W. Day J. M. D. Riches A. J. V. Singer K. I. Taylor L. A.
Diversity in High-Titanium Lunar Mare Basalts **[#1669]**
This abstract describes the diversity in high-Ti mare basalts.

Krawczynski M. J.   Sutton S. R.   Barr J. A.   Grove T. L.
Titanium Valence in Lunar Ultramafic Glasses and Olivine-Diogenites **[#1825]**
The valence of Ti in lunar glasses and olivine-diogenites is a function of melt composition and compatibility of Ti^{3+} in Fe-Mg minerals. The differences between glass and coexisting minerals suggests a non-quenchability of the Ti valence in glass.

Donohue P. H.   Neal C. R.
Apollo 17 High-Ti Basalt Crystal Size Distributions and Petrogenesis **[#2073]**
Crystal size distributions and geochemical data are presented for ilmenite in 16 Apollo 17 high-Ti basalts, encompassing all compositional types (A, B1, B2, C, D). This allows for constraints to be placed on petrogenetic history of these samples.

Fagan A. L.   Neal C. R.   Simonetti A.
Apollo 14 Olivine Vitrophyres: Geochemical Evidence for Heterogeneous Target Materials **[#2226]**
We suggest that, using textural and geochemical analyses, Apollo 14 olivine vitrophyre 14321,1486 provides evidence of a heterogenous target material consisting of high-Ti basalt, low-Ti basalt, and highlands material.

Liang Y.   Schiemenz A.   Parmentier E. M.
Melting and Melt Migration in a Heterogeneous Lunar Mantle: Physical Processes and Chemical Consequences **[#2241]**
Using numerical simulation we show that the distribution of key melt migration features, such as the depth of dunite channel, are strongly correlated with the amount and spatial distribution of the heterogeneous materials in the lunar mantle.

Weider S. Z.   Crawford I. A.   Joy K. H.
Impact Craters: Windows Through Lava Flows in Oceanus Procellarum **[#1300]**
Using Clementine multispectral data we have identified impact craters within a specific lava flow that have excavated material from a deeper and older lithology, their diameters can be used to estimate the thickness of the surface flow.

Hagerty J. J.   Hawke B. R.   Giguere T. A.   Gaddis L. R.   Lawrence D. J.
The Thorium Abundance Distribution of the Humorum Pyroclastic Deposit **[#2624]**
A large pyroclastic glass deposit has been identified in the southwestern part of Mare Humorum. We use forward modeling of Lunar Prospector Gamma Ray Spectrometer thorium data to place compositional and petrogenetic constraints on the deposit.

Kobayashi S.   Kobayashi M.   Hareyama M.   Hasebe N.   Shibamura E.   Yamashita N.   Karouji Y.   Okada T.   d'Uston C.   Gasnault O.   Forni O.   Reedy R. C.   Kim K. J.   Takeda H.   Arai T.   Sugihara T.   Dohm J. M.   Kaguya Gamma-Ray Spectrometer Team
The Lowest Thorium Region on the Lunar Surface Imaged by Kaguya Gamma-Ray Spectrometer **[#1795]**
The lowest Th region in the lunar farside occurs near the equatorial region (Zone A and B) and it should be noted that the regions well correspond to the lunar highest region and the thickest crust region recently measured by Kaguya mission.

Forni O.   Gasnault O.   d'Uston C.   Maurice S.   Hasebe N.   Yamashita N.   Kobayashi S.   Karouji Y.   Hareyama M.   Kobayashi M.   Reedy R. C.   Kim K. J.   SELENE GRS Team
Large Scale Potassium-Thorium Fractionation Around Imbrium **[#1944]**
We investigate the K/Th ratio using the GRS of Kaguya. We demonstrate that K and Th behaves differently at the lunar surface by means of ICA. We show that high K/Th ratio are encountered concentrically around the Imbrium event and suggest some explanation to that behaviour.

Narendranath S.   Sreekumar P.   Kellett B. J.   Joy K. H.   Howe C. J.   Crawford I. A.   Grande M.   Alha L.   Maddison B.   Huovelin J.   Erd C.   Athiray P. S.   Weider S. Z.   C1XS Team
Lunar Chemistry from Chandrayaan-1, C1XS Results from Southern Nearside Highlands of the Moon **[#1882]**
Results from the Chandrayaan-1 X-ray spectrometer (C1XS) flown on the Indian lunar mission from the analysis of a C3 flare for a region on the southern nearside highlands are presented.

Craddock P. R.   Dauphas N.   Clayton R. N.
Mineralogical Control on Iron Isotopic Fractionation During Lunar Differentiation and Magmatism **[#1230]**
We report Fe isotope values of mineral separates (pyroxene, plagioclase, ilmenite) in lunar mare basalt samples. The data identify possible controls on Fe isotope fractionation seen in lunar basalts produced by mantle differentiation and magmatism.

Armytage R. M. G.   Georg R. B.   Williams H. M.   Halliday A. N.
Terrestrial Silicon Isotope Composition of Lunar Rocks **[#1746]**
We present new high precision silicon isotope data for lunar rocks which are consistent with isotopic equilibration in the aftermath of the lunar forming impact.

Fitoussi C.   Bourdon B.   Pahlevan K.   Wieler R.
Si Isotope Constraints on the Moon-forming Impact **[#2653]**
The giant impact could have affected the Si isotope composition of the Moon, as it should have resulted in a vaporization of precursors of the lunar material. The analysis of Si isotopes in lunar rocks provides insights into the formation of Moon.

Seddio S. M.   Korotev R. L.   Jolliff B. L.   Zeigler R. A.
Comparing the Bulk Compositions of Lunar Granites, with Petrologic Implications **[#2688]**
Crystallization modeling to match the composition of lunar granite sample 12032,366-19 and compositions of other pristine lunar granites indicates extreme fractional crystallization of KREEP or a similarly compositionally evolved starting melt.

Fischer-Gödde M.   Becker H.   Wombacher F.
Highly Siderophile Element Abundances and 187Os/188Os in Lunar Impact Melt Rocks: Implications for Late Accretion Processes in the Earth-Moon System **[#2262]**
We report new highly siderophile element abundance and 187Os/188Os data for lunar impact melt rocks from Apollo 14, 16 and 17 landing sites, and the lunar meteorite DaG400.

Charlier B.   Namur O.   Grove T. L.
Anorthosite in the Sept Iles Layered Intrusion (Canada): Ideas for the Formation of the Lunar Crust **[#1231]**
Anorthosite formation processes and the accumulation of buoyant plagioclase at the base and the top of the 5000 km^2 Sept Iles layered intrusion are used as analogue to explain the origin of the vertically zoned lower and upper lunar crusts.

Uemoto K.   Ohtake M.   Haruyama J.   Matsunaga T.   Yokota Y.   Morota T.   Nakamura R.   Yamamoto S.   Iwata T.
Purest Anorthosite Distribution in the Lunar South Pole-Aitken Basin Derived from SELENE Multiband Imager **[#1635]**
In this study, we analyzed rock types of craters within The South Pole-Aitken (SPA) basin and investigated the distribution of purest anorthosite. From our analyzes, we confirmed that the anorthosite rocks present within the transient cavity.

Miura Yas.
Calicium-rich Plagioclases Formed by Giant Impact Event to the Lunar Crust **[#2462]**
The lunar crust with anorthositic compositions is considered to be derived from primordial Earth during impact, which is found in C, N and Cl elements of lunar basalts, and Ca-plagioclase formation at hot carbon dioxide gas at Mutsure-jima, Japan.

Edmunson J.   Cohen B. A.   Carpenter P.   Zeigler R. A.   Jolliff B. L.
Yttrium Silicate in Lunar Troctolitic Anorthosite 76335 **[#2627]**
An yttrium silicate was found in Mg-suite troctolitic anorthosite 76335. Major, minor, and trace element data are presented for the yttrium silicate.

LUNAR ORIGINS AND CHRONOLOGY

Zindler A.   Jacobsen S. B.
Rethinking Lunar Formation: Back to the Future? **[#2702]**
Review Giant Impact and arguments for formation of the Moon from the Earth's mantle.

Canup R. M.   Barr A. C.
Modeling Moon-forming Impacts; High-Resolution SPH and CTH Simulations **[#2488]**
We compare results from SPH and CTH simulations of Moon-forming impacts, in particular to determine the effect of resolution and simulation method on the fraction of orbiting protolunar disk material that originates from the impactor vs. the proto-Earth's mantle.

Crawford D. A.   Kipp M. E.
Giant Impact Theory for Origin of the Moon: High Resolution CTH Simulations **[#1405]**
We present high resolution simulations of the giant impact theory of lunar origin using adaptive mesh refinement, an improved ANEOS representation and self gravity. The calculation shows clumping, spiral shocks and streamer development.

Zhong S. J.
Are Mare Basalt Volcanism, Volatile Distribution in the Lunar Mantle, and Moonquakes Related? **[#2063]**
A new hypothesis on mare basalts, moonquakes, and lunar interior structures including volatile distributions is proposed. The new hypothesis is to be tested with new tidal deformation model that accounts for heterogeneous lunar mantle structure.

Pidgeon R. T.   Nemchin A. A.   Grange M. L.   Meyer C.
Evidence for a Lunar "Cataclysm" at 4.34 Ga from Zircon U-Pb Systems **[#1126]**
The dating of large impacts on the Moon is a major problem for lunar evolution. We discuss evidence from SIMS U-Pb analyses of zircons from lunar breccias, together with textural and mineral data, for an extremely large impact on the Moon at ~4.34Ga.

Connelly J. N.   Borg L. E.
Revisiting the Pb Isotopic System in Lunar Ferroan Anorthosite 60025 **[#1966]**
After extensive pre-cleaning and using a stepwise dissolution procedure, we have analyzed Pb from a mafic fraction from lunar ferroan anorthosite 60025 to determine a preliminary Pb-Pb crystallization age of 4382 ± 8 Ma.

Jacobsen S. B.   Ranen M. C.   Chakrabarti R.   Farkas J.   Huang S.   Parai R.   Yu G.   Zindler A.
The Isotopic Composition of the Lunar Crust and the Age and Origin of the Moon: Evidence from Lunar Soils **[#2596]**
Trace element and isotope data show that our lunar soil samples span the entire range of compositions from an >4.46 Ga old, almost pure highland end-member to a ~3.8 Ga KREEP end member.

Zhang A.   Hsu W.   Li X.   Li Q.   Tang G.   Jiang Y.
Cameca IMS-1280 Pb/Pb Dating of Baddeleyite in LAP 02224 **[#1080]**
This abstract reports baddeleyite Pb/Pb dating results of LAP 02224. Our data show that the crystallization age of LAP 02224 is much older than that from other methods (~3 to 3.1 Ga).

Arai T.   Yoshitake M.   Tomiyama T.   Niihara T.   Yokoyama T.   Kaiden H.   Misawa K.   Irving A. J.
Support for a Prolonged KREEP Magmatism: U-Pb Age Dating of Zircon and Baddeleyite in Lunar Meteorite NWA 4485 **[#2379]**
The U-Pb and Pb-Pb age spectrum of 4352–3922 Ma obtained from analyses of zircon and baddeleyite in a KREEP-rich lunar meteorite NWA 4485 supports a prolonged KREEP magmatism, which has been suggested from U-Pb isotopic studies of zircons in the Apollo non-mare samples.

A NEW MOON: VOLATILE SPECIES AROUND THE MOON

Gibson E. K. Pillinger C. T.
Re-Assessment of "Water on the Moon" After LCROSS **[#1829]**
Detection of water on the lunar surface by recent spacecraft in orbit and from impactors into permanently shadowed regions must take into account available information from past analysis of the Apollo sample collection. Solar wind production of volatiles must be considered.

Shearer C. K. Sharp Z. D. Brearley A. King P. L. Fischer T.
A "Dry" Versus a "Wet" Moon. The Effect of Potential Indigenous Water on the Composition of Lunar Volcanic Gases and Sublimates **[#1941]**
As another perspective for evaluating the controversy between a "wet" and "dry" Moon, we are examining the effect of variable water content on the composition of lunar volcanic gases and sublimation products.

Crotts A. P. S. Hummels C.
Outgassing/Regolith Interactions and Lunar Hydration **[#2079]**
A model of lunar interior outgassing successfully predicted that hydrated regolith would be found in a patchy distribution concentrated within ~20° of the poles, as detected by the Chandrayaan-1 M^3 and in hydrogen by epithermal neutron absorption.

Zhang Y. Wang K. L.
Bubble Growth in Lunar Basalts and Lunar Volatile Budget **[#1120]**
We will model bubble growth rates in lunar basaltic melts and examine the controlling factors. Various means to constrain volatile contents in the Moon will also be discussed.

Starukhina L. V. Shkuratov Y. G.
Simulation of 3-µm Absorption Band in Lunar Spectra: Water or Solar Wind Induced Hydroxyl? **[#1385]**
Theoretical simulation of 3-µm absorption bands in lunar reflectance spectra shows that chemical trapping of solar wind protons and formation of OH groups in the rims of lunar regolith particles can be responsible for the observed absorption.

Vilas F. Harvieux N. F. Jensen E. A. Jarvis K. S. Domingue D. L.
Search for 0.7-µm Absorption Feature in Galileo Lunmos 9 Images: Implications for Lunar Surface Composition **[#2136]**
Recent spacecraft observations show evidence of the 3-µm water of hydration absorption feature across the lunar surface. We examine Lunmos 9 and Lunmap 14 detections of an absorption feature at 0.7-µm suggesting oxidized iron in phyllosilicates.

Kim K. J. Reedy R. C. Drake D. M. Hasebe N.
Numerical Simulation of Gamma-Ray and Neutron Production in the Lunar Surface Using the MCNPX Code System **[#2420]**
The production of gamma-rays and neutrons in the lunar surface investigated by the MCNPX code is useful in understanding production mechanisms for secondary particle fluxes, especially both neutrons and gamma-rays in planetary surfaces.

Lawrence D. J. Feldman W. C. Elphic R. C. Maurice S. Hurley D. M. Miller R. S.
Sensitivity of Neutron Measurements to the Thickness and Abundance of Surfical Lunar Water **[#1471]**
Lunar Prospector neutron data do not show strong evidence for a H signature at Goldschmidt crater. Based on new neutron transport models, the thickness of the H-rich material detected by the NIR spectral data is less than 0.5 cm.

McClanahan T. P.   Mitrofanov I. G.   Boynton W. V.   Sagdeev R.   Trombka J. I.   Starr R. D.   Evans L. G.
Litvak M. L.   Chin G.   Garvin J.   Sanin A. B.   Malakhov A.   Milikh G. M.   Harshman K.
Finch M. J.   Nandikotkur G.
Correlation of Lunar South Polar Epithermal Neutron Maps: Lunar Exploration Neutron Detector and Lunar Prospector Neutron Spectrometer **[#1395]**
Research compares a corrected preliminary south polar epithermal rate map from the Lunar Reconnaissance Orbiter's Lunar Exploration Neutron Detector (LEND) with the Lunar Prospector Neutron Spectrometer epithermal rate map using several analytical techniques.

Sanin A.   Mitrofanov I.   Boynton W.   Chin G.   Demidov N.   Garvin J.   Golovin D.   Evans L.   Harshman K.
Kozyrev A.   Litvak M.   Malakhov A.   McClanahan T.   Milikh G.   Mokrousov M.   Nandikotkur G.
Nuzhdin I.   Sagdeev R.   Shevchenko V.   Shvetsov V.   Starr R.   Tretyakov V.   Trombka J.   Usikov D.
Varennikov A.   Vostrukhin A.
Mapping of Lunar Hydrogen According to the LEND Neutron Measurements Onboard the NASA LRO **[#2437]**
In this study we would like to present some preliminary estimations of hydrogen distribution along polar regions based on the LEND measurements of neutron flux from the Moon.

Bussey D. B. J.   McGovern J. A.   Spudis P. D.   Neish C.   Sorensen S.   Noda H.   Ishihara Y.
Lunar Polar Illumination Conditions Derived Using Kaguya Laser Data **[#2293]**
We have used the Kaguya laser-derived topography data to fully characterize the lunar polar illumination conditions. We have generated illumination profiles for the areas that receive the most illumination.

Wang K. L.   Xu Z.   Zhang Y.
Calibration for Infrared Measurements of Water in Apatite **[#1121]**
We report a study on calibration of infrared (IR) method to determine water concentration in apatite using the elastic recoil detection (ERD) method. The calibration will allow us to constrain water content in lunar and martian apatites using IR spectra.

Sharp Z. D.   Shearer C. K.   Barnes J. D.
The Chlorine Isotope Composition of the Moon **[#2424]**
The Cl isotope composition of lunar samples varies from –0.74 to +16.00‰. The high values are due to loss of the light isotope by solar wind bombardment, micrometeorite impact and/or higher (escape) velocities of the light HCl isotopologue.

Wetzel D.   Rutherford M. J.   Hauri E. H.   Saal A. E.
Carbon in Lunar Magmas: Abundance, Speciation and Role in Magmatic Processes **[#1827]**
The results of SIMS and RAMAN analyses on previous experiments and the results of new graphite-saturated experiments for both the A17 orange and A15 green glass compositions indicate the abundance, speciation, and role of carbon in lunar magmas.

A NEW MOON: LCROSS

Killen R. M.   Potter A. E.   Hurley D. M.   Plymate C.   Naidu S.
Observations of the LCROSS Impact Event from the McMath-Pierce Solar Telescope: Sodium and Dust **[#2333]**
We used the McMath-Pierce telescope to observe sodium ejected as a result of the LCROSS impact onto the Moon on Oct. 9, 2009. We also observed in light of two orthogonal polarizations to detect dust. We observed 2 kg of sodium but saw no evidence for dust.

Hastie M.   Bailey V.   Hinz P.   Callahan S.   Vaitheeswaran V.   Gibson D.   Porter D.   Vilas F.
LCROSS Impact Observations from the MMT Observatory **[#2501]**
MMT Observatory spectra and images of the LCROSS impact into the Cabeus Crater during spacecraft impact are described.

Storrs A. D. Colaprete A.
Observations of the LCROSS Lunar Impact from Hubble Space Telescope **[#2196]**
We present results of the HST observations in support of the impact of the LCROSS mission into a permanently shadowed crater near the south pole of the Moon.

Hurley D. M. Gladstone R. Retherford K. Stern S. Parker J. Kaufmann D. Egan A. Davis M. Versteeg M. Slater D. Miles P. Steffl A. Greathouse T. Feldman P. Pryor W. Hendrix A. Killen R. Potter A.
Modeling the Vapor Plume Expansion Resulting from the LCROSS Impact on the Moon **[#2308]**
We present simulations of the gas emitted in the LCROSS vapor plume.

Summy D. P. Goldstein D. B. Varghese P. L. Trafton L. M. Colaprete A.
Gas and Dust Dynamic Model of the LCROSS Impacts **[#2091]**
We present the latest developments in our model of the LCROSS impact plumes, focusing on new features designed to match results from LCROSS and LRO observations.

Artemieva N.
Magic of an Impact Plume — Insight from Numerical Modeling **[#1968]**
Numerical models are used to unveil some secrets of an impact plume and to clarify its role in the impact ejecta deposition. The Ries and Chicxulub craters are discussed.

Hermalyn B. Schultz P. H. Colaprete A. Shirley M. Ennico K.
LCROSS Ejecta Dynamics: Insight from Experiments **[#2095]**
The LCROSS mission impacted the Moon in a permanently shadowed region on October 9, 2009. This study presents initial results of an experimental campaign designed to understand and interpret the unique conditions of the LCROSS impact event.

Stubbs T. J. Wang Y. Mazarico E. Neumann G. A. Smith D. E. Zuber M. T. Torrence M. H.
Characterizing the Optical Shadowing at the Moon Using LOLA Topographic Data: Predictions for the LCROSS Impact **[#2410]**
We describe an optical shadowing model for the Moon that uses LOLA topographic data. Example predictions are shown for the time of the LCROSS impact.

Stubbs T. J. Wang Y. Farrell W. M. Halekas J. S. Vondrak R. R. Mazarico E. Neumann G. A. Smith D. E. Zuber M. T. Torrence M. H.
Characterizing the Plasma Shadowing and Surface Charging at the Moon Using LOLA Topographic Data: Predictions for the LCROSS Impact **[#2658]**
We describe a plasma shadowing code for the Moon that uses LOLA topographic data. The output is used with plasma wake and surface charging models to predict surface potentials. We show example predictions for the time of the LCROSS impact.

Neish C. D. Bussey D. B. J. Spudis P. Thomson B. Patterson G. W. Carter L. Mini-RF Science Team
Mini-RF Observations in Support of LCROSS **[#2075]**
Cabeus water; Observed by LCROSS, not SAR; No lunar skat[ing] rinks?

A NEW MOON: GEOLOGIC PROCESSES ON THE MOON

Oshigami S. Yamaguchi Y. Okuno S. Ono T. Ohtake M.
Subsurface Structure of Mare Serenitatis Observed with Lunar Radar Sounder and Multiband Imager Onboard Kaguya **[#1576]**
Radar reflectors are detected under a large area of Mare Serenitatis. Meanwhile, layered structures are discernible on some crater walls in mineral content maps of the mare. We discuss characteristics of the subsurface layers by comparing these data.

Shankar B.   Osinski G.   Antonenko I.   Stooke P. J.   Mest S.
Multispectral Study of the Schrödinger Impact Basin **[#2542]**
A multispectral study using Clementine UV-VIS data to determine the compositions of mapped geologic units within the Schrödinger Impact Basin.

Arnold J. A.   Glotch T. D.   Bandfield J. L.   Greenhagen B. T.   Lucey P. G.   Wyatt M.   Paige D.
Local-Scale Spectral Variability of the South Pole-Aitken Basin **[#2023]**
Preliminary results of mapping mafic materials within the SPA basin using data from the Diviner Lunar Radiometer Experiment.

Thaisen K. G.   Taylor L. A.   Head J. W.   Pieters C. M.   Isaacson P. J.   Kramer G. Y.   McCord T. B.   Staid M.   Petro N. E.
Geology of the Moscoviense Basin: Implications for the Character of the Highland Crust **[#2169]**
Combining M^3 spectral imagery, hi-resolution imagery, and new DEM to exploring the Moscoviense Basin may provide insights into the FHT crust and secondary magmatic process of the early Moon.

Dickson J. L.   Head J. W. III   Smith D. E.   Zuber M. T.   Neumann G.   Fassett C.   LOLA Team
Lunar Orientale Basin: Topographic Characterization from Lunar Orbiting Laser Altimeter (Lola) Data and Insights into Multi-Ringed Basin Formation **[#1031]**
Lunar Orbiting Laser Altimeter (LOLA) data have provided new insight into Orientale and the nature of multi-ring impact basin formation, the role of pre-existing topography, processes of ring formation, and the evolution of the inner depression.

Head J. W. III   Pieters C.   Staid M.   Mustard J.   Taylor L.   McCord T.   Isaacson P.   Klima R.   Petro N.   Clark R.   Nettles J.   Whitten J.   M3 Team
Morphology and Distribution of Volcanic Vents in the Orientale Basin from Chandrayaan-1 Moon Mineralogy Mapper (M^3) Data **[#1032]**
Moon Mineralogy Mapper (M^3) data have provided new insight into the distribution, morphology and morphometry of volcanic vents, such as sinuous rilles, in the Orientale basin and their relationship to ring structures and basin thermal evolution.

Whitten J.   Head J.   Staid M.   Pieters C.   Mustard J.   Taylor L.   McCord T.   Isaacson P.   Klima R.   Nettles J.   M3 Team
Characteristics, Affinities and Ages of Volcanic Deposits Associated with the Orientale Basin from Chandrayaan-1 Moon Mineralogy Mapper (M^3) Data: Mare Stratigraphy **[#1841]**
Orientale basin contains many volcanic deposits, including Mare Orientale, Lacus Veris, and Lacus Autumni have been redated using statistical crater counting techniques. Several new mare ponds have been identified in the western part of the basin.

Garry W. B.   Robinson M. S.   LROC Team
Observations of Flow Lobes in the Phase I Lavas, Mare Imbrium, the Moon **[#2278]**
The Phase I lavas in Mare Imbrium on the Moon have previously been defined only by albedo and color boundaries on the surface. We present LROC NAC images of flow lobes in the Phase I lavas and implications for emplacement parameters.

Xiao Z.   Zeng Z.   Ding N.   Hu C.
Origin of Pit Chains in the Floor of Lunar Copernican Craters — Example of Crater Copernicus, Aristarchus and Tycho. **[#1034]**
The inner crater floor pit chains in lunar Copernican craters are originated from the activity of faults while there are two possible formation mechanism of the round crater floor pit chains.

Xiao Z.   Zeng Z.   Xiao L.
Origin of Polygons in the Crater Floor of Tycho **[#1526]**
Polygons in the floor of crater Tycho are orignated from the uplift of subsurface magma while the source of the magma is still undetermined.

Korteniemi J.   Eldridge D. L.   Lough T.   Werblin L.   Singer K.   Kring D.
Assessment of Lunar Volcanic Morphological Diversity: Distribution of Floor-fractured Craters **[#1335]**
A survey of floor-fractured craters on the Moon from global data. They are locations where a multitude of volcanic deposits can be sampled, and they should thus be taken into account when considering landing sites for future missions.

Srisutthiyakorn N.   Kiefer W. S.   Kirchoff M.
Spatial Distribution of Volcanos in the Marius Hills and Comparison with Volcanic Fields on Earth and Venus **[#1185]**
The spatial concentration of volcanos in the Marius Hills on the Moon is comparable to the concentration in the Snake River Plains of Idaho and for a number of volcanic dome fields on Venus.

Gustafson J. O.   Bell J. F. III   Gaddis L. R.   Hawke B. R.   Robinson M. S.   LROC Science Team
Analysis of Pyroclastic Deposits on the Southeastern Limb of the Moon Using LROC and Clementine Spectral Reflectance Data **[#1862]**
LROC NAC, LROC WAC, and Clementine data are being used to study potential pyroclastic deposits. NAC and WAC data are used to examine morphology and confirm pyroclastic origin. WAC and Clementine data are used to constrain composition.

Hawke B. R.   Giguere T. A.   Lawrence S. J.   Campbell B. A.   Gaddis L. R.   Gustafson J. O.   Hagerty J. J.   Peterson C. A.   Robinson M. S.   LROC Team
LROC and Other Remote Sensing Studies of Pyroclastic Deposits in the Mare Humorum Region **[#1583]**
The two large regional pyroclastic deposits are dominated by pyroclastic glasses. LROC NAC images show that the thickest portion of the SWH deposit is dark, flat, smooth, and deficient in blocks >1m across.

Lough T.   Gregg T. K. P.
Geologic Mapping of the Aristarchus Plateau Region on the Moon **[#2370]**
We present preliminary mapping of a 13° × 10° area around Aristarchus plateau, located in Lunar Quadrangle 10, with the goal of inferring changes in magma properties and volcanic plumbing through detailed mapping of surficial deposits.

Morota T.   Haruyama J.   Ohtake M.   Matsunaga T.   Yokota Y.   Honda C.   Sugihara T.   Kimura J.   Ishihara Y.   Kawamura T.   Iwasaki A.   Saiki K.   Takeda H.
Mare Volcanism on the Farside and in the Orientale Region of the Moon **[#1309]**
Dating of lunar mare basalts is necessary for understanding the volcanic history of the Moon. Here we performed new crater counts in mare deposits on the farside and in the Orientale region, using new images obtained by SELENE Terrain Camera.

Payne C. J.   Spudis P. D.   Bussey B.   Thomson B. J.
Scattering Properties of Lunar Geological Units Revealed by the Mini-SAR Imaging Radar, Chandrayaan-1 Mission **[#1211]**
We have collected data from Mini-SAR orbital radar on the surface scattering properties of several lunar geological units of varying age and origin with the aim of understanding the physical properties of the surface of the Moon.

Mest S. C.   Berman D. C.   Petro N. E.
Geologic Mapping of Impact Crater Floor Deposits Near the Lunar South Pole **[#2363]**
Geologic mapping of impact crater floor deposits in the lunar South Pole quadrangle (LQ-30) is revealing (1) smooth, dark deposits interpreted to be mare, and (2) brighter, densely cratered deposits consisting of impact melt and/or mantled mare.

Hawke B. R.   Giguere T. A.   Bray V.   Lawrence S.   Tornabene L.   Denevi B. W.   Garry W. B.   Gaddis L. R.   Kestay L.   Robinson M.   LROC Science Team
Byrgius A Crater Impact Melts — An LROC Perspective **[#1611]**
LROC NAC images were used to investigate the origin, distribution, and modes of occurrence of impact melt at the lunar crater Byrgius A.

Denevi B. W.   Robinson M. S.   Lawrence S. J.   Keszthelyi L. P.   Hawke B. R.   Garry W. B.   Bray V.
Tornabene L. L.   LROC Team
Physical Constraints on Impact Melt Properties from LROC NAC Images **[#2582]**
A range of well-preserved impact melt flows observed on the outside of crater rims are studied in order to elucidate the physical properties of lunar impact melts.

Plescia J. B.   Bussey D. B. J.   Robinson M. S.   Paige D. A.
King Crater – Surface Properties Derived from Diviner, Mini-RF, and LROC Data **[#2160]**
King Crater displays anomalous thermal and radar properties. High resolution LROC images show these are associated with boulders and bedrock outcrops. This example illustrates how LRO data can be used to understand geologic details of a site.

Trang D.   Gillis-Davis J. J.   Williams K.   Bussey D. B. J.   Spudis P. D.   Carter L. M.   Neish C. D.
Thompson B.   Patterson W.
Using Mini-RF to Investigate the Anomalous UVVIS Spectrum in the Apollo and Plato Region **[#2652]**
Mini-RF radar data are used to examine the chemical and physical properties of both Apollo and Plato regions.

Campbell B. A.   Carter L. M.   Campbell D. B.   Nolan M.   Chandler J.   Ghent R. R.   Hawke B. R.
Anderson R. F.   Wells K.
Earth-Based S-Band Radar Mapping of the Moon: New Views of Impact Melt Distribution and Mare Physical Properties **[#1772]**
We present results at the halfway point of a campaign to map much of the Moon's near side using the 12.6-cm radar transmitter at Arecibo Observatory and receivers at the Green Bank Telescope.

Thomson B. J.   Spudis P. D.   Bussey D. B. J.   Carter L.   Kirk R. L.   Neish C.   Patterson G.   Raney R. K.
Winters H.   Mini-RF Team
Roughness and Radar Polarimetry of Lunar Polar Craters: Testing for Ice Deposits **[#2176]**
Results from the Mini-SAR radar instrument on Chandrayaan-1 indicate certain north polar craters on the Moon have polarization signatures consistent with ice. Roughness effects alone appear insufficient to explain the observations.

Patterson G. W.   Bussey D. B. J.   Spudis P. D.   Neish C. D.   Thomson B. J.   Carter L. M.   Raney K.
Williams K.   Mini-RF Science Team
The Geomorphology of the Lunar Surface as Seen by the Mini-RF Instrument on LRO **[#2316]**
Here we describe some of the unique capabilities of the Mini-RF radar instrument on LRO with regard to analyzing the geomorphology of the lunar surface.

Lawrence S. J.   Mechtley M.   Spudis P.   Bussey B.   Robinson M. S.
Coordinated Mini-RF and LROC Observations of the Lunar Surface **[#2689]**
We report on coordinated Mini-RF radar and LROC Narrow Angle Camera observations of the lunar surface.

Mazarico E.   Watters W. A.   Barnouin O. S.   Neumann G. A.   Zuber M. T.   Smith D. E.   LOLA Science Team
Depth-Diameter Ratios of Small Craters from LOLA Multi-Beam Laser Altimeter Data **[#2443]**
We characterize small craters using the unique cross-track topographic information of the LOLA data. We estimate the best-fit shape and the depth-to-diameter ratio, which inform us on formation processes and (shallower) secondary crater population.

Wells K. S.   Bell J. F. III
Characterization of Ejecta Facies of a Small Lunar Crater in Balmer Basin Using LROC Data **[#1932]**
Using a 0.93 m/pix Lunar Reconnaissance Orbiter Camera (LROC) Narrow Angle Camera (NAC) image, we investigate the distribution of impact ejecta of a small (D ~ 1 km) unnamed lunar primary crater located in Balmer Basin (–18.6°, 69.1°).

Sori M. M.   Zuber M. T.
Preliminary Measurement of Depth-to-Diameter Ratios of Lunar Craters in the Transition Regime Between Complex Craters and Multiringed Basins **[#2202]**
Impact craters on the Moon follow a size-morphology sequence. This study looks at those impact structures in the transition regime between complex craters and multiringed basins. The ratios of those structures' depth to diameter are measured.

Rosenburg M. A.   Aharonson O.   Smith D. E.   Zuber M. T.   Neumann G. A.   Torrence M. H.   Mazarico E.
Lunar Surface Roughness and Slope Statistics from LOLA **[#2502]**
The RMS slope and Hurst exponent over horizontal scales of ~56 meters to ~2.7 kilometers are calculated from LOLA altimetry measurements and used to quantitatively characterize the roughness properties of the lunar surface.

Barnouin O. S.   Smith D.   Zuber M.   Robinson M.   Neumann G.   Mazarico E.   Denevi B.   Duxbury T.   Turtle E.   LOLA Team   LROC Team
The Topographic Shape and Surface Roughness of a few Lunar Craters **[#1479]**
Topographic data measured from the Lunar Orbiter Laser Altimetry (LOLA) and the Lunar Reconnaissance Orbiter Camera (LROC) are used to assess the relationship between observed surface features and their topographic expressions within a few lunar craters.

Hiesinger H.   van der Bogert C. H.   Pasckert J. H.   Robinson M. S.   Klemm K.   Reiss D.   LROC Team
New Crater Size-Frequency Distribution Measurements for Copernicus Crater Based on Lunar Reconnaissance Orbiter Camera Images **[#2304]**
We have performed new crater size-frequency distribution measurements for melt pools, the floor, and the ejecta blanket of Copernicus crater.

Marchi S.   Bottke W. F.
New Insights on the Cratering History of Lunar Farside **[#1314]**
In order to achieve a better understanding of the early evolution of the Moon, we performed new crater counts on the oldest terrains on the lunar farside. Derived crater counts are here presented and analysed.

Morita S.   Asada N.   Demura H.   Hirata N.   Terazono J.   Ogawa Y.   Honda C.   Kitazato K.
Approach to Crater Chronology with Fourier Transform of Digital Terrain Model **[#1990]**
We validated the effect of crater position, diameter and number using the transformed images and their average values. As a result, it showed fourier transform of DTM may be able to be used for geological age estimation instead of crater counting.

Neumann G. A.   Mazarico E. M.   Lemoine F. G.   Smith D. E.   Zuber M. T.
What are Lunar Basins? **[#1712]**
Lunar basins have been characterized as circular craters > 300 km with no central peak defined by tectonic and volcanic features. LRO/LOLA observations allow re-examination and perhaps removal of some uncertain pre-Nectarian basins, and addition of others.

Ishihara Y.   Morota T.   Iwata T.   Matsumoto K.   Goossens S.   Sasaki S.
Lunar Large Impact Basin Structures and Implications for Thermal History **[#1559]**
We reconstruct excavate cavity geometry of large impact basins on the Moon (including farside basins) using the Kaguya crustal thickness model. We discuss the impact structures and thermal history.

Ambrose W. A.
Origin, Distribution and Chronostratigraphy of Asymmetric Secondary Craters and Ejecta Complexes in the Crisium Basin **[#1061]**
Asymmetric secondary craters in the Crisium Basin, differentiated from morphologically similar primary craters, constrain estimated ages of landforms and are instrumental in refining stratigraphic relationships in the basin.

Gan F. P.   Yu Y. M.   Yan B. K.
Primary Study of the Relationship Between the Lunar Surface Topography and Geological Informations **[#1303]**
The distributions of elements and minerals of the lunar surface are retrieved using Clementine data, and DEM model is retrieved using LIDAR data of Chang'E-1 satellite. Finally, the relationship between the compositions and topography of the lunar surface is analyzed.

EDUCATION AND PUBLIC OUTREACH: MOON

Wood C. A.   Reese D. D.   Ruberg L.   Harrison A.   Lightfritz C.   Avatrian, LLC
MoonWorld: Implementation of Virtual Lunar Exploration **[#1439]**
MoonWorld is an immersive virtual learning experience using Second Life. MoonWorld is realistically based on actual lunar landscapes, NASA spacesuits, base, rover and life support concepts, and mission objectives consistent with field exploration.

Reese D. D.   Wood C. A.
Learning Lunar Science Through the Selene Videogame **[#2260]**
Selene is a videogame to promote and assess learning of lunar science concepts. As players build and modify a Moon, Selene measures learning as it occurs. Selene is a model for 21st century learning and embedded assessment.

Shaner A. J.   Shupla C.   Shipp S.   Eriksson A.
MyMoon: Crossroads of Social Media and Lunar Science Exploration **[#2668]**
In July 2009 the Lunar and Planetary Institute (LPI) launched a lunar education new media portal, MyMoon. MyMoon utilizes social media platforms such as Twitter, Facebook, and Flickr to engage — and involve — the 18–35-year-old demographic in lunar science exploration.

Allen J.   Luckey M.   McInturff B.   Huynh P.   Tobola K.   Loftin L.
Lunar and Meteorite Sample Education Disk Program — Space Rocks for Classrooms, Museums, Science Centers, and Libraries **[#1707]**
NASA's Lunar and Meteorite Sample Education Disk Program has Lucite disks containing Apollo lunar samples and meteorite samples that are available for trained educators to borrow for use in classrooms, museums, science center, and libraries.

Joy K. H.   Lintott C. J.   Smith A. M.   Gay P.   Roberts D.   Fortson L.   Moon Zoo Team
Moon Zoo: Utilizing LROC Lunar Images for Lunar Science and Education **[#1620]**
Moon Zoo will be a citizen science project that will ask users to identify, classify, and measure the shape of features on the lunar surface to address key questions in lunar science.

Bleacher L. V.   Weir H.   Hsu B. C.   Roark J.   Keller J.
Utilizing Data from the Lunar Orbiter Laser Altimeter to Produce Products for Formal and Informal Education **[#1798]**
LOLA data is being incorporated into lessons on lunar geology and topography, used to produce tactile models for use in comparative planetology sets, and used with Gridview software that lets users examine and measure topographic features.

MARTIAN ALTERATION PROCESSES: EXPERIMENTAL, OBSERVATIONAL, AND THEORETICAL

Tomkinson T.   Needham A. W.   Johnson D.   Guillermier C.   Franchi I. A.   Hagermann A.
Wright I. P.   Grady M. M.
Determining the Carbon Isotopic Composition of ALH 84001 Rosettes with NanoSIMS **[#2717]**
Determining the carbon isotopic composition of ALH 84001 rosettes with NanoSIMS.

Fu Q.   Niles P. B.
Kinetic Isotope Fractionation Processes During Experimental Formation of Ca- and Mg-rich Carbonates: Implications for ALH 84001 **[#2474]**
In experiments simulating cooling and CO_2 degassing processes, chemically zoned Ca- and Mg-rich carbonates were formed. Kinetic isotope effect and rapid carbonate formation during CO_2–H_2O equilibration create large isotopic variations in carbonates.

Needham A. W.   Tomkinson T. O. R.   Guillermier C.   Abel R. L.   Franchi I. A.   Grady M. M.
Nakhlites and NanoSIMS via Micro-CT Characterisation **[#2643]**
The nakhlite meteorites contain mineral phases formed by aqueous processes. This study aims to combine isotopic analyses with three dimensional characterisation of the complex network of alteration veins.

Changela H. G.   Bridges J. C.
Secondary Minerals in the Nakhlites Formed at Varying Depths in an Impact Hydrothermal Cell **[#1407]**
Amorphous gel and Fe-smectite within the nakhlites show compositional fractionation consistent with varying depths of origin. They formed from neutral pH and progressively oxidised fluids during an impact hydrothermal/evaporation event.

Isobe H.   Yoshizawa M.
Iron Mineral Fine Particles Produced by Acidic Hydrothermal Alteration Experiments of the Synthetic Martian Basalt **[#1292]**
Acidic hydrothermal alteration experiments of synthetic iron-rich martian basalt revealed that iron mineral fine particles with quite characteristic morphology can be produced by alteration spots related to the martian volcanic activities.

Johnson J. R.   Herkenhoff K. E.   Bell J. F. III   Farrand W. H.   Ashley J.   Weitz C.   Squyres S. W.
Pancam Visible/Near-Infrared Spectra of Large Fe-Ni Meteorites at Meridiani Planum, Mars **[#1974]**
The MER Opportunity rover imaged three large Fe-Ni meteorites in 2009. Pancam reflectance spectra of coatings on the rocks are consistent with ferric oxides (e.g., np-hematite), suggestive of chemical weathering on portions of the meteorite surfaces.

Ashley J. W.   Golombek M. P.   Schröder C.   Fleischer I.   McCoy T. J.   Christensen P. R.
Parker T. J.   Athena Science Team
Morphologic Evidence for Mechanical and Chemical Weathering of Three New Iron-Nickel Meteorites on Mars — Process Insights for Meridiani Planum **[#2208]**
We describe the morphology of three new iron-nickel meteorites found by the Opportunity spacecraft on Mars, and provide preliminary results and their implications for an assessment of weathering features identified.

Fleischer I.   Klingelhöfer G.   Schröder C.   Mittlefehldt D. W.   Morris R. V.   Golombek M.   Ashley J. W.
In Situ Investigation of Iron Meteorites at Meridiani Planum, Mars **[#1791]**
The MER rover Opportunity has encountered four iron meteorites along its traverse in Meridiani Planum, three of them between July and October 2009. We present results on their chemistry, mineralogy and weathering.

Fleischer I.   Agresti D. G.   Klingelhöfer G.   Morris R. V.
Hematite at Meridiani Planum, Mars, Investigated by Simultaneous Fitting of MER Mössbauer Spectra **[#1805]**
Hematite was detected in the outcrop matrix and in small spherules encountered by the MER rover Opportunity at its landing site in Meridiani Planum. We investigate the properties of Meridiani hematite using simultaneous fitting of MER Mössbauer spectra.

Knak Jensen S.   Gunnlaugsson H. P.   Merrison J. M.   Nørnberg P.
Wind Mediated Oxidation of Pyrite: A Putative Mechanism for Sulfate Production on Mars **[#1279]**
A reaction for sulfate formation from pyrite under conditions similar to the present martian environment is reported.

Schwenzer S. P.   Kring D. A.
Evaluating the Effect of Sulfur on Alteration Assemblages in Impact Cratered Terrains on Mars **[#1614]**
Impact-generated hydrothermal systems are capable of forming a variety of alteration phases that may support habitable conditions. Depending on the protolith those are clays, other hydrous silicates, hematite, or even carbonates, sulfides, sulfates.

McCollom T. M.   Marcucci E.   Hynek B. M.
Combined Experimental and Theoretical Study of Acid-Sulfate Alteration of Basalt for Interpretation of Sulfate-rich Deposits on Mars **[#1380]**
Laboratory experiments and numerical modeling are used to explore acid-sulfate alteration as an analog to formation of sulfate-rich deposits on Mars.

Worsham E. W.   Niles P. B.   Kraft M. D.
Experimental Constraints on Low-Temperature Acid-Weathering of Olivine: Implications for Mars **[#2599]**
Subzero to low temperature acid-weathering of olivine is explored experimentally, taking into account pH, temperature, and dissolution effects. The findings are applied to possible acid-weathering on Mars in its often very low temperatures.

Sutter B.   Ming D. W.
Titanium Mass-Balance Analysis of Paso Robles Soils: Elemental Gains and Losses as Affected by Acid Alteration Fluids **[#2603]**
Titanium mass-balance analysis of Paso Robles soils indicated elemental gains as supplied by sulfuric acid alteration fluids. This suggests that open-system dissolution processes have operated in the Paso Robles soils.

McGlynn I. O.   Fedo C. M.   McSween H. Y.   Herkenhoff K. E.
Weathering Trends from Chemical and Textural Characteristics of Soils in Gusev Crater, Mars **[#2163]**
Soil compositions are combined with textual parameters to evaluate the extent of chemical weathering of basaltic sediments in Gusev Crater. Major theories of weathering pathways are evaluated in the context of a chemical-textural relationship.

Hanley J.   Berget D.   Chevrier V. F.
Thermodynamic Properties of Aqueous Chlorine Oxyanion Solutions and Their Applications to Mars **[#1971]**
The intermediate oxidized species of chlorine (between perchlorate and chloride) are studied for their relevance to martian surface geochemistry.

Nekvasil H.   Ustunisik G.   McCubbin F. M.   Lindsley D. H.
Experimental Simulation of Magmatic Hydrothermal Activity on Mars: I. High Temperature Alteration in the Presence of a Cl-and S-enriched Fluid **[#1774]**
Experimental alteration of a partly crystallized Humphrey basalt by Cl-and S- fluid exsolved from a magma of Backstay composition at mid-crustal levels produced a martian amphibolite.

Peng Z. X.   Wang A.   Jolliff B. L.
Hydrothermal Process on Mars — Mission Observations and a Laboratory Simulation Experiment **[#2586]**
We report a set of newly conducted simulation experiment for hydrothermal process on Mars and related secondary mineralogy with preliminary results.

Marion G. M.   Kargel J. S.   Crowley J. K.   Catling D. C.
Modeling Hydrothermal Systems on Mars **[#1393]**
The specific objective of this study was to create a FREZCHEM-like chemical thermodynamic model that would raise the upper temperature range from 25 to 100°C.

Gago-Duport L.   Fairén A. G.   Davila A. F.   Gil C.   McKay C. P.
Subsurface Diffusion of Salt-forming Cations on Early Mars **[#2452]**
The salts needed to balance the stoichiometry of the Noachian sediments characterized by the presence of clays never precipitated on early Mars, and the cations that could have formed these salts are mostly buried below the phyllosilicate layer.

Thompson A. K.   Greenwood J. P.
Kinetics of Hydrogen Isotope Exchange in Gypsum: Terrestrial and Planetary Applications **[#2569]**
Experimental determination of the rates of hydrogen isotope exchange of gypsum and water via vapor exchange and solution will be presented. Applications are related to martian *in situ* and sample return analyses, as well as gypsum in SNCs.

Robertson K. R.   Bish D. L.
Thermal Behavior of the Magnesium Perchlorate-H_2O System **[#1666]**
Perchlorate salts are inferred to exist as surface deposits on the martian surface. Our results show that the dehydration of this mineral is unlikely under current martian surface conditions and it thus represents a potentially important H_2O reservoir.

Sowe M.   Wendt L.   Kneissl T.   McGuire P. C.   Neukum G.
Hydrated Minerals in Aureum Chaos, Mars **[#2499]**
The stratigraphic relationship, extent and layering attitude of hydrated minerals within Aureum Chaos were analyzed in order to understand their formation. Therefore, high-resolution imagery, elevation, and spectral data were used.

McKeown N. K.   Bishop J. L.   Amador E.   Cuadros J.   Hillier S.   Makarewicz H.   Parente M.   Silver E. A.
Spectral Mixtures of Clays and Their Impact on CRISM Mineral Identifications **[#2510]**
Many CRISM spectra measured at Mawrth Vallis appear to be mixtures of montmorillonite with hydrated silica, kaolinite, or beidellite. Here we analyze spectra of quantified mixtures of these components and compare them to CRISM spectra.

Altheide T. S.   Chevrier V. F.
Mineralogical Characterization of Acid Weathered Phyllosilicates **[#2042]**
Acidic weathering of phyllosilicates with varying pHs of sulfuric acid solutions demonstrates geochemical relationship between sulfates and phyllosilicates, and may also help explain recent observations of phyllosilicate layered deposits on Mars.

Beehr A.   Catalano J.
Synthesis of Ferrous Iron Phyllosilicates and Subsequent Oxidation as an Analog for Martian Phyllosilicates **[#1498]**
Hydrothermal synthesis of ferrous iron phyllosilicates and subsequent oxidation by hydrogen peroxide in order to simulate the life cycle of a martian phyllosilicate.

Fairen A. G.   Chevrier V.   Abramov O.   Marzo G. A.   Gavin P.   Davila A. F.   Gross C.   Kneissl T.   Roush T. L.   Bishop J. L.   Tornabene L. L.   Dohm J. M.   Rodriguez J. A. P.   Schulze-Makuch D.   McKay C. P.
Toro Crater: First Evidence for Hesperian Phyllosilicates on Mars **[#2683]**
We propose that phyllosilicates inside Toro Crater have been formed after the impact excavation, i.e., during the Hesperian.

Popa C.   Esposito F.   Colangeli L.
Evidences for Phyllosilicate Alteration in Tithonium Chasma **[#2723]**
The work describes the alteration of mafic rocks in contact aureole of sulfate bearing deposits.

Dehouck E.   Mangold N.   Le Mouélic S.   Ansan V.   Gaudin A.   Poulet F.
Ismenius Cavus, Mars: A Deep Paleolake with Phyllosilicate-bearing Deposits **[#1217]**
Ismenius Cavus is a crater-like basin with three deltaic fans consistent with the presence of a 600-m-deep lake during the Hesperian period, which interior displays sedimentary deposits containing Fe/Mg phyllosilicates.

Perry K. A.   Bishop J. L.   McKeown N. K.
Mineralogy of Libya Montes, Mars and Applications of Phyllosiliate-Carbonate-Olivine Mixtures **[#2605]**
Libya Montes is an ancient terrain that holds clues to early martian alteration processes. We report the findings of phyllosilicate, carbonate, olivine, and pyroxene minerals. Clay and carbonate findings imply that Mars was an aqueous environment in the past.

Wilson J. H.   Mustard J. F.
Olivine and Phyllosilicate Detection in Taytay Crater, Mars **[#2516]**
CRISM data analysis reveals an olivine-rich unit within Taytay Crater that could be excavating material from a regionally extensive olivine-rich unit below.

Stewart S. T.   Kraus R. G.   Milliken R. E.   Tosca N. J.
Uncertainties in the Shock Devolatilization of Hydrated Minerals: A Nontronite Case Study **[#1919]**
Impact processes have modified the structure and spectra of hydrated minerals on Mars; our understanding of the onset and extent of modification remains poor. New and published shock recovery data on nontronite illustrate the difficulties.

PLANETARY AEOLIAN PROCESSES: DUNES, DUST, AND DEVILS

Hayward R. K.   Fenton L. K.   Tanaka K. L.   Titus T. N.   Christensen P. R.
Mars Global Digital Dune Database: Dune Volume Estimates in the North Polar Region **[#1109]**
We review methods used in selected previous estimates of north polar dune volume (1158 km^3 to 15,000 km^3) and present our preliminary estimates (1300 km^3 to 3600 km^3) and methods for comparison.

Coleman S. J.   Hayward R. K.   Barlow N. G.   Titus T. N.
Age Estimate of Martian Dunes Based on Possible Impact Feature **[#1368]**
We examine a suspected impact feature located on a dune field and utilize it to obtain an approximate age (1–10 Ma) for martian dune fields.

Savage C. J.   Radebaugh J.   Goodrich C.
Titan Dune Populations from Pattern Analysis of Dune Field Parameters **[#2530]**
Unlike many of Earth's linear dunes this study finds only a single population of linear dunes on Titan indicating that either there has been only one period of dune formation or all others have been erased.

Aliaga-Caro J. F.   Burr D. M.   White B. R.   Marshall J. R.   Greeley R.   Bridges N. T.
Cohesion Under Reduced Gravity and Implications for Titan Aeolian Sediment Transport: Preliminary Model and Results **[#1483]**
Reduced gravity influences angle of response via an increase in interparticle forces, with implications for aeolian sediment behavior on Titan. We present initial investigations modeling the effect of reduced gravity on cohesive forces.

Diniega S.   Byrne S.   Glasner K.
Niveo-Aeolian Process Interactions and Resultant Martian Polar Dune Morphology **[#2192]**
We hypothesize that the distinctive martian polar dune lee slope morphology is formed through a niveo-aeolian process. We will evaluate three formation hypotheses: ice-cementation of the dune core, seasonal frost sublimation, or reversing winds.

Cardinale M.   Komatsu G.   Pasculli A.
Mare Tyrrenium Region: Analysis of Dark Sand Dunes and Wind Direction Interpretations **[#1610]**
Our analysis of dune morphology in Mare Tyrrenium of Mars and GCM indicates that simple dunes are consistent with present wind conditions, but complex dunes reflect influences of local topography developing secondary wind flows not predicted by GCM.

Horgan B.   Bell J. F. III   Bourke M. C.
Dry Flow, Surface Cementation, and Ice Induration Features on Dunes in the North Polar Region of Mars **[#1325]**
In this study, we identify and map the distribution of features on dunes in the martian north polar erg, and show that many of these features are consistent with dunes that are ice-rich but still actively migrating.

Silvestro S.   Rossi A. P.   Flahaut J.   Fenton L. K.
Active and Fossil Dunes as Evidences of Different Aeolian Constructional Events in Gale Crater (Mars) **[#1838]**
We performed a geomorphological survey of Gale Crater (Mars). We identified different dune generations and a wide variety of aeolian features suggesting that several episodes of aeolian construction took place in this site.

Craddock R. A.   Howard A. D.   Tirsch D.   Zimbelman J. R.
Preliminary Analyses of Basaltic Dunes in the Ka'u Desert, Hawaii and Implications for Understanding Dunes on Mars **[#2164]**
Here we report the general physical and chemical characteristics of basaltic dunes located in the Ka'u Desert of Hawaii.

Tirsch D.   Craddock R. A.   Jaumann R.
Dark Dunes in Ka'u Desert (Hawaii) as Terrestrial Analogs to Dark Dunes on Mars **[#2121]**
In this work we compare spectra of sand samples of terrestrial dark dunes derived in Ka'u Desert (Hawaii) with that of dark martian dunes. We find indications for a similar origin of the dark sands.

Gardin E.   Bourke M. C.   Allemand P.   Quantin C.
Bright Features Suggest Possible Dark Dune Migration on Mars **[#2507]**
Observation of high albedo features in one dune field could be suggesting that liquid water was stable at equatorial area in the recent martian time.

Shockey K. M.   Zimbelman J. R.
Transverse Aeolian Ridges as Seen in HiRise Images **[#1423]**
Using Mars HiRise images, photoclinometry extracts profiles to characterize TARs geomorphologically.

Ramstad R.   Appel M.   Brown A. J.   McKay C. P.   Fredriksson S.
Mars in a Bulb: An Experimental Simulation of Martian Dark Dune Spots (DDSs) **[#1565]**
The mechanics behind the formation and evolution of dark dune spots (DDSs) has still not reached scientific consensus. From studying the phenomenology of DDSs a model is formulated and an experimental design to test it is presented in this paper.

Merrison J. P.   Gunnlaugsson H. P.   Holstein-Rathlou C.   Knak-Jensen S.   Nørnberg P.   Rasmussen K. R.
Sand Transport; a Source of Mineral Alteration on Mars **[#1664]**
The reddish color characterising martian dust could have formed through mechanical activation during sand transport. This is demonstrated by laboratory simulation.

O'Donnell K. H.   Howald T. V.   Schieber J.
Eolian Adhesion Crusts Produced During Experimental Abrasion of Sedimentary Rock — An Alternative Process for Martian Rock Varnish Formation? **[#1113]**
Iron-rich adhesion crusts resembling martian rock varnish are observed on rock surfaces during eolian abrasion experiments. These crusts seem to form in response to ambient humidity fluctuations and "impact sintering" of micron-sized particles.

Geissler P. E.   Daubar I. J.   McEwen A. S.   Bridges N. T.   Dundas C. M.
Eolian Degradation of Young Martian Craters **[#2591]**
HiRISE images of young martian craters show that surprisingly few changes took place during the global dust storm of 2007.

Siebach K.   Arvidson R.   Cabrol N.   Athena Science Team
Recent Spirit Results: Microscopic Imager Analysis of Particle Properties in Scamander Crater, West of Home Plate **[#2548]**
Images taken with the Spirit Rover's Microscopic Imager at its current location in Scamander Crater have been used to analyze particle properties of exposed subsurface soils. These data show angular sulfate-rich sand under eolian basaltic sand.

Holstein-Rathlou C.   Gunnlaugsson H. P.   Merrison J. P.   Nørnberg P.   Ellehoj M. D.   Bean K. M.
Lemmon M. T.   Tamppari L.   Smith P.
Time-dependent Dust Accumulation on the Mars Phoenix Wind Indicator **[#1811]**
Time dependent dust accumulation on the Telltale fibers was observed during the Phoenix mission. Removal of dust seems coupled with dust devil passings at the Phoenix landing site and investigations are underways to determine the wind speeds needed for the dust removal.

Holstein-Rathlou C.   Gunnlaugsson H. P.   Cantor B. A.   Ellehoj M. D.   Lange C. F.   Lemmon M.   Malin M. C.
Tamppari L.   Taylor P.   Merrison J. P.   Madsen M. B.   Nørnberg P.   Smith P.   Phoenix Science Team
On Dust Storms Observed at the Phoenix Landing Site **[#1837]**
In this contribution we discuss two different origins of dust activity at the Mars Phoenix landing site using lander data and images taken of the North Polar region on Mars by the Mars Color Imager onboard Mars Reconnaissance Orbiter.

Balme M. R.   Metzger S. M.   Pathare A.   Renno N.   Saca F.   Spiga A.7:00 p.m.   Towner M.
A New Field Study of Terrestrial Dust Devils with Application to Mars: Using a Stereo-Camera Survey and GIS to Calculate the Size-Frequency Distribution of Dust Devils in the Southwest USA **[#2349]**
We describe a new series of terrestrial field studies aimed at characterising dust devil intensity as a function of ambient meteorology. We present results from stereo imaging of dust devils that allow their size-frequency distribution to be accurately determined.

Metzger S.   Kurgansky M.   Montecinos A.   Villagran V.   Verdejo H.
Chasing Dust Devils in Chile's Atacama Desert **[#2564]**
We present field findings from Atacama Desert, Chile, of 35 dust devil encounters with three-dimensional sonic anemometry and thermal images.

Metzger S.   Balme M.   Pathare A.   Renno N.7:00 p.m.   Towner M.   Saca F.   Spiga A.
Dust Devil Sediment Loading, Wind Speeds and Pressure Excursions **[#2342]**
We present initial findings to directly sample dust devil vortices in Eldorado Valley, NV, June 2009 with over 130 direct (symmetrical, through the core) and nearby indirect encounters.

Pathare A.   Balme M.   Metzger S.   Spiga A.7:00 p.m.   Towner M.   Saca F.
Field Observations of the Size-Frequency Distribution of Terrestrial Dust Devils: Assessing the Power Law Hypothesis of Dust Devil Diameters **[#2325]**
Based on our recent new field observations of the size-frequency distribution of dust devils in Eloy, Arizona, and Eldorado Valley, Nevada, we assess the possible power law dependence of dust devil diameters.

MARTIAN POLAR PROCESSES: SEASONAL ICE AND POLAR LAYERED DEPOSITS

Brown A. J.   Calvin W. M.
MRO (CRISM/MARCI) Mapping of the North Pole — First Mars Year of Observations **[#1278]**
We have mapped the north polar region of Mars with using CRISM imaging spectrometer Multi-Spectral Polar dataset. We observe the north polar recession, reporting on the H_2O ice annulus and CO_2 and H_2O ice grain sizes as a function of season.

Appéré T.   Schmitt B.   Douté S.   Langevin Y.   Forget F.   Bibring J.-P.
Spring Evolution of Mars' Northern Seasonal Condensates from OMEGA on Mars Express **[#1071]**
We studied the MY 27-28 recession of the northern seasonal condensates on Mars from the OMEGA dataset (Mars Express). An evolution scenario is proposed from this analysis.

Koutnik M. R.   Winebrenner D. P.   Waddington E. D.   Pathare A. V.   Byrne S.
Equilibration Timescales for Ice Flow on Gemina Lingula Indicate Enhanced Flow at Low Temperatures **[#2272]**
With ice-flow enhancement comparable to that observed in Taylor Glacier, Antarctica, equilibration timescales for flow in Gemina Lingula, North Polar Layered Deposits are less than 5 million years, at basal temperatures only modestly warmer than today.

Christian S.   Holt J. W.   Choudhary P.   Fishbaugh K. E.   Plaut J. J.
Correlating High Resolution Radar Reflectors with Visible Layering of the Polar Layered Deposits, Mars **[#2372]**
High resolution radar reflectors from Shallow Radar (SHARAD) on the Mars Reconnaissance Orbiter have been modeled in three dimensions in order to attempt a quantitative correlation with optical layering.

Karlsson N. B.   Holt J. W.   Hindmarsh R. C. A.   Choudhary P.
Internal Layering of Gemina Lingula, North Polar Layered Deposits, Mars, and the Case for Ice Flow **[#1781]**
In this study we use SHARAD data retrieved from the southernmost tongue of the North Polar Layered Deposits on Mars to analyse the stratigraphy of the internal layers and compare them to modelled layers from a three-dimensional ice flow model.

Brothers T. C.   Holt J. W.   Christian S. W.   Choudhary P.
Investigating Subsurface Geomorphology of the Basal Unit of Planum Boreum, Mars with SHARAD to Constrain Early Erosional Processes **[#2590]**
We mapped the subsurface Planum Boreum Basal Unit (BU) on Mars using SHARAD. Mapping of this interface revealed many anomalous features in the BU, zones where accumulation alone cannot explain morphologies.

Fortezzo C. M.   Tanaka K. L.
Mapping Planum Boreum Unconformities Using Context Camera Mosaics **[#2554]**
Using Context Camera image mosaics of Planum Boreum, Mars, we located 308 exposed angular and parallel unconformities. Differential densities suggest latitude and elevation dependent preferential erosion of the Middle Amazonian layered deposits.

Nunes D. C.
Ice Flow and Mass Loss at the Martian Northern Polar Layered Deposits **[#2597]**
Thermomechanical models of the martian northern polar layered deposits are used to predict surface deformation and constrain ice ablation rates.

Herkenhoff K. E.   Fortezzo C.   Cushing G.   Kirk R. L.   Soderblom L. A.   Weller L.
Stratigraphy and Structure of the North Polar Layered Deposits on Mars **[#1566]**
Photoclinometric models of MOC springtime images allow the stratigraphy and structure of the north polar layered deposits on Mars to be quantitatively analyzed.

Li J.   Andrews-Hanna J. C.   Sun Y.   Zuber M. T.   Phillips R. J.   Plaut J. J.
Density Variations Within the South Polar Layered Deposits of Mars **[#2015]**
The south polar layered deposits (SPLD) constitute the largest known reservoir of surface water on Mars.
We invert for the lateral density variations in the layered deposits. The results suggest significant density variations within the SPLD.

Guallini L.   Rossi A. P.   Marinangeli L.
Evidences of Reverse Faults Within South Polar Layered Deposits in Promethei Lingula Region (Mars). A Possible Clue of "Ice-Cap" Migration? **[#1732]**
We identified reverse/transpressive faults within SPLD (Promethei Lingula). Their kinematic seems to be consistent with a past ice-cap migration (local?) towards its margins (ice-flow), perhaps influenced by interaction with bedrock (basal sliding).

Milkovich S. M.
Correlating Images and Radar at Promethei Lingula in the South Polar Layered Deposits of Mars **[#2142]**
Erosional features of individual layers exposed on the surface of Promethei Lingula, are examined in HiRISE images to gain insight into which layers cause radar reflections within SHARAD radargrams.

Aye K.-M.   Portyankina G.   Thomas N.
Semi-Automatic Measures of Activity in the Inca City Region of Mars Using Morphological Image Analysis **[#2707]**
Semi-automatic image feature extraction methods have been applied to a HiRISE data set covering two spring seasons of Inca City observations. The techniques used are being discussed and first results are shown and the ways forward to fully automatic methods are indicated.

Becerra P.   Byrne S.
Modeling the Formation of CO_2 Frost Halos in the South Polar Residual Cap of Mars **[#2097]**
We introduce a model for the formation of bright CO_2 frost halos seen by HiRISE on the edges of many "swiss cheese" features in the south polar residual cap of Mars.

Kereszturi A.   Schmidt F.   Vincendon M.
Searching for Water Ice in the Dark Dune Spots of Mars Using CRISM Data **[#1714]**
Observing dark dune spots on Mars in springtime, CRISM data show water ice is present as surface or atmospheric cristals there. This is compatible with the idea, that interfacial water or brine could produce flow-like features emanate from these spots.

Appel M.   Ramstad R.   Brown A. J.   McKay C. P.   Fredriksson S.
Potential Model for Dark Albedo Features in the Martian Polar Region Observed at 81°N 156°E **[#1562]**
Intriguing albedo features appear in the martian polar regions during local spring, e.g., dark dune spots. We studied a dune field at 81°N 156°E showing these features and here present a potential model for their formation.

Bérczi Sz.   Horváth A.   Kereszturi A.   Sik A.
Microstructure on the Surface of Dark Dunes in the Polar Region of Mars **[#1671]**
We propose possible near surface microstructures of the soil on polar dunes of Mars, connected to the dark dune spots' flow-like features, formed by the presence or movement of brines.

MARS ICE IN AND AROUND CRATERS

Bertilsson S. A. M.   Hajigholi M.   Brown A. J.   McKay C. P.   Fredriksson S.
Monitoring the Korolev Crater on Spring and Summer Images in the Martian Northern Polar Region with CTX and HiRISE **[#1569]**
Due to change of surface albedo in Korolev crater this work will analyze images of Korolev from different solar longitude, during spring and summer with CTX and HiRISE to map water ice and seasonal changes.

Luspay-Kuti A.   Kereszturi A.   Chevrier V. F.
Analysis of Frost Inside and Around Dokka Crater in the North Polar Region of Mars **[#2028]**
Properties of non-crater frost outliers around an am/pm HAE crater called Dokka are investigated.

Hajigholi M.   Bertilsson S. A. M.   Brown A. J.   McKay C. P.   Fredriksson S.
Monitoring Seasonal Behavior of Ices in the Craters in the Martian Northern Polar Region with CTX and HiRISE **[#1553]**
Seven martian craters in the Northern Polar Region have been monitored poleward of 60° in latitude to better understand ice behavior. The ice coverage has shown both expected and unexpected seasonal variations, during varying solar longitude.

Figueroa M.   Amara S.   Hendershot C.   Nagarajan S.   Nguyen T.   Prasad T.   Wilson R.
Determining a Trend in the Relation of Ice Deposits and Craters in the Martian Polar Region **[#1535]**
Small water ice deposits, present among the northern plains of the martian northern pole after the polar cap recedes in summer, have been studied to determine any correlation between the area covered by ice deposits and the area covered by craters.

Cornwall C.   Titus T. N.
Martian H_2O Ice Outliers in the Northern Plains **[#1107]**
"Ice patches" have been identified on Mars far from the northern residual cap using THEMIS, TES and CRISM observations. These deposits typically form on the northward-facing slopes of craters in early spring and disappear during late summer.

Pedersen G. B. M.
Observed Degradation Stages of Ring-Mold Craters (RMC): Geomorphic Evidence for Modification of Ice-rich Deposits in the Transition Zone Between Elysium and Utopia Basin, Mars **[#1790]**
Deposits with pits, depressions and RMCs observed north of Elysium rise are interpreted as degraded mixtures of ice and clastic material (CCF, LVF and LDA). Degradation stages of RMCs are an important tool for mapping dusty, deflated ice-rich units.

Maine A.   Kreslavsky M. A.   Orloff T. C.   Asphaug E.   Gray H.
Degradation of Small Craters in the High Latitudes of Mars **[#1556]**
Degradation of small craters in the high latitudes of Mars is very rapid. The activity of patterned ground, ground ice sublimation, formation of icy mantles, and eolian deposition contribute to the degradation sequence of the craters' geomorphology.

Kadish S. J.   Head J. W.   Barlow N. G.
The Formation Timescale and Ages of Mid-Latitude Pedestal Craters on Mars **[#1014]**
The ages and formation timescale of pedestal craters (Pd) have implications for the timing of ice-rich material accumulation at mid-latitudes on Mars. We show that most Pd are Amazonian in age, and formed from multiple episodes of ice-rich deposits.

TERRESTRIAL PLANET CRYOSPHERES: ICE TABLE, GLACIERS, AND PERIGLACIAL LANDFORMS

Levy J. S.   Head J. W.   Fassett C. I.   Fountain A. G.
Candidate Volcanic Ice-Cauldrons on Mars: Estimates of Ice Melt, Magma Volume, and Astrobiological Implications **[#1054]**
The morphological properties of two martian depressions suggest ice-cauldron formation. We conduct volumetric and calorimetric estimates showing that up to a cubic km of ice may have been removed in these depressions (melted and/or vaporized).

Hecht M. H.
Ice at the Phoenix Landing Site Part V: The Equilibrium Strikes Back **[#1481]**
Various types of ice found at the Phoenix cite (pore-filled, segregated, globules, and frost) are explained in terms of equilibrium physics.

Soare R. J.   Pearce G. D.   Séjourné A.
"Wet" Periglacial Processes, Ground Ice and a Revision of the Near-Surface Stratigraphy in Utopia Planitia, Mars **[#1506]**
Much attention has focused on whether the (late Amazonian) periglacial landscape of mid-UP, Mars is the product of "wet" thaw-related processes or of sublimation. We propose that the landscape substrate could have evolved only under a regime that includes "wet" conditions.

Saraiva J.   Bandeira L.   Pina P.
Mapping Properties of Periglacial Polygons on Mars **[#2027]**
The detailed characterization and mapping of small-scale polygons by automated methods in introduced.

Orloff T. C.   Kreslavsky M. A.   Asphaug E.
Rock Behavior on High-Latitude Patterned Ground Terrains of Mars **[#2184]**
Rocks organize in multiple configurations on martian high-latitude patterned ground terrain, but polygon margins are preferred to interiors. Rocks may also participate in multiple scales of patterning simultaneously in the same locale.

Mellon M. T.   Osterman G.   Searls M. L.
Geographic Variations in Polygonal Ground on Mars: Polygon Size and Its Relationship to Ground Ice **[#2067]**
We examine HiRISE images from the middle and high latitudes of Mars for polygonal patterns and measure characteristics with focus on the distribution of diameters. Observations are compared with theoretical models to assess the history of permafrost.

Gallagher C.   Balme M. R.
Landform Assemblages Indicative of Northern High Latitude Thaw on Mars **[#1623]**
We describe key results of a survey of 23 High Resolution Imaging Science Experiment (HiRISE) images covering 337° of longitude between 59°N and 79°N in which polycyclic morphogenesis reflecting freeze-thaw and liquid flow is evident.

Raitala J.   Aittola M.   Korteniemi J.   Öhman T.   Törmänen T.   Kukkonen S.
Possible Ice Lenses on Mars **[#1332]**
In a crater on Noachis Terra there are domes within a narrow crater floor unit. The unit is connected to a channel that breaches the crater rim. In this study we discuss of a possible pingo-like characteristics of the domes.

Pearce G.   Osinski G. R.   Soare R. J.
Intra-Crater Glacial Flow and Ice Mantling in Adamas Labyrinthus, Northern Plains of Mars **[#2490]**
We report a variety of possible glacial-like features that are found on northern outer-crater walls and within the channeled troughs of Adamas Labyrinthus. We suggest that this is consistent with region-wide late-Amazonian glacial conditions.

Parsons R. A.   Nimmo F.
Constraining the Timing of Lobate Debris Apron Emplacement at Martian Mid-Latitudes Using a Numerical Model of Ice Flow **[#1463]**
SHARAD observations constrain the thickness and dust content of lobate debris aprons (LDAs). Simulations of dust-free ice-sheet flow over a flat surface at 205 K for 10–100 m.y. give LDA lengths and thicknesses that are consistent with observations.

Fastook J. L.   Head J. W.   Madeleine J.-B.   Forget F.   Marchant D.
Modeling an Ice-rich Lobate Debris Apron in Deuteronilus Mensae **[#1823]**
Models help interpret observed glacial deposits and test formation scenarios. We examine a lobate debris apron recently proven to contain pure water ice. Two hypotheses are tested: alcove-only and collapse from a larger ice sheet driven by a GCM.

Fassett C. I.   Dickson J. L.   Head J. W.   Levy J. S.   Marchant D. R.
Supraglacial and Proglacial Valleys on Amazonian Mars **[#1892]**
In the mid-latitudes of Mars, small valleys are found in association with probable glacial deposits. We describe these features, which we interpret as proglacial or supraglacial valleys, formed by melting of glacial ice during the Amazonian.

Raack J.   Hiesinger H.   Reiss D.
Morphologic Map of Glacial and Periglacial Features in the Northwestern Argyre Basin, Mars **[#1998]**
We produced a morphological map of the northwestern rim of the Argyre Basin with focus on glacial and periglacial features. We report on features such as gullies, pingo-like forms and glacial remnants which are observed.

Krohn K.   van Gasselt S.   Neukum G.
High-Resolution Geologic and Geomorphologic Mapping of the Arsia Mons Fan-shaped Deposits **[#2207]**
We here report on a high-resolution geologic and geomorphologic mapping (1:50k) of the Arsia Mons fan-shaped deposits with emphasis on the chronostratigraphic relationships and definition of subunits.

Rutledge A. M.   Christensen P. R.
Seasonal Temperature Modeling of Near-Surface Ice Associated with Glacial Features in the Hellas Basin Region on Mars **[#2310]**
A thermal model using high-resolution temperature data from the Thermal Emission Imaging System (THEMIS) is applied to estimate near-surface water ice at lobate debris aprons on the eastern rim of Hellas Basin on Mars.

Boldt B.   Head J. W. III   Marchant D.   Wilson L.
Olympus Mons Debris-Covered Glaciers: Formation, Evolution and Volcano-Ice Interactions **[#1033]**
New data on the structure, accumulation zone, talus contributions, debris cover, terminal and lateral moraines, ages and volcano-ice interactions of the Late Amazonian tropical mountain glaciers along the western scarp of Olympus Mons are reported.

Kress A.   Head J. W.   Safaeinili A.   Holt J.   Plaut J.   Posiolova L.   Phillips R.   Seu R.   SHARAD Team
Age and Stratigraphic Relationships in Massif-Debris-Apron Terrain in Western Phlegra Montes, Mars **[#1166]**
SHARAD returns from lobate debris aprons (LDA) near Phlegra Montes may show similarly high ice contents to other LDA on Mars; geomorphology and surface ages of the deposits confirm this detection and support a debris-covered-glacier origin for LDA.

van Gasselt S.   Hauber E.   Rossi A.-P.   Dumke A.   Neukum G.
Geomorphology of the Tempe Terra Lobate Debris Aprons **[#2324]**
We here report on the landscape evolution of the Tempe Terra population of Lobate Debris Aprons with emphasis on a mantling deposit and recurrent degradation events.

Fairén A. G.   Davila A. F.   Lim D.   McKay C.
Icebergs on Early Mars **[#2478]**
The presence and distribution of boulders, clusters of boulders and chains of craters in the northern lowlands of Mars are consistent with iceberg transport and grounding in a global hydrosphere governed by ice-semicovered oceans, glaciers, icebergs and massive polar caps.

Kreslavsky M. A.   Head J. W.
Carbon Dioxide Glaciers in the Recent Geological History of Mars **[#1284]**
We interpret unusual features at high northern latitudes on Mars as drop moraines left by carbon dioxide glaciers that were active during recent low obliquity periods (0.6–3 Ma ago).

Putzig N. E.   Mellon M. T.   Herkenhoff K. E.   Phillips R. J.   Davis B. J.   Ewer K. J.
Near-Surface Ice Likely Cause of Thermal Anomaly in Martian North Polar Erg **[#2495]**
The anomalously low apparent thermal inertia of the north polar erg on Mars is attributed to a thermal effect of a layered surface with ~20 cm of normal sand over an ice-cemented substrate, obviating the need to invoke exotic agglomerations of dust.

MERCURY

Ziethe R.   Benkhoff J.
Mercury's Thermal Evolution, Dynamical Topography and Geoid **[#1728]**
We present thermal evolution models of Mercury and investigate the extention of a partial molten zone together with the topography and gravity field caused by interior dynamics.

Lu J.   Sun Y.   Toksoz M. N.   Zuber M. T.
Seismic Effects of the Caloris Impact: Insights into Mercury's Early Internal State **[#1991]**
We develop 1-D physically consistent structure models for Mercury and use advanced computational methods for the seismic source and wave propagation, to explore the effects of various parameters on the antipodal focusing seismic waves.

Preusker F.   Oberst J.   Phillips J.   Watters T. R.   Head J. W.   Zuber M. T.   Turner F. S.   Solomon S. C.
Digital Terrain Models of Mercury from MESSENGER Stereo Images **[#1789]**
Procedures have been developed to derive three separate digital terrain models from stereo images obtained by the MESSENGER narrow-angle camera during the spacecraft's three Mercury flybys of 2008 and 2009. They cover 33 percent of Mercury's surface.

Pashai P.   Izenberg N. R.   Gilles-Davis J. J.   Watters T. R.   Blewett D. T.   Solomon S. C.
A Mercury Crater with Volcanic and Tectonic Modification **[#1693]**
We explore possible formation histories a Mercury crater bisected by a compressional ridge and containing a central pit with evidence of pyroclastic volcanism.

Baker D. M. H.   Head J. W.   Prockter L. M.   Blewett D. T.   Denevi B. W.   Ernst C. M.   Watters T. R.
Peak-Ring Basins on Mercury: New MESSENGER Data and Implications for Basin Formation and Modification **[#1384]**
We assess MESSENGER flyby data to compile a database of peak-ring basins on Mercury, the transitions from complex crater to basin to multi-ring basin, and processes of modification of fresh peak-ring basins.

Schon S. C.   Head J. W.   Prockter L. M.   MESSENGER Science Team
Eminescu and the Transition to Peak-Ring Basins on Mercury **[#1263]**
Geologic mapping and analysis of Eminescu, a central peak-ring basin on Mercury, including smooth interior units.

Blewett D. T.   Denevi B. W.   Robinson M. S.   Ernst C. M.   Purucker M. E.   Gillis-Davis J. J.
A MESSENGER Look at Basin Antipodes on Mercury **[#1092]**
We examine basin antipodes on Mercury for occurrences of "hilly and lineated" terrain and unusual albedo markings.

Watters T. R.   Solomon S. C.   Robinson M. S.   Oberst J.   Preusker F.   MESSENGER Team
Evidence of Extension on Mercury Unrelated to Impact Basin Deformation **[#1477]**
Images obtained during MESSENGER's third flyby have revealed the first evidence of extension outside of l arge impact basins on Mercury. The extensional features are associated with a plateau bounded by an arcuate lobate scarp.

Orlando T. M.   Sprague A. L.   Grieves G. A.   Schriver D.   Trávníček P. M.   McLain J. L.   Starr R. D.
Electron Stimulated Desorption as a Source Mechanism for Ions in Mercury's Space Environment **[#2246]**
Electron-stimulated desorption experiments are performed using Na-bearing silicate targets to investigate nonthermal desorption and material removal processes on heterogeneous surfaces and interfaces under Mercury's conditions.

D´Amore M.   Helbert J.   Maturilli A.   Izenberg N. R.   Sprague A. L.   Holsclaw G. M.   Head J. W.   McClintock W. E.   Solomon S. C.
Compositional Units on Mercury from Principal Component Analysis of MESSENGER Reflectance Spectra **[#2016]**
We analyzed surface spectra from the Mercury Atmospheric and Surface Composition Spectrometer with a principal component approach and unsupervised classification techniques to identify and characterize surface units along the ground tracks.

Domingue D. L.   Murchie S. L.   Chabot N. L.   Denevi B. W.   Izenberg N. R.   Holsclaw G. M.
Analysis of the Dedicated Spectral Photometric Observations from MESSENGER's Third Mercury Flyby **[#2455]**
Analysis of the photometric observations obtained during MESSENGER's third flyby of Mercury are presented.

VENUS

Guseva E. N.
Comparision of the Volume of Rift-related Volcanic Rocks on Venus and Earth **[#1094]**
The regions of Atla and Beta rifts have significantly larger volumes of volcanic materials comparing with the Kenya-Ethiopian rifts. The much larger volumes of volcanic materials on Venus may be explained with some hypotheses.

Buz J. McGovern P.
Venusian Volcano Shapes: Implications for Edifice Evolution and the Internal Thermal State of Venus **[#1482]**
We attempt to relate shape characteristics of volcanos with magma source dimensions, supply rate, and thickness of the elastic lithosphere.

Senske D. A.
Tessera Terrain on Venus: Comparing Phoebe Regio and Tellus Tessera **[#1256]**
This analysis assesses and compares the morphologic and structural characteristics of Phoebe Regio and Tellus Tessera.

Gilmore M. S. Resor P. G. Ghent R. Senske D. A. Herrick R. R.
Mapping and Modeling of a Tessera Collision Zone, Tellus Regio, Venus **[#1769]**
SW Tellus Regio includes a zone of collision that incorporates several preexisting tessera fabrics and plains materials into the plateau. Lithospheric modeling based on structural wavelength yields high geotherms during tessera formation.

Orth C. P. Solomatov V. S.
Constraints on the Global Lithospheric Thickness of Venus in the Isostatic Stagnant Lid Approximation **[#2056]**
The isostatic stagnant lid approximation requires the stagnant lid to be in perfect isostatic equilibrium. This approximation is formulated on the basis of systematic two-dimensional calculations and is limited to long wavelengths.

Bleamaster L. F. III
Geologic Mapping of the Beta-Atla-Themis (BAT) Region of Venus: Batting a Thousand? **[#2408]**
Geologic mapping in the BAT region of Venus is characterizing potentially active sites of volcanism and tectonism including hundreds of coronae and several chasmata.

Tandberg E. R. Bleamaster L. F. III
Geologic Mapping of the Devana Chasma (V-29) Quadrangle, Venus: Preliminary Report **[#1816]**
Preliminary mapping results of the Devana Chasma (V-29) Quadrangle are presented, with an emphasis on rift formation styles in anomalously thick crust.

Barata M. T. Pina P. Saraiva J. Alves E. I.
Extraction of Craters and Ejecta from Venus SAR Imagery **[#1412]**
The present work is focused on a methodology for the detection of craters and ejecta deposits on Magel-lan SAR images of the surface of Venus, based on fractal dimension and morphological transforms.

Lambert J. L. Morookian J. Roberts T. Polk J. Smrekar S. Clegg S. M. Weins R. C. Dyar M. D. Treiman A.
Standoff LIBS and Raman Spectroscopy Under Venus Conditions **[#2608]**
High quality LIBS and Raman spectra of geologic samples held under Venus surface temperature (733 k) and pressure (92 bar) conditions have been acquired through a 1.5-m pathlength of simulated atmosphere (96.5% CO_2/3.5% N_2).

Ivanov M. A.   Head J. W.
Venus: The Apparent History of the Geoid **[#1057]**
We outline the possible history of the geoid of Venus analyzing the regional correlation (or lack of it) between the areal distribution of major stratigraphic units and the major features of the geoid of Venus.

Ding N.   Zeng Z.   Xiao Z.
An Assumption of the Formation Mechanism of Beta Plateau and Northern Devana Chasma,Venus **[#1296]**
We suppose that the pattern of double plume upwelling formed the Beta Plateau and northern Devana Chasma. As a result, the physical modeling validates the model of this pattern as a possible explanation.

Galgana G. A.   McGovern P. J.   Grosfils E. B.
The Interplay Between Flexural Stresses and Magma Reservoir Dynamics Beneath Large Venusian Volcanoes **[#2145]**
Flexural effects arising from continuous loads exerted by large volcanic edifices on Venus are studied. Numerical models that couple flexure with magma reservoir pressurization are used to analyze reservoir failure locations and predict lithosphere intrusion patterns.

Studd D.   Ernst R. E.   Samson C.   Grosfils E. B.   Head J. W.   Ivanov M. A.
Radiating Graben-Fissure Systems in Ulfrun Regio: A Contribution to the Venus Global Dyke Swarm Map Project **[#1950]**
We have undertaken to map all graben-fissure systems in the Ulfrun Regio area (0°–25°N, 200°–240°E) on Venus. We plan to establish the relative ages of radiating systems where they can be evaluated from cross-cutting and stratigraphic relationships.

MATERIAL ANALOGS: WHAT PLANET DID THAT COME FROM?

Hagerty J. J.   Clark S. E.   Hare T. M.   Hayward R. K.   Newsom H. E.   Wright S. P.   McHone J.
A New Repository for Drill Hole Samples and Remote Sensing Data from Meteor Crater, AZ **[#2213]**
A unique suite of samples from Meteor Crater have been collected by the USGS and are being made available to the scientific community. This collection will help to address unresolved issues regarding Meteor Crater and its associated ejecta deposits.

McHenry L. J.   Richardson C. D.   Hinman N. W.
Sulfate Minerals, Hematite, and Silica in Craters of the Moon, Idaho Basaltic Lava Tubes: A Potential Analog for Mars **[#1469]**
Lava tubes in the high-Fe basalts of Craters of the Moon, Idaho contain secondary silica, hematite, carbonate, and sulfate minerals. These formed through high and low temperature (and potentially biological) processes and could be analogous to Mars.

Hausrath E. M.
Characterization of Fumarolic Products in Nevada **[#2389]**
Hydrothermal alteration on Mars has been observed in meteorites and from orbital data and rovers. Alteration products and the weathering environment formed near fumaroles in Nevada are characterized to better interpret results from Mars.

Titus T. N.   Wynne J. J.   Ruby D.   Cabrol N.
The Atacama Desert Cave Shredder: A Case for Conduction Thermodynamics **[#1096]**
In the Atacama Desert, where caves are quite dry, the interior rock temperature should be a function of only the thermal conduction through the rock, which is driven by the mean temperature at the surface. In this paper, we test this hypothesis.

McAdam A. C.   Mahaffy P. R.   Blake D. F.   Ming D. W.   Franz H. B.   Eigenbrode J. L.
Steele A.   AMASE 2009 Team
Evolved Gas Analysis and X-Ray Diffraction of Carbonate Samples from the 2009 Arctic Mars Analog Svalbard Expedition: Implications for Mineralogical Inferences from the Mars Science Laboratory **[#2206]**
Carbonate analyses show that SAM evolved gas analysis will complement CheMin X-ray diffraction by supporting volatile-bearing mineral identification and providing information about trace phases below the XRD detection limit or amorphous phases.

Liu T.   Bish D. L.
Mineralogical Compositions of the Evaporites at Lewis Cliff Ice Tongue, Antarctica: A Potential Martian Analog **[#2024]**
The study on the formation of evaporite minerals in Antarctica under low-temperature conditions is an applicable analog to the hydrated evaporites on Mars which are used to document the evolution of natural waters from past water-rock interactions.

Marcucci E. C.   Hynek B. M.   McCollom T. M.   Rogers K. L.
Acid-Sulfate Weathering of Basalts at Cerro Negro Volcano, Nicaragua: An Early Mars Analog **[#2167]**
Cerro Negro, Nicaragua is a high temperature, low pH, S-rich environment, proposed to explain some acid-sulfate weathering on Mars. Simultaneously, we are analyzing field samples, laboratory experiments, theoretical modeling, and microbial studies.

Kuhlman K. R.   Janzen J. L.   Weingarten M.   Christensen M.   Yingst R. A.
Optical Microscopy of a Mars Analog from the 1996 Skei∂arársandur Jökulhlaup **[#2514]**
Here we present quantitative measures of the morphological features of sediment from the Mars analog 1996 Skei∂arársandur Jökulhlaup at the hand-lens and microscopic scales. These features represent basaltic volcano/water or ice interactions.

Kong W. G.   Wang A.   Chou I. M.
Determination of Phase Boundary Between Kornelite and Pentahydrated Ferric Sulfate by Humidity Buffer Technique and Raman Spectroscopy at 0.1 Mpa **[#2010]**
Phase boundary between kornelite and pentahydrated ferric sulfate in temperature-relative humidity space was obtained using a humidity buffer and Raman technology. The thermodynamic constants for this equilibrium were calculated and presented.

Choukroun M.   Castillo-Rogez J. C.   Young J. B.   Mielke R. E.
Preliminary Comparison Between the Dissipation in CO_2 Clathrates Hydrates and Water Ice **[#2172]**
We present new techniques for the synthesis and the characterization of clathrate hydrates, as well as preliminary mechanical measurements. We also compare the microstructure and the mechanical behavior of clathrate hydrate with that of water ice at the same conditions.

Cornell J. W.   Hausrath E. M.
Phosphate Mobility in a Mars Analog Environment **[#2141]**
Chemically weathered surfaces and secondary Fe and Al phosphates are observed in basalt flows from the Mars analog Craters of the Moon, ID. Understanding weathering in this environment should help us better understand phosphate mobility on Mars.

McHenry L. J.   Chevrier V. F.   Schröder C.
The Formation and Destruction of Jarosite in a Saline-Alkaline Paleolake Deposit: Implications for Mars **[#1476]**
Jarosite normally forms under acidic conditions, and has been used as evidence for acidic conditions on Mars. However, ephemeral jarosite occurs in zeolite-dominated altered tephra of a saline-alkaline paleolake deposit at Olduvai Gorge, Tanzania.

Lauer H. V. Jr.   Ming D. W.   Sutter B.   Mahaffy P. R.
Thermal and Evolved Gas Analysis of Calcite Under Reduced Operating Pressures: Implications for the 2011 MSL Sample Analysis at Mars (SAM) Instrument **[#2249]**
Operating pressure and carrier gas have an effect on the thermal and evolved gas behaviors of volatile-bearing phases. This study shows that volatile-bearing phases will have slightly higher thermal decomposition onset temperatures in SAM compared to TEGA.

Bishop J. L.   Makarewicz H. D.   Gates W. P.   McKeown N. K.   Hiroi T.
Beidellites: Spectral Properties and Importance for Mars **[#2080]**
Beidellites may be important phyllosilicates on Mars as they could be part of an alteration series between montmorillonite and higher temperature alteration minerals such as illite. The spectral properties of beidellites are presented.

Dukes C. A.   Baragiola R. A.
Effect of Water on the Surface Composition of Irradiated Minerals **[#2157]**
Sections of olivine and augite exposed to 10^{17} Ar cm^{-2} ion irradiation and then rinsed in water or exposed to a humid enviornment show up to 60% depletion of surface cations. This has implications for sample return and curation.

Hilchenbach M.   Lang T.   Neumann J.   Tarcea N.
Analysis of Mineral Soil Analog Samples with a Pulsed UV-Laser Source **[#1170]**
In this study we were focusing on setting up a new pulsed UV laser source combined with a laboratory Raman spectrometer and apply this setup to the analysis of powdered planetary mineral soil analog samples.

Durham W. B.   Pathare A. V.   Stern L. A.
Laboratory Measurements of Grain-Size-Sensitive Creep of Particulate-Laden Ice at Planetary Temperatures **[#2135]**
We investigate experimentally the effect of dust on the balance of grain-size-sensitive (GSS) vs grain-size-insensitive (GSI) creep mechanisms in ice, and find that small amounts of dust tend to inhibit GSS flow. Application is to Mars and icy moons.

Cleaves H. J. II   Dworkin J. P.
The Amino Acids Produced from HCN And Mixed HCN/HCHO Reactions: Analogues for Organic Chemistry In Extraterrestrial Bodies **[#2305]**
We report a synthetic model for the organics in carbonaceous chondrites from NH_3, HCHO, and HCN. We use LC-MS to study the reaction products and compare them with compounds in meteorites. This may help constrain conditions on carbonaceous chondrite parent bodies.

Rice M. S.   Cloutis E. A.   Crowley J. K.
Spectral Reflectance Changes Accompanying Long-Duration Exposure of Silica Sinter and Fe-Sulfates to Simulated Mars Surface Conditions **[#2576]**
To better understand the stability of silica-rich and Fe-sulfate materials under current martian surface conditions, we have subjected samples to long-duration simulated martian T, P and UV conditions.

Blewett D. T.   Nguyen N. V.   Lawrence S. J.
Iron Optical Constants and Reflectance Spectrometry of Planetary Surfaces **[#1051]**
We are making new measurements of the optical constants of iron, which are key inputs for radiative transfer modeling of the reflectance of planetary surfaces, including asteroids, the Moon, and Mercury.

Bower D. M.   Steele A.   Kater L.
Micro Raman Spectroscopic Investigations of the Nature and Provenance of Mineral and Carbonaceous Material in the 1.9 Gunflint Formation: Redefining D and G Carbon Parameters for the Detection of Biosignatures **[#2657]**
The unique mapping capabilities of micro Raman spectroscopy provide a greater view of the spatial relationships between carbonaceous materials and other features in ancient rocks. With this technique, the problem of carbon biogenicity can be addressed.

Quinn D. P.   Gillis-Davis J. J.   Lucey P. G.
Using Microsoft Excel for Hapke Modeling: A Technique to Simplify Calculations of Optical Constants and Reflectance Spectra **[#2426]**
Hapke radiative transfer modeling can be used to derive optical constants of from reflectance spectra. A method is developed to calculate imaginary indices of refraction in an Excel spreadsheet instead of expensive higher-level tools such as IDL.

Golden D. C.   Ming D. W.   Morris R. V.
Spherulitic Growth of Hematite Under Hydrothermal Conditions: Insights into the Growth Mechanism of Hematite Spherules in Meridiani Planum, Mars **[#2541]**
Morphological evolution of hematite spherules under acidic hydrothermal conditions is described. Two spehrule growth types are described based along with evidence for their occurence in Meridiani Planum, Mars.

Socki R. A.   Niles P. B.   Fu Q.   Gibson E. K. Jr.
Cryogenic Carbonate Formation on Mars: Clues from Stable Isotope Variations seen in Experimental Studies **[#2526]**
Experiments demonstrate carbonate formed cryogenically under martian conditions are enriched in ^{13}C over equilibrium values. If carbonate formation has persisted over the history of Mars we expect carbonate reservoirs to reflect this ^{13}C-enrichment.

Shepard M. K.
The Effects of Albedo and Compaction on the Opposition Surge of Laboratory Particulates **[#1742]**
Using bidirectional reflectance data of laboratory particulates acquired with the Bloomsburg University Goniometer (B.U.G.) Laboratory, we investigate the role of optical albedo and particulate compaction on the opposition surge.

Bonnet J.-Y.   Thissen R.   Frisari M.   Vuitton V.   Quirico E.   Le Roy L.   Fray N.   Cottin H.   Hörst S. M.   Yelle R.
HCN Polymers: Composition And Structure Revisited by High Resolution Mass Spectrometry **[#1334]**
Chemistry and structure of HCN polymers is poorly known instead of their planetary and prebiotic interest. We used a high resolution mass spectrometer LTO-OrbitrapXL to explore these analogs compositon and structure.

SPACECRAFT INSTRUMENTS

Blake D. F.   Vaniman D.   Anderson R.   Bish D.   Chipera S.   Chemtob S.   Crisp J.   DesMarais D. J.   Downs R.   Farmer J.   Feldman S.   Gailhanou M.   Ming D.   Morris R.   Stolper E.   Sarrazin P.   Treiman A.   Yen A.
Test and Delivery of the CheMin Mineralogical Instrument for Mars Science Laboratory '11 **[#1898]**
CheMin, an XRD/XRF instrument selected for flight on Mars Science Laboratory '11 has been tested and delivered to the MSL project. Diffraction and fluorescence data collected over a range of Mars-relevant temperature and pressure conditions will be presented.

Treiman A. H.   Robinson K. L.   Blake D. F.   Bish D.
Mineralogy Determinations by CheMin XRD, Tested on Ultramafic Rocks (Mantle Xenoliths) **[#1472]**
The CheMin XRD instrument, part of the MLS lander, can identify minerals and quantify their abundances in ultramafic rocks (like those at some proposed MSL landing sites).

Wiens R. C.   Clegg S. M.   Bender S.   Lanza N.   Barraclough B.   Perez R.   Forni O.   Maurice S.   ChemCam Team   Dyar M. D.   Newsom H.
Progress on Calibration of the ChemCam LIBS Instrument for the Mars Science Laboratory (MSL) Rover **[#2205]**
ChemCam underwent initial calibrations in late 2008 using rock powder standards; final lab calibrations will be in early 2010. Here we report analysis techniques and results from the ChemCam laser-induced breakdown spectroscopy (LIBS) instrument.

Perkins J. J. Sharma S. K. Lienert B. L. Misra A. K. Clegg S. M. Wiens R. C.
Improvement in Qualitative and Quantitaive LIBS Analysis of Elemental Compositions of Basalts **[#1517]**
We report here improvements in the qualitative classification and quantitative elemental compositions determination of rocks from the baseline corrected remote LIBS data with multivariate (PCA and PLS2) analysis.

Rauschenbach I. Jessberger E. K. Pavlov S. G. Schröder S. Hübers H.-W.
Calibration and Quantification of a Close-Up Mini-LIBS System for Planetary In-Situ Analysis **[#1658]**
We are developing a lightweight close-up LIBS instrument with a total mass of ~1 kg in flight-configuration. Here we report on a systematic performance study to determine the limits of detections and accuracies under martian atmospheric conditions.

Ishibashi K. Ohno S. Wada K. Senshu H. Kobayashi M. Arai T. Namiki N. Matsui T. Cho Y. Kamata S. Sugita S. Iijima Y. Tazawa S. Noda H. Sasaki S.
Effect of Spectral Quality on Laser-induced Breakdown Spectroscopy Measurements: The Precision of Elemental Abundance Prediction Using Partial Least Squares Regression **[#1719]**
We investigated the effect of S/N ratio and wavelength resolution of spectra on the prediction precision of elemental abundances in laser-induced breakdown spectroscopy measurements when partial least squares regression is used as an analysis method.

Cho Y. Sugita S. Ishibashi K. Ohno S. Kamata S. Kurosawa K. Sekine Y. Arai T. Kobayashi M. Senshu H. Wada K. Namiki N. Matsui T.
Effects of Laser Energy on LIBS Spectra **[#2158]**
LIBS spectra changes as laser fluence fluctuates, affecting the precision of analysis. Our experiments show that the spectral change may be predicted well with an LTE plasma with temperature proportional to a power-law function of laser fluence.

Cousin A. Maurice S. Forni O. Gasnault O. Dalmau J. Saccoccio M. Wiens R. ChemCamTeam
Laser Induced Breakdown Spectroscopy (LIBS) Library Under Martian Conditions **[#1983]**
ChemCam is part of the MSL rover to be launched in 2011 to investigate the martian surface geochemistry. The aim of this work is to build a library of LIBS emission lines in martian conditions and to develop software for analysis of ChemCam data.

Gallegos Z. E. Lanza N. L. Newsom H. E. Ollila A. M. King P. L. Osinski G. R. Clegg S. M. Wiens R. C. Vaniman D. T. Humphries S. D. McInroy R. E. Lee P.
Using Laser Induced Breakdown Spectroscopy (LIBS) to Assess Geologic Samples Associated with a Terrestrial Impact Structure as an Analogue for Future Planetary Explorations **[#2365]**
Determining the diversity of geologic materials in a complex impact structure using tools in the Mars Science Laboratory payload including ChemCam (LIBS and Remote Imager), CheMin (XRD), and APXS (XRF) and the MAHLI and MastCam cameras.

Blank J. G. Clegg S. M. Barefield J. E. McKay C. P. Wiens R. C.
Laboratory Exploration of Organic and Inorganic Carbon by Laser-induced Breakdown Spectroscopy (LIBS): Relevance for Planetary Astrobiology Missions **[#2485]**
We used LIBS and chemometric analysis to distinguish between organic and inorganic carbon in various samples (igneous rocks, carbonates, and kerogen-rich fertilizers), demonstrating the potential for ChemCam LIBS as an astrobiology tool for MSL.

Schröder S. Pavlov S. G. Hübers H.-W. Rauschenbach I. Jessberger E. K.
Analysis of Frozen Sulfate and Chloride Salt Solutions Using Laser-induced Breakdown Spectroscopy Under Martian Conditions **[#1842]**
We showed the feasibility of laser-induced breakdown spectroscopy to analyze different frozen salt solutions under martian conditions. We focused on chloride and sulphate salts which were found on Mars and could lower the freezing point of water.

Rehse S. J.   Miziolek A. W.   Collins L.   Torrione P.   Blank J.
A New Opportunity Using Elemental Microbiological Multi-Variate Analysis for the In Situ Identification of Astrobiological Materials **[#2231]**
Laser-induced breakdown spectroscopy is a spectrochemical technique that is part of the ChemCam package. Recent advances have allowed this technology to be utilized to identify biological organisms, including bacteria, in a technique we call EMMA.

Fabre C.   Maurice S.   Wiens R.   Sautter V.   ChemCam Team
ChemCam LIBS Instrument: Complete Characterization of the Onboard Calibration Silicate Targets (MSL Rover) **[#1835]**
This abstract presents the certification of the homogeneity, at the scale of laser spot sampling, of the different synthetic silicate glasses and the natural macusanite glass that will be mounted for the CHEM CAM instrument on the MSL rover.

Tucker J. M.   Dyar M. D.   Schaefer M. W.   Clegg S. M.   Wiens R. C.
Multivariate LIBS Analysis of Geologic Materials **[#1970]**
Because of the wealth of compositional data they contain, LIBS spectra can be used to determine chemical constituents of planetary materials. This study explores the best techniques for extracting quantitative information from geologic LIBS spectra.

Anderson R. B.   Morris R. V.   Clegg S. M.   Humphries S. D.   Weins R. C.   Bell J. F. III   Mertzman S. A.
Partial Least Squares and Neural Networks for Quantitative Calibration of Laser-Induced Breakdown Spectroscopy (LIBS) of Geologic Samples **[#2013]**
We have collected LIBS spectra of a diverse suite of well-characterized geologic samples and compare the performance of partial least squares regression and artificial neural networks in predicting quantitative sample compositions.

Humphries S. D.   Tucker J. M.   McInroy R. E.   Obrey S. J.   Wiens R. C.   Dyar M. D.   Clegg S. M.
A LIBS Elemental Emission Library for ChemCam at 7 m **[#2096]**
The focus of this paper is the development of a LIBS elemental spectral library under ChemCam's 7 m operating conditions. To facilitate elemental identification in data returned by ChemCam, a spectral library is being assembled of simple molecular forms.

Sobron P.   Alpers C. N.   Wang A.
LIBS/Raman Investigation of Mars-related Sulfates from Iron Mountain, California **[#2585]**
A combined LIBS/Raman (L/R) was used to investigate sulfates from Iron Mountain. We show a methodology to unambiguously identify sulfates that L/R proves to be a powerful combination for mineralogical/geochemical investigations of planetary bodies.

King P. L.   Gellert R.   Campbell J. L.   Hyde B. C.   Schofield C. D. M.   Perrett G.   Brown-Bury W.   Spilde M. S.   Boyd N.   Ollila A.   Lanza N.   Aran T.   McCutcheon W.   Newsom H.
Extended Calibrations for the APXS for the Mars Science Laboratory Mission **[#2539]**
We are using the laboratory MSL APXS to analyze materials with different textures, densities, and crystallographic orientation. We are testing APXS methods for analyzing light elements and rock coatings.

Litvak M. L.   Mitrofanov I. G.   Shvecov V. N.   Timoshenko G. N.   Kozyrev A. S.   Malakhov A. V.   Mokrousov M. I.   Sanin A. B.   Tretyakov V.   Vostrukhin A. A.   Golovin D.   Varenikov A. B.
DAN/MSL Instrument: First Field Tests **[#2021]**
Results of field tests of DAN/MSL instrument: detection of bound water in the subsurface.

Mahaffy P. R.   Glavin D. P.   Eigenbrode J. L.   Franz H.   Stern J.   Harpold D. N.   Brinckerhoff W. B.   Cabane M.   Coll P.   Szopa C.   Conrad P. G.   Webster C. R.   SAM Team
Calibration of the Sample Analysis at Mars (SAM) Instrument Suite for the 2011 Mars Science Laboratory **[#2130]**
The calibration of the flight unit if the Sample Analysis at Mars instrument suite for the 2011 Mars Science Laboratory is described. SAM provides chemical and isotopic analysis of organic and inorganic volatiles for atmospheric and solid samples.

Wimmer-Schweingruber R. F.   Martin C.   Kortmann O.   Boehm E.   Boettcher S.   Kharytonov A.   Ehresmann B.   Hassler D. M.   Zeitlin C.
Measuring Neutrons and Gamma Rays on Mars — The Mars Science Laboratory Radiation Assessment Detector MSL/RAD **[#2432]**
The Mars Science Laboratory (MSL) Radiation Assessment Detector (RAD) will measure the radiation environment including the neutral component on the martian surface. We present initial studies on the inversion of neutron calibration results.

Reedy R. C.   Boynton W. V.   Hamara D. K.   Evans L. G.   Brückner J.   Gasnault O.
Peaks in Germanium Planetary Gamma-Ray Spectra: An Update **[#2422]**
Improved techniques for fitting peaks in high energy resolution spectra from planetary gamma-ray spectrometer missions with Ge detectors are presented. Careful determination of continua and use of correct peak shapes are now done.

Brückner J.   Reedy R. C.   Englert P. A. J.   Drake D. M.
Analysis of Complex Gamma-Ray Spectra: Simulations for Planetary Gamma-Ray Spectroscopy of Solar-System Bodies **[#1608]**
Planetary gamma-ray spectroscopy provides data on chemical composition of solar-system bodies. To study the complexity of the gamma-ray spectra, experiments were performed by bombarding thick targets with protons and recording the gamma-rays.

Parsons A.   Bodnarik J.   Evans L.   Floyd S.   Lim L.   McClanahan T.   Namkung M.   Schweitzer J.   Starr R.   Trombka J.
Planetary Geochemistry Using Active Neutron and Gamma Ray Instrumentation **[#2553]**
We will present test data demonstrating the *in situ* bulk elementary composition measurement capabilities of the Pulsed Neutron Generator-Gamma Ray And Neutron Detector (PNG-GRAND) planetary geochemistry instrument.

Bodnarik J.   Evans L.   Floyd S.   Lim L.   McClanahan T.   Namkung M.   Parsons A.   Schweitzer J.   Starr R.   Trombka J.
A Unique Outside Neutron and Gamma Ray Instrumentation Development Test Facility at NASA's Goddard Space Flight Center **[#2581]**
A unique outdoor gamma ray and neutron instrumentation development test facility has been constructed at NASA's Goddard Space Flight Center for evaluating *in situ* gamma ray and neutron instrumentation designed for future planetary missions in a controlled environment.

Hardgrove C.   Moersch J. E.   Starr R.   McClanahan T.   Parsons A.
Simulations of Time-Dependent Neutron Scattering in Layered Materials Containing Hydrated Minerals **[#2473]**
Results of Monte Carle (MCNPX) simulations are presented for neutron die-away of several hydrated minerals detected on Mars. Composition, burial depth and mixing with regolith are considered with respect to their detectability by DAN.

Rodionov D.   Klingelhöfer G.   Blumers M.   Bernhardt B.   Fleischer I.   Gironés J.   Maul M.   Evlanov E.   Shlyk A.   d'Uston C.
In Situ Analysis of Iron Mineralogy on Phobos Surface by Moessbauer Spectroscopy **[#2261]**
Miniature Moessbauer Spectrometer (MIMOS II) is a powerful tool for *in situ* analysis of iron mineralogy. MIMOS successfully operates on the martian surface and now improved version is included in scientific payload of "Phobos-Grunt" mission.

Klingelhöfer G.   Blumers M.   Bernhardt B.   Lechner P.   Gironés-Lopez J.   Maul J.   Soltau H.   Strüder L.   Henkel H.
The Improved Miniaturized Mössbauer Spectrometer MIMOS IIA with Elemental Analysis Capability and Increased Sensitivity **[#2423]**
The instrument MIMOS IIA originally developed for the ESA ExoMars mission will use newly designed Si-Drift detectors with circular geometry (SDD) allowing high resolution X-ray fluorescence spectroscopy in parallel to Mössbauer measurements.

Sharma S. K. Misra A. K. Acosta T. Bates D. Lucey P. G.
Remote Raman Detection of Dark Minerals and Minerals in Hawaiian Basalts **[#1443]**
We present remote Raman spectral detection of hydrous dark minerals and minerals in basaltic rocks to a distance of 1 m with 10–30 s integration time with a compact Raman spectrograph.

Kong W. G. Wang A.
Planetary Laser Raman Spectroscopy for Surface Exploration on C/D-Type Asteroids — A Case Study **[#2730]**
A laser Raman spectroscopic study on Murchison and Allende meteorites provide detailed information on major, minor, and trace minerals information. This study demonstrates the feasibility of LR for surface exploration missions to C/D-type asteroids.

Rull F. Klingelhöfer G. Martinez-Frias J. Fleitcher I. Medina J. Sansano A.
In-Situ Raman, LIBS and Mössbauer Spectroscopy of Surface Minerals at Jaroso Ravine and Related Areas in Sierra Almagrera (Almeria-Spain) **[#2736]**
In this work we describe the results obtained from an *in situ* mineral analysis using Raman, LIBS and Mössbauer techniques during a field trip performed in the Jaroso Ravine area in September 2009.

De Sanctis M. C. Filacchione G. Capaccioni F. Piccioni G. Ammannito E. Capria M. T. Coradini A. Migliorini A. Battistelli E. Preti G.
SETA: An Imaging Spectrometer for Marco Polo Mission **[#1203]**
The aim of the SETA experiment is to perform imaging spectroscopy in the spectral range 400–3300 nm for a complete mapping of the Marco Polo target with a spectral sampling of at least 20 nm and a spatial resolution on the order of meters.

Maturilli A. Helbert J. D'Amore M.
Reflectance and Transmission Measurements in Support of the Emissivity Measurements in the Planetary Emissivity Laboratory (PEL) **[#1319]**
In the PEL a spectral library of emissivity measurements for planetary analogues, at high temperature and vacuum envoronment is built. Reflectance, transmission and emissivity measurement at room pressure and moderate temperatures are routinely performed in support.

Piccioni G. Filacchione G. Capaccioni F. Capria M. T. Cerroni P. De Sanctis M. C. Magni G. Stefani S. Zambelli M. Adriani A. Bellucci G. Boccaccini A. Coradini A. Grassi D. Nuccilli F. Palomba E. Tosi F. Turrini D. Fonti S. Poulet F. Berthé M. Bibring J. P. Eng P. Langevin Y. Nathues A. Titov D. Battistelli E. Calamai L. McCord T. Jaumann R. Helbert J. Sanchez-Lavega A. Debei S. Arnold G. Blaney D. Carlson R. Drossart P. Reuter D. Bolton S. Irwin P.
The Visible and Infrared Hyperspectral Imaging Spectrometer (VIRHIS): A Study for the EJSM Mission **[#1328]**
VIRHIS on JGO is an advanced imaging spectrometer in the 0.4-5.2 microns range. It is perfectly suitable to obtain a comprehensive picture of the Jupiter system by combining information of the surfaces of the Galilean satellites, the Jupiter's atmosphere, and other targets.

Mandrake L. Thompson D. R. Gilmore M. Castaño R.
Hii-HAT: An IDL/ENVI Toolkit for Rapid Hyperspectral Inquiry **[#1441]**
The Hii-HAT (Hyperspectral Image Interactive Helper and Analysis Tools) toolset in ENVI utilizes the novel superpixel concept to augment endmember discovery, mineral map formation, and automated neutral spectrum discovery in hyperspectral imagery.

Helbert J. Maturilli A. D'Amore M.
High-Temperature Emission Spectroscopy — The Planetary Emissivity Laboratory (PEL) at DLR Berlin **[#1502]**
After three years of intensive planning and a setup period of more than one year the PEL is close to completion. It will allow unique measurements with a strong focus on airless bodies and extreme conditions as for example BepiColombo and MESSENGER will encounter at Mercury.

Grunthaner P. J.   Bryson C.   DeFlores L.   Gill D.   Grunthaner F. J.   Kelly M.   Quinn R.   Taylor C. L.   White V.
Ambient-Pressure X-Ray Photoemission Spectrometer for Chemical Analysis of Planetary Surfaces **[#1914]**
Ambient-pressure XPS probes the surface chemistry of a rock/soil sample, including the atmospheric species interacting with the surface. It provides quantitative information on all elements, including the chemical state of each element (except H).

Reedy R. C.
Backgrounds in Bismuth Germanate (BGO) Gamma-Ray Spectrometers in Space **[#1917]**
The peaks from backgrounds in BGO detectors used as a main detector or from BGO in a main Ge detector were studied using space and laboratory measurements. Both prompt reactions and the decay of radionuclides make background peaks.

Chanover N. J.   Glenar D. A.   Voelz D.   Xiao X.   Tawalbeh R.   Boston P.   Brinckerhoff W.
Mahaffy P.   Getty S.
An AOTF-LDTOF Spectrometer Suite for In Situ Organic Detection and Characterization **[#1943]**
We discuss the development of a miniature near-infrared point spectrometer, operating from 2–4 µm, based on AOTF technology. It is paired with a laser desorption time-of-flight mass spectrometer for volatile or refractory organics detection.

Wang A.   Freeman J. J.   Sobron P.   Lambert J.
A Miniaturized Near Infrared Instrument for Detecting H_2O/OH, Sulfates, Carbonates and Organic Species During Planetary Surface Explorations **[#2018]**
We report the basic parameters of a newly developed miniaturized NIR sensor. It is small, light, robust, yet can provide rich science information for future planetary surface exploration missions to Mars, Moon, and asteroids.

Chemtob S. M.   Glotch T. D.   Rossman G. R.
ATR-IR Spectroscopy for In Situ Mineral Analysis on Planetary Surfaces: Steps Toward a Forward Model **[#2198]**
Attenuated total reflectance (ATR) is an FTIR method that has potential as a tool for quantitative mineralogy on future lander missions. We present new ATR spectra of silicates and initial efforts towards a forward model for ATR of mineral mixtures.

Bhartia R.   Fries M. D.   Hug W. H.   Reid R. D.   Beegle L. W.   Allwood A.   Lane A. L.
Salas E. C.   Nealson K. H.
Deep UV Native Fluorescence and Resonance Raman Imaging Spectroscopy for In-Situ Organic Detection **[#2674]**
Non invasive detection of organics utilizing optical methods has been limited. New laser technology in the deep UV enables enhanced detection capabilities for trace organics on surfaces by combining resonance Raman scattering and native fluorescence spectroscopic methods.

Glass B.   Thompson S.   Paulsen G.   Lee P.
Planetary Drill Concept Tests at Haughton Crater **[#2709]**
Field test results in a relevant planetary analog site are presented for 2009 tests of a conceptual planetary sampling rotary-percussive drill.

Zacny K.   Paulsen G.   Szczesiak M.   Glass B.   McKay C.   Santoro C.   Wilson J.   Craft J.
Rotary-Percussive Drill for Planetary Exploration and a 3.5 m Vacuum Chamber Enabling Full Scale Testing **[#2115]**
We present a 1-meter-class rotary-percussive drill and test results comparing rotary and rotary-percussive drilling in various formations. A 3.5-m large vacuum chamber build for testing drill systems to a depth of >1 m is also presented.

ElShafie A.   Chevrier V. F.   Ulrich R.   Roe L.
Penetration Testing in Martian Analog Material **[#1293]**
Penetration forces for different probes have been measured in different martian analog materials which enhances the required knowledge of the masses of the rovers or landers.

Schibler P.   Lognonne P.   de Raucourt S.
Planetary Protection Policy Applied to Planetary Seismometers Development **[#1165]**
The development of planetary seismometers must fulfill planetary protection requirements. COSPAR gives recommendations classified in five categories. The general approach to planetary protection compliance is to be defined at the very beginning.

Ciarletti V.   Clifford S. M.   Plettemeier D.   Corbell C.   Biancheri-Astier M.
The NetStation GPR: Lander- and Network-based 3-D Investigations of Subsurface Structure, Stratigraphy, and Volatile Distribution in Near- and Deep-Subsurface Planetary Environments **[#1518]**
The NetStation GPR is a stationary, impulse, multiband HF GPR, designed to conduct geologic and volatile-related investigations of planetary environments in both the near- and deep-subsurface, whether from a lander or geophysical network.

Kirby J. P.   Halabian S.   Kanik I.   Beegle L. W.   Roark S.   Lasnik J.   Soto J.
Automated Sample Handling and Processing on Future Mars Missions **[#2153]**
We report on the development of an Automated Sample Processing System that takes samples, extracts organics through solvent extraction, removing non-organic soluble species that are interferences and moves sample to multiple instruments for analysis.

Dreyer C. B.   Zacny K.   Anderson R. C.   Skok J.   Steele J.   Paulsen G.   Szczesiak M.   Schwendeman J.
A Rock Thin Section Device for Space Exploration **[#2573]**
The petrographic instrument, along with mobility, would result in the collection of a diversity of samples required to answer a very large number of scientific questions about many of the planetary bodies of current and future scientific interest.

Young K. E.   Hodges K. V.   Schmitt H. H.   Ford K. M.
Developing Advanced SmartTools for Advanced Planetary Field Geology **[#1918]**
We develop advanced “SmartTools” for planetary field geology, which will first be tested and implemented in terrestrial fieldwork. One tool is the “SmartStaff”, which could provide stability and situational awareness to astronauts on planetary surfaces.

Millar P. S.   Clark P. E.   Yeh P. S.   Cooper L.   Beaman B.   Feng S.   Ku J.   Young E. M.   Johnson M. A.
Technologically Optimized Science Packages for Planetary Surfaces **[#1253]**
Our optimized instrument package concept incorporates ultra low temperature/ultra low power electronics, low voltage power supplies, and distributed power systems to meet the challenges of operating on atmosphereless planetary surfaces.

Iwata T.   Imai K.   Misawa H.   Noda H.   Kondo T.   Nakajo T.   Takeuchi H.   Kumamoto A.   Tsuchiya F.   Nariyuki Y.   Asari K.   Kawano N.
A Study on the Moon-Earth Baseline Interferometry for Jovian Low Frequency Radio Observation **[#1677]**
Lunar Low Frequency Astronomy Telescope (LLFAST) is the Moon-Earth baseline interferometry which is a candidate mission instrument of Japan’s lunar explorer SELENE-2. It will shed light on the mechanism of Jovian radio sources.

Medley S. K.   Gregory D. A.   Sampson A. R.   Gaskin J. A.
Optimization of a Cold Field Emission Electron Gun for a Miniaturized Scanning Electron Microscope **[#2676]**
The field emission and the effects of aberrations of an electron gun will be examined, through simulations and testing of a prototype, to optimize the gun for a miniaturized scanning electron microscope.

Becker L.   Antione M.   Cornish T.   Pinnick V.   Cotter R.
The Search for Life on Mars Using the Mars Organic Molecule Analyzer “MOMA” **[#2345]**
Mars Organic Molecule Analyzer ‘MOMA’ combines Gas Chromatography (GC) and Laser Desorption (LD) to form ‘intact organic compounds that are mass analyzed using an Ion-Trap Mass Spectrometer (ITMS.

Scheld D. Marshall J. Mason L. Thompson P.
An Acoustic Particle Size Analyzer for Planetary Surfaces **[#1916]**
An acoustic method of determining the size of loose particles has been developed at the breadboard level. This is intended as a precursor to aflight instrument that can conduct grain-size analyses requiring no sample processing and handling.

Brinckerhoff W. B. Cornish T. J. Ecelberger S. A. Corrigan C. M. Ganesan A. L. Getty S. A. ten Kate I. L.
Advancement of a Compact Reflectron TOF-MS for Planetary Sample Analysis **[#2358]**
We present the status of our development of a miniature mass spectrometer for *in situ* planetary exploration. The spectrometer uses pulsed laser desorption and an advanced reflectron time-of-flight mass analyzer to detect elements and organics in solid samples.

Tomkinson T. Wolters S. D. Guthery B. W. Bohman A. F. Sund B. Sund A. T. Hagene J. K. Grady M. M.
Detection of Water and Magnesite with WATSEN: The Next Generation of Instrumentation for Mars **[#2719]**
Detection of water and magnesite with WATSEN: the next generation of instrumentation for Mars.

Anderson F. S. Nowicki K.
In-Situ Geochronometry: Improved LDRIMS Precision **[#1979]**
LDRIMS can now measure the isotope ratio of standards with 10 ppm net Sr to a precision of ±0.1%, with a sensitivity of $1:10^{10}$, in <15 minutes.

MISSION PLANS AND CONCEPTS

Benkhoff J.
The BepiColombo Mission to Explore Mercury **[#1743]**
BepiColombo is an ESA, JAXA interdisciplinary mission to explore the planet Mercury. Two spacecrafts, the Mercury Planetary Orbiter (MPO) and the Mercury Magnetospheric Orbiter (MMO), will be studying the planet and its environment and launched together in July 2014.

Balint T. S. Kerzhanovich V. V. Hall J. L. Baines K. H. Stephens S. K.
Four Aspects of a Venus Balloon Mission Concept **[#1301]**
Our poster explores four aspects of a typical Venus balloon mission concept using information design techniques, including a typical timeline; the atmospheric entry sequence; maps of the balloon's traverse path; and the material selection challenges.

Klaus K. Cook T. S. Smith D. B.
Small Body Landers for Near Earth Object Missions **[#1077]**
We are developing a small body lander product line that leverages the significant investments that have been made in the highly successful DARPA Orbital Express program.

Smith D. B. Klaus K. Caplin G. Elsperman M. S. Horsewood J.
Low Cost Multiple Near Earth Object Missions **[#1464]**
Our Commercial spacecraft are available with efficient high power solar arrays and hybrid propulsion systems (Chemical and Solar Electric) that make possible multiple Near Earth Object Missions within Discovery budget limits.

Ping J. S. Qian Z. H. Hong X. Y. Zheng W. M. Fung L. W. Liu Q. H. Zhang S. J. Shang K. Jian N. C. Shi X. Wang M. Y.
Brief Introduction About Chinese Martian Mission Yinghuo-1 **[#1060]**
The first Chinese Mars Probe Yinghuo-1 will explore the space weather of Mars.

Zhao H.
"Yinghuo-1"— Martian Space Environment Exploration Orbiter **[#1558]**
The first Chinese Mars orbiter, Yinghuo-1.

Chicarro A. F.
The European Robotic Exploration of the Planet Mars **[#1645]**
An overview of the European contribution to the new joint NASA-ESA Mars Exploration program will be given, in particular focusing on the 2016, 2018 and 2020 mission opportunities.

Foing B. H.   Barton A.   Blom J. K.   Mahapatra P.   Som S.   Jantscher B.   Page J.   Zegers T.   Stoker C.   Zavaleta J.   Poulakis P.   Visentin G.   Noroozi A.   Ehrenfreund P.   Mickolacjzak M.   Perrin A.   Chevrier S.   Direito S.   Dene A.   Voute S.   Olmedo A.   Groemer G.   Stumptner W.   Davies G.   van Westrenen W.   Koschny D.   Lebreton J. P.   Guglielmi M.   Freire M.   Walker R.   ILEWG ExoGeoLab Team N.   ILEWG Eifel Field Test Team N.
ExoGeoLab Lander, Rovers and Instruments: Tests at ESTEC & Eifel Volcanic Field **[#1701]**
We have built an ExoGeoLab lander demonstrator for future planetary missions, equipped with remotely operated instruments. We tested them at ESTEC and at an ILEWG field campaign at Eifel volcanic park in Germany in September 2009.

Ehrenfreund P.   Foing B. H.   Stoker C.   Zavaleta J.   Quinn R.   Blake D.   Martins Z.   Sephton M.   Becker L.   Orzechowska G.   van Sluis C.   Boche-Sauvan L.   Gross C.   Thiel C.   Wendt L.   Sarrazin P.   Mahapatra P.   Direito S.   Roling W.   EuroGeoMars MDRS Team
EuroGeoMars Field Campaign: Sample Analysis of Organic Matter and Minerals **[#1723]**
We report on the results of chemical, physical and astrobiological measurements of samples collected during the EuroGeoMars campaign at Utah Mars Desert Research Station (MDRS) in February 2009, as interdisciplinary preparation for a strategic search for life on Mars.

Hendrikse J.   Foing B. H.   Monaghan E.   Stoker C.   Zavaleta J.   Selch F.   Ehrenfreund P.   Wendt L.   Gross C.   Thiel C.   Peters S.   Borst A.   Sarrazin P.   Blake D.   Boche-Sauvan L.   Page J.   Pletser V.   Mahapatra P.   Wills D.   McKay C.   Davies G.   van Westrenen W.   Batenburg P.   Drijkoningen G.   Slob E.   Poulakis P.   Visentin G.   Noroozi A.   Gill E.   Guglielmi M.   Freire M.   Walker R.   ExoGeoLab Team   EuroGeoMars Team
Highlights from Remote Controlled Rover for EuroGeoMars MDRS Campaign **[#2435]**
The goal of the EuroGeoMars mission (from January 24 through February 28, 2009) was to validate a remote controlled rover for surface reconnaissance and extravehicular activity support and evaluate rover technical requirement for remote controlled reconnaissance from a habitat and *in situ* support.

Li R.   Wang W.   Tang M.   Tang P.   Coates A.   Muller J. P.   Griffiths A.   Paar G.   Oberst J.
ESA ExoMars Rover Localization and Topographic Mapping: Pre-Launch PanCam Modeling and Error Analysis **[#1819]**
This paper presents the concept of geometric modeling approaches for enhancing the localization and mapping capabilities of the ExoMars rover and advancing quantitative awareness of achievable accuracy.

Beaty D. W.   Allen C. C.
The Proposed Mars Astrobiology Explorer — Cacher [MAX-C] Rover: First Step in a Potential Sample Return Campaign **[#2571]**
The proposed MAX-C mission would be capable of yielding exciting *in situ* mission results in its own right as well as making significant feed-forward contributions to sample return, likely becoming the first step in a potential sample return campaign.

Feldman S. M.   Allwood A. C.   MEPAG Mid-Range Rover Science Analysis Group
Science Investigation Approach for the Proposed 2018 Mars Astrobiology Explorer–Cacher [MAX-C] Rover **[#2384]**
This poster presents a scientific measurement approach for the Mars Astrobiology Explorer-Cacher (MAX-C), a mission concept for the Mars 2018 launch opportunity, formulated by the MEPAG Mid-Range Rover Science Advisory Group (MRR-SAG).

Titus T. N.   Prettyman T. H.   Brown A.   Michaels T. I.   Colaprete A.
Mars Ice Condensation and Density Orbiter **[#1151]**
The Mars Ice Condensation and Density Obiter (MICADO) is meant to be relatively inexpensive and lightweight discovery-class mission. MICADO will have the capability to monitor the deposition of Mars seasonal ice and determine ice densities.

Billingsley L. J.   Miller D. P.
A Robotic Mission to Study Wet Gullies on Mars **[#1684]**
This poster will concentrate on the mobility requirements of a Mars rover, to make it from a safe landing area to a gully site appropriate for geological study.

Lee P.   Veverka J.   Bellerose J.   Boucher M.   Boynton J.   Braham S.   Gellert R.   Hildebrand A.   Manzella D.   Mungas G.   Oleson S.   Richards R.   Thomas P. C.   West M. D.
Hall: A Phobos and Deimos Sample Return Mission **[#1633]**
Hall is a proposed NASA-led New Frontiers-class international robotic lander and sample return mission to explore and return samples from the two moons of Mars, Phobos and Deimos.

McEwen A.   Turtle E.   Keszthelyi L.   Spencer J.   Thomas N.   Wurz P.   Christensen P.   Khurana K.   Glassmeier K.-H.   Auster U.   Furfaro R.   Davies A.   Nimmo F.   Moses J.   Bagenal F.   Kirk R.   Wieser M.   Barabash S.   Paranicus C.   Lorenz R.   Anderson B.   Showman A.   Sandel B.
Science Rationale for an Io Volcano Observer (IVO) Mission **[#1433]**
The IVO Discovery mission could provide detailed understanding of Io's currently active volcanism, the melt state of the mantle, tidal heating mechanism, tectonics, mass loss processes, and potential internal magnetic field.

Stofan E. R.   Lunine J. I.   Lorenz R. D.   Aharonson O.   Bierhaus E.   Clark B.   Griffith C.   Harri A-M.   Karkoschka E.   Kirk R.   Kantsiper B.   Mahaffy P.   Newman C.   Ravine M.   Trainer M.   Waite H.   Zarnecki J.
Exploring the Seas of Titan: The Titan Mare Explorer (TiME) Mission **[#1236]**
The Titan Mare Explorer (TiME) is a Discovery-class mission that would constrain Titan's active methane cycle as well as its intriguing prebiotic organic chemistry by providing *in situ* measurements from the surface of a Titan sea.

Epperly M. E.   Waite J. H.   Brockwell T. G.   Cronenberger J. O.   Klaus K. K.   Grayson G.
Titan Submersible Explorer —The Case for Subsurface Sampling of Titanian Lakes **[#1720]**
A team, led by Southwest Research Institute, has developed a mission concept to sample and analyze material from the bottom of Titan's lake. This poster and paper present the science and the feasibility of a submersible explorer concept.

Barnes J. W.   McKay C.   Lemke L.   Beyer R. A.   Radebaugh J.   Atkinson D.
AVIATR: Aerial Vehicle for In-Situ and Airborne Titan Reconnaissance **[#2551]**
This poster presents the scientific, engineering, and programmatic rationale behind a Titan airplane concept, AVIATR. The vehicle would explore Titan's geologic and lower atmospheric diversity over the course of a 1-year nominal mission.

Smith R. M.   Yozwiak A. W.   Lederer A. P.   Turtle E. P.
HORUS — Herschel Orbital Reconnaissance of the Uranian System **[#2471]**
A mission concept study of the uranian system is explored under the constraints of the NASA New Frontiers program. The study was designed and led by student interns at the Johns Hopkins University Applied Physics Laboratory.

Asphaug E.   Barucci A.   Belton M.   Bhaskaran S.   Brownlee D.   Carter L.   Castillo J.   Chesley S.   Chodas P.   Farnham T.   Gaskell R.   Gim Y.   Heggy E.   Klaasen K.   Kofman W.   Kreslavsky M.   Lisse C.   McFadden L.   Pettinelli E.   Plaut J.   Scheeres D.   Turtle E.   Weissman P.   Wu R.
Deep Interior Radar Imaging of Comets **[#2670]**
Deep Interior is a comet rendezvous mission using a high heritage planetary sounding radar to derive a high definition image of the global interior.

Klaus K.   Smith D. B.   Kaplan M. S.
Outer Planet Science Missions Enabled by Solar Power **[#1076]**
Our studies demonstrate that New Frontiers-class science missions to the Jupiter and Saturn systems are possible with commercial solar-powered spacecraft. A new solar array technology will be developed and demonstrated by DARPA that will provide even higher power.

Sollitt L. S.   Vilas F.
The Atsa Suborbital Observatory: Using Crewed Suborbital Spacecraft for a Low-Cost Space-Borne Telescope **[#2011]**
We discuss a human-tended suborbital flight program supporting NIR observations, suitable for a variety of solar system targets.

Blome H.-J.   Wilson T. L.
Cosmological Effects in Planetary Science **[#1019]**
Cosmological terms appearing in the local dynamics of planetary systems are examined for Friedmann-Lemaitre cosmologies. These are related to known spacecraft anomalies using the Hubble parameter and the deceleration parameter of Big Bang cosmology.

EDUCATION AND PUBLIC OUTREACH: MISSION PLANS AND CONCEPTS

Benfield M. P. J.   Turner M. W.   Runyon C. J.   Hakkila J.
The New Frontiers Academic AO Experiment **[#1986]**
The University of Alabama in Huntsville and the College of Charleston have embarked on an educational experiment called the Academic AO Project. This project seeks to simulate the NASA Announcement of Opportunity response process in the classroom.

Turner M. W.   Benfield M. P. J.   Runyon C. J.   Hakkila J.
The Mars Sample Return Integrated Product Team Academic Experiment **[#2009]**
The University of Alabama in Huntsville and the College of Charleston have embarked on an educational experiment called the Mars Sample Return Mission. This project seeks to simulate real-world engineering and science design and collaboration in the classroom.

DATA AND IMAGE SYSTEMS: PDS, GIS, WEB TOOLS, ETC.

Kirk R. L.   Becker T. L.   Garcia P.   Barrett J. M.   Stiles B. W.   LeGall A.   Janssen M. A.   Wye L.   Zebker H. A.   Cassini RADAR Science Team
Digital Map Products from the Cassini RADAR in the NASA Planetary Data System **[#2414]**
A new set of Titan maps, made from Cassini RADAR prime mission data, will be delivered early in 2010. Consistent presentation of diverse data sets in simple projections with extensive indexing should greatly facilitate comparative Titan research.

Kawamae W.   Hirata N.   Kitazato K.   Asada N.   Demura H.   Ogawa Y.   Honda C.   Terazono J. T.
Development of 3D Web-based Data Archive for Hayabusa Mission **[#1687]**
Data archive with more interactive interface for searching the data of Hayabusa mission is desired. The three-dimensional model allows users to search the specific area data of irregular shape body.

Hargitai H.
Mars Climate Zone Map Based on TES Data **[#1199]**
The abstract describes an experiment to construct a climate zone map of Mars, based on MGS TES and other datasets.

Wulf G.   van Gasselt S.   Walter S.   Neukum G.
Assessment of GIS-based Photometric Treatment of Planetary Image Data (HRSC) **[#2159]**
Photometric correction routines of planetary image data are developed and implemented using the ArcGIS framework with which the assessment, quantification and correction of photometric effects can be improved in an efficient way on an end-user level.

Stein T. C.   Arvidson R. E.   Heet T. L.   Wang J.
PDS Analyst's Notebook: Enriching Planetary Data Archives by Integrating Mission Data and Documents **[#1414]**
The PDS Analyst's Notebook (http://an.rsl.wustl.edu) provides access to the Mars Exploration Rover (MER), Mars Phoenix Lander, and Lunar Apollo surface mission data archives. In addition, a Notebook is being developed for the LCROSS mission.

Wang J.   Bennett K. J.   Scholes D. M.   Ward J. G.   Slavney S.   Guinness E. A.   Arvidson R. E.
Updates to the Orbital Data Explorer from the PDS Geosciences Node **[#2251]**
This abstract introduces WebGIS and map updates of NASA's PDS Geosciences Node's Orbital Data Explorer (ODE) for web-based orbital data search and download. Additional updates to support LRO data sets are also mentioned.

van Gasselt S.   Nass A.   Neukum G.
Data Infrastructure Requirements and Conceptual Database Model for Conducting and Organizing Geological and Geomorphological Mapping **[#2433]**
We here report on the logical and conceptual design of a geo-database-model implemented within a GIS framework for conducting and organizing geoscientific mapping.

Nass A.   van Gasselt S.   Jaumann R.   Asche H.
Developments in Planetary Mapping: GIS-based Implementation of International Standards for Digital Geological and Geomorphological Mapping **[#2383]**
We here report on current work focussing on the generation of a data model for geoscientific mapping with special emphasis on the implementation of international standards for symbolization.

Garcia P. A.   Isbell C. E.   Barrett J. M.   Gaddis L. R.
PDS Map-A-Planet Cartographic Web Services: The Latest Updates **[#2669]**
The NASA Planetary Data System (PDS) Map-A-Planet Web Service is a web-based data delivery system (mapaplanet.org) that serves a variety of digital cartographic map products. Here we describe MAP capabilities and data, and recent updates to both.

Akins S.   Raub R.   Hare T.   Blue J.
Web Feature Service for Planetary Nomenclature **[#1434]**
New technologies in the planetary nomenclature website.

EDUCATION AND PUBLIC OUTREACH: PROFESSIONAL DEVELOPMENT

Shipp S.   Dalton H.   CoBabe-Ammann E.   Wessen A.   Boonstra D.   Ristvey J.   Mackety D.
Get Involved in Planetary Science Education and Public Outreach **[#2318]**
The Planetary Science Education and Public Outreach (E/PO) Forum's role is to engage, support, and extend the community of E/PO professionals and scientists involved in planetary science education activities.

Shupla C.   Shipp S.   Asti P.   Bailey J.   Chambers L.   Pomeroy J.   Schultz G.   Slater T.   Slater S.   Smith D.   Stork D.   Waller W.
Institutes for Faculty Instructing Future Teachers **[#2281]**
A collaboration of scientists and educators have created two-day institutes for education and science faculty instructing future teachers: Faculty Institute for NASA Earth and Space Science Education (FINESSE).

Lebofsky L. A.   Anderson S. W.   Bleamaster L. F.   Canizo T. L.   Croft S. K.   Crown D. A.
Kortenkamp S.   Pierazzo E.
Professional Development Workshops for K–8 Teachers at the Planetary Science Institute **[#1192]**
The Planetary Science Institute offers professional development workshops for elementary and middle school teachers in Tucson, Arizona. These workshops provide teachers with in-depth content knowledge in astronomy, geology, and planetary science.

Cañizo T. L.   Anderson S. W.   Bleamaster L. F. III   Crown D. A.   Lebofsky L. A.
Evaluation Strategies for Professional Development Workshops for K–8 Teachers at the Planetary Science Institute **[#1164]**
The Planetary Science Institute, along with the Tucson Regional Science Center, offers professional development workshops for K–8 teachers in Tucson (AZ). This presentation discusses formative and summative evaluation strategies employed to assess our workshops.

STARDUST MISSION TO COMET WILD 2
Wednesday, 8:30 a.m. Waterway Ballroom 1

Chairs: **Hope Ishii and Andrew Westphal**

8:30 a.m. Brownlee D. E. * Joswiak D. Matrajt G. Ramien N. Bradley J. Ishii H. Westphall A. J. Gainforth Z.
The Nature of Moderately Fragmenting Comet Dust: Case Studies of Tracks 25 (Inti) and Track 77 **[#2146]**
TEM studies of 36 fragments from SD tracks 77 and Inti provide insight into moderately fragmenting comet dust. T77 fragments are chondrule derived while the Inti impactor was a mix of ~3-µm CAI nodules individually wrapped with 0.5-µm diopside rims.

8:45 a.m. Ishii H. A. * Stadermann F. J. Floss C. Joswiak D. Bradley J. P. Teslich N. Brownlee D. E. Matrajt G. MacPherson G. McKeegan K. D.
Lack of Evidence for In Situ Decay of Aluminum-26 in Comet 81P/Wild 2 CAI-like Refractory Particles 'Inti' and 'Coki' **[#2317]**
The comet 81P/Wild 2 CAI-like particles "Inti" and "Coki" show no evidence for initial ^{26}Al in TEM sections stabilized for NanoSIMS measurements by FIB. Implications for CAI history prior to incorporation in the comet are presented.

9:00 a.m. Joswiak D. J. * Brownlee D. E. Matrajt G. Messenger S. M. Ito M.
Stardust Track 130 Terminal Particle: Possible Al-rich Chondrule Fragment or Altered Amoeboid Olivine Aggregate **[#2119]**
The terminal particle from track 130 is composed of the refractory mineral assemblage Mg-rich olivine, Al- and Ti- bearing augite and anorthite and may be a fragment from an Al-rich chondrule or amoeboid olivine aggregate (altered).

9:15 a.m. Bridges J. C. * Changela H. G.
Refractory Chondrule Fragments with Carbonaceous Chondrite Affinities in Comet 81P/Wild2 **[#2058]**
Track #154 of Comet Wild 2 contains a refractory, 7–16 wt% Al_2O_3 Al-diopside (+ Fo, En) terminal grain. It is similar to a fragment of an Al-diopside rich chondrule from C-chondrites and is distinct from CAI refractory pyroxene.

9:30 a.m. Butterworth A. L. * Gainsforth Z. Bauville A. Bonal L. Brownlee D. E. Fakra S. C. Huss G. R. Joswiak D. Kunz M. Marcus M. A. Nagashima K. Ogliore R. C. Tamura N. Telus M. Tyliszczak T. Westphal A. J.
A Type IIA Chondrule Fragment from Comet 81P/Wild 2 in Stardust Track C2052,2,74 **[#2446]**
Coordinated analyses on a terminal particle, named Iris, from Stardust sample C2052,2,74, found it to be consistent with Type IIA chondrules. Methodologies used were in-aerogel XRF and Fe-XANES, followed by ultramicrotomy, STXM and TEM.

9:45 a.m. Stodolna J. * Jacob D. Leroux H.
Mineralogy of Stardust Track 80: Evidences for Aqueous Alteration and Igneous Process **[#1657]**
We report a TEM examination of a compressed wall piece from track 80. The sample shows a high variability of minerals from highly reduced silicates to oxidized components such as Fe-rich olivine, ulvöspinel and magnetite.

10:00 a.m. Wozniakiewicz P. J. * Ishii H. A. Kearsley A. T. Burchell M. J. Bradley J. P. Teslich N. Cole M. J.
Survivability of Cometary Phyllosilicates in Stardust Collections and Implications for the Nature of Comets **[#2357]**
In response to the recent report of phyllosilicates in comet 9P/Tempel 1, we explored survivability and alteration of phyllosilicates under Stardust hypervelocity collection conditions for comet 81P/Wild 2 dust and discuss the implications.

10:15 a.m. Westphal A. J. * Allen C. Bajt S. Bastien R. Bechtel H. Bleuet P. Borg J. Brenker F. Bridges J. Brownlee D. E. Burchell M. Burghammer M. Butterworth A. L. Cloetens P. Cody G. Ferroir T. Floss C. Flynn G. J. Frank D. Gainsforth Z. Grün E. Hoppe P. Hudson B. Kearsley A. Lai B. Lemelle L. Leroux H. Lettieri R. Marchant W. Nanz A. Nittler L. R. Ogliore R. Postberg F. Sandford S. A. Schmitz S. Silversmit G. Simionovici A. Srama R. Stadermann F. Stephan T. Stroud R. M. Susini J. Sutton S. Toucoulou R. Trieloff M. Tsou P. Tsuchiyama A. Tyliczszak T. Vekemans B. Vincze L. Warren J. Wagner S. Zevin D. Zolensky M. E. Stardust@home Dusters
Analysis of "Midnight" Tracks in the Stardust Interstellar Dust Collector: Possible Discovery of a Contemporary Interstellar Dust Grain **[#2050]**
We report on the results of analyses by synchrotron X-ray microprobe of four "midnight" tracks extracted from the Stardust Interstellar Collector. One particle is a candidate to be the first contemporary interstellar dust particle ever identified.

10:30 a.m. Leroux H. * Kearsley A. T. Troadec D.
Mineralogy of Wild 2 Residues in Micron-sized Craters from the STARDUST Al-Foils **[#1621]**
Electron transparent sections of micron-sized craters residues from Al-foils of Stardust were investigated by TEM. We show that impactors were multicomponent aggregates, mainly composed of crystalline material.

10:45 a.m. Stroud R. M. * Koch I. M. Bassim N. D. Piccard Y. N. Nittler L. R.
Structure and Composition of Comet Wild 2 Residues in Sub-Micron to Micron-Sized Craters **[#1792]**
We report on 89 new micrometer-sized and smaller craters that we identified by automated SEM mapping, and TEM analysis of cross-sections from 6 of these craters.

11:00 a.m. Leitner J. * Hoppe P. Heck P. R.
First Discovery of Presolar Material of Possible Supernova Origin in Impact Residues from Comet 81P/Wild 2 **[#1607]**
The oxygen isotopic compositions of cometary dust particles from 81P/Wild 2 have been analyzed by NanoSIMS in impact residues of 169 small impact craters (d<2µm) on Stardust Al foil C2037N. One ^{18}O-rich presolar signature has been detected.

11:15 a.m. Kearsley A. T. * Burchell M. J. Price M. C. Green S. F. Franchi I. A. Bridges J. C. Starkey N. Cole M. J.
Distinctive Impact Craters are Formed by Organic-rich Cometary Dust Grains **[#1435]**
Experimental impacts of organic-rich dust grains, fired at the Stardust-Wild 2 encounter velocity of 6 km/s, produce a distinctive surface texture in craters on Al foil, and leave a detectable light-element (C, N, O) trace from the impactor.

11:30 a.m. Fries M. * Steele A.
Comet 81P/Wild-2 Carbon — An Extraordinarily Diverse Suite of Materials **[#1083]**
Raman measurements of Comet 81P/Wild-2 particles reveal an extraordinary range of structure and chemistry consistent with formation and metamorphism of those materials under a similarly broad range of conditions.

EXPLORING THE MARTIAN CRUST: GEOLOGY, MINERALOGY, AND GEOCHEMISTRY
Wednesday, 8:30 a.m. Waterway Ballroom 4

Chairs: **Melissa Lane and William Farrand**

8:30 a.m. Squyres S. W. * Athena Science Team
Recent Scientific Results from Opportunity's Traverse Toward Endeavour Crater, Meridiani Planum, Mars **[#1757]**
This abstract provides an overview of the key scientific findings from the last year of operations of the Mars Exploration Rover Opportunity.

8:45 a.m. Crumpler L. * Arvidson R. Squyres S. Yingst A. McCoy T. DesMarais D. Cabrol N. Schröder C. Cohen B. Rice J. Jr. Ruff S. Morris R. Yen A. McEwen A. deSouza P. Athena Science Team
Overview of the Field Geologic Context of Mars Exploration Rover Spirit, Home Plate and Surroundings **[#2557]**
This work provides field context for APXS, MB, MI results of Spirit at Home Plate. High silica /sulfates, nanophase iron oxides, and hematite occur mostly in the lowest stratigraphic unit exposed along the axis of breached antiformal bedding.

9:00 a.m. McSween H. Y. *
Martian Rock and Soil Compositions from Orbit and the Ground: Why Can't We All Just Get Along? **[#1105]**
Chemical compositions of soils and alteration rinds on rocks are distinct from TES orbital data. Reconciling analyses of Mars surface materials from different techniques and at different scales is problematic.

9:15 a.m. Clark B. C. * Gellert R. Morris R. V. Ming D. W. Yen A. Arvidson R. E. Economou T.
The Enigmatic Global Martian Soil: Compositional Evidence from MER, Phoenix, Viking, MPF, MGS and Odyssey **[#1419]**
The existence of a global soil unit on Mars hinges on element profiles from five landers. Orbital and *in situ* data, including Phoenix, combine to explain the shortfall in Viking compositions, explicable as carbonate, H_2O, and minor elements.

9:30 a.m. Lane M. D. * Goodrich C. A.
High-Magnesian Olivine in the Argyre Rim: Derived from a Primitive Magma? **[#2094]**
High-Mg olivine (Fo80–90) units are mapped within the Argyre basin as part of an eroded annulus (uplifted basin rim). This high-Mg olivine, plus other minerals present, may represent primitive martian mantle-derived material similar to Y-980459.

9:45 a.m. Hamilton V. E. * McDowell M. L. Koeppen W. C.
Correlations Between Olivine Abundance and Thermal Inertia: Implications for Global Weathering and/or Alteration on Mars **[#2239]**
TES data show no global trend between thermal inertia and olivine abundance. But it is premature to conclude that all dark surfaces were once more mafic OR that olivine is not preferentially removed from olivine-enriched outcrops as they erode.

10:00 a.m. Howard D. A. * McSween H. Y.
Supporting Evidence for an Ultramafic Component of the Martian Crust **[#1679]**
Here we show that the recent CRISM spectrally derived ultramafic mineralogy in the Nili Fossae region is supported by THEMIS IR although the previously proposed mineral assemblage is not unique and the spectra can be matched without Mg-carbonate.

10:15 a.m. Ehlmann B. L. * Mustard J. F. Murchie S. L.
Geologic Setting of Serpentine Deposits on Mars **[#2235]**
Analyses of CRISM, HiRISE, and CTX data acquired to date show serpentine deposits on Mars are small, rare, and restricted to Noachian terrains. We detail the distribution of serpentine and the three distinct geologic settings in which it is found.

10:30 a.m. Skok J. R. * Mustard J. F. Tornabene L. L. Isaacson P. Murchie S. L.
Crystalline Igneous Crust of Mars: New Insights from the Southern Highlands **[#1926]**
High-resolution analysis of excavated mafic minerals from southern highland crater central peaks to constrain the formation of the primary crust of Mars.

10:45 a.m. Mittlefehldt D. W. * Gellert R. Herkenhoff K. E. Morris R. V. Clark B. C. Cohen B. A. Fleischer I. Jolliff B. L. Klingelhöfer G. Ming D. W. Yingst R. A. Athena Science Team
Marquette Island: A Distinct Mafic Lithology Discovered by Opportunity **[#2109]**
We will discuss the results of *in situ* investigation of a unique martian mafic lithology discovered by Opportunity on Meridiani Planum. You will be impressed.

11:00 a.m. Farrand W. H. * Lane M. D. Edwards B. R.
Analysis of Olivine and Augite Bearing Materials and Ice-related Features Found in Association with Domes on the Northern Plains of Mars **[#1965]**
CRISM and HiRISE data covering domes in western Arcadia and Utopia Planitiae were analyzed. MGM analysis indicates the presence of augite and Fe-rich olivine. Light-toned areas around the domes display a “brain terrain” morphology associated with the presence of ice.

11:15 a.m. Mustard J. F. * Ehlmann B. L.
Intact Stratigraphy Traversing the Phyllosilicate to Sulfate Eras at the Syrtis-Isidis Contact, Mars **[#2070]**
We analyze an intact stratigraphic section that captures the transition from early Mars where (alteration mineralogy dominated by phyllosilicate) to middle Mars (hydrous mineralogy is dominated by sulfates) where Syrtis lavas enter the Isidis Basin.

11:30 a.m. Hahn B. C. * McLennan S. M.
Regional Martian Crustal Heat Flow from Mars Odyssey Gamma-Ray Spectrometry **[#1371]**
Using radiogenic elemental abundances derived from Gamma-Ray Spectrometer (GRS) observations, we estimate the crustal component of martian heat flow for specific geologic features and regions, both present day and at the time of formation.

PLANETARY DYNAMICS AND TECTONICS
Wednesday, 8:30 a.m. Waterway Ballroom 5

Chairs: Andrew Dombard and Scott King

8:30 a.m. Roberts J. H. * Barnouin O. S.
The Effect of the Caloris Impact on the Mantle Dynamics of Mercury **[#1266]**
We investigate links between the Caloris impact, the volcanism within and surrounding the basin, and effects on Mercury’s dynamo. A Caloris-forming impact at expected velocities cannot significantly heat the core, and should not affect the dynamo.

8:45 a.m. Dombard A. J. * Phillips R. J.
Viscoelastic Finite-Element Simulations of the Flexure Under the North Polar Cap of Mars **[#1865]**
The thick lithosphere may be explained if the mantle and crust are subchondritic and if there is a strong depletion of heat-producing elements in the mantle, possibly a result of the formation of the crustal dichotomy via a giant impact.

9:00 a.m. Hood L. L. * Kiefer W. S. Langlais B.
Parallel Modeling of the Apollinaris Patera Magnetic and Gravity Anomalies **[#2006]**
Modeling of the A.P. magnetic anomaly is conducted to investigate whether a secondary concentration of magnetization exists at the construct itself. The gravity anomaly modeling is intended to investigate whether a significant buried load is implied.

9:15 a.m. Nahm A. L. * Schultz R. A.
A Test of Global Contraction Models for Mars Using Observations **[#2086]**
Based on observations of surface faults, we show that there is no evidence for a significant episode of global contraction on Mars. The amount of global contraction predicted by thermal models is larger than what is recorded by the surface faults.

9:30 a.m. King S. D. *
More Speculation on the Origin of Tharsis Rise **[#2007]**
Using three-dimensional temperature-dependent convection calculations I show how Tharsis might have formed as a result of small-scale convection at a step in lithosphere thickness.

9:45 a.m. Šrámek O. * Zhong S. J.
Link Between Tharsis and the Hemispheric Dichotomy — Testing the Model of Rotation of Lithosphere for Mars **[#2636]**
We present a series of models to test the "rotation of the lithosphere" hypothesis of Zhong (2009 Nature Geosci.) that links the evolution of Tharsis to the hemispheric dichotomy on Mars.

10:00 a.m. Bland M. T. * McKinnon W. B.
Folding on Europa: Clues to the Mechanical Behavior of Ice Lithospheres **[#2298]**
Models of folding of Europa's lithosphere indicate that producing even low-amplitude folds (~200 m) requires large strains (5–10%), larger than those previously assumed. Thus, large contractional strains may be hidden in low-amplitude deformation.

10:15 a.m. Han L. * Showman A. P.
Coupled Convection and Tidal Dissipation in Europa's Ice Shell: 2. Non-Newtonian Viscosity **[#1318]**
We present fully coupled simulation of convection and tidal heating to understand the impacts of non-Newtonian rheology on convection and tidal heating.

10:30 a.m. Schenk P. *
The Timing of Viscous Relaxation on Ganymede **[#2083]**
Mapping of the distribution of relaxed and unrelaxed craters on Ganymede show a distinct spatial pattern. Implications for Ganymede's thermal history will be discussed .

10:45 a.m. Hurford T. A. * Helfenstein P. Spencer J. R. Nimmo F.
Using CIRS Data to Constrain Enceladus' Libration State **[#1771]**
The mismatch between the theory of tidal shear heating and the observations of heat on Enceladus may be due to the neglect of physical librations. Here we fit the observed emitted power along the tiger stripes with a model of tidal shear heating.

11:00 a.m. Paganelli F. * Pappalardo R. Schubert G. Stiles B. Collins G. C. Mitchell K. Stofan E.
Preliminary Analysis of Structural Elements of Titan and Implications for Stress **[#2664]**
Titan possesses subtle but distinctive structural geological features. We use Cassini's synthetic aperture radar (SAR), HiSAR (a high-altitude single beam imaging mode), and SARTopo data of Titan with emphasis on the structural interpretation of tectonic elements.

11:15 a.m. Nimmo F. * Bills B. G.
Shell Thickness Variations and the Long Wavelength Topography of Titan **[#1068]**
Titan's global shape and gravity can be explained by shell thickness variations arising from tidal heating in a conductive ice shell.

11:30 a.m. Mitri G. * Pappalardo R. T. Stevenson D. J.
Evolution and Interior Structure of Titan **[#2229]**
We model the accretion, evolution and interior structure of Titan, using the gravity data as constraints.

NATURE OF THE LUNAR REGOLITH
Wednesday, 8:30 a.m. Waterway Ballroom 6

Chairs: Joshua Bandfield and Roy Christoffersen

8:30 a.m. Noble S. K. *
Examining the Uppermost Surface of the Lunar Regolith **[#1505]**
Understanding the properties of the uppermost surface of the lunar regolith is critical as it is the surface that is probed by remotely-sensed data. Our initial results suggest this surface may be enriched in ultrafine (<2 μm) grains.

8:45 a.m. Bandfield J. L. * Ghent R. R. Vasavada A. R. Paige D. A.
Mapping Lunar Surface Rock Abundance and Regolith Thermophysical Properties Using LRO Diviner Data **[#2012]**
Rock abundance and regolith fines temperatures are derived from nighttime Diviner multispectral thermal infrared measurements of the lunar surface. These data products can be used to determine and map the physical properties of the lunar regolith.

9:00 a.m. Ghent R. R. * Bandfield J. L. Koziar J. N. Vasavada A. R. Paige D. A.
Physical Properties of Lunar Impact Ejecta: Comparisons Between LRO Diviner and Earth-based Radar Measurements **[#1889]**
We report on comparisons between Earth-based radar observations and LRO Diviner thermal IR measurements of lunar impact ejecta. We seek to establish a relationship between areal and volumetric rock abundance in crater ejecta deposits.

9:15 a.m. Campbell B. A. * Hawke B. R. Campbell D. B.
The Serenitatis We Never Knew: 70-cm Radar Reveals Rugged Mare Deposits **[#1225]**
We present new 70-cm radar data for Mare Serenitatis that greatly improve our capability to map variations in lava morphology beneath the regolith, and discuss the implications of these results for flow emplacement conditions.

9:30 a.m. Fa W. * Heggy E. Wieczorek M. A.
Modeling Radar Scattering from the Lunar Surface and Analysis of the Effect of Roughness and Ice Inclusions on CPR Values **[#1137]**
We developed a model for radar scattering from the lunar reoglith layer using vector radiative transfer theory. From this model, both the radar backscattering coefficient and the circular polarization ratio can be predicted analytically as a function of regolith parameters.

9:45 a.m. Thompson T. W. * Ustinov E. A. Heggy E.
Modeling Radar Scattering from Icy Lunar Regoliths **[#1169]**
Models for backscattering from icy lunar regoliths are developed for cases where a thin regolith covers the ice and where the ice occupies small patches within a larger radar pixel for comparison with modeled backscatter from blocky crater ejecta.

10:00 a.m. Allen C. C. * Greenhagen B. T. Paige D. A.
LRO Diviner Soil Composition Measurements — Lunar Sample "Ground Truth" **[#1733]**
Diviner observations of the Apollo and Luna landing sites support the use of Christiansen feature values to indicate soil composition. Continuing observations and experiments will derive soil compositions across the Moon based on sample ground truth.

10:15 a.m. Zhang S. * Keller L. P.
Formation of Ilmenite Rims in Lunar Soils: Vapor Deposition, Irradiation and Thermal Effects **[#1432]**
Analysis of the Fe/Ti/O chemical variations in the ilmenite rims in lunar soils implies that the rims, in addition to vapor deposition and irradiation, require an impact-related thermal event in order to explain their mineralogy and microstructure.

10:30 a.m. Li S. * Li L.
Radiative Transfer Modeling of Lunar Soil Reflectance for Accommodating the Effects of Roughness and Temperature **[#2168]**
A Hapke's model accommodating the effect of temperature and roughness was implemented and its effectiveness was demonstrated with the data for two representative Apollo samples 15071 and 71061 from the lunar Soil Characterization Consortium dataset.

10:45 a.m. Christoffersen R. * Keller L. P. Dukes C. Rahman Z. Baragiola R.
Experimental Investigation of Space Radiation Processing in Lunar Soil Ilmenite: Combining Perspectives from Surface Science and Transmission Electron Microscopy **[#1532]**
The effect of space radiation processing on lunar ilmenite has been investigated using combined XPS *in situ* irradiation and surface analysis and FE-STEM imaging and analysis.

11:00 a.m. Kiely C. * Kiely C. J.
An X-Ray Ultramicroscopy Study of Apollo 11 Lunar Regolith **[#1118]**
Sub-micron resolution images of the internal structure (using X-ray ultramicroscopy) and external morphology (using SEM) of lunar regolith particles will be presented side-by-side. Rotational movies of individual particles will also be shown.

11:15 a.m. Chen S. B. * Meng Z. G.
Lunar Regolith Depth Measurement by Passive Microwave Radiometer Onboard Chang'E Orbitor **[#1632]**
The lunar regolith depths are retrieved by passive microwave radiometer onboard Chang'E Orbitor, China.

11:30 a.m. Wang Z. * Li Y. Jiang J. Li J.
A Estimation of The Lunar Surface Temperature, Dielectric Constant, Regolith Thickness and Helium-3 Content Retrieved from Brightness Temperature by CE-1 Microwave Sounder **[#1124]**
CEMLS is the first passive microwave radiometer on lunar orbit. The method of retrieving lunar surface geophysical parameters are discussed, and the retrievals of surface temperature, dielectric constant, regolith thickness and He_3 content are given.

ORIGINS OF PRESOLAR GRAINS
Wednesday, 1:30 p.m. Waterway Ballroom 1

Chairs: **Michael Savina and Tom Zega**

1:30 p.m. Stadermann F. J. * Zhao X. Daulton T. L. Isheim D. Seidman D. N. Heck P. R. Pellin M. J. Savina M. R. Davis A. M. Stephan T. Lewis R. S. Amari S.
Atom-Probe Tomographic Study of the Three-Dimensional Structure of Presolar Silicon Carbide and Nanodiamonds at Atomic Resolution **[#2134]**
We present a promising new analytical approach for the study of presolar grains which makes it possible to reconstruct the full three-dimensional structure of an analysis volume and visualize elemental distributions in their spatial context.

1:45 p.m. Zinner E. * Gyngard F. Lin Y.
Ti-44 and V-49 in SiC Grains of Type X Revisited **[#1360]**
^{44}Ti/48Ti and 49V/51V ratios inferred from ^{44}Ca and 49Ti excesses as well as Ti isotopic ratios from presolar SiC grains of type X are compared with theoretical calculations of the interior compositions of Type II supernovae.

2:00 p.m. Hoppe P. * Gröner E. Huth J. Amari S.
Presolar SiC Grains from Supernovae with Unusual Silicon- and Sulfur-Isotopic Compositions **[#1082]**
A NanoSIMS ion imaging survey of small presolar SiC grains led to the identification of three SN grains with unusual Si- and S-isotopic ratios. These characteristics add to the complexity of SN grains and represent challenges for future SNII models.

2:15 p.m. Savina M. R. * Levine J. Stephan T. Dauphas N. Davis A. M. Knight K. B. Pellin M. J.
Chromium Isotopes in Presolar SiC Grains **[#2568]**
The Cr isotopic composition of presolar SiC grains does not account for the anomalies noted in leachates of carbonaceous chondrites, nor does it agree with s-process nucleosynthesis models. It may be reflective of the origin material in the star that produced the grains.

2:30 p.m. Hynes K. M. * Amari S. Bernatowicz T. J. Lebsack E.
Microanalytical Investigations of Presolar SiC of Type AB **[#2074]**
We report the results of a coordinated NanoSIMS and TEM study, including isotopic, structural, chemical, and subgrain data, on four SiC AB grains. The stellar origin of these grains is believed to be both J stars and born-again AGB stars.

2:45 p.m. Croat T. K. * Jadhav M. Lebsack E. Bernatowicz T. J.
Microstructural Differences Among the Isotopic Groups of Low-Density Orgueil Graphites **[#1867]**
We find difference among the isotopic groups of low-density Orgueil graphites in terms of their structure and in the types of internal grains contained. TEM results are presented from one 13C-rich graphite, one nearly solar graphite, and two SN graphites.

3:00 p.m. Meier M. M. M. * Heck P. R. Amari S. Baur H. Wieler R.
He-4 and Ne-22 in Individual High-Density Presolar Graphite Grains from the Murchison Meteorite **[#1741]**
We have analyzed 18 presolar graphite grains from the Murchison KFC1 density fraction. We confirm the low fraction (~7%) of 22Ne-rich grains found by Kehm et al. 1996 and report the first detection of ^{4}He in a graphite grain of this density fraction.

3:15 p.m. Gyngard F. * Nittler L. R. Stadermann F. J. Zinner E.
The Smoking Gun: ^{44}Ti in an ^{16}O-rich Presolar Spinel Grain **[#1152]**
We report here the discovery of an extremely ^{16}O-rich spinel grain from the Murray meteorite which also has radiogenic ^{44}Ca from the decay of ^{44}Ti, unequivocal evidence for origin in a supernova.

3:30 p.m. Zega T. J. * Alexander C. M. O'D. Nittler L. R. Stroud R. M.
The Microstructure of a Presolar Spinel Grain **[#2055]**
We report TEM data on a third presolar spinel grain. It appears to be a non-stoichiometric single crystal and may have formed under non-equilibrium conditions.

3:45 p.m. Nittler L. R. * Qin L. Alexander C. M. O'D. Wang J. Carlson R. Staderman F. J.
Extreme Uncorrelated ^{54}Cr, ^{17}O, and ^{18}O Enrichments in Sub-Micron Orgueil Grains **[#2071]**
We report several sub-micron oxide grains in an Orgueil acid residue with extreme ^{54}Cr enrichments but normal O, and numerous presolar oxide grains, some with extreme ^{17}O or ^{18}O enrichments. The origin of the ^{54}Cr-rich grains is unresolved.

4:00 p.m. Nguyen A. N. * Messenger S. Ito M. Rahman Z.
Mg Isotopic Measurement of FIB-isolated Presolar Silicate Grains **[#2413]**
The Mg isotopic compositions of rare presolar silicates are analyzed to assess their stellar sources. Surrounding grains of solar composition were removed prior to analysis by focused ion beam milling, resulting in isotopic measurements undiluted by neighboring materials.

4:15 p.m. Bose M. * Floss C. Stadermann F. J. Stroud R. M. Speck A. K.
The Origin of Presolar Silica Grains in AGB Stars **[#1812]**
We have found two presolar silica grains in ALH A77307, which exhibit excesses in ^{17}O but are normal in ^{18}O. Silicon-oxide grains probably form during rapid cooling under non-equilibrium conditions in O-rich AGB stars with low Mg/Si ratios.

4:30 p.m. Floss C. * Stadermann F. J.
Presolar Silicate and Oxide Grains in the Ungrouped Carbonaceous Chondrite Adelaide: Effects of Thermal Annealing **[#1251]**
The Adelaide C chondrite has lower abundances of O-anomalous grains than other primitive meteorites. Fe contents in its presolar silicates are also distinctly elevated. Both are likely the result of thermal annealing experienced by this meteorite.

DIFFERENTIATED METEORITES
Wednesday, 1:30 p.m. Waterway Ballroom 4

Chairs: Tomohiro Usui and Joseph Goldstein

1:30 p.m. Bland P. A. * Ciesla F. J.
The Impact of Nebular Evolution on Volatile Depletion Trends Observed in Differentiated Objects **[#1817]**
We model disk evolution in the early solar system, and show that the level of volatile depletion observed in magmatic irons may be explained by incomplete condensation from a "hot" disk at 0.5–1.5AU, on a timescale entirely consistent with Hf-W ages.

1:45 p.m. Goldstein J. I. * Yang J. Michael J. R. Kotula P. G. Scott E. R. D.
Thermal History and Origin of the IVB Iron Meteorites and Their Parent Asteroid **[#1210]**
Metallographic cooling rates for the IVB iron asteroidal body vary by a factor of 10 and increase directly with increasing Ni content. The mantle of the parent IVB asteroid was probably removed while the outer part of the core was still liquid.

2:00 p.m. Meyer C. * Becker H. Wombacher F. Wiechert U.
Abundances of Lithophile Trace Elements in Iron Meteorites **[#1912]**
A multi element technique using a sector field ICP MS was applied for analyzing iron meteorite FeNi alloy as well as phosphide and sulfide rich inclusions. We focus on lithophile and siderophile elements, particularly of magmatic irons.

2:15 p.m. Ziegler K. * Young E. D. Schauble E. A.
Silicon Isotope Fractionation Between Silicate and Metal in Meteorites **[#2222]**
Measurements of Si isotope ratios of the silicate and metal phases of meteorites are shown. New laser ablation results confirm previously measured large fractionations (acid digestion technique) and a $\Delta^{30}Si$ silicate-metal–temperature relationship.

2:30 p.m. van Acken D. * Humayun M. Brandon A. D. Peslier A.
In Situ Determination of Siderophile Trace Elements in Metals and Sulfides in Enstatite Achondrites **[#1153]**
Laser ablation ICP-MS analysis of metals and sulfides in a number of enstatite achondrites reveals siderophile element fractionation consistent with solid metal/liquid metal partitioning and different regions of origin in the solar nebula.

2:45 p.m. Moynier F. * Paniello R. Gounelle M. Albarede F. Podosek F. Zanda B.
Zn Isotopic Study of Enstatite Meteorites **[#1180]**
We investigate the degree of isotopic fractionation of Zn in aubrites, EL chondrites and EH chondrites and its implication on the evolution of their parent bodies.

3:00 p.m. Hans U. * Kleine T. Bourdon B.
Rb-Sr Chronology of Volatile Depletion of the Angrite and Eucrite Parent Bodies **[#2680]**
We present new Rb-Sr data for angrites and eucrites to discuss volatile depletion in their parent bodies.

3:15 p.m. Wee B. S. * Yamaguchi A. Ebihara M.
Platinum Group Elements in Howardites and Polymict Eucrites: Implications for Impactors on the HED Parent Body **[#1886]**
This work presents PGE data of polymict breccias and discusses the origin of impactor materials that caused wide spread brecciation on the parent body in the early solar system.

3:30 p.m. Day J. M. D. * Qin L. Rumble D. Walker R. J. Irving A. J. Ash R. D. Piccoli P. M.
Highly Siderophile Element Abundance Variations in Diogenites Determined from Mineral-Scale and Whole-Rock Investigations **[#1942]**
Diogenites preserve five orders of magnitude variation in absolute HSE abundances. Petrologic and geochemical observations are presented to better understand the cause of this variation, and its consequences for planetary accretion and differentiation.

3:45 p.m. Spivak-Birndorf L. J. * Bouvier A. Wadhwa M. Bland P. A. Spurný P.
Trace Element Geochemistry and Chronology of the Bunburra Rockhole Basaltic Achondrite **[#2274]**
We report rare earth element abundances (measured by ion microprobe) in pyroxene and plagioclase from the unique Bunburra Rockhole basaltic achondrite. We also report results of an investigation on the Al-Mg and Pb-Pb chronometers in this meteorite.

4:00 p.m. Park J. * Nyquist L. E. Bogard D. D. Garrison D. H. Shih C.-Y. Reese Y. D.
An ~4.35 Ga Ar-Ar Age for GRA 8 and the Complex Chronology of Its Parent Body **[#1365]**
Ar-Ar ages of GRA8 plag lie in a narrow range for stepped ^{39}Ar release. An age of ~4344 Ma applies to 14–47% of the release. We interpret this age as the time of subsolidus re-equilibration, and discuss it in the context of the history of the GRA PB.

4:15 p.m. Shearer C. K. * Burger P. V. Papike J. J. Sharp Z. D.
Fluids on Differentiated Asteroids. Evidence from Phosphates in GRA 06128 and GRA 06129 **[#1928]**
Meteorite pairs GRA 06128 and 06129 have provided a rather unique view of early asteroidal magmatism. Additional textural, chemical, and isotopic observations suggest that they may provide insights into the nature and history of fluids on a differentiated asteroid.

4:30 p.m. Usui T. * Jones J. H. Mittlefehldt D. W.
Low-Degree Partial Melting Experiments of CR and H Chondrite Compositions: Implications for Asteroidal Magmatism Recorded in GRA 06128 and GRA 06129 **[#1186]**
Low-degree partial melts of chondrites, generated under oxidizing conditions, are silica-undersaturated and cannot be parental to GRA 06128/9 that is interpreted to originate from a low-degree partial melt from a volatile-rich oxidized asteroid.

IMPACTS ON THE MOON, MARS, AND BEYOND
Wednesday, 1:30 p.m. Waterway Ballroom 5

Chairs: **Mark Burchell and Jamie Kimberley**

1:30 p.m. Richardson J. E. * Thomas P. C.
Uncovering the Saturnian Impactor Population via Small Satellite Cratering Records **[#1523]**
We utilize a detailed cratered terrain evolution model to determine the size-frequency distribution of a common impactor population for three of the small Saturnian satellites, based upon their current crater density distributions.

1:45 p.m. Schmedemann N. * Galuba G. Neukum G. Denk T. Wagner R. Hartmann O.
Size-Frequency Distributions (SFD) of Impact Craters on Saturnian Satellites and of the Body Diameters of Possible Impactors **[#1989]**
This presentation is about the relationships between impact cratering on saturnian satellites, saturnian irregular satellites, Kuiper Belt objects and asteroids.

2:00 p.m. Shimaki Y. * Arakawa M. Yasui M.
Experimental Study on the Collisional Disruption of Sintered Snowball with Various Porosity **[#1630]**
We did impact experiments of sintered snowball with various porosity to study the re-accumulation process of icy bodies. We found that sticking occurred at the porosity larger than 60% and re-accumulation condition did not change with porosity.

2:15 p.m. Housen K. R. * Holsapple K. A.
Asteroids Without Ejecta **[#2354]**
Laboratory measurements show that target porosity reduces ejecta velocities. As a result, large craters on porous bodies can form without ejecta blankets.

2:30 p.m. Boyce J. M. * Barlow N. Mouginis-Mark P. M. Stewart S. T.
Rampart Craters on Ganymede Europa, Mars and Earth: Implications for Layered (Fluidized) Ejecta Emplacement **[#1444]**
Analysis of rampart craters on Ganymede, Europa, Mars and Earth suggests that none of the simple models for ejecta fluidization entirely fit the observed data.

2:45 p.m. Damptz A. L. * Glaze L. S. Baloga S. M.
A New Analysis of Rampart Crater Ejecta Thickness Profiles on Mars **[#1241]**
We provide quantitative characterization of rampart crater deposits. A key new measurement is the radial rampart thickness profile and shape. Results indicate rampart size and shape may be influenced by the composition of the impact target material.

3:00 p.m. Baloga S. M. * Fagents S. A. Glaze L. S. Mouginis-Mark P. J.
Shallow-Wave Approach to Emplacement of Layered Crater Ejecta on Mars **[#2294]**
A shallow-wave model for the overland flow of ejecta from impact craters on Mars is presented. The model provides a unifying framework for the formation of single, double, and multiple layer ejecta deposits.

3:15 p.m. Mouginis-Mark P. J. * Garbeil H.
Geologic and Topographic Mapping of Tooting Crater, Mars, from HiRISE and CTX Data: Rim Slumping Controls the Distribution of Impact Melt, Pitted Terrain, Mudflows and Cavity Dewatering **[#1497]**
CTX and HiRISE data of Tooting crater, Mars, reveal a strong link between ejecta volume, rim slumping, and the distribution of pitted terrain and floor fractures. Tooting provides a benchmark against which fresh large craters on Mars can be studied.

3:30 p.m. Nycz J. C. * Hildebrand A. R.
Using HiRISE Digital Elevation Models to Investigate the Peripheral Peak Ring Morphology in the Martian Impact Crater Tooting **[#1982]**
HiRiSE DEM's were generated which cover the collapsed rim in the impact crater Tooting. These were used to palinspastically restore the crater rim, develop a model of rim failure, and numerically model the strength properties of the near subsurface.

3:45 p.m. Schwenzer S. P. * Abramov O. Allen C. C. Clifford S. Filiberto J. Kring D. A. Lasue J. McGovern P. J. Newsom H. E. Treiman A. Vaniman D. T. Wiens R. C. Wittmann A.
Exploring Martian Impact Craters: What They Can Reveal About the Subsurface and Why They are Important in the Search for Life **[#1589]**
On Noachian Mars, impact craters were frequent, could have penetrated an existing cryosphere and potentially hosted hydrothermal systems. Therefore, they are important targets to explore the subsurface and potential habitats on Noachian terrain.

4:00 p.m. Andrews-Hanna J. C. *
Arabia Terra, Mars: A Partial Ring Structure Around the Borealis Basin and Implications for the Mechanism of Multi-Ring Basin Formation **[#2615]**
A comparison of the topography of Arabia Terra with lunar and martian multiring basins suggests that Arabia Terra is a partial ring structure around the Borealis impact basin in the lowlands, and provides insight into the mechanism of ring formation.

4:15 p.m. van der Bogert C. H. * Hiesinger H. McEwen A. S. Dundas C. Bray V. Robinson M. S. Plescia J. B. Reiss D. Klemm K. LROC Team
Discrepancies Between Crater Size-Frequency Distributions on Ejecta and Impact Melt Pools at Lunar Craters: An Effect of Differing Target Properties? **[#2165]**
We measured CSFDs for the lunar crater Jackson. The impact melt pools and ejecta have model ages of 85 Ma and 150 Ma, respectively. We show the discrepancy may be explained by differences in target properties, rather than an actual age difference.

4:30 p.m. Bray V. J. * Tornabene L. L. Caudill C. Rizk B. McEwen A. S. Hawke B. R. Giguere T. A. Garry W. B. Kestay L. van der Bogert C. H. Robinson M. LROC Team
Impact Melt Movement in Lunar Craters **[#2371]**
We are conducting mapping and analysis of small-scale flows, ponds and veneers in lunar craters to help us piece together the distribution, timing of emplacement, and cooling histories of different types of melt deposits.

SPECIAL SESSION: A NEW MOON: SPECTRAL CONSTRAINTS ON LUNAR CRUSTAL COMPOSITION
Wednesday, 1:30 p.m. Waterway Ballroom 6

Chairs: Peter Isaacson and Noah Petro

1:30 p.m. Greenhagen B. T. * Lucey P. G. Glotch T. D. Bandfield J. L. Allen C. C. Bowles N. E. Thomas I. R. Wyatt M. B. Donaldson Hanna K. L. Paige D. A.
Global Distribution of Lunar Silicates from the Diviner Lunar Radiometer **[#2382]**
The Diviner lunar radiometer has made the first direct global measurement of silicate mineralogy of the lunar surface using multispectral thermal emission mapping. We have found exposures of unusual lithologies and a lack of olivine-rich mantle materials.

1:45 p.m. Glotch T. D. * Lucey P. G. Bandfield J. L. Greenhagen B. T. Thomas I. R. Elphic R. C. Bowles N. E. Wyatt M. B. Allen C. C. Donaldson Hanna K. L. Paige D. A.
Identification of Highly Silicic Features on the Moon **[#1780]**
Diviner has detected several features on the Moon with highly silicic compositions. These geologic settings of these features suggest formation of highly evolved lithologies from both extrusive volcanic and intrusive processes.

2:00 p.m. Lucey P. G. * Paige D. A. Greenhagen B. T. Bandfield J. L. Glotch T. D.
Comparison of Diviner Christiansen Feature Position and Visible Albedo: Composition and Space Weathering Implications **[#1600]**
Diviner finds that the Christiansen Feature is correlated with visible albedo. This indicates that terrains of similar albedos share similar mafic mineral contents; major variations in Mg are not indicated.

2:15 p.m. Donaldson Hanna K. L. * Wyatt M. B. Paige D. A. Greenhagen B. T. Head J. W. Pieters C. M.
Lunar Mare Basalts: Insights Using Diviner Thermal Infrared Data **[#2396]**
Thermal infrared data from the Diviner Lunar Radiometer Experiment on the LRO is used to make regional maps of derived compositions and thermophysical properties. In this preliminary study, measurements of the lunar maria are analyzed to see what insight they provide.

2:30 p.m. Isaacson P. J. * Pieters C. M. Clark R. N. Head J. W. Klima R. L. Petro N. E. Staid M. I. Sunshine J. M. Taylor L. A. Thaisen K. G. Tompkins S.
Remote Compositional Analyses of Lunar Olivine-rich Lithologies Using Moon Mineralogy Mapper (M^3) Data **[#1809]**
We have applied techniques developed for laboratory spectra of lunar olivines to spectra collected by M^3. Our work suggests that the olivines analyzed to date are more Fe-rich than those in primitive Mg-suite rocks from the Apollo collection.

2:45 p.m. Dhingra D. * Pieters C. M. Isaacson P. Staid M. Mustard J. Klima R. Taylor L. A. Kramer G. Nettles J. M3 Team
Spectroscopic Signature of the High Titanium Basalts at Mare Tranquillitatis from Moon Mineralogy Mapper (M^3) **[#2494]**
High-Ti basalts at Mare Tranquillitatis have been studied using M^3 data to explore spectral effects of ilmenite utilizing near IR properties. The results from Mare Tranquillitatis are compared with low-Ti basalts at Mare Serenitatis.

3:00 p.m. Yamamoto S. * Nakamura R. Matsunaga T. Ogawa Y. Ishihara Y. Morota T. Hirata N. Ohtake M. Hiroi T. Yokota Y. Haruyama J.
Global Distribution of Olivine Exposures on the Moon Revealed by SELENE Spectral Profiler **[#1646]**
Here, we report the global distribution of olivine exposures, possibly originating from the lunar mantle as discovered by Spectral Profiler onboard the Japanese lunar explorer SELENE (Kaguya).

3:15 p.m. Bugiolacchi R. * Mall U. Bhatt M. McKenna-Lawlor S.
A Fresh Look at the Copernicus Crater Central Peak Region Through High-Resolution NIR Data from the SIR-2 Instrument on Chandrayaan-1 **[#1609]**
We looked at the NIR reflectance spectral characteristics of surface materials in the central peaks region of the Copernicus crater using high spectral and spatial resolution data from the SIR-2 instrument on board of the Chandrayaan-1 lunar mission.

3:30 p.m. Mustard J. F. * Pieters C. M. Isaacson P. J. Head J. W. Klima R. L. Petro N. E. Staid M. Sunshine J. M. Runyon C. Taylor L. A.
Compositional Characteristics of the Aristarchus Crater from (M^3) Data **[#2000]**
Aristarchus Crater, astride a mare-highland contact, exposes diverse mineralogy in a region of extensive rilles and dark mantle deposits. Here we show the first results of compositional diversity for Aristarchus Crater as seen from M^3.

3:45 p.m. Klima R. L. * Pieters C. M. Isaacson P. J. Head J. W. Staid M. Taylor L. A. Petro N. E. Sunshine J. M.
Global Distribution and Composition of Low-Ca Pyroxenes on the Moon as Viewed by the Moon Mineralogy Mapper **[#1485]**
High spectral and spatial resolution Moon Mineralogy Mapper (M^3) data is enabling quantitative characterization of pyroxene composition on the lunar surface. We present results of a global survey of low-Ca pyroxenes, focusing on their Mg-Fe ratios.

4:00 p.m. Riner M. A. * Lucey P. G. Neumann G. A. Mazarico E.
Mapping Low-Calcium Pyroxene Using LOLA **[#2292]**
LOLA is not commonly thought to be a mineralogic sensor, but its data can be used to map the relative abundance of magnesian low-calcium pyroxene through detection of changes in spectral reflectance with temperature.

4:15 p.m. Nettles J. W. * Besse S. Boardman J. Combe J-Ph. Clark R. Dhingra D. Isaacson P. Klima R. Kramer G. Petro N. E. Pieters C. M. Staid M. Taylor L. A.
Progress Toward A New Lunar Optical Maturity Measure Based on Moon Mineralogy Mapper (M^3) Data **[#2217]**
Efforts are ongoing to leverage the high spectral resolution and coverage of M^3 data to produce a new optical maturity index that better estimates the effects of space weathering on lunar spectra.

4:30 p.m. Hendrix A. R. * Vilas F. Retherford K. D. Gladstone G. R.
Ultraviolet Spectroscopy of the Moon: Clues About Composition and Weathering **[#2451]**
We present results from a study combining several UV lunar data sets, including IUE, Galileo and LRO/LAMP, to investigate compositional variations and weathering effects across the surface of the Moon.

PLANETARY ATMOSPHERES
Wednesday, 1:30 p.m. Montgomery Ballroom

Chairs: James Lyons and Aymeric Spiga

1:30 p.m. Zahnle K. * Freedman R. Catling D.
Is There Methane on Mars? **[#2456]**
Variable methane on Mars at ~10 ppb is an extraordinary claim. Published reports rely on spectral lines where potential for confusion with telluric lines is most severe, while reports for more favorable wavelengths are consistent with no methane.

1:45 p.m. Ishimaru R. * Komatsu G. Matsui T.
Solar Insolation-induced Destabilization of Subsurface Clathrates on Mars: Implications for the Martian Atmospheric Methane **[#1580]**
We consider the destabilization of subsurface clathrates due to solar insolation as a release mechanism of CH_4 on Mars. Factors (e.g., latitude distribution and composition of clathrates) controlling the destabilization of clathrates are discussed.

2:00 p.m. Chizek M. R. * Murphy J. R. Kahre M. A. Haberle R. M. Marzo G. A.
A Short-lived Trace Gas in the Martian Atmosphere: A General Circulation Model of the Likelihood of Methane **[#1527]**
We use the NASA Ames General Circulation model to explore trace gas production, transport, and destruction in the martian atmosphere in order to study the required production magnitude and destruction lifetime of the recently published methane observations.

2:15 p.m. Pankine A. A. * Mischna M. A. Tamppari L. K.
Simulated Water Vapor Transport During Martian Northern Summer and Interpretation of the MGS TES Observations **[#2545]**
Water vapor transport in martian northern polar summer is simulated with GCM and compared to MGS TES results. Plumes of vapor are driven by off-cap circulation, but meridional circulation appears weak to explain vapor increase in midlatitudes.

2:30 p.m. Wordsworth R. * Forget F. Millour E. Madeleine J.-B. Eymet V. Haberle R.
Three-Dimensional Modelling of the Early Martian Climate and Water Cycle **[#1913]**
We perform GCM modelling of the early martian climate. CO_2 condensation, cloud formation, and a water cycle are included. New CO_2 continuum opacity data predicts reduced warming, but this is partially compensated by local water vapor feedbacks.

2:45 p.m. Soto A. * Richardson M. I. Newman C. E.
Global Constraints on Rainfall on Ancient Mars: Oceans, Lakes, and Valley Networks **[#2397]**
We investigate the patterns of precipitation for the types of climates that might have existed during ancient Mars.

3:00 p.m. Kite E. S. * Rafkin S. C. R. Michaels T. I. Manga M.
Mesoscale Simulation of Atmospheric Response to Chaos Terrain Formation **[#1171]**
We report preliminary results from MRAMS (Mars Regional Atmospheric Modeling System) simulations intended to test the hypothesis that localized precipitation during chaos terrain formation formed inverted channel networks on the plateau adjacent to Juventae Chasma.

3:15 p.m. Spiga A. * Lewis S. R. Forget F. Millour E. Montabone L. Madeleine J.-B.
The Impact of Katabatic Winds on Martian Thermal Inertia Retrievals **[#1533]**
Maps of apparent thermal inertia exhibit spatial structures, which we show are not related to soil properties but to the nighttime warming of the surface by the atmosphere adiabatically heated by katabatic winds.

3:30 p.m. Hirschmann M. M. *
Oxidized or Reduced Early Atmospheres of Terrestrial Planets? Magma Ocean Atmosphere Control and the Importance of Metal-Magma Equilibration **[#1260]**
Early terrestrial atmospheres are influenced by interactions with magma oceans, which could impose either oxidizing or reduced conditions. Key variables include the depth of magma reaction with Fe, and the effect of pressure on Fe^{3+}/Fe^{2+} in magmas.

3:45 p.m. Suckale J. * Elkins-Tanton L. T.
The Possibility of Catastrophic Degassing and Implications for the Formationof Early Atmospheres **[#1678]**
We hypothesize that solidification of magma oceans proceeds in two stages: Initially, degassing is negligible and solidification rapid. Later, volatile enrichment triggers catastrophic degassing and sudden formation of a significant early atmosphere.

4:00 p.m. Valencia D. * Ikoma M. Guillot T. Nettlemann N.
Composition and Fate of Short-Period Super-Earths: The Case of CoRoT-7b **[#1872]**
With structure and evolution models, we show that exoplanet CoRoT-7b can either be rocky (although depleted in iron relative to Earth), or volatile-rich with at most 10% of vapor by mass. Its mass loss is $\sim 10^{11}$ g/s, and its origin unconstrained.

4:15 p.m. Walker A. C. * Goldstein D. B. Moore C. H. Varghese P. L. Trafton L. M. Stewart B. D.
Modeling the Sublimation-driven Atmosphere of Io with DSMC **[#1548]**
Io's sublimation-driven atmosphere is modeled using the Direct Simulation Monte Carlo (DSMC) method. The effects of plasma heating, planetary rotation, inhomogeneous surface frost, molecular residence time, and surface temperature distribution are investigated.

4:30 p.m. Moore C. H. * Goldstein D. B. Varghese P. L. Trafton L. M.
Io's UV-V Eclipse Emission: Implications for Pele-type Plumes **[#2353]**
Simulations of Io's NUV-V emission in eclipse show that S_2-rich giant plumes' S_2 concentrations and activity levels effect the absolute brightness and the east/west intensity ratio across Io allowing for plume activity to be determined from observed spectra.

SOLAR WIND, VOLATILE ELEMENTS, AND ORGANICS
Thursday, 8:30 a.m. Waterway Ballroom 1

Chairs: **Veronika S. Heber and Roger Wiens**

8:30 a.m. McKeegan K. D. * Kallio A. P. A. Heber V. S. Jarzebinski G. Mao P. H. Coath C. D. Kunihiro T. Wiens R. Allton J. Burnett D. S.
Genesis SiC Concentrator Sample Traverse: Confirmation of ^{16}O-Depletion of Terrestrial Oxygen **[#2589]**
We report oxygen isotope data for a traverse of the Genesis concentrator target. The Sun is ^{16}O-enriched relative to the Earth and inner solar system.

8:45 a.m. Heber V. S. * Wiens R. C. Vogel N. Baur H. Wieler R. McKeegan K. D. Burnett D. S.
Genesis Concentrator Target: Isotopic and Elemental Fractionation of Implanted Solar Wind Characterized and Quantified by Ne Isotopes and the Ne/Ar Ratio in SiC **[#1067]**
The Ne isotopic composition measured in the concentrator target will be used correct the instrumental mass fractionation induced by the concentration process to obtain the definitive oxygen isotopic composition of the solar wind.

9:00 a.m. Wiens R. C. * Reisenfeld D. B. Heber V. S. Burnett D. S.
Solar Wind Fractionation — Isotopic and Elemental — and Implications for Solar Compositions and Future Genesis Analyses **[#2125]**
Fractionation between solar wind and the solar photosphere is substantial, both for elements and isotopes. GENESIS measurements are key to understanding these fractionations, which will in turn provide more accurate solar compositions.

9:15 a.m. Vogel N. * Baur H. Burnett D. S. Heber V. S. Wieler R.
Isotopic and Elemental Compositions of Ar, Kr, and Xe in Bulk, Slow, and Fast Solar Wind Targets from Genesis **[#1893]**
We present new heavy noble gas isotopic and elemental data from Genesis targets exposed to the bulk, the fast, and the slow solar wind. Implications on fractionation effects between the Sun and the solar wind will be discussed.

9:30 a.m. Meshik A. P. * Hohenberg C. M. Pravdivtseva O. V. Allton J. H. Jurewicz A. J. G. Burnett D. S.
Solar Wind Krypton in Polished Aluminum Genesis Collector: Currect Status **[#1876]**
We present and discuss the Kr isotopic composition of solar wind measured in the Genesis collector using an 8-multiplier mass spectrometer.

9:45 a.m. Yabuta H. * Amari S. Matsuda J. Hasegawa N. Kilcoyne A. L. D.
Carbon-XANES Analyses of Q-Gas Rich Fractions from the Allende Meteorite **[#1202]**
The Q gas (the planetary noble gas)-rich carbonaceous fraction with the density of 1.65 g/cm^3 from Allende meteorite was analyzed by Carbon-XANES. We concluded that Q gas could be concentrated in sp^3 carbon-rich material.

10:00 a.m. Veryovkin I. V. * Tripa C. E. Zinovev A. V. King B. V. Pellin M. J. Burnett D. S.
Sensitive Multielement RIMS Depth Profiling of Genesis Solar Wind Collectors **[#2579]**
We report multielement (Mg, Ca and Cr) RIMS depth profiling analyses of Genesis solar wind collectors using an optimized approach, “mesa” depth profiling, that yields superior depth resolution and dynamic range.

10:15 a.m. Kallio A. P. A. * McKeegan K. D. Jarzebinski G. Mao P. H. Kunihiro T. Coath C. D. Heber V. S. Burnett D. S. Wiens R. C.
Nitrogen Isotopic Composition of Solar Wind Returned by the Genesis Mission **[#2481]**
New nitrogen isotopic data from a silicon carbide target of the Genesis solar wind concentrator.

10:30 a.m. Aléon J. *
Multiple Origins of Nitrogen Isotopic Anomalies in Meteorites and Comets **[#1342]**
N isotopic anomalies in primitive chondrites and comets can be explained by (1) ion-molecule reactions in the solar protoplanetary disk, (2) a late protosolar ^{15}N-rich component and (3) an interstellar D-rich component.

10:45 a.m. De Gregorio B. T. * Nittler L. R. Stroud R. M. Alexander C. M. O'D. Bassim N. Cody G. D. Kilcoyne A. L. D. Milam S. Nuevo M. Sandford S. A. Zega T. J.
Isotopic and Chemical Variation of Organic Nanoglobules in Primitive Meteorites **[#2108]**
We find that although most organic nanoglobules are chemically distinct from surrounding insoluble organic matter (IOM), only a minority of nanoglobules are enriched in ^{15}N relative to bulk IOM.

11:00 a.m. Piani L. * Robert F. Derenne S. Thomen A. Bourot-Denise M. Mostefaoui S. Marrocchi Y. Meibom A.
The Organic Matter in the Less Metamorphized Enstatite Chondrite Sahara 97096: Isotopic Composition and Spatial Distribution **[#1736]**
Highly ^{15}N enriched hotspots are detected in Sahara 97096 IOM; with different properties than carbonaceous chondrites hotspots. An i*n situ* study indicates that $^{15}N/^{14}N$ ratio is not influenced by any specific association with inorganic phases.

11:15 a.m. Clemett S. J. * Nakamura-Messenger K. Thomas-Keprta K. L. Messenger S. McKay D. S.
The Spatial Distribution and Mineralogical Association of Organics in the Tagish Lake and Bells Carbonaceous Chondrites **[#2347]**
We have used two-step laser mass spectrometry to map, *in situ*, the spatial distribution of organics in the matrices of the Tagish Lake and Bells carbonaceous chondrites.

11:30 a.m. Remusat L. * Le Guillou C. Thomen A. Rouzaud J.-N. Guan Y. Eiler J.
Relationships Between Graphite and Organic Matter in the Abee Enstatite Chondrite; a TEM and NanoSIMS Study **[#1400]**
We characterized the morphology and isotopic properties of carbonaceous phases in Abee EH4 acid residue. Two populations of graphites coexist with amorphous organic matter depleted in D and ^{13}C. They have likely been formed by two different processes.

MARS: FLUVIAL GEOMORPHOLOGY AND PROCESSES
Thursday, 8:30 a.m. Waterway Ballroom 4

Chairs: Rossman Irwin and John Grant

8:30 a.m. Di Achille G. * Hynek B. M.
The Case of an Integrated Global Hydrosphere on Early Mars: Clues from the Distribution of Ancient Deltas and Valley Networks **[#2366]**
Global database of known martian deltaic deposits and valley networks are used in conjunction with the topography from MOLA for testing the occurrence of a global hydrosphere and of an ancient ocean on early Mars. We present results of such test.

8:45 a.m. Stepinski T F. Luo W. *
Global Pattern of Dissection on Mars and the Northern Ocean Hypothesis **[#1350]**
Global distribution of valley networks on Mars is accounted for by a weather pattern that follows from the existence of a northern ocean; precipitation is restricted to the regions located directly south of the dichotomy boundary.

9:00 a.m. Irwin R. P. III * Craddock R. A. Howard A. D. Flemming H. L.
Topographic Controls on Martian Valley Networks: Implications for Climate Change During the Noachian Period **[#2436]**
Topographic controls on martian valley networks are mostly large, early Noachian features that underwent slow aqueous weathering and erosion in an arid to hyperarid Noachian paleoclimate, followed by valley entrenchment around the Noachian/Hesperian transition.

9:15 a.m. Jaumann R. * Nass A. Tirsch D. Reiss D. Neukum G.
Valleys in the Martian Libya Montes: Evidence for Episodic Erosion Events **[#1629]**
A valley network in the western Libya Montes exhibits significant detail about water release processes and duration of erosional activities.

9:30 a.m. Mangold N. * Ansan V.
A Series of Fluvial Valleys, Depositional Fans and Transient Lakes in West Ismenius Lacus Region, Mars **[#1188]**
A series of valleys and fans suggest the presence of standing bodies of water and the occurrence of episodic fluvial activity well after the usual Early Mars period considered to have been warmer.

9:45 a.m. Grudzinski B. P. * Luo W.
Estimating Hydraulic Conductivity from Drainage Patterns Derived from a DEM — A Case Study in the Mare Tyrrhenum Quadrangle on Mars **[#1178]**
This study provides a direct estimate for hydraulic conductivity based on drainage patterns derived from a DEM for Mars and is also the first study (to the best of our knowledge) that provides spatial variability of hydraulic conductivity on Mars.

10:00 a.m. Grant J. A. * Buczkowski D. Irwin R. P. III Siebach K.
A Lake in Uzboi Vallis and Implications for Late Noachian Climate on Mars **[#1834]**
A geologically short-lived lake in Uzboi Vallis exceeded 4000 cubic km and was fed by runoff from precipitation associated with a perhaps global hydrologic system active during the late Noachian on Mars.

10:15 a.m. Warner N. H. * Gupta S. Lin S. Kim J. Muller J. P. Morley J.
Late Noachian to Hesperian Climate Change on Mars: Evidence from Crater Lakes and Thermokarst Terrain Near Ares Vallis **[#1320]**
We suggest that the presence of Hesperian-age crater outlet channels in association with Hesperian-age alas-lake type thermokarst features requires climate conditions that were favorable for the transient occurrence of stable surface liquid water.

10:30 a.m. El Maarry M. R. * Markiewicz W. Mellon M. Goetz W.
Crater Floor Polygons (CFPs): Signs of Desiccated Paleolakes on Mars? **[#1650]**
Crater floor polygons on Mars are globally mapped. Physical modeling suggests that thermal stresses are not responsible for formation of these polygons, and as such, we propose desiccation to be the main driving mechanism for formation.

10:45 a.m. Schon S. C. * Head J. W. Fassett C. I.
Lacustrine Facies Classification Systems: Application and Implications for Noachian Climate and Hydrology **[#2328]**
A lithofacies and basin classification scheme constrains Noachian paleoclimate and hydrology.

11:00 a.m. Enns D. C. * Harvey R. P. Howard A. D.
Breaching Martian Craters **[#2065]**
We have simulated martian crater and fluvial interactions with MARSSIM. We have found that breaching a crater rim is possible given certain settings.

11:15 a.m. Kostama V.-P. * Ivanov M. A. Raitala J. Törmänen T. Korteniemi J.
The Sources of Martian Outflow Channels: Water Reservoirs or Accumulation of Ice Bearing Deposits? A Case Study of Hellas Basin Valles **[#1995]**
The deposition of ice-bearing materials at different levels during the growth of the lava plateau in Hesperia-Hellas Trough offers a better explanation to the key features of the Valles structures.

11:30 a.m. Wilkinson M. J. * McGovern P. J.
Megafans and Paleo-Megafans in Amazonis and Northwest Tharsis: Implications for Fluvial Processes, Surface Geology, and Spreading of the Olympus Mons Volcano **[#2253]**
Megafan sediments of Amazonis may have repeatedly provided decollement conditions that have produced the distinctive shape and tectonism of both the Olympus Mons edifice and its flanking landslides (aureole deposits).

IGNEOUS AND VOLCANIC PROCESSES ON TERRESTRIAL BODIES IN THE SOLAR SYSTEM
Thursday, 8:30 a.m. Waterway Ballroom 5

Chairs: Thomas Prettyman and Ernst Hauber

8:30 a.m. Farkaš J. * Huang S. Jacobsen S. B.
Mass-dependent Calcium Isotope Composition of Solar System Objects **[#2266]**
This study discusses Ca isotope compositions, $^{44}Ca/^{40}Ca$ and $^{44}Ca/^{42}Ca$ ratios, of various terrestrial materials (basalts, dunite, mantle pyroxenes, accessory apatites), igneous rocks from Moon, Mars and Vesta, and Ca-Al-rich inclusions from Allende.

8:45 a.m. Prettyman T. H. * McSween H. Y. Jr. Raymond C. A. Feldman W. C. Li J.-Y. McFadden L. A. Russell C. T. Tricarico P.
Dawn's GRaND to Reveal the Complex Geochemistry of Vesta **[#2299]**
Is Vesta's composition more diverse than implied by the HED meteorites? Find out what the NASA Dawn mission's gamma ray and neutron detector (GRaND) can reveal about planetary igneous processes on a virtual visit to Vesta.

9:00 a.m. Michaut C. *
Dynamics of Laccolith Intrusions, with Applications to Earth and Moon **[#1084]**
The dynamics of magma spreading below an elastic crust is modeled and predicts three different intrusion morphologies. Laccoliths on Earth and candidate intrusive domes on the Moon are well explained by the morphology predicted in the elastic regime.

9:15 a.m. Karlstrom L. * Manga M. Matsuyama I.
Martian Magmatic Plumbing and the Spacing Between Tharsis Montes Shield Volcanoes **[#2339]**
We present a model for the development of discrete volcanic centers via melt focusing by magma chambers. We apply this model to the spacing of Tharsis Montes shield volcanoes, and test the effects of Tharsis loading and True Polar Wander stresses.

9:30 a.m. Zolotov M. Yu. *
Chemistry of Magmatic Volatiles and Explosive Volcanism on Mercury **[#1246]**
Solubilities of S, C, Cl and N in reduced magmas and potential degassing mechanisms are discussed with application to Mercury's volcanism. Nitrogen could be a major volcanic gas on Mercury and other gases are S_2, CS_2 and CO.

9:45 a.m. Glaze L. S. * Baloga S. M. Wimert J.
Volcanic Eruptions from Linear Vents on Earth, Venus and Mars: Comparisons with Central Vent Eruptions **[#1147]**
Vent geometry plays a significant role in the ability of an explosive eruption to sustain a buoyant, convective plume. Only the Earth's atmosphere can sustain convective plumes reaching tens of kilometers in altitude over a broad range of eruptive conditions.

10:00 a.m. Filiberto J. * Gross J. Treiman A. H.
Basaltic Pyroclastic Deposits on Earth and Mars: Constraints for Robotic Exploration of Martian Pyroclastic Deposits **[#1936]**
We investigate the Trailbridge basaltic ignimbrite, compare it to several possible basaltic pyroclastics on Mars, and place constraints on types of data we would need to recognize a pyroclastic deposit on Mars.

10:15 a.m. Zimbelman J. R. * Garry W. B. Crumpler L. S. Bleacher J. E. Self S.
Field Investigation of Inflated Pahoehoe Basalt Lava Flows, with Application to Lava Flows on Other Planets **[#1826]**
Field studies of the 1859 Mauna Loa lava flow in Hawaii and the McCartys lava flow in New Mexico were conducted to document topographic and textural aspects of inflated lava flows. The results should be helpful for identifying inflated flows on other planetary surfaces.

10:30 a.m. Bleacher J. E. * de Wet A. P. Garry W. B. Zimbelman J. R. Trumble M. E.
Volcanic or Fluvial: Comparison of an Ascraeus Mons, Mars, Braided and Sinuous Channel with Features of the 1859 Mauna Loa Flow and Mare Imbrium Flows **[#1612]**
A channel on Ascraeus Mons, previously suggested to indicate fluvial activity, is shown in its entirety. Distal portions indicate that this feature is of a volcanic origin despite similarities in the proximal sections to fluvial features.

10:45 a.m. Keszthelyi L. P. *
Formation of Sinuous Rilles on the Moon and Mars **[#2385]**
Recent lessons from HiRISE observations of Mars suggest that sinuous rilles were not formed by giant turbulent floods of lava. Instead, sustained flow over a mechanically weak substrate may be the key.

11:00 a.m. Hurwitz D. M. * Fassett C. I. Head J. W. Wilson L.
A Lava Channel Within an Elysium Planitia Impact Crater: Mechanics of Flow and Origin **[#1021]**
We describe a channel observed in an Elysium Planitia impact crater and constrain the viscosity and velocity of the lava that formed the channel. We can thus explore whether thermal or mechanical erosion was responsible for channel formation.

11:15 a.m. Richardson J. A. * Bleacher J. E. Baptista A. R.
Identification of Volcanic Ridge in Northern Syria Planum, Mars: Constraint on Geologic History of Syria **[#1427]**
We identify a new volcanic feature in north Syria Planum that is composed of 17 small vents together forming a northeast-trending ridge at the summit of the plateau. This feature represents a migration of Syria volcanism or a unique magma production event.

11:30 a.m. Hauber E. * Brož P. Jagert F.
Plains Volcanism on Mars: Ages and Rheology of Lavas **[#1298]**
Ages of plains volcanism in Tharsis, Mars, range from <<100 Ma to ~ 3 Ga, with most ages being clustered in the very late Amazonian. Rheologic analyses based on lava flow morphometry indicate fluid lavas with low viscosities and low yield strengths.

LARGE IMPACT BASINS ON THE MOON
Thursday, 8:30 a.m. Waterway Ballroom 6

Chairs: **Patrick McGovern and Peter Schultz**

8:30 a.m. Zuber M. T. * Smith D. E. Neumann G. A. Lemoine F. G. Mazarico E. Garrick-Bell I. Head J. W.
Contribution of Major Basins to the Long-Wavelength Shape of the Moon from the Lunar Orbiter Laser Altimeter (LOLA) **[#2022]**
We characterize the contribution of the largest lunar basins to the long-wavelength lunar shape using new observations from the Lunar Orbiter Laser Altimeter (LOLA), as well as consideration of gravity.

8:45 a.m. McGovern P. J. * Litherland M. M.
Loading Stresses and Magma Ascent In and Around Large Lunar Impact Basins: Scenarios for the Emplacement of Mare Basalts **[#2724]**
We show that the filling of large lunar impact basins with mare basalts creates a mechanical response beyond their rims that greatly facilitates magma ascent, and discuss the implications for the evolution of various maria.

9:00 a.m. Balcerski J. A. * Hauck S. A. II Dombard A. J. Turtle E. P.
The Influence of Local Thermal Anomalies on Large Impact Basin Relaxation **[#2535]**
Several lunar basins appear to be superisostatically compensated, yet the causes for, and the preservation of, this state are poorly understood. We investigate the role of impact and KREEP-derived thermal anomalies on large impact basin relaxation.

9:15 a.m. Namiki N. *
Admittance and Correlation of Localized Gravity and Topography of Freundlich-Sharonov Basin of the Moon **[#1885]**
New global data sets obtained by Kaguya are used to localize gravity and topography of Freundlich-Sharonov basin on far side of the Moon. Calculated admittance and correlation give clues to understand internal structure of the far side basins.

9:30 a.m. Schultz P. H. * Papamarcos S.
Evolving Flowfields from Imbrium and Orientale Impacts **[#2480]**
Secondary craters and grooves from the Orientale and Imbrium Basins reveal an evolving flow field related the angle of impact. Moreover, extensions of distal grooves reveal the size of the objects that formed these basins.

9:45 a.m. Head J. W. III * Pieters C. Boardman J. Burratti B. Cheek L. Clark R. Combe J.-P. Fassett C. Green R. Hicks M. Isaacson P. Klima R. Kramer G. Lundeen S. Malaret E. McCord T. Mustard J. Nettles J. Petro N. Runyon C. Staid M. Sunshine J. Taylor L. Tompkins S. Varanasi P.
The Lunar Orientale Basin: Structure and Crustal Mineralogy from Chandrayaan-1 Moon Mineralogy Mapper (M^3) Data **[#1030]**
Moon Mineralogy Mapper (M^3) data have provided new insight into the lunar Orientale basin and the nature of multi-ring impact basin formation, depth of sampling, impact melt characteristics, crustal structure and processes of ring formation.

10:00 a.m. Potter R. W. K. * Collins G. S. Kring D. A. Kiefer W. McGovern P.
Constraining the Size of the South Pole-Aitken Basin Impact **[#1700]**
We compare the dimensions of the compositional and gravity anomalies of the South Pole-Aitken basin with the results of hydrocode simulations of giant lunar impact basin formation to constrain the size of the SPA impact.

10:15 a.m. Sasaki S. * Ishihara Y. Araki H. Noda H. Hanada H. Matsumoto K. Goossens S. Namiki N. Iwata T. Ohtake M.
Structure of the Lunar South Pole-Aitken Basin from Kaguya (SELENE) Gravity/Topography **[#1691]**
KAGUYA gravity and topography data are used to characterize the structure of South Pole-Aitken basin. Previously proposed elliptic basin shape was confirmed by crustal thickness. The thinner region with 30km crust is offset from the basin center.

10:30 a.m. Kim K. J. * Dohm J. M. Williams J.-P. Ruiz J. Yu B.-H. Hare T. M. Hasebe N. Yamashita N. Karouji Y. Kobayashi S. Hareyama M. Shibamura E. Kobayashi M. d'Uston C. Gasnault O. Forni O. Reedy R. C.
Investigation of the South Pole-Aitken Basin Region using GIS and SELENE Elemental Information **[#2040]**
Using Geographic Information Systems (GIS), we performed comparative analysis among stratigraphic information and the Kaguya (SELENE) GRS data of the South Pole-Aitken basin and surroundings.

10:45 a.m. Petro N. E. * Sunshine J. Pieters C. Klima R. Boardman J. Besse S. Head J. Isaacson P. Taylor L. Tompkins S.
Lower Crustal Materials Exposed in the Apollo Basin Revealed Using Moon Mineralogy Mapper (M^3) Data **[#1802]**
Moon Mineralogy Mapper data show the interior of the Apollo Basin to contain distinct anorthositic and noritic materials, which might represent unique exposures of lower crustal material that were not excavated by the South Pole-Aitken Basin (SPA).

11:00 a.m. Zeigler R. A. * Jolliff B. L. Korotev R. L.
Petrography and Pairing Relationships of Lunar Meteorites Sayh al Uhaymir 449 and Dhofar 925, 960, and 961 **[#1985]**
Similarities among their lithic clast populations definitively indicate that despite bulk compositional differences, Dhofar 925, 960, and 961 are paired and strongly suggest that SaU 449 is also paired.

11:15 a.m. Liu D. * Jolliff B. L. Zeigler R. A. Wan Y. Zhang Y. Dong C. Korotev R. L.
A 3.91 Billion Year Age for Apollo 12 High-Thorium Impact-Melt Breccias: Products of Imbrium, or an Older Impact Basin in the Procellarum KREEP Terrane? **[#2477]**
SHRIMP-II dating of zircons within fragments of Apollo 12 high-Th IMB yield $^{207}Pb/^{206}Pb$ crystallization ages of 3.913±7 Ga, the same age as the IMB lithology in lunar meteorite SaU 169, and older than the accepted age range of the Imbrium Basin.

11:30 a.m. Grange M. L. * Nemchin A. A. Jourdan F.
Review of Ages of Lunar Impact Rocks: Implication to the Timing of Serenitatis and Imbrium Impacts and the LHB Model **[#1275]**
Ages obtained on lunar breccias have been reviewed in order to isolate reliable and precise data that can be used to constrain the timing of major impacts. Revised ages for Imbrium and Serenitatis and impact rate affecting the Moon are proposed.

COSMIC DUST AND COMETARY MATTER
Thursday, 1:30 p.m. Waterway Ballroom 1

Chair: **Lindsay Keller**

1:30 p.m. Messenger S. * Keller L. P. Nakamura-Messenger K. Nguyen A.
History of Nebular Processing Traced by Silicate Stardust in IDPs **[#2483]**
We have identified two presolar silicate grains as polycrystalline assemblages, or equilibrated aggregates. These grains occur in a stardust-rich interplanetary dust particle (IDP). We propose these grains were annealed in the solar nebula.

1:45 p.m. Keller L. P. * Loeffler M. J. Christoffersen R. Dukes C. Rahman Z. Baragiola R.
Irradiation of FeS: Implications for the Lifecycle of Sulfur in the Interstellar Medium and Presolar FeS Grains **[#1172]**
We performed irradiation experiments on FeS to simulate interstellar exposure and analyzed the resulting material using X-ray photoelectron spectroscopy and transmission electron microscopy.

2:00 p.m. Busemann H. * Spring N. Crowther S. A. Claydon J. L. Gilmour J. D. Nittler L. R.
Abundant Primordial Xenon in Interplanetary Dust Particles from the Comet Grigg-Skjellerup Collection **[#1947]**
We compare Xe abundances in IDPs from the Grigg-Skjellerup collection (GSC) and regular IDPs. The large Xe abundance proves the particular character of some GSC-IDPs. The detected amount most likely indicates the presence of primordially trapped Xe.

2:15 p.m. Ogliore R. C. * Butterworth A. L. Fakra S. C. Gainsforth Z. Marcus M. A. Westphal A. J.
Comparing the Oxidation State of Fe in Comet 81P/Wild 2 and CP-IDPs **[#1929]**
Using Fe K-edge XANES, we directly compare the oxidation state of Fe in 15 CP-IDPs to 194 fragments in 11 Stardust tracks.

2:30 p.m. Flynn G. J. * Wirick S. Keller L. P. Jacobsen C. Sandford S. A.
Organic Coatings on Individual Grains in CP IDPs: Implications for the Formation Mechanism of Pre-Biotic Organic Matter and for Grain Sticking in the Early Solar System **[#1079]**
Individual grains in CP IDPs have coatings of organic matter critical to aggregation in the nebula with properties inconsistent with formation by mineral specific catalysis but consistent with irradiation of carbon-bearing ices on grain surfaces.

2:45 p.m. Aguiar J. A. * Sandford S. A. Browning N. D. Bradley J. P.
Detection of Organic Compounds with One-Nanometer Spatial Resolution **[#1901]**
Using monochromated scanning transmission electron microscopy and electron energy loss spectroscopy we have detected organics detected with 1-nm spatial resolution.

3:00 p.m. Dobrica E. * Engrand C. Leroux H. Duprat J.
Investigation of Ultracarbonaceous Antarctic Micrometeorites by Analytical Transmission Electron Microscopy **[#1613]**
Ultracarbonaceous micrometeorites were studied by TEM in order to understand the mineralogy and petrology of probable cometary grains. GEMS, and spherical objects with an igneous signature similar to chondrules were observed in these samples.

ROCKS, LIFE, AND BIOSIGNATURES
Thursday, 3:15 p.m. Waterway Ballroom 1

Chairs: Kathie Thomas-Keprta and John Parnell

3:15 p.m. Abramov O. * Mojzsis S. J.
Thermal, Physical, and Biological Effects of Impact Bombardments on Noachian Mars **[#2402]**
We apply an established bombardment model to Noachian Mars. Our analysis shows that although Mars would have been completely resurfaced, its crust would not have melted, and the impacts would have been on the whole beneficial to microbial life.

3:30 p.m. Treiman A. H. * Essene E. J.
Metamorphic Origin of Sub-Micron Magnetite Crystals in ALH 84001: Reevaluation of Equilibria, Thermochemistry, and Experiments **[#1159]**
Magnetite grains in ALH 84001, cited as evidence of martian life, could have formed abiotically by thermal decomposition of Fe-rich carbonates. Thomas-Keprta et al. (2009) criticize this abiotic hypothesis; their criticisms lack merit and do not disprove the hypothesis.

3:45 p.m. Thomas-Keprta K. L. * Clemett S. J. Wentworth S. J. McKay D. S. Gibson E. K. Jr.
New Insights into the Origin of Magnetite Crystals in ALH 84001 Carbonate Disks **[#1064]**
Comparison of new TEM results with decomposition studies of sideritic carbonates conducted under a range of heating scenarios suggests that the magnetite nanocrystals in ALH 84001 carbonate disks are not the products of thermal decomposition.

4:00 p.m. Brown I. I. * Bryant D. A. Thomas-Keprta K. L. Tringe S. G. Sarkisova S. A. Galindo C. Jr. Malley K. Sosa O. Garrison D. H. Mckay D. S.
Biogeochemical Activity of Siderophilic Cyanobacteria and Insights from Their Genomes: Implication for the Development of New Biosignatures **[#1512]**
Siderophilic (iron-loving) cyanobacteria were shown to use phosphates for sequestration of internal Fe pool. The analysis of the genomes of siderophilic cyanobacteria indicates putative links between physical and molecular biosignatures.

4:15 p.m. Johnson A. P. * Onstott T. C. Pratt L. M. Pfiffner S. Vishnivetskaya T. A. Bryan R. A. White L. Radtke K. Chan E. Tronnick S. Borgonie G. Mancinelli R. Rothschild L. Rogoff D.
Microorganism and Organic Biomarker Survival as a Function of Depth in a Mars Analog Regolith after Exposure to Mars Surface Conditions **[#1531]**
Microorganism and relevant biomarkers were exposed to several weeks of simulated martian conditions while embedded within a synthetic Mars analog regolith. Survival of organisms and biomarkers was related to burial depth and UV exposure with time.

4:30 p.m. Parnell J. * Boyce A. J.
Follow the Methane: The Search for Deep Biospheres on Mars and Earth **[#1087]**
Methane seepages indicate gas pathways that could fuel microbial sulfate reduction at depth. Sulfur isotope studies can indicate microbial activity in the ancient deep biosphere on Earth, and could be applied to seek ancient deep biosphere on Mars.

SPECIAL SESSION: CHARACTERIZING NEAR-EARTH OBJECTS
Thursday, 1:30 p.m. Waterway Ballroom 4

Chairs: Andrew Cheng and Dan Scheeres

1:30 p.m. Cheng A. * Barnouin O. S.
Eros and Itokawa Comparisons: NEAR Shoemaker and Hayabusa **[#2747]**
NEAR and Hayabusa have studied two S-type near-Earth asteroids with similar compositions, but with distinct internal structures and surface geologies. What does surface geology, in the form of lineaments, craters, and small surface features, tell us about strength and cohesion?

2:00 p.m. Yoshikawa M. * Kawaguchi J. Yano H.
Asteroid Sample Return Mission Hayabusa, Its Engineering Challenges and Scientific Results **[#2746]**
Asteroid explorer Hayabusa will come back to the Earth in June 2010. We overcame many engineering difficulties and obtained many scientific data about the tiny S-type asteroid Itokawa. We summarize engineering and the scientific results of Hayabusa.

2:30 p.m. Benner L. A. M. *
Arecibo and Goldstone Radar Imaging of Near-Earth Asteroid **[#2748]**
Radar is the most powerful ground-based astronomical technique for studying the physical properties of near-Earth objects and for refining their orbits, principally through its ability to achieve resolutions as fine as several meters/pixel that can spatially resolve small objects.

3:00 p.m. Mainzer A. K. * Bauer J. M. Masiero J. Grav T. Cutri R. McMillan R. Walker R. Wright E. L. WISE Team
NEOWISE — The WISE Near Earth Object Survey **[#2534]**
The WISE spacecraft is expected to observe roughly 700 near-Earth objects, more than a third newly discovered. These measurements will provide a relatively unbiased and uniform sampling of this small body sub-population down to sizes of a few hundred meters.

3:30 p.m. Emery J. P. * Fernández Y. R. Kelley M. S. Hergenrother C. Ziffer J. Lauretta D. S. Drake M. J. Campins H.
Thermophysical Characterization of Potential Spacecraft Target (101955) 1999 RQ36 **[#2282]**
We report on thermal emission measurements of 1999 RQ36 from Spitzer. The derived size is in agreement with radar measurements, and we find a moderately high thermal inertia and homogeneous surface properties.

3:45 p.m. Gaskell R. W. * Barnouin O. S. Scheeres D. J.
The NEAR Shoemaker Landing on Eros **[#2093]**
NEAR imaging and NLR data are being used to determine the spacecraft's approach trajectory and final landing site.

4:00 p.m. Binzel R. P. * Morbidelli A. Merouane S. DeMeo F. E. Birlan M. Vernazza P. Thomas C. A. Rivkin A. S. Bus S. J. Tokunaga A. T.
Good Vibrations: Recent Near-Earth Encounters as the Missing Piece of the S-Asteroid and Ordinary Chondrite Meteorite Puzzle **[#1226]**
Close Earth encounters that induce seismic shaking of near-Earth asteroids are found to produce surfaces free of space weathering. These "Q-type asteroids" are direct spectral matches to the most commonly falling meteorites, the ordinary chondrites.

4:15 p.m. Gaffey M. J. * Reddy V.
Mineralogical Diversity in the S-Type NEA Population **[#1864]**
Mineralogically diagnostic spectral parameters derived from VNIR spectra of near-Earth asteroids confirm previous suggestions that LL-chondrite-like assemblages appear overrepresented in the NEA population relative to the meteorite fall population.

4:30 p.m. Scheeres D. J. * Hartzell C. M.
The Relevance and Role of Cohesive Forces for Small Asteroids **[#1839]**
A comparison of forces at asteroids shows that van der Waals cohesion between regolith grains is significant. Consideration of this effect as a function of grain size suggests a new model for the terminal evolution of rubble pile asteroids.

4:45 p.m. Jacobson S. A. * Scheeres D. J.
The Evolution of Binary Asteroids Formed by Spin Fission **[#2098]**
The mass ratio determines the evolution after a YORP spin-fission event. High mass ratio systems (>0.2) evolve to a tidally locked state. Low mass ratio systems (<0.2) disrupt, but may undergo secondary fission events that can stabilize the system.

5:00 p.m. Lasue J. * De Sanctis M. C. Capria M. T. Turrini D. Coradini A.
Thermal Model of Comet Nuclei: Implications for Rosetta **[#1675]**
We investigate the effect of shape, orbital history, obliquity and dust covering on the thermal properties and the activity of Comet 67P/Churyumov-Gerasimenko. Implications for the Rosetta mission timeline are derived.

SEVERAL SPECIES OF VARIOUSLY SIZED ICY CHUNKS GATHERED TOGETHER AROUND GIANT PLANETS AND EVOLVING OVER TIME
Thursday, 1:30 p.m. Waterway Ballroom 5

Chairs: **Karly Pitman and Gerald Patterson**

1:30 p.m. Lorenz R. D. * Newman C. Lunine J. I. Cassini RADAR Team
Why Titan's Lakes Have Been Smooth So Far — and May Be About to Get Rough **[#1112]**
No waves seen so far.Could Titan Lakes be viscous or just calm season?

1:45 p.m. Estrada P. R. * Durisen R. H.
An Improved Model for Modeling the Coupled Structural and Compositional Evolution of Saturn's Rings Due to Meteoroid Bombardment **[#2686]**
We report on the development of a new code for modeling the structural and pollution evolution of Saturn's rings, in tandem, due to the ballistic transport of micrometeorite impact ejecta.

2:00 p.m. Chen E. M. A. * Glatzmaier G. A. Nimmo F.
Modeling the Dynamics of Icy Satellite Subsurface Oceans with Focus on Implications for Spacecraft Observables **[#1454]**
We present numerical simulations of the behavior of subsurface oceans on multiple icy satellites. Spacecraft observables such as the magnetic field likely contain signals associated with ocean circulation.

2:15 p.m. Shirley J. H. * Dalton J. B. Prockter L. M. Kamp L. W.
Signatures of the Radiolytic Sulfur Cycle on Europa: A New Tool for Integrated Compositional and Stratigraphic Investigations **[#2395]**
A spatial gradient of H_2SO_4 hydrate abundance is evident on the anti-jovian hemisphere of Europa. Locations that depart significantly from the regional trend may represent surfaces where radiolytic processing has not reached equilibrium.

2:30 p.m. Loeffler M. J. * Hudson R. L. Moore M. H.
Ion Irradiation of Sulfuric Acid: Implication for Its Stability on Europa **[#1240]**
The Galileo NIMS detected regions on Europa's surface that may contain sulfuric acid mixed in water ice. We studied the radiation stability of sulfuric acid.

2:45 p.m. Buratti B. J. * Faulk S. P. Mosher J. A. Clark R. N. Brown R. H. Baines K. H. Nicholson P. D.
A Search for Activity on Mimas, Tethys, and Dione with the Cassini Visual and Infrared Mapping Spectrometer **[#1389]**
Observations of the forward-scattered component of the solar phase curves of Mimas, Tethys, and Dione places a limit on plume activity of less than 1% that of Enceladus.

3:00 p.m. Ciarniello M. * Capaccioni F. Filacchione G. Coradini A. Cerroni P. Tosi F. Stephan K.
Spectrophotometric Analysis of Rhea Surface Scattering Properties **[#1643]**
We did spectrophotometric analysis of VIMS data for Rhea, the second largest satellite of Saturn, applying the Hapke model to retrieve informations about the surface characteristics of the planet: presence of contaminants, grain size and roughness.

3:15 p.m. Hansen G. B. * Romain J.
Water Ice Grain Sizes and CO_2 on the Tiger Stripes of Enceladus from Cassini/VIMS Observations **[#2646]**
We are modeling the grain size of water snow on Enceladus, particularly in the tiger stripe region, and looking for CO_2 and other materials in VIMS spectra.

3:30 p.m. McKinnon W. B. *
Argon-40 Degassing from Titan and Enceladus: A Tale of Two Satellites **[#2718]**
Titan and Enceladus are very different worlds in terms of ^{40}Ar degassing efficiency, but not necessarily the way one might think.

3:45 p.m. Wood C. A. * Radebaugh J. D. Stofan E. Zebker H.
Titan's Xanadu: Ancient and Young **[#2221]**
Xanadu is the largest and most anomalous region of Titan. It has the highest concentration of impact craters, but they are all concentrated in the eastern quarter. Xanadu contains both the oldest terrain on Titan and very young surfaces.

4:00 p.m. Wall S. Hayes A. * Bristow C. Lorenz R. Stofan E. Lunine J. Le Gall A. Janssen M. Lopes R. Wye L. Soderblom L. Paillou P. Aharonson O. Zebker H. Farr T. Mitri G. Kirk R. Mitchell K. Notarnicola C. Casarano D. Ventura B.
The Earthlike Shoreline Morphology of Titan's Ontario Lacus **[#1466]**
Ontario Lacus' shoreline features include Earth-like rivers, deltas and flooded topography. Ontario is a dynamic lake, similar in many ways to terrestrial lakes, with active shoreline processes.

4:15 p.m. Langhans M. * Jaumann R. Stephan K. Brown R. H. Buratti B. J. Clark R. Baines K. H. Nicholson P. D. Lorenz R. D. Sotin C.
Valley Formation from Methane Convective Storms on Titan **[#1709]**
Precipitation in the form of episodic thunderstorms is suspected to cause fluvial erosion at the surface of Titan. Valley morphology provides hints to verify whether episodic storm events accounts for the presence of valleys.

4:30 p.m. Moore J. M. * Howard A. D. Schenk P. M. Pappalardo R. T.
Titan: Can Fluvial Erosion Patterns Tell Us Anything About Initial Landforms and Regional Landscapes? **[#1167]**
We report on our effort to recognize initial (e.g., endogenic) landforms subjected to Titan's weather. Our model results indicate that drainage patterns were initiated when Titan had substantially more regional relief than the icy Galilean satellites.

SPECIAL SESSION: A NEW MOON: LUNAR VOLCANISM AND IMPACT CHRONOLOGY
Thursday, 1:30 p.m. Waterway Ballroom 6

Chairs: Harald Hiesinger and Lisa Gaddis

1:30 p.m. Spudis P. D. * Bussey D. B. J. Butler B. Carter L. Chakraborty M. Gillis-Davis J. Goswami J. Heggy E. Kirk R. Neish C. Nozette S. Patterson W. Robinson M. Raney R. K. Thompson T. Thomson B. J. Ustinov E.
Results of the Mini-SAR Imaging Radar, Chandrayaan-1 Mission to the Moon **[#1224]**
The Mini-SAR imaging radar on India's Chandrayaan-1 mission mapped more than 90% of both poles of the Moon. Scattering properties suggest that water ice is present in some permanently shadowed craters near the north pole.

1:45 p.m. Robinson M. S. * Thomas P. C. Braden S. E. Lawrence S. J. Garry W. B. LROC Team
High Resolution Imaging of Ina: Morphology, Relative Ages, Formation **[#2592]**
Meter scale geomorphic analysis of the interior of the enignmatic lunar feature known as Ina.

2:00 p.m. Lawrence S. J. * Stopar J. D. Hawke B. R. Gaddis L. R. Robinson M. S. Denevi B. W. Giguere T. A. Jolliff B. L. Braden S. E. LROC Team
LROC Observations of the Marius Hills **[#1906]**
High-resolution LROC NAC imagery and stereo observations are providing important new insights into the volcanic history of the Marius Hills region.

2:15 p.m. Besse S. * Sunshine J. M. Pieters C. M. Petro N. E. Staid M. Deepak D. Head J. Isaacson P. M3 Team
New Observations of the Marius Hills Complex from Moon Mineralogy Mapper (M^3) **[#1361]**
Observations of the Marius Hills complex with M^3 reveal a plateau with a weaker 1 µm from the surrounding mare. Domes are distinct from the mare of the plateau with the weakest 1 µm band. Olivine signature is found inside the crater Marius.

2:30 p.m. Braden S. E. * Robinson M. S. Tran T. Gengl H. Lawrence S. J. Hawke B. R.
Morphology of Gruithuisen and Hortensius Domes: Mare vs. Nonmare Volcanism **[#2677]**
Digital elevation models derived from stereo image pairs acquired with the Lunar Reconnaissance Orbiter Narrow Angle Camera allow for a detailed comparison of the stratigraphy and morphology of Gruithuisen Gamma and three of the Hortensius Domes.

2:45 p.m. Staid M. I. * Pieters C. M. Boardman J. Head J. W. Sunshine J. Taylor L. A. Isaacson P. Besse S. Klima R. L. Kramer G. Y. Dhingra D.
Regional and Temporal Variations in the Western Mare Basalts: New Observations from the Moon Mineralogy Mapper **[#2002]**
The last major phases of lunar volcanism produced spectrally unique basalts on the western near side of the Moon. The Moon Mineralogy Mapper on Chandrayaan-1 has provided detailed new measurements to assess the mineralogy of these basalts.

3:00 p.m. Carter L. M. * Gillis-Davis J. J. Bussey D. B. J. Spudis P. D. Neish C. D. Thompson B. J. Patterson G. W. Raney R. K. Mini-RF Science Team
Mini-RF Observations of a Sample of Large Lunar Pyroclastic Deposits **[#1563]**
We present new radar data of large lunar pyroclastic deposits obtained using the Mini-RF instruments on Chandrayaan-1 and Lunar Reconnaissance Orbiter, including the Orientale pyroclastic.

3:15 p.m. Gaddis L. * Robinson M. S. Hawke B. R. Giguere T. Keszthelyi L. Gustafson J. O. Bell J. F. III LROC Science Team
Lunar Pyroclastic Volcanism at Atlas Crater as Viewed by LROC **[#2059]**
LROC data of Atlas Crater reveal major differences between two pyroclastic deposits in the crater floor. Evidence for different eruption styles between the two deposits and possible multiple eruptive episodes at the southern vent is presented.

3:30 p.m. Hiesinger H. * van der Bogert C. H. Robinson M. S. Klemm K. Reiss D.
New Crater Size-Frequency Distribution Measurements for Tycho Crater Based on Lunar Reconnaissance Orbiter Camera Images **[#2287]**
We have performed new crater size-frequency distribution measurements for melt pools, the floor, and the ejecta blanket of Tycho crater. While the pools and the floor are about the same age, the ejecta blanket shows older ages.

3:45 p.m. Huang J. * Xiao L. Yang J. Dong Y. S.
New Model Ages of Mare Material in Sinus Iridum, Moon **[#1184]**
Here we present new absolute model ages of mare material in Sinus Iridum by CSFD method derived from data of Chinese first lunar orbiter Chang'E-1 (CE-1).

4:00 p.m. Hirata N. * Haruyama J. Ohtake M. Matsunaga T. Yokota Y. Morota T. Honda C. Ogawa Y. Kitazato K. Shibata Y. Sugihara T. Miyamoto H. Demura H. Asada N.
Remote Sensing Study of a Large Lunar Crater Jackson **[#1585]**
We investigated a large lunar crater Jackson with LISM/SELENE data to reconstruct the impact event forming the crater from distributions of its ejecta and other associated features.

4:15 p.m. Plescia J. B. * Robinson M. S. Paige D. A.
Giordano Bruno: The Young and the Restless **[#2038]**
Giordano Bruno (22 km diameter) has a transitional morphology between simple and complex. Craters on the ejecta may be secondaries formed by the GB impact and thus may not be useful for determining absolute age.

4:30 p.m. Werner S. C. * Medvedev S.
Lunar Rayed Craters **[#1058]**
Global cratering statistics of young rayed impact craters suggests that other geological processes such as space weathering or target composition modified the ray visibility, and any possible asymmetric crater rates were obscured if they existed.

POSTER SESSION II
Thursday, 7:00 p.m. Town Center Exhibit Area

ICE AND DUST

Yasui M. Arakawa M.
Mechanical Strength of Small Icy Bodies with Residual Porosity Less Than 30% **[#1618]**
We did deformation experiments of ice-silica mixtures with various silica mass contents and porosities to study the strength of small icy bodies. We found that the strength became smaller as silica mass content or porosity increased.

Wakita S. Sekiya M.
Thermal Evolution of Icy Planetesimals in the Early Solar System **[#1291]**
The thermal evolution of the icy planetesimals for a wide range of parameters is numerically performed. It is found that the initial ratio of $^{26}Al/^{27}Al$ is the key parameter for the chemical reactions to take place or not, and its timing.

Boice D. C. Martinez S. E.
Physico-Chemical Modeling of the Coma of Comet C/2004 Q2 (Machholz) **[#2733]**
Modeling is central to understand the important physical and chemical processes that operate in cometary comae. Details of these processes are presented in the inner coma of Comet Machholz, including thermodynamics and gas-phase chemistry throughout this region.

Moriarty D. Hibbitts C. A. Lisse C. M. Dyar M. D. Harlow G. Ebel D. Peale R.
Near–Far IR Spectra of Sulfide Minerals Relevant to Comets **[#2447]**
Sample preparation procedures and preliminary results from our IR spectroscopy (~2–200 µm) of sulfides relevant to comets, in support of analyzing Spitzer Space Telescope data from the Deep Impact mission.

Kohout T. Kosterov A. Haloda J. Halodova P. Zboril R.
Magnetic Properties of Cometary Bodies and Detection Limits of the Rosetta Space Mission **[#1048]**
We provide review of magnetic properties of sulphides within cometary material and model magnetic interactions of comets with interplanetary magnetic field. The results are compared to detection limits of the Rosetta space mission.

Kelley M. S. Woodward C. E. Harker D. E. Wooden D. H. Reach W. T. Fernández Y. R.
Comet Dust Diversity in Ground-based and Spitzer Space Telescope Mid-Infrared Spectra **[#2375]**
We examine the composition of comet dust from mid-infrared spectra to assess the efficiency of mixing of dust and planetesimals in the comet formation zone.

Reach W. T.
Structure of the Zodiacal Cloud Along the Earth's Orbit **[#1499]**
Using Spitzer Space Telescope observations of the brightness of the ecliptic poles, we measured the structure of the Earth's resonant dust ring, showing Earth is trailed by a cloud 0.2 AU away and 0.08 AU wide, along the Earth's orbit.

Ipatov S. I.
Delivery of Dust Particles and Small Bodies to Planets **[#1267]**
The probabilities of collisions of migrating small bodies and dust particles produced by these bodies with all planets were calculated. The delivery of water and volatiles to planets is discussed based on the probabilities.

Miljkovic K. Mason N. J. Zarnecki J. C.
Environmental Effects on Dust Around Europa **[#1346]**
We investigate the effects of environmental conditions at Europa and the variations in Europa's surface properties on the dust population around it, showing that the surface composition could be preserved in the dust ejected to orbital altitudes.

STARDUST MISSION TO COMET WILD 2

Jurewicz A. J. G.   Jones S. M.   Zolensky M.   Frank D.   Dupray L.   deHoog B.
Stardust Aerogel Baseline Data: Recovery and Use **[#1897]**
We report on pre-flight Stardust aerogel data being recovered for use by the scientific community. In addition, pre- and post-flight densities for select cells are compared. Density profiles of some cells changed significantly enough to affect models of particle capture.

Price M. C.   Kearsley A. T.   Burchell M. J.   Abel R.   Cole M. J.
Comet Wild 2 Dust: How Particle Structure and Composition are Reflected in the Shape of Stardust Aerogel Tracks **[#1313]**
Laboratory shots of artificial mineral aggregates at ~6 km/s give Type C (bulbous) aerogel tracks. Larger grains in a fine mineral matrix makeType B. Some purely organic particles also create Type C tracks, implying volatile expansion is important.

Meshik A. P.   Hohenberg C. M.   Pravdivtseva O. V.
Spallogenic Neon in the Exposed Layer of Stardust Aerogel — Submicron Dust or Surface Artifact? **[#2706]**
Small but statistically significant excess of ^{21}Ne is found in outer layer of Stardust aerogel exposed to the comet.

Ogliore R. C.   Butterworth A. L.   Doran A.   Gainsforth Z.   Scholl A.   Westphal A. J.   Young A.
Photoemission Electron Microscopy of Stardust Cometary Foils **[#2572]**
We present results from photoemission electron microscopy (PEEM) analysis of Stardust cometary foil craters. In addition, we explain how this instrument is well-suited for analysis of Stardust interstellar foil craters.

Kearsley A. T.   Westphal A. J.   Stadermann F. J.   Armes S. P.   Ball A. D.   Borg J.   Bridges J. C.   Brownlee D. E.   Burchell M. J.   Chater R. J.   Davis A. M.   Floss C.   Flynn G.   Gainsforth Z.   Grün E.   Heck P.   Hoppe P.   Hörz F.   Howard L. E.   Howe G.   Huss G. R.   Huth J.   Landgraf M.   Leitner J.   Leroux H.   Nittler L.   Ogliore R.   Postberg F.   Price M. C.   Srama R.   Stroud R.   Trieloff M.   Trigo-Rodriguez J.   Sandford S. A.   Stephan T.   Sternovsky Z.   Tsou P.   Zolensky M. E.
Finding Interstellar Particle Impacts on Stardust Aluminium Foils: The Safe Handling, Imaging and Analysis of Samples Containing Femtogram Residues **[#1593]**
Hypervelocity shots and numerical simulations show the likely form of Stardust interstellar particle impacts on Al foil. A robust holder for sample handling in preliminary examination is now available, with a protocol for contamination monitoring.

Stadermann F. J.   Floss C.   Lam H. Y. M.   Price M. C.   Burchell M. J.   Kearsley A. T.
Identifying Off-Normal Hypervelocity Impacts in Aluminum Foil by Auger Imaging: Implications for the Examination of the Interstellar Collector **[#1349]**
We show that thin impact sprays can be used to identify off-normal hypervelocity impacts. The measurement of these sprays by Auger imaging is non-destructive and has the potential to provide information that is not otherwise available.

Gainsforth Z.   Butterworth A. L.   Bonal L.   Brownlee D. E.   Fakra S. C.   Huss G. R.   Joswiak D.   Kunz M.   Marcus M. A.   Nagashima K.   Ogliore R. C.   Tamura N.   Telus M.   Tyliszczak T.   Westphal A. J.
Integrating Analytical Techniques for Analysis of Comet 81P/Wild2 in Stardust Track C2052,2,74 **[#2698]**
Stardust case study examining sample preparation, experimental issues and instrumental prioritization.

Greenberg M.   Ebel D. S.   Ramcharan S.   Hein P.   Newville M.   Lanzirotti A.   Zolensky M. E.
Nondestructive XRF and Quantitative Volumetric Image Analysis of Stardust Tracks 140, 151 & 152 **[#2346]**
We present a full textural analysis of three whole Stardust tracks, with an emphasis placed on three-dimensional, nondestructive methods. Implications of data on hypervelocity impacts modeling and Stardust material processing will be discussed as well.

Sanders N. E. Velbel M. A.
The Size Distribution of Stardust Metal Sulfide Droplets **[#1175]**
The size distribution of nanoscale Fe-Ni-S droplets has been determined from TEM images of melted Stardust grains. This distribution could aid the interpretation of capture modification and the composition of the incident cometary material.

Matrajt G. Messenger S. Ito M. Wirick S. Flynn G. Joswiak D. Brownlee D.
TEM, XANES and NanoSIMS Characterization of Carbonaceous Phases from Individual Stardust and IDP Particles **[#1564]**
We present chemical and isotopic data on four different carbon morphologies found in IDPs and Stardust samples.

Milam S. N. Nuevo M. Sandford S. A. Cody G. D. Kilcoyne A. L. D. Stroud R. M. DeGregorio B. T.
Comparison of the Organic Composition of Cometary Samples with Residues Formed from the UV Irradiation of Astrophysical Ice Analogs **[#2078]**
We present C-, N-, and O-XANES results of organic residues produced in the laboratory from the UV irradiation of astrophysical ice analogs containing H_2O, CO, CH_3OH, NH_3, in order to mimic processes that may occur in comets.

Burchell M. J. Cole M. J. Price M. C. Kearsley A. T. Nixon A.
Glycine Survival in Hypervelocity Impacts in the Laboratory into Aerogel and onto Aluminium Foil **[#1637]**
Survival of glycine under impact at 6 km/s is tested with aerogel and aluminium targets. SEM-EDX shows residue in al craters but Raman spectroscopy finds no signals for glycine.

Stodolna J. Jacob D. Burchell M. J. Leroux H.
Collect-induced Microstructure Modifications in Stardust Samples: Some Experimental Evidences **[#1659]**
Olivine and pyroxene samples have been experimentally shot in aerogel reproducing Wild2 material capture conditions. The TEM investigation improves the understanding of the collect-induced microstructure modifications.

COSMIC DUST AND COMETARY MATTER

Poppe A. R. James D. Jacobsmeyer B. Horányi M.
Measurements of the Interplanetary Dust Population by the Venetia Burney Student Dust Counter on the New Horizons Mission **[#1219]**
We present measurements of the interplanetary dust population from 2.5 to 15 A.U. made by the Venetia Burney Student Dust Counter on the New Horizons mission.

Bell S. W. Lasue J. Stepinski T.
Automated Classification of Stratospheric Dust **[#2622]**
We have applied data mining techniques to the JSC Cosmic Dust Catalog Volume 16 cluster particles. We have demonstrated a technique capable of reproducing the separation between cosmic and contaminant particles.

Lasue J. Stepinski T. F. Bell S. W.
Automatic Classification of Interplanetary Dust Particles **[#2054]**
We present an automatic classification of the IDPs collected by NASA-JSC based on their EDS spectra. Agglomerative clustering and the Sammon's map algorithms are used to visualize relationships between the clusters.

Sekigawa C. Keller L. P.
The Mineralogy, Petrography and Chemistry of Comet Dust: Sulfides **[#2405]**
Our measurements focused on the sulfide grains to determine the mineralogy, mineral compositions and grain sizes for several interplanetary dust particles (IDPs) in order to provide a database for comparison with other primitive meteoritic materials.

Nakamura-Messenger K.   Messenger S.   Ito M.   Keller L. P.   Clemett S. J.   Jones J. H.   Klöck W.
Zolensky M.   Tatsuoka H.
Si Isotopes of Brownleeite **[#1900]**
To evaluate the origin of the newly discovered mineral, Brownleeite (MnSi) and the associated LIME olivine, we performed isotopic analyses using the NASA/JSC nanoSIMS ion microprobe. Si isotopic data indicate that they are probable solar system products rather than Stardust.

Floss C.   Stadermann F. J.   Mertz A. F.   Wopenka B.
Anatomy of an Isotopically Primitive IDP from the 55P/Tempel-Tuttle Targeted Collector: Quantitative Auger Measurements of C and N Abundances in N-Anomalous Hotspots **[#1330]**
Kerogen standards were measured to get C and N sensitivity factors for quantifying Auger elemental spectra of carbonaceous matter. Application to N-anomalous areas in a primitive IDP shows an inverse correlation of N abundances with ^{15}N-enrichments.

Trappitsch R.   Leya I.
Modeling the Recoil Loss of Cosmogenic Nuclides in Micrometeorites **[#1852]**
We present a purely physical model to quantify recoil losses in all types of grains and all types of irradiation environments where the maximum projectile energy is below 245 MeV.

Taylor S.   Jones K. W.   Hornig C.   Herzog G. F.
Porosity of Micrometeorites Measured by Tomography **[#1909]**
Vesicles in micrometeorites show up clearly in the micro-tomographic images. The shape and distribution of vesicles are tightly linked to specific textural types and provide an independent criterion for classifying micrometeorites.

Taylor S.   Delaney J. S.   Herzog G. F.
A CAI Micrometeorite **[#1205]**
SP-155 is a 200 µm × 150 µm CAI found in the South Pole water well micrometeorite collection. Its core resembles Type A and B1 CAIs except that it contains no melilite. SP-155 is much larger than any previously reported CAI or refractory phases found in MM and IDPs.

Doi M.   Nakamoto T.   Nakamura T.   Yamauchi Y.
Three-Dimensional Shapes of Cosmic Spherules: Deformation of Dust Particles Molten in the Earth Atmosphere **[#1560]**
We measured the 3-D shape of once molten stony cosmic spherules. Also, we theoretically modeled the deformation of cosmic spherules and compared the calculation and observation results. We found that the model may explain the observed results.

Sears D. W. G.   Craig J. P.
Thermoluminescence and the History of Cometary Particles **[#1404]**
TL studies provide a wide variety of data on tiny samples not obtainable by other methods.

ORIGINS OF PRESOLAR GRAINS

Gilmour J. D.   Holland G.   Turner G.   Verchovsky A. B.   Fisenko A. V.   Semjonova L. F.
Observation and Implications of Iodine (with Iodine-129) Associated with Presolar Xenon Components in Meteoritic Nanodiamonds **[#1662]**
Iodine with live ^{129}I is shown to be associated with the P3 and P6 (but not HL) xenon components in nanodiamonds at I/Xe ratios >100× higher than expected for average galactic material. This suggests a distinct, chemically selective trapping process.

Garvie L. A. J.
Where are the Nanodiamonds in the Primitive Meteorites? Preliminary TEM Results **[#1388]**
Transmission electron microscopy and electron-energy loss spectroscopy is used to find nanodiamonds in the primitive meteorite matrix materials.

Otsuki K.
Origin of Xe-H Component in Presolar Diamond **[#1652]**
Possible origin of Xe-H component in presorlar diamond is discussed. Theoretical calculations are compared with measured $^{134}Xe/^{136}Xe$ ratio. Further isotope analysis of diamond can be a strong constraint of this model.

Heck P. R.   Pellin M. J.   Davis A. M.   Martin I.   Renaud L.   Benbalagh R.   Isheim D.   Seidmann D. N.   Hiller J.   Stephan T.   Lewis R. S.   Savina M. R.   Mane A.   Elam J.   Stadermann F. J.   Zhao X.   Daulton T. L.   Amari S.
Atom-Probe Tomographic Analyses of Presolar Silicon Carbide Grains and Meteoritic Nanodiamonds — First Results on Silicon Carbide **[#2112]**
We present first results of laser-assisted atom-probe tomography of presolar silicon carbide grains and describe our effort to analyze the chemical compositions of individual meteoritic nanodiamonds.

Wopenka B.   Jadhav M.   Lebsack E.   Zinner E.
Raman and Isotopic Studies of Large Presolar SiC Grains **[#1390]**
Raman spectra correlate with grain morphology: euhedral grains are cubic, grains with smooth, blocky morphology are hexagonal. An unusually large (30 µm) polycrystalline cubic X grain has wide Raman peaks, indicative of crystallographic disorder.

King A.   Henkel T.   Rost D.   Lyon I.
Trace Element Depth-Profiles in Presolar SiC **[#1976]**
TOFSIMS has been systematically used to study the distribution of trace elements in seven presolar SiC grains. There is evidence to suggest that some trace elements may have been implanted into the grains.

Croat T. K.   Lebsack E.   Bernatowicz T. J.
Pristine SiC Candidates: Spectral Imaging and Auger Investigations **[#1891]**
We describe a new spectral imaging method to locate pristine SiCs (those prepared without acid dissolution) from within Murchison matrix material. We present images,X-ray and Auger electron spectra from pristine SiCs, which show carbonaceous surface coatings.

Zinner E.   Gyngard F.   Nittler L. R.
Automated C and Si Isotopic Analysis of Presolar SiC Grains from the Indarch Enstatite Chondrite **[#1359]**
We report C and Si isotopic ratios of presolar SiC and Si_3N_4 grains from the Indarch enstatite chondrite obtained by automated NanoSIMS analysis. One unusual SiC grain with large $^{29,30}Si$, ^{12}C and and ^{15}N excesses originated in a Type II supernova.

Jadhav M.   Amari S.   Zinner E.   Maruoka T.
Presolar Graphite Grains from Orgueil: Some Unresolved Issues **[#1035]**
We highlight some of the problems we encountered while studying presolar graphite grains from Orgueil and trying to constrain the nucleosynthetic processes in their stellar sources.

Vollmer C.   Hoppe P.
First Fe Isotopic Measurement of a Highly ^{17}O-enriched Stardust Silicate **[#1200]**
We report on NanoSIMS Fe isotopic measurements of thirteen stardust silicates from the Acfer 094 meteorite. Most of the stardust silicates have solar $^{54}Fe/^{56}Fe$ ratios, but one highly ^{17}O-enriched silicate is significantly depleted in ^{54}Fe.

Le Guillou C.   Brearley A. J.   Brunner C. E.   Floss C.   Stadermann F. J.
FIB Extraction and TEM Analysis of Presolar Grains from the CR3 Chondrite MET 00426 **[#2602]**
The preliminary results of an integrated NanoSIMS/FIB/TEM study of isotopically anomalous C and O grains from the CR chondrite MET 00426 are presented.

Davidson J.   Busemann H.   Franchi I. A.   Grady M. M.
Presolar Grain Inventories of the Ungrouped C3 Adelaide and the CV3 RBT 04133 **[#2230]**
Here we report the presolar grain inventories (silicates, oxides, SiC, and other C-anomalous phases) determined for Adelaide (an ungrouped C3 chondrite) and RBT 04133 (a mildly thermally altered CV3) by NanoSIMS raster ion imaging.

Zhao X.   Stadermann F. J.   Floss C.   Bose M.   Lin Y.
Characterization of Presolar Grains from the Carbonaceous Chondrite Ningqiang **[#1431]**
Five Fe-rich presolar silicates (115 ppm) and one possible SiC (1 ppm) were found in the Ningqiang C chondrite. Two of the silicates are unusually large (~1 µm). Secondary alteration (metasomatism) may account for the Fe-enrichment of the silicates.

Meyer B. S.   Johnson J. P.
Internal Equilibration Rate of ^{186}Re and Presolar Grains **[#2654]**
We compute the effective internal equilibration rate of ^{186}Re. Calculations Os abundances in s-process calculations do not need modification for branching through the ^{186}Re isomer for comparison with presolar grain data.

SOLAR WIND, VOLATILE ELEMENTS, AND ORGANICS

Verchovsky A. B.   Franchi I. A.
Measurements of Nitrogen in the Genesis Concentrator Target Materials: Sources of Contamination N **[#2127]**
We analysed the sources of contamination N for the gold cross and DLC Genesis concentrator targets using published and our own data. We found that the contamination sources for the materials are different.

Becker R. H.
Solar Wind ^{15}N/^{14}N from Genesis — A Tale of Two Values **[#2469]**
Values for solar wind nitrogen of –385‰ and +320‰ have been reported from Genesis samples in the past year. These values represent a factor of two difference in ^{15}N/^{14}N. Possible explanations for the discrepancy are considered.

Heber V. S.   Guan Y.   Jurewicz A. J. G.   Kallio A. P.   Olinger C.   Woolum D. S.
McKeegan K. D.   Burnett D. S.
Solar Wind Elemental Fractionation: Genesis C and O Fluences by Backside SIMS Profiling — Preliminary Data **[#2234]**
We here report the first successful analyses of C and O fluences from Genesis. Backside depth profiling with SIMS is a strong tool to detect shallowly implanted solar wind in spite of large surface contamination.

Cetina C.   Demoranville L. T.   Grabowski K. S.   Knies D. L.
Evaluation of Standards for Silicon Analysis in Germanium Genesis Collectors by SIMS-AMS **[#2729]**
Recent efforts at the NRL SIMS-AMS facility have focused on Si measurements towards evaluating the possibility of Si analysis in Genesis collectors. We have begun to evaluate the use of the Ge substrate material for Genesis measurements.

King B. V.   Veryovkin I. V.   Zinovev A. V.   Tripa C. E.   Pellin M. J.   Toyoda N.   Yamada I.   Schmeling M.
Ion Beam Removal of Surface Contamination in Genesis Samples **[#1975]**
Surface contamination of Genesis samples limits our ability to accurately measure solar wind fluences. We show using AFM, TXRF, interferometry and RIMS depth profiling that cluster ion sputtering can successfully remove such contamination.

Olinger C. T.   Wiens R. C.
Interpreting Measured Solar Wind Implant Profiles Through Simulation **[#2219]**
SRIM simulations provide a tool for understanding differences in solar wind compositions inferred from different measurements of Genesis materials and differences between short-term Genesis exposures and long-term lunar exposures to solar wind.

Kuhlman K. R.   Lyon I.   Burnett D. S.
Genesis Cleaning and Particle Analysis Techniques: An Update **[#1822]**
We are experimenting with various methods for cleaning difficult sample and using a secondary electron microscope with energy dispersive spectroscopy to analyze submicron particulates that are recalcitrant to removal.

Schmeling M.
Analysis of Genesis Sample Surface Contamination by Total Reflection X-Ray Fluorescence Spectrometry **[#1682]**
Laboratory based TXRF has been used to analyze Genesis flight samples for surface contamination. After initial cleaning substantial contaminations remained but additional acid cleaning could remove most of these.

Rieck K.   Jurewicz A. J. G.   Wadhwa M.   Burnett D. S.   Hervig R.   Wiens R.
SIMS Measurements of Mg Isotopes in the Solar Wind **[#2391]**
Using Genesis collector materials, we investigate whether or not solar wind (SW) Mg isotopes are fractionated compared to the photospheric composition.

Yurimoto H.   Itoh S.   Ebata S.
Oxygen Isotopic Composition of Stellar Wind from the Protosun **[#1098]**
We report bimodal distribution of O isotopic composition from metal grains in a gas-rich chondrite. The ^{16}O-rich component seems to be trapped solar wind of the protosun. The composition suggests no signature of self-pollution in the solar system.

Yamada A.   Nanbu S.   Kasai Y.   Ozima M.
Qauntum Chemical Calculations on Photo-Dissociation; Isotope Effect of the Rotational Levels of the Ground State O_2 Molecules with Relevance to Exotic Oxygen in Lunar Metals **[#1653]**
To reveal the mechanism of MIF oxygen, we calculate photo-dissociation cross section of O_2 by using the quantum dynamics simulations and estimate isotopic ratio of dissociated oxygen atoms for comparison with exotic oxygen in lunar metals.

Vogel N.   Baur H.   Bochsler P.   Bühler F.   Grimberg A.   Wieler R.
New Analyses of Helium, Neon, and Argon in Aluminum Foils of the Apollo Solar Wind Composition Experiment **[#1907]**
We present new analyses of solar wind He, Ne, and Ar obtained by UV laser ablation of Apollo 15 foils. The new data will be compared to those obtained ~40 years ago and to Genesis solar wind data. Agreements and potential discrepancies will be discussed.

Amari S.   Matsuda J.
Noble Gas Analysis of Q-rich Fractions from Orgueil and Allende **[#1570]**
We analyzed noble gases in HF-HCl and pyridine-treated residues from Orgueil and Allende by step-wise heating. After the pyridine treatment, 27–45% of the heavy noble gases were lost in the Orgueil residue, while there was no substantial loss in the Allende residue.

Spring N.   Vogel N.   Baur H.   Wieler R.   Alexander C. M. O'D.   Busemann H.
Pyridine Treatment of Insoluble Organic Matter from Chondrites Krymka and Vigarano — No Effects on the Noble Gas Carrier Phase Q **[#2640]**
We examine the effect of pyridine on phase Q in macromolecular organic matter in chondrites Krymka and Vigarano. Our results show no Q-gas loss. Such loss has been found in Orgueil, although attribute this to presolar grain loss.

Crowther S. A.   Busemann H.   Gilmour J. D.
Distribution and Abundance of Q-Xe Carriers in Acfer 094 Matrix **[#1895]**
The Xe concentrations in individual 10–40 µm samples of Acfer 094 matrix have been measured. The derived distribution is compared with models to estimate the distribution of Q-Xe carriers, suggesting that for a typical 500 nm grain size, ~1 grain in (1-10)E3 is a carrier.

Nuth J. A.   Johnson N. M.   Meshik A.   Hohenberg C.
Trapping Planetary Noble Gases During the Fischer-Tropsch-type Synthesis of Organic Materials **[#1232]**
We will report measurements of the noble gas trapping in macromolecular carbon coatings formed via FTT reactions on silicate smokes.

Kimura Y.   Saito M.
Synthesis of Organic Hollow Globules Based on Singular Phenomena of Nanoparticles **[#1599]**
We duplicated organic hollow globules founding in carbonaceous chondrite in a laboratory. Our results suggest the globules can be produced in circumstellar environments and are possibly the final products in the evolution of carbonaceous matter.

Matsumoto T.   Tsuchiyama A.   Nakamura-Messenger K.   Zolensky M. E.   Nakano T.   Uesugi K.
Search for Organic Nanoglobules in Carbonaceous Chondrites Using Microtomography **[#1960]**
We identified organic nanoglobules in carbonaceous chondrites non-destructively using X-ray microtomography. Some globules were confirmed by TEM. We may examine whether or not fluids are preserved in the hollows of the globules for a further study.

Thomen A.   Remusat L.   Robert F.   Meibom A.   Mostefaoui S.
Chemical and Nitrogen Isotopic Composition of the Hotspots in Orgueil Insoluble Organic Matter **[#2472]**
A NanoSims study shows the relations between the CN/C ionic ratio and (1) the sample topography or (2) the departure from the steady state Cesium implantation. These relations has profound implications for the interpretations of this ratio measured in extraterrestrial materials.

Rost D.   Busemann H.   Henkel T.   King A.   Spring N.   Alexander C. M. O'D.   Lyon I.
First Results from the Study of Extracted Insoluble Organic Matter with C60-ToF-SIMS **[#1973]**
We present our first measurements of IOM residues analyzed with time-of-flight secondary ion mass spectrometry utilizing C_{60}^+ primary ions.

Robert F.   Thomen A.   Anquetil Ch.   Derenne S.   Hassouni K.
Hydrogen Isotopic Exchange Rates Between D_3^+ and Aliphatic, Aromatic and Benzilic C-H Bonds **[#1206]**
The hydrogen isotopic fractionation factors measured between the three types of C-H bonds identified in the IOM were reproduced in laboratory conditions.

FORMATION OF THE BUILDING BLOCKS OF PLANETARY BODIES

Rubin A. E.
Comparative Chondrule-ology: Evidence for Multiple Melting of Chondrules in Dusty Environments **[#1011]**
Chondrite groups with large chondrules have few RP+C types, many enveloping compound chondrules, many chondrules with thick igneous rims, and few sulfide-bearing type-I chondrules. Chondrite groups with small chondrules have the opposite properties.

Konrad K.   Ebel D. S.   McKnight S. V.
X-Ray Image Analysis of Clast Size and Abundance in Acfer 094 **[#1447]**
Image analysis of clasts in X-ray mapped (10.5 sq. mm, 1 µm/pxl) unique, primitive chondrite Acfer 094 reveals 51.2 vol% matrix, 38.9% chondrules, 2.8% CAIs, 4.0% AOAs. The composition confirms that it is unique and should remain ungrouped.

Sherman K. M.   Friedrich J. M.   Ebel D. S.   Rivers M. S.
Methods for Direct Measurement of Chondrule Size, Morphology and Density **[#2313]**
Size, shape, and density of groups and individual chondrules, are measured through varous two-dimensional and three-dimensional techniques. Three-dimensional tomography images and serially sectioned slices of Semarkona (LL3.0) are quantified for application to astrophysical modeling.

Singerling S. A.   Glazner A. F.   Singletary S. J.   Pavelsky T. M.   Tacker R. C.
Textural Mineral Mapping of the Farmville Meteorite Using GIS Software **[#1884]**
We analyzed the ordinary chondrite meteorite, Farmville, on an SEM and created X-ray images which were then treated as Landsat multispectral images using ENVI software. The result was a textural mineral map, useful for phase distribution analysis.

Herd R. K.   Samson C.   Dixon L.   Cooke A.   Hunt P. A.
Testing and Extending a New Classification Scheme for Chondrules **[#2026]**
A new descriptive, product based classification scheme for chondrules, derived from study of 370 chondrules in a single polished thin section of Saratov (L4), is being tested on a second section and refined for use on similar grade meteorites.

Kurat G.   Varela M. E.   Zinner E.
Chondrule Tieschitz XII Revisited: Reading a Very Old Logbook **[#1315]**
Chondrule Tieschitz XII (Tie XII) was recently re-investigated with an ion micro-probe. Tie XII perfectly fit the PLC model (Varela and Kurat, 2009) and the theoretical predictions of phase condensation in a non-canonical solar nebula [*Ebel,* 2006].

Chaussidon M.   Villeneuve J.
Constraints on the Origin of Refractory Olivines in Allende Type I Chondrules from their Oxygen Isotopic Composition **[#1626]**
Developments of high precision oxygen isotopic analysis by multi-collector ion microprobe allow to test whether Mg-rich relict olivines in type I chondrules from Allende could originate from the disruption of a few prexisting planetesimals.

Kurahashi E.   Hezel D.   Russell S. S.
Petrological Studies of Type I Chondrules in Primitive CR Chondrites **[#1634]**
Bulk elemental abundance ranges of Type I chondrules of CR chondrites are similar to those of CO Type I chondrules except iron. Higher abundance of iron of CR Type Is suggests they formed in higher oxidizing region relative to CO Type I chondrules.

Villeneuve J.   Chaussidon M.   Libourel G.
Timing of Formation of FeO-poor Olivines from Allende Chondrules: Evidence from Mg Isotopic Compositions **[#1801]**
We used our high precision ion probe procedure for the measurement of the ^{26}Al-^{26}Mg systematics to study the Mg isotopic composition of FeO-poor olivines from the Allende carbonaceous chondrite. The goal was to constrain the Mg model age of FeO-poor olivines.

Jacquet E.   Alard O.   Gounelle M.
Trace Element Analyses of Silicates and Glass in Renazzo (CR2) Chondrules **[#1739]**
Irrespective of textural type, olivine REE content measured by LA ICPMS are on the order of 0.01× CI for LREE and subchondritic for HREE. Such fractionation might indicate rapid cooling.

Morlok A.   Sutton Y. C.   Braithwaite N.   Grady M. M.
Experiments in Chondrule Formation: Simulations of Gas-Grain Collisions Using Plasma Arcs **[#1764]**
To investigate the formation of chondrules in gas-grain collisions, we conducted experiments where mineral mixtures were melted in plasma arcs. First results already show silicate-rich spheres quite similar to chondrules.

Chiba H.   Tachibana S.   Nagahara H.   Ozawa K.
Reaction Experiments of Forsterite with Si-rich Gas in Molecular-Beam Epitaxity Type Vacuum Furnace **[#2531]**
We carried out experiments on a reaction between forsterite and Si-rich gas at temperatures close to formation temperatures of enstatite in protoplanetary disks and circumstellar environments using a molecular-beam epitaxy type vacuum furnace.

Das J. P.   Goswami J. N.   Pravdivtseva O. V.   Meshik A. P.   Hohenberg C. M.
Cosmogenic Neon in Individual Chondrule Fragments: Records of Pre-Compaction Exposure **[#1961]**
This first ever study on 41 splits of chondrules show that ^{21}Ne CRE ages in 11 splits are high compared to that of host, ranging from 5–35 Ma. Splits from same chondrule show different CRE ages. We conclude that the excess is due to early active Sun.

Morris M. A.   Desch S. J.   Ciesla F. J.
Preliminary Assessment of Chondrule Cooling Rates in Planetesimal Bow Shocks, Including the Heating Effects of H_2 Recombination **[#2393]**
A preliminary assessment of the planetesimal bow shock model, examining the effects of recombination of hydrogen on chondrule cooling rates. We find that it remains unlikely that planetesimal bow shocks were the mechanism responsible for the formation of most chondrules.

Miura H.   Yokoyama E.   Nagashima K.   Tsukamoto K.
Demonstration of Chondrule Melt Solidification by Numerical Simulation **[#1663]**
We carried out numerical simulation of crystallization from a supercooled chondrule melt sphere. We report one successful simulation result in which crystalization pattern very similar to internal texture of BO chondrule was reproduced.

CHONDRITES

Lipman M. D.   Strait M. M.   Flynn G. J.   Durda D. D.
New Information from Impact Disruption Experiments of Chondritic Meteorites **[#2442]**
Comparing measurement methods for dents and holes in disrupted meteorite samples.

Durda D. D.   Movshovitz N.   Richardson D. C.   Asphaug E.   Rawlings A. R.   Vest C.
Large-Scale Experiments to Determine the Coefficient of Restitution for Meter-Scale Granite Spheres **[#1896]**
We present results from an extensive series of large-scale experiments to measure the coefficient of restitution for impacts between 1-m diameter granite spheres with collision speeds up to ~2 m/s.

Fagan T. J.   Kataoka S.   Yoshida A.   Norose K.
Transition to Low Oxygen Fugacities in the Solar Nebula Recorded by EH3 Chondrite ALHA 81189 **[#1534]**
ALH A81189 may be the most primitive EH3 chondrite. However, variations in chondrule types suggest that it is not the metamorphic protolith of other EH3 chondrites. ALH A81189 formed at slightly higher oxygen fugacities than other EH3s.

Schepker T. J.   Ruzicka A. M.
X-Ray Diffraction as a Tool for the Classification of Equilibrated Ordinary Chondrites **[#2644]**
XRD-determined d_{130} values can be used with confidence to discriminate between equilibrated ordinary chondrites of different groups, and to estimate olivine Fa contents, provided scan times are sufficiently long.

Duffy C. M.   Bland P. A.   Abel R. L.   Twelker E.
Grain-size Analysis of CBa Gujba Using 3-D Computed Tomography Methods **[#1800]**
The origin of CBs is still a matter of debate. Three-dimensional graphical representations of particular phases (>1800 grains were analysed) enable grain size frequency distributions to be determined, which may assist in constraining an origin by condensation.

Riches A. J. V.   Liu Y.   Zhang A.   Taylor L. A.
Description of Newly -Identified CV3 Chondrites: Salient Textural and Mineralogical characteristics **[#2561]**
This abstract presents the preliminary results of two newly identified oxidized-CV3 chondrites.

Patzer A.   Pack A.
Investigation of Refractory Lithophile Trace Elements in the Leoville CV3 Meteorite **[#1590]**
We will present comprehensive geochemical data of the reduced CV3 chondrite Leoville. In particular, we will investigate the inventory of refractory lithophile trace elements and deduce constraints on condensation processes and the formational history of the meteorite.

Hutson M. L.   Ruzicka A. M.
Jungo 001, Jungo 002, Jungo 003, and Big Horn Mountains: Four New Chondrites from Nevada and Arizona Which Contain a Variety of Unusual Petrographic Features **[#1878]**
Four newly classified chondrites from Nevada and Arizona show one or more unusual petrographic features, including conjugate fractures, a complexly textured olivine-rich clast, silicate-bearing troilite, and bimodal weathering.

Troiano J.   Rumble D. III   DiRaimo A. G.   Rivers M. S.   Friedrich J. M.
Compositional Studies of Three Low-FeO Ordinary Chondrites **[#1815]**
We detail our efforts to investigate the oxygen isotopic and whole rock trace element abundances in the low-FeO ordinary chondrites Burnwell, LAP 04575, and EET 96031. Our data supports a common origin for most low-FeO and H chondrites.

Archer G. J.   Reeves D. W.   Taylor L. A.   McSween H. Y.
A New Equilibrated Ordinary Chondrite from North West Africa **[#2300]**
We describe and classify a newly recovered L5/6 chondrite from North West Africa.

McCausland P. J. A.   Brown P. G.   Hildebrand A. R.   Flemming R. L.   Barker I.   Moser D. E.
Renaud J.   Edwards W.
Fall of the Grimsby H5 Chondrite **[#2716]**
Meteorites fell in the area of Grimsby, Ontario on the early evening of Sept. 25, 2009. The bright fireball event was well recorded by a camera network, radar and infrasound and thus far 13 fragments of a fresh H5 chondrite have been recovered.

Fries M.   Fries J.
Partly Cloudy with a Chance of Chondrites — Studying Meteorite Falls Using Doppler Weather Radar **[#1179]**
We present Doppler weather radar as a new method for locating meteorite falls. This locates meteorites within a few kilometers of the ground, provides some characterization in flight, and functions for new falls and archived events back to 1992.

Tan D.   Harvey R. P.   Caffee M.   Osinski G.
Limited Fluctuations of East Antarctic Interior in Late Pliocene, and Influences on Meteorite Concentrations **[#2416]**
Cosmogenic exposure age dating in the Miller Range indicate that the East Antarctic Ice sheet interior has few fluctuations in the past 2 m.y., which is significant for meteorite concentration.

Corrigan C. M.   Welzenbach L. C.   McCoy T. J.
The Antarctic Meteorites: Classification and Curation at the Smithsonian Institution **[#2332]**
Here we describe the current state of classification and curation of the Antarctic Meteorite Program at the Smithsonian Institution.

Bourot-Denise M.   Zanda B.   Marrocchi Y.   Greenwood R. C.   Pont S.   Hewins R. H.   Franchi I. A.   Cornen G.
Paris: The Slightly Altered, Slightly Metamorphosed CM that Bridges the Gap Between CMs and Cos **[#1683]**
A fresh, 1.3 kilo stone was found in Paris. It is a CM chondrite with metal, Fe-sulfide, FeS-rich PCPs and relict mesostasis and is ~3.0 ± 0.1. Petrographic and oxygen isotope evidence indicates that it has affinities with the CO chondrites.

Wittmann A.   Kring D. A.   Friedrich J. M.   Troiano J.   Macke R. J.   Britt D. T.   Swindle T. D.
Weirich J. R.   Rumble D. III
Highly Porous and Compositionally Intermediate Ordinary Chondrite LAP 031047 **[#1848]**
LAP 031047 is a highly porous ordinary chondrite with a very young Ar-Ar age, and oxygen isotopic, and bulk and silicate mineral composition intermediate between H- and L-chondrites: Shock-lithified debris of a distinct ordinary chondrite asteroid?

Isa J.   Rubin A. E.   Wasson J. T.
Petrology and Bulk Chemistry of R Chondrites: New Data **[#2525]**
New INAA data show that R chondrites of all petrologic types are isochemical. R3 PRE 95411 contains numerous awaruite grains; R6 Y 980702 has a fine-grained granoblastic matrix; MET 01149 is reclassified as R3.

Bunch T. E.   Rumble D. III   Wittke J. H.   Irving A. J.   Pitt D.
Multilithologic, Extra-Ordinary Chondrite Northwest Africa 5717: Further Evidence for Unrecognized Metal-Poor, Non-Carbonaceous Chondritic Parent Bodies **[#1280]**
This unusual meteorite is a blend of two chondritic lithologies, neither of which resembles H, L, LL or carbonaceous chondrites.

Craig J. P.   Sears D. W. G.
Natural and Induced Thermoluminescence Data for Twenty-five 10–15 µm Particles from the LL3.0 Ordinary Chondrite Semarkona: Implications for the Nature and History of Primitive Solar System Material **[#1401]**
We report on the NTL and ITL properties of 25-µm grains of the LL3.0 ordinary chondrite Semarkona. We have seen the radiation history for these particles are uniform but the thermal history varies for such small samples in close proximity to each other.

Abreu N. M.   Nuth J. A. III
Laboratory-created Chondritic Matix: TEM Study of Nanophase Fe-Sulfides and Magnetite Embedded in Fe-rich Amorphous Silicates **[#1128]**
We produced materials resembling the matrices of type 3.0 chondrites by direct disequilibrium condensation from a gas. These experiments may also be relevant to the chemistry following the impacts of sulfide grains into aerogel.

Hezel D. C.   Howard L. E.
First Topographic High-Resolution Data of Carbonaceous Chondrite Matrices Using FEG SEM **[#1804]**
High-resolution imaging reveals detailed structural and petrological information. Porous matrices such as in CV and CO chondrites might still contain primitive material, whereas dense matrices such as in CM, CR, CH and CB chondrites were altered.

Lehner S. W.   Buseck P. B.
TEM Study of the Submicrometer-sized Fraction of Matrix in Sahara 97072 (EH3) and ALH 84170 (EH3) **[#1880]**
The submicrometer fraction of EH3 matrix contains areas of both amorphous and extremely fine-grained silica-rich material hosting submicron-sized clasts of minerals typical of the EH chondrites including schreibersite unassociated with Fe-Ni metal.

Scheffler F.   Fritz J.   Greshake A.
High-Pressure Phases of Chromite in L6-Chondrites and Martian Meteorites **[#1204]**
In a comparative study of chromites and their high-pressure polymorphs in L6-chondrites and chromite-bearing martian meteorites we studied their occurrence and discuss their formation history.

THERMAL AND AQUEOUS PROCESSES ON CHONDRITE PARENT BODIES

Harrison K. P.   Grimm R. E.
Thermal History of the H-Chondrite Parent Body Reconsidered **[#1794]**
We present a broad survey of available H-chondrite age and cooling rate data which, together with thermal and dynamical simulations, constrain the early history of the parent body.

Komatsu M.   Fagan T.   Watanuki H.   Norose K.   Matsui K.   Wakai H.
Variable Equilibration in Silicates and Sulfides in Enstatite Chondrites: Implications for Metamorphic and Nebular Reaction Histories **[#1522]**
Textures, EPMA and EBSD results from a set of enstatite chondrites indicate that pyroxenes from metamorphosed ECs preserve near-peak compositions, whereas troilite compositions continued to change during post-metamorphic-peak cooling.

Jones R. H.   Dreeland L.
Phosphate Minerals in the LL6 Chondrite, St. Séverin **[#1972]**
Merrillite and chlorapatite in St. Séverin both show compositional heterogeneity, including variable FeO contents and F/Cl ratios. At least some phosphate grain growth appears to postdate peak metamorphism, possibly in the presence of fluids.

Le Gac Y.   Benedix G. K.   Bland P. A.   Lyon I.   Henkel T.   Rost D.   Russell S. S.
A 750µm-Wide Sub-Hexagonal Clast in the Matrix of Orgueil **[#1940]**
We report an unusual regular-sided clast in the matrix of Orgueil (CI1), around 0.75 mm in diameter. We use SEM, EMPA and ToF-SIMS techniques to study this clast, and discuss its potential origins.

Blinova A.   Herd C. D. K.
Insights into the Mineralogy of the Tagish Lake Meteorite Through EPMA, XRD and CL **[#2140]**
We present new EPMA, XRD and CL data on the new lithologies from the Tagish Lake C2 carboneceous chondrite.

Petitat M.   Gounelle M.
Magnetite Content and Carbonate Mineralogy as Constraints for Parent Body Hydrothermal Alteration **[#1673]**
We present a mineralogical study of magnetite and carbonates from various C1s and C2s in order to improve our understanding of the relationships between these two minerals and between these meteorite groups.

Mironenko M. V.   Zolotov M. Yu.   Marshakov A. I.   Yurasova T. A.   Rybkina A. A.
Dissolution Rate of Kamacite: Electrochemical Study Under Anoxic Aqueous Conditions **[#1403]**
We report dissolution rate of kamacite from the Sikhote-Alin iron meteorite in neutral anoxic water at 25°C and discuss implications for aqueous processes in parent bodies of carbonaceous chondrites.

Palmer E. E.   Lauretta D. S.
A Kamacite Alteration Index for CM Chondrites **[#2211]**
We establish an alteration scale for aqueous alteration of kamacite on CM chondrites. Kamacite alters into tochilinite and P-rich sulfides. We use the width of the tochilinite rim to establish the degree of alteration.

Howard K. T.   Benedix G. K.   Bland P. A.   Greenwood R. C.   Franchi I. A.   Cressey G.
Correlated Modal Mineralogy, Aqueous Alteration and Oxygen Isotope Composition of CM Chondrites **[#1595]**
In this study we move beyond defining alteration sequences in CM chondrites towards understanding the relationship between modal mineralogy, the extent of aqueous alteration and O-isotope compositions.

Sugiura N.   Ichimura K.   Fujiya W.   Takahata N.
A Progress Report on the Mn/Cr Relative Sensitivity for Carbonate Measured with a NanoSIMS **[#1617]**
Mn/Cr relative sensitivity for a synthetic calcite was measured by SIMS. The relative Mn/Cr sensitivity is time-dependent. The time-averaged RSF for the calcite spot analysis is significantly lower than that for San Carlos olivine.

Tyra M. A.   Brearley A. J.   Matzel J.   Hutcheon I. D.
Types and Timescales of Secondary Carbonate in CR1 Chondrite GRO 95577 **[#2614]**
GRO 95577 is the only CR chondrite classified as type 1. We show that it possesses multiple carbonate phases (calcite, dolomite, and high Fe, Mn, and Mg "siderite"). We analyzed the short-lived Mn/Cr system (NanoSIMS) within the "siderite" and present preliminary results.

Pravdivtseva O.   Meshik A.   Hohenberg C. M.
Possible Late and/or Prolonged Aqueous Alteration in CR Chondrites Parent Body **[#2285]**
The I-Xe system in two studied Acfer 059 chondrules indicates that it may have been reset by aqueous alteration about 55 Ma after formation of CAIs.

Varela M. E.   Kurat G.   Zinner E.   Hoppe P.
Dark Inclusion Allende 4884-2B Provides New Insights on the Formation of Fayalitic Olivine **[#1317]**
We combine a chemical and petrographic study of the Allende DI 4884-2B and a ATEM study of Allende DI All-AF (NHM, Vienna) in order to get new insights onto the genesis of these objects.

Ford R. L.   Brearley A. J.
Discovery of Vesuvianite and Kaolinite Formed During the Alteration of Melilite in an Allende Type A CAI: Characterization by FIB/TEM **[#1402]**
While examining alteration in Allende CAIs, we observed margarite, grossular, vesuvianite and kaolinite. This is the first reporting of kaolinite and vesuvianite in an Allende CAI, further constraining alteration conditions for Allende CAIs.

NEAR-EARTH OBJECTS

Gaffey M. J.
Space Weathering and the Analysis of Asteroid Reflectance Spectra **[#2144]**
Space weathering on asteroids 243 Ida and 433 Eros differs from each other and from the Moon. This adversely affects curve matching analyses, but not analyses based on diagnostic spectral parameters such as band centers and band area ratios.

Nimura T.   Hiroi T.   Pieters C. M.   Abe M.
An Application of a Unified Model of Intimate Mixing, Space Weathering, and Modified Gaussian Deconvolution to a Ground-based Spectra of Asteroids **[#2711]**
The purpose of this study is to make a unified model of intimate mixing, space weathering, and modeified Gaussian model for estimating the composition, structure, and degree of space weathering and apply it to some ground based spectra of asteroids.

Okada T.   Fukuhara T.   Nakamura R.   Sekiguchi T.   Hasegawa S.   Kitazato K.   Taguchi M.   Imamura T.   Helbert J.   Hayabusa 2 Mid-Infrared Imager Team
Mid-Infrared Imaging for Surface Thermal Inertia and Material of Near-Earth Asteroid in Hayabusa-2 **[#2132]**
A mid-infrared imager is now proposed for thermal emission imaging of a C-class NEO in Hayabusa-2. The instrument is based on the LIR (long-infrared imager) onboard Akatsuki, adding a 8-point filter wheel will extend its observational function for material classification.

Takeuchi H.   Miyamoto H.   Maruyama S.
Origins of Bright Spots on the Surface of Boulders Covering Asteroid Itokawa. **[#1578]**
We examine the enigmatic features (bright spots) observed on the surface of boulders on asteroid Itokawa and conclude that bright spots are micro-craters formed by impacts of micrometeoroids on the surfaces of boulders.

Maruyama S.   Miyamoto H.   Takeuchi H.   Oku M.
Evidence for Global-Scale Inverse Grading of Regolith Materials on Asteroid Itokawa **[#1577]**
We analyzed the asteroid Itokawa to assess the nature and structure of the surface material. Detailed geological mapping was performed using high-resolution images. The results imply the existence of a global inverse graded regolith layer.

Korycansky D. G.   Asphaug E.
Rubble-Pile Calculations with the Open Dynamics Engine: Benchmarks and Angle-of-Repose Tests **[#1156]**
We present benchmarks and angle-of-repose tests for simulations of rigid-body dynamics using the Open Dynamics Engine (ODE).

Hartmann O.   Neukum G.
Impact-Chronology Model as Mass-Estimate Method for Impacted Masses on Planetary Surfaces **[#2082]**
The estimate of impacted masses on the surfaces of planetary bodies by application of recent lunar-like impact-chronology models will lead to the mass-depletion and time-constraints of the major impactor-source which is considered to be the asteroid belt.

Clark C. S.   Clark P. E.
Using Boundary-based Mapping to Determine the Underlying Structure for Itokawa and Other Small Bodies **[#1264]**
We apply the constant scale natural boundary mapping technique to Itokawa, a very small, low density, and rough object interpreted as a rubble pile, as part of our ongoing effort for morphological, dynamic, and historical classification of asteroids.

BOOM! HIGH-ENERGY IMPACTS

Lisse C. M.   Chen C. H.   Wyatt M. C.   Morlok A.   Thebault P.   Orton G. S.   Fletcher L. N.   Fujiwara H.   Bridges J. C.   Elkins-Tanton L. T.   Gaidos E. J.   Trang D.
Silica Debris Star Systems — Spitzer Evidence for Lunar Formation Events & Crustal Stripping or Magma Oceans & Late Heavy Bombardments? **[#2390]**
Recent work (*Lisse et al.,* 2009) has detected amorphous silica and SiO gas around 12-m.y.-old HD 172555, at the right age to form rocky planets. Here we discuss the location, lifetime, and source of the material, using inferences gleaned from HD 172555 and three new silica systems.

Roark S.   Cottingham C.   Dissly R.   Scheeres D.   Petr V.   Housen K.
Explosive Surface Pods for Cratering Experiments on Small Bodies **[#2100]**
This poster will describe the development and application of simple, inexpensive explosive surface pods for small body rendezvous missions.

Flynn G. J.   Durda D. D.   Minnick M. A.   Strait M. M.
Disruption Experiments on Porous Pumice Targets: Implications for Cratering and Disruption of Porous Asteroids like Mathilde **[#1078]**
Hypervelocity impact experiments into two pumice targets demonstrate that high porosity targets are more resistant to disruption and support the production of significantly larger craters than can be produced on low porosity materials.

Plesko C. S.   Weaver R. P.   Clement R. R. C.   Bradley P. A.   Huebner W. F.   Conlon L.
Energy Deposition in an Asteroid-like Target from a Stand-Off Nuclear Burst **[#2453]**
We model the deposition of energy from a 100 kt nuclear stand-off burst onto a basaltic asteroid using the RAGE hydrocode and the MCNP particle transport code.

Bradley P. A.   Plesko C. S.   Weaver R. P.   Clement R. R. C.   Guzik J. A.   Pritchett-Sheets L. A.   Huebner W. F.
Initial Parameter Study of the Response of Simple Asteroid or Cometary Nuclei Models to a Nuclear Burst **[#2540]**
One of the great challenges facing humanity is how to mitigate the threat from a potentially hazardous object (PHO). Our initial parameter study shows that we can deflect a simple PHO model with lead times of less than one year.

Weaver R. P.   Plesko C. S.   Dearholt W. R.
Los Alamos Hydrocode Models of Asteroid Destruction by an Internal Explosion **[#1729]**
We use the Los Alamos hydrocode xRAGE to calculate the disruption of realistic asteroid shapes from an internal explosion of 1–10 Mt. Realistic material equations of state and material fracture models are used.

Korycansky D. G.   Plesko C. S.
Re-Aggregation Times of Potentially Hazardous Object Fragments After a Hazard Mitigation Impulse **[#1456]**
We examine re-accretion times for potentially hazardous objects following the outcome of mitigation strategies, by modeling the disruption and re-aggregation of polyhedron-element rubble piles after the application of an impulsive applied velocity field.

LUNAR DUST

Glenar D. A.   Stubbs T. J.   Hahn J.   Vondrak R.
Did Clementine Observe Lunar Horizon Glow? **[#2735]**
The Clementine Star Tracker data set is being analyzed using an accurate scattering simulation code, in order to quantify the spatial distribution of horizon glow due to exospheric dust. Results of the work now underway will be presented.

Hartzell C. M.   Scheeres D. J.
The Implications of Lunar Water on Electrostatic Dust Levitation **[#2470]**
The recent discovery of increased water in colder terminator regions of the Moon can lower the cohesive forces between regolith particles there and lead to the preferential levitation of particles from the terminators, especially at sunrise.

Poppe A. R.   Horányi M.
Simulations of the Lunar Photoelectron Sheath and Associated Dust Grain Levitation Equilibria **[#1218]**
We simulate the lunar photoelectron sheath via a one-dimensional particle-in-cell code. Test particle studies of dust grain levitation are also presented.

Wohl C. J.   Lin Y.   Belcher M. A.   Atkins B. M.   Connell J. W.
Development of Materials and Evaluation Methods Concerning Lunar Dust Adhesion **[#1089]**
Lunar dust strongly adheres to surfaces due to both its physical properties and environmental factors. Mitigation strategies involving materials generation and modification will be presented along with techniques to evaluate their efficacy.

Dove A.   Dickson S.   Robertson S.   Sternovsky Z.   Wang X.   Horányi M.
Characterization of a UV-generated Photoelectron Sheath **[#2406]**
We measure the characteristics of the photoelectron sheath generated by UV radiation from a xenon excimer lamp above a photoemitting surface in vacuum.

Jackson T. L.   Farrell W. M.   Delory G. T.   Stubbs T. J.   Collier M. R.   Halekas J. S.   Vondrak R. R.
Astronaut and Object Charging on the Lunar Surface **[#2368]**
An astronaut or rover moving along the lunar surface will collect charge. In lunar craters, dissipation times for this charge are great compared to the dayside of the Moon. This work will advance the lunar surface charging model by incorporating a tribo-charging source.

Cooper B. L.   McKay D. S.   Riofrio L. M.   Taylor L. A.   Gonzalez C. P.
Lunar Dust Separation for Toxicology Studies **[#2297]**
We have developed a method for extracting respirable dust from Apollo lunar soils. This method meets stringent requirements that the soil must be kept dry, and must conserve and recover the maximum amount of both respirable dust and coarser soil.

Rask J. C.   McCrossin C. G.   Tranfield E.   Loftus D. J.
Persistent Chemical Reactivity of Quartz Generated by Mechanical Grinding Relevant to Lunar Dust Activation and Toxicity Studies **[#2672]**
We used mechanical grinding to generate radicals in silica, as a model for lunar dust. We observed persistence of these radicals for more than seven weeks, in contrast to previous reports of 30 hours, a finding that may have implications for lunar dust toxicity and ISRU.

LUNAR REGOLITH

Thompson M.   Christoffersen R.
The Smallest Lunar Grains: Analytical TEM Characterization of the Sub-Micron Size Fraction of a Mare Soil **[#2191]**
Analytical TEM observations show the sub-micron size fraction of a mature mare soil is highly enriched in glass grains, including spherules, relative to the larger size fractions, including the sub 10 micron size fraction as a whole.

Greenberg G.   Kiely C.   Kiely C. J.
Apollo 11 Lunar Regolith (10084-47) Revisted — A Novel Optical Microscopy Study **[#1119]**
Using oblique lighting conditions, along with the processing of a through-focal series of frames, has allowed us to obtain high resolution color micrographs of lunar regolith particles showing detail never thought possible with an optical microscope.

Cooper B. L.   McKay D. S.   Riofrio L. M.   Taylor L. A.   Gonzalez C. P.
Sub-10-Micron and Respirable Particles in Lunar Soils **[#2279]**
Grain size analyses of Apollo 11 soil 10084 by a laser diffraction technique shows that this soil contains roughly 2% by volume in the respirable (2.5 µm and below) grain size, in agreement with our prior estimates based on extrapolation of sieve data.

Ostrach L. R.   Robinson M. S.
Effects of Seismic Shaking on Grain Size and Density Sorting with Implications for Constraining Lunar Regolith Bulk Composition **[#2521]**
Does the lunar regolith exhibit compositional sorting at the few 100 µm to 10 cm depth scale? We report on experiments modeling a bimodal granular mixture of materials with strong density contrasts and varying grain sizes.

Jiang J.   Wang Z.   Li Y.   Zhang W.   Zhang Y.
The Microwave Anomalies of the Lunar Far-Side and South Pole — The Chang'E-1 Microwave Sounder (CELMS) Results **[#1176]**
CELMS shows the farside TBL is lower than the nearside, while the regolith thickness is thicker. The dielectric constant in the area 40S-70S, 159W-150E is fairly low. CELMS shows that it cannot rule out the possibility of water existing at the lunar pole.

Jin Y. Q.   Fa W.   Wieczorek M. A.
Preliminary Analysis of Microwave Brightness Temperature of the Lunar Surface from Chang-E 1 Multi-Channel Radiometer Observation and Inversion of Regolith Layer Thickness **[#1331]**
Using Chang'E-1 microwave radiometer observation, a global regolith thickness map was inverted and the global abundance of ^{3}He in the regolith was estimated.

Heggy E.   Fa W.   Thompson T. W.   Ustinov E.   Bussey B.   Spudis P.
Exploring Dielectric Properties of the Lunar Cratonic Fills from the Mini-RF Observations Onboard Chandrayaan and LRO **[#2031]**
We explore potential subsurface ice enrichment and compositional variations in lunar crater fills in the shadowed and illuminated areas using the Mini-RF SAR data on Chandrayaan and LRO.

LUNAR RADIATION

De Angelis G.   Dachev Ts. P.   Tomov B.   Matviichuk Yu.   Dimitrov P.   Spurny F.
A Comparison Between Models of the Moon Radiation Environment and the Data from the RADOM Experiment Onboard the Indian Chandrayaan-1 Satellite **[#1711]**
Models of radiation environment due to Galactic Cosmic Rays (GCR) and Solar Particle Events (SPE) on the Moon have been developed, and compared with data from the RADOM investigation onboard the ISRO Chandrayaan-1 spacecraft.

Case A. W.   Spence H. E.   Golightly M. J.   Kasper J. C.   Blake J. B.   Mazur J.6:30 p.m.
Townsend L.   Zeitlin C.
Variations in the Galactic Cosmic Ray Flux at the Moon: Effects of the Magnetotail and Solar Wind Structures **[#2606]**
This paper will use data from the CRaTER instrument on the Lunar Reconnaissance Orbiter (LRO) to investigate the magnetosphere's influence on the flux of GCR in low lunar orbit.

LUNAR GEOPHYSICS

Lillis R. J.   Halekas J. S.   Stewart S. T.   Louzada K. L.   Purucker M. E.   Manga M.
Lunar Impact Demagnetization: New Constraints from Monte Carlo Modeling and Multiple Altitude Magnetic Field Data **[#1511]**
We fit observed radial magnetic field profiles from the Lunar Prospector ER and MAG data sets to those predicted by Fourier domain modeling of impact demagnetization signatures to constrain impact parameters and crustal magnetization properties.

Grott M.   Knollenberg J.
The Apollo Thermal Conductivity Experiment Revisited **[#1102]**
We reassess the Apollo thermal conductivity measurements and conclude that regolith disruption by the rotary-percussion drill system probably caused the discordant thermal conductivity readings obtained by different methods.

Williams J. G.   Boggs D. H.   Ratcliff J. T.
Lunar Fluid Core Moment **[#2336]**
New data improves lunar science results. A fluid core and tidal dissipation are inferred from dissipation effects on orientation. Detection of core-mantle boundary flattening and fluid core moment are additional evidence for a fluid core.

Lawrence J. F.   Johnson C. L.
Synthetic Seismograms with High-Frequency Scattering for the Moon **[#2701]**
We investigate the seismic scattering effects of a highly heterogeneous regolith layer on the Moon, and how shallow heterogeneity effects high-frequency seismograms.

Kiefer W. S.
Gravity Constraints on the Subsurface Structure of the Marius Hills: A Sharper View of the Magmatic Pluming System Based on Improved Topography Data and New Lunar Density Measurements **[#1274]**
Gravity observations require the presence of a thick, high density batholith beneath much of the Marius Hills. The likely cause is basalt that has flooded the pore space within the brecciated anorthosite crust.

Yang H. W.   Zhao W. J.   Wu Z. H.
Derivation of Lunar Gravity Anomalies and Its Indispensable Effects in Lunar Interior Structure Research and Future Plans **[#1187]**
Derivation of lunar gravity model from orbit data. An effective method for lunar gravity reduction is described. How to apply gravity anomaly to interpretation and future plans. A lunar gravity anomaly map based on the SELENE data is displayed.

Kamata S.   Sugita S.   Abe Y.   Ishihara Y.   Harada Y.   Namiki N.   Iwata T.   Hanada H.   Araki H.
Viscoelastic Deformation of Lunar Basins: Implications for Lunar Farside Thermal History Based on Selenodetic Data of Kaguya **[#1727]**
Using our newly developed numerical code for viscoelastic motion of a Maxwell body, we analyzed the result of lunar farside gravity and topography data obtained by Kaguya, yielding several important constraints on lunar farside thermal history.

Macke R. J.   Kiefer W. S.   Britt D. T.   Consolmagno G. J.
Density, Porosity and Magnetic Susceptibility of Lunar Rocks **[#1252]**
We measured bulk and grain density, porosity and magnetic susceptibility for five Apollo lunar samples and three meteorites of lunar origin. We discuss the results of those measurements.

A NEW MOON: SPECTRAL CONSTRAINTS ON LUNAR CRUSTAL COMPOSITION

Petro N. E.   Gaddis L. R.   Rodriguez S. R.
Mapping Global Lunar Basalt Compositions with Clementine UVVIS and NIR Data **[#2628]**
With the online release of a calibrated and coregistered Clementine NIR global mosaic (100 m/pixel nominal resolution, 1100–2000 nm in four bands) both UVVIS and NIR data can now be used for detailed spectral characterization of lunar mare basalts.

Antonenko I.   Osinski G. R.
Automated Detection of Basalt Spectra in Clementine Lunar Data **[#2237]**
We empirically developed an automated method for detecting fresh basalt spectra in Clementine UVVIS data. Application of this method to a large study area consistently identified basalt spectra on the ejecta and/or slopes of selected craters.

Bhattacharya S.   Chauhan P.   Rajawat A. S.   Ajai   Kiran Kumar A. S.
Study of Central Part of Mare Moscoviense Using Chandrayaan-1 Hyperspectral Imager (HySI) Data **[#1870]**
Study of mare and highland units across the central part of Mare Moscoviense based on spectral parameters as applied on hyperspectral HySI data from Chandrayaan-1 mission with implication of multiple basaltic source regions and mantle heterogeneity.

Kubo N.   Namiki N.   Ohtake M.   Yamaji A.   Haruyama J.   Matsunaga T.
Layering and Thickness of Basalitic Lava Flows in Mare Humorum: New Spectral Analysis of Multiband Imager Data of Kaguya (SELENE) **[#1915]**
n this study, using spectral image data of Multiband Imager (MI) onboard Kaguya (SELENE), we estimate both thicknesses of mare basalt and lava flow units in Mare Humorum.

Kobayashi Y.   Ohtake M.   Haruyama J.   Matsunaga T.   Iwata T.   Morota T.   Yokota Y.
Yamamoto S.   Kitazato K.
Estimating Composition of Dark Mantle Deposit in Schrödinger Basin Using SELENE Spectral Data **[#1636]**
Dark Mantle Deposit (DMD) regions are considered to contain glassy or crystallized pyroclastic beads. We used the spectrum data acquired by SELENE Multi-band Imager to analyze a DMD in Schrödinger basin, and estimated the composition of the DMD.

Cloutis E. A.
Basalt-Ilmenite Mixtures: Spectral Reflectance Changes as a Function of Grain Size and Ilmenite Abundance **[#1139]**
Reflectance spectra of basalt + ilmenite mixtures show measurable differences, particularly in the UV region, that can potentially be used to constrain ilmenite abundances.

Liu F.   Shi J.   Li Q.   Rong Y.
Lunar Titanium Characterization Based on Chang'E (CE-1) Interference Imaging Spectrometer (IIM) Imagery and RELAB Spectra **[#1642]**
FWHM, absorption position, absorption depth, absorption area and absorption asymmetry are used to characterize titanium spectral features by Chang'E-1 and RELAB data around Apollo 17 and 16 landing sites.

Cheek L. C.   Pieters C. M.   Clark R. N.   Isaacson P. J.   McCord T. B.   Nettles J. W.   Petro N. E.
Sunshine J. M.   Taylor L. A.
The Goldschmidt Region as Viewed from Moon Mineralogy Mapper (M^3) Data **[#1962]**
The geology of the region near Goldschmidt crater on the northern lunar nearside has been investigated using M^3 data. The spectral character of local soils is heterogeneous and is influenced by material excavated by large nearby craters.

Cheek L. C.   Pieters C. M.   Parman S. W.   Cooper R.
Anorthite Synthesis Experiments with Applications to Lunar Spectroscopy **[#2438]**
Experiments to synthesize a suite of plagioclase samples for reflectance studies have produced Fe-bearing anorthite with broad absorption features in the near-IR.

Wyatt M. B.   Donaldson Hanna K. L.   Paige D. A.   Greenhagen B. T.   Helbert J.   Maturilli A.
Diviner Observations of Pure Plagioclase Regions as Identified by SELENE and the Moon Mineralogy Mapper **[#2498]**
Diviner thermal infrared observations of plagioclase regions on the Moon are analyzed along with laboratory emissivity spectra of the plagioclase solid solution series to determine if plagioclase compositional variations exist on the lunar surface.

Song E.   Bandfield J. L.   Glotch T. D.   Lucey P. G.   Greenhagen B. T.   Paige D. A.
Investigating Lunar Central Peak Compositions Using LRO Diviner Thermal Infrared Measurements **[#2578]**
Multispectral thermal IR measurements from Diviner were used to analyze compositional variability of impact crater central peaks. Compositional variations can be distinguished, but the effects of space weathering dominate spectral features.

Chauhan P.   Srivastava N.   Pieters C. M.   Ajai   Kiran Kumar A. S.   Navalgund R. R.   Head J. W.   Petro N.
Runyon C.   Goswami J. N.
Integrated Analysis of Topographically High Mafic Exposures at Apollo–17 Landing Site Using Data from Imaging Sensors on Chandrayaan–1 **[#1606]**
Mafic exposures at topographically high locations surrounding Apollo 17 landing site have been studied using imaging sensors onboard Chandrayaan -1 (TMC, HySI, and M^3). Compositionally, most of them have been found to be noritic.

Boardman J. W.   Pieters C. M.   Green R. O.   Clark R. N.   Sunshine J.   Combe J.-P.   Isaacson P.   Lundeen S. R.
Malaret E.   McCord T.   Nettles J.   Petro N. E.   Varanasi P.   Taylor L.
A New Lunar Globe as Seen by the Moon Mineralogy Mapper: Image Coverage, Spectral Dimensionality and Statistical Anomalies **[#1716]**
NASA's Moon Mineralogy Mapper, flown on ISRO's Chandrayaan-1, collected a global imaging spectrometry data set. We explore the M^3 coverage, the principal components of the whole data set and the detection of anomalous areas, revealing a new Moon.

Matsunaga T.   Ohtake M.   Haruyama J.   Yamamoto S.   Ogawa Y.   Nakamura R.   Yokota Y.   Morota T.
Honda C.   Abe M.   Nimura T.   Hiroi T.   Arai T.   Saiki K.   Takeda H.   Hirata N.   Kodama S.   Sugihara T.
Demura H.   Asada N.   Terazono J.   Otake H.
Updates on Scientific Results and Products of SELENE Spectral Profiler **[#2242]**
Updates on scientific results and products of the SELENE Spectral Profiler (SP) will be given. Scientific results highlight recently published papers and ongoing research. Status of available products and a plan for future products will be presented.

Haruyama J.   Hara S.   Hioki K.   Morota T.   Yokota Y.   Shirao M.   Hiesinger H.   van der Bogert C. H.
Miyamoto H.   Iwasaki A.   Ohtake M.   Saito Y.   Matsunaga T.   Nakanotani S.   Pieters C. M.   Lucey P. G.
New Discoveries of Lunar Holes in Mare Tranquillitatis and Mare Ingenii **[#1285]**
We recently reported the discovery of a vertical hole at Marius Hills region on the Moon in data acquired by SELENE Cameras. Here we report new discoveries of two additional deep holes in Mare Tranquillitatis and Mare Ingenii.

Tsuboi N.   Sugita S.   Hiroi T.   Nagata K.   Okada M.
A New Modified Gaussian Model (MGM) Using the Cross-Validation Method **[#1744]**
We propose a new MGM that can determine the optimum number of Gaussians, using the cross-validation. This method can detect the presence of olivine in OLV-OPX mixtures and may become a very useful tool for analyzing planetary spectra.

Yan B. K.   Wang R. S.   Gan F. P.   Wang Z. C.
Minerals Mapping of the Lunar Surface With Clementine UV-VIS-NIR Data Based on Spectra Unmixing Method and Hapke Model **[#1295]**
The distribution of clinopyroxene, orthopyroxene, olivine, ilmenite, and plagioclase on the lunar surface has been mapped with Clementine UV/VIS/NIR data. The results were validated using mineral composition data of Apollo samples.

Combe J.-Ph.   McCord T. B.   Kramer G. Y.   Pieters C. M.   Taylor L. A.   Petro N. E.   Boardman J. W.   Mustard J. F.   Sunshine J. M.   Tompkins S.   Green R. O.   M3 Team
Mixing of Surface Materials Investigated by Spectral Mixture Analysis with the Moon Mineralogy Mapper **[#2215]**
Lithological and mineralogical mapping of lunar surface is one main goal of the Moon Mineralogy Mapper imaging spectrometer. Spectral mixture analysis provides large scale maps of the main components that show diverse mare units and mineral contents.

Li L.   Li S.
Deriving Lunar Mineral Abundance Maps from Clementine Multispectral Imagery **[#2189]**
The effectiveness of the genetic algorithms (GA)-partial least square (PLS) regression for mapping lunar mineralogy was demonstrated using the Clementine UV-VIS-NIR image of the lunar surface covering eastern nearside maria.

Thomas I. R.   Bowles N. E.   Greenhagen B. T.   Glotch T. D.   Donaldson Hanna K. L.   Wyatt M. B.   Bandfield J. L.   Paige D. A.
Emission Measurements of Lunar Analogues for Interpretation of Returning Data from the Diviner Lunar Radiometer on NASA's Lunar Reconnaissance Orbiter **[#1364]**
Mineral emission spectra are altered by the lunar environment, therefore a new spectral database is being made of many lunar analogue minerals, which can then be compared to data returned from Diviner in order to constrain lunar surface composition.

Green R. O.   Pieters C. M.   Boardman J.   Eastwood M.   Mouroulis P.   Lundeen S.   White M.
Assessment of the Complete Moon Mineralogy Mapper Data Set and On-Orbit Validation of the Spectral Calibration **[#2190]**
We present assessment of the complete Moon Mineralogy Mapper imaging spectrometer data set that covers more than 95% of the Moon as well as on-orbit validation of the spectral calibration.

Green R. O.   Boardman J.   Pieters C. M.   Clark R.   M3 Team
An Algorithm for Estimation and Correction of the Thermal Emitted Radiance with Preservation of Spectral Structure in Data Measured by the Moon Mineralogy Mapper **[#2331]**
An novel algorithm for estimation and correction of the thermal emitted radiance with preservation of spectral structure in data measured by the Moon Mineralogy Mapper is present with initial test results.

Holsclaw G.   Snow M.   Hendrix A.   McClintock W.
The LASP Lunar Albedo Measurement and Analysis from SOLSTICE (LLAMAS) **[#2696]**
Description of ultraviolet lunar irradiance dataset from SOLSTICE.

Nefian A. V.   Kim T.   Broxton M.   Beyer R.   Moratto Z.
Towards Albedo Reconstruction from Apollo Metric Camera Imagery **[#1555]**
The goal of this research is to model the image formation process and extract the albedo information using digital elevation and surface reflectance models. This paper describes our results on lunar albedo reconstruction from images captured by the Apollo missions.

Denevi B. W.   Robinson M. S.   Hapke B. W.   Lawrence S. J.   Wiseman S. M.   Jolliff B. L.   LROC Team
Global Ultraviolet Through Visible Color Observations of the Moon with the Lunar Reconnaissance Orbiter Wide Angle Camera **[#2263]**
This study focuses on initial results from the LROC Wide Angle Camera, which provides a rich new dataset for the study of the photometric properties of the Moon and variations in ultraviolet-visible reflectance.

Mall U.   Korokhin V.   Shkuratov Yu.
Photometric Investigations Using the SIR-2 Data of the Chandrayaan-1 Mission **[#1616]**
NIR data from the SIR-2 point spectrometer on Chandrayaan-1 allow to estimate the phase function of lunar maria. We present a photometric correction technique for the SIR-2 data and show a comparison with Clementine UVIS data and first results.

Hicks M. D.   Buratti B. J.   Staid M.   Pieters C.   Nettles J.   Boardman J. W.   Sunshine J.
A Visible and Infrared Spectrophotometric Model for the Moon Based on ROLO and Chandrayaan-1 Moon Mineralogical Mapper Data **[#2076]**
We present a photometric model of the Moon from 430 nm to 3000 nm based on ground-based ROLO observations. This model is used for first-order phase reddening and absorption band attenuation correction.

Yokota Y.   Matsunaga T.   Ohtake M.   Haruyama J.   Nakamura R.   Yamamoto S.   Ogawa Y.   Morota T.   Honda C.   Saiki K.   Nagasawa K.   Kitazato K.   Sasaki S.   Iwasaki A.   Demura H.   Hirata N.
Refinement of Lunar Vis/NIR Phase Curve Acquired by SELENE Spectral Profiler **[#2532]**
The SELENE Spectral Profiler (SP) acquired lunar visible to NIR spectral data at a spatial resolution of 500 m. we report refined results of the phase curves derived from SP data.

Clark R. N.   Pieters C. M.   Taylor L. A.   Petro N. E.   Isaacson P. J.   Nettles J. W.   Combe J. P. M^3 Team
Rayleigh Scattering in Reflectance Spectra of the Moon **[#2337]**
Rayleigh scattering is observed in the lunar surface with Moon Mineralogy Mapper data.

Lucey P. G.
Nanophase Iron that Darkens but Does Not Redden: A Mie-Hapke Model **[#1604]**
Mie theory is used to compute the absorption properties of nanophase iron inclusions of any size including those that darken but do not redden. This approach reproduces experimental results better than prior approaches.

Garrick-Bethell I.   Head J. W. III   Pieters C. M.
Spectral Properties of Lunar Swirls and Their Formation by Dust Transport **[#2675]**
Albedo anomalies on the Moon associated with crustal magnetic fields can be explained by dust transport processes.

Kramer G.   Combe J.-P.   McCord T.   Harnett E.   Hawke B. R.   Blewett D.
An Investigation into the Effects of the Magnetic Anomaly on Regional Space Weathering at Mare Ingenii and Its Influence on the Spectra of the Basalts and Lunar Swirls **[#2594]**
Our analysis of Mare Ingenii points to the importance of solar wind implanted protons in creating $npFe^0$ on the lunar surface both within and outside the influence of a magnetic field.

Coman E. I.   Blewett D. T.   Hawke B. R.   Gillis-Davis J. J.   Purucker M. E.
Lunar Swirls and Crustal Magnetic Anomalies: Further Examination of the Link **[#1222]**
This report presents additional results from our ongoing study of the lunar swirls, their relation to lunar crustal magnetic anomalies, and the phenomenon of space weathering on airless rocky bodies of the solar system.

Kramer G.   Combe J.-P.   McCord T.   Pieters C.   Head J.   Taylor L.   Staid M.
Colorful Views of the Moon: Comparing Spectra from Clementine and the Moon Mineralogy Mapper **[#2338]**
M^3 spectra derived from immature craters show a significantly increased spectral contrast compared with their Clementine counterparts. The M^3 dataset improves our ability to interpret mineralogy, petrology, surface and subsurface processes.

LUNAR CARTOGRAPHY, STEREOGRAMMETRY, AND IMAGING SYSTEMS

Hargitai H. I.   Shingareva K. B.   Golodnikova I. Y.   Gede M.
Historic Soviet Planetary Maps Online **[#1209]**
The abstract describes a special collection group of the International Planetary Cartography Database: historic Soviet maps digitized and made available online.

Stooke P. J.
Early LROC Views of Lunar 'Heritage' Sites **[#1116]**
Early LROC images show some old hardware locations including Apollo and Surveyor sites. The images are used to improve EVA traverse maps and to identify the discarded Surveyor 3 retro-rocket. Future opportunities to observe other items are discussed.

Ping J. S.   Su S. L.   Huang Q.
Recent Selenodetic Progress in Chang'E Lunar Mission **[#1059]**
Chang'E-1 lunar orbiter discovered middle scale geological features like basins and volcanos.

Ning X.   Chang X.   Zhang J.   King B.
Digital Photogrammetric Mapping Near the South Pole of the Moon Based on Clementine Images and ULCN2005 **[#1099]**
A pilot project using Clementine imagery to create a DTM and topographic map of a portion of the southern polar region of the Moon is presented.

Archinal B. A.   Duxbury T. C.   Scholten F.   Oberst J.   Danton J.   Robinson M. S.   Smith D. E.   Neumann G. A.   Zuber M.   LROC Team   LOLA Team
Tying LRO Data to the Fundamental Lunar Laser Ranging Reference Frame **[#2609]**
We describe plans for tying together LRO LROC and LOLA data in the fundamental Lunar Laser Ranging reference frame. This will allow for the use of such data and indeed all lunar data to the fullest possible potential for science and exploration.

Rosiek M. R.   Lawrence S. J.   Robinson M. S.   Close W.   Grunsfeld J.   Ingram R.   Jefferson L.   Locke S.   Mitchell R.   Scarsella T.   White M.   Archinal B. A.   Hare T.   Redding B. L.   Galuszka D. M.   Hopkins M.
Topographic Data Derived from Scans of the Original Apollo Panoramic Flight Film **[#2506]**
JSC and ASU are creating a digital archive of the Apollo flight films. Panoramic stereo models are useful for topographic mapping. Image resolution varies from 1–2 m/pixel. Expected vertical accuracy of the topographic data is 0.5–1.5 m.

Tran T.   Howington-Kraus E.   Archinal B.   Rosiek M.   Lawrence S. J.   Gengl H.   Nelson D.   Robinson M. S.   Beyer R.   Li R.   Oberst J.   Mattson S.   LROC Science Team
Generating Digital Terrain Models from LROC Stereo Images with SOCET SET **[#2515]**
LRO is acquiring high-resolution stereo pairs used to generate DTMs. We describe the methodology and error analysis used to reduce the stereo images to the topographic products.

Beyer R. A.   Archinal B.   Chen Y.   Edmundson K.   Harbour D.   Howington-Kraus E.   Li R.   McEwen A.   Mattson S.   Moratto Z.   Oberst J.   Rosiek M.   Scholten F.   Tran T.   Robinson M.   LROC Team
LROC Stereo Data — Results of Initial Analysis **[#2678]**
This analysis of LROC DTMs by different groups using different techniques on similar data allows an important initial comparison of derived camera parameters and an assessment of LROC DTM quality.

Oberst J.   Scholten F.   Matz K.-D.   Roatsch T.   Wählisch M.   Haase I.   Gläser P.   Gwinner K.   Robinson M. S.   LROC Team
Apollo 17 Landing Site Topography from LROC NAC Stereo Data — First Analysis and Results **[#2051]**
The LROC NAC camera onboard the LRO mission provides stereo data with a ground scale of 0.5–1.5 m. We used our DLR photogrammetric processing system to compute a digital terrain model (DTM) of the Apollo 17 landing site and show first results.

Scholten F. Oberst J. Matz K.-D. Roatsch T. Wählisch M. Robinson M. S. LROC Team
Towards Global Lunar Topography using LROC WAC Stereo Data **[#2111]**
The LROC WAC camera onboard the LRO mission provides systematic across-track stereo overlap. We present the current status with regard to the derivation of a global lunar DTM with a resolution of 200–500 m using our DLR photogrammetric processing system.

Kirk R. L. Cook D. Howington-Kraus E. Barrett J. M. Becker T. L. Neish C. D. Thomson B. J. Bussey D. B. J. Mini-RF Science Team
Radargrammetry with Chandrayaan-1 and LRO Mini-RF Images of the Moon: Controlled Mosaics and Digital Topographic Models **[#2428]**
Rigorous geometric modeling will allow us to make highly accurate image mosaics and detailed topographic maps, even in permanently shadowed regions, from data provided by the first two synthetic aperture radars to orbit the Moon.

Conrad A. R. Wooden D. Lucey P. Campbell R. D. Goodrich R. Merline W. J. Chapman C. R.
Diffraction Limited Images of the Lunar Surface with Keck Adaptive Optics **[#2533]**
On Oct 30, 2009, we locked the Keck-II AO system on a sunlit peak near the Moon's terminator and acquired NIR images. With this demonstration, observers may now propose for observing time to investigate open questions in lunar science.

Dong Y. S. Huang D. H. Xiao L. Huang J. Liu J. T.
Chang'E-1 CCD Image Processing and Database Construction **[#1627]**
We processed the Chang'E-1 CCD images to stand format for the end user. A database for the images and mosaic data was designed.

Mattson S. Robinson M. McEwen A. Bartels A. Bowman-Cisneros E. Li R. Lawver J. Tran T. Paris K. LROC Team
Early Assessment of Spacecraft Jitter in LROC-NAC **[#1871]**
Jitter in LROC-NAC images is analyzed based on previous methods for characterizing and correcting jitter in HiRISE images. Jitter effects on Digital Terrain Models are noted. This study has implications for the future design of similar cameras.

Mahanti P. Tran T. Tschimmel M. Robinson M. S. Humm D. LROC Team
Focal Plane Temperature Prediction for the Lunar Reconnaissance Orbiter Narrow Angle Camera **[#1521]**
The Lunar Reconnaissance Orbiter Narrow Angle Camera is acquiring high resolution images of the Moon. An adaptive prediction model of the CCD focal plane temperature is being used for image acquisition commanding to get better quality images.

McKerracher P. L. Jensen J. R. Sequeira H. B. Raney R. K. Schulze R. C. Bussey D. B. J. Butler B. J. Neish C. D. Palsetia M. Patterson G. W. Spudis P. D. Thomson B. J. Turner F. S.
Mini-RF Calibration, a Unique Approach to On-Orbit Synthetic Aperture Radar System Calibration **[#2352]**
The Mini-RF program consists of two dual-polarized Mini-RF Synthetic Aperture Radars (SARs) on the LRO and Ch-1 missions. Both missions achieved lunar orbit and imaged the lunar surface. This report describes the first calibrations of Mini-RF.

Williams D. R. Hills H. K. Guinness E. A. Lowman P. D. Taylor P. T.
PDS Lunar Data Node Restoration of Apollo In-Situ Surface Data **[#1690]**
We describe the ongoing work of the PDS Lunar Data Node at the NSSDC in restoring Apollo surface data that were originally on older media and in obsolete formats. We will also discuss work on Apollo orbital data sets.

Terazono J.   Nakamura R.   Kodama S.   Yamamoto N.   Demura H.   Hirata N.   Ogawa Y.   Haruyama J.
Ohtake M.   Matsunaga T.   Suzuki T.   Hayashi T.
WISE-CAPS: An Integrated and Secure Web-based Environment for Analysis and Browsing of Lunar and Planetary Data **[#1516]**
We are now constructing a Web-GIS based framework called "WISE-CAPS," a virtual research environment to share and browse the data under secured data access. This presentation will address on current implementation status and future prospective.

ONCE AND FUTURE MOON: MISSIONS AND INSTRUMENTS

Jolliff B. L.   Alkalai L.   Pieters C. M.   Head J. W. III   Papanastassiou D. A.   Bierhaus E. B.
Sampling the South Pole-Aitken Basin: Objectives and Site Selection Criteria **[#2450]**
Science objectives for South Pole-Aitken Basin sample return drive site selection strategies. Key criteria include obtaining a large number of melt rocks for age dating and maximizing diversity, including depth variations and volcanic materials.

Cohen B. A.   Coker R. F.
Pulling Marbles from a Bag: Deducing the Regional Impact History of the SPA Basin from Impact-Melt Rocks **[#2475]**
So much depends upon/impact-melt rocks/gleaned from a scoop sample/inside the SPA basin.

Fagan A. L.   Ennis M. E.   Pogue J. N.   Porter S.   Snape J. F.   Neal C. R.   Kring D. A.
Science-rich Mission Sites Within South Pole-Aitken Basin, Part 1: Antoniadi Crater **[#2467]**
We suggest that Antoniadi Crater is an ideal location to achieve the concepts and goals outlined in the 2007 NRC report, Scientific Context for Exploration of the Moon. We outline the achievable goals at three potential landing sites within Antoniadi Crater.

Snape J. F.   Fagan A. L.   Ennis M. E.   Pogue J. N.   Porter S.   Neal C. R.   Kring D. A.
Science-rich Mission Sites Within South Pole-Aitken Basin, Part 2: Von Kármán Crater **[#1857]**
We have identified Von Kármán Crater, within the South Pole-Aitken Basin, as a target for future manned lunar exploration. The potential for *in situ* scientific studies was evaluated for three specific landing sites in the crater.

Ennis M. E.   Fagan A. L.   Pogue J. N.   Porter S.   Snape J. F.   Kring D. A.
Lunar Farside Volcanism: Potential Sampling Localities Within South Pole-Aitken Basin **[#2512]**
The National Research Council outlined specific goals for the future of lunar exploration in a 2007 report. A number of localities within South Pole-Aitken Basin are presented where we can begin to address many of the goals pertaining to volcanism.

Korteniemi J.   Eldridge D. L.   Singer K.   Lough T.   Werblin L.   Kring D.
Volcanic Landing Sites on the Moon: The Compact and Diverse Harbinger Region **[#1339]**
We map out potential landing sites on the Harbinger region (25.71°N, 44.47°W) for future missions. Most open lunar science questions can be addressed there, particularly ones concerning volcanism, internal activity, dating and impact processes.

Weisbin C. R.   Clark P.   Adumitroaie V.   Mrozinski J.   Shelton K.   Hua H.   Smith J. H.   Elfes A.
Lincoln W.   Silberg R.
Formulation, Modeling and Analysis of a Mission to the Moon's Schrodinger Crater **[#1473]**
We formulate ~90 day lunar mission, Shackleton to Schrodinger Crater and back, covering ~1100 km achieving ~80% targeted science value. When value of enhancing science activities is added, mission science rises to nearly twice the targeted value.

Lough T.   Korteniemi J.   Eldridge D. L.   Singer K.   Werblin L.   Kring D. A.
Mission Options to Explore the Flux and Evolution of Lunar Volcanism Through Space and Time **[#2537]**
We outline criteria to determine mission options and identify four example lunar landing sites that explore the flux and evolution of lunar volcanism with the goal of understanding the thermal and chemical development of the Moon.

Jolliff B. L.   Wiseman S. A.   Lawrence S. J.   Tran T. N.   LROC Science Team
Scientific Return from Systematic Imaging of the Constellation Exploration Sites: Compton-Belkovich Example **[#2412]**
NASA's Constellation Program identified 50 sites for detailed imaging by LRO that represent a wide range of features of interest for human/scientific exploration. The Compton-Belkovich "thorium anomaly" site is shown as an example of science context.

Arya A. S.   Rajasekhar R. P.   Ajai   Kiran Kumar A. S.   Navalgund R. R.
Identification of Lunar Volcanic Tubes, a Potential Site for Human Settlement Using 3D Chandryaan 1 – TMC Data **[#1484]**
This paper presents three dimensional analysis over a volcanic tube in Oceanus Procellurum using high resolution Chandrayaan-1 TMC data for the identification potential site for human settlement.

Xiong S. Q.   Yan B. K.   Gan F. P.   Wang Z. C.
The Choice of the Lunar Landing Sites and Preliminary Analysis of Several Sites **[#1304]**
Three sites are chosen based on the lunar exploration achievements and problems, and are analyzed using LIDAR and CCD data of Chang'E-1 satellite as well as Clementine UV-VIS data.

Yamada R.   Garcia R.   Calvet M.   Gagnepain-Beyneix J.
Design of an Optimized Seismic Network for Future Lunar Missions **[#1619]**
We will describe how to design an optimized seismic network for future lunar missions. We designed the positions of new seismic stations to satisfy principal scientific objectives. In this presentation, some examples of the network will be indicated.

Neal C. R.   Banerdt W. B.   Alkalai L.
LUNETTE: Establishing a Lunar Geophysical Network Without Nuclear Power Through a Discovery-Class Mission **[#2710]**
The LUNETTE concept uses new power management technology to offer a non-nuclear alternative. It will provide detailed information on the interior of the Moon through seismic, thermal, electromagnetic, and precision laser ranging measurements.

Currie D. G.   Dell'Agnello S.   Delle Monache G.
A Lunar Laser Reflector for the 21st Century **[#2269]**
The Apollo Lunar Laser Reflectors after forty years are limiting the range accuracy. The science objectives, the design, the thermal and optical simulation and field testing of the new retroreflector array for lunar ranging will be presented.

Mumm E.   Zacny K.   Kumar N.   Hedlund M.   Smrekar S.   Morgan P.   Nagihara S.   Shasho J.   Pierides A.   Milam B.
Heat Flow Probes for Small Lunar Lander **[#2128]**
We have been developing two innovative heat-flow probe systems: percussive and pneumatic-proboscis. Each system consists of two parts: (1) a method of reaching 3 m depth in lunar regolith, and (2) a method of deploying thermal sensors.

Moreschini P.   Rutberg M.   Zacny K.   Paulsen G.
DIHeDRAL: Downhole Regolith Interrogation with He-assisted Drill and Laser Induced Breakdown Spectroscopy System **[#1722]**
We describe DIHeDRAL, a downhole LIBS system designed to be integrated into a 3-m-class drill, currently under development at Honeybee Robotics. DiHeDRAL allows subsurface access providing information on the composition of lunar soil.

Scheld D. Marshall J. R. Mason L. C. Martin J. P.
In-Situ Geologic Analyzer for Lunar and Martian Surface **[#1539]**
An instrument is presented with a triple system to work as a robotic geologist on remote planetary surfaces. MICA is a miniature instrument that employs X-ray scattering and visual imaging to determine nondestructively the mineralogy of a rock sample *in situ*.

Campbell A. E. Thaisen K. G. Gaskin J. A. Jerman G. A. Taylor L. A.
Miniaturized Scanning Electron Microscope for the Moon: Energy Dispersive X-Ray Spectroscopy Studies **[#2201]**
NASA Marshall Space Flight Center and colleagues have been developing a miniaturized SEM with chemical analysis capability (EDS). Our interest is to understand the limiting instrument capabilities and appropriate science.

Lanza N. L. Deans M. C. Clegg S. M. Humphries S. D. McInroy R. E. Wiens R. C. Newsom H. E. Ollila A. M.
Evaluating LIBS as a Geochemical Reconnaissance Tool for the K10 Lunar Rover **[#2613]**
Materials were collected from Black Point Lava Flow (BPLF) in Arizona and analyzed with LIBS in the laboratory to evaluate this technique for future use on the K10 lunar rover. These results were compared to bulk analyses carried out in previous studies.

Corsaro R. D. Liou J.-C. Giovane F. Burtchell M. Pisacane V. Lagakos N. Williams E. Stansbery E.
Micrometeoroid and Lunar Secondary Ejecta Flux Measurement: Comparison of Three Acoustic Systems **[#1108]**
We examine the inherent capability of three large-area acoustic sensor systems and their applicability for micrometeoroids and lunar secondary ejecta detection and characterization for future lunar exploration activities.

Segura T. L. Lo A. S. Eller H. Dailey D. Drucker E. Wehner J.
Secondary Payloads Using the LCROSS Architecture **[#2673]**
We describe several secondary planetary mission concepts that could be accommodated by an LCROSS-based ESPA spacecraft.

Laufer R. Hyde T. W. Matthews L. Lachenmann M. Herdrich G. Srama R. Roeser H.-P.
A Baylor University Payload Contribution to the Universitaet Stuttgart Moon Orbiter LUNAR MISSION BW1 **[#2105]**
The LUNAR MISSION BW1 is an academic small lunar orbiting satellite of the Universitaet Stuttgart, Germany. As part of a collaborative agreement between Baylor University and the Universitaet Stuttgart, an instrument contribution is under consideration.

Li R. He S. Tang P. Skopljak B. Yilmaz A. Jiang J. Banks M. S. Oman C.
Development of a Lunar Astronaut Spatial Orientation and Information System **[#1782]**
This paper presents the progress of the development of a Lunar Astronaut Spatial Orientation and Information System (LASOIS) to continuously provide spatial orientation and navigation information to astronauts for reducing spatial disorientation.

Crawford I. A. Joy K. H. Cousins C. R. Grindrod P. Snape J. Weider S. Z. White O. Lupisella M. L. Petro N. E.
Enhancing the Probability of Making Serendipitous Discoveries from a Pressurized Lunar Rover **[#1272]**
A scientific benefit of returning humans to the Moon is the increased opportunity for serendipitous discoveries. Here we identify design requirements for a pressurized rover which will increase the probability of making such discoveries.

Kókány A. Pál P. Pintér Cs. Urbán I.
Practical Realization of Robot Technology Constructed to Promote Work on the Moon **[#1143]**
The purpose of our researches is the practical realization of lunar work in view of Moon environment as well as utilization of our innovations and technologies in robot designing.

Cohen B. A.   Bassler J. A.   Hammond M. S.   Harris D. W.   Hill L. A.   Kirby K. W.   Morse B. J.
Mulac B. D.   Morse C. L. B.
Robotic Lunar Landers for Science and Exploration **[#2616]**
Soaring toward the Moon, robotic landers will seed cloudbursts of knowledge.

Angelopoulos V.   Lillis R.   Sibeck D. G.   Halekas J.   Delory G. T.   Khurana K. K.   Russell C. T.
McFadden J. P.   Bonnell J.   Larson D.
ARTEMIS, A Two Spacecraft, Planetary and Heliospheric Lunar Mission **[#1425]**
ARTEMIS is re-targeting two of NASA's five THEMIS satellites into coordinated, lunar equatorial orbits. It will make the first systematic, two-point observations of the lunar space and planetary environment starting in April 2011.

Graham P.   Snyder G.   OpenLuna Science Team
OpenLuna: An "Open Source", Privately Funded, Return to the Moon Mission **[#2721]**
The OpenLuna Foundation seeks to return mankind to the lunar surface through private enterprise, using open-source strategies. We will launch a stepped series of robotic and limited manned missions leading to outpost construction. Your Moon, your mission. Get involved.

Kobayashi M.   Ohashi H.   Sasaki S.   Shibata H.   Iwai T.   Fujii M.   Nogami K.   Kimura H.
Nakamura M.   Hirai T.
Lunar Dust Monitor for the Orbiter of the next Japanese Lunar Mission SELENE2 **[#1964]**
A dust particle detector is proposed to be onboard the orbiter of SELENE-2 mission. We summarize the significance of circumlunar dust and report an overview of our instrument proposed to accompany the SELENE-2 mission.

Munsat T.   Sternovsky Z.   Robertson S.   Grün E.   Horanyi M.
Lunar Dust Transport Package **[#2538]**
We present the Lunar Dust Transport Package, a proposed instrument suite to investigate dusty plasma processes on the lunar surface, including spatial and size distributions of levitated/transported dust grains, and surface plasma characterization.

Delory G. T.   Elphic R. C.   Colaprete A.   Mahaffy P.   Horanyi M.
The LADEE Mission: The Next Step After the Discovery of Water on the Moon **[#2459]**
We discuss how the LADEE mission will contribute to our knowledge of the origin and evolution of lunar volatiles.

PLANETARY ATMOSPHERES

Shuvalov V.
Atmospheric Erosion Induced by Oblique Impacts **[#1191]**
The aim of the present study is to calculate the loss of atmospheric air in oblique impacts of large (1–30 km) asteroids and comets.

Maurette M.
Cracking the Elemental Genetic Code of the Atmospheric Noble Gases: The "Missing" ^{36}Ar and ^{84}Kr **[#1114]**
The accretion of hydrous-carbonaceous meteoroids with sizes of 50–200 µm rightly predicts the total burdens of ^{20}Ne and ^{132}Xe in the terrestrial atmosphere. However, the huge excesses of both ^{36}Ar and ^{84}Kr (15×) required additional "spikes" of cometary gases.

Economou T. E.   Pierrehumbert R. T.
Mars Atmosphere Argon Density Measurements on MER Missions **[#2179]**
Although there is no meteorology instrument on either of the MER rovers, using the on board Alpha Particle X-ray Spectrometer on both rovers, we were able to measure the argon density variation in the martian atmosphere as a function of seasons.

Niles P. B. Boynton W. V. Hoffman J. H. Ming D. W. Hamara D. Phoenix Science Team
Carbon and Oxygen Stable Isotope Measurements of Martian Atmospheric CO_2 by the Phoenix Lander **[#2315]**
The Phoenix lander has measured the isotopic composition of martian atmospheric CO_2 to a precision better than 0.5%. This is consistent with previous results and has wide implications for understanding the past and current climate history of Mars.

Longhi J.
Some Phase Equilibrium Systematics of Martian Volatiles **[#2039]**
Binary pressure (P) – temperature (T) phase diagrams were constructed for the N_2-, CH_4-, and SO_2-H_2O systems making use of published triple points, critical points, and limited experimental determination of univariant equilibria.

Leeman J. R. Blackburn D. G. Elwood Madden M. E. Ulrich R. Chevrier V.
CO_2 Clathrate Dissociation Rates Below the Freezing Point of Water **[#1418]**
Gas hydrates represent large carbon reservoirs on Mars. Here low temperature rates of carbon dioxide hydrate dissociation are reported and reaction mechanisms determined.

Root M. J. Gainey S. R. Elwood Madden M. E.
Assessment of Hydrate Reservoirs as Potential Methane Sources on Mars **[#1705]**
This work aims to summarize the rates for methane hydrate dissociation in the literature and determine if dissociation of methane hydrate reservoirs could provide fluxes of methane comparable to seasonal methane plumes observed on Mars.

Schuerger A. C. Clausen C. Britt D.
Methane Evolution from UV-Irradiated Spacecraft Materials Under Simulated Martian Conditions: Implications for the MSL Mission **[#2092]**
Methane evolution by solar UV irradiation of spacecraft materials may interfere with the sensitivity of the SAM instrument on MSL to detect CH_4.

Chevrier V. F. Hanley J. Rivera-Valentin E.
Regolith Control of Atmospheric Water Vapor on Mars from Analysis of Phoenix TECP Data **[#2559]**
Preliminary detailed analysis of Phoenix TECP data shows that the humidity cycle is partly controlled by phase changes of magnesium perchlorate hydrates. Moreover, calculations suggest that adsorption may be also responsible for humidity variations.

Saruya T. Toyota T. Baratoux D. Kurita K.
The Exchanges of Water Vapor Between the Atmosphere and the Surface of Mars **[#1306]**
PFS observed the variation of water vapor in the atmosphere of Mars. It showed two local maximums of water at Tharsis and Arabia Terra. We will discuss the possibility of atmosphere-surface exchanges of water at Arabia Terra.

Teal D. A. Murphy J. R. Kahre M. A.
Martian Middle-Latitude Atmospheric Stationary Waves as Manifested in MRO MCS Retrieved Temperature Data **[#2630]**
Stationary waves in Mars' atmosphere at middle latitudes will be investigated via analyses of Mars Reconnaissance Orbiter derived atmospheric temperatures.

Wiseman S. M. Arvidson R. E. Morgan F. Wolff M. J. Morris R. V. McGuire P. C. Murchie S. L. Mustard J. F. Seelos F. P. Smith M. D.
Radiative Transfer Modeling of the Empirical 'Volcano Scan' Atmospheric Correction: Discussion of Artifacts **[#2461]**
Atmospheric correction of spectra acquired by MRO CRISM is important for interpretation of surface spectral properties. We use DISORT modeling to simulate the commonly used empirical volcano scan correction method and identify potential artifacts.

Lemmon M. T.
Martian Cirrus-like Hazes at the Phoenix Landing Site **[#2377]**
Phoenix SSI images show water ice hazes late in the mission. Diffraction by the ice particles constrains the effective radius to 20–50 µm. Diurnal changes in water vapor exceed the cloud abundance, and daily adsorption of ~15 µm of water in the soil is suggested.

Bean K. M.   Lemmon M. T.
Nighttime Optical Depth Patterns from the Mars Exploration Rovers **[#1730]**
Using images from the Mars Exploration Rovers, the nocturnal optical depth variations can be better characterized. Trends searched for include an increase due to water ice cloud formation and a decrease due to large particle settling in a calmer boundary layer.

Merrison J. P.   Gunnlaugsson H. P.   Holstein-Rathlou C.   Knak Jensen S.   Nørnberg P.   Rasmussen K. R.
Formation and Properties of the Martian Dust Aerosol **[#1651]**
The suspension of mineral dust in the martian atmosphere has a major effect on the planets climate. This presentation outlines the current level of understanding of mineral grain transport on Mars and some of the technology involved in this research.

Sciamma-O'Brien E.   Carrasco N.   Szopa C.   Buch A.   Cernogora G.
Titan's Atmosphere: An Optimal Gas Mixture for Aerosol Production? **[#2522]**
This study presents the latest results obtained in PAMPRE, a plasma experiment developed to simulate experimentally Titan's atmosphere. It has allowed the determination of the experimental parameters needed to produce tholins in conditions similar to Titan's atmosphere.

Devaraj K.   Steffes P. G.
Laboratory Measurements of Microwave Properties of Ammonia Under Deep Jovian Atmospheric Conditions **[#1875]**
Over 500 lab measurements of the 1.5-6-GHz properties of ammonia have been made under simulated deep jovian atmospheric conditions (pressures up to 100 bars and temperatures upto 450 K) using a high-pressure measurement system built at Georgia Tech.

Espley J. R.   Morgan D. D.   Christou A.   Farrell W.   Grebowsky J.   Gurnett D.   Plaut J.
MARSIS Observations of the 2009 Martian Geminid Meteor Shower: Null Results **[#2187]**
MARSIS observations during the predicted martian Geminid meteor shower showed no obvious effects on the martian ionosphere.

Spiga A.   Pathare A.   Balme M.   Renno N.   Saca F.   Halleaux D.   Metzger S.
In Situ Studies of Terrestrial Dust Devils and Ambient Meteorology: Field Measurements of Vorticity **[#1327]**
The main purpose of the work described in this abstract is to relate measured ambient vertical vorticity with simultaneous observations of dust devil size and frequency.

Saca F. A.   Renno N. O.   Halleaux D. G.   Rogacki S.   Gillespie R.   Musko S.
A Portable Instrument for Atmospheric Measurements **[#1767]**
We describe a new instrument for making accurate measurements in atmospheric systems. It consists of a Prandtl tube capable of measuring static and stagnation pressures, various sensors, and supporting electronics.

Renno N. O.   Halleaux D. G.   Saca F.   Rogacki S.   Gillespie R.   Musko S.
A Generalization of Bernoulli's Equation to Convective Vortices **[#1745]**
Measurements of the static and stagnation pressures with an innovative instrument proved a generalization of Bernouilli's equation to convective systems.

McDoniel W. J.   Goldstein D.   Varghese P.   Trafton L.   Stewart B.
DSMC Modeling of the Plume Pele on Io **[#2623]**
Pele's vent, as imaged by Galileo, is modeled with DSMC, and an asymmetric plume results which better matches observations than do simulations from a simple disk-source.

MARS REMOTE SENSING: TECHNIQUE DEVELOPMENT

Teodoro L. F. A.   Eke V. R.   Elphic R. C.   Feldman W. C.
Pixon Goes to Mars: Improved Spatial Resolution of Mars Odyssey Epithermal Neutron Data **[#2742]**
We apply a pixon code to the Mars Odyssey Neutron Spectrometer (MONS) at polar locations with the aim of deconvolving the MONS point spread function and producing higher resolution hydrogen maps.

Bandeira L.   Ding W.   Stepinski T. F.
Automatic Detection of Sub-km Craters Using Shape and Texture Information **[#1144]**
A new algorithm utilizes shape and texture information in high resolution orbital images to detect subkilometer craters on Mars with a detection rate >82%.

Kneissl T.   van Gasselt S.   Neukum G.
New Software Tool for Map-Projection-Independent Crater Size-Frequency Determination in ArcGIS **[#1638]**
In order to simplify correct measurements of crater-size frequency distributions on planetary surfaces we developed an extension for ESRI's ArcGIS to determine the diameters of impact craters independently of the map projection of the image basis.

Kneissl T.   van Gasselt S.   Neukum G.
*Measurement of Strike and Dip of Geologic Layers from Remote Sensing Data —
New Software Tool for ArcGIS* **[#1640]**
The only way to get information about the attitude of geologic layers on planetary surfaces is the use of remote sensing data. The developed ArcGIS extension provides a user-friendly interface for measuring strike and dip of layers using DTM data.

Dumke A.   Spiegel M.   van Gasselt S.   Neu D.   Neukum G.
*Systematic Processing of High-Resolution Digital Terrain Model Quadrangels on the Basis of
Mars-Express HRSC Data* **[#1980]**
Since December 2003, the European Space Agency's (ESA) Mars Express (MEX) orbiter has been investigating Mars. The High Resolution Stereo Camera (HRSC), one of the scientific experiments onboard MEX, is a pushbroom stereo color scanning instrument.

Walter S.   Neukum G.
*A New Frontend Implementation for the Mars Mapserver Prototype, Based on the Open Source
p.mapper/MapScript Framework* **[#2193]**
In this work, we present a new frontend for the existing data sets served by the Mars Mapserver prototype. This new frontend is based on the Open Source p.mapper/MapScript framework and includes improved functionality together with an advanced dynamic user interface.

Walter S.   Neukum G.
*Systematic Processing of HRSC Imagery for the Correction of Shading Effects Using Photometric Models on
Pixel-Scale Surface Orientation* **[#2182]**
We want to present our approach for the systematic correction of shading effects on level 4 HRSC imagery using simple and approved photometric models applied on the real surface orientation derived by the associated HRSC-DTM.

Maki J. N.   Arvidson R. E.
Image Illumination Geometry and the Appearance of Surface Texture **[#2491]**
A series of Mars Exploration Rover (MER) Spirit Navcam images of the surface acquired at different solar elevation angles helps to illustrate the relationship between time of day and visible textural detail.

Zinzi A.   Palomba E.   Rinaldi G.   D'Amore M.
Effect of Martian Suspended Dust on Albedo Measurements from the MGS-TES Data **[#1598]**
Suspended dust on Mars influences albedo measurements by orbiting instruments, but not necessary the real surface albedo. The aim of this study is to characterize the role of suspended aerosols on albedo measurement by remote sensing instruments.

Portyankina G.   Vincendon M.   Thomas N.   Aye K.-M.
Recovery of Surface Reflectance from Atmospheric Aerosol Contribution: Application to HiRISE Images **[#1582]**
To ensure correct comparison of surface reflectance in images taken on different dates we propose to adapt the procedure of recovery of surface reflectance spectra originally developed for OMEGA observations. It proved applicable and useful for HiRISE observations.

EDUCATION AND PUBLIC OUTREACH: MARS REMOTE SENSING

Grigsby B.   Capages C.   Christensen P. R.   Murchie S.   Turney D.   Beisser K.   Seelos F.   Seelos K.   Harvel C.   Barnouin-Jha O.   Patterson W.   McGovern A.   Buczkowski D.   Malaret E.   Hash C.   Zufall A.
Students Conducting Authentic Research: Beta Test Results of the Mars Exploration Student Data Teams **[#1259]**
The Mars Exploration Student Data Teams (MESDT) program, created by Arizona State University's Mars Education Program, focuses on immersing teams of high school students in an authentic research Science, Technology, Engineering and Mathematics (STEM)-based experience.

Viviano C. E.   Moersch J. E.   McSween H. Y.
Using JMARS as a Teaching Tool in Undergraduate Planetary Courses **[#2463]**
We have utilized the JMARS program in the laboratory portion of the planetary geosciences course at the University of Tennessee. We review several ways we have applied JMARS tools, including a crater counting and a rover geologic traverse project.

Beyer R. A.   McArthur G.   Heyd R.   Deardorff D. G.   Gulick V.   HiRISE Team
HiRISE Web-based Public Suggestion Tool **[#2458]**
The new HiRISE public suggestion tool is a website that anyone can log in to and make target suggestions that have the potential to be imaged by HiRISE.

MARS: GEOLOGIC, GEOMORPHIC, AND LANDING SITE MAPPING

Skinner J. A. Jr.   Tanaka K. L.
Sub-dividing the Geology of Vastitas Borealis, Mars: Evidence for a Varied Record of Amazonian Deposition and Erosion **[#2734]**
We observe multiple lines of evidence that allude to the existence of unique outcrops of materials that superpose previously mapped Early Amazonian geologic units.

Tanaka K. L.   Rodriguez J. A. P.   Fortezzo C. M.   Hayward R. K.   Skinner J. A. Jr.
Nature of Hesperian Resurfacing in the Scandia-North Polar Region of Mars **[#2323]**
Formational hypotheses based on preliminary observations and first-year mapping results of the Scandia-North Polar Region of Mars. The map area includes the Scandia Cavi, Scandia Tholi, Scandia Colles, northern Alba Patera, and Vastitas Borealis.

Hielscher F. J.   Hiesinger H.   Erkeling G.   Ivanov M. A.   Reiss D.
Distribution and Classification of Thumbprint Terrain in Isidis Planitia, Mars **[#2394]**
We have produced the most detailed map of thumbprint terrain in the Isidis basin currently available. We have performed detailed morphometric measurements of thumbprint terrain.

Ivanov M. A.   Erkeling G.   Hiesinger H.   Hielscher F. J.   Reiss D.
Major Episodes of the Geological History of Isidis Planitia, Mars **[#1294]**
We describe morphology of the mapped units in Isidis Planitia and its immediate surroundings, give age estimates for them, and formulate the major steps in the geologic history of the region.

Zimbelman J. R.
Geologic Mapping of the MC-23 NW Quadrangle: Emplacement and Erosion of the Lower Member of the Medusae Fossae Formation on Mars **[#1157]**
The lower member of the Medusae Fossae Formation (MFF) has two mappable subdivisions within the quadrangle, including several outliers interpreted to be MFF materials. Layering in outliers is similar to layering in nearby portions of globally mapped MFF deposits.

Komatsu G.   Ori G. G.   Cardinale M.   Dohm J. M.   Baker V. R.   Vaz D. A.   Ishimaru R.   Namiki N.   Matsui T.
The Search for Methane Gas Emission Features on Mars **[#1355]**
The methane gas in martian atmosphere is likely to have derived from the surface of the planet through unknown processes. We conducted an investigation to identify possible methane emission features beginning with the suggested source areas.

Harrold B. C.   King D. T. Jr.   Marzen L. J.
Remote Sensing Applications for the Martian Fretted Terrain **[#2004]**
The fretted terrain is located along the global escarpment. ArcGIS 9.x and MOLA was used to geoprocess and overlay images along with personal geodatabases to organization thousands of features to access the blocks present orientation/location.

Williams K. K.
Geomorphic Mapping of MTMs -20022 and -20017: South of Jones Crater, Mars **[#2645]**
The area south of Jones Crater in Margaritifer Terra, Mars, is being geomorphologically mapped in order to understand the relative timing of fluvial, impact, and depositional processes.

Mest S. C.   Crown D. A.
Geologic Mapping of the Reull Vallis Source Area in Southern Hesperia Planum, Mars **[#1945]**
Geologic mapping of MTMs -30247, -35247 and -40247 characterizes the upper reaches of the Reull Vallis system, including its source area and main canyon. Crater size-frequency distributions are being generated for mapped units for age determinations.

Crown D. A.   Bleamaster L. F. III   Mest S. C.   Mustard J. F.   Vincendon M.
Geologic Mapping of the NW Rim of Hellas Basin, Mars: Evidence for an Ancient Buried Landscape **[#1888]**
Geologic mapping and investigations of impact craters on the NW Hellas rim reveal an extensively buried landscape and suggest that regional sedimentary deposition extended beyond the topographic margin of Hellas basin and well into the surrounding highlands.

Williams D. A.   Bleacher J. E.   Shean D.   Byrne P. K.   Greeley R.   Tanaka K. L.   Musiol S.
Geologic Mapping of Olympus Mons: A New Project to Investigate the Evolution of a Martian Shield Volcano **[#1053]**
We discuss the goals, objectives and data sources for our project to produce a new 1:1,000,000 geologic map of Olympus Mons.

Parker T. J.   Golombek M. P.   Powell M. W.
Geomorphic/Geologic Mapping, Localization, and Traverse Planning at the Opportunity Landing Site, Mars **[#2638]**
Mapping of the Opportunity traverse, using the project's planning tool, "maestro," and GIS software. Experience gained by the science and engineering teams will be invaluable for planning and conducting future mobile explorer missions to Mars and other planetary bodies.

Gwinner K.   Oberst J.   Jaumann R.   Neukum G.
Regional HRSC Multi-Orbit Digital Terrain Models for the Mars Science Laboratory Candidate Landing Sites **[#2727]**
Regional DTM at 50 m resolution have been derived from multi-orbit HRSC data. Characteristics and related methods are reported.

Golombek M.   Grant J.   Vasavada A. R.   Grotzinger J.   Watkins M.   Kipp D.   Noe Dobrea E.   Griffes J.   Parker T.   Kirk R.   Fergason R.   Beyer R.   Huertas A.   Milliken R.   Sun Y.
Landing Sites Under Consideration for Mars Science Laboratory **[#2407]**
Detailed scientific investigations of target materials and surface characteristics are focusing on four potential landing sites (Holden, Gale and Eberswalde craters and Mawrth Vallis) for the Mars Science Laboratory.

SPIRIT: DIGGING UP THE DIRT

Rice J. W. Jr.   Greeley R.   Li R.   Wang W.   Crumpler L.   Farrand W. H.   Athena Science Team
Geomorphology of the Columbia Hills Complex: Landslides, Volcanic Vent, and Other Home Plates **[#2566]**
Spirit has been exploring the Columbia Hills region of Gusev Crater for over five and a half years. New observations from both the surface and orbit have revealed landslides, a possible volcanic vent, and additional Home Plate-like materials.

Cabrol N. A.   Grin E. A.   Herkenhoff K. E.   Weitz C. M.   de Souza P.   Athena Science Team
Gusev Soil Analysis: Methods, Inventory, and Database **[#1182]**
We present results for soils at Gusev from landing to Troy and the sedimentology database for the MER mission that is being organized and will be made available to the planetary community for, i.e., modeling and landing site selection activities.

Yingst R. A.   Crumpler L. S.   Li R.   de Souza P.   Athena Science Team
Shape, Roundness and Texture of Particles Along the Spirit Rover Traverse from Sol 750 to Sol 1824 **[#1276]**
Particle morphologies can be assessed quantitatively and qualitatively to classify rock types. Here we assess the size, shape, roundness and texture of pebble- to cobble-sized clasts along the Spirit rover traverse from sol 750 to sol 1824.

Lira C.   Saraiva J.   Pina P.
Full Granulometric Curves of Meridiani Soils **[#2043]**
The full granulometric curves of Meridiani soils obtained by a mathematical morphology approach are presented.

Sullivan R.   Anderson R.   Biesiadecki J.   Bond T.   Stewart H.
Cohesions and Friction Angles of Martian Regolith from MER Wheel Trenches and Wheel Scuffs **[#1879]**
We analyzed all MER wheel trenches and wheel scuffs along both MER traverses to derive cohesions and friction angles for martian regolith. Friction angles at both MER sites are 30-37 degrees; cohesions generally are 10 kPa or less.

Lichtenberg K. A.   Arvidson R. E.   Lindemann R.   Iagnemma K.   Bennett K. J.   Trease B.   Richter L.   Scharringhausen M.
Rover Mobility at the “Troy” Site, Mars: A Modeling Perspective **[#2295]**
Preliminary rover mobility simulations using MCS Adams have successfully replicated a number of behaviors seen in ground-based rover testing and with MER-Spirit on Mars; deformable soil interactions will aid in mobility predictions for future rovers.

MARS: FLUVIAL GEOMORPHOLOGY AND PROCESSES

Howard A. D.   Moore J. M.
Young Mid-Latitude Martian Valleys: Evidence from Newton and Gorgonum Basins **[#1115]**
Shallowly incised valleys on the floor of Newton and Gorgonum basins date to the late Hesperian to early Amazonian. Flow was sourced from runoff from ice deposits on the basin rim. A contemporaneous ice-covered lake was present in the center of Gorgonum.

Yamaguchi Y.   Miyamoto H.   Tanaka K. L.   Dohm J. M.   Hare T. M.
Detailed Mapping and Statistical Analysis of Noachian and Post-Noachian Valley Networks: Implications to the History of Martian Surface Environment **[#1775]**
We find correlation between the mean slopes and the drainage densities of martian valley networks in distant Noachian and post-Noachian terrains through detailed mapping investigation and quantitative analysis, which indicates mostly rainfall-origin.

Matsubara Y.   Howard A. D.
Hydrologic Analysis of Noachian Lakes in the Southern Highlands of Mars **[#1288]**
A hydrologic model using the ratio of runoff to evaporation was developed to estimate stream flow and lake distribution on southern highland. Our preliminary results of possible conditions required to form fluvial features seen on Mars are presented.

Rivera-Valentin E. G.   Ulrich R.   Chevrier V. F.   Altheide T. S.   Wray J. J.
Dynamic Modeling of Martian Paleolake Stability **[#1446]**
We conduct a stability study of martian paleolakes by modeling heat and mass transfer and incorporating simultaneously running processes such as sublimation, freezing, and diffusion-advection. Preliminary results show the effects of soil deposits.

Altheide T. S.   Chevrier V. F.   Rivera-Valentin E. G.   Wray J. J.
Geochemical Modeling of the Evaporation of an Ancient Paleolake in Columbus Crater, Terra Sirenum, Mars **[#2479]**
A geochemical modeling approach is used to determine the longevity of liquid water in a potential paleolake scenario, in an attempt to investigate the habitable nature of early Mars.

Williams R. M. E.   Rogers A. D.   Chojnacki M.   Hardgrove C.   Boyce J.
Episodic Alluvial Fan Formation in Western Terra Tyrrhena, Mars **[#2185]**
Alluvial fans within an unnamed crater in far western Terra Tyrrhena show morphological, thermal and spectral variations that indicate episodic formation.

Lucchitta B. K.
Slippery Slopes on Ceti Mensa, West Candor Chasma, Mars: Analysis of a Lobate Deposit **[#1075]**
A lobate deposit on the north side of Ceti Mensa is composed of rounded blocks that appear to have slid on a malleable substrate. Sliding features elsewhere on the mensa suggest that gravity gliding contributed to the domal shape of this ILD stack.

MARS: GULLIES AND SLOPE STREAKS

Morgan G. A.   Head J. W. III   Dickson J. L.   Marchant D. R.   Levy J. S.
Gully Formation on Mars and Earth: The Transition from Glacial Activity to Gully Depositional Phases **[#1044]**
We test theories of Mars gully formation by examining gullies found superposed on glacial deposits on Mars and Earth. Many gullies form in environments favoring long-term snow/ice accumulation; stratigraphic relations favor top-down melting during warming climatic periods.

Reiss D.   Hauber E.   Hiesinger H.   Jaumann R.   Trauthan F.   Preusker F.   Zanetti M.   Ulrich M.   Johnsson A.   Johansson L.   Olvmo M.   Carlsson E.   Johansson H. A. B.   McDaniel S.
Terrestrial Gullies on Svalbard as Planetary Anologs for Mars **[#1665]**
We compare the morphology of terrestrial gully analogs from Svalbard with martian gullies in order to constrain which formation process might be dominant on Mars, i.e., fluvial and/or debris flow processes.

Johnsson A.   Johansson L.   Zanetti M.   Reiss D.   Hauber E.   Hiesinger H.   Ulrich R. M.   Olvmo M.   Carlsson E.   Jaumann R.   Trauthan F.   Preusker F.   Johansson H. A. B.   McDaniel S.
The Origin of Stripe-like Patterns on Martian Gully Slopes; Using Svalbard Advent Valley as a Mars Analogue **[#2492]**
Features on Mars resembling terrestrial stripes have been observed on gully slopes in recent HiRISE images. Stripes on Earth are indicators of freeze and thaw processes. On Mars they could point to niches where soil moisture temporally occurs.

Kincy L.   Currit C.   Butler D.   Fuhrmann S.
A Spatial Analysis of Gullies on Mars **[#2743]**
The spatial dispersion of gullies is determined to be clustered away from the equator. Evidence is found that indicates gullies are found in areas high in iron and chlorine, low in water, potassium, and silicon. Brine as the likely fluid source for gullies on Mars.

Barbieri L.   Dickson J. L.   Head J. W.   Dyar M. D.
Deciphering Late-Amazonian Climate Change on Mars: Evidence for Episodic Gully Activity Preserved in Gully Fan Stratigraphy **[#2745]**
HiRISE data have revealed examples of stratigraphy in the fans of martian gullies. We show examples of fan deposits that require multiple episodes of activity. In this way gully fans provide an opportunity to document shifts in the martian climate.

Conway S. J.   Balme M. R.   Murray J. B.   Towner M. C.   Okubo C.   Grindrod P. M.
Geomorphic Analysis of the Formation Processes of Martian Gullies **[#1881]**
We present quantitive geomorphic analyses of high resolution digital elevation models of gully systems on Mars. Our methods allowed good discrimination between processes on Earth, and on Mars debris flow is identified as the dominant process.

Conway S. J.   Balme M. R.7:00 p.m.   Towner M. C.   Murray J. B.
Can Water Move Sediment on Present-Day Mars? Insights into Gully Formation from Laboratory Simulations **[#1894]**
We describe experiments designed to study sediment transport by liquid water under the current low temperature-pressure on Mars. We find that these flows: are erosive, flow faster and further than on Earth, and produce unique sedimentary features.

Dixon J. C.   Howe K. L.   Coleman K. A.
Periglacial Hillslope Analogs for Martian Gully Formation **[#2392]**
This paper examines the appropriateness of periglacial hillslope processes as analogs for the formation of gullies on Mars. Specifically, the suitability of debris flows and slush flows are examined.

Howe K. L.   Dixon J. C.   Chevrier V. F.
Effects of Viscosity on the Morphology of Martian Flow Features **[#1706]**
Although studied for decades, the formation mechanism of slope streaks is still unclear. By altering the viscosity of a fluid, our group has created slope streak features that match many characteristics of Mars slope streaks.

Coleman K. A.   Dixon J.   Howe K. L.   Chevrier V. F.
Slushflows as Analogs for Martian Gully Formation **[#2741]**
Simulations performed in our flume with variable water volume supported slushflows as a viable Earth analog for martian gullies based on the water volumes included in the simulations that approximate martian gullies.

Kossacki K. J.   Markiewicz W. J.
Interfacial Liquid Water On Mars: Can It Form Hill Gullies? **[#1702]**
We model both the diurnal and the seasonal cycle of the interfacial liquid water in the context of a possible mechanism for formation of the so called hill gullies.

Reiss D.   Erkeling G.   Bauch K. E.   Hiesinger H.
Evidence for Present Day Gully Activity on the Russell Crater Dune Field, Mars **[#2152]**
Based on the morphology, spectral data and thermal modeling we conclude that the gully changes might be due to transient melting of small amounts of H_2O-ice around LS ~210° triggering small debris flows.

Kereszturi A.
Gullies, Flow Features and Spider Arms for Climate Reconstruction on Mars —
Proposal for Complex Map Generation **[#2102]**
We review four groups of high latitude features ("classical" gullies, gullies on dunes, small meandering trenches, VLF-flow features) as tools in climate reconstruction for the past million years.

Addison B. C.   Chevrier V. F.   Dixon J. C.   Howe K. L.
Experimental Simulations of Martian Gullies using $MgSO_4$ Brine Solution **[#1399]**
To help us better understand the processes creating martian gullies, we simulated gully morphologies using $MgSO_4$ brine solutions. We also determined whether sulfates are detectable on the surface and/or subsurface of these gullies.

Grindrod P. M.   Warner N.   Gupta S.
Gully Morphology in Hydrated Deposits in Candor Mensa **[#1312]**
We use a HiRISE DEM to discuss the morphology of gully-like features in Candor Mensa. Our observations fit well with a groundwater model of formation, in which chemical, as well as physical, erosion appears to be significant.

Hart S. D.   Gulick V. C.   Ishikawa S. T.   Barnhart C. J.   Parsons R. A.
Detailed Topographic and Morphometric Analysis of Lyot's Central Peak Gullies **[#2662]**
A detailed study of gullies on the central peak of Lyot Crater. Morphometric analysis was done using HiRISE images, MOLA data, and a HiRISE derived DTM. We also estimate gully volume and channel discharge calculations based on channel geometries.

Yakovlev V.
Slope Streaks on Mars — Gravity-Capillary Displays of Water **[#1333]**
We proposed the hypothesis about the slope streaks formation on Mars as a result of the mineralized water wave passing along the cavities, formed by the subsurface sublimation of the saline ice, without the lateral energy and substance transferring.

EXPLORING THE MARTIAN CRUST: GEOLOGY, MINERALOGY, AND GEOCHEMISTRY

McLennan S. M.   Boynton W. V.   Karunatillake S.   Hahn B. C.   Taylor G. J.   Mars Odyssey GRS Team
Distribution of Sulfur on the Surface of Mars Determined by the 2001 Mars Odyssey
Gamma Ray Spectrometer **[#2174]**
Mars Odyssey GRS has mapped sulfur in the upper half meter of the martian surface. Correlations with H constrain the role of hydrated sulfates and the linear regression with Cl indicates differential mobility for S and Cl in the near surface.

Dyar M. D.   Lane M. D.   Glotch T.   Hiroi T.   Wopenka B.   Klima R.   Bishop J. L.   Pieters C.   Sunshine J.
Marchand G. J.   Seaman S. J.
Spectroscopy of Yamato 984028 **[#1831]**
UV-, visible-, near-, and mid-IR reflectance, thermal (mid-IR) emission, attenuated total reflectance, transmission FTIR, Raman and Mössbauer spectral results of whole rock and mineral separates from Y-984028 are reported.

Minitti M. E.   Hamilton V. E.
Searching for Basaltic to Intermediate Igneous Glasses in Martian Surface Materials **[#1810]**
To investigate the presence of intermediate to basaltic glasses on Mars, we created a suite of glasses and deconvolved regional martian TES spectra with a spectral library containing the glasses. The glasses do not appear in the modeled mineralogies.

Clenet H.   Pinet P. C.   Daydou Y.   Flahaut J.   Bibring J.-P.   Rosemberg C.   Ceuleneer G.   Allemand P.
Mafic Minerals Mapping on Mars and Chemical Composition Characterization Using a Systematic Approach Based on the Modified Gaussian Model (MGM) **[#1656]**
We developed a systematic approach based on the MGM in VNIR wavelengths domain. Automatic initialization allows us to map mafic minerals abundances on martian terrains. We also characterize more precisely olivine and pyroxenes chemical compositions.

Farrand W. H.   Johnson J. R.   Bell J. F. III   Yingst R. A.   Weitz C. M.
Distinguishing Martian "Erratics" from Meteorites at Meridiani Planum Using Pancam: Comparing Marquette Island to Meridiani Cobbles **[#1935]**
Opportunity Pancam multispectral imaging of the martian erratic rock Marquette Island is described. The spectral character of Marquette Island is compared to that of other objects encountered by the Mars Exploration Rovers.

Nettles J. W.   Wyatt M. B.   Mustard J. F.
Combining TES And OMEGA Datasets at Regional Scales to Constrain Surface Compositions: Preliminary Results **[#2508]**
Global scale NIR and TIR spectroscopic studies of primary martian surface composition roughly agree. But on regional scales, questions remain. We are attempting to reconcile TES and OMEGA results to constrain the martian surface on regional scales.

Edwards C. S.   Rogers A. D.   Bandfield J. L.   Christensen P. R.
Volcanic Origin of Flat Floored, Bedrock Containing Craters on Mars **[#1543]**
Using THEMIS, CRISM, and TES data it was found that flat floored, bedrock containing craters are more mafic than the surrounding regolith material. These and morphologic data suggest that impact associated volcanism is a likely formation mechanism.

Ody A.   Poulet F.   Bibring J.-P.   Gondet B.   Langevin Y.   Carter J.   Vincendon M.   Jouglet D.
Global Mineralogical Mapping of the Martian Surface from OMEGA/MEx: An Update **[#1905]**
In 2007, the observations acquired by OMEGA/Mex provided a first analysis of the global distribution of some surface materials. Here we reassess the detection of these minerals in the light of the analysis of new data acquired since the publication of 2007.

Brown A. J.   Hook S. J.   Baldridge A. M.   Crowley J. F.   Bridges N. T.   Thomson B. J.   Marion G. M. de Souza Filho C. R.   Bishop J. L.
Hydrothermal Formation of Clay-Carbonate Alteration Assemblages in the Nili Fossae Region of Mars **[#2124]**
We report here on a formation hypothesis for carbonates detected in the Nili Fossae Region near Syrtis Major. Our favored hypothesis is talc-carbonate hydrothermal alteration, similar to that seen in ultramafic units in Western Australia.

Michalski J. R.   Niles P. B.   Poulet F.   Carter J.   Baldridge A.   Bibring J.-P.
Updated Global Mapping of Martian Sulfates with Mars Express OMEGA Data: New Data, New Perspectives **[#1959]**
We report on updated global mapping of sulfate minerals on Mars using Mars Express OMEGA. Spectral data are being infused with other global datasets to interpret trends in the occurrence and context of martian sulfates.

Goetz W.   Hviid S. F.   Madsen M. B.   Pike W. T.   Hecht M. H.   Morris R. V.   Leer K.   Drube L.   Sykulska H.   Herkenhoff K. E.   Cabrol N. A.   Keller H. U.   Markiewicz W. J.   Arvidson R. E.   Smith P. H.
Comparison of Some Phoenix and Gusev Soil Types: Inferences on Possible Origin and Global Distribution **[#2738]**
The comparison of soil particles at the Phoenix landing site and in Gusev Crater provides clues on their origin and global distribution. Some unusual Phoenix particles are possibly of (more) local origin, as they appear to be absent in Gusev dunes.

Smith M. R.   Bandfield J. L.   Gillespie A. R.
Aqueous Alteration of Granitoid-bearing Terrains in Northwest Syrtis Major, Mars: Evidence for Alteration Gradients in a Hydrothermal Environment **[#2194]**
We investigate a mineral assemblage in NW Syrtis Major consisting of hydrated (phyllosilicates, hydrated silica, and zeolites) and granitoid (quartz and plagioclase) materials and assess its origin as a plutonically driven hydrothermal system.

Rampe E. B.   Kraft M. D.   Sharp T. G.   Golden D. C.   Ming D. W.
Thermal Infrared Emission Spectroscopy of Synthetic Allophane and Its Potential Formation on Mars **[#1938]**
We synthesized allophane, a terrestrial aqueous alteration product, and measured a thermal IR emission spectrum for the public spectral library. The use of this spectrum in martian spectral models can help constrain chemical alteration environments.

Hanley J.   Chevrier V. F.   Davis B. L.   Altheide T. S.   Francis A.
Reflectance Spectra of Low-Temperature Chloride and Perchlorate Hydrates and Their Relevance to the Martian Surface **[#1953]**
Near-infrared spectra of hydrated chlorides and perchlorates show spectral features that should allow for identification on Mars.

Bishop J. L.   Makarewicz H. D.   Perry K. A.   McKeown N. K.   Parente M.   Tornabene L. L.   Swayze G. A.   Clark R. N.   Mustard J. F.   Murchie S. L.   McEwen A. S.
Mineralogy of Libya Montes and the Southern Isidis Planitia Region: CRISM Detection of Clay, Carbonate, Olivine and Pyroxene, and Correlation with HiRISE Imagery **[#2147]**
Analyses of CRISM images of Libya Montes have revealed ancient phyllosilicate- and carbonate-bearing outcrops covered by an olivine-rich unit with pyroxene-rich material on top. Distinct textures are observed in HiRISE images for these geologic units.

Ruff S. W.   Bandfield J. L.
Refinement and Discovery with Mini-TES Spectra in Gusev Crater **[#2411]**
Refinements to Mini-TES spectra involving corrections for dust provide improved results. Fortuitous observations of the Gusev plains by Mini-TES now demonstrate for the first time the presence of olivine-rich Adirondack Class basalts to the east of the Columbia Hills.

Popa C.   Esposito F.   Colangeli L.
New Landing Site Proposal for Mars Science Laboratory (MSL) in Xanthe Terra **[#1807]**
The work describes the advantages of choosing this landing site.

Thollot P.   Mangold N.   LeMouélic S.   Milliken R. E.   Roach L. H.   Mustard J. F.
Recent Hydrated Minerals in Noctis Labyrinthus Chamata, Mars **[#1873]**
We examine spectral and imaging data over Noctis Labyrinthus in search for hydrated minerals. Possible spectral matches include sulfates, phyllosilicates and hydrated silica. Alteration ages may range between late Hesperian and late Amazonian.

Le Deit L.   Flahaut J.   Quantin C.   Allemand P.
Geological Setting of Different Phyllosilicate-rich Deposits Exposed on the Surrounding Plateaus and in the Walls of Valles Marineris, Mars **[#1146]**
We identified Al- and Fe/Mg-phyllosilicate-rich deposits on the surrounding plateaus and in the walls of Valles Marineris. We report on the morphology, the mineralogical composition, and the spatial distribution of these deposits.

Viviano C. E.   Moersch J. E.   Piatek J. L.
Stratigraphic Relationships in the Phyllosilicate-rich Materials of Tyrrhena Terra, Mars **[#2550]**
We use a THEMIS phyllosilicate index to map exposures of phyllosilicate-rich materials in Tyrrhena Terra. We find evidence for phyllosilicate-bearing ejecta blankets in at least two locations, and in basement materials exposed by fluvial incision.

Karunatillake S.   McLennan S. M.   Mars Exploration Rover Team
Relationships Between Chemical Trends and Grain Size in Gusev Soils **[#1382]**
Key goals are to classify Gusev soil by grain size; characterize each class chemically; make inferences with differences and similarities across the classes; and discuss the viability of binary (and/or ternary) mixing models to explain compositional variations.

Carter J.   Poulet F.   Bibring J.-P.   Murchie S.
Discovery, Mapping and Analysis of Hydrous Silicate-bearing Deposits in Northern Plains of Mars **[#1850]**
Thanks to CRISM and OMEGA spectral imagery data, we report the detection of hydrous-silicate bearing minerals in northern plain craters of Mars.

Barnhart C. J.   Nimmo F.
The Role of Impact Excavation in Distributing Clays Over Noachian Surfaces **[#1097]**
We present an impact excavation model for the delivery of pre-existing, buried clays to the martian surface. Our results could explain clays associated with ejecta deposits and may reveal clues about the stratigraphy of the upper Noachian crust.

Mercer C. M.   Cohen B. A.
Principal Components Analysis of Reflectance Spectra Returned by the Mars Exploration Rover Opportunity **[#1377]**
This study analyzes the variability among Pancam 13-Filter spectra of rocks at Meridiani Planum. By understanding which rock characteristics cause this variance, we may be able to regain the capability to remotely identify locally unique rocks.

Cull S. C.   Arvidson R. E.   Seelos F. IV   Wolff M. J.
Photometric Properties of Soils at the Mars Phoenix Landing Site: Preliminary Analysis from CRISM EPF Data **[#1416]**
Using data from CRISM's Emission Phase Function observations, we attempt to constrain Phoenix soil scattering properties, including soil grain size, single-scattering albedo, and surface phase function.

Jensen H. B.   Glotch T. D.
Near Infrared Spectral Analysis of Mixtures of Halite and Labradorite for Application to Putative Chloride Deposits Observed by CRISM **[#1436]**
By investigating the effect of adding labradorite to halite on near infrared diffuse reflectance spectra, this investigation explains the red spectral slope viewed in the ratioed CRISM spectral data of putative chloride deposit regions on Mars.

Seelos K. D.   Barnouin O. S.   CRISM Team
Huygens Crater and the Highland Terrains in Western Tyrrhena Terra: Mineralogic Mapping with CRISM Data **[#2400]**
Preliminary mapping of Huygens crater and vicinity with CRISM data reveals expansive olivine-bearing plains, distinctive pyroxene-bearing outcrops, and widespread occurrences of phyllosilicate that may shed light on Noachian crustal stratigraphy in the southern highlands.

Parente M. Bishop J. L.
Extracting Endmember Spectra from CRISM Images: Comparison of New DiREX Image Transform Technique with MNF **[#2633]**
We present the DiREX dimensionality reduction technique that preserves the mixing structure of the hyperspectral scene and separates unique spectral species. The technique outperformed the more traditional MNF on an endmember extraction task.

Bridges N. T. Seelos F. P. Hook S. J. Baldridge A. M. Thomson B. J.
Simulating CRISM and HiRISE Data Using Airborne Hyperspectral Imagery: Lessons Learned from Ground Truth **[#1887]**
We have generated synthetic CRISM spectral summary parameter maps and HiRISE color images of analog study sites using converted airborne hyperspectral data.

MARS: THE SEDIMENTARY ROCK RECORD

Pondrelli M. Rossi A. P. Ori G. G. van Gasselt S.
Sedimentary Volcanoes in the Crommelin Crater Area, Mars **[#1149]**
We report the discovery of possible sedimentary volcanos located in many spots in the Crommelin crater area.

McGowan E. M. McGill G. E.
The Utopia/Isidis Overlap; Possible Conduit for Mud Volcanism **[#1070]**
Both Utopia basin and Isidis basin are ancient overlapping multi-ringed impact basins. Where these two structures overlap is a large population of pitted cones, which could be the result of mud volcanism facilitated by the underlying structures.

Oehler D. Z. Allen C. C.
Evidence for Basinwide Mud Volcanism in Acidalia Planitia, Mars **[#1009]**
40,000 mud volcano-like mounds are estimated to occur in southern Acidalia. They may reflect a major event in the history of the lowlands and may provide a means of tapping samples from deep zones of potential astrobiological significance.

Amador E. S. Allen C. C. Oehler D. Z.
Regional Mapping and Spectral Analysis of Mounds in Acidalia Planitia, Mars **[#1037]**
Regional mapping and spectral analysis of over 18,000 high albedo mounds across Acidalia Planitia, Mars has provided us with clues to better understand the geologic processes that led to their formation. These mounds appear to best resemble terrestrial mud volcanos.

Chojnacki M. Moersch J. Wray J. J. Burr D. M.
The Stratigraphy, Composition and Thermophysical Properties of Endeavour Crater, Meridiani Planum, Mars, from Orbital Remote Sensing **[#2175]**
Endeavour crater, Meridiani Planum, Mars, is the current destination for the Opportunity rover. We are performing detailed mapping of Endeavour crater and report morphologic and spectral differences from locations previously visited by the rover.

Clevy J. R. Kattenhorn S. A.
Water Equivalent Hydrogen Abundance at Endeavour Crater: A Timely Example of Sub-Kilometer Epithermal Neutron Resampling **[#2482]**
In this study we evaluate the results of resampling epithermal neutrons to create sub-kilometer hydrogen abundance maps of the area around Opportunity’s next target, Endeavour Crater.

Hill K. S. Bridges J. C. Tragheim D. G. Smith K. B. Davies S. J.
CRISM Studies of Interior Layered Deposits in Arabia Terra, Mars **[#2227]**
CRISM studies of interior layered deposits (ILD) in Arabia Terra and elsewhere suggest localised concentrations of hydrous minerals. This is consistent with deposition of hydrous minerals, e.g., from brines after ILD deposition.

Weitz C. M.   Lane M.   Noe Dobrea E.   Roach L.   Knudson A.
Distribution and Formation of Crystalline Gray Hematite in Eastern Valles Marineris **[#2264]**
We have mapped out the distribution of gray hematite in Capri Chasma, identified geologic units associated with the hematite, and proposed modes of formation for hematite in Capri Chasma.

Weitz C. M.   Bishop J. L.   Roach L.   Milliken R. E.   Rodriguez J. A.
Mineralogy and Morphology of Light-toned Deposits in Noctis Labyrinthus **[#2240]**
We have analyzed 10 light-toned deposits in troughs of Noctis Labyrinthus that vary morphologically and mineralogically throughout Noctis, suggesting that there may be multiple processes with variable amounts of water that have emplaced and/or altered units in each trough.

Sefton-Nash E.   Catling D. C.
An Integrated Study of Light-toned Layered Outcrops (LLOs) in Iani Chaos **[#1957]**
We describe the morphological, mineralogical and thermal characteristics of light-toned layered outcrops in Iani Chaos. Using an integrated, GIS-based approach, we study their relationship with chaotic terrain and discuss plausible formation methods.

Hughes A. C. G.   Murchie S. L.   Seelos F. P.   Seelos K. D.   Buczkowski D. L.
Burr D. M.   CRISM Science Team
CRISM and HiRISE Observations of Two New Phyllosilicate-bearing Fan Deposits on Mars **[#2248]**
We report the first results of a systematic investigation of fan deposits on Mars. Two new fans have been identified to contain phyllosilicates and exhibit subhorizontal layering similar to that in Holden, Eberswalde, and Jezero craters.

Hughes C. G.   Ramsey M. S.
Super-Resolution of Martian Chloride Sites and the Associated Mineral Assemblages **[#2284]**
This study investigates the applicability of the super-resolution technique to enhance the THEMIS thermal infrared data of a chloride deposit in Terra Syrenum using visible data. The result is a radiometrically-accurate TIR dataset at a spatial resolution of 36 m/pixel.

Sailer D. S.   Jowell A. R.   Kelley A. K.   Heyer A. L.   Furest A. J.   Pokuri K.
Thermal Modeling for Playa and Unconsolidated Sediments **[#1142]**
This abstract is on the topic of discovering the thermal properties of a playa. Being able to distinguish the thermal properties of unconsolidated sediment and playa will allow for scientists to be able to detect the presence of water.

Kelley E. M.   Heyer K. M.   Erb A. E.
Thermal Modeling of Mixed Sediments **[#1122]**
An examination of the thermal inertia of mixed sediments.

Griffes J. L.   Grotzinger J. P.   Milliken R. E.
Working Towards a Classification Scheme for Sedimentary Rocks on Mars **[#2737]**
A systematic study for the purpose of distinguishing various types of sedimentary rocks on Mars.

Törmänen T.   Ivanov M.   Raitala J.   Korteniemi J.   Kostama V.-P.
End-Member Morphologies of Volcanic and Sedimentary Layered Rocks on Mars from the High-Resolution Images **[#1310]**
The first results of a systematic photogeological study to look at the characteristic morphology of the layers formed by volcanic processes (especially emplacement of lava flows) and due to deposition and sedimentation on Mars.

Rodriguez J. A. P.   Tanaka K. L.   Berman D. C.
Geochronologic Implications of Non-Random Distribution of Pedestal Craters in the Circum-Polar Plains of Gemini Scopuli, Mars **[#2387]**
We describe a population of pedestal craters in the north polar plains of Mars, which may have formed as a result of the collapse of volatile-rich sedimentary deposits during the Late Hesperian.

MARS CRATERS: IMPACTS, DEMAGNETIZATION, COUNTS, AND CATALOGS

Fassett C. I.   Head J. W.
Conditions on Early Mars: Scenarios, Transitions and Events **[#1951]**
Major events and transitions occurred on early Mars, including the shutdown of the magnetic dynamo, impact basin formation, erosion of valleys, and changes in weathering (to name a few). We explore scenarios for the sequence and timing of events.

Lillis R. J.   Halekas J. S.   Stewart S. T.   Louzada K. L.   Purucker M. E.   Manga M.
Impact Demagnetization at Mars: New Constraints from Monte Carlo Modeling and Multiple Altitude Magnetic Field Data **[#1514]**
We fit observed radial magnetic field profiles from Mars Global Surveyor ER and MAG data to those predicted by Fourier domain modeling of impact demagnetization signatures to constrain impact parameters and crustal magnetization properties.

Frey H. V.
Lessons Learned from Large Impact Basins on Mars **[#1145]**
Large impact basins on Mars provide important constraints on early martian and early solar system evolution, including the nature of the Late Heavy Bombardment, the origin of the crustal dichotomy and the demise of the global magnetic field on Mars.

Frey H. V.
A Minimum Crater Retention Age for the Proposed "Borealis Basin" on Mars **[#1136]**
A crater retention age (CRA) for the Borealis Basin on Mars based on both N(300) CRAs of large basins and the N(1000) CRA of the area inside and outside Borealis suggests it formed before all the large impact basins now recognized, perhaps 4.3 BYA.

Williams J.-P.   Aharonson O.   Pathare A. V.
The Production of Small Primary Craters on Mars **[#2574]**
A Monte Carlo simulation of small projectiles in the martian atmosphere demonstrates that ablation and deceleration can have as significant influence on the population of small craters.

Berman D. C.   Crown D. A.   Joseph E. C. S.   Chuang F. C.
Impact Craters as Stratigraphic Markers Using CTX-based Crater Size-Frequency Distributions **[#1163]**
With the availability of new high-resolution datasets for Mars, ages of individual impact craters can be estimated from counts of small craters superposed on their ejecta blankets and used as local stratigraphic markers.

Nava R. A.   Skinner J. A. Jr.
GIS-based Analysis of Secondary Craters as Stratigraphic Markers, Mars **[#2699]**
We present the developmental successes and operational performance of a GIS-based computer program that analyzes the spatial relationships of secondary craters with potential parent craters to assist with Mars geologic mapping.

Tornabene L. L.   McEwen A. S.   Caudill C.   Osinski G. R.   Wray J. J.   Marzo G. A.   Mustard J. F.   Skok J. R.   Grant J. A.   Mattson S.
A Crater-exposed Bedrock Database for Mars with Applications for Determining the Composition and Structure of the Upper Crust **[#1737]**
Craters expose both shallow and deeper-seated bedrock in their rims, wall-terraces, and central uplifts, so they may provide some insights into the regional and global composition and structure of the martian upper crust.

Barlow N. G.
Central Pit, Central Peak, and Elliptical Craters in the Martian Northern Hemisphere: New Results from the Revised Catalog of Large Martian Impact Craters **[#1065]**
New analysis of central pit, central peak, and elliptical craters finds that pit craters are concentrated on volcanic units, pit and peak diameters display a linear relation with crater diameter, and elliptical craters show no obvious orientation changes with time.

Robbins S. J. Hynek B. M.
Progress Towards a New Global Catalog of Martian Craters and Layered Ejecta Properties, Complete to 1.5 km **[#2257]**
We present a ~290,000-crater database of Mars with topographic information and our progress toward completing ejecta and interior morphology and morphometry by the end of 2010.

Lončarić S. Salamunićcar G.
Extensions of the Framework for Evaluation of Crater Detection Algorithms Based on New Algorithm for Registration of Craters and GT-115225 Catalogue **[#1417]**
The framework for evaluation of crater detection algorithms (CDAs) was extended with (1) a new algorithm for registration of craters; and (2) a new catalogue with 127172 craters, which is the extension of the previous GT-115225 catalogue.

Salamunićcar G. Lončarić S.
Basic Principles and Prototype of Crater Detection Algorithm for Detection of Craters from Global Mosaics of Visual Images for the Whole Mars **[#1421]**
Prototype of the crater detection algorithm (CDA), which should be capable to process global mosaics of visual images, was developed. This includes a new method of reconstruction of digital topography from a visual image.

Salamunićcar G. Vinković D. Karbonini L. Vojković M. Lončarić S.
Differences in Distribution in GT-115225 Global Catalogue of Martian Craters Between Shallow and Deep Craters and Between Large and Small Craters **[#1426]**
The new GT-115225 catalogue of martian craters was analyzed using 1/128° MOLA data and Topography-Profile Diagrams (TPDs). The results are newly discovered differences in distribution between shallow and deep and between large and small craters.

Vojković M. Karbonini L. Vinković D. Salamunićcar G. Lončarić S.
Laboratory Craters and their Comparison with Craters from GT-115225 Global Catalogue of Martian Impact Craters **[#1428]**
We present the results of comparison between explosion-induced laboratory craters and GT-115225 catalogue. Laboratory craters fit into the gravity regime and we show that they follow the same depth/diameter relationship as the young martian craters.

MARTIAN METEORITES AND IGNEOUS PROCESSES

Cartwright J. A. Burgess R. Gilmour J. D. Turner G.
Ar and Cl-bearing Hydrous Fluids in Nakhlites **[#2214]**
Analysis of nakhlite meteorites suggests the presence of trapped Ar as a fluid within the samples. Crystallisation ages of two nakhlites are reported.

Bogard D. D. Garrison D. H. Park J.
Chlorine Abundances in Martian Meteorites **[#1074]**
Chlorine abundances obtained from Ar-Ar dating analyses are reported for whole rock and mineral separates of 16 martian meteorites.

Franz H. B.   Farquhar J.   Irving A. J.
Acid Volatile Sulfur Isotopic Composition of Seven Shergottites from Northwest Africa **[#2341]**
We report here the isotopic composition of acid volatile sulfur from several martian meteorites from Northwest Africa, as part of a comprehensive study to characterize the isotopic composition of sulfur-bearing mineral phases in martian meteorites.

Anand M.   Parkinson I. J.
Variations in Light Lithophile Elements (Li, B, Be) and Lithium Isotopes in Martian Pyroxenes and Olivines: Roles of Degassing and Diffusion **[#2362]**
We have measured and modelled light lithophile elements and Li isotopic composition in pyroxenes and olivines from newly discovered martian meteorites to assess the roles of various processes involved in martian magmatic history.

Ustunisik G.   Nekvasil H.   McCubbin F. M.   Lindsley D. H.
The Effect of S and Cl on Mineral Stability in Martian Magmas **[#1761]**
Experiments on the effect of Cl and S on mineral stability in magma of Backstay composition indicates suppression of olivine, plagioclase, and amphibole stability.

Martin A. M.   Righter K.
Experimental Constraints on the Stability of Clinopyroxene + Magnesite in Iron Bearing Planetary Mantles: Implications for Nakhlite Formation **[#2419]**
We performed experiments on Fe/C interactions in planetary mantles. Melting of magnesite + clinopyroxene at 1.8 GPa–1100° to 1300°C produces a CaO-, CO_2-rich melt in equilibrium with olivine and cpx that have similar compositions as nakhlite minerals.

Arauza S. J.   Jones J. H.   Le L.   Mittlefehldt D. W.
Is EETA79001 Lithology B a True Melt Composition? **[#1429]**
The presence of olivine in experiments on the Lithology B composition precludes it from being a true melt. Natural Lith B contains no olivine.

Karner J. M.   Papike J. J.   Sutton S. R.   Burger P. V.   Shearer C. K.   Le L.   Newville M.   Choi Y.
Partitioning of Eu Between Augite and a Highly Spiked Martian Basalt Composition as a Function of Oxygen Fugacity (IW-1 to FMQ): Determination of Eu2+/Eu3+ Ratios by XANES **[#1022]**
Valence state partitioning of Eu between augite and melt.

Koizumi E.   Mikouchi T.   Monkawa A.   Kurihara T.   Miyamoto M.
Micro FT/IR Analysis of Brown Olivines in Martian Meteorites **[#1575]**
We analyzed the spectra of martian meteorites with brown olivine by micro FT/IR, and the olivine from shock-recovery experiment under 40 GPa by ATR. The results indicate that the midinfrared reflectance of olivine correspond to their darkness.

He Q.   Xiao L.   McSween H. Y.
Melt Inclusions in the Second Chassignite NWA 2737 **[#1344]**
Olivine crystals in the second known chassignite contain a diverse array of trapped melt inclusions that may record the evolution of its parent magma.

Stephen N. R.   Benedix G. K.   Bland P. A.   Howard K. T.   Hamilton V. E.
Modal Mineralogy of the Martian Meteorite Zagami **[#2367]**
In this abstract we show that modal mineralogy of Zagami as determined by thin section may not be representative. We will present the modal mineralogy as determined by an XRD method. An accurate mode can be used as a calibration for deconvolutions of thermal infrared data.

Ennis M. E.   McSween H. Y.   Patchen A.   Taylor L. A.
Zoning of Phosphorus Within the Olivines of the Olivine-Phyric Shergottite Dhofar 019 **[#2404]**
The results of phosphorus zoning mapping of olivine grains contained within the olivine-phyric shergottite Dhofar 019 and implications for martian magma crystallization history and evolution.

Irving A. J.   Kuehner S. M.   Herd C. D. K.   Gellissen M.   Rumble D. III   Lapen T. J.   Ralew S.   Altmann M.
Olivine-bearing Diabasic Shergottite Northwest Africa 5990: Petrology and Composition of a New Type of Depleted Martian Igneous Rock **[#1833]**
Petrologic, elemental and Nd isotope characteristics of a depleted permafic shergottite, which bridges the gap between most olivine-phyric shergottites and QUE 94201.

Irving A. J.   Kuehner S. M.   Herd C. D. K.   Gellissen M.   Korotev R. L.   Puchtel I.   Walker R. J.   Lapen T.   Rumble D. III
Petrologic, Elemental and Multi-Isotopic Characterization of Permafic Olivine-Phyric Shergottite Northwest Africa 5789: A Primitive Magma Derived from Depleted Martian Mantle **[#1547]**
We report on an extensive petrological-chemical study of a very primitive depleted shergottite, which is similar in many (but not all) respects to Yamato 980459/98497.

Basu Sarbadhikari A.   Goodrich C. A.   Liu Y.   Taylor L. A.
Melt Inclusions in Olivine-Phyric Shergottite LAR 06319: Important Considerations in Using Melt Inclusions to Retrieve Parent Magmas **[#1369]**
This work focuses on melt inclusions in coarse olivine grains in LAR 06319 which does not have a cumulate component and its melt inclusions present a relatively simple case that allows us to address several methodological issues.

Burger P. V.   Shearer C. K.   Papike J. J.
Origin of Low-Ca Pyroxene Megacrysts in Martian Basalts. Comparisons Among the Composition of Minerals in RBT 04262 **[#2053]**
We compare mineral compositions in three textures observed in martian meteorite RBT 04262 to gain a better understanding of the origin of megacrysts in shergottites, the petrogenesis of martian basalts, and the nature of the martian crust.

Hui H.   Peslier A. H.   Lapen T. J.   Shafer J.   Brandon A.   Irving A.
Enriched Shergottite NWA 5298 as an Evolved Parent Melt: Trace Element Inventory **[#1851]**
NWA 5298 is a highly evolved, enriched basaltic shergottite. The trace element study provides strong evidence for closed-system magmatic behavior of NWA 5298. NWA 5298 may represent a LREE enriched and oxidized parental liquid.

Marks N. E.   Borg L. E.   Gaffney A. M.   DePaolo D.
The Relationship of Northwest Africa 4468 to the Other Incompatible Element-enriched Shergottites Inferred from its Rb-Sr and Sm-Nd Isotopic Systematics **[#2064]**
We present Rb-Sr and Sm-Nd age determinations for the LREE-enriched shergottite NWA 4468.

Agresti D. G.   Morris R. V.
Mineralogy of SNC Meteorite EET 79001 by Simultaneous Fitting of Mössbauer Backscatter Spectra **[#2577]**
We measured nine samples of SNC EET 79001 with a MIMOS II backscatter Mössbauer spectrometer similar to those in use on Mars.

Satake W.   Mikouchi T.   Miyamoto M.
Iron Micro-XANES Measurement of Maskelynite in Shergottites: An Update **[#1902]**
Fe micro-XANES measurement of maskelynite in shergottites gave the Fe^{3+}/(Fe^{2+} and Fe^{3+}) ratios ranging 0.1–0.9. We found that they are well correlated with redox states suggested from geochemical characteristics.

Kurihara T.   Mikouchi T.   Yamaguchi A.   Sekine T.   Miyamoto M.
High Temperature Shock Experiment of San Carlos Olivine: Implications for the Formation of Nano-Particles in Olivine from Martian Meteorites **[#1655]**
We performed high temperature shock experiments of olivine to reproduce nano-particles in martian meteorites. Fe-Ni nano-particles instead of magnetite were observed in olivines from preheated samples.

Sutton S. R.   Rao M. N.   Nyquist L. E.
Oxidation States of GRIM Glasses in EET79001 Based on Vanadium Valence **[#1747]**
Mean vanadium valences determined by microXANES for gas-rich impact-melt (GRIM) glasses in EET 79001 ranged from 3.0 to 3.6. Mean fO_2 ranged from IW-1.2 to IW+1.4. Variable oxidation state is consistent with impact reduction of regolith precursors.

Rao M. N.   Hoppe P.   Sutton S. R.   Nyquist L. E.   Huth J.
Sulfur Isotopes in Gas-rich Impact-Melt Glasses in Shergottites **[#1161]**
Sulfur isotope studies in gas-rich impact-melt glasses in shergottites indicate that sulfate is reduced to sulfide during impact melting and quenching.

Ross D. K.   Ito M.   Rao M. N.   Hervig R.   Williams L. B.   Nyquist L. E.   Peslier A.
Jarosite in the Shergottite QUE 94201 **[#1154]**
Hydrogen isotope ratios in the hydrous alteration mineral jarosite have been measured by ion probe, in the shergottite QUE 94201. Hydrogen isotope ratios indicate that jarosite was formed in Antarctica, or that hydrogen isotopes reequilibrated with Antarctic water.

Chennaoui Aoudjehane H.   Jambon A.   Boudouma O.
A Cathodoluminescence Study of Silica and K-Feldspar in the Nakhlite MIL 03346 and NWA 5790 **[#1934]**
We propose in this work to constrain the intensity of the shock in nakhlites, by using cathodoluminescence spectroscopy on silica phases that occurs on the mesostasis. CL spectra has been collected from NWA 5790 and compared to spectrum collected on MIL 03346.

Schrader C. M.   Cohen B. A.   Donovan J. J.   Vicenzi E. P.
A High Resolution Microprobe Study of EET A79001 Lithology C **[#2441]**
We present initial findings from a high-resolution electron microprobe study of impact melt from martian meteorite EET A79001. We investigate martian soil composition, near-surface processes, and the generation of impact melt.

Nishiizumi K.   Caffee M. W.
A Tale of Two Shergottites: RBT 04261 and RBT 04262 **[#2276]**
The two shergottites RBT 04261 and RBT 04262 were presumed to be paired based on similar textures and mineral compositions. Cosmogenic radionuclide ages indicate that they are different falls and that the objects were separate entities in space.

ENVIRONMENTS FOR LIFE AND ITS PRESERVATION, FOSSILS, AND LOOK-ALIKES

Dohm J. M.   Miyamoto H.   Ori G. G.   Komatsu G.   Pondrelli M.   Kim K. J.   Anderson R. C.   Fairén A. G.   Hare T. M.   Williams P.   Ruiz J.   Davila A. F.   McGuire P. C.   Mahaney W. C.   Schulze-Makuch D.   Fink W.   Boston P.   Di Achille G.   Glamoclija M.   Allen C.   Oehler D.   Baker V. R.   Maruyama S.   Ip F.   Wheelock S. J.
Linkage Among Geology, Hydrology, Climate, and Life on Earth Point to Possible Life-containing Environments on Mars **[#2360]**
On Earth, biology, hydrology, and geology are often interwoven such that certain types of life are often linked with specific geologic, hydrologic, and climatic conditions. Through Earth, we discuss potential life-containing environments on Mars.

Marnocha C. L.   Chevrier V. F.   Ivey D. M.
Sulfate-reducing Bacteria as a Model for Life in the Martian Subsurface **[#1536]**
We suggest sulfate-reducing bacteria as a model for life in the martian subsurface. This study seeks to determine the survival of sulfate-reducing bacteria in Mars-like conditions and to identify potential biosignatures produced in these conditions.

Glamoclija M.   Fogel M. L.   Kish A.   Steele A.
Microbial Signatures from the Dune Field at White Sands National Monument, New Mexico **[#2527]**
White Sands National Monument (New Mexico) is studied as a terrestrial analog to gypsum rich dunes from Mars. Microbial signatures from the dune field are investigated to assess a variety and distribution of available habitats.

Ziegler K.   Coleman M. L.   Mielke R. E.   Young E. D.
Sources and Contributions of Oxygen During Microbial Pyrite Oxidation: The Triple Oxygen Isotopes of Sulfate as a Biosignature **[#2245]**
Microbial pyrite oxidation experiments in spiked water and the triple oxygen isotopes of resulting sulfate suggest that $\Delta^{17}O_{SO4}$ signatures can trace microbial vs. inorganic sulfate formation, and, therefore, have the potential as biosignature.

Blanco A.   Zavala F. J.   Hernández-Ávila J.   Maurrasse F.   Duque-Botero F.   Ramírez-Cardona M.
Microbial Preservation in Sedimentary Pyrite from Cretaceous Organic-Matter-rich Carbonate Mudstone: A Preliminary Report **[#2487]**
The main purpose of this work is to provide a general description of these fossil microorganisms in order to increase its documentation in the stratigraphic record, for further comparisons with both terrestrial and/or extraterrestrial biomorphic structures.

Krestina N.   Petaev M. I.   Jacobsen S.
Search for Microfossils in Carbonaceous Chondrites **[#1949]**
We present the preliminary results of FESEM and NanoSIMS studies of extraterrestrial “fossils” aimed at the development of a technique for distinguishing biotic from abiotic objects.

Miura Yas.
Characteristics of Fine Bacteria-like Texture Formed by Iron Meteorite by Atmosphere Reaction **[#2489]**
Spherule-chained texture of nano-grains with Fe, Ni, C and Cl is found in the Kuga iron meteorite, which are greatly different than the martian meteorite. Fine texture of the Kuga meteorite is example of fossil-like texture.

Schieber J.
Progressive Silicification of Iron Microbes — Preliminary Observations from a Two Year Experiment **[#1106]**
Iron microbe mats were stored at 50°C in a silica-rich solution for two years and intermittently examined by SEM. The results suggest a high potential for morphological preservation of iron microbes in silica precipitating environments.

Delano J. W.   Tailby N. D.   Aldersley M. F.   Watson E. B.   Joshi P. C.   Ferris J. P.
Could Montmorrillonites Have Played a Role in the Formation of Prebiotic Molecules on the Early Earth? **[#2425]**
Montmorillonite may have served as a mineral catalyst for building complex, prebiotic molecules on the early Earth. Only a subset of all montmorillonites that have been investigated are observed to be catalytic.

Glavin D. P.   Aubrey A. D.   Callahan M. P.   Dworkin J. P.   Elsila J. E.   Parker E. T.   Bada J. L.
Extraterrestrial Amino Acids in the Almahata Sitta Meteorite **[#1042]**
An unusual distribution of two- to six-carbon aliphatic amino acids was identified in the Almahata Sitta meteorite. The amino acid enantiomeric ratios were racemic, suggesting that these compounds are indigenous to the meteorite.

SATELLITES AND THEIR PLANETS

Crow-Willard E. N.   Pappalardo R. T.
Global Geological Mapping of Enceladus **[#2715]**
We will present a global geological map of Enceladus, and interpretations of the stratigraphy and geological history that our mapping implies.

Yeoh S. K.   Kizer J. R.   Goldstein D. B.   Varghess P. L.   Trafton L. M.
Modeling the Gas/Particle Plume of Enceladus **[#2635]**
A water vapor composite plume was detected over the south pole of Enceladus in 2005. A hybrid model of the gas/particle plume is constructed using the DSMC method and a free-molecular model.

Rambaux N.   Castillo-Rogez J. C.   Williams J. G.   Karatekin O.
Librational Response of Enceladus to Its Interior Structure **[#1883]**
We will present the rotational motion of Enceladus perturbed by planetary perturbations and tidal torques and describe the main librations and short librations at 1.37 days amplitude for various interior models (computed with the Andrade model).

Patthoff D. A.   Kattenhorn S. A.
Old Tiger Stripes and the South Polar Dichotomy on Enceladus **[#2099]**
Our detailed fracture and fold maps explore the relationship between the present day tiger stripes and old, non active tiger stripes and the dichotomy which surrounds the most active region of the SPT on Enceladus.

Kirchoff M. R.   Schenk P.
Global Impact Cratering Record of Saturn's Moon Dione: Constraining the Geological History **[#1455]**
We use the global impact crater distribution to constrain the geological history of Saturn's moon Dione. Of particular interest are the extent, formation time, and formation processes of the smooth plains and wispy terrains.

Burleigh K. J.   Helfenstein P.   Carcich B.   Veverka J.   Thomas P.   West R.   Denk T.   Neukum G.
Linear Polarization and Albedo Reconnaissance for Regolith Texture on Saturn's Moon Iapetus **[#2607]**
We demonstrate the sensitivity of the Cassini Images Science Subsystem Narrow Angle Camera polarization images by revealing Umov's law. We make linear polarization (%P) and albedo images of Iapetus and plot %P vs. albedo from DN values of corresponding pixels.

Martin E. S.   Jurdy D. M.
Iapetus: Construction and Analysis of a Global Crater Database **[#1437]**
Notwithstanding in-depth studies focused on Iapetus, no global digital database of craters exists. This work has mapped and recorded the location and diameter of craters (>1 km) on Iapetus into a global crater database.

Blackburn D. G.   Buratti B. J.   Ulrich R.   Mosher J.
A Bolometric Bond Albedo Map of Iapetus from the Merger of Cassini VIMS and Voyager ISS Data **[#1242]**
We took advantage of the solar phase angle and wavelength coverage of the Cassini VIMS instrument to calculate the phase integrals and construct a bolometric Bond albedo map for Iapetus, supplementing coverage in the north with Voyager ISS.

Pitman K. M.   Buratti B. J.   Mosher J. A.
Bolometric Bond Albedos For Saturnian Satellites From Cassini VIMS: Leading and Trailing Hemispheres **[#2035]**
We present values of disk-integrated bolometric Bond albedo, phase integrals, and geometric albedos, derived using Cassini VIMS solar phase curves at 7-15 wavelengths, for the saturnian satellites Rhea, Dione, Tethys, Mimas, and Enceladus.

Filacchione G.   Capaccioni F.   Clark R. N.   Cruikshank D. P.   Coradini A.   Cerroni P.   Ciarniello M.   Tosi F.
Nicholson P. D.   McCord T. B.   Brown R. H.   Buratti B. J.   Nelson R. M.   Jaumann R.   Stephan K.
Spectral Classes and Surface Properties of the Saturnian Satellites Retrieved from Cassini-VIMS Disk-integrated Observations **[#1704]**
Analysis of the saturnian satellites disk-integrated observations returned by the VIMS experiment onboard Cassini. This investigation is focused on VIS spectral slopes and IR absorption bands variability.

Sharp P. W.   Castillo-Rogez J. C.   Grazier K. R.
Coupled Geophysical and Orbital Evolution of Saturn's Satellites **[#2238]**
We discuss preliminary results using coupled geophysical and orbital modeling for Mimas, Enceladus, Tethys, Dione, Rhea, and Iapetus.

Fukuzaki S.   Sekine Y.   Sugita S.   Genda H.   Kadono T.   Matsui T.
Has Titan's Atmospheric N_2 been replenished from Crustal NH_3 Through Cometary Impacts? **[#1731]**
We evaluate the role of impact-induced N_2 production through cometary impacts after the accretion from reduced nitrogen-bearing materials proposed to be contained in Titan's crust, NH_3-H_2O ice ,for the replenishment of N_2 to the atmosphere over Titan's history (~ 4.5 Gyr).

Harris C. C.   Matthews L. S.   Hyde T. W.
The Development of a Probabilistic Model for Tholin Aggregation in Titan's Atmosphere **[#2334]**
A numerical model of coagulation of tholin particles in Titan's atmosphere includes the fractal geometry of the aggregates. Dipole charge interactions during collisions cause particles to rotate affecting the coagulation rate and the subsequent morphology of the grains.

Cornet T.   Le Mouélic S.   Bourgeois O.   Rodriguez S.   Sotin C.   Barnes J. W.   Brown R. H.   Baines K. H.   Buratti B. J.   Clark R. N.   Nicholson P. D.
Observation of Ontario Lacus on Titan with Cassini/VIMS at 17 Months Interval **[#1370]**
We are investigating an empirical method to correct the photometric and atmospheric effects in VIMS images of Titan's surface. This method is applied to T38 and T51 Ontario Lacus observations to determine whether surface changes occured between these two flybys.

Stephan K.   Jaumann R.   Brown R. H.   Soderblom J. M.   Soderblom L. A.   Barnes J. W.   Sotin C.   Griffith C. A.   Kirk R. L.   Baines K. H.   Buratti B. J.   Clark R. N.   Lytle D. M.   Nelson R. M.   Nicholson P. D.
Detection of a Specular Reflection on Titan by Cassini-VIMS **[#1692]**
We present the detection of a specularly reflected signal from Titan's surface associated with Kraken Mare, which indicates a liquid surface that is smooth on the scale of the observed VIMS signal at 5 μm.

Malaska M.   Radebaugh J.   Lorenz R.   Mitchell K.   Farr T.   Stofan E.
Identification of Karst-like Terrain on Titan from Valley Analysis **[#1544]**
Valley network terrains in Titan's southern high latitudes show several characteristics that are similar to defined karst terrains on Earth.

Mitchell K. L.   Stiles B. W.   Kirk R. L.   Stofan E. R.   Cassini RADAR Team
Refinement of the Cassini Titan RADAR Mapper SARTopo Technique for Local Studies of Lakes **[#2740]**
We refine the SARTopo method for extraction of topographic from Cassini RADAR data of Titan for local studies. Our results reveal details in the morphology around polar lakes on Titan that were only previously possible using stereo or radarclinometric methods.

Dalton J. B.
A Cryogenic Reflectance Spectroscopy Facility for Characterization of Candidate Icy Satellite Surface Compounds in Support of Spacecraft Observations **[#1710]**
The Planetary Ice Characterization Laboratory at JPL has been established in order to provide relevant spectral measurements for determination of material abundances and distributions from visible and near infrared imaging spectroscopy of icy satellites.

Yamashita Y.   Arakawa M.   Kato M.
The Rheological Properties of Polycrystalline Nitrogen and Methane: Implications for Tectonic Process on Triton **[#1685]**
To investigate the evolution process of planetary surfaces in outer solar system, rheological properties of polycrystalline nitrogen and methane were studied by means of an uniaxial deformation system with a cryostat.

Desch S.   Porter S.
Amphitrite: A Twist on Triton's Capture **[#2625]**
We propose Triton was captured by Neptune while it orbited a 2 $M_{\oplus}$ planet, Amphitrite, that then collided with either Neptune or Uranus. We present relevant dynamical calculations and discuss observational consequences for Uranus and Neptune.

Burton M. E.   Dougherty M. K.   Russell C. T.
Saturn's Internal Planetary Magnetic Field **[#2273]**
Based on Cassini magnetic field measurements we have detected a range of planetary rotation periods for which there is a measurable non-axisymmetric field component and derive models of Saturn's internal planetary magnetic field based on this rate.

Cao H.   Russell C. T.   Joy S. P.   Yu A. Z. Y.   Leinweber H. K.
Galileo Observations of Jupiter's Intrinsic Magnetic Field **[#1155]**
Previously unmodeled Galileo magnetic measurements, obtained interior to Io, are examined to determine their suitability for extending the modeled field to higher orders and to compare with Pioneer 11 measurements to constrain the secular variation.

Selvans Z. A.   Pappalardo R. T.
Geological Superposition Networks on Europa: A Corroboration of the Nonsynchronous Rotation Hypothesis **[#2610]**
A Geological Superposition Network (GSN) constructed from the linear tectonic features on Europa shows superposition relationships strongly corroborating prograde nonsynchronous rotation (NSR) of <180°, where ~40% of the mapped features are attributable to NSR.

Quick L. C.   Barnouin O. S.   Patterson G. W.   Prockter L. M.
Constraints on the Detection of Cryovolcanic Plumes on Europa **[#2247]**
This abstract will provide new insights on imaging requirements necessary to detect plumes on Europa, should they exist.

Kay J. P.   Kattenhorn S. A.
An Open-Source GUI for Calculating Icy Moon Tidal Stresses Using SatStress **[#2046]**
We have used the open-source program SatStress to develop a graphic user interface (GUI) for calculating tidal stresses on the surface of a satellite with both elastic and viscoelastic rheology. SatStress GUI will eventually be open-source.

Phillips C. B.   Dalton J. B.
Scattered Light Correction to Galileo Europa Data and Quantitative Spectral Comparisons **[#2661]**
We are combining the SSI and NIMS datasets for Europa, by performing a scattered light correction to provide a quantitative calibration to the SSI color data to allow for direct comparisons with NIMS.

Keszthelyi L. P.   Jaeger W. L.   Okubo C.
Paterae on Io: Insights from Slope Stability Analysis **[#2244]**
The near-vertical walls of paterae on Io require that the upper crust be composed of material with significant cohesion, such as basalt or cold sulfur. We continue to investigate if low-density sulfur/sulfur dioxide snow is also an option.

Barth B.   Radebaugh J.   McKean A.
Distribution and Comparison of Io's Paterae: Areas, Effective Diameters, and Active Volcanism. **[#2666]**
Accurate areas and effective diameters for Io's paterae were found using ArcGIS. Black material area measurements within paterae were also done and help us understand release of Io's heat.

Veeder G. J.   Davies A. G.   Matson D. L.   Johnson T. V.   Williams D. A.   Radebaugh J.
Io: The Dark Paterae Component of Heat Flow **[#1221]**
We focus on the heat flow contribution from dark paterae on Io. We have estimated the areas of dark material within 130 paterae. We have analyzed their bimodal spatial distribution to constrain their total power.

Cheng A. F. *   Weaver H. A.   Nguyen L.   Hamilton D. P.   Stern S. A.   Throop H. B.
A New Ring or Ring Arc of Jupiter? **[#2549]**
New Horizons LORRI observations of Himalia reveal a streak-like, extended emission feature that is interpreted as a new ring of Jupiter.

PLANETARY DYNAMICS AND TECTONICS

Neesemann A.   van Gasselt S.   Hauber E.   Neukum G.
Insights to the Evolution of the Tempe Terra Region, Mars: Refinements of Geologic and Tectonic Units **[#2685]**
The tectonic and volcanic history of Mars is mainly concentrated on the Tharsis rise. As a further contribution to a better understanding of this region we chose Tempe Terra with its complex pattern of graben and faults to estimate changes in orientation with time.

Fueten F.   Robinson A.   Stesky R.   MacKinnon P.   Hauber E.   Zegers T.   Gwinner K.
Dip of Chasm Wall Faults in Ophir Chasma, Valles Marineris, Mars **[#1449]**
The mean dip of normal fault facets within the walls of Ophir Chasma is approximately 36°. We suggest that the shallow faults were initiated as thrust faults during a localized uplift phase of the basin formation and reactivated as normal faults.

Birnie C.   Fueten F.   Stesky R.   Hauber E.   Zegers T.   Gwinner K.
Fracture Orientations Within HiRISE Images of Ceti Mensa, West Candor Chasma, Mars **[#1753]**
Fracture morphology and orientations measured within HiRISE images around Ceti Mensa show a large variation in orientation and are generally not parallel to the proposed trend of the major basin-forming faults.

Chadwick D. J.
Deflection of Lava Flow Directions Relative to Modern Topographic Slopes in the Tharsis Region of Mars: Indications of Post-Flow Subsidence **[#2444]**
High-resolution topographic data and imagery are used to identify angular deviations between lava flow directions and topographic slopes.

Kattenhorn S. A.   Meyer J. A.
Magmatic Dikes and Megafloods: A Protracted History of Interactions Between Magma and Subsurface Ice, Cerberus Fossae, Mars **[#1271]**
A protracted period of dike intrusion away from Elysium Mons, Mars, resulted in a segmented fracture system (Cerberus Fossae) that induced multiple megafloods as intruding magma interacted with subsurface ice.

Craft K.   Lowell R.   Germanovich L.
Dike Emplacement and Hydrothermal Circulation on Mars **[#2583]**
Using a finite element program, we model a dike propagating on Mars and calculate how the resulting surrounding stresses affect circulation in an adjacent porous medium. We also investigate the melting of an ice layer overlying the porous medium.

Wyrick D. Y.   Buczkowski D. L.   Bleamaster L. F.   Collins G. C.
Pit Crater Chains Across the Solar System **[#1413]**
Pit crater chains exist on a range of planetary bodies — from small asteroids to icy moons to large terrestrial planets — raising important questions about formation mechanisms and near-surface crustal properties of solid bodies in our solar system.

Kneuer C. B.   Lang N. P.
Formation and Evolution of the Peneus Patera Caldera **[#2429]**
Here we present our initial results on the evolution of the Peneus Patera caldera.

Schumacher S.   Zegers T. E.
Chaotic Terrain and Its Constraints on the Surface Heat Flux of Mars **[#1345]**
Geological analysis of Aram Chaos on Mars suggests that this chaotic terrain could have formed by the collapse of an underground lake. We show how this concept can be used to constrain the surface heat flux during the Hesperian.

Wenkert D. D.   Nunes D. C.
Gravitational Signatures of Large Martian Craters **[#2044]**
Recent improvements in Mars' gravity field model make it possible to analyze the effects of smaller impact basins than previously possible. We are analyzing the effects of larger impact craters (small basins) on the gravity field.

Han S.-C.   Mazarico E.   Lemoine F. G.
Towards Improved Regional and Global Gravity Fields on Mars by Means of Localized Harmonic Analysis **[#2504]**
We present the ongoing progress towards improved Mars gravity fields to understand the density structure of the martian crust and polar layered deposits by optimally resolving the geopotential from radio tracking data.

Reese C. C.   Solomatov V. S.
Early Martian Dynamo Generation due to Giant Impacts **[#1948]**
Giant impacts produce localized melt regions facilitating rapid iron-silicate segregation. Impactor iron heated by the collision can carry thermal energy to the core and establish conditions favorable for core cooling and dynamo generation.

Reese C. C.   Orth C. P.   Solomatov V. S.
Impact Origin for the Martian Crustal Dichotomy: Half-Emptied or Half-Filled? **[#1988]**
We suggest an alternative impact origin for the martian crustal dichotomy in which impact generated melt floods the excavated cavity, produces thickened crust, and generates an antipodal topographic basin.

Milbury C.   Schubert G.
Modeling of Mars' Large-Scale Crustal Magnetization **[#2288]**
We present a very simple model of the crustal magnetization in order to match the large-scale features of the magnetic field observations.

King S. D.
The Influence of Core Radius on the Planform of Stagnant Lid Convection **[#1749]**
The transitional radius between roll and plume modes of stagnant lid convection will be discussed.

Michel N.   Forni O.
The Role of Phase Transitions in the Martian Mantle **[#1190]**
In that work, we want to improve the study of phase transitions, adding the core cooling, the decay of radioactive elements, and a temperature and depth dependant viscosity to the two-dimensional numerical model, with two different sizes of the martian core.

Kohlstedt D. L.   Schneider S. E.
Experimental Constraints on the Strength of the Lithospheres of Terrestrial Planets **[#1846]**
To better constrain the flow law used to described deformation of the lithospheres of terrestrial planets, we have performed deformation experiments on crystals of San Carlos olivine at lower temperatures and higher stresses than previous studies.

Wagner R. J.   Neukum G.   Giese B.   Roatsch T.   Denk T.   Wolf U.   Porco C. C.
The Geology of Rhea: A First Look at the ISS Camera Data from Orbit 121 (Nov. 21, 2009) in Cassini's Extended Mission **[#1672]**
In orbit 121 of Cassini's Extended Mission, the ISS cameras aboard the spacecraft observed the trailing hemisphere of Saturn's icy satellite Rhea. In this paper we present a first look at geologic features in this area, especially of tectonic structures.

Singer K. N.   McKinnon W. B.   Schenk P. M.
Pits, Spots, Uplifts, and Small Chaos Regions on Europa: Evidence for Diapiric Upwelling from Morphology and Morphometry **[#2195]**
Feature size and topographic expression were determined for pits, uplifts, spots, and subcircular chaos on Europa in the ~200 m/px RegMaps. The results support a diapiric formation and place lower limits on ice shell thickness when features formed.

Rudolph M. L.   Manga M.
Damage Mechanics Model for Making Ridges on Icy Satellites **[#2087]**
We apply a damage mechanics model to the problem of ridge formation. Preliminary results indicate that this model is capable of producing ridge-like topography.

Preuss L. J.   Barr A. C.
Dominant Wavelength of Small-Scale Folds Between Enceladus' South Polar Tiger Stripes **[#1487]**
High-resolution images of Enceladus' south polar terrain reveal regions of small-scale folds between Damascus and Baghdad sulci. We will present the results of a systematic study of the folding wavelength using Fourier transform methods.

Olgin J.   Smith-Konter B. R.   Pappalardo R. T.
Investigating the Limits of Enceladus's Tidally Driven Tiger Stripe Failure Scenario: Exploration of Ice Shell Thickness, Coefficient of Friction, and Fault Depth **[#2085]**
We compute Coulomb failure conditions to assess likely failure criteria at Enceladus's tiger stripes, exploring a suite of model parameters (e.g., ice shell thickness, fault depth, frictional coefficient) that inhibit or promote shear fault failure.

Patterson G. W.   Prockter L. M.
Investigating the Rigidity of Europa's Lithosphere by Modeling Plate Motion **[#2183]**
We are using plate motion modeling to determine the magnitude and extent of non-rigid behavior present within several plate systems on Europa.

Wasiak F. C.   Hames H.   Chevrier V.   Blackburn D. G.
Characterizing the Stability of Titan's Northern Lakes Using Image Analysis and Mass Transfer Modeling **[#1538]**
We search for evidence of change in Titan's northern lake region utilizing Cassini data analyzed with GIS, and explore a new mass transfer model suitable for evaporation/sublimation of methane/ethane under Titan conditions.

Matson D. L.   Johnson T. V.   Lunine J. I.   Castillo-Rogez J. C.
Enceladus' Interior: A Liquid Circulation Model **[#1698]**
We investigate a model for Enceladus' interior in which the requirements of supplying water, gas and dust, to the eruptive plumes and matching the observed heat flow are accomplished by a relatively deeply circulating brine solution.

Bunte M. K.   McNamara A. K.   Greeley R.
Investigating Ice Shell Convection with a Lower Boundary Defined by Changes in Phase and Composition: Implications for Europa **[#2523]**
We present thermochemical convection models of the ice shell of Europa. We investigate the ability of new ice to form at the lower boundary of the ice shell and examine the behavior of diapirs in relation to a highly viscous surface lid.

Castillo-Rogez J.   Lunine J. I.
Titan's Core Structure Constrained by Cassini Observations **[#2449]**
We explore possible evolution models for Titan's core, constrained by Cassini observations, for different initial conditions on the nature of its silicate component.

IGNEOUS AND VOLCANIC PROCESSES ON TERRESTRIAL BODIES IN THE SOLAR SYSTEM

Dominguez G.   Wilkins G.   Thiemens M. H.
Modeling the Isotopic Fractionation of Magnesium and Calcium in High Temperature Thermal Gradients from First Principles **[#2123]**
A fundamental model of isotope specific diffusion in high-temperature (T > 1000°C) systems was developed and tested. We find that differences in zero point energy of isotopes leads to isotopic fractionation in high-temperature thermal gradients.

Mikouchi T. Sugiyama K. Kato Y. Yamaguchi A. Koizumi E. Kaneda K.
Mineralogy of Calcium Silico-Phosphates in Angrites Compared with Related Phases in Heated Eucrite and Synthetic Analog **[#2343]**
We analyzed Ca silico-phosphates in angrites and found that they have a graserite structure by EBSD and Raman study. The related phases in experimentally heated eucrite and synthetic analog are slightly different in both composition and structure.

Stanley B. D. Mounier M. T. Hirschmann M. M.
Experimental Investigation of CO_2 Solubility in Martian Basalts with Varied Oxidation State and Applications to Martian Atmospheric Evolution **[#1667]**
We investigate the solubility of carbon dioxide in martian analogue basaltic melts at varying oxygen fugacities to constrain the magmatic outgassing fluxes of carbon dioxide during martian atmospheric evolution.

Jowell A. H. Davis S. J. Stein A. J. Erb Z. S. Oliver B. L. Eckert-Erdheim A. M.
Thermal Modeling of Mafic and Ultramafic Igneous Rocks **[#1740]**
Experimental data suggests the thermal inertias of tested rocks are in the following increasing order: vesicular basalt, massive basalt, altered peridotite. Weathered surfaces mask the thermal signatures of all rocks tested.

Wilson L. Head J. W.
Lunar Magmatism and Volcanism: Theory of Magma Generation, Ascent, Intrusion and Eruption **[#1100]**
We review current understanding of lunar volcanic processes to pinpoint issues needing theoretical and observational study. Contrasting eruption conditions of mare lava flows and sinuous rilles throw light on depths and volumes of magma sources.

Mikosz J. A. Dombard A. J.
A Global Search for Actively Forming Coronae on Venus **[#2037]**
By comparing geophysical and geologic maps, we identify 13 coronae that may currently be active. Extrapolating globally, there could be 26–32 coronae forming at present. Venus may lose a significant fraction of its heat via corona formation.

Leone G. Wilson L. Davies A. G.
The Geothermal Gradient of Io: Consequences for Lithosphere Structure and Volcanic Eruptive Activity **[#1130]**
We re-evaluate Io's temperature structure with temperature-dependent thermal parameters to find the depths at which sulphur volatiles, buried by volcanic activity, melt to be mixed into later magmas, affecting eruption rates and intrusion depths.

Giacomini L. Carli C. Massironi M. Sgavetti M.
Morphological and Spectral Analysis for the Daedalia Planum Geological Mapping **[#1594]**
Our study has been focused on the Daedalia Planum geological mapping. THEMIS, MOC, HiRISE images were analyzed to perform a stratigraphic and morphological analysis. OMEGA data revealed spectral differences that permitted improvement of our mapping.

Ramsey M. S. Crown D. A.
Thermophysical and Spectral Variability of Arsia Mons Lava Flows **[#1111]**
Lava flows on the SW apron of Arsia Mons have a multitude of textures and thermophysical characteristics in THEMIS data. Despite moderately high albedo, the spectral diversity appears to be directly related to flow emplacement and composition.

Davies A. G. Keszthelyi L. P. Harris A. J. L.
The Thermal Signature of Volcanic Eruptions on Io and Earth — Implications for a Future Mission to Io **[#1396]**
We present a new methodology (which we term the "thermal signature") of classifying ongoing high-temperature volcanic eruptions in low spatial resolution remote sensing data which is effective for both Io and Earth observations.

Leverington D. W.
Volcanic Interpretations of the Martian Outflow Channels are Consistent with Surface Mineralogy **[#1282]**
Though not supportive of aqueous processes of outflow channel formation, the surface mineralogy of Mars appears consistent with volcanic mechanisms of system development.

Hurwitz D. M. Head J. W. Wilson L. Hiesinger H.
Lunar Sinuous Rilles: Analysis of Morphology, Topography, and Mineralogy, and Implications for a Thermal Erosion Origin **[#1056]**
Characteristic measurements of lunar sinuous rilles are used to determine flow velocity, erosion regime, and vertical/lateral erosion rates that occurred during rille formation. These parameters provide key insights into the origin of sinuous rilles.

Wilson L. Head J. W. III
Conditions in Lunar Eruptions Producing Sinuous Rilles **[#1101]**
We used Hulme's erosion model to analyze eight lunar sinuous rille channels to infer conditions in the volcanic eruptions forming them. Ten-fold smaller volume fluxes than for mare lava flows, plus steeper ground slopes, distinguish rilles from flows.

Giguere T. A. Wilson L. Hawke B. R.
Magmatic Origin for Rima Hyginus: Implications for Its Feeder Dike **[#1129]**
Our results strongly support the idea that all of the major structural features of the Hyginus rille are the direct consequences of a shallow dike intrusion.

Weber A. K. Head J. W. Saal A. E. Weinreich T. Wilson L.
Volatiles in Lunar Fire Fountaining Eruptions and the Effect of Rotation on Droplets in Free Flight **[#1208]**
This presentation deals with the rotational aspect of liquid magma droplets while in flight, during emplacement of fire fountaining eruptions. Samples from the Apollo 15 and 17 missions were analyzed for this research.

Kerber L. Head J. W. III Madeleine J. B. Wilson L. Forget F.
The Distribution of Ash from Ancient Explosive Volcanoes on Mars **[#1006]**
A martian explosive eruption model is combined with a global circulation model to simulate the dispersal of tephra from major martian volcanoes. Implications for friable layered deposits are discussed.

Farrell A. K. Lang N. P.
Distribution of Explosive and Effusive Volcanic Deposits at Apollinaris Patera, Mars **[#2072]**
We present our initial results on the distribution of explosive and effusive deposits at Apollinaris Patera, Mars.

Platz T. Kneissl T. Hauber E. Le Deit L. Michael G. G. Neukum G.
Total Volume Estimates of Volcanic Material of the Elysium Volcanic Region **[#2476]**
Our ongoing study comprises total volume estimates of material erupted at martian volcanic centers. Here, results for the Elysium volcanic region are presented with implications for its outgassing history.

Bleacher J. E. Richardson J. A. Richardson P. W. Glaze L. S. Baloga S. M. Greeley R. Hauber E. Lillis R. J.
Updates to the Catalog of Tharsis Province Small Volcanic Vents, Mars **[#1615]**
This abstract reports on the ongoing efforts to catalog small volcanic vents in the Tharsis province of Mars, and the scientific implications of these observations for South Tharsis, Olympus Mons, and Syria Planum.

Stofan E. R. Glaze L. S.
Analysis of Flank Vents at Large Venusian Volcanoes **[#1337]**
Flank eruptions provide a window to a volcano's plumbing system. We assess flank vents on large volcanoes on Venus to determine the degree of randomness in their locations and use any systematic behavior to provide insight into formation mechanisms.

Baptista A. R.   Craddock R. A.
The Galapagos and Hawaii Volcanoes: Two Analogues of Syria Planum on Mars **[#1768]**
This study will establish an analogous eruptive and emplacement history of the range of shield volcanos and volcanic provinces found both on Syria Planum, Mars, and on the Galapagos and Kilauea, Hawaii, volcanos on Earth.

Pasckert J. H.   Hiesinger H.   Reiss D.
Rheology and Age of Lava Flows on Elysium Mons, Mars **[#1903]**
We present results of our study of the rheologies and ages of lava flows on the Elysium Mons volcano, Mars.

Williams D. A.   Keszthelyi L. P.   Crown D. A.   Geissler P. E.   Schenk P. M.   Yff J.   Jaeger W. L.
Volcanism on Io: Results from Global Geologic Mapping **[#1351]**
Here we highlight some of the results from global geologic mapping of Io.

Dundas C. M.   Keszthelyi L.   Bray V. J.   McEwen A. S.
The Cratering Record of Young Platy-ridged Lava on Mars: Implications for Material Properties **[#2486]**
Target properties can affect the cratering record of planetary surfaces. We investigate the implications of this effect for the cratering record of martian platy-ridged lava with varying crater densities.

Crown D. A.   Ramsey M. S.   Berman D. C.
Mapping Arsia Mons Lava Flow Fields: Insights into Flow Emplacement Processes and Flow Field Development **[#2225]**
This study utilizes high-resolution images combined with topographic and thermal infrared data to produce detailed maps of flow fields south of Arsia Mons that provide new insights into flow emplacement processes and flow field development.

Robbins S. J.   Di Achille G.   Hynek B. M.
Dating the Most Recent Episodes of Volcanic Activity from Mars' Main Volcanic Calderae **[#2252]**
We have dated the most recent volcanism on Mars through crater-counting with CTX mosaics of the calderae of Mars' major volcanic complexes.

Xiao L.   Huang J.   Christensen P. R.   Williams D. A.   Greeley R.   Wang C. Z.   Xu W. B.   Yang J.   He Q.   Ruff S.
The Possibly Oldest Volcanoes on Mars **[#1173]**
This study shows numerous Early Noachian (>4.0 Ga) small volcanoes preserved in the heavily cratered southern highlands. They are possibly the oldest shield volcanos on Mars.

ENVIRONMENTAL ANALOGS: WHAT PLANET ARE YOU ON?

Lofgren G. E.   Hörz F.   D-RATS SSR   Bell M. S.   Cohen B. A.   Eppler D. B.   Evans C. A.   Hodges K. V.   Hynek B. M.   Gruener J. E.   Kring D. A.   Hurtado J. M.   Lee P.   Ming D. W.   Rice J. W.
Science Support Room Operations During Desert RATS 2009 **[#2081]**
The DRATS 2009 field exercise provided operational experience that will help define science requirements for a science support room for future lunar surface operations. Lessons learned emphasize the continued collaboration between science, engineering, and operations.

Garry W. B.   Bleacher J. E.
Field Geology Conducted from the Lunar Electric Rover, NASA Desert RATS 2009: Strategies for Human Surface Science Operations on the Moon **[#2209]**
Science operations on the Moon will need to take advantage of new vehicles, suits, and technology. We present field geology strategies implemented during NASA's Desert RATS 2009 field test of the Lunar Electric Rover in Arizona.

Calaway M. J.   Evans C. A.   Bell M. S.
GeoLab 2010 Hardware in NASA's Pressurized Excursion Module **[#1908]**
Hardware for a geological laboratory is being constructed for NASA's Habitat Demonstration Unit–1 in a Pressurized Excursion Module configuration for analog testing at NASA's annual Desert Research and Technology Studies in late summer 2010.

Evans C. A.   Bell M. S.   Calaway M. J.
GeoLab in NASA's First Generation Pressurized Excursion Module: Operational Concepts **[#1480]**
We discuss a prototype GeoLab integrated into a Pressurized Excursion Module and tested in the 2010 DesertRATS analog test. GeoLab collects preliminary data on samples, addressing concepts for prioritization and curation of future lunar samples.

Phaneuf M.   Germain M.   Williamson M-C.   Hipkin V.
WebGIS Tools Applied to Science Traverse Planning and the Geospatial Analysis of Terrestrial Analogue Sites **[#2162]**
The Canadian space agency (CSA) is currently developing a geospatial architecture intended for planetary and terrestrial analogue databases and a WebGIS for traverses planning for extravehicular activities.

Clark P. E.   Bleacher J.   Mest S.   Petro N.
Comparison of Geological Field Work for Similar Investigations at Different Landing Sites and for Different Architectures at the Same Landing Sites **[#1261]**
We have demonstrated that suitable architectures for exploration are very site-dependent by developing a series of scenarios for a range of targets with very different density and distribution of features under investigation.

Clark P. E.
Applying the Apollo Breakthrough in Field Work Methodology for Planetary Surfaces **[#1255]**
The extraordinary challenge faced in planning Apollo, the first human expeditions to the surface of another solar system body, led to the development of a distinctive and effective approach to geological field work applicable to future missions.

Shimizu K.   Stefanov W. L.   Evans C. A.
Assessment of a Handheld Forward Looking (FLIR) Infrared Camera as a Potential Lunar Field Geology Tool **[#1546]**
The primary goal of this study is to assess the usefulness of FLIR cameras in determining rock abundance for geologic hazard assessment, and to develop data collection procedures appropriate to lunar surface sorties.

Ximenes S. W.   Mardon A. A.   Baiden G.   Osinski G. R.   Ghafoor N.   Gurtuna O.   Prévot A.   Daly M. G.
Lava Tube Analog Mission for Lunar Science and Human Performance Studies **[#2575]**
A terrestrial analog site for science research and testing of mission operations to lunar subsurface sites is proposed for investigating required science measurements with human performance objectives simulating robotic and human "first contact" with a lunar lava tube.

Boche-Sauvan L.   Foing B. H.   Stoker C.   Ehrenfreund P.   Wendt L.   Gross C.   Thiel C.   Peters S.   Borst A.   Zavaleta J.   Sarrazin P.   Blake D.   Page J.   Pletser V.   Monaghan E.   Mahapatra P.   Noroozi A.   Giannopoulos P.   Calzada A.   Walker R.   Zegers T.   ExoGeoLab   ILEWG ExoHab Team   EuroGeoMars Team
ILEWG ExoHab & EuroGeoMars Campaigns: Habitability & Human Operations **[#1759]**
We studied concepts for a minimal Moon-Mars habitat, focussing on the system aspects and as an evolving architecture. We validated experimentally the Habitat and Laboratory ExoHab concept constraints during EuroGeoMars campaign in Utah desert research station.

Groemer G.   Stumptner W.   Foing B.   Blom J. K.   Perrin A.   Mikolajczak M.   Chevrier S.   Direito S.   Olmedo-Soler A.   Zegers T. E.   Scheer D.   Bickert K.   Schildhammer D.   Jantscher B.   Mahapatra P.   MECA Team
ILEWG Eifel 2009 Campaign: Astronaut Extravehicular Surface/Subsurface Activities and Human Aspects **[#1680]**
The ILEWG organised a field campaign on 26–30 Sep 2009 with partners in Mendig, Germany, in the volcanic Eifel region. They tested their systems as simulation of lunar or planetary human and robotic mission operations, and for the first time in a subterranean lavadome.

Shiro B. R.   Ferrone K. L.
In Situ Geophysical Exploration by Humans in Mars Analog Environments **[#2052]**
We completed three experiments to better understand the challenges astronauts will face when studying the martian subsurface. These included a passive seismometer deployment and electromagnetic survey on Devon Island and an active seismic survey in Utah.

Stoker C. R.   Zavaleta J.   Bell M.   Direto S.   Foing B.   Blake D.   Kim S.
Drilling on the Moon and Mars: Developing the Science Approach for Subsurface Exploration with Human Crews **[#2697]**
The paper describes first results from DOMEX, an analog mission to develop the approach for using human crews to perform science activities on the Moon and Mars involving exploration and sampling of the subsurface.

Gross C.   Wendt L.   McGuire P. C.   Bonnici A.   Foing B. H.   Souza-Egipsy V.   Bose R.   Walter S.   Ormö J.   Díaz-Martínez E.   Oesker M.   Ontrup J.   Haschke R.   Ritter H.
The Cyborg Astrobiologist: Testing a Novelty Detection Algorithm at the Mars Desert Research Station (MDRS), Utah **[#2457]**
Herein we present a computer vision algorithm, based in part on an artificial neural network capable of identifying novel, previously unseen areas of geological or astrobiological scenery.

Borst A.   Peters S.   Foing B. H.   Stoker C.   Wendt L.   Gross C.   Zavaleta J.   Sarrazin P.   Blake D.   Ehrenfreund P.   Boche-Sauvan L.   Page J.   McKay C.   Batenburg P.   Drijkoningen G.   Slob E.   Poulakis P.   Visentin G.   Noroozi A.   Gill E.   Guglielmi M.   Freire M.   Walker R.   Sabbatini M.   Pletser V.   Monaghan E.   Ernst R.   Oosthoek J.   Mahapatra P.   Wills D.   Thiel C.   Lebreton J. P.   Zegers T.   Chicarro A.   Koschny D.   Vago J.   Svedhem H.   Davies G.   Westenberg A.   Edwards J.   ExoGeoLab Team   EuroGeoMars Team
Geochemical Results from EuroGeoMars MDRS Utah 2009 Campaign **[#2744]**
We report on the geochemistry investigations during the EuroGeoMars Campaign at the MDRS station in Utah. A total of ~150 samples from different lithologies were analyzed using advanced and miniaturized instruments (XRF, Raman, and spectrometers).

Bell M. S.   Todd B.   Schultz M. K.
NEEMO— NASA Extreme Environment Mission Operations **[#1997]**
During NEEMO (NASA's Extreme Environment Mission Operations) a crew of Aquanauts lives aboard the Aquarius Undersea Lab for up to fourteen days and conducts a variety of "Moon walks" to test Lunar Surface Systems mission operations concepts.

Bérczi Sz.   Hudoba Gy.   Lang A.   Varga T. P.   Józsa S.   Szakmány Gy.   Erdélyi I.   Kiss D.   Nickl I.   Panyi T.   Varga T. N.   Hegyi S.   Pataki T.
How We Used NASA Lunar Samples in Lunar Analog Field Trip at the Tapolca Basin Basalt Flows, Balaton-Highlands, Hungary in Comparisons with Apollo 15 Layered Outcrop and Apollo 12 Basalt Samples **[#1358]**
Lunar analog Tapolca Basin basalt mountains were visited in field works for comparisons to Apollo 12 and Apollo 15 field geology and petrography for students, studying geological setting, stratification of eruptions, and textural characteristics.

Singer K. I.   Eldridge D. L.   Korteniemi J.   Lough T.   Werblin L.   Kring D. A.
Using ArcGIS to Identify Landing Sites with Diverse Mare Basalt Compositions **[#2520]**
We use ArcGIS to provide detailed global maps of compositional information combined with stratigraphic and volcanic features that will assist mission planners in locating sites with unsampled volcanic products.

Steele A.   Amundsen H. E. F.   Conrad P.   Benning L.   AMASE '09 Team
Arctic Mars Analogue Svalbard Expedition (AMASE) 2009 **[#2398]**
The Arctic Mars Analogue Svalbard Expeditions (AMASE) 2009 was the latest of a series of expeditions that are NASA ASTEP and ESA funded and have as among their primary goals sample acquisition, collection and caching on rover platforms.

Rull F.   Sansano A.   Sobron P.   AMASE ’08 ’09 Team
In-Situ Raman-LIBS Analysis of Regolithes During AMASE 2008 and 2009 Expeditions **[#2731]**
Resume of Raman and LIBS anaysis performed during AMASE 2008 and 2009 by the RLS Exomars Spanish Team.

Pina P.   Vieira G.   Christiansen H. H.   Barata M. T.   Saraiva J.   Bandeira L.   Lira C.   Benavente N.   Mora C.   Neves M.   Jorge M.   Ferreira A.
Analysis of Polygonal Terrains on Mars Based on Svalbard Analogues **[#1372]**
Description of project ANAPOLIS (2010–2012), whose subject consists of the analysis of martian polygonal terrains based on terrestrial analogues from Svalbard.

Tamppari L. K.   Anderson R. M.   Archer D.   Douglas S.   Kounaves S. P.   McKay C. P.   Ming D. W.   Moore Q.   Quinn J. E.   Smith P. H.   Stroble S.   Zent A. P.
McMurdo Dry Valleys, Antarctica — A Mars Phoenix Mission Analog **[#2464]**
A comprehensive study of the the best Mars analog site on Earth — the McMurdo Dry Valleys, Antarctica — was conducted and results are presented and comparisons to Mars made.

Quinn J. E.   Ming D. W.   Morris R. V.   Douglas S.   Kounaves S. P.   McKay C. P.   Tamppari L. K.   Smith P. H.   Zent A. P.   Archer P. D. Jr.
Mineralogy of Antarctica Dry Valley Soils: Implications for Pedogenic Processes on Mars **[#2403]**
The Antarctic Dry Valleys (ADVs) are one of the best terrestrial analogs for the climatic conditions on Mars. The goal of this study was to characterize the alteration mineralogy of select ADV soils, which may have implications for pedogenic processes on Mars.

Salvatore M. R.   Wyatt M. B.   Mustard J. F.   Head J. W.   Marchant D. R.
Near-Infrared Spectral Diversity of the Ferrar Dolerite in Beacon Valley, Antarctica: Implications for Martian Climate & Surface Compositions **[#2290]**
Spectroscopic studies of Beacon Valley, Antarctica, reveal a range of secondary alteration minerals that have developed in a cold, dry, and stable environment. These results have implications for the development of similar minerals on Mars.

Wyatt M. B.   Head J. W.   Marchant D. R.   Harvey R. P.   Christensen P. R.   Salvatore M. R.   Horodyskyj U. N.
Orbital Spectral Mapping of Surface Compositions in the Antarctic Dry Valleys: Regional Distributions of Secondary Mineral-Phases as Climate Indicators and Implications for Mars **[#2275]**
The Antarctic Dry Valleys are an ideal location to examine links between surface compositions and climate variables in a Mars-like, hyper-arid, cold-polar desert. We report results from ongoing field work and laboratory and orbital spectroscopy.

Levy J. S.   Fountain A. G.   Head J. W.   Marchant D. R.
Physical Controls on Antarctic Dry Valleys Permafrost Geomorphology and Soil Ecosystem Habitability: Cold-Desert Processes and Mars Astrobiological Implications **[#1055]**
We present new observations of the physical, chemical, and morphologic properties of Antarctic Dry Valleys permafrost environments as basis for analysis of permafrost terrain on Mars. Climate history and astrobiological implications are discussed.

Horodyskyj U. N.   Wyatt M. B.
Spectral and Chemical Variations in Rocks and Soils from Iceland’s Interior: Implications for Surface and Sub-Surface Weathering Processes in the Martian Northern Plains **[#2178]**
We analyze surface and subsurface materials from Iceland’s interior to understand terrestrial weathering and apply this to observations from the martian lowlands.

Ehlmann B. L.   Mustard J. F.   Bish D. L.
Weathering and Hydrothermal Alteration of Basalts in Iceland: Mineralogy from VNIR, TIR, XRD and Implications for Linking Mars Orbital and Surface Data **[#1858]**
How do single mineral identifications (Fe/Mg smectite, hydrated silica) relate to rock modal mineralogy? Our analysis of spectrally Mars-like samples from Iceland emulates orbital data linked to *in situ* data such as will be measured by MSL’s ChemMin.

Boisson J.   Heggy E.   Clifford S.   Anglade A.   Yoshikawa K.
Radar Sounding of Temperate Permafrost in Alaska: Analogy to the Martian Mid-Lattitude Ice-Rich Terrains **[#2060]**
To quantify the different loss mechanisms observed in the martian radar data, we conducted radar and resistivity soundings on a permafrost terrain in Fairbanks (AK, USA), a region which has been recognized as terrestrial analogs to Mars.

Mahapatra P.   Foing B.   Direito S.   Gomez F.   Rull F.
CAREX Rio Tinto Field Workshop: Instruments, Sample Collection and Analysis **[#1374]**
At Rio Tinto, a Mars analogue site, Raman and fibre-optic spectrometers were successfully used to select appropriate rock and soil samples, and detect minerals for which it is interesting to study the associated microorganisms for innovative molecular biology techniques.

Kirkland L. E.   Herr K. C.   Adams P. M.
Disparities Between Geological Interpretations of Visible vs. Thermal-Infrared Airborne Hyperspectral Imagery of Schooner Crater **[#1695]**
This Mars analog study shows results from the first simultaneous airborne measurements of reflective (0.4–2.4 µm) and thermal-infrared (7.5–13 µm) hyperspectral imagery of a Mars analog crater, the 260-m-diameter Schooner crater, Nevada Test Site.

Chan M. A.   Nicoll K.   Ormö J.   Okubo C. H.   Komatsu G.
Utah's Geologic and Geomorphic Terrestrial Analogs to Mars: A Training Ground for Future Robotic and Human Missions to Mars **[#1110]**
Utah has many ancient and modern examples of diverse terrestrial environments and geomorphic expressions. These examples are valuable resources for exploratory and robotic missions to Mars.

Gavin P.   Chevrier V.   Sayyed M. R. G.   Islam R.
Spectral Analysis of Deccan Paleosols, India: Analog for Phyllosilicates on Mars **[#1904]**
XRD and NIR reflectance spectra of the Deccan bole beds are compared to spectra of heated phyllosilicates and used as an analog to thermally altered phyllosilicates on Mars.

Anderson L. D.   Izawa M. R. M.   Bebout G. E.   Bridge N. J.   Banerjee N. R.
Hydrothermal Alteration of 2.7 Ga Basaltic Andesites and Implications for Past Fluid-Rock Interactions on Mars **[#1668]**
A ca. 2701 Ma outcrop of greenschist-facies metabasites in the Abitibi greenstone belt of Canada provides an analogue for studying Earth and martian-like hydrothermal fluid interactions with mafic lavas at sites possibly hosting microorganisms.

Hardgrove C.   Whisner S. C.   Williams R. M. E.   Moersch J. E.   Chojnacki M.   Rogers D.
Remote Thermophysical Observations of Terrestrial Inverted Relief Features **[#2497]**
Inverted channels and sinuous ridges are well studied features on Earth and are being considered as analogs for their putative martian counterparts. Here we present preliminary results of a thermal infrared investigation of these features on Earth.

Nowicki S. A.
Thermal Inertia of Planetary Analogs Using MODIS Diurnal Observations **[#2434]**
Using diurnal, daily observations from the MODIS instruments, a new method for mapping surface characteristics is proving to be applicable at Mars analog sites in arid regions.

Petruny L. M.
Life on Mars — A Terrestrial Analogue for Martian Intertidal Stromatolites? **[#1410]**
Digitate stromatolites serve as a potential terrestrial analogue for yet-to-be discovered martian intertidal stromatolites.

Bonaccorsi R. McKay C. P.
Habitability Potential and Living Biomass of Clay Minerals: Astrobiology Investigations for MSL11 Landing Sites Candidates **[#2714]**
We present biosignatures-based, e.g., Lipopolisaccarides biomass as proxy for habitability potential in clays from arid/hyperarid desert analogs (Atacama, Death Valley). The MSL11 mission will focus on phyllosilicate minerals as targets for past/present life.

Gleeson D. F. Anderson M. S. Pappalardo R. T. Wright K. W. Templeton A. S.
Investigating Sulfur as a Biosignature and Indicator of Habitability at an Arctic Analog to Europa **[#1967]**
Sulfur-rich materials on the icy surface of Europa have the potential to contain biosignatures representative of processes occurring within the ice shell or ocean. We explore the biogenicity of sulfur minerals from the surface of an Arctic glacier.

Laufer R. Hyde T. W. Matthews L. Herdrich G. Srama R. Roeser H.-P.
Establishing an Environmental Simulation Facility for Lunar Dust Research **[#2118]**
CASPER, Baylor University, will establish new space research facilities in the fields of interstellar dust, orbital debris and microgravity and lunar environment research.

Nornberg P. Merrison J. P. Gunnlaugsson H. P.
The New Danish/ESA Mars Simulation Wind Tunnel at Aarhus University **[#1641]**
This paper will present a new Mars wind tunnel that can work under simulated martian surface conditions with a dusty atmosphere. It will be used for research projects, instrument development, testing and calibration.

EDUCATION AND PUBLIC OUTREACH: ENVIRONMENTAL ANALOGS

Rask J. C. McKay C. P. Schwert D. Clambey G. Lepper K. De Leon P. Bieri S.
Spaceward Bound North Dakota **[#2695]**
We report on Spaceward Bound North Dakota, an educational program designed to inspire and train students and teachers in the exploration of scientifically interesting geologic features in the upper midwest as an analog for exploration of Mars.

EDUCATION AND PUBLIC OUTREACH: MISCELLANEOUS

Urquhart M. L. Kisunzu P. K. Hairston M.
A Quest for True Integration of Science and Mathematics Education in the Context of NASA-sponsored Space Science Educational Outreach **[#2401]**
We are taking a new look at our NASA-sponsored space science educational outreach for the CINDI mission from the perspective of meeting the needs of mathematics educators to strengthen the connections between science and mathematics for students.

Choudhuri A. Borrok D. M. Hurtado J. M. Jr. Shafirovich E.
UTEP Center for Space Exploration Technology Research: Integrated Science and Engineering Approach to Propulsion, In-Situ Resource Utilization, and Planetary Science and Aerospace Education **[#2682]**
The purpose of this presentation is to disseminate information on the Center for Space Exploration Technology Research (cSETR), established at the University of Texas at El Paso (UTEP), effective October 1, 2009.

Lebofsky L. A. McCarthy D. W. Higgins M. L. Lebofsky N. R.
Near Infrared Camera (NIRCam): Making Models, Building Understanding **[#1856]**
The Astronomy Camp for Girl Scout Leaders is an E/PO program sponsored by NASA's JWST. We have developed a long-term relationship with adult trainers from GSUSA Councils that directly benefits troops in general science education and STEM concepts.

Lang Á.   Cseh R.   Varga T.   Szalay K.   Erdélyi S.   Erdősi F.   Nickl I.   Panyi T.   Kiss D.   Bérczi Sz.
Optical-Chemistry Experiment Measuring Gases Liberated by Heating from the "Planetary" Soil by the Husar-5 NXT-based Rover Model of The Széchenyi István High School, Sopron, Hungary **[#2139]**
We report about the new chemical measuring experiment built on the HUSAR-5 rover model. Our rover used optical lens as classical heating experiment and used CO gas-sensor in measuring chemical components liberated by heating from the soil.

Gaboriaud A.   Maurice S.   Cabane M.   Rubaud M.   Rivola S.   Canceill S.   Escande A.   Barthes L.   Roualdes G.   Exbrayat M.   Grasset L.   Serfass Denis A.
Students Designed and Built a Full-Scale Working Replica of the MSL Curiosity Rover **[#1778]**
CNES (France) decided to build a full-scale working replica of the MSL Rover, in partnership with CNRS and the Toulouse educational district. More than 200 students and 30 teachers from 15 technical schools worked on the design and construction of this replica.

Bueter D.   Musiol S.   Neukum G.
Educational Outreach Activities at the Planetary Sciences and Remote Sensing Group, Freie Universitaet Berlin **[#1952]**
The European mission "Mars Express" has been successfully operating since 2003. Images and terrain model data based on the High Resolution Stereo Camera experiment (HRSC) and processed at DLR and FUB are regularly presented to a broad audience.

THERMAL AND AQUEOUS PROCESSES ON CHONDRITE PARENT BODIES
Friday, 8:30 a.m.   Waterway Ballroom 1

Chairs: **Molly McCanta and Mark Tyra**

8:30 a.m. Davison T. M. * Collins G. S. Ciesla F. J. O'Brien D. P.
Heating Planetesimals by Impacts **[#1725]**
We estimate the cumulative heating caused by a population of projectiles impacting a planetesimal. Global heating before disruption is impossible, but a significant proportion of the fragments formed in a disruptive collision may be strongly heated.

8:45 a.m. Scott E. R. D. * Mandell D. Yang J. Goldstein J. I. Krot T. Taylor G. J.
Metamorphism and Impacts on the Parent Asteroid of H Chondrites **[#1529]**
Cooling rates of H3–6 chondrites inferred from the dimensions of cloudy taenite intergrowths are consistent with published metallographic cooling rates and suggest that H chondrites cooled in a concentrically layered body that was modified by impact.

9:00 a.m. Sprung P. * Göpel C. Kleine T. Van Orman J. A. Bourdon B.
A Hf-W Perspective on the Thermal Evolution of the L Chondrite Parent Body **[#1921]**
The synthesis of chronometers whose closure temperatures span a wide range enables the reconstruction of the thermal history of planetary bodies. We present ^{182}Hf-^{182}W and ^{207}Pb-^{206}Pb evidence for similarities between the thermal evolution of H6 and L6 chondrites.

9:15 a.m. Kebukawa Y. * Cody G. D. Alexander C. M. O'D.
Composition Diversity of Organic Matter in Type 1, 2 and 3 Chondrites by Infrared Spectroscopy **[#2047]**
An IR study of 22 chondritic organic solids (IOM) reveals a complex history related to parent body processing. IR spectra uniquely reveal two distinct classes of type 3 IOM that are not easily explained by mineralogical designations of class and group.

9:30 a.m. Orthous-Daunay F.-R. * Quirico E. Beck P. Brissaud O. Schmitt B.
Structural and Functional Micro-Infrared Survey of Pristine Carbonaceous Chondrites Insoluble Organic Matter **[#1803]**
We present a mid-infrared study of C2 and C1 chondrites IOM. All have similar aliphatic structure at 50°C under 10^{-7} mbar. Oxidized functions are depleted in less altered chondrites. 300°C heating in ambient air turns aliphatic chains to esters.

9:45 a.m. Bonal L. * Huss G. R. Nagashima K.
Hydrogen Isotopic Composition of the Water in CR Chondrites **[#1442]**
We report the hydrogen isotopic composition of the phyllosilicates in five CR chondrites and focus on the isotopic exchange between water and organic matter during asteroidal aqueous alteration.

10:00 a.m. Brearley A. J. * Martinez C.
Ubiquitous Exsolution of Pentlandite and Troilite in Pyrrhotite from the TIL 91722 CM2 Carbonaceous Chondrite: A Record of Low Temperature Solid State Processes **[#1689]**
SEM and TEM studies show that submicron exsolution of pentlandite and troilite occurred at very low temperatures in pyrrhotite in the TIL 91722 CM2 chondrite. The exsolution occurred below 373 K on the CM chondrite parent body.

10:15 a.m. Berger E. L. * Zega T. J. Lauretta D. S.
Microstructures of CI-Chondrite Pyrrhotite and Cubanite **[#1160]**
TEM analyses of CI-chondrite sulfides establish the presence of orthorhombic cubanite and 4C monoclinic pyrrhotite. These crystal structures constrain low-temperature formation conditions.

10:30 a.m. Tyra M. A. * Matzel J. Brearley A. J. Hutcheon I. D.
Variability in Carbonate Petrography and NanoSIMS $^{53}Mn/^{53}Cr$ Systematics in Paired CM1 Chondrites ALH 84051, ALH 84049, and ALH 84034 **[#2687]**
We present carbonate petrographical, chemical, and Mn/Cr radioisotope compositions of three paired CM1 chondrites (ALH 84051, ALH 84049, and ALH 84034). In spite of an abundance of chemical and presumably spatial variability, the carbonate ages seem well-constrained.

10:45 a.m. Fujiya W. * Sugiura N. Ichimura K. Takahata N. Sano Y.
Mn-Cr Ages of Carbonates in Murchison and ALH 83100 CM Chondrites **[#1644]**
We report Mn-Cr ages of carbonates in Murchison and ALH 83100 CM chondrites. Ages of carbonates in the two meteorites are similar, indicating relatively short duration of aqueous alteration in CM chondrites.

11:00 a.m. Jogo K. * Nakamura T. Ito M. Messenger S.
Mn-Cr Systematics of secondary Fayalites in the CV3 Carbonaceous Chondrites A 881317, MET 00430 and MET 01074 **[#1573]**
We report NanoSIMS ^{53}Mn-^{53}Cr isotopic measurements of fayalites in three CV3 chondrites. Obtained initial $^{53}Mn/^{55}Mn$ ratios are identical with those of other CV3 fayalites, indicating aqueous alteration have simultaneously occurred in CV3 asteroids.

11:15 a.m. Jones R. H. * Brearley A. J.
Late-Stage Fluids on the LL Chondrite Parent Body: Evidence from Feldspar in the LL4 Chondrites Bo Xian and Bjurböle **[#2133]**
Plagioclase in Bo Xian and Bjurböle shows ubiquitous evidence for alteration subsequent to grain growth, in the form of nephelinitization and dissolution reactions. Fluids were present in the late stages of metamorphism on the LL parent body.

11:30 a.m. McCanta M. C. * Treiman A. H.
Evaluation of Reported Graphite in the R Chondrites LAP 02238/03645: Resolution of a Redox Riddle **[#1394]**
The reporting of graphite in two R chondrites is evaluated due to potential redox issues, i.e., the presence of a reduced phase in an oxidized meteorite group. The phase identified as graphite is an alteration phase containing an oxide-sulfate mix.

MARS: DEPOSITION AND EROSION OF THE STRATIGRAPHIC RECORD
Friday, 8:30 a.m. Waterway Ballroom 4

Chairs: Jeffrey Andrews-Hanna and Martha Gilmore

8:30 a.m. Andrews-Hanna J. C. *
Hydrologic Evolution of Early Mars: Secular and Periodic Climate Forcing and Implications for the Sedimentary Record **[#2660]**
Hydrological models are used to investigate the evolution of the hydrologic-climatic system of early Mars, driven by secular loss of water and periodic perturbations from orbital forcing, and the resulting geomorphic and sedimentary record.

8:45 a.m. Lewis K. W. * Aharonson O. Grotzinger J. P. McEwen A. S. Kirk R. L.
Global Significance of Cyclic Sedimentary Deposits on Mars **[#2648]**
Quasiperiodic stratigraphy has now been identified in widespread sedimentary deposits across the surface of Mars. We will discuss the significance of this observation, along with possible depositional timescales and origins.

9:00 a.m. Harrison S. K. * Balme M. R. Hagermann A. Murray J. B. Muller J. - P.
Mapping Medusae Fossae Formation Materials in the Southern Highlands of Mars **[#1681]**
We provide evidence for a greater southern extent than previously mapped for the Medusae Fossae Formation of equatorial Mars.

9:15 a.m. Zabrusky K. J. * Andrews-Hanna J. C.
Reconstructing the Original Volume and Extent of the Sedimentary Deposits of Meridiani Planum and Arabia Terra **[#2529]**
We extend the current Meridiani Planum deposits by using morphological and geological evidence to find similar eroded remains throughout Arabia Terra. A smooth surface is then fitted to these remains in order to estimate the original deposit volume.

9:30 a.m. Grindrod P. M. * Balme M. R.
Groundwater Processes in Hebes Chasma, Mars **[#1311]**
We discuss the possible role of topography-driven groundwater upwelling in Hebes Chasma, and the effects of evaporation-driven crystallization on the nature of hydrated mineral formation.

9:45 a.m. Gilmore M. S. * Greenwood J. P. Bishop J. L.
Sulfates in Iani Chaos, Mars **[#2374]**
Monohydrated and polyhydrated sulfates are found in Iani Chaos and attributed to at least two episodes of deposition.

10:00 a.m. Fergason R. L. * Gaddis L. R.
Hematite-bearing Low Albedo Materials in Candor Chasma, Mars: Variations in Physical Properties and Implications **[#1474]**
We mapped low albedo materials within Candor Chasma to constrain the physical properties of these hematite-bearing units, identify decadal changes in their location, and develop hypotheses describing the post-emplacement history of these materials.

10:15 a.m. Massé M. * Bourgeois O. Le Mouélic S. Verpoorter C. Le Deit L.
Origin of Martian Circum-Polar Gypsum-bearing Deposits **[#1138]**
From an integrated morphological and spectroscopic compositional analyze, we demonstrate that polar and circum-polar deposits are sublimation tills derived from the North Polar Cap.

10:30 a.m. Baldridge A. M. * Hook S. J. Bridges N. T. Thomson B. J. Clarke J . D. A.
Phyllosilicate and Sulfate Layering in Interplaya Dunes; Analogs for Mars Intercrater Deposits **[#2268]**
Mineral maps of playas in WA indicate that layered phyllosilicates and sulfates concentrate in the central playa as aeolian features that may be analogous to the thick sequences of layered, crater-hosted martian sedimentary materials.

10:45 a.m. Carter J. A. * Poulet F. Bibring J.-P. Murchie S. Ansan V. Mangold N.
Mineralogy of Layered Deposits in Terby Crater, N. Hellas Planitia **[#1866]**
We report the co-detection of Fe/Mg-rich phyllosilicates and zeolites or poly-hydrated sulfates in layered mesas in Terby crater.

11:00 a.m. Rice M. S. * Bell J. F. III
Geologic Mapping of the Proposed Mars Science Laboratory (MSL) Landing Ellipse in Eberswalde Crater **[#2524]**
Eberswalde Crater has been selected as a high-priority candidate landing site for the Mars Science Laboratory. Here we characterize the geology of the proposed landing ellipse within the Eberswalde Basin.

11:15 a.m. Stillman D. E. * Grimm R. E.
Mechanisms for the Attenuation of SHARAD Energy **[#2143]**
The attenuation of SHARAD energy over the majority of the martian surface can be explained by absorption of energy via adsorbed water on high surface area minerals and/or scattering losses created by density contrast of 0.4–0.6 g/cc.

11:30 a.m. Heggy E. * Boisson J. Grima C. Clifford S. M. Gim Y. Frigeri A. Plaut J. J.
Exploring Bulk Compositions of Large Equatorial Basins Fills on Mars Using MARSIS and SHARAD Data **[#1289]**
We performed three-dimensional regional attenuation maps of the shallow subsurface of Amazonis and Isidis basins constraining their fill bulk composition and exploring the hypothesis on their origin and the validity of the paleo-ocean hypothesis.

MARTIAN IGNEOUS PROCESSES
Friday, 8:30 a.m. Waterway Ballroom 5

Chairs: Christopher Herd and Mariek Schmidt

8:30 a.m. Lapen T. J. * Brandon A. D. Righter M. Shafer J. Irving A. J.
A Hybridized Martian Mantle Source for Shergottites **[#2448]**
Here we show Lu-Hf and Sm-Nd isotopic evidence for a hybridized upper-mantle source of shergottites as well as ALH 84001.

8:45 a.m. Peslier A. H. * Hnatyshin D. Herd C. D. K. Walton E. L. Brandon A. D. Lapen T. J. Shafer J.
A More Reduced Mantle Source for Enriched Shergottites; Insights from Olivine-Phyric Shergottite LAR 06319 **[#1503]**
LAR 06319 detailed oxybarometry shows that a basaltic melt becomes more oxidized during differentiation. The first crystallized assemblages are used to redefine the oxygen fugacity of the enriched shergottite mantle source to the value of FMQ-2.

9:00 a.m. Hutchins K. I. * Agee C. B. Draper D. S.
High Pressure Experiments Yield Insight into an Early Magma Ocean on Mars **[#1525]**
Borg and Draper (2003) modeled crystallization of the martian mantle from an early, global magma ocean. We are in the process of experimentally testing this model and present our results thus far.

9:15 a.m. Schmidt M. E. * McCoy T. J.
Heterogeneities in the Martian Mantle Through Time: Clues from Meteorites and Gusev Basalts **[#1336]**
The composition of martian basalts reflect their mantle source at the time of extraction. Geochemical data combined with age information are used to interpret how the martian mantle has evolved with time.

9:30 a.m. Filiberto J. * Dasgupta R. Kiefer W. S. Treiman A. H.
High Pressure Phase Equilibrium Investigation of the Home Plate Pyroclastic Basalt Fastball and Application to Melting in the Martian Mantle **[#1238]**
We have investigated the phase equilibria of a Home Plate pyroclastic basalt and show that it is represents a primary mantle-derived magma, estimate the plausible mantle melt fraction, and constrain the potential temperature of the martian mantle.

9:45 a.m. Gross J. * Treiman A. H. Filiberto J. Robinson K. L.
Primitive Olivine-Phyric Shergottite NWA 5789: Petrography, Mineral Chemistry and Cooling History Imply a Magma Similar to Yamato 980459 **[#1813]**
Petrography, mineral chemistry and cooling history of NWA 5789 and comparison to Yamato 980459 imply that both meteorites are primitive and crystallized from the same type of magma. Primitive melts help elucidate the geology and geochemistry of Mars.

10:00 a.m. Shafer J. T. * Brandon A. D. Lapen T. J. Righter M. Peslier A. H.
Sm-Nd Age and REE Systematics of Larkman Nunatak 06319: Closed System Fractional Crystallization of a Shergottite Magma **[#1726]**
The Sm/Nd age of LAR 06319 is 180 ± 13 Ma. It is a member of the enriched shergottite group. REE contents of pyroxene are consistent with fractional crystallization of a single magma and not with assimilation of a crustal component into a depleted magma.

10:15 a.m. Riches A. J. V. * Liu Y. Day J. M. D. Puchtel I. S. Rumble D. III McSween H. Y. Jr Walker R. J. Taylor L. A.
Highly-Siderophile Element Abundances and Re-Os Isotopic Systematics of Lherzolitic Shergottite Yamato 984028 **[#2618]**
We report HSE abundances and Re-Os isotopic compositions of a newly recognized lherzolitic-shergottite, Yamato 984028, and explore the petrogenetic constraints determined by these elements.

10:30 a.m. Goodrich C. A. * Treiman A. H. Filiberto J. Jercinovic M. J.
The Nakhla Parent Magma: Old Problems, New Approaches **[#1387]**
We reevaluate evidence that melt trapped in early olivine in Nakhla had very high K and K/Na ratio.

10:45 a.m. Jambon A. Barrat J. A. Bollinger C. Sautter V. * Boudouma O. Greenwood R. C. Franchi I. A. Badia D.
Northwest Africa 5790. Top Sequence of the Nakhlite Pile **[#1696]**
NWA 5790 is a recently discovered nakhlite. Its mineralogy, petrology and geochemistry suggest that it is the topmost sequence of the nakhlite lava pile.

11:00 a.m. Williams C. D. * Wadhwa M. Bell D. R. Hervig R.
Light Lithophile Element Microdistributions in Pyroxenes of the Martian Meteorites **[#2641]**
We report here Li, B and Be distributions in pyroxenes of three shergottites (Shergotty and Zagami, and SaU 005) and the nakhlite Yamato 000593 to assess the role of magmatic degassing, igneous fractionation and subsolidus diffusion processes in their petrogenesis.

11:15 a.m. Channon M. B. * Stolper E. M. Eiler J. M.
Oxygen Isotope Compositions of Mineral Separates from SNC Meteorites: Constraints on SNC Parental Magmas **[#2212]**
We present measurements of $\delta^{18}O$ and $\Delta^{17}O$ in mineral separates from SNC meteorites; these data define oxygen isotope compositions of their parent magmas and constrain abundances of aqueously altered crustal materials in their sources.

11:30 a.m. Herd C. D. K. * Stern R. A. Walton E. L. Li J. Bibby C.
TEM and SEM-CL Analysis of Baddeleyite in NWA 3171: Geochronological Implications for Martian Meteorites **[#2280]**
Using a FIB plan-view liftout method for TEM sample preparation, and TEM and SEM-CL analysis of baddeleyite in the NWA 3171 shergottite, we provide insights into baddeleyite petrogenesis and implications for U-Pb geochronology of martian meteorites.

INTERIOR OF THE MOON
Friday, 8:30 a.m. Waterway Ballroom 6

Chairs: **Lon Hood and Mark Wieczorek**

8:30 a.m. Hood L. L. *
Central Magnetic Anomalies of Nectarian-aged Lunar Impact Basins: Possible Evidence for an Early Core Dynamo **[#1954]**
More detailed regional maps of central magnetic anomalies in a series of Nectarian-aged lunar basins are presented. The anomalies have characteristics consistent with thermoremanent magnetization of impact melt in a large-scale, steady magnetizing field.

8:45 a.m. Shea E. K. * Weiss B. P. Tikoo S. M. Grove T. L. Fuller M.
Evidence for a Lunar Core Dynamo at 3.7 Ga from Mare Basalt 10020? **[#2204]**
We present a new paleomagnetic study of an extremely high coercivity, unshocked lunar rock, mare basalt 10020. Our initial results suggest it has a stable NRM likely acquired over timescales that are long relative to impact-produced fields.

9:00 a.m. Tikoo S. M. * Weiss B. P. Buz J. Garrick-Bethell I. Grove T. L. Gattaccaea J.
Ancient Lunar Dynamo: Absence of Evidence is Not the Evidence of Absence **[#2705]**
The lack of evidence of for a lunar dynamo in many Apollo samples is not evidence for the absence of a dynamo.

9:15 a.m. Wieczorek M. A. * Weiss B. P.
Testing the Lunar Dynamo Hypothesis Using Global Magnetic Field Data **[#1625]**
We show that the lunar magnetic anomalies observed from orbit are consistent with the magnetization of mare basalts and metal-rich impact melts in the presence of a strong ancient lunar dynamo.

9:30 a.m. Purucker M. E. * Nicholas J. B.
A New Map of the Internal Magnetic Field of the Moon and Its Implications **[#2291]**
An improved model of the internal magnetic field of the Moon is developed. The power spectra of the new model contains a heretofore unseen change in slope which may be a manifestation of an early lunar dynamo.

9:45 a.m. Steinberger B. * Werner S. C. Kohout T.
Deep vs. Shallow Origin of Gravity Anomalies and Topography on the Moon **[#1694]**
If density anomalies in both viscous mantle and elastic lithosphere can be modelled as “white noise,” we can compute the “expected” lunar geoid spectrum and explain degrees 2–5 including the flattening term, as mainly due to mantle density anomalies.

10:00 a.m. Watters T. R. * Robinson M. S. Beyer R. A. Bell J. F. Pritchard M. E. Banks M. E. Turtle E. P. Williams N. R. LROC Team
Lunar Thrust Faults: Implications for the Thermal History of the Moon **[#1863]**
Images from the Lunar Reconnaissance Orbiter Camera (LROC) have revealed previously undetected, small-scale thrust fault scarps. The spatial distribution of the newly viewed and previously known scarps suggests they are globally distributed.

10:15 a.m. Nagihara S. * Saito Y. Taylor P. T.
Reexamination of the Apollo 15 Heat Flow Data Toward Understanding Potential Causes of the Long-Term Subsurface Warming Observed **[#1353]**
The lunar surface and subsurface temperature records from the Apollo 15 site have been reexamined for further understanding potential causes of the subsurface warming observed.

10:30 a.m. Siegler M. A. * Paige D. A. Keihm S. J. Vasavada A. R. Ghent R. R. Bandfield J. L. Snook K. J.
Apollo Lunar Heat Flow Experiments and the LRO Diviner Radiometer **[#2650]**
We examine the Apollo 15 heat flow experiment in light of new measurements from the LRO Diviner Lunar Radiometer, a detailed model of the probe, and a ray tracing thermal model to examine the effects of orbit and topography on the heat flow probe.

10:45 a.m. Weber R. C. * Lin P. Garnero E.
A Seismic Search for the Lunar Core **[#1977]**
We reassess the Apollo deep moonquake seismograms to search for putative seismic phase arrivals from the lunar core. This work should allow us to constrain the core radius and the seismic velocity contrast of the core-mantle boundary.

11:00 a.m. Kawamura T. * Kobayashi N. Tanaka S. Lognonné P. Gagnepain -Beyneix J.
Search for Farside Deep Moonquakes: Source Determination of Unlocated Deep Moonquakes with Apollo 17 Lunar Surface Gravimeter **[#1766]**
We located deep moonquakes that were not unlocatable from the previous lunar seismic data set by using the Apollo 17 Lunar Surface Gravimeter as an additional seismometer.

11:15 a.m. Ong L. * Melosh H. J.
Reorientation of the Moon Due to South Pole-Aitken Basin Ejecta **[#1363]**
As a result of the massive global ejecta blanket produced by the South Pole-Aitken basin, the Moon experiences a major reorientation that places the impact basin near the South Pole where we observe it today.

11:30 a.m. Bills B. G. * Moore W. B. Siegler M. A. Paige D. A.
Lunar Obliquity During a Cassini-State Transition **[#1752]**
The obliquity values attained by the Moon, during a Cassini-state transition, depend sensitively upon the poorly known values of the degree two gravity field at that time. This transition is a key event in the retention of polar volatiles.

FORMATION OF THE BUILDING BLOCKS OF PLANETARY BODIES
Friday, 1:30 p.m. Waterway Ballroom 1

Chairs: Scott Whattam and Alex Ruzicka

1:30 p.m. Whattam S. A. * Hewins R. H. Devouard B.
Refractory Inclusions as Precursors of Chondrules: Initial Results from Melting Experiments **[#2032]**
One hour of isothermal heating of synthetic CAI and olivine preserves distinct CAI and olivine domains at 1250°–1550°C; complete CAI melting and PO texture development occurs by 1600°C. Type I chondrules could be made from condensate olivine + CAI, or AOA.

1:45 p.m. Alexander C. M. O'D. *
Constraining Chondrule Thermal Histories Using the Kinetics of Olivine Dissolution and Crystallization **[#2181]**
The preliminary results of a model of diffusive dissolution/crystallization are presented. Only dissolution of olivine is considered, first in experiments with basalt and then in chondrule melts.

2:00 p.m. Richter F. M. * Mendybaev R. A. Christensen J. Ebel D.
Laboratory Experiments Bearing on the Evolution of Type IA and IIA Chondrules **[#2562]**
Evaporation experiments using chondrule-like liquids as starting compositions are used to place constraints on the processes and conditions for the origin and evolution of Type IA and Type IIA chondrules.

2:15 p.m. Srivastava A. * Inatomi Y. Tsukamoto K. Miura H.
In-situ Visualization of Experimentally Reproduced Chondrule Textures from Crystallizing Silicate Melts **[#1045]**
We present *in situ* visualization of crystallization process of supercooled silicate melts. Schlieren and shadowgraph techniques are employed to visualize the crystallization process. The primary objective is to image convection and prediction of chondrule textures in real time.

2:30 p.m. Wick M. J. * Jones R. H.
Experimental Study of Type I Chondrule Formation in CO3 Chondrites: What Conditions are Necessary for Plagioclase Crystallization? **[#1925]**
Chondrule analog experiments were conducted to reproduce plagioclase-bearing type I chondrules observed in CO3 chondrites. Textures/compositions are very similar to natural chondrules; however, plagioclase was not produced in these experiments.

2:45 p.m. Schrader D. L. * Connolly H. C. Jr. Lauretta D. S.
On the Nebular and Aqueous Signatures in the CR Chondrites **[#1262]**
We report a synthesis of our ongoing investigation into the nebular and aqueous signatures of the CR chondrites, designed to address their pre- and post-accretion history as constrained by their opaque phases.

3:00 p.m. Ruzicka A. * Floss C. Hutson M.
Accretion and Melting of Dust to Form Ferroan Chondrules in Ordinary Chondrites **[#1956]**
Chemical and petrographic data suggest that fine-grained agglomeratic olivine inclusions (AOIs) include both unmelted and melted types and likely were precursors to some ferroan (Type II) chondrules in ordinary chondrites.

3:15 p.m. Hewins R. H. * Zanda B. Bendersky C.
Sodium in Semarkona Type II Chondrules **[#1703]**
Na in chondrules increases more from bulk to mesostasis more than can be due to fractionation. Equilibrium Na partitioning exists between olivine rims and interstitial glass. Type II chondrules were open to evaporation and recondensation of Na.

3:30 p.m. Fedkin A. V. * Grossman L.
Condensation of the High-FeO Silicates in Primitive Chondrites: Still a Problem **[#1448]**
Olivine with significant XFa cannot form in water-rich solar gas, even using new, higher Fe-Mg diffusion coefficients. It could form if supersaturation of Fe metal occurred, but this is unlikely due to homogeneous condensation of more refractory phases.

3:45 p.m. Nakashima D. * Ushikubo T. Kita N. T. Nagao K.
Mineralogy, Chemistry, and Oxygen Isotopic Compositions of Chondrules from the SaU 290 CH3 Chondrite **[#2259]**
Mineralogy, chemistry, and oxygen isotope ratios of chondrules from SaU 290 (CH3) were investigated. O isotopic heterogeneity among the chondrules may reflect O isotopic variation of the nebular gaseous reservoir temporally or spatially.

4:00 p.m. Lehner S. W. * Buseck P. R.
Silica-rich Chondrules in ALH 84170 and Sahara 97072 EH3 Meteorites: Evidence for Sulfidation of Silicates **[#1855]**
Silica-rich chondrules in EH3 meteorites contain tridymite, niningerite, and troilite associated with enstatite and olivine and no Fe-Ni metal. We interpret these assemblages as evidence for the formation of niningerite by sulfidation of silicates.

4:15 p.m. Weisberg M. K. * Ebel D. S. Kimura M. Kita N. T. Nakashima D.
Petrology and Oxygen Isotopes of Chondrules in the Kota Kota EH3 Chondrite **[#1756]**
Oxygen isotopes of most Kota Kota chondrules plot along the TF line and some overlap the OC field on a 3-isotope plot. ^{16}O-rich values in EH3s form a new mixing line. EH3 chondrules formed from a distinct oxygen reservoir and show mixing behavior.

4:30 p.m. Ushikubo T. * Kimura M. Nakashima D. Kita N. T.
A Combined Study of the Al-Mg Systematics and O Isotope Ratios of Chondrules from the Primitive Carbonaceous Chondrite Acfer 094 **[#1491]**
We measured the Al-Mg systematics of type I chondrules from Acfer 094. Inferred initial $^{26}Al/^{27}Al$ ratios are about 5e-6 and no correlation between initial $^{26}Al/^{27}Al$ ratios and O isotope ratios are observed.

4:45 p.m. Humayun M. * Connolly H. C. Jr. Rubin A. E. Wasson J. T.
Elemental Distribution in Metal from the CR Chondrites Acfer 059 and PCA 91082 **[#1840]**
There has been intense debate on the origin of metal rimming chondrules in CR chondrites. We present new siderophile element data that significantly redefines the direction of future discourse on the subject.

MARS: TIMING OF RECENT AND OLDER GEOLOGIC PROCESSES
Friday, 1:30 p.m. Waterway Ballroom 4

Chairs: **Serina Diniega and Ralph Harvey**

1:30 p.m. Morgan G. A. * Head J. W. III Marchant D. Dickson J. Levy J.
Sources of Water for Gulley Formation in the Antarctic Dry Valleys: Multi-Year Analysis of Precipitation and Temperature in the South Fork of Upper Wright Valley and Implications for the Origin of Gullies on Mars **[#1043]**
We study Mars gully analogs in the Antarctic Dry Valleys and report on the differences in precipitation, temperature profiles, meltwater sources, and level of fluvial activity in the gullies over a four-year period, and discuss application to Mars.

1:45 p.m. Dickson J. L. * Head J. W. Fassett C. I. Levy J. S. Morgan G. A.
The Life Cycle of Young Gullies on Mars: Gullies as a Transient Product of Ice-rich Mantle Emplacement and Removal **[#1002]**
We propose a model for gully evolution on Mars: (1) deposition of ice-rich mantle; (2) erosion of that mantle by surface melting; (3) removal of the mantle, erasing the record of gully activity. This accounts for the lack of older gullies on Mars.

2:00 p.m. Diniega S. * Byrne S. Bridges N. T. Dundas C. M. McEwen A. S.
Present-Day Martian Dune Gully Activity **[#2216]**
We identified gullies within 18 dune fields in the southern hemisphere, and gully activity within seven fields. We constrain the timing of activity to late southern winter, which is most consistent with seasonal frost-driven gully evolution theories.

2:15 p.m. Dundas C. M. * McEwen A. S. Diniega S. Byrne S.
New and Recent Gully Activity on Mars as Seen by HiRISE **[#2114]**
HiRISE observes recent deposits associated with many martian gullies. We discuss the properties of these deposits, the timing of their formation (when known), and the implications for gully formation and evolution.

2:30 p.m. King C. M. * Schorghofer N. Wagstaff K. L.
Martian Slope Streaks Form Sporadically Throughout the Year **[#1542]**
Time constraints for the formation of dark slope streaks on Mars are derived from multi-overlap orbital images. We find that slope streaks form sporadically throughout the year, which has implications for possible triggering mechanisms.

2:45 p.m. Wagstaff K. L. * Panetta J. Ansar A. Bunte M. Greeley R. Pendleton Hoffer M. Schörghofer N.
Change Detection in Mars Orbital Images Using Dynamic Landmarking **[#2555]**
We developed a content-based analysis of Mars orbital images to automatically identify landmarks (impact craters, dust devil tracks, slope streaks, etc.) and then detect changes in the landmarks. This method detects both new and vanished features.

3:00 p.m. Ivanov B. A. Melosh H. J. * McEwen A. S. HiRISE Team
New Small Impact Craters in High Resolution HiRISE Images - III **[#2020]**
The database for ~70 “new” dated craters has been processed. Percentage of single/multiple cratering, dark halo width, and air shock wave traces at the surface are discussed.

3:15 p.m. Daubar I. J. * McEwen A. S. Byrne S. Dundas C. M. Kennedy M. Ivanov B. A.
The Current Martian Cratering Rate **[#1978]**
MRO has now confirmed 100 new primary martian impact sites. We describe the detection rate, estimate global impact rates, analyze seasonal trends, and compare the size-frequency distribution to model isochrons.

3:30 p.m. Kress A. * Head J. W. Fassett C. I.
Ridges in the Dorsa Argentea Formation: Geomorphology and Age Assessment from Buffered Crater Counting **[#2355]**
The Dorsa Argentea ridges have been interpreted as eskers, and we analyze these ridges using buffered crater counting to better estimate when such potential eskers may have formed and what implications their age has for the history of ice on Mars.

3:45 p.m. Erkeling G. * Hiesinger H. Reiss D. Hielscher F. J. Ivanov M. A.
Stratigraphy of the Amenthes Region, Mars: Time Limits for the Formation of Volcanic and Water-related Deposits **[#2014]**
The area of Amenthes (95°/115°E and 15°N/5°S) has been affected by a large variety of geologic processes. We present the first results of our morphologic and stratigraphic investigations in the northwestern part of Amenthes.

4:00 p.m. Harvey R. P. * Griswold J.
Burial, Exhumation, Metamorphism and Other Dastardly Deeds Exposed at the Hesperian/Noachian Boundary in the Southern Nili Fossae Region **[#2045]**
The physical geology of southeast Nili Fossae suggests that Syrtis Major lavas once buried a significant portion of the region and were later removed, with nasty implications for local metamorphic history and mineralogy (some already confirmed).

4:15 p.m. Platz T. * Michael G. G. Neukum G.
Confident Thickness Estimates for Planetary Surface Deposits from Concealed Crater Populations **[#2348]**
An improved technique is presented to determine more accurately surface deposit thicknesses utilising crater size-frequency distributions. This technique enables thickness estimates of deposits that fully cover their underlying unit.

4:30 p.m. Stepinski T. F. *
Geographical Distribution of Crater Depths on Mars **[#1845]**
Global maps of crater depths on Mars are constructed using a new dataset that lists depths of >75,000 craters. Distribution of crater depths is interpreted in terms of cryosphere extent, and the locations of deepest craters on Mars are identified.

SMALL BODY ORIGIN, EVOLUTION, AND COMPOSITION
Friday, 1:30 p.m. Waterway Ballroom 5

Chairs: **Paul Warren and Daniel Durda**

1:30 p.m. Cuzzi J. N. * Hogan R. C. Bottke W. F.
Towards Initial Mass Functions for Asteroids and Kuiper Belt Objects **[#1861]**
We present a scenario for primary accretion in turbulence of 20–200 km diameter inner and outer solar system primitive bodies directly from freely-floating, but size-sorted, nebula particles, which also helps explain the nearly Myr variance in formation age of chondrules in a given chondrite.

1:45 p.m. Dwyer C. A. * Nimmo F. Asphaug E. O'Brien D. P.
Erosion During Accretion: Consequences for Planetary Iron-Silicate Ratios and Tungsten Isotope Anomalies **[#2271]**
We model the chemical effects of impact erosion using an N-body model of late-stage accretion. Planetary Fe:Si ratios are generally increased and mantle tungsten isotope anomalies are also affected.

2:00 p.m. Bottke W. F. * Vokrouhlicky D. Nesvorny D. Minton D. Morbidelli A. Brasser R.
The E-Belt: A Possible Missing Link in the Late Heavy Bombardment **[#1269]**
We propose that the primordial asteroid belt once had an stable extension thatstretched to Mars. If true, its elimination 3.9 billion years ago during giant planet migration may have produced much of the late heavy bombardment.

2:15 p.m. Warren P. H. *
The Inevitability of a Thick, Strongly Insulating Megaregolith on Bodies of Order 100-km to Moon-like in Size **[#2465]**
By modeling ejecta accumulation starting from assumed (a) largest cratering event and (b) power-law size distribution, I show that development of a km(+) thick insulating megaregolith is inevitable even for planetesimals as small as 100 km in diameter.

2:30 p.m. Sanchez P. * Scheeres D. J. Swift M. R.
Impact Driven Size Sorting in Self-gravitating Granular Aggregates **[#2634]**
Impact driven size segregation is simulated to understand size sorting on asteroids; our studies indicate a more complex mechanism than the previously suggested Brazil Nut Effect.

2:45 p.m. Britt D. T. Macke R. J. Kiefer W. Consolmagno G. J.
An Overview of Achondrite Density, Porosity and Magnetic Susceptibility **[#1869]**
Achondrites represent a huge range of parent bodies, mineralogies, formation conditions, and physical evolution. This work compares new measurements of the density, porosity, and magnetic susceptibility of achondrite meteorites and lunar samples.

3:00 p.m. Strait M. M. * Consolmagno G. J. SJ
Visualizing Porosity in Meteorites **[#2258]**
A look at the appearance of porosity in meteorites. It is found that the measurement of porosity must include a visual aspect to fully understand the process.

3:15 p.m. Dunn T. L. * McCoy T. J. Sunshine J. M. McSween H. Y. Jr.
A Coordinated Mineralogical, Spectral, and Compositional Study of Ordinary Chondrites: Implications for Asteroid Spectroscopic Classification **[#1750]**
Here we examine a large suite of ordinary chondrites, in which spectral and mineralogical data have been measured, to establish relationships between spectral parameters (BAR, Band centers) and mineralogical parameters (abundances and composition).

3:30 p.m. Castillo-Rogez J. C. * Schmidt B. E.
Geophysical Evolution of the Themis Family Parent Body **[#2632]**
We model the geophysical evolution of the Themis family parent body. This study is motivated by the recent detection of water ice at the surface of 24 Themis, the first detection of free water on the surface of an asteroid.

3:45 p.m. Schmidt B. E. * Castillo-Rogez J. C.
Evolution of Large, Water-rich Planetesimals: Implications for the Variety of C-type Asteroids **[#2378]**
We model the evolution of large water-rich asteroids, including Pallas, the Themis family parent body and other C-type bodies. We evaluate the role of composition and time of formation and illuminate possible genetic relationships between C-types.

4:00 p.m. Fieber-Beyer S. K. * Gaffey M. J. Kelley M. S. Reddy V. Reynolds C. M. Hicks T.
Near-Infrared Spectroscopy of 3:1 Kirkwood Gap Asteroids 695 Bella, 714 Ulula, and 3066 McFadden **[#1500]**
This research explores possible links between three asteroids located near the 3:1 resonance (695 Bella, 714 Ulula, and 3066 McFadden) and potential meteorite analogs in the terrestrial collections.

4:15 p.m. Durda D. D. * Enke B. L. Merline W. J. Richardson D. C. Asphaug E. Bottke W. F. Jr.
Comparing the Properties of Observed Main-Belt Asteroid Binaries and Modeled Escaping Ejecta Binaries (EEBs) from Numerical Simulations **[#2558]**
Parameters of modeled asteroid satellite systems are compared with observed properties of main-belt asteroid pairs to provide clues to better understand the origin and evolution of these systems.

4:30 p.m. Grav T. * Bauer J. M. Mainzer A. K. Cutri R. Masiero J. McMillan R. Walker R. Wright E. L. WISE Team
Preliminary Results of Jupiter Trojans Observed with WISE **[#2587]**
We will present the preliminary results of detections of Jupiter Trojans from the first two months of WISE scan operations and discuss such topics as size distribution, relative abundances and comparison with other solar system populations.

4:45 p.m. Moldovan R. * Matthews J. M. Gladman B. Bottke W. F. Vokrouhlicky D.
Searching for Trojan Asteroids in the HD 209458 System: Spacebased MOST Photometry and Dynamical Modeling **[#1168]**
We have searched MOST satellite photometry of the star HD 209458 for Trojan asteroid swarms dynamically coupled with the system's transiting planet HD 209458b. Our results set an upper limit on the optical depth and mass of Trojans in this system.

PETROLOGIC CHARACTERIZATION OF THE MOON
Friday, 1:30 p.m. Waterway Ballroom 6

Chairs: Juliane Gross and Mirjam van Kan Parker

1:30 p.m. Barr J. A. * Grove T. L.
Primordial Lunar Mantle Melts and Assimilated Magma Ocean Cumulates: Implications for the Depth of the Lunar Magma Ocean Based on Ultramafic Glass Compositions **[#2427]**
We have developed a model to predict the chemistry of primordial lunar mantle melts. These model melts can be used in mixing calculations to help constrain the depth of magma ocean cumulates, and by association the depth of the lunar magma ocean.

1:45 p.m. Elardo S. M. * Draper D. S. Shearer C. K.
Magma Ocean Composition and the Lunar Mantle: Implications for the Source Lithologies of the Highlands Magnesian Suite **[#1450]**
Experiments have been conducted on two bulk Moon compositions to assess whether the earliest cumulates from the lunar magma ocean could have served as the source lithologies for the Mg-rich, Ni, Co and Cr- poor mafic silicates of the Mg-suite.

2:00 p.m. Sakai R. * Kushiro I. Nagahara H. Ozawa K. Tachibana S.
Chemical Composition of Lunar Magma Ocean Constrained by High Pressure Experiments **[#2066]**
We report our attempts to constrain bulk chemical compositions of lunar magma ocean based on experimental constraints from physical properties of magma that can float anorthite to form the lunar anorthosite crust.

2:15 p.m. van Kan Parker M. * Mason P. Liebscher A. Frei D. van Sijl J. Blundy J. Franz G. van Westrenen W.
Trace Element Evolution During Lunar Magma Ocean Crystallisation **[#1588]**
We present new experimental results on orthopyroxene-melt and ilmenite-melt partitioning that can be used for predictive modelling of lunar magma ocean crystallisation of major and trace elements.

2:30 p.m. Sunshine J. M. * Besse S. Petro N. E. Pieters C. M. Head J. W. Taylor L. A. Klima R. L. Isaacson P. J. Boardman J. W. Clark R. C. M3 Team
Hidden in Plain Sight: Spinel-rich Deposits on the Nearside of the Moon as Revealed by Moon Mineralogy Mapper (M^3) **[#1508]**
The Moon Mineralogy Mapper has revealed a new, unique, and unexpected spinel-rich lithology on the central nearside. These spinel-rich deposits are found only among the Sinus Aestuum pyroclastic deposits and are notably absent from nearby Rima Bode.

2:45 p.m. Pieters C. M. * Boardman J. Buratti B. Clark R. Combe J. P. Green R. Goswami J. N. Head J. W. Hicks M. Isaacson P. Klima R. Kramer G. Kumar K. Lundeen S. Malaret E. McCord T. B. Mustard J. Nettles J. Petro N. Runyon C. Staid M. Sunshine J. Taylor L. A. Thaisen K. Tompkins S. Varanasi P.
Identification of a New Spinel-rich Lunar Rock Type by the Moon Mineralogy Mapper (M^3) **[#1854]**
Diffuse and widely separated regions along the highly feldspathic inner ring of Moscoviense Basin exhibit unusual mineral components. One composition is a new rock type dominated by Mg-spinel with no detectible mafic silicates (<5%).

3:00 p.m. Neal C. R. * Fagan A. L. Oshrin J. C.
Differentiating Between Pristine Mare Basalts and Impact Melts Using Quantitative Petrography **[#1647]**
Lunar impact melts and pristine mare basalts have similar textures. We present a quantitative study of lunar melt rock textures via crystal size distributions to demonstrate distinguish impact melts from pristine mare basalts.

3:15 p.m. Taylor G. J. * Martel L. M. Spudis P. D.
Apollo 15 KREEP Basalts and Emplacement of the Apennine Bench Formation **[#1510]**
The Apennine Bench Formation, represented by Apollo 15 KREEP basalts, is composed of a range of compositionally similar but not identical pahoehoe lava flows.

3:30 p.m. O'Sullivan K. M. * Neal C. R.
Exploring the Petrogenesis of Apollo 12 Ilmenite Suite Basalts **[#2322]**
We report crystal size distributions along with major and trace element abundances of pyroxene and ilmenite to determine the petrogenesis of these samples.

3:45 p.m. Gross J. * Treiman A. H.
New Insights into the Complex History of Lunar Highlands: ALHA 81005 Under Reinvestigation **[#2180]**
Lunar meteorites represent the Moon's crust better than returned mission samples. This reinvestigation of ALH A81005 improves our understanding of unsampled areas and enlarges our knowledge of lunar highland rock types and the Moon's early history.

4:00 p.m. Ohtake M. * Matsunaga T. Takeda H. Yokota Y. Yamamoto S. Morota T. Ogawa Y. Hiroi T. Nakamura R. Haruyama J.
Distribution of Purest Anorthosite on the Entire Lunar Surface **[#1628]**
We surveyed the distribution of the purest anorthosite over the entire lunar surface by using reflectance spectra derived by the SELENE Spectral Profiler. Results indicate a homogeneous distribution of the purest anorthosite.

4:15 p.m. Korotev R. L. * Jolliff B. L. Zeigler R. A.
On the Origin of the Moon's Feldspathic Highlands, Pure Anorthosite, and the Feldspathic Lunar Meteorites **[#1440]**
If anorthosite consisting of nearly 100% plagioclase occurs globally at depth in the lunar crust, why is it rare in the ~37 feldspathic lunar meteorites?

4:30 p.m. Nyquist L. E. * Shih C.-Y. Reese Y. D. Park J. Bogard D. D. Garrison D. H. Yamaguchi A.
Lunar Crustal History Recorded in Lunar Anorthosites **[#1383]**
Variations in ages and initial 143Nd/144Nd of lunar anorthosites show they do not all derive from the LMO. "Old" Ar-Ar ages for anorthosites in lunar meteorites suggest the "lunar cataclysm" may be a localized phenomenon.

PRINT-ONLY PRESENTATIONS

SOLAR AND PRESOLAR DUST

Fisenko A. V.   Verchovsky A. B.   Semjonova L. F.   Wright I. P.
Bimodal Thermal Release of Noble Gases from Meteoritic Nanodiamonds: Are P3 Noble Gases Likely Evolves at Higher Temperatures? **[#2008]**
HL in the nanodiamonds not formed at implantation of P3 and a highly anomalous supernova ejects. It has been formed at the mixing of the supernova and isotopically normal components before implantation and this has been implanted independently of P3.

Rietmeijer F. J. M.
Fe-Ni-S Compositions After Background Correction: An Ongoing Study of the Properties of Wild 2 Smallest Sulfide Grains in Quenched Superheated Aerogel **[#1239]**
Background-corrected FeNiS grains dispersed in silica glass are low-S low-Ni FeNiS, Ni-free FeS ($40<S<60$), and rare FeS_2 and FeS_4 compounds. They are the quenched melt droplets and vapor condensates of instantaneously disintegrated Wild 2 sulfides.

Semjonova L. F.   Fisenko A. V.
Once Again About ^{129}Xe in Meteoritic Nanodiamonds* **[#1307]**
Based on relations of ^{129}Xe* and ^{132}Xe-P3 contents in nanodiamonds has shown that the model of surface-connected ^{129}I in diamond grains is more preferable than model of simultaneously capture of iodine and P3 gases as a result of the implantation.

Ustinova G. K.
On Possible Solar Origin of Meteoritic Nanodiamonds **[#1050]**
It is shown that the nanodiamond population with anomalous Xe-HL, which is observed in meteorites, was generated at the front of the explosive shock wave from SnIa in the process of formation of the solar system, and, therefore, that is not presolar.

COSMOCHEMICAL ORIGINS

Bagulya A. V.   Vladimirov M. S.   Goncharova L. A.   Ivliev A. I.   Kalinina G. V.   Kashkarov L. L.
Konovalova N. S.   Okat'eva N. M.   Polukhina N. G.   Roussetski A. S.   Starkov N. I.
Abundance of the Super-Heavy ($Z>55$) Galactic Cosmic Ray Nuclei by the Meteorite Track Data: Comparison with the Satellite Apparatus Measuring and the Sun and Solar System Values **[#1597]**
Track parameters in olivine crystals from pallasite Marjalahti were recorded. Some results of comparison of obtained nucleus abundance distribution data with the results of satellite apparatus measuring and Sun and solar system values are presented.

Jabeen I.   Kusakabe M.   Nakamura T.   Nagao K.
Oxygen Isotope Study to Explore the Extent of Aqueous Alteration in Chondrules from Allende CV3 Chondrite **[#1958]**
Oxygen isotopes are studied in different types of chondrules from Allende CV3 chondrite. The trend of oxygen isotopes in these chondrules is compared with that of anhydrous and hydrous phases to look into degree of aqueous alteration in them.

Shornikov S. I.   Yakovlev O. I.
A Study of CAI Melt Composition Changing During Evaporation **[#1408]**
We study the composition changes in CAI and lunar basalt melts at evaporation. The developed approach was based on own experimental thermodynamic data. Redox conditions influence on evaporation rate and residual melt composition is shown.

DIFFERENTIATED BODIES

Geissman J.   Shearer C. K.
Magnetic Properties of Primitive Achondritic Meteorites GRA 06128 and GRA 06129 **[#2186]**
The intent of this abstract is to examine the magnetic properties of GRA 06128 to gain insights into its evolving mineral assemblage and the environment under which GRA obtained its magnetism.

Lorenz C. A.   Ivanova M. A.   Teplyakova S. N.   Kononkova N. A.   Roshina I. A.
Sadilenko D. A.   Abdrakhimov A. M.
Composition and Genesis of Pyroxenite Xenolith from the Toufassour Mesosiderite **[#1197]**
A large pyroxenite xenolith was found among the fragments of Toufassour mesosiderite. This pyroxenite was formed during the fractional crystallization of high-magnesium source after the cumulative sedimentation of olivine.

Moggi-Cecchi V.   Pratesi G.   Franchi I. A.   Greenwood R. C.
NWA 4415 and 4416: Two New Enstatite Chondrites from Northwest Africa **[#2621]**
Two new enstatite chondrites, NWA 4415 and 4416, have been recovered in Northwest Africa. Recovery, textural and compositional data suggest a classification as enstatite chondrites (EL6) and a possible pairing.

Pratesi G.   Moggi-Cecchi V.   Franchi I. A.   Greenwood R. C.
NWA 4537: A New Aubrite from Northwest Africa **[#2720]**
A new aubrite has been discovered in Northwest Africa. Textural, compositional and isotopic data are provided.

Shukolyukov A.   Lugmair G.   Day J. M. D.   Walker R. J.   Rumble D. III   Nakashima D.   Nagao K.   Irving A. J.
Constraints on the Formation Age, Highly Siderophile Element Budget and Noble Gas Isotope Compositions of Northwest Africa 5400: An Ultramafic Achondrite with Terrestrial Isotopic Characteristics **[#1492]**
Mn-Cr isotope systematics, abundances and isotopic composition of highly siderophile elements, and noble gas and oxygen isotope compositions suggest that NWA 5400 is a moderately ancient ultramafic achondrite with terrestrial oxygen and ^{54}Cr isotopic compositions.

Teplyakova S. N.   Kostitsyn Y. A.   Kononkova N. N.
Differentiate Precursor for Silicate Inclusions In the Elga Iron Meteorite **[#1686]**
We studied 17 silicate inclusions in IIE Elga irons by electron microprobe and LA-ICP-MS. The bulk compositions of the Elga SIs are enriched in Si, K, Na, and Rb, Nb and could be formed during intensive differentiation process.

SMALL BODIES

Alexeev V. A.
Some Peculiarities of Isotopic Ratios of Noble Gases in Fossil Meteorites of Sweden **[#1039]**
The found features in distributions of noble gas contents and of exposure ages in the fossil meteorites of Sweden imply the falling single meteorite shower instead of the intensive flux of meteorites to Earth during ~1–2 Ma about 470 Ma ago.

Ammannito E.   De Sanctis M. C.   Coradini A.
Spectral Images of HEDS: A Statistical Approach to Select Spectral Types **[#1495]**
The purpose of this work is to perform a spectral characterization of HEDs using the same spectral resolution of the spectrometer of the Dawn mission. It will be used together with the data from Dawn to study the relation between Vesta and HEDs.

Díaz M. J.   Madiedo J. M.   Trígo-Rodríguez J. M.   Moreno-Vargas J.   López L.   Escalona F.   Gómez C.
Analysis of a Potential Meteorite-dropping Event over Spain in 2009 **[#1501]**
We present here the first results of the analysis of a potential meteorite-dropping event recorded by the Spanish Meteor Network (SPMN) that took place over southwest Spain on May 12, 2009.

Ghosh A.
A Thermal Evolution Model of a Magma Ocean on Asteroid 4 Vesta **[#2570]**
We present a thermal evolution model of a magma ocean on 4 Vesta.

Gorin V. D.   Alexeev V. A.   Ivliev A. I.   Kalinina G. K.   Kashkarov L. L.   Kuyunko N. S.   Sadilenko D. A.
Some Results of the Cosmic-Ray Influence in Ash Creek L6 Chondrite **[#1040]**
The Ash Creek L6 chondrite: Cosmogenic radionuclides, thermoluminescence, and tracks of VH nuclei data are discussed.

Kolesnikov D. V.   Perov N. I.
On the Method of Searching for Undiscovered Hazardous Comets and Meteoroids Colliding with Terrestrial Type Planets **[#1013]**
A model of forecasting appearances of as undiscovered yet minor celestial bodies as well hazardous for Earth's civilization but unobservable comets, based on the hypothesis of interaction of these bodies and major planets, is presented.

Machii N.   Nakamura A. M.   Fujii Y.
Impact Disruption Experiments of Sintered Glass Beads Aggregate Consisting of Millimeter-Size Particles **[#2069]**
We conducted impact experiments of targets consisting of 100–400 glass beads bonded by sintering. The strength was measured for two-body beads. They were catastrophically disrupted into monomers, for which two-dimensional ejection velocities were determined.

Madiedo J. M.   Ortiz J. L.   Castro-Tirado A.   Díaz M. J.   Trigo-Rodríguez J. M.
On the Development of Robotic CCD Video Meteor Observing Stations in Spain **[#1504]**
We summarize here the significant improvements we have made to robotize the video meteor observing stations operated by the Spanish Meteor Network.

Moreno-Ventas J.   Trigo-Rodríguez J. M.   Alonso-Azcárate J.   Zamorano J.   Izquierdo J.   Ocaña F.   Castro-Tirado A. J.   Llorca J.   Madiedo J. M.   Montanyá J.   Van der Velde O.   Lacruz J.   Pujols P.   Cortés J.
Large Meteoroids on Minor Cometary Streams: Recent Events Detected by the Spanish Fireball Network **[#1718]**
Sublimation and disruption in cometary nuclei are both mechanisms producing meteoroids. Using fireball observations we find out the size of final products and orbital parameters, to understand the processes that deliver meteorites to the Earth.

Rikhtehgar A.   Velichko F. P.
Phase Function of Brightness of NEA 1627 Ivar **[#2528]**
We present the magnitude-phase dependence of NEA 1627 Ivar obtained from observations of a more south hemisphere of the asteroid's surface in the range of phase angle from about of 0.6° to 31.6°.

Shevchenko V. G.   Belskaya I. N.   Tereschenko I. A.
The Diversity of the Opposition Effect of Dark Asteroids **[#1131]**
Analisys of the OE of dark asteroids was performed. The correlations of the OE amplitude of low albedo asteroids with color index s-b and albedo were found.

Slyuta E. N.
Physical-Mechanical Anisotropy of Ordinary Chondrites and the Shape of Small Rocky Bodies **[#1103]**
The shape parameters and morphology of small rocky bodies of the solar system, apparently, are not random shot and may depend substantially also on the internal composition and structure of these bodies.

Trigo-Rodríguez J. M.   Lacruz J.   Sánchez A.   Rodriguez D.   García-Hernández A.
Follow-Up of Comet-Asteroid Transition Object 107P Wilson-Harrington During Its 2009 Return to Perihelium **[#1193]**
We have been monitoring 107P comet-asteroid transition object during its 2009 return to perihelium. We have been unable of identifying any trace of cometary activity until December 8, 2009.

Weidenschilling S. J.
Were Asteroids Born Big? An Alternative Scenario **[#1453]**
The size-frequency distribution of the asteroids can be produced by collisional growth starting with small bodies of sizes ~ 0.1 km.

SATELLITES AND RINGS

D'Aversa E.   Bellucci G.   Altieri F.   Carrozzo F. G.
Statistical Perspectives on the Study of the Ring Spokes of Saturn **[#2197]**
Spokes on the Saturn rings have recently been observed at infrared wavelengths for the first time, with unexpected findings. A perspective statistical study of spokes with the Cassini/VIMS spectrometer is outlined.

Ruskol E. L.   Dorofeeva V. A.
Some Remarks on the Thermal Evolution of Enceladus **[#1212]**
We present arguments suggest that long-lived radioactivity and the tidal friction acting throughout the history of the solar system could be responsible for the modern state of Enceladus.

Stryk T.   Stooke P. J.
Transit and Shadow Transit of Neptune by Despina **[#1849]**
Despina, a small inner satellite of Neptune, has been found in a previously overlooked Voyager 2 image sequence which includes a shadow transit across the planet and in one frame a satellite transit.

PLANETARY ATMOSPHERES

Tejfel V. G.   Vdovichenko V. D.   Karimov A. M.   Kharitonova G. A.   Kirienko G. A.
Saturn At and Between the Equinoxes 1995 and 2009 **[#1250]**
The results of space and time variations of the methane absorption from Saturn's spectrophotometry in 1995–2009 are described.

MERCURY

Holin I. V.
Spin Dynamics and Deep Interior of Mercury from Earth-based HSDI **[#1038]**
Mercury's core can be in intermediate state which can be specified and studied to high precision by Earth-based radar.

Riner M. A.   McCubbin F. M.   Lucey P. G.   Taylor G. J.   Gillis-Davis J. J.
Mercury Surface Composition: Integrating Petrologic Modeling and Remote Sensing Data **[#2218]**
We integrate petrologic modeling with remote sensing data to constrain Mercury's surface composition and explain a potential petrologic conflict between proposed high FeO opaque oxides with coexisting low FeO silicates.

IMPACTS

Arif Md.   Misra S.   Basavaiah N.
Rock Magnetic Characterization of Target Basalts at Lonar Crater, India **[#1571]**
The present work reports the characterization of rock magnetic properties of shocked and unshocked target basalts occuring around the Lonar crater, India.

Bose T.   Misra S.   Banerjee K. S.   Chakroborty S.   Newsom H.   Reddy K.
Gamma (γ) – Ray Mapping of Ejecta around Lonar Asteroid Impact Crater, India. **[#1549]**
The problem of ejecta mapping of weathering modified terrestrial craters is explored using γ-ray mapping by handheld GM counter supported by U, Th, and K data of various surface types for Lonar crater, India.

Kimberley J.   Ramesh K. T.
A Scaled Model Describing the Compressive Strength of Geologic Materials **[#2543]**
A micromechanics based model for describing the rate dependent compressive strength of brittle geological materials is developed and expressed in terms of non-dimensional parameters.

Krzesinska A.
Oblique Impact-induced (Shock-related) Shearing and Frictional Melting in Pultusk (H5) Chondrite **[#1140]**
In Pultusk (H5) dark clast has cataclastic texture and light clast shows evidences for shearing. Boundary of clasts shows evidences of melting. In whole sample silicates are of S2-S3 stage. Pultusk may have been deformed at oblique impact-related shearing.

Levin B. W.   Vishnevsky S. A.   Palchik N. A.
Underwater Depressions on the Bottom of the Tatarsky Strait, the Sea of Japan (Western Coast of the Sakhalin Island, Russia): Possible Marine Impact Craters **[#1189]**
Two deep underwater depressions on the bottom of the Tatarsky strait, the Sea of Japan are supposed to be the new marine impact craters.

Louzada K. L.   Stewart S. T.   Weiss B. P.
Shock Demagnetization of Single Domain Magnetite **[#1937]**
Single-domain (SD) magnetite is an important contender for martian crustal magnetization. We report new shock demagnetization data on SD-magnetite bearing chiton teeth.

Michael G.   Neukum G.
Planetary Surface Dating from Crater Size-Frequency Distribution Measurements: Differential Forms of Production Function Polynomials **[#1920]**
We present expressions for the transformation of reverse-cumulative impact crater production function polynomials into the Hartmann (root-2 incremental) and R-plot presentations.

Nagy Sz.   Bérczi Sz.   Józsa S.   Gucsik A.   Veres M.
Olivine and Pyroxene High-Pressure Polymorphs in Melt Veins of the Strongly Shocked NWA 5011 Meteorite Sample **[#1228]**
In this abstract, we report the firstly observed ringwoodite-majorite-glassy material assemblages from the NWA 5011 highly shocked meteorite, and a transition boundary zone by ringwoodite lamellae, along a peripheral part of the shock vein.

Naumov M. V.
Impact-generated Sulfide Ore from the Suavjarvi Impact Structure, Russian Karelia **[#1117]**
The data about massive pyrite-chalcopyrite-pyrrhotite ores from the 16-km-sized Suavjarvi impact structure are reported. This ore cements polymict impact breccia and contains about 0.75% Cu.

Spray J. G.   Boonsue S.
Quartz-Coesite-Stishovite Relations in Shock Veins from the Vredefort Impact Structure **[#2312]**
The spatial and temporal relationships between the SiO_2 polymorphs quartz, coesite and stishovite are presented based on field emission–scanning electron microscopy, Raman spectroscopy and electron backscattered diffraction data.

Takasawa S.   Nakamura A. M.   Kadono T.   Arakawa M.   Dohi K.   Ohno S.   Seto Y.   Maeda M.   Hironaka Y.   Sakaiya T.   Fujioka S.   Sano T.   Shigemori K.   Machii N.   Setoh M.   Takeuchi T.
Ejecta Size Distribution from Hypervelocity Impact Cratering of Planetary Materials **[#1194]**
We conducted impact experiments to study ejection process of planetary materials at collision velocity higher than 10 km/s using a GEKKO XII-HIPER laser. We show the size distribution of ejecta, which ranged from a few µm to tens of µm in diameter.

Valter A. A.   Pisansky A. I.
The Rate of Astroblemes Discovery and One Example of the Significance of Such Structures for Archaeology **[#1069]**
Empirical formulas for crater discovery rate are determined. The reserve of astroblemes yet to be discovered is estimated. The significance of the Ilintsy astrobleme (Ukraine) for archaeology is shown.

Vishnevsky S.
Popigai ZH-Glasses: Origin by Initial H_2O Irregularities, Unstable Shock Flow and Quenching **[#1026]**
Interesting fine-banded impact glasses known in some astroblemes and among some tektite strewn fields are highly-mobile products of initial shock melting and mixing, bearing the traces of unstable microflow preserved by quenching.

MOON

Abdrakhimov A. M.   Basilevsky A. T.
Re-Examination of Lunokhod Sites: Panoramas and Aims for LROC Investigations **[#2173]**
Lunokhod 1 and 2 panoramas were digitized. Analyses of panoramas could define three lunar landscape types: mare plain, highland, joint fissure area. High resolution LRO camera will help us to locate Lunokhod 1 site and refine both rover traverses.

Eldridge D. L.   Korteniemi J.   Lough T.   Singer K. I.   Werblin L.   Kring D. A.
Sampling the Youngest and Oldest Mare Basalts: Important Lunar Regions **[#1486]**
Basalts spanning the duration of lunar mare volcanism are incompletely sampled. Presented here is a brief summary of the current knowledge of mare basalt ages and a set of exploration targets where the youngest and oldest mare basalts may be found.

Evans R.   Lena R.   Wöhler C.   Berezhnoy A.
Mons Hansteen: Morphometry, Petrographic Mapping, and Mode of Emplacement **[#1475]**
This contribution describes the determination of the morphometric and rheologic properties of the lunar highland dome Mons Hansteen. Furthermore, the abundances of several elements are estimated for Mons Hansteen based on multispectral imagery.

Garvin J. B.   Mitrofanov I.   Smith D. E.   Malakhov A.   Zuber M. T.   Neumann G.   Sanin A.   Mazarico E.
Lunar Polar Hydrogen Correlations with Impact Crater Geometry from LRO LEND and LOLA Observations **[#2224]**
Spatial clustering analysis of lunar polar region impact crater geometric properties measured from LRO LOLA together with neutron fluxes measured from LRO LEND indicates that there are associations between state of crater degradation and estimated regolith hydrogen content.

Gerasimenko S. Yu.   Kaydash V. G.   Shkuratov Yu. G.   Opanasenko N. V.   Velikodsky Yu. I.   Korokhin V. V.
Phase Angle Ratio Images of Color Index C (610/480 nm) of West Portion of the Lunar Nearside **[#1445]**
We map the color index phase ratios for the lunar nearside. At phase angles 2°–50° the color index C (610/480 nm) of highlands grows with phase angle faster than that for maria. The opposite effect is observed at larger phase angles, 50°–95°.

Korokhin V. V.   Velikodsky Yu. I.   Shkuratov Yu. G.   Kaydash V. G.   Gerasimenko S. Yu.   Opanasenko N. V.
Comparison Between Kaguya (Selene) Altimetry Data and Lunar Topography Retrieved from Photoclinometry **[#1356]**
A new technique to map the zonal component of the lunar topography slopes using telescopic photometry imagery and to correct photometric data for the topography influence is proposed. We compare our map with the Kaguya laser altimetry (LALT) data.

Kozlova E. A.   Lazarev E. N.
Crater Cabeus as Possible Cold Trap for Volatiles Near South Pole of the Moon **[#1779]**
Crater Cabeus has been chosen by NASA as a target for impact experiment of LCROSS mission. On the basis of topographical data from KAGUYA we made a topographical model of Cabeus, the illumination map for crater and investigate the temperature distribution in crater.

Lena R.   Woehler C.   Phillips J.   Berezhnoy A.
An Effusive Lunar Dome in the Light Plains of the Crater Meton **[#1470]**
A lunar effusive dome is identified on the floor of the crater Meton on typical light plains material, suggesting the occurrence of non-mare volcanism in the light plains regions.

Li X.   Wang S.   Tang H.   Zheng Y.
Primitive Results from Passive Microwave Exploration in Chinese Chang'e Lunar Mission **[#1036]**
A microwave radiometer was loaded in the Chinese Chang'E lunar mission and a lot of data was received. By analyzing these data, some characteristics of brightness temperature and primitive results have been obtained.

Lu Y.
Correlations Between Iron Abundances and Lunar Surface Features: Crater Kepler Area **[#1258]**
Since iron is one of the major mineral forming elements on the Moon, iron abundance can show composition and the stratigraphy of the lunar crust details, and it can help us to understand the formation, distribution and variety of lunar mare basalts.

McKay D. S.   Wentworth S. J.   Thomas-Keprta K. L.   Ross K.   Clemett S. J.
Volcanic Coatings on Picritic Apollo 17 Glasses: Submicrometer-Deposits of Fe-, Cr-Metal **[#2509]**
We are investigating the origin and evolution of volcanic surface coatings on Apollo 15 green and Apollo 17 black glasses.

Mendell W. W.   Noble S. K.
The Epiregolith **[#1348]**
Successful models of the non-Lambertian character of lunar surface albedo and emissivity imply the existence of a lattice-like layer, several particles thick, where photon interactions occur and which may be the product of grain charging by the solar wind.

Mendell W. W.
How Cold Are the Floors of Lunar Polar Shadowed Craters? **[#1352]**
The epiregolith in permanently shadowed polar regions may have a very fine size distribution, leading to greatly reduced emissivity at wavelengths >100 µm. Diviner readings in this situation may not be a reliable representation of the physical temperature.

Nemchin A. A.   Whitehouse M. J.   Grange M. L.   Muhling J. R.
High U-Pb Ratios in the Source of Low-Ti Volcanic Glass Beads from the Apollo 14 Soil **[#1836]**
Green volcanic glass beads from the Apollo 14 soil sample indicate high U-Pb ratios in their source, suggesting that the mantle sources of magmas forming glass beads and mare basalts could be similar.

Parmentier E. M.   Liang Y.
Formation of Pure Anorthosite During Lunar Magma Ocean Solidification: Implications for the Melt-Solid Segregation Process **[#1824]**
SELENE remote sensing data indicate nearly pure anorthosite in crater central peaks. Segregation of plagioclase from denser mafic minerals by shearing in granular flow and by migration of residual liquid from a compacting solid matrix are examined.

Pugacheva S. G. Sv.   Shevchenko V. V. Vl.
The Chemical Composition of Regolith at the Moon's South Pole, According to Data of Lunar Prospector and Lunar Reconnaisance Orbiter Missions **[#1297]**
Comparative evaluation of the chemical composition of the soil matters in the lunar craters with "cold traps."

Richard D. T.   Glenar D. A.   Stubbs T. J.   Davis S. S.   Colaprete A.
Light Scattering in the Lunar Orbital Environment by Non-Spherical Dust Grains **[#2704]**
We compute the scattering properties of non-spherical lunar dust grain models using the Discrete Dipole Approximation (DDA) for use in data analysis of optical diagnostics recorded in the lunar environment.

Slyuta E. N.   Abdrakhimov A. M.   Basilevsky A. T.   Lazarev E. N.   Dolgopolov V. P.   Sheikhet A. I.
Landing Sites for the Russian Luna-Resurs Mission to the Moon **[#1141]**
Considering that mission will be in October 2012, two landing sites have been selected, both in the south pole region: #1 (basic), and #2 (back-up).

Tang H.   Wang S.   Li X.
Experimental Simulation of Nanophase Iron Production in Lunar Space Weathering **[#1041]**
In the study, an experiment using microwave heating and magnetron sputtering techniques to simulating nanophase iron both in glass phase and on the grain surface is proposed.

Velikodsky Yu. I.   Opanasenko N. V.   Akimov L. A.   Korokhin V. V.   Shkuratov Yu. G.   Kaydash V. G.
Kharkiv Absolute Photometry of the Moon **[#1760]**
A two-month series of quasi-simultaneous imaging photometric observations of the Moon and the Sun has been performed at Maidanak. New values of lunar albedo have been obtained. They turn out about 15–25% higher than that in previous works.

Wang L.   Xiang S.   Gao J.   Lin X.   Lv Z.   Huang Y.   Huang D.
The Discovery of Water on Lunar: Indication on Searching for Life on it **[#1592]**
The discovery of water on the Moon: Indication on searching for life on it.

Wöhler C.   Lena R.   Pau K. C.
Lunar Intrusive Domes on the Floor of Grimaldi and Near Aristillus **[#1478]**
In this contribution we examine two large lunar domes of probably intrusive origin. The morphometric properties of the domes are derived, and geophysical parameters (intrusion depth, magma pressure) are estimated based on modelling.

PLANETARY DIFFERENTIATION, DYNAMICS, AND TECTONICS

Futó P.
Detailed Internal Structure Model for Super-Earths in case of Earth-like Composition **[#1024]**
It was expected that 1–2% uncertainty in planet mass and radius would be able to reasonably determine not only main composition of iron/silicate planets, but also conclude the substantial parameters of their interior structure.

Kobayashi D.   Sprenke K. F.
Geometric Analysis of Lineation Patterns in the Martian Magnetic Field **[#1452]**
Through a geometric analysis, we have found that the lineations in the martian magnetic field form small circles about two distinct poles, a result consistent with our hypothesis that the magnetic anomalies on Mars represent hotspot tracks on ancient Mars.

Kósik Sz.   Karátson D.   Farkas A.
A Hypothesis for Martian Topography, Tectonics and Volcanism **[#1248]**
We present a theory for development of martian crustal dichotomy, based on plume volcanism of Tharsis.

Sharkov E. V.   Bogatikov O. A.
Evolution of Tectonomagmatic Processes on Terrestrial Planets: Key for Understanding of Their Formation and Development **[#1027]**
Terrestrial planets were developed at the same scenario, subjected cardinal change of tectonomagmatic processes at the middle stages of evolution. It can be possible if (1) they originally were heterogeneous or (2) downward heating of them had occurred.

Wasserburg G. J.   Caro G.   Papanastassiou D. A.
^{40}Ca Isotopic Evolution of the Oceans and Crust and the Major Role of Hydrothermal Circulation Over Geologic Time **[#1924]**
Using precise ^{40}Ca measurements we show that hydrothermal exchange from ongoing volcanism, subduction, and sea-floor spreading appears as the dominating agent in the chemical composition of sea water over almost all of geologic time.

MARS

Coleman N.
Spectacular Cataracts (Dry Falls) on the Floor of Kasei Valles, Mars **[#1174]**
The largest known cataracts exist on the floor of Kasei Valles. These spectacular dry falls have a vertical relief of ~500 m, and may have migrated by headward erosion as much as 250 km. They are characterized using THEMIS images and MOLA data.

Deák M.
The Methodology of Finding Lava Tubes with the Use of Remote Detection on Mars, on the Example of a Newly Found Cave **[#1507]**
To find entrances to lava tubes on Mars using remote detection, multispectral images, thermal infrared images and elevation data are needed. Using them makes it possible to find new caves, as it is shown on the example of a new one, the “Catherine.”

Hobbs S. W.   Paull D. J.   Bourke M. C.
Aeolian Processes and Dune Morphology In Gale Crater **[#1561]**
We used thermal inertia data, dune slip-face morphology and mesoscale modelling to analyse the dune fields in Gale Crater.

Jackson R. G.   Sanders N. H.   Ward C. C.   Ward F. R.   Benson S. M.   Lee N. F.
Autonomous Temperature Data Acquisition Compared to Existing Thermal Models of Different Sediments **[#1362]**
Our team wanted to improve sampling methods for experiments on the thermal properties of martian sediments. We built a robot that could take the data autonomously over a period of days, and then compared them to existing models.

Lanz J. K.   Wagner R.   Wolf U.   Neukum G.   Kröchert J.
Volcanic Rift Zone and Associated Cinder Cone Field in Utopia Planitia, Mars **[#1366]**
We have analyzed a small area in SW Utopia Planitia that shows striking similarities to rift zone volcanos on Earth. The area exhibits eruptive fissures, cinder cones, and dyke swarms indicating rifting and magmatic activity prior to the deposition of VBF material.

Malin M. C.   Caplinger M. A.   Edgett K. S.   Ghaemi F. T.   Ravine M. A.   Schaffner J. A.   Baker J. M.   Bardis J. D.   DiBiase D. R.   Maki J. N.   Willson R. G.   Bell J. F. III   Dietrich W. E.   Edwards L. J.   Hallet B.   Herkenhoff K. E.   Heydari E.   Kah L. C.   Lemmon M. T.   Minitti M. E.   Olson T. S.   Parker T. J.   Rowland S. K.   Schieber J.   Sullivan R. J.   Sumner D. Y.   Thomas P. C.   Yingst R. A.
The Mars Science Laboratory (MSL) Mast-mounted Cameras (Mastcams) Flight Instruments **[#1123]**
The Mars Science Laboratory has two color science mast cameras with 15° and 5° fields of view (FOV). They take 1200 × 1600 RGB and science filter images, with JPEG and lossless compression, into 8-Gigabyte buffers.

Miyamoto M.   Mikouchi T.   Satake W.   Koizumi E.   Kaiden H.
The Cooling Rate of Several Olivine-Phyric Shergottites on the basis of Fe-Mg Zoning in Olivine **[#1554]**
We have developed a model to calculate the cooling rate and burial depth by using the Fe-Mg zoning of olivine and applied this model to calculating the cooling rate and burial depth for several olivine-phyric shergottites.

Molina A.   de Pablo M. A.   Ramos M.
Testing THEMIS-derived Brightness Temperature by MINI-TES (Spirit) Data **[#1150]**
Most of the data from Mars comes from orbital sensors, but only few missions had reached the surface of the planet. Spirit sensor, called Mini-TES, provides most direct data (more reliable therefore) and allow to compare them with orbital ones (such as THEMIS).

Papike J. J.   Karner J. M.   Shearer C. K.   Burger P. V.
Valence State Partitioning of V Between Augite/Melt Crystallized from a Highly Spiked Martian Basalt Composition as a Function of Oxygen Fugacity (IW-1 to FMQ) **[#1010]**
This abstract explores the partitioning of vanadium between augite and melt in a highly-spiked QUE 94201 composition, at each of four different fO_2 values (IW-1, IW, IW+1, FMQ).

Pendleton Hoffer M.   Greeley R.
Bright Tracks on Mars: Alternate Dust Devil Tracks **[#2713]**
Some linear, curved and "curlicue" albedo features on Mars are attributed to the tracks left by the passage of dust devils.

Shean D. E.
Evidence for Widespread Removal of Martian Mid-Latitude "Fill" Material **[#1509]**
Evidence is presented for each of the archetypal mid-latitude "fill" material settings (crater and lineated valley fill, aprons, viscous flow features) suggesting that this material was thicker and laterally more extensive in the relatively recent past.

Shih C.-Y.   Nyquist L. E.   Reese Y.   Jambon A.
Sm-Nd Isotopic Studies of Two Nakhlites, NWA 5790 and Nakhla **[#1367]**
Sm-Nd ages for Nakhla and the mesostasis-rich nakhlite NWA 5790 are 1.38±0.07 and 1.38±0.10 Ga, respectively. Model calculations suggest nakhlite parental magmas were derived from LREE-depleted, garnet-bearing sources by small percentages of melting.

Syzyakova L.   Perov N. I.
Size Distributions of Martian Craters **[#1025]**
Function for martian crater size distribution is considered that (a) is applied to finite and infinite distributions; (b) approximates of small diameters and about the point contrary flexure; (c) turns asymptotically into by standard power law.

Thompson D. R.   Castaño R.   Wettergreen D.
Compression Ratio as Indicator of Scientist Preference for Rover Images **[#1287]**
Spacecraft performing onboard image analysis can prioritize interesting data for downlink and potentially improve science return. Images' compressed size (a rough measure of "visual information") correlates strongly with desirable content.

Tsang S. W. R.
The Trade Winds of Mars **[#1012]**
This abstract examines yardangs to study wind patterns on Mars.

White O. L.   Stofan E. R.
An Estimation of the Theoretical MARSIS Aquifer Detection Depth **[#1220]**
A theoretical aquifer detection depth of MARSIS is estimated based on extrapolation of its penetration ability at other martian geological settings. The resulting estimate does not constrain the distribution of martian aquifers.

de Pablo M. A.   Caprarelli G.
Possible Subglacial Volcanoes in Nepenthes Mensae, Eastern Hemisphere, Mars **[#1584]**
We report our observations of 50 hilly features in Nepenthes Mensae, Mars, what we interpret to be possible moberg ridges, formed by fissural eruption of lava under thick ice layer. We finally discuss some of their geological implications.

EXOBIOLOGY

Gibson E. K. Jr.   McKay D. S.   Thomas-Keprta K. L.   Clemett S. J.   Pillinger C. T.
Wright I. P.   Verchovsky A. P.
Reduced Martian Carbon: Evidence from Martian Meteorites **[#1062]**
The search for reduced carbon species on the martian surface has been enhanced with the identification of reduced carbon components within martian meteorites of different ages. Reduced carbon has been identified in materials ranging from 3.9 Ga to as young as 600,000 Ma.

Perov N. I.   Kondratieva A. V.
Localization of Boundaries of Life of the Earth's Type in the Star Clusters **[#1028]**
The stable four body celestial mechanical central configurations of the "hot" objects and a "warm" planet with ratio of mass $m_2/m_1 = m_3/m_1 > 367.0540108$, $m_0/m_1 \sim 0$ and for the temperature 223 K < T < 323 K on the surface of the planet m_0 are under consideration.

Thomas-Keprta K. L.   Clemett S. J.   Le L.   Ross K.   McKay D. S.   Gibson E. K. Jr.
Characterization of Spitsbergen Disks by Transmission Electron Microscopy and Raman Spectroscopy **[#1063]**
Characterized by TEM and Raman, significant chemical and physical differences exist between the disks found in the fractures and pore spaces of peridotite xenoliths and basalts in Spitsbergen and the carbonates present in martian meteorite ALH 84001.

ENVIRONMENTAL AND MATERIAL ANALOGS

He X. X.   Xiao L.   Huang J.   Wan C. H.   Wu T.   Gao R.   Yan S. W.   He Q.
Lunar Regolith Simulant CUG-1A **[#1183]**
CUG-1A, a new lunar regolith simulant was produceed under the sponsors of China University of Geosciences (Wuhan), is very similar to the Apollo 14 soil for the chemical and phycial properties. It is an additional simulant for lunar soil chemistry and engineering studies.

Hörz F.   Lofgren G. E.   Eppler D. E.   Ming D.
Lunar Surface Operations with Dual Rovers **[#1234]**
Future long-range lunar surface traverses will utilize two rovers; we suggest that these vehicles be configured individually to pursue independent, yet highly complementary tasks.

Lin X.   Gao J.   Xiang S.   Wang L.   Lv Z.   Zhang X.   Huang Y.   Huang D.
Extremophiles Research for Lunar Outpost **[#1574]**
We hope to build an artificial recycling ecosystem like the "Biosphere 2," our main consideration was how to use some extremophiles on the Earth to improve the lunar soil condition, making it more conducive for plants.

Lofgren G. E.   Horz F.
Multiple Approaches to Down Sizing of the Lunar Sample Return Collection **[#2062]**
Future samples from the Moon will be a scientific treasure that will be mined for decades. We must expend every effort to maximize the quality of that collection with highly trained crews, appropriate analytical instruments, and effective ground support.

EDUCATION AND PUBLIC OUTREACH

Kabai S.   Bérczi Sz.
Space Science Education by Mathematica Demonstrations: Interactive Design of Moving Space Probe Elements Mechanics by Foldable and Extendable Structures for Space Applications **[#2340]**
By the interactive Mathematica Demonstrations of the Wolfram Research several mechanics for space probe operation and motion simulations were studied as space robotics and science educational program.

Mizser A.
Outreach Activity in Planetary Science and Astrobiology in the International Year of Astronomy in Hungary **[#1322]**
We summarize our results in outreach activity related to planetary science and astrobiology in the International Year of Astronomy (IYA2009) in Hungary.

Sipos A.   Vizi P. G.
Simulated Mars Rover Model Competition 2009–2010 **[#2649]**
This is a competition of applied engineering sciences.

DATA AND IMAGE SYSTEMS

Hare T. M.
A Case for a PDS Supported Cartographic Raster Library **[#2728]**
This abstract simply outlines a recommendation for the IPDA and PDS to consider long-term support for a community driven raster library for geospatial data holdings.

Loomis A. C.   Huffman J. N.   Head J. W.   Fassett C. I.   Dickson J. L.   Forsberg A. S.
Visualization of Planetary Data with ADVISER: Applications to the Moon and Beyond **[#2090]**
We briefly touch on the ADVISER toolset, which has been used in the past for the interactive visualization and exploration of Mars, and we then discuss its application to the new planetary datasets coming back from the Moon.

Moratto Z. M.   Broxton M. J.   Beyer R. A.   Lundy M.   Husmann K.
Ames Stereo Pipeline, NASA's Open Source Automated Stereogrammetry Software **[#2364]**
The Intelligent Robotics Group (IRG) at NASA Ames have released open source software to perform stereogrammetry called the Ames Stereo Pipeline. The abstract outlines the use, an example result from, and how to get the software.

SPACECRAFT CONCEPTS

Mardon C. A.   Mardon A. A.
Rappelling Techniques in Low Gravity on the Moon in a Spacesuit **[#2692]**
Rapelling techniques in spacesuits.

PROGRAM AUTHOR INDEX

** Denotes speaker*

Abdrakhimov A. M.	Print Only: Differentiated Bodies
Abdrakhimov A. M.	Print Only: Moon
Abe M.	Near-Earth Objects Posters, Thu, p.m., Town Center Exhibit Area
Abe M.	A New Moon: Spectral Constraints Posters, Thu, p.m., Town Center Exhibit Area
Abe Y.	Lunar Geophysics Posters, Thu, p.m., Town Center Exhibit Area
Abel R.	Stardust Mission Posters, Thu, p.m., Town Center Exhibit Area
Abel R. L.	Achondrites Posters, Tue, p.m., Town Center Exhibit Area
Abel R. L.	Martian Alteration Processes Posters, Tue, p.m., Town Center Exhibit Area
Abel R. L.	Chondrites Posters, Thu, p.m., Town Center Exhibit Area
Abramov O.	Martian Alteration Processes Posters, Tue, p.m., Town Center Exhibit Area
Abramov O.	Impacts on the Moon, Mars, and Beyond, Wed, p.m., Waterway Ballroom 5
Abramov O. *	Rocks, Life, and Biosignatures, Thu, p.m., Waterway Ballroom 1
Abreu N. M.	Water in the Solar System: Primitive Bodies, Mon, p.m., Waterway Ballroom 6
Abreu N. M.	Chondrites Posters, Thu, p.m., Town Center Exhibit Area
Achilles C. N.	Experimental Constraints on Martian Alteration Processes, Mon, p.m., Waterway Ballroom 4
Acosta T.	Spacecraft Instruments Posters, Tue, p.m., Town Center Exhibit Area
Adams P. M.	Environmental Analogs Posters, Thu, p.m., Town Center Exhibit Area
Adcock C. T.	Experimental Constraints on Martian Alteration Processes, Mon, p.m., Waterway Ballroom 4
Addison B. C.	Mars: Gullies and Slope Streaks Posters, Thu, p.m., Town Center Exhibit Area
Adolph L.	Impact Ejecta Posters, Tue, p.m., Town Center Exhibit Area
Adriani A.	Spacecraft Instruments Posters, Tue, p.m., Town Center Exhibit Area
Adumitroaie V.	Once and Future Moon Posters, Thu, p.m., Town Center Exhibit Area
Agee C. B.	Planetary Differentiation, Mon, a.m., Waterway Ballroom 5
Agee C. B.	Planetary Differentiation Posters, Tue, p.m., Town Center Exhibit Area
Agee C. B.	Martian Igneous Processes, Fri, a.m., Waterway Ballroom 5
Agresti D. G.	Martian Alteration Processes Posters, Tue, p.m., Town Center Exhibit Area
Agresti D. G.	Martian Meteorites Posters, Thu, p.m., Town Center Exhibit Area
Aguiar J. A. *	Cosmic Dust, Thu, p.m., Waterway Ballroom 1
Aharonson O.	A New Moon: LRO Results, Mon, a.m., Waterway Ballroom 6
Aharonson O.	A New Moon: Geologic Processes Posters, Tue, p.m., Town Center Exhibit Area
Aharonson O.	Mission Plans and Concepts Posters, Tue, p.m., Town Center Exhibit Area
Aharonson O.	Several Species of Icy Chunks, Thu, p.m., Waterway Ballroom 5
Aharonson O.	Mars Craters Posters, Thu, p.m., Town Center Exhibit Area
Aharonson O.	Mars: Deposition and Erosion, Fri, a.m., Waterway Ballroom 4
Ahmed M.	Parent Cloud and Solar Nebula, Mon, a.m., Waterway Ballroom 1
Aittola M.	Terrestrial Planet Cryospheres Posters, Tue, p.m., Town Center Exhibit Area
Ajai	A New Moon: Spectral Constraints Posters, Thu, p.m., Town Center Exhibit Area
Ajai	Once and Future Moon Posters, Thu, p.m., Town Center Exhibit Area
Akimov L. A.	Print Only: Moon
Akins S.	Data and Image Systems Posters, Tue, p.m., Town Center Exhibit Area
Alard O.	Formation of Building Blocks Posters, Thu, p.m., Town Center Exhibit Area
Albarede F.	Iron and Stony Iron Meteorites Posters, Tue, p.m., Town Center Exhibit Area
Albarede F.	Differentiated Meteorites, Wed, p.m., Waterway Ballroom 4
Albrecht A.	Cosmic-Ray Exposure Dating Posters, Tue, p.m., Town Center Exhibit Area
Aldersley M. F.	Environments for Life Posters, Thu, p.m., Town Center Exhibit Area
Aléon J. *	Solar Wind, Volatile Elements, and Organics, Thu, a.m., Waterway Ballroom 1
Alexander C. M. O'D.	Parent Cloud and Solar Nebula, Mon, a.m., Waterway Ballroom 1
Alexander C. M. O'D.	Radionuclides and Early Solar System Chronology, Tue, a.m., Waterway Ballroom 1
Alexander C. M. O'D.	Ureilitic Asteroids: Almahata Sitta, Tue, p.m., Waterway Ballroom 1
Alexander C. M. O'D.	Cosmic-Ray Exposure Dating Posters, Tue, p.m., Town Center Exhibit Area
Alexander C. M. O'D.	Origins of Presolar Grains, Wed, p.m., Waterway Ballroom 1
Alexander C. M. O'D.	Solar Wind, Volatile Elements, and Organics, Thu, a.m., Waterway Ballroom 1
Alexander C. M. O'D.	Solar Wind, Volatile Elements, and Organics Posters, Thu, p.m., Town Center Exhibit Area
Alexander C. M. O'D.	Thermal and Aqueous Processes on Chondrite Parent Bodies, Fri, a.m., Waterway Ballroom 1
Alexander C. M. O'D. *	Formation of Building Blocks, Fri, p.m., Waterway Ballroom 1
Alexeev V. A.	Print Only: Small Bodies
Alha L.	Lunar Petrology and Geochemistry Posters, Tue, p.m., Town Center Exhibit Area
Aliaga-Caro J. F.	Planetary Aeolian Processes Posters, Tue, p.m., Town Center Exhibit Area
Alkalai L.	Once and Future Moon Posters, Thu, p.m., Town Center Exhibit Area
Allemand P.	Martian Alteration Processes, Mon, a.m., Waterway Ballroom 4
Allemand P.	Planetary Aeolian Processes Posters, Tue, p.m., Town Center Exhibit Area
Allemand P.	Exploring the Martian Crust Posters, Thu, p.m., Town Center Exhibit Area
Allen C.	A New Moon: LRO Results, Mon, a.m., Waterway Ballroom 6

Athena Science Team	Martian Alteration Processes, Mon, a.m., Waterway Ballroom 4
Athena Science Team	Martian Alteration Processes Posters, Tue, p.m., Town Center Exhibit Area
Athena Science Team	Exploring the Martian Crust, Wed, a.m., Waterway Ballroom 4
Athena Science Team	Spirit Posters, Thu, p.m., Town Center Exhibit Area
Athiray P. S.	Lunar Petrology and Geochemistry Posters, Tue, p.m., Town Center Exhibit Area
Atkins B. M.	Lunar Dust Posters, Thu, p.m., Town Center Exhibit Area
Atkinson D.	Mission Plans and Concepts Posters, Tue, p.m., Town Center Exhibit Area
Aubrey A. D.	Environments for Life Posters, Thu, p.m., Town Center Exhibit Area
Auster U.	Mission Plans and Concepts Posters, Tue, p.m., Town Center Exhibit Area
Austin D. E.	Impact Experiments Posters, Tue, p.m., Town Center Exhibit Area
Avatrian, LLC	E/PO: Moon Posters, Tue, p.m., Town Center Exhibit Area
Aye K.-M.	Mars Polar Processes, Tue, p.m., Waterway Ballroom 4
Aye K.-M.	Martian Polar Processes Posters, Tue, p.m., Town Center Exhibit Area
Aye K.-M.	Mars Remote Sensing Techniques Posters, Thu, p.m., Town Center Exhibit Area
Bada J. L.	Environments for Life Posters, Thu, p.m., Town Center Exhibit Area
Badia D.	Martian Igneous Processes, Fri, a.m., Waterway Ballroom 5
Bagenal F.	Mission Plans and Concepts Posters, Tue, p.m., Town Center Exhibit Area
Bagulya A. V.	Print Only: Cosmochemical Origins
Baiden G.	Environmental Analogs Posters, Thu, p.m., Town Center Exhibit Area
Bailey J.	E/PO: Professional Development Posters, Tue, p.m., Town Center Exhibit Area
Bailey M. J.	Impact Ejecta Posters, Tue, p.m., Town Center Exhibit Area
Bailey V.	A New Moon: LCROSS Posters, Tue, p.m., Town Center Exhibit Area
Baines K. H.	Mission Plans and Concepts Posters, Tue, p.m., Town Center Exhibit Area
Baines K. H.	Several Species of Icy Chunks, Thu, p.m., Waterway Ballroom 5
Baines K. H.	Satellites and Their Planets Posters, Thu, p.m., Town Center Exhibit Area
Bajt S.	Stardust Mission to Comet Wild 2, Wed, a.m., Waterway Ballroom 1
Baker D. M. H. *	Terrestrial Planet Cryospheres, Tue, a.m., Waterway Ballroom 4
Baker D. M. H.	Mercury Posters, Tue, p.m., Town Center Exhibit Area
Baker J. M.	Print Only: Mars
Baker V. R.	Mars: Geologic, Geomorphic, etc., Posters, Thu, p.m., Town Center Exhibit Area
Baker V. R.	Environments for Life Posters, Thu, p.m., Town Center Exhibit Area
Balcerski J. A. *	Large Impact Basins on the Moon, Thu, a.m., Waterway Ballroom 6
Baldridge A.	Exploring the Martian Crust Posters, Thu, p.m., Town Center Exhibit Area
Baldridge A. M.	Exploring the Martian Crust Posters, Thu, p.m., Town Center Exhibit Area
Baldridge A. M. *	Mars: Deposition and Erosion, Fri, a.m., Waterway Ballroom 4
Balint T. S.	Mission Plans and Concepts Posters, Tue, p.m., Town Center Exhibit Area
Ball A. D.	Stardust Mission Posters, Thu, p.m., Town Center Exhibit Area
Balme M.	Planetary Aeolian Processes Posters, Tue, p.m., Town Center Exhibit Area
Balme M.	Planetary Atmospheres Posters, Thu, p.m., Town Center Exhibit Area
Balme M. R.	Planetary Aeolian Processes Posters, Tue, p.m., Town Center Exhibit Area
Balme M. R.	Terrestrial Planet Cryospheres Posters, Tue, p.m., Town Center Exhibit Area
Balme M. R.	Mars: Gullies and Slope Streaks Posters, Thu, p.m., Town Center Exhibit Area
Balme M. R.	Mars: Deposition and Erosion, Fri, a.m., Waterway Ballroom 4
Baloga S. M. *	Impacts on the Moon, Mars, and Beyond, Wed, p.m., Waterway Ballroom 5
Baloga S. M.	Igneous and Volcanic Processes, Thu, a.m., Waterway Ballroom 5
Baloga S. M.	Igneous and Volcanic Processes Posters, Thu, p.m., Town Center Exhibit Area
Bandeira L.	Terrestrial Planet Cryospheres Posters, Tue, p.m., Town Center Exhibit Area
Bandeira L.	Mars Remote Sensing Techniques Posters, Thu, p.m., Town Center Exhibit Area
Bandeira L.	Environmental Analogs Posters, Thu, p.m., Town Center Exhibit Area
Bandfield J. L.	A New Moon: LRO Results, Mon, a.m., Waterway Ballroom 6
Bandfield J. L.	A New Moon: Geologic Processes Posters, Tue, p.m., Town Center Exhibit Area
Bandfield J. L. *	Nature of the Lunar Regolith, Wed, a.m., Waterway Ballroom 6
Bandfield J. L.	A New Moon: Spectral Constraints, Wed, p.m., Waterway Ballroom 6
Bandfield J. L.	A New Moon: Spectral Constraints Posters, Thu, p.m., Town Center Exhibit Area
Bandfield J. L.	Exploring the Martian Crust Posters, Thu, p.m., Town Center Exhibit Area
Bandfield J. L.	Interior of the Moon, Fri, a.m., Waterway Ballroom 6
Banerdt W. B.	Once and Future Moon Posters, Thu, p.m., Town Center Exhibit Area
Banerjee K. S.	Print Only: Impacts
Banerjee N. R.	Environmental Analogs Posters, Thu, p.m., Town Center Exhibit Area
Banks M. E.	Terrestrial Planet Cryospheres, Tue, a.m., Waterway Ballroom 4
Banks M. E.	Interior of the Moon, Fri, a.m., Waterway Ballroom 6
Banks M. S.	Once and Future Moon Posters, Thu, p.m., Town Center Exhibit Area
Baptista A. R.	Igneous and Volcanic Processes, Thu, a.m., Waterway Ballroom 5
Baptista A. R.	Igneous and Volcanic Processes Posters, Thu, p.m., Town Center Exhibit Area
Barabash S.	Mission Plans and Concepts Posters, Tue, p.m., Town Center Exhibit Area
Baragiola R.	Nature of the Lunar Regolith, Wed, a.m., Waterway Ballroom 6
Baragiola R.	Cosmic Dust, Thu, p.m., Waterway Ballroom 1

Baragiola R. A.	Water in the Solar System: Moon, Tue, p.m., Waterway Ballroom 6
Baragiola R. A.	Material Analogs Posters, Tue, p.m., Town Center Exhibit Area
Barata M. T.	Venus Posters, Tue, p.m., Town Center Exhibit Area
Barata M. T.	Environmental Analogs Posters, Thu, p.m., Town Center Exhibit Area
Baratoux D.	Planetary Atmospheres Posters, Thu, p.m., Town Center Exhibit Area
Barbieri L.	Mars: Gullies and Slope Streaks Posters, Thu, p.m., Town Center Exhibit Area
Bardis J. D.	Print Only: Mars
Barefield J. E.	Venus, Mon, p.m., Waterway Ballroom 5
Barefield J. E.	Spacecraft Instruments Posters, Tue, p.m., Town Center Exhibit Area
Barker I.	Chondrites Posters, Thu, p.m., Town Center Exhibit Area
Barlow N.	Impacts on the Moon, Mars, and Beyond, Wed, p.m., Waterway Ballroom 5
Barlow N. G.	Impact Craters Posters, Tue, p.m., Town Center Exhibit Area
Barlow N. G.	Planetary Aeolian Processes Posters, Tue, p.m., Town Center Exhibit Area
Barlow N. G.	Mars Ice and Craters Posters, Tue, p.m., Town Center Exhibit Area
Barlow N. G.	Mars Craters Posters, Thu, p.m., Town Center Exhibit Area
Barnes J. D.	A New Moon: Volatile Species Posters, Tue, p.m., Town Center Exhibit Area
Barnes J. W.	Mission Plans and Concepts Posters, Tue, p.m., Town Center Exhibit Area
Barnes J. W.	Satellites and Their Planets Posters, Thu, p.m., Town Center Exhibit Area
Barnhart C. J.	Mars: Gullies and Slope Streaks Posters, Thu, p.m., Town Center Exhibit Area
Barnhart C. J.	Exploring the Martian Crust Posters, Thu, p.m., Town Center Exhibit Area
Barnouin O. S.	Characterizing Near-Earth Objects, Thu, p.m., Waterway Ballroom 4
Barnouin O. S. *	Mercury, Tue, p.m., Montgomery Ballroom
Barnouin O. S.	Impact Experiments Posters, Tue, p.m., Town Center Exhibit Area
Barnouin O. S.	A New Moon: Geologic Processes Posters, Tue, p.m., Town Center Exhibit Area
Barnouin O. S.	Planetary Dynamics and Tectonics, Wed, a.m., Waterway Ballroom 5
Barnouin O. S.	Characterizing Near-Earth Objects, Thu, p.m., Waterway Ballroom 4
Barnouin O. S.	Exploring the Martian Crust Posters, Thu, p.m., Town Center Exhibit Area
Barnouin O. S.	Satellites and Their Planets Posters, Thu, p.m., Town Center Exhibit Area
Barnouin-Jha O.	Impact Craters Posters, Tue, p.m., Town Center Exhibit Area
Barnouin-Jha O.	E/PO: Mars Remote Sensing Posters, Thu, p.m., Town Center Exhibit Area
Barr A. C. *	Planetary Differentiation, Mon, a.m., Waterway Ballroom 5
Barr A. C.	Planetary Differentiation Posters, Tue, p.m., Town Center Exhibit Area
Barr A. C.	Lunar Origins and Chronology Posters, Tue, p.m., Town Center Exhibit Area
Barr A. C.	Planetary Dynamics and Tectonics Posters, Thu, p.m., Town Center Exhibit Area
Barr J. A.	Lunar Petrology and Geochemistry Posters, Tue, p.m., Town Center Exhibit Area
Barr J. A. *	Petrologic Characterization of the Moon, Fri, p.m., Waterway Ballroom 6
Barraclough B.	Spacecraft Instruments Posters, Tue, p.m., Town Center Exhibit Area
Barrat J. A.	Martian Igneous Processes, Fri, a.m., Waterway Ballroom 5
Barrett J. M.	Data and Image Systems Posters, Tue, p.m., Town Center Exhibit Area
Barrett J. M.	Lunar Cartography, Stereogrammetry, and Imaging Posters, Thu, p.m., Town Center Exhibit Area
Bart G. D.	A New Moon: LCROSS, Chandrayaan, Chang'E, Tue, a.m., Waterway Ballroom 6
Bartels A.	Lunar Cartography, Stereogrammetry, and Imaging Posters, Thu, p.m., Town Center Exhibit Area
Barth B.	Satellites and Their Planets Posters, Thu, p.m., Town Center Exhibit Area
Barthes L.	E/PO: Miscellaneous Posters, Thu, p.m., Town Center Exhibit Area
Barton A.	Mission Plans and Concepts Posters, Tue, p.m., Town Center Exhibit Area
Bartosova K.	Impactite Petrology and Ages Posters, Tue, p.m., Town Center Exhibit Area
Barucci A.	Mission Plans and Concepts Posters, Tue, p.m., Town Center Exhibit Area
Basavaiah N.	Print Only: Impacts
Basilevsky A. T.	Print Only: Moon
Basilevsky A. T. *	Venus, Mon, p.m., Waterway Ballroom 5
Basilevsky A. T.	Lunar Meteorites Posters, Tue, p.m., Town Center Exhibit Area
Basov D.	Laboratory Instruments and Samples Posters, Tue, p.m., Town Center Exhibit Area
Bassim N.	Solar Wind, Volatile Elements, and Organics, Thu, a.m., Waterway Ballroom 1
Bassim N. D.	Stardust Mission to Comet Wild 2, Wed, a.m., Waterway Ballroom 1
Bassler J. A.	Once and Future Moon Posters, Thu, p.m., Town Center Exhibit Area
Bastien R.	Stardust Mission to Comet Wild 2, Wed, a.m., Waterway Ballroom 1
Basu A. R.	Impact Ejecta Posters, Tue, p.m., Town Center Exhibit Area
Basu Sarbadhikari A.	Martian Meteorites Posters, Thu, p.m., Town Center Exhibit Area
Batenburg P.	Mission Plans and Concepts Posters, Tue, p.m., Town Center Exhibit Area
Batenburg P.	Environmental Analogs Posters, Thu, p.m., Town Center Exhibit Area
Bates D.	Spacecraft Instruments Posters, Tue, p.m., Town Center Exhibit Area
Battistelli E.	Spacecraft Instruments Posters, Tue, p.m., Town Center Exhibit Area
Bauch K. E.	Mars: Gullies and Slope Streaks Posters, Thu, p.m., Town Center Exhibit Area
Bauer J. M.	Small Body Missions Posters, Tue, p.m., Town Center Exhibit Area
Bauer J. M.	Characterizing Near-Earth Objects, Thu, p.m., Waterway Ballroom 4
Bauer J. M.	Small Bodies, Fri, p.m., Waterway Ballroom 5
Baur H.	Origins of Presolar Grains, Wed, p.m., Waterway Ballroom 1

Baur H.	Solar Wind, Volatile Elements, and Organics, Thu, a.m., Waterway Ballroom 1
Baur H.	Solar Wind, Volatile Elements, and Organics Posters, Thu, p.m., Town Center Exhibit Area
Bauville A.	Stardust Mission to Comet Wild 2, Wed, a.m., Waterway Ballroom 1
Beaman B.	Spacecraft Instruments Posters, Tue, p.m., Town Center Exhibit Area
Bean K. M.	Planetary Aeolian Processes Posters, Tue, p.m., Town Center Exhibit Area
Bean K. M.	Planetary Atmospheres Posters, Thu, p.m., Town Center Exhibit Area
Beaty D. W.	Mission Plans and Concepts Posters, Tue, p.m., Town Center Exhibit Area
Bebout G. E.	Environmental Analogs Posters, Thu, p.m., Town Center Exhibit Area
Becerra P.	Martian Polar Processes Posters, Tue, p.m., Town Center Exhibit Area
Bechtel H.	Stardust Mission to Comet Wild 2, Wed, a.m., Waterway Ballroom 1
Beck A. W.	Achondrites Posters, Tue, p.m., Town Center Exhibit Area
Beck P. *	Water in the Solar System: Primitive Bodies, Mon, p.m., Waterway Ballroom 6
Beck P.	Thermal and Aqueous Processes on Chondrite Parent Bodies, Fri, a.m., Waterway Ballroom 1
Becker H.	Lunar Petrology and Geochemistry Posters, Tue, p.m., Town Center Exhibit Area
Becker H.	Differentiated Meteorites, Wed, p.m., Waterway Ballroom 4
Becker L.	Impact Ejecta Posters, Tue, p.m., Town Center Exhibit Area
Becker L.	Spacecraft Instruments Posters, Tue, p.m., Town Center Exhibit Area
Becker L.	Mission Plans and Concepts Posters, Tue, p.m., Town Center Exhibit Area
Becker R. H.	Solar Wind, Volatile Elements, and Organics Posters, Thu, p.m., Town Center Exhibit Area
Becker T. L.	Data and Image Systems Posters, Tue, p.m., Town Center Exhibit Area
Becker T. L.	Lunar Cartography, Stereogrammetry, and Imaging Posters, Thu, p.m., Town Center Exhibit Area
Beckett J. R.	Formation of First Solar System Solids, Mon, p.m., Waterway Ballroom 1
Beckett J. R.	Radionuclides and Early Solar System Chronology, Tue, a.m., Waterway Ballroom 1
Beckett J. R.	Formation of First Solar System Solids Posters, Tue, p.m., Town Center Exhibit Area
Beegle L. W.	Laboratory Instruments and Samples Posters, Tue, p.m., Town Center Exhibit Area
Beegle L. W.	Spacecraft Instruments Posters, Tue, p.m., Town Center Exhibit Area
Beehr A.	Martian Alteration Processes Posters, Tue, p.m., Town Center Exhibit Area
Beisser K.	E/PO: Mars Remote Sensing Posters, Thu, p.m., Town Center Exhibit Area
Belcher M. A.	Lunar Dust Posters, Thu, p.m., Town Center Exhibit Area
Bell D. R.	Iron and Stony Iron Meteorites Posters, Tue, p.m., Town Center Exhibit Area
Bell D. R.	Martian Igneous Processes, Fri, a.m., Waterway Ballroom 5
Bell J. III	Planetary Aeolian Processes, Tue, p.m., Waterway Ballroom 4
Bell J. F.	Interior of the Moon, Fri, a.m., Waterway Ballroom 6
Bell J. F. III	Print Only: Mars
Bell J. F. III	A New Moon: Geologic Processes Posters, Tue, p.m., Town Center Exhibit Area
Bell J. F. III	Martian Alteration Processes Posters, Tue, p.m., Town Center Exhibit Area
Bell J. F. III	Planetary Aeolian Processes Posters, Tue, p.m., Town Center Exhibit Area
Bell J. F. III	Spacecraft Instruments Posters, Tue, p.m., Town Center Exhibit Area
Bell J. F. III	A New Moon: Lunar Volcanism, Thu, p.m., Waterway Ballroom 6
Bell J. F. III	Exploring the Martian Crust Posters, Thu, p.m., Town Center Exhibit Area
Bell J. F. III	Mars: Deposition and Erosion, Fri, a.m., Waterway Ballroom 4
Bell M. S.	Environmental Analogs Posters, Thu, p.m., Town Center Exhibit Area
Bell S. W.	Cosmic Dust Posters, Thu, p.m., Town Center Exhibit Area
Bellerose J.	Mission Plans and Concepts Posters, Tue, p.m., Town Center Exhibit Area
Bellucci G.	Print Only: Satellites and Rings
Bellucci G.	Spacecraft Instruments Posters, Tue, p.m., Town Center Exhibit Area
Belskaya I. N.	Print Only: Small Bodies
Belton M.	Mission Plans and Concepts Posters, Tue, p.m., Town Center Exhibit Area
Benavente N.	Environmental Analogs Posters, Thu, p.m., Town Center Exhibit Area
Benbalagh R.	Origins of Presolar Grains Posters, Thu, p.m., Town Center Exhibit Area
Bender S.	Spacecraft Instruments Posters, Tue, p.m., Town Center Exhibit Area
Bendersky C.	Formation of Building Blocks, Fri, p.m., Waterway Ballroom 1
Benecchi S. D.	Main Belt Posters, Tue, p.m., Town Center Exhibit Area
Benedix G. K.	Achondrites Posters, Tue, p.m., Town Center Exhibit Area
Benedix G. K.	Thermal and Aqueous Processes Posters, Thu, p.m., Town Center Exhibit Area
Benedix G. K.	Martian Meteorites Posters, Thu, p.m., Town Center Exhibit Area
Benfield M. P. J.	E/PO: Mission Plans and Concepts Posters, Tue, p.m., Town Center Exhibit Area
Benkhoff J.	Mercury Posters, Tue, p.m., Town Center Exhibit Area
Benkhoff J.	Mission Plans and Concepts Posters, Tue, p.m., Town Center Exhibit Area
Benner L. A. M. *	Characterizing Near-Earth Objects, Thu, p.m., Waterway Ballroom 4
Bennett K. J.	Data and Image Systems Posters, Tue, p.m., Town Center Exhibit Area
Bennett K. J.	Spirit Posters, Thu, p.m., Town Center Exhibit Area
Benning L.	Environmental Analogs Posters, Thu, p.m., Town Center Exhibit Area
Benson S. M.	Print Only: Mars
Bérczi Sz.	Print Only: Impacts
Bérczi Sz.	Print Only: Education and Public Outreach
Bérczi Sz.	Lunar Meteorites Posters, Tue, p.m., Town Center Exhibit Area

Bishop J. L.	Exploring the Martian Crust Posters, Thu, p.m., Town Center Exhibit Area
Bishop J. L.	Mars: Sedimentary Rock Record Posters, Thu, p.m., Town Center Exhibit Area
Bishop J. L.	Mars: Deposition and Erosion, Fri, a.m., Waterway Ballroom 4
Blackburn D. G.	Planetary Atmospheres Posters, Thu, p.m., Town Center Exhibit Area
Blackburn D. G.	Satellites and Their Planets Posters, Thu, p.m., Town Center Exhibit Area
Blackburn D. G.	Planetary Dynamics and Tectonics Posters, Thu, p.m., Town Center Exhibit Area
Blagburn D. J.	Laboratory Instruments and Samples Posters, Tue, p.m., Town Center Exhibit Area
Blair D. M. *	Mercury, Tue, p.m., Montgomery Ballroom
Blake D.	Mission Plans and Concepts Posters, Tue, p.m., Town Center Exhibit Area
Blake D.	Environmental Analogs Posters, Thu, p.m., Town Center Exhibit Area
Blake D. F.	Material Analogs Posters, Tue, p.m., Town Center Exhibit Area
Blake D. F.	Spacecraft Instruments Posters, Tue, p.m., Town Center Exhibit Area
Blake J. B.	Lunar Radiation Posters, Thu, p.m., Town Center Exhibit Area
Blanco A.	Environments for Life Posters, Thu, p.m., Town Center Exhibit Area
Bland M. T. *	Planetary Dynamics and Tectonics, Wed, a.m., Waterway Ballroom 5
Bland P. A.	Achondrites Posters, Tue, p.m., Town Center Exhibit Area
Bland P. A.	Impact Ejecta Posters, Tue, p.m., Town Center Exhibit Area
Bland P. A. *	Differentiated Meteorites, Wed, p.m., Waterway Ballroom 4
Bland P. A.	Chondrites Posters, Thu, p.m., Town Center Exhibit Area
Bland P. A.	Thermal and Aqueous Processes Posters, Thu, p.m., Town Center Exhibit Area
Bland P. A.	Martian Meteorites Posters, Thu, p.m., Town Center Exhibit Area
Blaney D.	Spacecraft Instruments Posters, Tue, p.m., Town Center Exhibit Area
Blank J. G.	Spacecraft Instruments Posters, Tue, p.m., Town Center Exhibit Area
Bleacher J.	Environmental Analogs Posters, Thu, p.m., Town Center Exhibit Area
Bleacher J. E. *	Igneous and Volcanic Processes, Thu, a.m., Waterway Ballroom 5
Bleacher J. E.	Mars: Geologic, Geomorphic, etc., Posters, Thu, p.m., Town Center Exhibit Area
Bleacher J. E.	Igneous and Volcanic Processes Posters, Thu, p.m., Town Center Exhibit Area
Bleacher J. E.	Environmental Analogs Posters, Thu, p.m., Town Center Exhibit Area
Bleacher L. V.	E/PO: Moon Posters, Tue, p.m., Town Center Exhibit Area
Bleamaster L. F.	E/PO: Professional Development Posters, Tue, p.m., Town Center Exhibit Area
Bleamaster L. F.	Planetary Dynamics and Tectonics Posters, Thu, p.m., Town Center Exhibit Area
Bleamaster L. F. III	Venus Posters, Tue, p.m., Town Center Exhibit Area
Bleamaster L. F. III	E/PO: Professional Development Posters, Tue, p.m., Town Center Exhibit Area
Bleamaster L. F. III	Mars: Geologic, Geomorphic, etc., Posters, Thu, p.m., Town Center Exhibit Area
Bleuet P.	Stardust Mission to Comet Wild 2, Wed, a.m., Waterway Ballroom 1
Blewett D.	A New Moon: Spectral Constraints Posters, Thu, p.m., Town Center Exhibit Area
Blewett D. T.	Mercury, Tue, p.m., Montgomery Ballroom
Blewett D. T.	Main Belt Posters, Tue, p.m., Town Center Exhibit Area
Blewett D. T.	Mercury Posters, Tue, p.m., Town Center Exhibit Area
Blewett D. T.	Material Analogs Posters, Tue, p.m., Town Center Exhibit Area
Blewett D. T.	A New Moon: Spectral Constraints Posters, Thu, p.m., Town Center Exhibit Area
Blichert-Toft J.	Iron and Stony Iron Meteorites Posters, Tue, p.m., Town Center Exhibit Area
Blinova A.	Thermal and Aqueous Processes Posters, Thu, p.m., Town Center Exhibit Area
Blom J. K.	Mission Plans and Concepts Posters, Tue, p.m., Town Center Exhibit Area
Blom J. K.	Environmental Analogs Posters, Thu, p.m., Town Center Exhibit Area
Blome H.-J.	Mission Plans and Concepts Posters, Tue, p.m., Town Center Exhibit Area
Blue J.	Data and Image Systems Posters, Tue, p.m., Town Center Exhibit Area
Blumers M.	Spacecraft Instruments Posters, Tue, p.m., Town Center Exhibit Area
Blundy J.	Petrologic Characterization of the Moon, Fri, p.m., Waterway Ballroom 6
Boardman J.	Water in the Solar System: Moon, Tue, p.m., Waterway Ballroom 6
Boardman J.	A New Moon: Spectral Constraints, Wed, p.m., Waterway Ballroom 6
Boardman J.	Large Impact Basins on the Moon, Thu, a.m., Waterway Ballroom 6
Boardman J.	A New Moon: Lunar Volcanism, Thu, p.m., Waterway Ballroom 6
Boardman J.	A New Moon: Spectral Constraints Posters, Thu, p.m., Town Center Exhibit Area
Boardman J.	Petrologic Characterization of the Moon, Fri, p.m., Waterway Ballroom 6
Boardman J. W.	A New Moon: Spectral Constraints Posters, Thu, p.m., Town Center Exhibit Area
Boardman J. W.	Petrologic Characterization of the Moon, Fri, p.m., Waterway Ballroom 6
Boccaccini A.	Spacecraft Instruments Posters, Tue, p.m., Town Center Exhibit Area
Boche-Sauvan L.	Mission Plans and Concepts Posters, Tue, p.m., Town Center Exhibit Area
Boche-Sauvan L.	Environmental Analogs Posters, Thu, p.m., Town Center Exhibit Area
Boche-Sauvan L.	Mission Plans and Concepts Posters, Tue, p.m., Town Center Exhibit Area
Boche-Sauvan L.	Environmental Analogs Posters, Thu, p.m., Town Center Exhibit Area
Bochsler P.	Solar Wind, Volatile Elements, and Organics Posters, Thu, p.m., Town Center Exhibit Area
Bodnarik J.	Spacecraft Instruments Posters, Tue, p.m., Town Center Exhibit Area
Boehm E.	Spacecraft Instruments Posters, Tue, p.m., Town Center Exhibit Area
Boehnhardt H.	Small Body Missions Posters, Tue, p.m., Town Center Exhibit Area
Boesenberg J. S.	Laboratory Instruments and Samples Posters, Tue, p.m., Town Center Exhibit Area

Castillo-Rogez J. C. *	Small Bodies, Fri, p.m., Waterway Ballroom 5
Castro-Tirado A. J.	Print Only: Small Bodies
Catalano J.	Martian Alteration Processes Posters, Tue, p.m., Town Center Exhibit Area
Catling D.	Planetary Atmospheres, Wed, p.m., Montgomery Ballroom
Catling D. C.	Martian Alteration Processes, Mon, a.m., Waterway Ballroom 4
Catling D. C.	Martian Alteration Processes Posters, Tue, p.m., Town Center Exhibit Area
Catling D. C.	Mars: Sedimentary Rock Record Posters, Thu, p.m., Town Center Exhibit Area
Caudill C.	Impacts on the Moon, Mars, and Beyond, Wed, p.m., Waterway Ballroom 5
Caudill C.	Mars Craters Posters, Thu, p.m., Town Center Exhibit Area
Cernogora G.	Planetary Atmospheres Posters, Thu, p.m., Town Center Exhibit Area
Cerroni P.	Spacecraft Instruments Posters, Tue, p.m., Town Center Exhibit Area
Cerroni P.	Several Species of Icy Chunks, Thu, p.m., Waterway Ballroom 5
Cerroni P.	Satellites and Their Planets Posters, Thu, p.m., Town Center Exhibit Area
Cetina C.	Solar Wind, Volatile Elements, and Organics Posters, Thu, p.m., Town Center Exhibit Area
Ceuleneer G.	Exploring the Martian Crust Posters, Thu, p.m., Town Center Exhibit Area
Chabot N. L. *	Planetary Differentiation, Mon, a.m., Waterway Ballroom 5
Chabot N. L.	Mercury Posters, Tue, p.m., Town Center Exhibit Area
Chadwick D. J.	Planetary Dynamics and Tectonics Posters, Thu, p.m., Town Center Exhibit Area
Chakrabarti R. *	Radionuclides and Early Solar System Chronology, Tue, a.m., Waterway Ballroom 1
Chakrabarti R.	Impact Ejecta Posters, Tue, p.m., Town Center Exhibit Area
Chakrabarti R.	Impactite Petrology and Ages Posters, Tue, p.m., Town Center Exhibit Area
Chakrabarti R.	Lunar Origins and Chronology Posters, Tue, p.m., Town Center Exhibit Area
Chakraborty M.	A New Moon: Lunar Volcanism, Thu, p.m., Waterway Ballroom 6
Chakraborty S. *	Parent Cloud and Solar Nebula, Mon, a.m., Waterway Ballroom 1
Chakroborty S.	Print Only: Impacts
Chambers L.	E/PO: Professional Development Posters, Tue, p.m., Town Center Exhibit Area
Chan E.	Rocks, Life, and Biosignatures, Thu, p.m., Waterway Ballroom 1
Chan M. A.	Environmental Analogs Posters, Thu, p.m., Town Center Exhibit Area
Chandler J.	A New Moon: Geologic Processes Posters, Tue, p.m., Town Center Exhibit Area
Chang J.	A New Moon: LCROSS, Chandrayaan, Chang'E, Tue, a.m., Waterway Ballroom 6
Chang X.	Lunar Cartography, Stereogrammetry, and Imaging Posters, Thu, p.m., Town Center Exhibit Area
Changela H. G.	Martian Alteration Processes Posters, Tue, p.m., Town Center Exhibit Area
Changela H. G.	Stardust Mission to Comet Wild 2, Wed, a.m., Waterway Ballroom 1
Channon M. B. *	Martian Igneous Processes, Fri, a.m., Waterway Ballroom 5
Chanover N. J.	Spacecraft Instruments Posters, Tue, p.m., Town Center Exhibit Area
Chapman C. R.	Mercury, Tue, p.m., Montgomery Ballroom
Chapman C. R.	Lunar Cartography, Stereogrammetry, and Imaging Posters, Thu, p.m., Town Center Exhibit Area
Chappelow J. E.	Impacts Modeling Posters, Tue, p.m., Town Center Exhibit Area
Charlier B.	Lunar Petrology and Geochemistry Posters, Tue, p.m., Town Center Exhibit Area
Chater R. J.	Stardust Mission Posters, Thu, p.m., Town Center Exhibit Area
Chauhan P.	A New Moon: Spectral Constraints Posters, Thu, p.m., Town Center Exhibit Area
Chaussidon M.	Radionuclides and Early Solar System Chronology Posters, Tue, p.m., Town Center Exhibit Area
Chaussidon M.	Formation of Building Blocks Posters, Thu, p.m., Town Center Exhibit Area
Che C. *	Experimental Constraints on Martian Alteration Processes, Mon, p.m., Waterway Ballroom 4
Cheek L.	Large Impact Basins on the Moon, Thu, a.m., Waterway Ballroom 6
Cheek L. C.	A New Moon: Spectral Constraints Posters, Thu, p.m., Town Center Exhibit Area
ChemCam Team	Spacecraft Instruments Posters, Tue, p.m., Town Center Exhibit Area
Chemtob S.	Spacecraft Instruments Posters, Tue, p.m., Town Center Exhibit Area
Chemtob S. M.	Spacecraft Instruments Posters, Tue, p.m., Town Center Exhibit Area
Chen B.	Planetary Differentiation, Mon, a.m., Waterway Ballroom 5
Chen C. H.	BOOM! Posters, Thu, p.m., Town Center Exhibit Area
Chen E. M. A. *	Several Species of Icy Chunks, Thu, p.m., Waterway Ballroom 5
Chen H. W.	Formation of First Solar System Solids Posters, Tue, p.m., Town Center Exhibit Area
Chen J. C.	Formation of First Solar System Solids Posters, Tue, p.m., Town Center Exhibit Area
Chen J. H.	Parent Cloud and Solar Nebula, Mon, a.m., Waterway Ballroom 1
Chen J. H.	Planetary Differentiation, Mon, a.m., Waterway Ballroom 5
Chen J. H.	Isotopes and REEs Posters, Tue, p.m., Town Center Exhibit Area
Chen S. B.*	Nature of the Lunar Regolith, Wed, a.m., Waterway Ballroom 6
Chen Y.	Lunar Cartography, Stereogrammetry, and Imaging Posters, Thu, p.m., Town Center Exhibit Area
Cheng A. F. *	Characterizing Near-Earth Objects, Thu, p.m., Waterway Ballroom 4
Cheng A. F. *	Satellites and Their Planets Posters, Thu, p.m., Town Center Exhibit Area
Chennaoui Aoudjehane H.	Martian Meteorites Posters, Thu, p.m., Town Center Exhibit Area
Chesley S.	Mission Plans and Concepts Posters, Tue, p.m., Town Center Exhibit Area
Chevrier S.	Mission Plans and Concepts Posters, Tue, p.m., Town Center Exhibit Area
Chevrier S.	Environmental Analogs Posters, Thu, p.m., Town Center Exhibit Area
Chevrier V. *	Experimental Constraints on Martian Alteration Processes, Mon, p.m., Waterway Ballroom 4
Chevrier V.	Impact Experiments Posters, Tue, p.m., Town Center Exhibit Area

Cohen B. A.	Environmental Analogs Posters, Thu, p.m., Town Center Exhibit Area
Coker R. F.	Once and Future Moon Posters, Thu, p.m., Town Center Exhibit Area
Colangeli L.	Martian Alteration Processes Posters, Tue, p.m., Town Center Exhibit Area
Colangeli L.	Exploring the Martian Crust Posters, Thu, p.m., Town Center Exhibit Area
Colaprete A.	Print Only: Moon
Colaprete A. *	A New Moon: LCROSS, Chandrayaan, Chang'E, Tue, a.m., Waterway Ballroom 6
Colaprete A.	A New Moon: LCROSS Posters, Tue, p.m., Town Center Exhibit Area
Colaprete A.	Mission Plans and Concepts Posters, Tue, p.m., Town Center Exhibit Area
Colaprete A.	Once and Future Moon Posters, Thu, p.m., Town Center Exhibit Area
Colaprete T.	A New Moon: LCROSS, Chandrayaan, Chang'E, Tue, a.m., Waterway Ballroom 6
Cole M. J.	Impact Models and More, Tue, p.m., Waterway Ballroom 5
Cole M. J.	Stardust Mission to Comet Wild 2, Wed, a.m., Waterway Ballroom 1
Cole M. J.	Stardust Mission Posters, Thu, p.m., Town Center Exhibit Area
Coleman K. A.	Mars: Gullies and Slope Streaks Posters, Thu, p.m., Town Center Exhibit Area
Coleman M. L.	Environments for Life Posters, Thu, p.m., Town Center Exhibit Area
Coleman N.	Print Only: Mars
Coleman S. J.	Planetary Aeolian Processes Posters, Tue, p.m., Town Center Exhibit Area
Coll P.	Spacecraft Instruments Posters, Tue, p.m., Town Center Exhibit Area
Collier M. R.	Lunar Dust Posters, Thu, p.m., Town Center Exhibit Area
Collins G. C.	Planetary Dynamics and Tectonics, Wed, a.m., Waterway Ballroom 5
Collins G. C.	Planetary Dynamics and Tectonics Posters, Thu, p.m., Town Center Exhibit Area
Collins G. S.	Impacts Modeling Posters, Tue, p.m., Town Center Exhibit Area
Collins G. S.	Large Impact Basins on the Moon, Thu, a.m., Waterway Ballroom 6
Collins G. S.	Thermal and Aqueous Processes on Chondrite Parent Bodies, Fri, a.m., Waterway Ballroom 1
Collins L.	Spacecraft Instruments Posters, Tue, p.m., Town Center Exhibit Area
Coman E. I.	A New Moon: Spectral Constraints Posters, Thu, p.m., Town Center Exhibit Area
Combe J. P.	A New Moon: Spectral Constraints Posters, Thu, p.m., Town Center Exhibit Area
Combe J. P.	Petrologic Characterization of the Moon, Fri, p.m., Waterway Ballroom 6
Combe J.-P.	Martian Alteration Processes, Mon, a.m., Waterway Ballroom 4
Combe J.-P.	Large Impact Basins on the Moon, Thu, a.m., Waterway Ballroom 6
Combe J.-P.	A New Moon: Spectral Constraints Posters, Thu, p.m., Town Center Exhibit Area
Combe J.-Ph.	Water in the Solar System: Moon, Tue, p.m., Waterway Ballroom 6
Combe J.-Ph.	A New Moon: Spectral Constraints Posters, Thu, p.m., Town Center Exhibit Area
Combe J-Ph.	A New Moon: Spectral Constraints, Wed, p.m., Waterway Ballroom 6
Conlon L.	BOOM! Posters, Thu, p.m., Town Center Exhibit Area
Connell J. W.	Lunar Dust Posters, Thu, p.m., Town Center Exhibit Area
Connelly J. N.	Lunar Origins and Chronology Posters, Tue, p.m., Town Center Exhibit Area
Connolly H. C. Jr	Formation of First Solar System Solids Posters, Tue, p.m., Town Center Exhibit Area
Connolly H. C. Jr.	Formation of First Solar System Solids, Mon, p.m., Waterway Ballroom 1
Connolly H. C. Jr.*	Radionuclides and Early Solar System Chronology, Tue, a.m., Waterway Ballroom 1
Connolly H. C. Jr.	Formation of First Solar System Solids Posters, Tue, p.m., Town Center Exhibit Area
Connolly H. C. Jr.	Formation of Building Blocks, Fri, p.m., Waterway Ballroom 1
Conrad A. R.	Lunar Cartography, Stereogrammetry, and Imaging Posters, Thu, p.m., Town Center Exhibit Area
Conrad P.	Environmental Analogs Posters, Thu, p.m., Town Center Exhibit Area
Conrad P. G.	Spacecraft Instruments Posters, Tue, p.m., Town Center Exhibit Area
Consolmagno G. J.	Lunar Geophysics Posters, Thu, p.m., Town Center Exhibit Area
Consolmagno G. J.	Small Bodies, Fri, p.m., Waterway Ballroom 5
Conway S. J.	Mars: Gullies and Slope Streaks Posters, Thu, p.m., Town Center Exhibit Area
Cook D.	Lunar Cartography, Stereogrammetry, and Imaging Posters, Thu, p.m., Town Center Exhibit Area
Cook D. L.	Iron and Stony Iron Meteorites Posters, Tue, p.m., Town Center Exhibit Area
Cook M.	Impact Experiments Posters, Tue, p.m., Town Center Exhibit Area
Cook T. S.	Mission Plans and Concepts Posters, Tue, p.m., Town Center Exhibit Area
Cooke A.	Formation of Building Blocks Posters, Thu, p.m., Town Center Exhibit Area
Cooper B. L.	Lunar Dust Posters, Thu, p.m., Town Center Exhibit Area
Cooper B. L.	Lunar Regolith Posters, Thu, p.m., Town Center Exhibit Area
Cooper F. J.	Ground Truth Galore: Terrestrial Impact Craters, Tue, a.m., Waterway Ballroom 5
Cooper F. J.	Impactite Petrology and Ages Posters, Tue, p.m., Town Center Exhibit Area
Cooper L.	Spacecraft Instruments Posters, Tue, p.m., Town Center Exhibit Area
Cooper R.	A New Moon: Spectral Constraints Posters, Thu, p.m., Town Center Exhibit Area
Coradini A.	Print Only: Small Bodies
Coradini A.	Water in the Solar System: Primitive Bodies, Mon, p.m., Waterway Ballroom 6
Coradini A.	Spacecraft Instruments Posters, Tue, p.m., Town Center Exhibit Area
Coradini A.	Characterizing Near-Earth Objects, Thu, p.m., Waterway Ballroom 4
Coradini A.	Several Species of Icy Chunks, Thu, p.m., Waterway Ballroom 5
Coradini A.	Satellites and Their Planets Posters, Thu, p.m., Town Center Exhibit Area
Corbell C.	Spacecraft Instruments Posters, Tue, p.m., Town Center Exhibit Area
Cordier C.	Achondrites Posters, Tue, p.m., Town Center Exhibit Area

Cornell J. W.	Material Analogs Posters, Tue, p.m., Town Center Exhibit Area
Cornen G.	Chondrites Posters, Thu, p.m., Town Center Exhibit Area
Cornet T.	Satellites and Their Planets Posters, Thu, p.m., Town Center Exhibit Area
Cornish T.	Spacecraft Instruments Posters, Tue, p.m., Town Center Exhibit Area
Cornwall C.	Mars Ice and Craters Posters, Tue, p.m., Town Center Exhibit Area
Corrigan C. M.	Spacecraft Instruments Posters, Tue, p.m., Town Center Exhibit Area
Corrigan C. M.	Chondrites Posters, Thu, p.m., Town Center Exhibit Area
Corsaro R. D.	Once and Future Moon Posters, Thu, p.m., Town Center Exhibit Area
Cortés J.	Print Only: Small Bodies
Cosarinsky M.	Cosmic-Ray Exposure Dating Posters, Tue, p.m., Town Center Exhibit Area
Costard F.	Terrestrial Planet Cryospheres, Tue, a.m., Waterway Ballroom 4
Cotter R.	Spacecraft Instruments Posters, Tue, p.m., Town Center Exhibit Area
Cottin H.	Material Analogs Posters, Tue, p.m., Town Center Exhibit Area
Cottingham C.	BOOM! Posters, Thu, p.m., Town Center Exhibit Area
Cottrell R. D.	Iron and Stony Iron Meteorites Posters, Tue, p.m., Town Center Exhibit Area
Cousin A.	Spacecraft Instruments Posters, Tue, p.m., Town Center Exhibit Area
Cousins C. R.	Once and Future Moon Posters, Thu, p.m., Town Center Exhibit Area
Craddock P. R.	Lunar Petrology and Geochemistry Posters, Tue, p.m., Town Center Exhibit Area
Craddock R. A.	Planetary Aeolian Processes Posters, Tue, p.m., Town Center Exhibit Area
Craddock R. A.	Mars: Fluvial Geomorphology and Processes, Thu, a.m., Waterway Ballroom 4
Craddock R. A.	Igneous and Volcanic Processes Posters, Thu, p.m., Town Center Exhibit Area
Craft J.	Spacecraft Instruments Posters, Tue, p.m., Town Center Exhibit Area
Craft K.	Planetary Dynamics and Tectonics Posters, Thu, p.m., Town Center Exhibit Area
Craig J. P.	Cosmic Dust Posters, Thu, p.m., Town Center Exhibit Area
Craig J. P.	Chondrites Posters, Thu, p.m., Town Center Exhibit Area
Craig M. A.	Impact Experiments Posters, Tue, p.m., Town Center Exhibit Area
CRaTER Science Team	A New Moon: LRO Results, Mon, a.m., Waterway Ballroom 6
Crawford D. A.	Lunar Origins and Chronology Posters, Tue, p.m., Town Center Exhibit Area
Crawford I. A.	Lunar Petrology and Geochemistry Posters, Tue, p.m., Town Center Exhibit Area
Crawford I. A.	Lunar Meteorites Posters, Tue, p.m., Town Center Exhibit Area
Crawford I. A.	Lunar Petrology and Geochemistry Posters, Tue, p.m., Town Center Exhibit Area
Crawford I. A.	Once and Future Moon Posters, Thu, p.m., Town Center Exhibit Area
Cremonese G.	Mercury, Tue, p.m., Montgomery Ballroom
Cressey G.	Impact Ejecta Posters, Tue, p.m., Town Center Exhibit Area
Cressey G.	Thermal and Aqueous Processes Posters, Thu, p.m., Town Center Exhibit Area
CRISM Science Team	Mars: Sedimentary Rock Record Posters, Thu, p.m., Town Center Exhibit Area
CRISM Team	Martian Alteration Processes, Mon, a.m., Waterway Ballroom 4
CRISM Team	Exploring the Martian Crust Posters, Thu, p.m., Town Center Exhibit Area
Crisp J.	Spacecraft Instruments Posters, Tue, p.m., Town Center Exhibit Area
Croat T. K. *	Origins of Presolar Grains, Wed, p.m., Waterway Ballroom 1
Croat T. K.	Origins of Presolar Grains Posters, Thu, p.m., Town Center Exhibit Area
Croft S. K.	E/PO: Impacts Posters, Tue, p.m., Town Center Exhibit Area
Croft S. K.	E/PO: Professional Development Posters, Tue, p.m., Town Center Exhibit Area
Cronenberger J. O.	Mission Plans and Concepts Posters, Tue, p.m., Town Center Exhibit Area
Crósta A. P.	Impact Craters Posters, Tue, p.m., Town Center Exhibit Area
Crotts A. P. S.	A New Moon: Volatile Species Posters, Tue, p.m., Town Center Exhibit Area
Crowley J. F.	Exploring the Martian Crust Posters, Thu, p.m., Town Center Exhibit Area
Crowley J. K.	Martian Alteration Processes Posters, Tue, p.m., Town Center Exhibit Area
Crowley J. K.	Material Analogs Posters, Tue, p.m., Town Center Exhibit Area
Crown D. A.	E/PO: Professional Development Posters, Tue, p.m., Town Center Exhibit Area
Crown D. A.	Mars: Geologic, Geomorphic, etc., Posters, Thu, p.m., Town Center Exhibit Area
Crown D. A.	Mars Craters Posters, Thu, p.m., Town Center Exhibit Area
Crown D. A.	Igneous and Volcanic Processes Posters, Thu, p.m., Town Center Exhibit Area
Crowther S. A.	Cosmic Dust, Thu, p.m., Waterway Ballroom 1
Crowther S. A.	Solar Wind, Volatile Elements, and Organics Posters, Thu, p.m., Town Center Exhibit Area
Crow-Willard E. N.	Satellites and Their Planets Posters, Thu, p.m., Town Center Exhibit Area
Cruikshank D. P.	Satellites and Their Planets Posters, Thu, p.m., Town Center Exhibit Area
Crumpler L. *	Exploring the Martian Crust, Wed, a.m., Waterway Ballroom 4
Crumpler L.	Spirit Posters, Thu, p.m., Town Center Exhibit Area
Crumpler L. S.	Igneous and Volcanic Processes, Thu, a.m., Waterway Ballroom 5
Crumpler L. S.	Spirit Posters, Thu, p.m., Town Center Exhibit Area
Cseh R.	E/PO: Miscellaneous Posters, Thu, p.m., Town Center Exhibit Area
Cuadros J.	Martian Alteration Processes Posters, Tue, p.m., Town Center Exhibit Area
Cui H. Y.	A New Moon: LCROSS, Chandrayaan, Chang'E, Tue, a.m., Waterway Ballroom 6
Cull S. C.	Exploring the Martian Crust Posters, Thu, p.m., Town Center Exhibit Area
Currie D. G.	Once and Future Moon Posters, Thu, p.m., Town Center Exhibit Area
Currit C.	Mars: Gullies and Slope Streaks Posters, Thu, p.m., Town Center Exhibit Area

Day J. M. D.	Lunar Petrology and Geochemistry Posters, Tue, p.m., Town Center Exhibit Area
Day J. M. D. *	Differentiated Meteorites, Wed, p.m., Waterway Ballroom 4
Day J. M. D.	Martian Igneous Processes, Fri, a.m., Waterway Ballroom 5
Daydou Y.	Exploring the Martian Crust Posters, Thu, p.m., Town Center Exhibit Area
De Angelis G.	Lunar Radiation Posters, Thu, p.m., Town Center Exhibit Area
De Gregorio B. T. *	Solar Wind, Volatile Elements, and Organics, Thu, a.m., Waterway Ballroom 1
de Leeuw N. H.	Water in the Solar System: Primitive Bodies, Mon, p.m., Waterway Ballroom 6
De Leon P.	E/PO: Environmental Analogs Posters, Thu, p.m., Town Center Exhibit Area
de Leuw S.	Parent Cloud and Solar Nebula, Mon, a.m., Waterway Ballroom 1
de Lophem T-L.	Small Body Missions Posters, Tue, p.m., Town Center Exhibit Area
de Pablo M. A.	Print Only: Mars
de Raucourt S.	Spacecraft Instruments Posters, Tue, p.m., Town Center Exhibit Area
De Sanctis M. C.	Print Only: Small Bodies
De Sanctis M. C.	Water in the Solar System: Primitive Bodies, Mon, p.m., Waterway Ballroom 6
De Sanctis M. C. *	Mercury, Tue, p.m., Montgomery Ballroom
De Sanctis M. C.	Spacecraft Instruments Posters, Tue, p.m., Town Center Exhibit Area
De Sanctis M. C.	Characterizing Near-Earth Objects, Thu, p.m., Waterway Ballroom 4
de Souza P.	Spirit Posters, Thu, p.m., Town Center Exhibit Area
de Souza Filho C. R.	Exploring the Martian Crust Posters, Thu, p.m., Town Center Exhibit Area
de Wet A. P.	Igneous and Volcanic Processes, Thu, a.m., Waterway Ballroom 5
Deák M.	Print Only: Mars
Deans M. C.	Once and Future Moon Posters, Thu, p.m., Town Center Exhibit Area
Deardorff D. G.	E/PO: Mars Remote Sensing Posters, Thu, p.m., Town Center Exhibit Area
Dearholt W. R.	BOOM! Posters, Thu, p.m., Town Center Exhibit Area
Debei S.	Spacecraft Instruments Posters, Tue, p.m., Town Center Exhibit Area
Deepak D.	A New Moon: Lunar Volcanism, Thu, p.m., Waterway Ballroom 6
DeFlores L.	Spacecraft Instruments Posters, Tue, p.m., Town Center Exhibit Area
Defouilloy C.	Iron and Stony Iron Meteorites Posters, Tue, p.m., Town Center Exhibit Area
DeGregorio B. T.	Stardust Mission Posters, Thu, p.m., Town Center Exhibit Area
deHoog B.	Stardust Mission Posters, Thu, p.m., Town Center Exhibit Area
Dehouck E.	Experimental Constraints on Martian Alteration Processes, Mon, p.m., Waterway Ballroom 4
Dehouck E.	Martian Alteration Processes Posters, Tue, p.m., Town Center Exhibit Area
DeJong E. M.	A New Moon: LRO Results, Mon, a.m., Waterway Ballroom 6
Delaney J. S.	Achondrites Posters, Tue, p.m., Town Center Exhibit Area
Delaney J. S.	Cosmic Dust Posters, Thu, p.m., Town Center Exhibit Area
Delano J. W.	Environments for Life Posters, Thu, p.m., Town Center Exhibit Area
Delbó M.	Small Body Missions Posters, Tue, p.m., Town Center Exhibit Area
Dell'Agnello S.	Once and Future Moon Posters, Thu, p.m., Town Center Exhibit Area
Delle Monache G.	Once and Future Moon Posters, Thu, p.m., Town Center Exhibit Area
Delory G. T.	Water in the Solar System: Moon, Tue, p.m., Waterway Ballroom 6
Delory G. T.	Lunar Dust Posters, Thu, p.m., Town Center Exhibit Area
Delory G. T.	Once and Future Moon Posters, Thu, p.m., Town Center Exhibit Area
DeMeo F. E.	Characterizing Near-Earth Objects, Thu, p.m., Waterway Ballroom 4
Demidov N.	A New Moon: Volatile Species Posters, Tue, p.m., Town Center Exhibit Area
Demoranville L. T.	Solar Wind, Volatile Elements, and Organics Posters, Thu, p.m., Town Center Exhibit Area
Demura H.	A New Moon: Geologic Processes Posters, Tue, p.m., Town Center Exhibit Area
Demura H.	Data and Image Systems Posters, Tue, p.m., Town Center Exhibit Area
Demura H.	A New Moon: Lunar Volcanism, Thu, p.m., Waterway Ballroom 6
Demura H.	A New Moon: Spectral Constraints Posters, Thu, p.m., Town Center Exhibit Area
Demura H.	Lunar Cartography, Stereogrammetry, and Imaging Posters, Thu, p.m., Town Center Exhibit Area
Dene A.	Mission Plans and Concepts Posters, Tue, p.m., Town Center Exhibit Area
Denevi B.	A New Moon: Geologic Processes Posters, Tue, p.m., Town Center Exhibit Area
Denevi B. W.	Mercury, Tue, p.m., Montgomery Ballroom
Denevi B. W.	A New Moon: Geologic Processes Posters, Tue, p.m., Town Center Exhibit Area
Denevi B. W.	Mercury Posters, Tue, p.m., Town Center Exhibit Area
Denevi B. W.	A New Moon: Lunar Volcanism, Thu, p.m., Waterway Ballroom 6
Denevi B. W.	A New Moon: Spectral Constraints Posters, Thu, p.m., Town Center Exhibit Area
Denk T.	Impacts on the Moon, Mars, and Beyond, Wed, p.m., Waterway Ballroom 5
Denk T.	Satellites and Their Planets Posters, Thu, p.m., Town Center Exhibit Area
Denk T.	Planetary Dynamics and Tectonics Posters, Thu, p.m., Town Center Exhibit Area
Denneau L.	Small Body Missions Posters, Tue, p.m., Town Center Exhibit Area
DePaolo D.	Martian Meteorites Posters, Thu, p.m., Town Center Exhibit Area
DePaolo D. J.	Isotopes and REEs Posters, Tue, p.m., Town Center Exhibit Area
DePaolo D. J.	Formation of First Solar System Solids Posters, Tue, p.m., Town Center Exhibit Area
Derenne S.	Solar Wind, Volatile Elements, and Organics, Thu, a.m., Waterway Ballroom 1
Derenne S.	Solar Wind, Volatile Elements, and Organics Posters, Thu, p.m., Town Center Exhibit Area
Desch S.	Satellites and Their Planets Posters, Thu, p.m., Town Center Exhibit Area

Dyar M. D. *	Water in the Solar System: Primitive Bodies, Mon, p.m., Waterway Ballroom 6
Dyar M. D.	Water in the Solar System: Moon, Tue, p.m., Waterway Ballroom 6
Dyar M. D.	Venus Posters, Tue, p.m., Town Center Exhibit Area
Dyar M. D.	Spacecraft Instruments Posters, Tue, p.m., Town Center Exhibit Area
Dyar M. D.	Ice and Dust Posters, Thu, p.m., Town Center Exhibit Area
Dyar M. D.	Mars: Gullies and Slope Streaks Posters, Thu, p.m., Town Center Exhibit Area
Dyar M. D.	Exploring the Martian Crust Posters, Thu, p.m., Town Center Exhibit Area
Dyl K. A. *	Formation of First Solar System Solids, Mon, p.m., Waterway Ballroom 1
Dypvik H.	Ground Truth Galore: Terrestrial Impact Craters, Tue, a.m., Waterway Ballroom 5
Dypvik H.	Impactite Petrology and Ages Posters, Tue, p.m., Town Center Exhibit Area
Eastwood M.	A New Moon: Spectral Constraints Posters, Thu, p.m., Town Center Exhibit Area
Ebata S.	Solar Wind, Volatile Elements, and Organics Posters, Thu, p.m., Town Center Exhibit Area
Ebel D.	Ice and Dust Posters, Thu, p.m., Town Center Exhibit Area
Ebel D.	Formation of Building Blocks, Fri, p.m., Waterway Ballroom 1
Ebel D. S.	Planetary Differentiation, Mon, a.m., Waterway Ballroom 5
Ebel D. S.	Laboratory Instruments and Samples Posters, Tue, p.m., Town Center Exhibit Area
Ebel D. S.	Formation of First Solar System Solids Posters, Tue, p.m., Town Center Exhibit Area
Ebel D. S.	Stardust Mission Posters, Thu, p.m., Town Center Exhibit Area
Ebel D. S.	Formation of Building Blocks Posters, Thu, p.m., Town Center Exhibit Area
Ebel D. S.	Formation of Building Blocks, Fri, p.m., Waterway Ballroom 1
Ebihara M.	Differentiated Meteorites, Wed, p.m., Waterway Ballroom 4
Ecelberger S. A.	Spacecraft Instruments Posters, Tue, p.m., Town Center Exhibit Area
Eckert-Erdheim A. M.	Igneous and Volcanic Processes Posters, Thu, p.m., Town Center Exhibit Area
Economou T.	Exploring the Martian Crust, Wed, a.m., Waterway Ballroom 4
Economou T. E.	Planetary Atmospheres Posters, Thu, p.m., Town Center Exhibit Area
Edgar L. A. *	Planetary Aeolian Processes, Tue, p.m., Waterway Ballroom 4
Edgett K. S.	Print Only: Mars
Edmundson K.	Lunar Cartography, Stereogrammetry, and Imaging Posters, Thu, p.m., Town Center Exhibit Area
Edmunson J.	Laboratory Instruments and Samples Posters, Tue, p.m., Town Center Exhibit Area
Edmunson J.	Lunar Petrology and Geochemistry Posters, Tue, p.m., Town Center Exhibit Area
Edwards B. R.	Exploring the Martian Crust, Wed, a.m., Waterway Ballroom 4
Edwards C. S.	Exploring the Martian Crust Posters, Thu, p.m., Town Center Exhibit Area
Edwards J.	Environmental Analogs Posters, Thu, p.m., Town Center Exhibit Area
Edwards L. J.	Print Only: Mars
Edwards W.	Chondrites Posters, Thu, p.m., Town Center Exhibit Area
Egan A.	A New Moon: LCROSS Posters, Tue, p.m., Town Center Exhibit Area
Ehlmann B. L. *	Exploring the Martian Crust, Wed, a.m., Waterway Ballroom 4
Ehlmann B. L.	Environmental Analogs Posters, Thu, p.m., Town Center Exhibit Area
Ehrenfreund P.	Mission Plans and Concepts Posters, Tue, p.m., Town Center Exhibit Area
Ehrenfreund P.	Environmental Analogs Posters, Thu, p.m., Town Center Exhibit Area
Ehresmann B.	Spacecraft Instruments Posters, Tue, p.m., Town Center Exhibit Area
Eigenbrode J. L.	Material Analogs Posters, Tue, p.m., Town Center Exhibit Area
Eigenbrode J. L.	Spacecraft Instruments Posters, Tue, p.m., Town Center Exhibit Area
Eiler J.	Water in the Solar System: Moon, Tue, p.m., Waterway Ballroom 6
Eiler J.	Solar Wind, Volatile Elements, and Organics, Thu, a.m., Waterway Ballroom 1
Eiler J. M.	Isotopes and REEs Posters, Tue, p.m., Town Center Exhibit Area
Eiler J. M.	Martian Igneous Processes, Fri, a.m., Waterway Ballroom 5
Eke V. R.	Water in the Solar System: Moon, Tue, p.m., Waterway Ballroom 6
Eke V. R.	Mars Remote Sensing Techniques Posters, Thu, p.m., Town Center Exhibit Area
El Maarry M. R. *	Mars: Fluvial Geomorphology and Processes, Thu, a.m., Waterway Ballroom 4
Elam J.	Origins of Presolar Grains Posters, Thu, p.m., Town Center Exhibit Area
Elardo S. M. *	Petrologic Characterization of the Moon, Fri, p.m., Waterway Ballroom 6
Elder C. M. *	Impact Models and More, Tue, p.m., Waterway Ballroom 5
Eldridge D. L.	Print Only: Moon
Eldridge D. L.	A New Moon: Geologic Processes Posters, Tue, p.m., Town Center Exhibit Area
Eldridge D. L.	Once and Future Moon Posters, Thu, p.m., Town Center Exhibit Area
Eldridge D. L.	Environmental Analogs Posters, Thu, p.m., Town Center Exhibit Area
Elfes A.	Once and Future Moon Posters, Thu, p.m., Town Center Exhibit Area
Eliason E. M.	A New Moon: LRO Results, Mon, a.m., Waterway Ballroom 6
Elis V. R.	Impact Models and More, Tue, p.m., Waterway Ballroom 5
Elkins-Tanton L. T.	Planetary Differentiation, Mon, a.m., Waterway Ballroom 5
Elkins-Tanton L. T. *	Water in the Solar System: Moon, Tue, p.m., Waterway Ballroom 6
Elkins-Tanton L. T.	Planetary Atmospheres, Wed, p.m., Montgomery Ballroom
Elkins-Tanton L. T.	BOOM! Posters, Thu, p.m., Town Center Exhibit Area
Ellehoj M. D.	Planetary Aeolian Processes Posters, Tue, p.m., Town Center Exhibit Area
Eller H.	Once and Future Moon Posters, Thu, p.m., Town Center Exhibit Area
Elliott T.	Radionuclides and Early Solar System Chronology, Tue, a.m., Waterway Ballroom 1

Elphic R. C.	A New Moon: LRO Results, Mon, a.m., Waterway Ballroom 6
Elphic R. C. *	Water in the Solar System: Moon, Tue, p.m., Waterway Ballroom 6
Elphic R. C.	A New Moon: Volatile Species Posters, Tue, p.m., Town Center Exhibit Area
Elphic R. C.	A New Moon: Spectral Constraints, Wed, p.m., Waterway Ballroom 6
Elphic R. C.	Once and Future Moon Posters, Thu, p.m., Town Center Exhibit Area
Elphic R. C.	Mars Remote Sensing Techniques Posters, Thu, p.m., Town Center Exhibit Area
ElShafie A.	Spacecraft Instruments Posters, Tue, p.m., Town Center Exhibit Area
Elsila J. E.	Environments for Life Posters, Thu, p.m., Town Center Exhibit Area
Elsperman M. S.	Mission Plans and Concepts Posters, Tue, p.m., Town Center Exhibit Area
Elwood Madden M. E. *	Experimental Constraints on Martian Alteration Processes, Mon, p.m., Waterway Ballroom 4
Elwood Madden M. E.	Planetary Atmospheres Posters, Thu, p.m., Town Center Exhibit Area
Emery J. P.	Main Belt Posters, Tue, p.m., Town Center Exhibit Area
Emery J. P. *	Characterizing Near-Earth Objects, Thu, p.m., Waterway Ballroom 4
Eng P.	Spacecraft Instruments Posters, Tue, p.m., Town Center Exhibit Area
Englert P. A. J.	Spacecraft Instruments Posters, Tue, p.m., Town Center Exhibit Area
Engrand C.	Impact Ejecta Posters, Tue, p.m., Town Center Exhibit Area
Engrand C.	Cosmic Dust, Thu, p.m., Waterway Ballroom 1
Enke B. L.	Small Bodies, Fri, p.m., Waterway Ballroom 5
Ennico K.	A New Moon: LCROSS, Chandrayaan, Chang'E, Tue, a.m., Waterway Ballroom 6
Ennico K.	A New Moon: LCROSS Posters, Tue, p.m., Town Center Exhibit Area
Ennis M. E.	Once and Future Moon Posters, Thu, p.m., Town Center Exhibit Area
Ennis M. E.	Martian Meteorites Posters, Thu, p.m., Town Center Exhibit Area
Enns D. C. *	Mars: Fluvial Geomorphology and Processes, Thu, a.m., Waterway Ballroom 4
Eory M.	Parent Cloud and Disk Processes Posters, Tue, p.m., Town Center Exhibit Area
Epperly M. E.	Mission Plans and Concepts Posters, Tue, p.m., Town Center Exhibit Area
Eppler D. B.	Environmental Analogs Posters, Thu, p.m., Town Center Exhibit Area
Eppler D. E.	Print Only: Environmental and Material Analogs
Erb A. E.	Mars: Sedimentary Rock Record Posters, Thu, p.m., Town Center Exhibit Area
Erb Z. S.	Igneous and Volcanic Processes Posters, Thu, p.m., Town Center Exhibit Area
Erd C.	Lunar Petrology and Geochemistry Posters, Tue, p.m., Town Center Exhibit Area
Erdélyi I.	Environmental Analogs Posters, Thu, p.m., Town Center Exhibit Area
Erdélyi S.	E/PO: Miscellaneous Posters, Thu, p.m., Town Center Exhibit Area
Erdosi F.	E/PO: Miscellaneous Posters, Thu, p.m., Town Center Exhibit Area
Erickson A.	Iron and Stony Iron Meteorites Posters, Tue, p.m., Town Center Exhibit Area
Eriksson A.	E/PO: Moon Posters, Tue, p.m., Town Center Exhibit Area
Erkeling G.	Mars: Geologic, Geomorphic, etc., Posters, Thu, p.m., Town Center Exhibit Area
Erkeling G.	Mars: Gullies and Slope Streaks Posters, Thu, p.m., Town Center Exhibit Area
Erkeling G. *	Mars: Timing of Geologic Processes, Fri, p.m., Waterway Ballroom 4
Ernst C. M.	Mercury, Tue, p.m., Montgomery Ballroom
Ernst C. M.	Impact Experiments Posters, Tue, p.m., Town Center Exhibit Area
Ernst C. M.	Mercury Posters, Tue, p.m., Town Center Exhibit Area
Ernst R.	Environmental Analogs Posters, Thu, p.m., Town Center Exhibit Area
Ernst R. E.	Venus Posters, Tue, p.m., Town Center Exhibit Area
Escalona F.	Print Only: Small Bodies
Escande A.	E/PO: Miscellaneous Posters, Thu, p.m., Town Center Exhibit Area
Espley J. R.	Planetary Atmospheres Posters, Thu, p.m., Town Center Exhibit Area
Esposito F.	Martian Alteration Processes Posters, Tue, p.m., Town Center Exhibit Area
Esposito F.	Exploring the Martian Crust Posters, Thu, p.m., Town Center Exhibit Area
Essene E. J.	Rocks, Life, and Biosignatures, Thu, p.m., Waterway Ballroom 1
Estrada P. R. *	Several Species of Icy Chunks, Thu, p.m., Waterway Ballroom 5
EuroGeoMars MDRS Team	Mission Plans and Concepts Posters, Tue, p.m., Town Center Exhibit Area
EuroGeoMars Team	Mission Plans and Concepts Posters, Tue, p.m., Town Center Exhibit Area
EuroGeoMars Team	Environmental Analogs Posters, Thu, p.m., Town Center Exhibit Area
Evans C. A.	Environmental Analogs Posters, Thu, p.m., Town Center Exhibit Area
Evans L.	A New Moon: LRO Results, Mon, a.m., Waterway Ballroom 6
Evans L.	A New Moon: Volatile Species Posters, Tue, p.m., Town Center Exhibit Area
Evans L.	Spacecraft Instruments Posters, Tue, p.m., Town Center Exhibit Area
Evans L. G.	Mercury, Tue, p.m., Montgomery Ballroom
Evans L. G.	A New Moon: Volatile Species Posters, Tue, p.m., Town Center Exhibit Area
Evans L. G.	Spacecraft Instruments Posters, Tue, p.m., Town Center Exhibit Area
Evans R.	Print Only: Moon
Evlanov E.	Spacecraft Instruments Posters, Tue, p.m., Town Center Exhibit Area
Ewer K. J.	Terrestrial Planet Cryospheres Posters, Tue, p.m., Town Center Exhibit Area
Exbrayat M.	E/PO: Miscellaneous Posters, Thu, p.m., Town Center Exhibit Area
ExoGeoLab	Environmental Analogs Posters, Thu, p.m., Town Center Exhibit Area
ExoGeoLab Team	Mission Plans and Concepts Posters, Tue, p.m., Town Center Exhibit Area
ExoGeoLab Team	Environmental Analogs Posters, Thu, p.m., Town Center Exhibit Area

Fernández Y. R.	Ice and Dust Posters, Thu, p.m., Town Center Exhibit Area
Ferrari S.	Mercury, Tue, p.m., Montgomery Ballroom
Ferreira A.	Environmental Analogs Posters, Thu, p.m., Town Center Exhibit Area
Ferrière L.	Impactite Petrology and Ages Posters, Tue, p.m., Town Center Exhibit Area
Ferris J. P.	Environments for Life Posters, Thu, p.m., Town Center Exhibit Area
Ferroir T.	Stardust Mission to Comet Wild 2, Wed, a.m., Waterway Ballroom 1
Ferrone K. L.	Environmental Analogs Posters, Thu, p.m., Town Center Exhibit Area
Feyh N.	Experimental Constraints on Martian Alteration Processes, Mon, p.m., Waterway Ballroom 4
Fieber-Beyer S. K.	Main Belt Posters, Tue, p.m., Town Center Exhibit Area
Fieber-Beyer S. K. *	Small Bodies, Fri, p.m., Waterway Ballroom 5
Fiethe B.	Venus, Mon, p.m., Waterway Ballroom 5
Figueroa M.	Mars Ice and Craters Posters, Tue, p.m., Town Center Exhibit Area
Fikes J.	Laboratory Instruments and Samples Posters, Tue, p.m., Town Center Exhibit Area
Filacchione G.	Mercury, Tue, p.m., Montgomery Ballroom
Filacchione G.	Spacecraft Instruments Posters, Tue, p.m., Town Center Exhibit Area
Filacchione G.	Several Species of Icy Chunks, Thu, p.m., Waterway Ballroom 5
Filacchione G.	Satellites and Their Planets Posters, Thu, p.m., Town Center Exhibit Area
Filiberto J.	Impacts on the Moon, Mars, and Beyond, Wed, p.m., Waterway Ballroom 5
Filiberto J. *	Igneous and Volcanic Processes, Thu, a.m., Waterway Ballroom 5
Filiberto J. *	Martian Igneous Processes, Fri, a.m., Waterway Ballroom 5
Finch M. J.	A New Moon: Volatile Species Posters, Tue, p.m., Town Center Exhibit Area
Fink D.	Cosmic-Ray Exposure Dating Posters, Tue, p.m., Town Center Exhibit Area
Fink W.	Environments for Life Posters, Thu, p.m., Town Center Exhibit Area
Fischer T.	A New Moon: Volatile Species Posters, Tue, p.m., Town Center Exhibit Area
Fischer-Gödde M.	Lunar Petrology and Geochemistry Posters, Tue, p.m., Town Center Exhibit Area
Fisenko A. V.	Print Only: Solar and Presolar Dust
Fisenko A. V.	Origins of Presolar Grains Posters, Thu, p.m., Town Center Exhibit Area
Fishbaugh K.	Mars Polar Processes, Tue, p.m., Waterway Ballroom 4
Fishbaugh K. E.	Martian Polar Processes Posters, Tue, p.m., Town Center Exhibit Area
Fitoussi C.	Lunar Petrology and Geochemistry Posters, Tue, p.m., Town Center Exhibit Area
Flahaut J. *	Martian Alteration Processes, Mon, a.m., Waterway Ballroom 4
Flahaut J.	Planetary Aeolian Processes Posters, Tue, p.m., Town Center Exhibit Area
Flahaut J.	Exploring the Martian Crust Posters, Thu, p.m., Town Center Exhibit Area
Fleeming G. M. II	Laboratory Instruments and Samples Posters, Tue, p.m., Town Center Exhibit Area
Fleischer I.	Martian Alteration Processes Posters, Tue, p.m., Town Center Exhibit Area
Fleischer I.	Spacecraft Instruments Posters, Tue, p.m., Town Center Exhibit Area
Fleischer I.	Exploring the Martian Crust, Wed, a.m., Waterway Ballroom 4
Fleitcher I.	Spacecraft Instruments Posters, Tue, p.m., Town Center Exhibit Area
Flemming H. L.	Mars: Fluvial Geomorphology and Processes, Thu, a.m., Waterway Ballroom 4
Flemming R. L.	Impact Experiments Posters, Tue, p.m., Town Center Exhibit Area
Flemming R. L.	Chondrites Posters, Thu, p.m., Town Center Exhibit Area
Fletcher L. N.	BOOM! Posters, Thu, p.m., Town Center Exhibit Area
Floss C.	Lunar Meteorites Posters, Tue, p.m., Town Center Exhibit Area
Floss C.	Stardust Mission to Comet Wild 2, Wed, a.m., Waterway Ballroom 1
Floss C. *	Origins of Presolar Grains, Wed, p.m., Waterway Ballroom 1
Floss C.	Stardust Mission Posters, Thu, p.m., Town Center Exhibit Area
Floss C.	Cosmic Dust Posters, Thu, p.m., Town Center Exhibit Area
Floss C.	Origins of Presolar Grains Posters, Thu, p.m., Town Center Exhibit Area
Floss C.	Formation of Building Blocks, Fri, p.m., Waterway Ballroom 1
Floyd S.	Spacecraft Instruments Posters, Tue, p.m., Town Center Exhibit Area
Flynn G.	Stardust Mission Posters, Thu, p.m., Town Center Exhibit Area
Flynn G. J.	Stardust Mission to Comet Wild 2, Wed, a.m., Waterway Ballroom 1
Flynn G. J. *	Cosmic Dust, Thu, p.m., Waterway Ballroom 1
Flynn G. J.	Chondrites Posters, Thu, p.m., Town Center Exhibit Area
Flynn G. J.	BOOM! Posters, Thu, p.m., Town Center Exhibit Area
Fogel M. L.	Environments for Life Posters, Thu, p.m., Town Center Exhibit Area
Foing B.	Environmental Analogs Posters, Thu, p.m., Town Center Exhibit Area
Foing B. H.	Mission Plans and Concepts Posters, Tue, p.m., Town Center Exhibit Area
Foing B. H.	Environmental Analogs Posters, Thu, p.m., Town Center Exhibit Area
Folco L.	Achondrites Posters, Tue, p.m., Town Center Exhibit Area
Folco L.	Impact Ejecta Posters, Tue, p.m., Town Center Exhibit Area
Fonti S.	Spacecraft Instruments Posters, Tue, p.m., Town Center Exhibit Area
Foote E. J.	A New Moon: LRO Results, Mon, a.m., Waterway Ballroom 6
Foote M. C.	A New Moon: LRO Results, Mon, a.m., Waterway Ballroom 6
Foote M. C.	A New Moon: LCROSS, Chandrayaan, Chang'E, Tue, a.m., Waterway Ballroom 6
Ford K. M.	Spacecraft Instruments Posters, Tue, p.m., Town Center Exhibit Area
Ford R. L.	Thermal and Aqueous Processes Posters, Thu, p.m., Town Center Exhibit Area

Grady M. M.	Formation of Building Blocks Posters, Thu, p.m., Town Center Exhibit Area
Graff T. G.	Experimental Constraints on Martian Alteration Processes, Mon, p.m., Waterway Ballroom 4
Graham P.	Once and Future Moon Posters, Thu, p.m., Town Center Exhibit Area
Grande M.	Lunar Petrology and Geochemistry Posters, Tue, p.m., Town Center Exhibit Area
Grange M. L.	Print Only: Moon
Grange M. L.	Lunar Origins and Chronology Posters, Tue, p.m., Town Center Exhibit Area
Grange M. L. *	Large Impact Basins on the Moon, Thu, a.m., Waterway Ballroom 6
Grant J.	Mars: Geologic, Geomorphic, etc., Posters, Thu, p.m., Town Center Exhibit Area
Grant J. A. *	Mars: Fluvial Geomorphology and Processes, Thu, a.m., Waterway Ballroom 4
Grant J. A.	Mars Craters Posters, Thu, p.m., Town Center Exhibit Area
Grasset L.	E/PO: Miscellaneous Posters, Thu, p.m., Town Center Exhibit Area
Grassi D.	Spacecraft Instruments Posters, Tue, p.m., Town Center Exhibit Area
Grau T.	Cosmic-Ray Exposure Dating Posters, Tue, p.m., Town Center Exhibit Area
Grav T.	Small Body Missions Posters, Tue, p.m., Town Center Exhibit Area
Grav T.	Characterizing Near-Earth Objects, Thu, p.m., Waterway Ballroom 4
Grav T. *	Small Bodies, Fri, p.m., Waterway Ballroom 5
Gray H.	Terrestrial Planet Cryospheres, Tue, a.m., Waterway Ballroom 4
Gray H.	Mars Ice and Craters Posters, Tue, p.m., Town Center Exhibit Area
Grayson G.	Mission Plans and Concepts Posters, Tue, p.m., Town Center Exhibit Area
Grazier K. R.	Satellites and Their Planets Posters, Thu, p.m., Town Center Exhibit Area
Greathouse T.	A New Moon: LCROSS Posters, Tue, p.m., Town Center Exhibit Area
Grebowsky J.	Planetary Atmospheres Posters, Thu, p.m., Town Center Exhibit Area
Greeley R.	Print Only: Mars
Greeley R.	Planetary Aeolian Processes Posters, Tue, p.m., Town Center Exhibit Area
Greeley R.	Mars: Geologic, Geomorphic, etc., Posters, Thu, p.m., Town Center Exhibit Area
Greeley R.	Spirit Posters, Thu, p.m., Town Center Exhibit Area
Greeley R.	Planetary Dynamics and Tectonics Posters, Thu, p.m., Town Center Exhibit Area
Greeley R.	Igneous and Volcanic Processes Posters, Thu, p.m., Town Center Exhibit Area
Greeley R.	Mars: Timing of Geologic Processes, Fri, p.m., Waterway Ballroom 4
Green R.	Large Impact Basins on the Moon, Thu, a.m., Waterway Ballroom 6
Green R.	Petrologic Characterization of the Moon, Fri, p.m., Waterway Ballroom 6
Green R. O.	Water in the Solar System: Moon, Tue, p.m., Waterway Ballroom 6
Green R. O.	A New Moon: Spectral Constraints Posters, Thu, p.m., Town Center Exhibit Area
Green S. F.	Small Body Missions Posters, Tue, p.m., Town Center Exhibit Area
Green S. F.	Stardust Mission to Comet Wild 2, Wed, a.m., Waterway Ballroom 1
Greenberg G.	Lunar Regolith Posters, Thu, p.m., Town Center Exhibit Area
Greenberg M.	Stardust Mission Posters, Thu, p.m., Town Center Exhibit Area
Greenhagen B. T.	A New Moon: LRO Results, Mon, a.m., Waterway Ballroom 6
Greenhagen B. T.	A New Moon: LCROSS, Chandrayaan, Chang'E, Tue, a.m., Waterway Ballroom 6
Greenhagen B. T.	A New Moon: Geologic Processes Posters, Tue, p.m., Town Center Exhibit Area
Greenhagen B. T.	Nature of the Lunar Regolith, Wed, a.m., Waterway Ballroom 6
Greenhagen B. T. *	A New Moon: Spectral Constraints, Wed, p.m., Waterway Ballroom 6
Greenhagen B. T.	A New Moon: Spectral Constraints Posters, Thu, p.m., Town Center Exhibit Area
Greenwood J. P. *	Water in the Solar System: Moon, Tue, p.m., Waterway Ballroom 6
Greenwood J. P.	Martian Alteration Processes Posters, Tue, p.m., Town Center Exhibit Area
Greenwood J. P.	Mars: Deposition and Erosion, Fri, a.m., Waterway Ballroom 4
Greenwood R. C.	Print Only: Differentiated Bodies
Greenwood R. C.	Chondrites Posters, Thu, p.m., Town Center Exhibit Area
Greenwood R. C.	Thermal and Aqueous Processes Posters, Thu, p.m., Town Center Exhibit Area
Greenwood R. C.	Martian Igneous Processes, Fri, a.m., Waterway Ballroom 5
Gregg T. K. P.	A New Moon: Geologic Processes Posters, Tue, p.m., Town Center Exhibit Area
Gregory D. A.	Achondrites Posters, Tue, p.m., Town Center Exhibit Area
Gregory D. A.	Spacecraft Instruments Posters, Tue, p.m., Town Center Exhibit Area
Greshake A.	Chondrites Posters, Thu, p.m., Town Center Exhibit Area
Grieve R. A. F.	Ground Truth Galore: Terrestrial Impact Craters, Tue, a.m., Waterway Ballroom 5
Grieves G.	Water in the Solar System: Primitive Bodies, Mon, p.m., Waterway Ballroom 6
Grieves G. *	Water in the Solar System: Moon, Tue, p.m., Waterway Ballroom 6
Grieves G. A.	Mercury Posters, Tue, p.m., Town Center Exhibit Area
Griffes J.	Mars: Geologic, Geomorphic, etc., Posters, Thu, p.m., Town Center Exhibit Area
Griffes J. L.	Mars: Sedimentary Rock Record Posters, Thu, p.m., Town Center Exhibit Area
Griffith C.	Mission Plans and Concepts Posters, Tue, p.m., Town Center Exhibit Area
Griffith C. A.	Satellites and Their Planets Posters, Thu, p.m., Town Center Exhibit Area
Griffiths A.	Mission Plans and Concepts Posters, Tue, p.m., Town Center Exhibit Area
Grigsby B.	E/PO: Mars Remote Sensing Posters, Thu, p.m., Town Center Exhibit Area
Grima C.	Mars: Deposition and Erosion, Fri, a.m., Waterway Ballroom 4
Grimberg A.	Solar Wind, Volatile Elements, and Organics Posters, Thu, p.m., Town Center Exhibit Area
Grimm R. E. *	Terrestrial Planet Cryospheres, Tue, a.m., Waterway Ballroom 4

Guo W.	A New Moon: LCROSS, Chandrayaan, Chang'E, Tue, a.m., Waterway Ballroom 6
Gupta S.	Mars: Fluvial Geomorphology and Processes, Thu, a.m., Waterway Ballroom 4
Gupta S.	Mars: Gullies and Slope Streaks Posters, Thu, p.m., Town Center Exhibit Area
Gurnett D.	Planetary Atmospheres Posters, Thu, p.m., Town Center Exhibit Area
Gurov E. P.	Ground Truth Galore: Terrestrial Impact Craters, Tue, a.m., Waterway Ballroom 5
Gurtuna O.	Environmental Analogs Posters, Thu, p.m., Town Center Exhibit Area
Guseva E. N.	Venus Posters, Tue, p.m., Town Center Exhibit Area
Gustafson J. O.	A New Moon: Geologic Processes Posters, Tue, p.m., Town Center Exhibit Area
Gustafson J. O.	A New Moon: Lunar Volcanism, Thu, p.m., Waterway Ballroom 6
Guthery B. W.	Spacecraft Instruments Posters, Tue, p.m., Town Center Exhibit Area
Guzik J. A.	BOOM! Posters, Thu, p.m., Town Center Exhibit Area
Gwinner K.	Lunar Cartography, Stereogrammetry, and Imaging Posters, Thu, p.m., Town Center Exhibit Area
Gwinner K.	Mars: Geologic, Geomorphic, etc., Posters, Thu, p.m., Town Center Exhibit Area
Gwinner K.	Planetary Dynamics and Tectonics Posters, Thu, p.m., Town Center Exhibit Area
Gyngard F. *	Origins of Presolar Grains, Wed, p.m., Waterway Ballroom 1
Gyngard F.	Origins of Presolar Grains Posters, Thu, p.m., Town Center Exhibit Area
Gyollai I.	Lunar Meteorites Posters, Tue, p.m., Town Center Exhibit Area
Haack H.	Cosmic-Ray Exposure Dating Posters, Tue, p.m., Town Center Exhibit Area
Haase I.	Lunar Cartography, Stereogrammetry, and Imaging Posters, Thu, p.m., Town Center Exhibit Area
Haberer S.	Ureilites Posters, Tue, p.m., Town Center Exhibit Area
Haberle R. M.	Planetary Atmospheres, Wed, p.m., Montgomery Ballroom
Hagene J. K.	Spacecraft Instruments Posters, Tue, p.m., Town Center Exhibit Area
Hagermann A.	Martian Alteration Processes Posters, Tue, p.m., Town Center Exhibit Area
Hagermann A.	Mars: Deposition and Erosion, Fri, a.m., Waterway Ballroom 4
Hagerty J. J.	Lunar Petrology and Geochemistry Posters, Tue, p.m., Town Center Exhibit Area
Hagerty J. J.	A New Moon: Geologic Processes Posters, Tue, p.m., Town Center Exhibit Area
Hagerty J. J.	Material Analogs Posters, Tue, p.m., Town Center Exhibit Area
Hagiya K.	Ureilitic Asteroids: Almahata Sitta, Tue, p.m., Waterway Ballroom 1
Hagiya K.	Ureilites Posters, Tue, p.m., Town Center Exhibit Area
Hahn B. C. *	Exploring the Martian Crust, Wed, a.m., Waterway Ballroom 4
Hahn B. C.	Exploring the Martian Crust Posters, Thu, p.m., Town Center Exhibit Area
Hahn J.	Lunar Dust Posters, Thu, p.m., Town Center Exhibit Area
Hairston M.	E/PO: Miscellaneous Posters, Thu, p.m., Town Center Exhibit Area
Hajigholi M.	Mars Ice and Craters Posters, Tue, p.m., Town Center Exhibit Area
Hakkila J.	E/PO: Mission Plans and Concepts Posters, Tue, p.m., Town Center Exhibit Area
Halabian S.	Spacecraft Instruments Posters, Tue, p.m., Town Center Exhibit Area
Halekas J.	Once and Future Moon Posters, Thu, p.m., Town Center Exhibit Area
Halekas J. S.	A New Moon: LCROSS Posters, Tue, p.m., Town Center Exhibit Area
Halekas J. S.	Lunar Dust Posters, Thu, p.m., Town Center Exhibit Area
Halekas J. S.	Lunar Geophysics Posters, Thu, p.m., Town Center Exhibit Area
Halekas J. S.	Mars Craters Posters, Thu, p.m., Town Center Exhibit Area
Hall J. L.	Mission Plans and Concepts Posters, Tue, p.m., Town Center Exhibit Area
Halleaux D. G.	Planetary Atmospheres Posters, Thu, p.m., Town Center Exhibit Area
Hallet B.	Print Only: Mars
Halliday A. N.	Lunar Petrology and Geochemistry Posters, Tue, p.m., Town Center Exhibit Area
Haloda J.	Ice and Dust Posters, Thu, p.m., Town Center Exhibit Area
Halodova P.	Ice and Dust Posters, Thu, p.m., Town Center Exhibit Area
Hamara D.	Planetary Atmospheres Posters, Thu, p.m., Town Center Exhibit Area
Hamara D. K.	Spacecraft Instruments Posters, Tue, p.m., Town Center Exhibit Area
Hames H.	Planetary Dynamics and Tectonics Posters, Thu, p.m., Town Center Exhibit Area
Hamilton D. P.	Satellites and Their Planets Posters, Thu, p.m., Town Center Exhibit Area
Hamilton V. E.	Experimental Constraints on Martian Alteration Processes, Mon, p.m., Waterway Ballroom 4
Hamilton V. E. *	Exploring the Martian Crust, Wed, a.m., Waterway Ballroom 4
Hamilton V. E.	Exploring the Martian Crust Posters, Thu, p.m., Town Center Exhibit Area
Hamilton V. E.	Martian Meteorites Posters, Thu, p.m., Town Center Exhibit Area
Hammond M. S.	Once and Future Moon Posters, Thu, p.m., Town Center Exhibit Area
Hamura T.	A New Moon: LCROSS, Chandrayaan, Chang'E, Tue, a.m., Waterway Ballroom 6
Han L. *	Planetary Dynamics and Tectonics, Wed, a.m., Waterway Ballroom 5
Han S.-C.	Planetary Dynamics and Tectonics Posters, Thu, p.m., Town Center Exhibit Area
Hanada H.	Large Impact Basins on the Moon, Thu, a.m., Waterway Ballroom 6
Hanada H.	Lunar Geophysics Posters, Thu, p.m., Town Center Exhibit Area
Hanley J.	Martian Alteration Processes Posters, Tue, p.m., Town Center Exhibit Area
Hanley J.	Planetary Atmospheres Posters, Thu, p.m., Town Center Exhibit Area
Hanley J.	Exploring the Martian Crust Posters, Thu, p.m., Town Center Exhibit Area
Hans U. *	Differentiated Meteorites, Wed, p.m., Waterway Ballroom 4
Hansen C. J.	Mars Polar Processes, Tue, p.m., Waterway Ballroom 4
Hansen C. J. *	Mars Polar Processes, Tue, p.m., Waterway Ballroom 4

Hassler D. M.	Spacecraft Instruments Posters, Tue, p.m., Town Center Exhibit Area
Hassler S. W.	Impact Models and More, Tue, p.m., Waterway Ballroom 5
Hassouni K.	Solar Wind, Volatile Elements, and Organics Posters, Thu, p.m., Town Center Exhibit Area
Hastie M.	A New Moon: LCROSS Posters, Tue, p.m., Town Center Exhibit Area
Hauber E. *	Terrestrial Planet Cryospheres, Tue, a.m., Waterway Ballroom 4
Hauber E.	Terrestrial Planet Cryospheres Posters, Tue, p.m., Town Center Exhibit Area
Hauber E. *	Igneous and Volcanic Processes, Thu, a.m., Waterway Ballroom 5
Hauber E.	Mars: Gullies and Slope Streaks Posters, Thu, p.m., Town Center Exhibit Area
Hauber E.	Planetary Dynamics and Tectonics Posters, Thu, p.m., Town Center Exhibit Area
Hauber E.	Igneous and Volcanic Processes Posters, Thu, p.m., Town Center Exhibit Area
Hauck S. A. II*	Mercury, Tue, p.m., Montgomery Ballroom
Hauck S. A. II	Large Impact Basins on the Moon, Thu, a.m., Waterway Ballroom 6
Hauri E. H.	A New Moon: Volatile Species Posters, Tue, p.m., Town Center Exhibit Area
Hausrath E. M.	Experimental Constraints on Martian Alteration Processes, Mon, p.m., Waterway Ballroom 4
Hausrath E. M.	Material Analogs Posters, Tue, p.m., Town Center Exhibit Area
Hawke B. R.	Lunar Petrology and Geochemistry Posters, Tue, p.m., Town Center Exhibit Area
Hawke B. R.	A New Moon: Geologic Processes Posters, Tue, p.m., Town Center Exhibit Area
Hawke B. R.	Nature of the Lunar Regolith, Wed, a.m., Waterway Ballroom 6
Hawke B. R.	Impacts on the Moon, Mars, and Beyond, Wed, p.m., Waterway Ballroom 5
Hawke B. R.	A New Moon: Lunar Volcanism, Thu, p.m., Waterway Ballroom 6
Hawke B. R.	A New Moon: Spectral Constraints Posters, Thu, p.m., Town Center Exhibit Area
Hawke B. R.	Igneous and Volcanic Processes Posters, Thu, p.m., Town Center Exhibit Area
Hawkesworth C. J.	Planetary Differentiation, Mon, a.m., Waterway Ballroom 5
Hayabusa 2 Mid-Infrared Imager Team	Near-Earth Objects Posters, Thu, p.m., Town Center Exhibit Area
Hayano Y.	A New Moon: LCROSS, Chandrayaan, Chang'E, Tue, a.m., Waterway Ballroom 6
Hayashi T.	Lunar Cartography, Stereogrammetry, and Imaging Posters, Thu, p.m., Town Center Exhibit Area
Hayden L. A.	Planetary Differentiation Posters, Tue, p.m., Town Center Exhibit Area
Hayes A. *	Several Species of Icy Chunks, Thu, p.m., Waterway Ballroom 5
Hayes A. G.	Planetary Aeolian Processes, Tue, p.m., Waterway Ballroom 4
Hayne P. O.	A New Moon: LRO Results, Mon, a.m., Waterway Ballroom 6
Hayne P. O. *	A New Moon: LCROSS, Chandrayaan, Chang'E, Tue, a.m., Waterway Ballroom 6
Hayward R. K.	Planetary Aeolian Processes Posters, Tue, p.m., Town Center Exhibit Area
Hayward R. K.	Material Analogs Posters, Tue, p.m., Town Center Exhibit Area
Hayward R. K.	Mars: Geologic, Geomorphic, etc., Posters, Thu, p.m., Town Center Exhibit Area
He Q.	Print Only: Environmental and Material Analogs
He Q.	Martian Meteorites Posters, Thu, p.m., Town Center Exhibit Area
He Q.	Igneous and Volcanic Processes Posters, Thu, p.m., Town Center Exhibit Area
He S.	Once and Future Moon Posters, Thu, p.m., Town Center Exhibit Area
He X. X.	Print Only: Environmental and Material Analogs
Head J.	A New Moon: Geologic Processes Posters, Tue, p.m., Town Center Exhibit Area
Head J.	Large Impact Basins on the Moon, Thu, a.m., Waterway Ballroom 6
Head J.	A New Moon: Lunar Volcanism, Thu, p.m., Waterway Ballroom 6
Head J.	A New Moon: Spectral Constraints Posters, Thu, p.m., Town Center Exhibit Area
Head J. III	A New Moon: LRO Results, Mon, a.m., Waterway Ballroom 6
Head J. W.	A New Moon: Geologic Processes Posters, Tue, p.m., Town Center Exhibit Area
Head J. W.	Terrestrial Planet Cryospheres Posters, Tue, p.m., Town Center Exhibit Area
Head J. W.	A New Moon: Spectral Constraints, Wed, p.m., Waterway Ballroom 6
Head J. W.	Igneous and Volcanic Processes Posters, Thu, p.m., Town Center Exhibit Area
Head J. W.	Print Only: Data and Image Systems
Head J. W.	Terrestrial Planet Cryospheres, Tue, a.m., Waterway Ballroom 4
Head J. W.	Water in the Solar System: Moon, Tue, p.m., Waterway Ballroom 6
Head J. W.	Mercury, Tue, p.m., Montgomery Ballroom
Head J. W.	Mars Ice and Craters Posters, Tue, p.m., Town Center Exhibit Area
Head J. W.	Terrestrial Planet Cryospheres Posters, Tue, p.m., Town Center Exhibit Area
Head J. W.	Mercury Posters, Tue, p.m., Town Center Exhibit Area
Head J. W.	Venus Posters, Tue, p.m., Town Center Exhibit Area
Head J. W.	A New Moon: Spectral Constraints, Wed, p.m., Waterway Ballroom 6
Head J. W.	Mars: Fluvial Geomorphology and Processes, Thu, a.m., Waterway Ballroom 4
Head J. W.	Igneous and Volcanic Processes, Thu, a.m., Waterway Ballroom 5
Head J. W.	Large Impact Basins on the Moon, Thu, a.m., Waterway Ballroom 6
Head J. W.	A New Moon: Lunar Volcanism, Thu, p.m., Waterway Ballroom 6
Head J. W.	A New Moon: Spectral Constraints Posters, Thu, p.m., Town Center Exhibit Area
Head J. W.	Mars: Gullies and Slope Streaks Posters, Thu, p.m., Town Center Exhibit Area
Head J. W.	Mars Craters Posters, Thu, p.m., Town Center Exhibit Area
Head J. W.	Igneous and Volcanic Processes Posters, Thu, p.m., Town Center Exhibit Area
Head J. W.	Environmental Analogs Posters, Thu, p.m., Town Center Exhibit Area
Head J. W.	Mars: Timing of Geologic Processes, Fri, p.m., Waterway Ballroom 4

Hiller J.	Origins of Presolar Grains Posters, Thu, p.m., Town Center Exhibit Area
Hillier S.	Martian Alteration Processes Posters, Tue, p.m., Town Center Exhibit Area
Hills H. K.	Lunar Cartography, Stereogrammetry, and Imaging Posters, Thu, p.m., Town Center Exhibit Area
Hindmarsh R. C. A.	Martian Polar Processes Posters, Tue, p.m., Town Center Exhibit Area
Hines R.	E/PO: Meteorites Posters, Tue, p.m., Town Center Exhibit Area
Hinman N. W.	Material Analogs Posters, Tue, p.m., Town Center Exhibit Area
Hinz P.	A New Moon: LCROSS Posters, Tue, p.m., Town Center Exhibit Area
Hioki K.	A New Moon: Spectral Constraints Posters, Thu, p.m., Town Center Exhibit Area
Hipkin V.	Environmental Analogs Posters, Thu, p.m., Town Center Exhibit Area
Hirai T.	Once and Future Moon Posters, Thu, p.m., Town Center Exhibit Area
Hirata N.	A New Moon: Geologic Processes Posters, Tue, p.m., Town Center Exhibit Area
Hirata N.	Data and Image Systems Posters, Tue, p.m., Town Center Exhibit Area
Hirata N.	A New Moon: Spectral Constraints, Wed, p.m., Waterway Ballroom 6
Hirata N. *	A New Moon: Lunar Volcanism, Thu, p.m., Waterway Ballroom 6
Hirata N.	A New Moon: Spectral Constraints Posters, Thu, p.m., Town Center Exhibit Area
Hirata N.	Lunar Cartography, Stereogrammetry, and Imaging Posters, Thu, p.m., Town Center Exhibit Area
Hirata T.	Iron and Stony Iron Meteorites Posters, Tue, p.m., Town Center Exhibit Area
HiRISE Team	E/PO: Mars Remote Sensing Posters, Thu, p.m., Town Center Exhibit Area
HiRISE Team	Mars: Timing of Geologic Processes, Fri, p.m., Waterway Ballroom 4
Hiroi T.	Ureilites Posters, Tue, p.m., Town Center Exhibit Area
Hiroi T.	Material Analogs Posters, Tue, p.m., Town Center Exhibit Area
Hiroi T.	A New Moon: Spectral Constraints, Wed, p.m., Waterway Ballroom 6
Hiroi T.	Near-Earth Objects Posters, Thu, p.m., Town Center Exhibit Area
Hiroi T.	A New Moon: Spectral Constraints Posters, Thu, p.m., Town Center Exhibit Area
Hiroi T.	Exploring the Martian Crust Posters, Thu, p.m., Town Center Exhibit Area
Hiroi T.	Petrologic Characterization of the Moon, Fri, p.m., Waterway Ballroom 6
Hironaka Y.	Print Only: Impacts
Hironaka Y.	Impact Experiments Posters, Tue, p.m., Town Center Exhibit Area
Hirschmann M. M.	Planetary Differentiation Posters, Tue, p.m., Town Center Exhibit Area
Hirschmann M. M. *	Planetary Atmospheres, Wed, p.m., Montgomery Ballroom
Hirschmann M. M.	Igneous and Volcanic Processes Posters, Thu, p.m., Town Center Exhibit Area
Hnatyshin D.	Martian Igneous Processes, Fri, a.m., Waterway Ballroom 5
Hobbs S. W.	Print Only: Mars
Hochleitner R.	Ureilites Posters, Tue, p.m., Town Center Exhibit Area
Hodges K. V.	Ground Truth Galore: Terrestrial Impact Craters, Tue, a.m., Waterway Ballroom 5
Hodges K. V.	Impactite Petrology and Ages Posters, Tue, p.m., Town Center Exhibit Area
Hodges K. V.	Spacecraft Instruments Posters, Tue, p.m., Town Center Exhibit Area
Hodges K. V.	Environmental Analogs Posters, Thu, p.m., Town Center Exhibit Area
Hoffman E. J. *	Water in the Solar System: Primitive Bodies, Mon, p.m., Waterway Ballroom 6
Hoffman J. H.	Planetary Atmospheres Posters, Thu, p.m., Town Center Exhibit Area
Hoffmann V. H.	Ureilites Posters, Tue, p.m., Town Center Exhibit Area
Hofmann B.	Cosmic-Ray Exposure Dating Posters, Tue, p.m., Town Center Exhibit Area
Hogan R. C.	Small Bodies, Fri, p.m., Waterway Ballroom 5
Hohenberg C.	Solar Wind, Volatile Elements, and Organics Posters, Thu, p.m., Town Center Exhibit Area
Hohenberg C. M.	Solar Wind, Volatile Elements, and Organics, Thu, a.m., Waterway Ballroom 1
Hohenberg C. M.	Stardust Mission Posters, Thu, p.m., Town Center Exhibit Area
Hohenberg C. M.	Formation of Building Blocks Posters, Thu, p.m., Town Center Exhibit Area
Hohenberg C. M.	Thermal and Aqueous Processes Posters, Thu, p.m., Town Center Exhibit Area
Holdsworth D. W.	Laboratory Instruments and Samples Posters, Tue, p.m., Town Center Exhibit Area
Holin I. V.	Print Only: Mercury
Holland G.	Origins of Presolar Grains Posters, Thu, p.m., Town Center Exhibit Area
Holsapple K. A.	Impacts Modeling Posters, Tue, p.m., Town Center Exhibit Area
Holsapple K. A.	Impacts on the Moon, Mars, and Beyond, Wed, p.m., Waterway Ballroom 5
Holsclaw G.	A New Moon: Spectral Constraints Posters, Thu, p.m., Town Center Exhibit Area
Holsclaw G. M.	Mercury, Tue, p.m., Montgomery Ballroom
Holsclaw G. M.	Mercury Posters, Tue, p.m., Town Center Exhibit Area
Holstein-Rathlou C.	Planetary Aeolian Processes Posters, Tue, p.m., Town Center Exhibit Area
Holstein-Rathlou C.	Planetary Atmospheres Posters, Thu, p.m., Town Center Exhibit Area
Holt J.	Terrestrial Planet Cryospheres Posters, Tue, p.m., Town Center Exhibit Area
Holt J. W.	Terrestrial Planet Cryospheres, Tue, a.m., Waterway Ballroom 4
Holt J. W.	Mars Polar Processes, Tue, p.m., Waterway Ballroom 4
Holt J. W. *	Mars Polar Processes, Tue, p.m., Waterway Ballroom 4
Holt J. W.	Martian Polar Processes Posters, Tue, p.m., Town Center Exhibit Area
Holzheid A.	Impactite Petrology and Ages Posters, Tue, p.m., Town Center Exhibit Area
Honda C.	A New Moon: Geologic Processes Posters, Tue, p.m., Town Center Exhibit Area
Honda C.	Data and Image Systems Posters, Tue, p.m., Town Center Exhibit Area
Honda C.	A New Moon: Lunar Volcanism, Thu, p.m., Waterway Ballroom 6

Hynek B. M.	Martian Alteration Processes Posters, Tue, p.m., Town Center Exhibit Area
Hynek B. M.	Material Analogs Posters, Tue, p.m., Town Center Exhibit Area
Hynek B. M.	Mars: Fluvial Geomorphology and Processes, Thu, a.m., Waterway Ballroom 4
Hynek B. M.	Mars Craters Posters, Thu, p.m., Town Center Exhibit Area
Hynek B. M.	Igneous and Volcanic Processes Posters, Thu, p.m., Town Center Exhibit Area
Hynek B. M.	Environmental Analogs Posters, Thu, p.m., Town Center Exhibit Area
Hynes K. M. *	Origins of Presolar Grains, Wed, p.m., Waterway Ballroom 1
Iagnemma K.	Spirit Posters, Thu, p.m., Town Center Exhibit Area
Ichimura A. I.	Water in the Solar System: Moon, Tue, p.m., Waterway Ballroom 6
Ichimura K.	Thermal and Aqueous Processes Posters, Thu, p.m., Town Center Exhibit Area
Ichimura K.	Thermal and Aqueous Processes on Chondrite Parent Bodies, Fri, a.m., Waterway Ballroom 1
Iijima Y.	Spacecraft Instruments Posters, Tue, p.m., Town Center Exhibit Area
Iizuka T.	Radionuclides and Early Solar System Chronology, Tue, a.m., Waterway Ballroom 1
Ikoma M.	Planetary Atmospheres, Wed, p.m., Montgomery Ballroom
ILEWG Eifel Field Test Team	Mission Plans and Concepts Posters, Tue, p.m., Town Center Exhibit Area
ILEWG ExoGeoLab Team	Mission Plans and Concepts Posters, Tue, p.m., Town Center Exhibit Area
ILEWG ExoHab Team	Environmental Analogs Posters, Thu, p.m., Town Center Exhibit Area
Imai K.	Spacecraft Instruments Posters, Tue, p.m., Town Center Exhibit Area
Imamura T.	Near-Earth Objects Posters, Thu, p.m., Town Center Exhibit Area
Inatomi Y.	Formation of Building Blocks, Fri, p.m., Waterway Ballroom 1
Ingram R.	Lunar Cartography, Stereogrammetry, and Imaging Posters, Thu, p.m., Town Center Exhibit Area
Ip F.	Environments for Life Posters, Thu, p.m., Town Center Exhibit Area
Ipatov S. I.	Ice and Dust Posters, Thu, p.m., Town Center Exhibit Area
Ireland T.	Laboratory Instruments and Samples Posters, Tue, p.m., Town Center Exhibit Area
Ireland T. R.	Radionuclides and Early Solar System Chronology, Tue, a.m., Waterway Ballroom 1
Irisawa K.	Iron and Stony Iron Meteorites Posters, Tue, p.m., Town Center Exhibit Area
Irving A.	Martian Meteorites Posters, Thu, p.m., Town Center Exhibit Area
Irving A. J.	Print Only: Differentiated Bodies
Irving A. J.	Planetary Differentiation, Mon, a.m., Waterway Ballroom 5
Irving A. J.	Achondrites Posters, Tue, p.m., Town Center Exhibit Area
Irving A. J.	Lunar Meteorites Posters, Tue, p.m., Town Center Exhibit Area
Irving A. J.	Lunar Origins and Chronology Posters, Tue, p.m., Town Center Exhibit Area
Irving A. J.	Differentiated Meteorites, Wed, p.m., Waterway Ballroom 4
Irving A. J.	Chondrites Posters, Thu, p.m., Town Center Exhibit Area
Irving A. J.	Martian Meteorites Posters, Thu, p.m., Town Center Exhibit Area
Irving A. J.	Martian Igneous Processes, Fri, a.m., Waterway Ballroom 5
Irwin P.	Spacecraft Instruments Posters, Tue, p.m., Town Center Exhibit Area
Irwin R. P. III*	Mars: Fluvial Geomorphology and Processes, Thu, a.m., Waterway Ballroom 4
Isa J.	Chondrites Posters, Thu, p.m., Town Center Exhibit Area
Isaacson P.	A New Moon: Geologic Processes Posters, Tue, p.m., Town Center Exhibit Area
Isaacson P.	Exploring the Martian Crust, Wed, a.m., Waterway Ballroom 4
Isaacson P.	A New Moon: Spectral Constraints, Wed, p.m., Waterway Ballroom 6
Isaacson P.	Large Impact Basins on the Moon, Thu, a.m., Waterway Ballroom 6
Isaacson P.	A New Moon: Lunar Volcanism, Thu, p.m., Waterway Ballroom 6
Isaacson P.	A New Moon: Spectral Constraints Posters, Thu, p.m., Town Center Exhibit Area
Isaacson P.	Petrologic Characterization of the Moon, Fri, p.m., Waterway Ballroom 6
Isaacson P. J.	Water in the Solar System: Moon, Tue, p.m., Waterway Ballroom 6
Isaacson P. J.	Lunar Meteorites Posters, Tue, p.m., Town Center Exhibit Area
Isaacson P. J.	A New Moon: Geologic Processes Posters, Tue, p.m., Town Center Exhibit Area
Isaacson P. J. *	A New Moon: Spectral Constraints, Wed, p.m., Waterway Ballroom 6
Isaacson P. J.	A New Moon: Spectral Constraints Posters, Thu, p.m., Town Center Exhibit Area
Isaacson P. J.	Petrologic Characterization of the Moon, Fri, p.m., Waterway Ballroom 6
Isachsen C. E.	Impact Experiments Posters, Tue, p.m., Town Center Exhibit Area
Isbell C. E.	Data and Image Systems Posters, Tue, p.m., Town Center Exhibit Area
Isheim D.	Origins of Presolar Grains, Wed, p.m., Waterway Ballroom 1
Isheim D.	Origins of Presolar Grains Posters, Thu, p.m., Town Center Exhibit Area
Ishibashi K.	Laboratory Instruments and Samples Posters, Tue, p.m., Town Center Exhibit Area
Ishibashi K.	Spacecraft Instruments Posters, Tue, p.m., Town Center Exhibit Area
Ishihara Y.	A New Moon: Volatile Species Posters, Tue, p.m., Town Center Exhibit Area
Ishihara Y.	A New Moon: Geologic Processes Posters, Tue, p.m., Town Center Exhibit Area
Ishihara Y.	A New Moon: Spectral Constraints, Wed, p.m., Waterway Ballroom 6
Ishihara Y.	Large Impact Basins on the Moon, Thu, a.m., Waterway Ballroom 6
Ishihara Y.	Lunar Geophysics Posters, Thu, p.m., Town Center Exhibit Area
Ishii H.	Stardust Mission to Comet Wild 2, Wed, a.m., Waterway Ballroom 1
Ishii H. A.	Radionuclides and Early Solar System Chronology, Tue, a.m., Waterway Ballroom 1
Ishii H. A. *	Stardust Mission to Comet Wild 2, Wed, a.m., Waterway Ballroom 1
Ishikawa S. T.	Mars: Gullies and Slope Streaks Posters, Thu, p.m., Town Center Exhibit Area

Johnsson A.	Terrestrial Planet Cryospheres, Tue, a.m., Waterway Ballroom 4
Johnsson A.	Mars: Gullies and Slope Streaks Posters, Thu, p.m., Town Center Exhibit Area
Jolley D. W.	Ground Truth Galore: Terrestrial Impact Craters, Tue, a.m., Waterway Ballroom 5
Jolliff B. L.	A New Moon: LRO Results, Mon, a.m., Waterway Ballroom 6
Jolliff B. L.	Water in the Solar System: Moon, Tue, p.m., Waterway Ballroom 6
Jolliff B. L.	Lunar Meteorites Posters, Tue, p.m., Town Center Exhibit Area
Jolliff B. L.	Lunar Petrology and Geochemistry Posters, Tue, p.m., Town Center Exhibit Area
Jolliff B. L.	Martian Alteration Processes Posters, Tue, p.m., Town Center Exhibit Area
Jolliff B. L.	Exploring the Martian Crust, Wed, a.m., Waterway Ballroom 4
Jolliff B. L.	Large Impact Basins on the Moon, Thu, a.m., Waterway Ballroom 6
Jolliff B. L.	A New Moon: Lunar Volcanism, Thu, p.m., Waterway Ballroom 6
Jolliff B. L.	A New Moon: Spectral Constraints Posters, Thu, p.m., Town Center Exhibit Area
Jolliff B. L.	Once and Future Moon Posters, Thu, p.m., Town Center Exhibit Area
Jolliff B. L.	Petrologic Characterization of the Moon, Fri, p.m., Waterway Ballroom 6
Jones A. P.	Ureilites Posters, Tue, p.m., Town Center Exhibit Area
Jones J. H.	Planetary Differentiation, Mon, a.m., Waterway Ballroom 5
Jones J. H.	Planetary Differentiation Posters, Tue, p.m., Town Center Exhibit Area
Jones J. H.	Differentiated Meteorites, Wed, p.m., Waterway Ballroom 4
Jones J. H.	Cosmic Dust Posters, Thu, p.m., Town Center Exhibit Area
Jones J. H.	Martian Meteorites Posters, Thu, p.m., Town Center Exhibit Area
Jones K. W.	Cosmic Dust Posters, Thu, p.m., Town Center Exhibit Area
Jones R. H.	Thermal and Aqueous Processes Posters, Thu, p.m., Town Center Exhibit Area
Jones R. H. *	Thermal and Aqueous Processes on Chondrite Parent Bodies, Fri, a.m., Waterway Ballroom 1
Jones R. H.	Formation of Building Blocks, Fri, p.m., Waterway Ballroom 1
Jones S. M.	Stardust Mission Posters, Thu, p.m., Town Center Exhibit Area
Jorge M.	Environmental Analogs Posters, Thu, p.m., Town Center Exhibit Area
Joseph E. C. S.	Mars Craters Posters, Thu, p.m., Town Center Exhibit Area
Joshi P. C.	Environments for Life Posters, Thu, p.m., Town Center Exhibit Area
Joswiak D.	Stardust Mission to Comet Wild 2, Wed, a.m., Waterway Ballroom 1
Joswiak D.	Stardust Mission Posters, Thu, p.m., Town Center Exhibit Area
Joswiak D. J. *	Stardust Mission to Comet Wild 2, Wed, a.m., Waterway Ballroom 1
Jouglet D.	Exploring the Martian Crust Posters, Thu, p.m., Town Center Exhibit Area
Jourdan F. *	Ground Truth Galore: Terrestrial Impact Craters, Tue, a.m., Waterway Ballroom 5
Jourdan F.	Impactite Petrology and Ages Posters, Tue, p.m., Town Center Exhibit Area
Jourdan F.	Large Impact Basins on the Moon, Thu, a.m., Waterway Ballroom 6
Jowell A. H.	Igneous and Volcanic Processes Posters, Thu, p.m., Town Center Exhibit Area
Jowell A. R.	Mars: Sedimentary Rock Record Posters, Thu, p.m., Town Center Exhibit Area
Joy K. H.	Lunar Petrology and Geochemistry Posters, Tue, p.m., Town Center Exhibit Area
Joy K. H.	Lunar Meteorites Posters, Tue, p.m., Town Center Exhibit Area
Joy K. H.	Lunar Petrology and Geochemistry Posters, Tue, p.m., Town Center Exhibit Area
Joy K. H.	E/PO: Moon Posters, Tue, p.m., Town Center Exhibit Area
Joy K. H.	Once and Future Moon Posters, Thu, p.m., Town Center Exhibit Area
Joy S. P.	Satellites and Their Planets Posters, Thu, p.m., Town Center Exhibit Area
Józsa S.	Print Only: Impacts
Józsa S.	Environmental Analogs Posters, Thu, p.m., Town Center Exhibit Area
Jull A. J. T.	Cosmic-Ray Exposure Dating Posters, Tue, p.m., Town Center Exhibit Area
Jurdy D. M.	Satellites and Their Planets Posters, Thu, p.m., Town Center Exhibit Area
Jurewicz A. J. G.	Solar Wind, Volatile Elements, and Organics, Thu, a.m., Waterway Ballroom 1
Jurewicz A. J. G.	Stardust Mission Posters, Thu, p.m., Town Center Exhibit Area
Jurewicz A. J. G.	Solar Wind, Volatile Elements, and Organics Posters, Thu, p.m., Town Center Exhibit Area
Jutzi M. *	Vesta and Dawn, Tue, p.m., Waterway Ballroom 1
Kabai S.	Print Only: Education and Public Outreach
Kadish S. J. *	Terrestrial Planet Cryospheres, Tue, a.m., Waterway Ballroom 4
Kadish S. J.	Mars Ice and Craters Posters, Tue, p.m., Town Center Exhibit Area
Kadono T.	Print Only: Impacts
Kadono T.	A New Moon: LCROSS, Chandrayaan, Chang'E, Tue, a.m., Waterway Ballroom 6
Kadono T.	Impact Experiments Posters, Tue, p.m., Town Center Exhibit Area
Kadono T.	Satellites and Their Planets Posters, Thu, p.m., Town Center Exhibit Area
Kaguya Gamma-Ray Spectrometer Team	Lunar Petrology and Geochemistry Posters, Tue, p.m., Town Center Exhibit Area
Kah L. C.	Print Only: Mars
Kahan D. S.	Mercury, Tue, p.m., Montgomery Ballroom
Kahre M. A.	Planetary Atmospheres, Wed, p.m., Montgomery Ballroom
Kahre M. A.	Planetary Atmospheres Posters, Thu, p.m., Town Center Exhibit Area
Kaiden H.	Print Only: Mars
Kaiden H.	Lunar Origins and Chronology Posters, Tue, p.m., Town Center Exhibit Area
Kalinina G. K.	Print Only: Small Bodies
Kalinina G. V.	Print Only: Cosmochemical Origins

Kalleson E. *	Ground Truth Galore: Terrestrial Impact Craters, Tue, a.m., Waterway Ballroom 5
Kalleson E.	Impactite Petrology and Ages Posters, Tue, p.m., Town Center Exhibit Area
Kallio A. P.	Solar Wind, Volatile Elements, and Organics Posters, Thu, p.m., Town Center Exhibit Area
Kallio A. P. A. *	Solar Wind, Volatile Elements, and Organics, Thu, a.m., Waterway Ballroom 1
Kaltenbach A.	Radionuclides and Early Solar System Chronology, Tue, a.m., Waterway Ballroom 1
Kamata S.	Spacecraft Instruments Posters, Tue, p.m., Town Center Exhibit Area
Kamata S.	Lunar Geophysics Posters, Thu, p.m., Town Center Exhibit Area
Kammer J. A.	Water in the Solar System: Primitive Bodies, Mon, p.m., Waterway Ballroom 6
Kamp L. W.	Several Species of Icy Chunks, Thu, p.m., Waterway Ballroom 5
Kaneda K.	Igneous and Volcanic Processes Posters, Thu, p.m., Town Center Exhibit Area
Kanik I.	Spacecraft Instruments Posters, Tue, p.m., Town Center Exhibit Area
Kantsiper B.	Mission Plans and Concepts Posters, Tue, p.m., Town Center Exhibit Area
Kapit J.	Martian Alteration Processes, Mon, a.m., Waterway Ballroom 4
Kaplan M. S.	Mission Plans and Concepts Posters, Tue, p.m., Town Center Exhibit Area
Karatekin O.	Satellites and Their Planets Posters, Thu, p.m., Town Center Exhibit Area
Karátson D.	Print Only: Planetary Differentiation
Karbonini L.	Mars Craters Posters, Thu, p.m., Town Center Exhibit Area
Karczemska A.	Ureilites Posters, Tue, p.m., Town Center Exhibit Area
Kargel J. S.	Martian Alteration Processes Posters, Tue, p.m., Town Center Exhibit Area
Karimov A. M.	Print Only: Planetary Atmospheres
Karkoschka E.	Mission Plans and Concepts Posters, Tue, p.m., Town Center Exhibit Area
Karlsson N. B.	Martian Polar Processes Posters, Tue, p.m., Town Center Exhibit Area
Karlstrom L. *	Igneous and Volcanic Processes, Thu, a.m., Waterway Ballroom 5
Karner J. M.	Print Only: Mars
Karner J. M.	Martian Meteorites Posters, Thu, p.m., Town Center Exhibit Area
Karouji Y.	Lunar Meteorites Posters, Tue, p.m., Town Center Exhibit Area
Karouji Y.	Lunar Petrology and Geochemistry Posters, Tue, p.m., Town Center Exhibit Area
Karouji Y.	Large Impact Basins on the Moon, Thu, a.m., Waterway Ballroom 6
Karunatillake S.	Exploring the Martian Crust Posters, Thu, p.m., Town Center Exhibit Area
Kasai Y.	Solar Wind, Volatile Elements, and Organics Posters, Thu, p.m., Town Center Exhibit Area
Kashkarov L. L.	Print Only: Cosmochemical Origins
Kashkarov L. L.	Print Only: Small Bodies
Kasper J. C.	Lunar Radiation Posters, Thu, p.m., Town Center Exhibit Area
Kataoka S.	Chondrites Posters, Thu, p.m., Town Center Exhibit Area
Kater L.	Material Analogs Posters, Tue, p.m., Town Center Exhibit Area
Kato M.	Satellites and Their Planets Posters, Thu, p.m., Town Center Exhibit Area
Kato Y.	Igneous and Volcanic Processes Posters, Thu, p.m., Town Center Exhibit Area
Kattenhorn S. A.	Impact Craters Posters, Tue, p.m., Town Center Exhibit Area
Kattenhorn S. A.	Mars: Sedimentary Rock Record Posters, Thu, p.m., Town Center Exhibit Area
Kattenhorn S. A.	Satellites and Their Planets Posters, Thu, p.m., Town Center Exhibit Area
Kattenhorn S. A.	Planetary Dynamics and Tectonics Posters, Thu, p.m., Town Center Exhibit Area
Kaufmann D.	A New Moon: LCROSS Posters, Tue, p.m., Town Center Exhibit Area
Kawaguchi J.	Characterizing Near-Earth Objects, Thu, p.m., Waterway Ballroom 4
Kawakita H.	A New Moon: LCROSS, Chandrayaan, Chang'E, Tue, a.m., Waterway Ballroom 6
Kawamae W.	Data and Image Systems Posters, Tue, p.m., Town Center Exhibit Area
Kawamura T.	A New Moon: Geologic Processes Posters, Tue, p.m., Town Center Exhibit Area
Kawamura T. *	Interior of the Moon, Fri, a.m., Waterway Ballroom 6
Kawano N.	Spacecraft Instruments Posters, Tue, p.m., Town Center Exhibit Area
Kay J. P.	Satellites and Their Planets Posters, Thu, p.m., Town Center Exhibit Area
Kaydash V. G.	Print Only: Moon
Ke S.	Radionuclides and Early Solar System Chronology Posters, Tue, p.m., Town Center Exhibit Area
Kearsley A.	Stardust Mission to Comet Wild 2, Wed, a.m., Waterway Ballroom 1
Kearsley A. T.	Impact Models and More, Tue, p.m., Waterway Ballroom 5
Kearsley A. T.	Stardust Mission to Comet Wild 2, Wed, a.m., Waterway Ballroom 1
Kearsley A. T. *	Stardust Mission to Comet Wild 2, Wed, a.m., Waterway Ballroom 1
Kearsley A. T.	Stardust Mission Posters, Thu, p.m., Town Center Exhibit Area
Kebukawa Y. *	Thermal and Aqueous Processes on Chondrite Parent Bodies, Fri, a.m., Waterway Ballroom 1
Keihm S. J.	Interior of the Moon, Fri, a.m., Waterway Ballroom 6
Keiser S. A.	Parent Cloud and Solar Nebula, Mon, a.m., Waterway Ballroom 1
Keller H. U.	Exploring the Martian Crust Posters, Thu, p.m., Town Center Exhibit Area
Keller J.	A New Moon: LRO Results, Mon, a.m., Waterway Ballroom 6
Keller J.	E/PO: Moon Posters, Tue, p.m., Town Center Exhibit Area
Keller L. P.	Formation of First Solar System Solids Posters, Tue, p.m., Town Center Exhibit Area
Keller L. P.	Nature of the Lunar Regolith, Wed, a.m., Waterway Ballroom 6
Keller L. P.	Cosmic Dust, Thu, p.m., Waterway Ballroom 1
Keller L. P. *	Cosmic Dust, Thu, p.m., Waterway Ballroom 1
Keller L. P.	Cosmic Dust Posters, Thu, p.m., Town Center Exhibit Area

Keller N. S.	Planetary Differentiation, Mon, a.m., Waterway Ballroom 5
Kellett B. J.	Lunar Petrology and Geochemistry Posters, Tue, p.m., Town Center Exhibit Area
Kelley A. K.	Mars: Sedimentary Rock Record Posters, Thu, p.m., Town Center Exhibit Area
Kelley E. M.	Mars: Sedimentary Rock Record Posters, Thu, p.m., Town Center Exhibit Area
Kelley M. S.	Vesta and Dawn, Tue, p.m., Waterway Ballroom 1
Kelley M. S.	Characterizing Near-Earth Objects, Thu, p.m., Waterway Ballroom 4
Kelley M. S.	Ice and Dust Posters, Thu, p.m., Town Center Exhibit Area
Kelley M. S.	Small Bodies, Fri, p.m., Waterway Ballroom 5
Kelley S. P.	Ground Truth Galore: Terrestrial Impact Craters, Tue, a.m., Waterway Ballroom 5
Kelley S. P.	E/PO: Meteorites Posters, Tue, p.m., Town Center Exhibit Area
Kelly M.	Spacecraft Instruments Posters, Tue, p.m., Town Center Exhibit Area
Kenkmann T.	Ground Truth Galore: Terrestrial Impact Craters, Tue, a.m., Waterway Ballroom 5
Kenkmann T.	Impact Experiments Posters, Tue, p.m., Town Center Exhibit Area
Kenkmann T.	Impact Craters Posters, Tue, p.m., Town Center Exhibit Area
Kennedy M.	Mars: Timing of Geologic Processes, Fri, p.m., Waterway Ballroom 4
Kerber L.	Igneous and Volcanic Processes Posters, Thu, p.m., Town Center Exhibit Area
Kereszturi A.	Martian Polar Processes Posters, Tue, p.m., Town Center Exhibit Area
Kereszturi A.	Mars Ice and Craters Posters, Tue, p.m., Town Center Exhibit Area
Kereszturi A.	Mars: Gullies and Slope Streaks Posters, Thu, p.m., Town Center Exhibit Area
Kerzhanovich V. V.	Mission Plans and Concepts Posters, Tue, p.m., Town Center Exhibit Area
Kestay L.	A New Moon: Geologic Processes Posters, Tue, p.m., Town Center Exhibit Area
Kestay L.	Impacts on the Moon, Mars, and Beyond, Wed, p.m., Waterway Ballroom 5
Keszthelyi L.	Mission Plans and Concepts Posters, Tue, p.m., Town Center Exhibit Area
Keszthelyi L.	A New Moon: Lunar Volcanism, Thu, p.m., Waterway Ballroom 6
Keszthelyi L.	Igneous and Volcanic Processes Posters, Thu, p.m., Town Center Exhibit Area
Keszthelyi L. P.	A New Moon: Geologic Processes Posters, Tue, p.m., Town Center Exhibit Area
Keszthelyi L. P. *	Igneous and Volcanic Processes, Thu, a.m., Waterway Ballroom 5
Keszthelyi L. P.	Satellites and Their Planets Posters, Thu, p.m., Town Center Exhibit Area
Keszthelyi L. P.	Igneous and Volcanic Processes Posters, Thu, p.m., Town Center Exhibit Area
Kharitonova G. A.	Print Only: Planetary Atmospheres
Kharytonov A.	Spacecraft Instruments Posters, Tue, p.m., Town Center Exhibit Area
Khurana K.	Mission Plans and Concepts Posters, Tue, p.m., Town Center Exhibit Area
Khurana K. K.	Once and Future Moon Posters, Thu, p.m., Town Center Exhibit Area
Kiefer W.	Large Impact Basins on the Moon, Thu, a.m., Waterway Ballroom 6
Kiefer W.	Small Bodies, Fri, p.m., Waterway Ballroom 5
Kiefer W. S.	A New Moon: Geologic Processes Posters, Tue, p.m., Town Center Exhibit Area
Kiefer W. S.	Planetary Dynamics and Tectonics, Wed, a.m., Waterway Ballroom 5
Kiefer W. S.	Lunar Geophysics Posters, Thu, p.m., Town Center Exhibit Area
Kiefer W. S.	Martian Igneous Processes, Fri, a.m., Waterway Ballroom 5
Kiely C. *	Nature of the Lunar Regolith, Wed, a.m., Waterway Ballroom 6
Kiely C.	Lunar Regolith Posters, Thu, p.m., Town Center Exhibit Area
Kiely C. J.	Nature of the Lunar Regolith, Wed, a.m., Waterway Ballroom 6
Kiely C. J.	Lunar Regolith Posters, Thu, p.m., Town Center Exhibit Area
Kilcoyne A. L. D.	Solar Wind, Volatile Elements, and Organics, Thu, a.m., Waterway Ballroom 1
Kilcoyne A. L. D.	Stardust Mission Posters, Thu, p.m., Town Center Exhibit Area
Killen R.	A New Moon: LCROSS Posters, Tue, p.m., Town Center Exhibit Area
Killen R. M.	Water in the Solar System: Moon, Tue, p.m., Waterway Ballroom 6
Killen R. M.	Mercury, Tue, p.m., Montgomery Ballroom
Killen R. M.	A New Moon: LCROSS Posters, Tue, p.m., Town Center Exhibit Area
Kim J.	Water in the Solar System: Moon, Tue, p.m., Waterway Ballroom 6
Kim J.	Mars: Fluvial Geomorphology and Processes, Thu, a.m., Waterway Ballroom 4
Kim K. J.	Lunar Petrology and Geochemistry Posters, Tue, p.m., Town Center Exhibit Area
Kim K. J.	A New Moon: Volatile Species Posters, Tue, p.m., Town Center Exhibit Area
Kim K. J. *	Large Impact Basins on the Moon, Thu, a.m., Waterway Ballroom 6
Kim K. J.	Environments for Life Posters, Thu, p.m., Town Center Exhibit Area
Kim S.	Environmental Analogs Posters, Thu, p.m., Town Center Exhibit Area
Kim T.	A New Moon: Spectral Constraints Posters, Thu, p.m., Town Center Exhibit Area
Kim W.	Mars Polar Processes, Tue, p.m., Waterway Ballroom 4
Kimberley J.	Print Only: Impacts
Kimberley J.	Impact Experiments Posters, Tue, p.m., Town Center Exhibit Area
Kimura H.	Parent Cloud and Disk Processes Posters, Tue, p.m., Town Center Exhibit Area
Kimura H.	Once and Future Moon Posters, Thu, p.m., Town Center Exhibit Area
Kimura J.	Iron and Stony Iron Meteorites Posters, Tue, p.m., Town Center Exhibit Area
Kimura J.	A New Moon: Geologic Processes Posters, Tue, p.m., Town Center Exhibit Area
Kimura M.	Formation of Building Blocks, Fri, p.m., Waterway Ballroom 1
Kimura Y.	Solar Wind, Volatile Elements, and Organics Posters, Thu, p.m., Town Center Exhibit Area
Kincy L.	Mars: Gullies and Slope Streaks Posters, Thu, p.m., Town Center Exhibit Area

Lu J.	Mercury Posters, Tue, p.m., Town Center Exhibit Area
Lu Y.	Print Only: Moon
Lucchitta B. K.	Mars: Fluvial Geomorphology and Processes Posters, Thu, p.m., Town Center Exhibit Area
Lucey P.	Lunar Cartography, Stereogrammetry, and Imaging Posters, Thu, p.m., Town Center Exhibit Area
Lucey P. G.	Print Only: Mercury
Lucey P. G.	A New Moon: LRO Results, Mon, a.m., Waterway Ballroom 6
Lucey P. G.	A New Moon: LCROSS, Chandrayaan, Chang'E, Tue, a.m., Waterway Ballroom 6
Lucey P. G.	A New Moon: Geologic Processes Posters, Tue, p.m., Town Center Exhibit Area
Lucey P. G.	Material Analogs Posters, Tue, p.m., Town Center Exhibit Area
Lucey P. G.	Spacecraft Instruments Posters, Tue, p.m., Town Center Exhibit Area
Lucey P. G.	A New Moon: Spectral Constraints, Wed, p.m., Waterway Ballroom 6
Lucey P. G. *	A New Moon: Spectral Constraints, Wed, p.m., Waterway Ballroom 6
Lucey P. G.	A New Moon: Spectral Constraints Posters, Thu, p.m., Town Center Exhibit Area
Luckey M.	E/PO: Moon Posters, Tue, p.m., Town Center Exhibit Area
Lugmair G.	Print Only: Differentiated Bodies
Lundeen S.	Large Impact Basins on the Moon, Thu, a.m., Waterway Ballroom 6
Lundeen S.	A New Moon: Spectral Constraints Posters, Thu, p.m., Town Center Exhibit Area
Lundeen S.	Petrologic Characterization of the Moon, Fri, p.m., Waterway Ballroom 6
Lundeen S. R.	A New Moon: Spectral Constraints Posters, Thu, p.m., Town Center Exhibit Area
Lundy M.	Print Only: Data and Image Systems
Lunine J.	Impacts Modeling Posters, Tue, p.m., Town Center Exhibit Area
Lunine J.	Several Species of Icy Chunks, Thu, p.m., Waterway Ballroom 5
Lunine J. I.	Planetary Aeolian Processes, Tue, p.m., Waterway Ballroom 4
Lunine J. I.	Mission Plans and Concepts Posters, Tue, p.m., Town Center Exhibit Area
Lunine J. I.	Several Species of Icy Chunks, Thu, p.m., Waterway Ballroom 5
Lunine J. I.	Planetary Dynamics and Tectonics Posters, Thu, p.m., Town Center Exhibit Area
Luo W. *	Mars: Fluvial Geomorphology and Processes, Thu, a.m., Waterway Ballroom 4
Lupisella M. L.	Once and Future Moon Posters, Thu, p.m., Town Center Exhibit Area
Luspay-Kuti A.	Mars Ice and Craters Posters, Tue, p.m., Town Center Exhibit Area
Lv Z.	Print Only: Moon
Lv Z.	Print Only: Environmental and Material Analogs
Lynett P.	Impact Models and More, Tue, p.m., Waterway Ballroom 5
Lyon I.	Origins of Presolar Grains Posters, Thu, p.m., Town Center Exhibit Area
Lyon I.	Solar Wind, Volatile Elements, and Organics Posters, Thu, p.m., Town Center Exhibit Area
Lyon I.	Thermal and Aqueous Processes Posters, Thu, p.m., Town Center Exhibit Area
Lyons J. R. *	Parent Cloud and Solar Nebula, Mon, a.m., Waterway Ballroom 1
Lyons J. R.	Parent Cloud and Disk Processes Posters, Tue, p.m., Town Center Exhibit Area
Lytle D. M.	Satellites and Their Planets Posters, Thu, p.m., Town Center Exhibit Area
M3 Team	A New Moon: Spectral Constraints Posters, Thu, p.m., Town Center Exhibit Area
M3 Team	A New Moon: Geologic Processes Posters, Tue, p.m., Town Center Exhibit Area
M3 Team	A New Moon: Spectral Constraints, Wed, p.m., Waterway Ballroom 6
M3 Team	A New Moon: Lunar Volcanism, Thu, p.m., Waterway Ballroom 6
M3 Team	A New Moon: Spectral Constraints Posters, Thu, p.m., Town Center Exhibit Area
M3 Team	Petrologic Characterization of the Moon, Fri, p.m., Waterway Ballroom 6
Ma C.	Formation of First Solar System Solids Posters, Tue, p.m., Town Center Exhibit Area
Ma P.	Cosmic-Ray Exposure Dating Posters, Tue, p.m., Town Center Exhibit Area
Ma T.	A New Moon: LCROSS, Chandrayaan, Chang'E, Tue, a.m., Waterway Ballroom 6
Machii N.	Print Only: Small Bodies
Machii N.	Print Only: Impacts
Mackay S. L.	Terrestrial Planet Cryospheres, Tue, a.m., Waterway Ballroom 4
Macke R. J.	Chondrites Posters, Thu, p.m., Town Center Exhibit Area
Macke R. J.	Lunar Geophysics Posters, Thu, p.m., Town Center Exhibit Area
Macke R. J.	Small Bodies, Fri, p.m., Waterway Ballroom 5
Mackety D.	E/PO: Professional Development Posters, Tue, p.m., Town Center Exhibit Area
MacKinnon P.	Planetary Dynamics and Tectonics Posters, Thu, p.m., Town Center Exhibit Area
MacPherson G.	Stardust Mission to Comet Wild 2, Wed, a.m., Waterway Ballroom 1
MacPherson G. J. *	Radionuclides and Early Solar System Chronology, Tue, a.m., Waterway Ballroom 1
MacPherson G. J.	Formation of First Solar System Solids Posters, Tue, p.m., Town Center Exhibit Area
Madden A. S.	Experimental Constraints on Martian Alteration Processes, Mon, p.m., Waterway Ballroom 4
Maddison B.	Lunar Petrology and Geochemistry Posters, Tue, p.m., Town Center Exhibit Area
Madeleine J. B.	Igneous and Volcanic Processes Posters, Thu, p.m., Town Center Exhibit Area
Madeleine J.-B.	Terrestrial Planet Cryospheres Posters, Tue, p.m., Town Center Exhibit Area
Madeleine J.-B.	Planetary Atmospheres, Wed, p.m., Montgomery Ballroom
Mader D.	Impactite Petrology and Ages Posters, Tue, p.m., Town Center Exhibit Area
Madiedo J. M.	Print Only: Small Bodies
Madsen M. B.	Planetary Aeolian Processes Posters, Tue, p.m., Town Center Exhibit Area
Madsen M. B.	Exploring the Martian Crust Posters, Thu, p.m., Town Center Exhibit Area

Maeda M.	Print Only: Impacts
Magni G.	Spacecraft Instruments Posters, Tue, p.m., Town Center Exhibit Area
Magri C.	Vesta and Dawn, Tue, p.m., Waterway Ballroom 1
Mahaffy P.	Spacecraft Instruments Posters, Tue, p.m., Town Center Exhibit Area
Mahaffy P.	Mission Plans and Concepts Posters, Tue, p.m., Town Center Exhibit Area
Mahaffy P.	Once and Future Moon Posters, Thu, p.m., Town Center Exhibit Area
Mahaffy P. R.	Material Analogs Posters, Tue, p.m., Town Center Exhibit Area
Mahaffy P. R.	Spacecraft Instruments Posters, Tue, p.m., Town Center Exhibit Area
Mahaney W. C.	Environments for Life Posters, Thu, p.m., Town Center Exhibit Area
Mahanti P.	Lunar Cartography, Stereogrammetry, and Imaging Posters, Thu, p.m., Town Center Exhibit Area
Mahapatra P.	Mission Plans and Concepts Posters, Tue, p.m., Town Center Exhibit Area
Mahapatra P.	Environmental Analogs Posters, Thu, p.m., Town Center Exhibit Area
Mahapatra P.	Mission Plans and Concepts Posters, Tue, p.m., Town Center Exhibit Area
Mahapatra P.	Environmental Analogs Posters, Thu, p.m., Town Center Exhibit Area
Maine A.	Terrestrial Planet Cryospheres, Tue, a.m., Waterway Ballroom 4
Maine A.	Mars Ice and Craters Posters, Tue, p.m., Town Center Exhibit Area
Mainzer A. K.	Small Body Missions Posters, Tue, p.m., Town Center Exhibit Area
Mainzer A. K. *	Characterizing Near-Earth Objects, Thu, p.m., Waterway Ballroom 4
Mainzer A. K.	Small Bodies, Fri, p.m., Waterway Ballroom 5
Makarewicz H.	Martian Alteration Processes Posters, Tue, p.m., Town Center Exhibit Area
Makarewicz H. D.	Material Analogs Posters, Tue, p.m., Town Center Exhibit Area
Makarewicz H. D.	Exploring the Martian Crust Posters, Thu, p.m., Town Center Exhibit Area
Maki J. N.	Print Only: Mars
Maki J. N.	Mars Remote Sensing Techniques Posters, Thu, p.m., Town Center Exhibit Area
Makide K. *	Radionuclides and Early Solar System Chronology, Tue, a.m., Waterway Ballroom 1
Malakhov A.	Print Only: Moon
Malakhov A.	A New Moon: LRO Results, Mon, a.m., Waterway Ballroom 6
Malakhov A.	A New Moon: Volatile Species Posters, Tue, p.m., Town Center Exhibit Area
Malakhov A. V.	Spacecraft Instruments Posters, Tue, p.m., Town Center Exhibit Area
Malaret E.	Martian Alteration Processes, Mon, a.m., Waterway Ballroom 4
Malaret E.	Large Impact Basins on the Moon, Thu, a.m., Waterway Ballroom 6
Malaret E.	A New Moon: Spectral Constraints Posters, Thu, p.m., Town Center Exhibit Area
Malaret E.	E/PO: Mars Remote Sensing Posters, Thu, p.m., Town Center Exhibit Area
Malaret E.	Petrologic Characterization of the Moon, Fri, p.m., Waterway Ballroom 6
Malaska M.	Satellites and Their Planets Posters, Thu, p.m., Town Center Exhibit Area
Malin M. C.	Print Only: Mars
Malin M. C.	A New Moon: LRO Results, Mon, a.m., Waterway Ballroom 6
Malin M. C.	Planetary Aeolian Processes Posters, Tue, p.m., Town Center Exhibit Area
Mall U.	A New Moon: Spectral Constraints, Wed, p.m., Waterway Ballroom 6
Mall U.	A New Moon: Spectral Constraints Posters, Thu, p.m., Town Center Exhibit Area
Malley K.	Rocks, Life, and Biosignatures, Thu, p.m., Waterway Ballroom 1
Malone L.	Impactite Petrology and Ages Posters, Tue, p.m., Town Center Exhibit Area
Mancinelli R.	Rocks, Life, and Biosignatures, Thu, p.m., Waterway Ballroom 1
Mandell D.	Thermal and Aqueous Processes on Chondrite Parent Bodies, Fri, a.m., Waterway Ballroom 1
Mandrake L.	Spacecraft Instruments Posters, Tue, p.m., Town Center Exhibit Area
Mane A.	Origins of Presolar Grains Posters, Thu, p.m., Town Center Exhibit Area
Manga M.	Planetary Atmospheres, Wed, p.m., Montgomery Ballroom
Manga M.	Igneous and Volcanic Processes, Thu, a.m., Waterway Ballroom 5
Manga M.	Lunar Geophysics Posters, Thu, p.m., Town Center Exhibit Area
Manga M.	Mars Craters Posters, Thu, p.m., Town Center Exhibit Area
Manga M.	Planetary Dynamics and Tectonics Posters, Thu, p.m., Town Center Exhibit Area
Mangold N.	Experimental Constraints on Martian Alteration Processes, Mon, p.m., Waterway Ballroom 4
Mangold N.	Martian Alteration Processes Posters, Tue, p.m., Town Center Exhibit Area
Mangold N. *	Mars: Fluvial Geomorphology and Processes, Thu, a.m., Waterway Ballroom 4
Mangold N.	Exploring the Martian Crust Posters, Thu, p.m., Town Center Exhibit Area
Mangold N.	Mars: Deposition and Erosion, Fri, a.m., Waterway Ballroom 4
Mann U.	Planetary Differentiation, Mon, a.m., Waterway Ballroom 5
Manzella D.	Mission Plans and Concepts Posters, Tue, p.m., Town Center Exhibit Area
Mao P. H.	Solar Wind, Volatile Elements, and Organics, Thu, a.m., Waterway Ballroom 1
Marangoni Y. R.	Impact Models and More, Tue, p.m., Waterway Ballroom 5
Marchand G. J.	Exploring the Martian Crust Posters, Thu, p.m., Town Center Exhibit Area
Marchant D.	Terrestrial Planet Cryospheres Posters, Tue, p.m., Town Center Exhibit Area
Marchant D.	Mars: Timing of Geologic Processes, Fri, p.m., Waterway Ballroom 4
Marchant D. R. *	Terrestrial Planet Cryospheres, Tue, a.m., Waterway Ballroom 4
Marchant D. R.	Terrestrial Planet Cryospheres Posters, Tue, p.m., Town Center Exhibit Area
Marchant D. R.	Mars: Gullies and Slope Streaks Posters, Thu, p.m., Town Center Exhibit Area
Marchant D. R.	Environmental Analogs Posters, Thu, p.m., Town Center Exhibit Area

Mazarico E.	A New Moon: LCROSS Posters, Tue, p.m., Town Center Exhibit Area
Mazarico E.	A New Moon: Geologic Processes Posters, Tue, p.m., Town Center Exhibit Area
Mazarico E.	A New Moon: Spectral Constraints, Wed, p.m., Waterway Ballroom 6
Mazarico E.	Large Impact Basins on the Moon, Thu, a.m., Waterway Ballroom 6
Mazarico E.	Planetary Dynamics and Tectonics Posters, Thu, p.m., Town Center Exhibit Area
Mazarico E. M.	A New Moon: Geologic Processes Posters, Tue, p.m., Town Center Exhibit Area
Mazur J.	Lunar Radiation Posters, Thu, p.m., Town Center Exhibit Area
McAdam A. C.	Material Analogs Posters, Tue, p.m., Town Center Exhibit Area
McArthur G.	E/PO: Mars Remote Sensing Posters, Thu, p.m., Town Center Exhibit Area
McCanta M. C. *	Thermal and Aqueous Processes on Chondrite Parent Bodies, Fri, a.m., Waterway Ballroom 1
McCarthy D. W.	E/PO: Miscellaneous Posters, Thu, p.m., Town Center Exhibit Area
McCausland P. J. A.	Laboratory Instruments and Samples Posters, Tue, p.m., Town Center Exhibit Area
McCausland P. J. A.	Chondrites Posters, Thu, p.m., Town Center Exhibit Area
McClanahan T.	A New Moon: LRO Results, Mon, a.m., Waterway Ballroom 6
McClanahan T.	A New Moon: Volatile Species Posters, Tue, p.m., Town Center Exhibit Area
McClanahan T.	Spacecraft Instruments Posters, Tue, p.m., Town Center Exhibit Area
McClanahan T. P.	A New Moon: Volatile Species Posters, Tue, p.m., Town Center Exhibit Area
McCleese D. J.	A New Moon: LRO Results, Mon, a.m., Waterway Ballroom 6
McClintock W.	A New Moon: Spectral Constraints Posters, Thu, p.m., Town Center Exhibit Area
McClintock W. E.	Mercury, Tue, p.m., Montgomery Ballroom
McClintock W. E.	Mercury Posters, Tue, p.m., Town Center Exhibit Area
McCollom T. M.	Martian Alteration Processes Posters, Tue, p.m., Town Center Exhibit Area
McCollom T. M.	Material Analogs Posters, Tue, p.m., Town Center Exhibit Area
McCord T.	A New Moon: Geologic Processes Posters, Tue, p.m., Town Center Exhibit Area
McCord T.	Spacecraft Instruments Posters, Tue, p.m., Town Center Exhibit Area
McCord T.	Large Impact Basins on the Moon, Thu, a.m., Waterway Ballroom 6
McCord T.	A New Moon: Spectral Constraints Posters, Thu, p.m., Town Center Exhibit Area
McCord T. B. *	Water in the Solar System: Moon, Tue, p.m., Waterway Ballroom 6
McCord T. B.	A New Moon: Geologic Processes Posters, Tue, p.m., Town Center Exhibit Area
McCord T. B.	A New Moon: Spectral Constraints Posters, Thu, p.m., Town Center Exhibit Area
McCord T. B.	Satellites and Their Planets Posters, Thu, p.m., Town Center Exhibit Area
McCord T. B.	Petrologic Characterization of the Moon, Fri, p.m., Waterway Ballroom 6
McCoy T.	Exploring the Martian Crust, Wed, a.m., Waterway Ballroom 4
McCoy T. J.	Radionuclides and Early Solar System Chronology, Tue, a.m., Waterway Ballroom 1
McCoy T. J.	Mercury, Tue, p.m., Montgomery Ballroom
McCoy T. J.	Martian Alteration Processes Posters, Tue, p.m., Town Center Exhibit Area
McCoy T. J.	Chondrites Posters, Thu, p.m., Town Center Exhibit Area
McCoy T. J.	Martian Igneous Processes, Fri, a.m., Waterway Ballroom 5
McCoy T. J.	Small Bodies, Fri, p.m., Waterway Ballroom 5
McCrossin C. G.	Lunar Dust Posters, Thu, p.m., Town Center Exhibit Area
McCubbin F. M.	Print Only: Mercury
McCubbin F. M. *	Water in the Solar System: Moon, Tue, p.m., Waterway Ballroom 6
McCubbin F. M.	Martian Alteration Processes Posters, Tue, p.m., Town Center Exhibit Area
McCubbin F. M.	Martian Meteorites Posters, Thu, p.m., Town Center Exhibit Area
McCutcheon W.	Spacecraft Instruments Posters, Tue, p.m., Town Center Exhibit Area
McDaniel S.	Mars: Gullies and Slope Streaks Posters, Thu, p.m., Town Center Exhibit Area
McDoniel W. J.	Planetary Atmospheres Posters, Thu, p.m., Town Center Exhibit Area
McDonough W. F.	Ureilites Posters, Tue, p.m., Town Center Exhibit Area
McDonough W. F.	Planetary Differentiation, Mon, a.m., Waterway Ballroom 5
McDonough W. F.	Planetary Differentiation Posters, Tue, p.m., Town Center Exhibit Area
McDowell M. L.	Exploring the Martian Crust, Wed, a.m., Waterway Ballroom 4
McElhoney K.	Martian Alteration Processes, Mon, a.m., Waterway Ballroom 4
McEwen A.	Mars Polar Processes, Tue, p.m., Waterway Ballroom 4
McEwen A.	Planetary Aeolian Processes, Tue, p.m., Waterway Ballroom 4
McEwen A.	Mission Plans and Concepts Posters, Tue, p.m., Town Center Exhibit Area
McEwen A.	Exploring the Martian Crust, Wed, a.m., Waterway Ballroom 4
McEwen A.	Lunar Cartography, Stereogrammetry, and Imaging Posters, Thu, p.m., Town Center Exhibit Area
McEwen A. S.	A New Moon: LRO Results, Mon, a.m., Waterway Ballroom 6
McEwen A. S.	Terrestrial Planet Cryospheres, Tue, a.m., Waterway Ballroom 4
McEwen A. S.	Impact Craters Posters, Tue, p.m., Town Center Exhibit Area
McEwen A. S.	Planetary Aeolian Processes Posters, Tue, p.m., Town Center Exhibit Area
McEwen A. S.	Impacts on the Moon, Mars, and Beyond, Wed, p.m., Waterway Ballroom 5
McEwen A. S.	Exploring the Martian Crust Posters, Thu, p.m., Town Center Exhibit Area
McEwen A. S.	Mars Craters Posters, Thu, p.m., Town Center Exhibit Area
McEwen A. S.	Igneous and Volcanic Processes Posters, Thu, p.m., Town Center Exhibit Area
McEwen A. S.	Mars: Deposition and Erosion, Fri, a.m., Waterway Ballroom 4
McEwen A. S.	Mars: Timing of Geologic Processes, Fri, p.m., Waterway Ballroom 4

Moersch J. E.	Exploring the Martian Crust Posters, Thu, p.m., Town Center Exhibit Area
Moersch J. E.	Environmental Analogs Posters, Thu, p.m., Town Center Exhibit Area
Moggi-Cecchi V.	Print Only: Differentiated Bodies
Möhlmann D. T. F.	Experimental Constraints on Martian Alteration Processes, Mon, p.m., Waterway Ballroom 4
Mohrig D.	Mars Polar Processes, Tue, p.m., Waterway Ballroom 4
Mohr-Westheide T.	Impactite Petrology and Ages Posters, Tue, p.m., Town Center Exhibit Area
Moilanen J.	Impactite Petrology and Ages Posters, Tue, p.m., Town Center Exhibit Area
Mojzsis S. J.	Rocks, Life, and Biosignatures, Thu, p.m., Waterway Ballroom 1
Mokrousov M.	A New Moon: LRO Results, Mon, a.m., Waterway Ballroom 6
Mokrousov M.	A New Moon: Volatile Species Posters, Tue, p.m., Town Center Exhibit Area
Mokrousov M. I.	Spacecraft Instruments Posters, Tue, p.m., Town Center Exhibit Area
Moldovan R. *	Small Bodies, Fri, p.m., Waterway Ballroom 5
Molina A.	Print Only: Mars
Monaghan E.	Environmental Analogs Posters, Thu, p.m., Town Center Exhibit Area
Monaghan E.	Mission Plans and Concepts Posters, Tue, p.m., Town Center Exhibit Area
Monaghan E.	Environmental Analogs Posters, Thu, p.m., Town Center Exhibit Area
Monegato G.	Impact Craters Posters, Tue, p.m., Town Center Exhibit Area
Monkawa A.	Martian Meteorites Posters, Thu, p.m., Town Center Exhibit Area
Montabone L.	Planetary Atmospheres, Wed, p.m., Montgomery Ballroom
Montanyá J.	Print Only: Small Bodies
Montecinos A.	Planetary Aeolian Processes Posters, Tue, p.m., Town Center Exhibit Area
Montes-Hernandez G.	Water in the Solar System: Primitive Bodies, Mon, p.m., Waterway Ballroom 6
Monteux J.	Planetary Differentiation Posters, Tue, p.m., Town Center Exhibit Area
Moon Zoo Team	E/PO: Moon Posters, Tue, p.m., Town Center Exhibit Area
Moore C. H.	Planetary Atmospheres, Wed, p.m., Montgomery Ballroom
Moore C. H. *	Planetary Atmospheres, Wed, p.m., Montgomery Ballroom
Moore J. M. *	Several Species of Icy Chunks, Thu, p.m., Waterway Ballroom 5
Moore J. M.	Mars: Fluvial Geomorphology and Processes Posters, Thu, p.m., Town Center Exhibit Area
Moore M. H.	Several Species of Icy Chunks, Thu, p.m., Waterway Ballroom 5
Moore Q.	Environmental Analogs Posters, Thu, p.m., Town Center Exhibit Area
Moore W. B.	Vesta and Dawn, Tue, p.m., Waterway Ballroom 1
Moore W. B.	Interior of the Moon, Fri, a.m., Waterway Ballroom 6
Mora C.	Environmental Analogs Posters, Thu, p.m., Town Center Exhibit Area
Moratto Z.	A New Moon: Spectral Constraints Posters, Thu, p.m., Town Center Exhibit Area
Moratto Z.	Lunar Cartography, Stereogrammetry, and Imaging Posters, Thu, p.m., Town Center Exhibit Area
Moratto Z. M.	Print Only: Data and Image Systems
Morbidelli A.	Characterizing Near-Earth Objects, Thu, p.m., Waterway Ballroom 4
Morbidelli A.	Small Bodies, Fri, p.m., Waterway Ballroom 5
Moreno-Vargas J.	Print Only: Small Bodies
Moreno-Ventas J.	Print Only: Small Bodies
Moreschini P.	Once and Future Moon Posters, Thu, p.m., Town Center Exhibit Area
Morgan D. D.	Planetary Atmospheres Posters, Thu, p.m., Town Center Exhibit Area
Morgan F.	Planetary Atmospheres Posters, Thu, p.m., Town Center Exhibit Area
Morgan G. A.	Terrestrial Planet Cryospheres, Tue, a.m., Waterway Ballroom 4
Morgan G. A.	Mars: Gullies and Slope Streaks Posters, Thu, p.m., Town Center Exhibit Area
Morgan G. A. *	Mars: Timing of Geologic Processes, Fri, p.m., Waterway Ballroom 4
Morgan J. V.	Impacts Modeling Posters, Tue, p.m., Town Center Exhibit Area
Morgan P.	Once and Future Moon Posters, Thu, p.m., Town Center Exhibit Area
Moriarty D.	Ice and Dust Posters, Thu, p.m., Town Center Exhibit Area
Moriarty D.	Water in the Solar System: Primitive Bodies, Mon, p.m., Waterway Ballroom 6
Morita S.	A New Moon: Geologic Processes Posters, Tue, p.m., Town Center Exhibit Area
Morley J.	Mars: Fluvial Geomorphology and Processes, Thu, a.m., Waterway Ballroom 4
Morlok A.	Formation of Building Blocks Posters, Thu, p.m., Town Center Exhibit Area
Morlok A.	BOOM! Posters, Thu, p.m., Town Center Exhibit Area
Morookian J.	Venus Posters, Tue, p.m., Town Center Exhibit Area
Morota T.	Lunar Meteorites Posters, Tue, p.m., Town Center Exhibit Area
Morota T.	Lunar Petrology and Geochemistry Posters, Tue, p.m., Town Center Exhibit Area
Morota T.	A New Moon: Geologic Processes Posters, Tue, p.m., Town Center Exhibit Area
Morota T.	A New Moon: Spectral Constraints, Wed, p.m., Waterway Ballroom 6
Morota T.	A New Moon: Lunar Volcanism, Thu, p.m., Waterway Ballroom 6
Morota T.	A New Moon: Spectral Constraints Posters, Thu, p.m., Town Center Exhibit Area
Morota T.	Petrologic Characterization of the Moon, Fri, p.m., Waterway Ballroom 6
Moroz L. V.	Venus, Mon, p.m., Waterway Ballroom 5
Morris M. A.	Formation of First Solar System Solids, Mon, p.m., Waterway Ballroom 1
Morris M. A.	Formation of Building Blocks Posters, Thu, p.m., Town Center Exhibit Area
Morris M. R.	Parent Cloud and Solar Nebula, Mon, a.m., Waterway Ballroom 1
Morris R.	Spacecraft Instruments Posters, Tue, p.m., Town Center Exhibit Area

Mustard J.	Petrologic Characterization of the Moon, Fri, p.m., Waterway Ballroom 6
Mustard J. F.	Martian Alteration Processes, Mon, a.m., Waterway Ballroom 4
Mustard J. F.	Water in the Solar System: Moon, Tue, p.m., Waterway Ballroom 6
Mustard J. F.	Martian Alteration Processes Posters, Tue, p.m., Town Center Exhibit Area
Mustard J. F.	Exploring the Martian Crust, Wed, a.m., Waterway Ballroom 4
Mustard J. F. *	Exploring the Martian Crust, Wed, a.m., Waterway Ballroom 4
Mustard J. F. *	A New Moon: Spectral Constraints, Wed, p.m., Waterway Ballroom 6
Mustard J. F.	A New Moon: Spectral Constraints Posters, Thu, p.m., Town Center Exhibit Area
Mustard J. F.	Planetary Atmospheres Posters, Thu, p.m., Town Center Exhibit Area
Mustard J. F.	Mars: Geologic, Geomorphic, etc., Posters, Thu, p.m., Town Center Exhibit Area
Mustard J. F.	Exploring the Martian Crust Posters, Thu, p.m., Town Center Exhibit Area
Mustard J. F.	Mars Craters Posters, Thu, p.m., Town Center Exhibit Area
Mustard J. F.	Environmental Analogs Posters, Thu, p.m., Town Center Exhibit Area
Muttik N.	Impact Ejecta Posters, Tue, p.m., Town Center Exhibit Area
Muttik N.	Impactite Petrology and Ages Posters, Tue, p.m., Town Center Exhibit Area
Myers J.	Small Body Missions Posters, Tue, p.m., Town Center Exhibit Area
Nagahara H. *	Parent Cloud and Solar Nebula, Mon, a.m., Waterway Ballroom 1
Nagahara H.	Formation of Building Blocks Posters, Thu, p.m., Town Center Exhibit Area
Nagahara H.	Petrologic Characterization of the Moon, Fri, p.m., Waterway Ballroom 6
Nagao K.	Print Only: Cosmochemical Origins
Nagao K.	Print Only: Differentiated Bodies
Nagao K.	Formation of Building Blocks, Fri, p.m., Waterway Ballroom 1
Nagarajan S.	Mars Ice and Craters Posters, Tue, p.m., Town Center Exhibit Area
Nagasawa K.	A New Moon: Spectral Constraints Posters, Thu, p.m., Town Center Exhibit Area
Nagashima K. *	Formation of First Solar System Solids, Mon, p.m., Waterway Ballroom 1
Nagashima K.	Radionuclides and Early Solar System Chronology, Tue, a.m., Waterway Ballroom 1
Nagashima K.	Radionuclides and Early Solar System Chronology Posters, Tue, p.m., Town Center Exhibit Area
Nagashima K.	Formation of First Solar System Solids Posters, Tue, p.m., Town Center Exhibit Area
Nagashima K.	Impact Ejecta Posters, Tue, p.m., Town Center Exhibit Area
Nagashima K.	Stardust Mission to Comet Wild 2, Wed, a.m., Waterway Ballroom 1
Nagashima K.	Stardust Mission Posters, Thu, p.m., Town Center Exhibit Area
Nagashima K.	Formation of Building Blocks Posters, Thu, p.m., Town Center Exhibit Area
Nagashima K.	Thermal and Aqueous Processes on Chondrite Parent Bodies, Fri, a.m., Waterway Ballroom 1
Nagata K.	A New Moon: Spectral Constraints Posters, Thu, p.m., Town Center Exhibit Area
Nagihara S.	Once and Future Moon Posters, Thu, p.m., Town Center Exhibit Area
Nagihara S. *	Interior of the Moon, Fri, a.m., Waterway Ballroom 6
Nagy Sz.	Print Only: Impacts
Nagy Sz.	Lunar Meteorites Posters, Tue, p.m., Town Center Exhibit Area
Nahm A. L. *	Planetary Dynamics and Tectonics, Wed, a.m., Waterway Ballroom 5
Naidu S.	Main Belt Posters, Tue, p.m., Town Center Exhibit Area
Naidu S.	A New Moon: LCROSS Posters, Tue, p.m., Town Center Exhibit Area
Nakajo T.	Spacecraft Instruments Posters, Tue, p.m., Town Center Exhibit Area
Nakamoto T.	Cosmic Dust Posters, Thu, p.m., Town Center Exhibit Area
Nakamura A. M.	Print Only: Small Bodies
Nakamura A. M.	Print Only: Impacts
Nakamura M.	Once and Future Moon Posters, Thu, p.m., Town Center Exhibit Area
Nakamura N.	Laboratory Instruments and Samples Posters, Tue, p.m., Town Center Exhibit Area
Nakamura R.	A New Moon: LCROSS, Chandrayaan, Chang'E, Tue, a.m., Waterway Ballroom 6
Nakamura R.	Lunar Meteorites Posters, Tue, p.m., Town Center Exhibit Area
Nakamura R.	Lunar Petrology and Geochemistry Posters, Tue, p.m., Town Center Exhibit Area
Nakamura R.	A New Moon: Spectral Constraints, Wed, p.m., Waterway Ballroom 6
Nakamura R.	Near-Earth Objects Posters, Thu, p.m., Town Center Exhibit Area
Nakamura R.	A New Moon: Spectral Constraints Posters, Thu, p.m., Town Center Exhibit Area
Nakamura R.	Lunar Cartography, Stereogrammetry, and Imaging Posters, Thu, p.m., Town Center Exhibit Area
Nakamura R.	Petrologic Characterization of the Moon, Fri, p.m., Waterway Ballroom 6
Nakamura T.	Print Only: Cosmochemical Origins
Nakamura T.	Main Belt Posters, Tue, p.m., Town Center Exhibit Area
Nakamura T.	Cosmic Dust Posters, Thu, p.m., Town Center Exhibit Area
Nakamura T.	Thermal and Aqueous Processes on Chondrite Parent Bodies, Fri, a.m., Waterway Ballroom 1
Nakamura-Messenger K.	Formation of First Solar System Solids Posters, Tue, p.m., Town Center Exhibit Area
Nakamura-Messenger K.	Solar Wind, Volatile Elements, and Organics, Thu, a.m., Waterway Ballroom 1
Nakamura-Messenger K.	Cosmic Dust, Thu, p.m., Waterway Ballroom 1
Nakamura-Messenger K.	Cosmic Dust Posters, Thu, p.m., Town Center Exhibit Area
Nakamura-Messenger K.	Solar Wind, Volatile Elements, and Organics Posters, Thu, p.m., Town Center Exhibit Area
Nakano T.	Solar Wind, Volatile Elements, and Organics Posters, Thu, p.m., Town Center Exhibit Area
Nakanotani S.	A New Moon: Spectral Constraints Posters, Thu, p.m., Town Center Exhibit Area
Nakashima D.	Print Only: Differentiated Bodies

Nakashima D.	Laboratory Instruments and Samples Posters, Tue, p.m., Town Center Exhibit Area
Nakashima D.	Formation of Building Blocks, Fri, p.m., Waterway Ballroom 1
Nakashima D. *	Formation of Building Blocks, Fri, p.m., Waterway Ballroom 1
Nakata F.	Main Belt Posters, Tue, p.m., Town Center Exhibit Area
Namiki N.	Laboratory Instruments and Samples Posters, Tue, p.m., Town Center Exhibit Area
Namiki N.	Spacecraft Instruments Posters, Tue, p.m., Town Center Exhibit Area
Namiki N.	Large Impact Basins on the Moon, Thu, a.m., Waterway Ballroom 6
Namiki N. *	Large Impact Basins on the Moon, Thu, a.m., Waterway Ballroom 6
Namiki N.	Lunar Geophysics Posters, Thu, p.m., Town Center Exhibit Area
Namiki N.	A New Moon: Spectral Constraints Posters, Thu, p.m., Town Center Exhibit Area
Namiki N.	Mars: Geologic, Geomorphic, etc., Posters, Thu, p.m., Town Center Exhibit Area
Namkung M.	Spacecraft Instruments Posters, Tue, p.m., Town Center Exhibit Area
Namur O.	Lunar Petrology and Geochemistry Posters, Tue, p.m., Town Center Exhibit Area
Nanbu S.	Solar Wind, Volatile Elements, and Organics Posters, Thu, p.m., Town Center Exhibit Area
Nandikotkur G.	A New Moon: LRO Results, Mon, a.m., Waterway Ballroom 6
Nandikotkur G.	A New Moon: Volatile Species Posters, Tue, p.m., Town Center Exhibit Area
Nanz A.	Stardust Mission to Comet Wild 2, Wed, a.m., Waterway Ballroom 1
Narcisi B.	Impact Ejecta Posters, Tue, p.m., Town Center Exhibit Area
Narendranath S.	Lunar Petrology and Geochemistry Posters, Tue, p.m., Town Center Exhibit Area
Nariyuki Y.	Spacecraft Instruments Posters, Tue, p.m., Town Center Exhibit Area
Nass A.	Data and Image Systems Posters, Tue, p.m., Town Center Exhibit Area
Nass A.	Mars: Fluvial Geomorphology and Processes, Thu, a.m., Waterway Ballroom 4
Nathues A.	Vesta and Dawn, Tue, p.m., Waterway Ballroom 1
Nathues A.	Main Belt Posters, Tue, p.m., Town Center Exhibit Area
Nathues A.	Small Body Missions Posters, Tue, p.m., Town Center Exhibit Area
Nathues A.	Spacecraft Instruments Posters, Tue, p.m., Town Center Exhibit Area
Naumov M. V.	Print Only: Impacts
Nava R. A.	Mars Craters Posters, Thu, p.m., Town Center Exhibit Area
Navalgund R. R.	Once and Future Moon Posters, Thu, p.m., Town Center Exhibit Area
Navalgund R. R.	A New Moon: Spectral Constraints Posters, Thu, p.m., Town Center Exhibit Area
Neal C. R.	Lunar Petrology and Geochemistry Posters, Tue, p.m., Town Center Exhibit Area
Neal C. R.	Once and Future Moon Posters, Thu, p.m., Town Center Exhibit Area
Neal C. R. *	Petrologic Characterization of the Moon, Fri, p.m., Waterway Ballroom 6
Nealson K. H.	Spacecraft Instruments Posters, Tue, p.m., Town Center Exhibit Area
Nebel O.	Planetary Differentiation, Mon, a.m., Waterway Ballroom 5
Needham A. W.	Martian Alteration Processes Posters, Tue, p.m., Town Center Exhibit Area
Neesemann A.	Planetary Dynamics and Tectonics Posters, Thu, p.m., Town Center Exhibit Area
Nefian A. V.	A New Moon: Spectral Constraints Posters, Thu, p.m., Town Center Exhibit Area
Neish C.	A New Moon: LRO Results, Mon, a.m., Waterway Ballroom 6
Neish C.	A New Moon: Volatile Species Posters, Tue, p.m., Town Center Exhibit Area
Neish C.	A New Moon: Geologic Processes Posters, Tue, p.m., Town Center Exhibit Area
Neish C.	A New Moon: Lunar Volcanism, Thu, p.m., Waterway Ballroom 6
Neish C. D.	A New Moon: LCROSS Posters, Tue, p.m., Town Center Exhibit Area
Neish C. D.	A New Moon: Geologic Processes Posters, Tue, p.m., Town Center Exhibit Area
Neish C. D.	A New Moon: Lunar Volcanism, Thu, p.m., Waterway Ballroom 6
Neish C. D.	Lunar Cartography, Stereogrammetry, and Imaging Posters, Thu, p.m., Town Center Exhibit Area
Nekvasil H.	Water in the Solar System: Moon, Tue, p.m., Waterway Ballroom 6
Nekvasil H.	Martian Alteration Processes Posters, Tue, p.m., Town Center Exhibit Area
Nekvasil H.	Martian Meteorites Posters, Thu, p.m., Town Center Exhibit Area
Nelson D.	Lunar Cartography, Stereogrammetry, and Imaging Posters, Thu, p.m., Town Center Exhibit Area
Nelson M. J.	Impact Ejecta Posters, Tue, p.m., Town Center Exhibit Area
Nelson R. M.	Satellites and Their Planets Posters, Thu, p.m., Town Center Exhibit Area
Nemchin A. A.	Print Only: Moon
Nemchin A. A.	Lunar Origins and Chronology Posters, Tue, p.m., Town Center Exhibit Area
Nemchin A. A.	Large Impact Basins on the Moon, Thu, a.m., Waterway Ballroom 6
Nesvorny D.	Small Bodies, Fri, p.m., Waterway Ballroom 5
Nettlemann N.	Planetary Atmospheres, Wed, p.m., Montgomery Ballroom
Nettles J.	A New Moon: Geologic Processes Posters, Tue, p.m., Town Center Exhibit Area
Nettles J.	A New Moon: Spectral Constraints, Wed, p.m., Waterway Ballroom 6
Nettles J.	Large Impact Basins on the Moon, Thu, a.m., Waterway Ballroom 6
Nettles J.	A New Moon: Spectral Constraints Posters, Thu, p.m., Town Center Exhibit Area
Nettles J.	Petrologic Characterization of the Moon, Fri, p.m., Waterway Ballroom 6
Nettles J. W.	Water in the Solar System: Moon, Tue, p.m., Waterway Ballroom 6
Nettles J. W. *	A New Moon: Spectral Constraints, Wed, p.m., Waterway Ballroom 6
Nettles J. W.	A New Moon: Spectral Constraints Posters, Thu, p.m., Town Center Exhibit Area
Nettles J. W.	Exploring the Martian Crust Posters, Thu, p.m., Town Center Exhibit Area
Neu D.	Mars Remote Sensing Techniques Posters, Thu, p.m., Town Center Exhibit Area

Nimmo F.	Exploring the Martian Crust Posters, Thu, p.m., Town Center Exhibit Area
Nimmo F.	Small Bodies, Fri, p.m., Waterway Ballroom 5
Nimura T.	Near-Earth Objects Posters, Thu, p.m., Town Center Exhibit Area
Nimura T.	A New Moon: Spectral Constraints Posters, Thu, p.m., Town Center Exhibit Area
Ninagawa K.	Impact Experiments Posters, Tue, p.m., Town Center Exhibit Area
Ning X.	Lunar Cartography, Stereogrammetry, and Imaging Posters, Thu, p.m., Town Center Exhibit Area
Nishiizumi K.	Ureilitic Asteroids: Almahata Sitta, Tue, p.m., Waterway Ballroom 1
Nishiizumi K.	Martian Meteorites Posters, Thu, p.m., Town Center Exhibit Area
Nissinboim A.	Laboratory Instruments and Samples Posters, Tue, p.m., Town Center Exhibit Area
Nittler L.	Stardust Mission Posters, Thu, p.m., Town Center Exhibit Area
Nittler L. R.	Radionuclides and Early Solar System Chronology, Tue, a.m., Waterway Ballroom 1
Nittler L. R.	Mercury, Tue, p.m., Montgomery Ballroom
Nittler L. R.	Stardust Mission to Comet Wild 2, Wed, a.m., Waterway Ballroom 1
Nittler L. R.	Origins of Presolar Grains, Wed, p.m., Waterway Ballroom 1
Nittler L. R. *	Origins of Presolar Grains, Wed, p.m., Waterway Ballroom 1
Nittler L. R.	Solar Wind, Volatile Elements, and Organics, Thu, a.m., Waterway Ballroom 1
Nittler L. R.	Cosmic Dust, Thu, p.m., Waterway Ballroom 1
Nittler L. R.	Origins of Presolar Grains Posters, Thu, p.m., Town Center Exhibit Area
Nixon A.	Stardust Mission Posters, Thu, p.m., Town Center Exhibit Area
NLSI-DREAM Team	Water in the Solar System: Moon, Tue, p.m., Waterway Ballroom 6
Noble S. K.	Print Only: Moon
Noble S. K. *	Nature of the Lunar Regolith, Wed, a.m., Waterway Ballroom 6
Noda H.	A New Moon: Volatile Species Posters, Tue, p.m., Town Center Exhibit Area
Noda H.	Spacecraft Instruments Posters, Tue, p.m., Town Center Exhibit Area
Noda H.	Large Impact Basins on the Moon, Thu, a.m., Waterway Ballroom 6
Noe Dobrea E.	Mars: Geologic, Geomorphic, etc., Posters, Thu, p.m., Town Center Exhibit Area
Noe Dobrea E.	Mars: Sedimentary Rock Record Posters, Thu, p.m., Town Center Exhibit Area
Noe Dobrea E. Z. *	Martian Alteration Processes, Mon, a.m., Waterway Ballroom 4
Nogami K.	Once and Future Moon Posters, Thu, p.m., Town Center Exhibit Area
Nolan M.	A New Moon: Geologic Processes Posters, Tue, p.m., Town Center Exhibit Area
Nolan M. C.	Vesta and Dawn, Tue, p.m., Waterway Ballroom 1
Noll K. S.	Main Belt Posters, Tue, p.m., Town Center Exhibit Area
Nornberg P.	Environmental Analogs Posters, Thu, p.m., Town Center Exhibit Area
Nørnberg P.	Martian Alteration Processes Posters, Tue, p.m., Town Center Exhibit Area
Nørnberg P.	Planetary Aeolian Processes Posters, Tue, p.m., Town Center Exhibit Area
Nørnberg P.	Planetary Atmospheres Posters, Thu, p.m., Town Center Exhibit Area
Noroozi A.	Mission Plans and Concepts Posters, Tue, p.m., Town Center Exhibit Area
Noroozi A.	Environmental Analogs Posters, Thu, p.m., Town Center Exhibit Area
Noroozi A.	Mission Plans and Concepts Posters, Tue, p.m., Town Center Exhibit Area
Noroozi A.	Environmental Analogs Posters, Thu, p.m., Town Center Exhibit Area
Norose K.	Chondrites Posters, Thu, p.m., Town Center Exhibit Area
Norose K.	Thermal and Aqueous Processes Posters, Thu, p.m., Town Center Exhibit Area
Notarnicola C.	Several Species of Icy Chunks, Thu, p.m., Waterway Ballroom 5
Nowicki K.	Spacecraft Instruments Posters, Tue, p.m., Town Center Exhibit Area
Nowicki S. A.	Environmental Analogs Posters, Thu, p.m., Town Center Exhibit Area
Nozette S.	A New Moon: LRO Results, Mon, a.m., Waterway Ballroom 6
Nozette S.	A New Moon: Lunar Volcanism, Thu, p.m., Waterway Ballroom 6
Nuccilli F.	Spacecraft Instruments Posters, Tue, p.m., Town Center Exhibit Area
Nuevo M.	Ureilitic Asteroids: Almahata Sitta, Tue, p.m., Waterway Ballroom 1
Nuevo M.	Solar Wind, Volatile Elements, and Organics, Thu, a.m., Waterway Ballroom 1
Nuevo M.	Stardust Mission Posters, Thu, p.m., Town Center Exhibit Area
Nugent C. R. *	Vesta and Dawn, Tue, p.m., Waterway Ballroom 1
Nunes D. C.	Martian Polar Processes Posters, Tue, p.m., Town Center Exhibit Area
Nunes D. C.	Planetary Dynamics and Tectonics Posters, Thu, p.m., Town Center Exhibit Area
Nuñez J. I.	Laboratory Instruments and Samples Posters, Tue, p.m., Town Center Exhibit Area
Nuth J.	Parent Cloud and Disk Processes Posters, Tue, p.m., Town Center Exhibit Area
Nuth J. A.	Solar Wind, Volatile Elements, and Organics Posters, Thu, p.m., Town Center Exhibit Area
Nuth J. A. III	Chondrites Posters, Thu, p.m., Town Center Exhibit Area
Nuzhdin I.	A New Moon: LRO Results, Mon, a.m., Waterway Ballroom 6
Nuzhdin I.	A New Moon: Volatile Species Posters, Tue, p.m., Town Center Exhibit Area
Nycz J. C. *	Impacts on the Moon, Mars, and Beyond, Wed, p.m., Waterway Ballroom 5
Nyquist L.	Lunar Meteorites Posters, Tue, p.m., Town Center Exhibit Area
Nyquist L. E.	Print Only: Mars
Nyquist L. E.	Laboratory Instruments and Samples Posters, Tue, p.m., Town Center Exhibit Area
Nyquist L. E.	Cosmic-Ray Exposure Dating Posters, Tue, p.m., Town Center Exhibit Area
Nyquist L. E.	Differentiated Meteorites, Wed, p.m., Waterway Ballroom 4
Nyquist L. E.	Martian Meteorites Posters, Thu, p.m., Town Center Exhibit Area

Quinn J. E.	Environmental Analogs Posters, Thu, p.m., Town Center Exhibit Area
Quinn R.	Spacecraft Instruments Posters, Tue, p.m., Town Center Exhibit Area
Quinn R.	Mission Plans and Concepts Posters, Tue, p.m., Town Center Exhibit Area
Quinn R. C.	Martian Alteration Processes, Mon, a.m., Waterway Ballroom 4
Quirico E.	Water in the Solar System: Primitive Bodies, Mon, p.m., Waterway Ballroom 6
Quirico E.	Material Analogs Posters, Tue, p.m., Town Center Exhibit Area
Quirico E.	Thermal and Aqueous Processes on Chondrite Parent Bodies, Fri, a.m., Waterway Ballroom 1
Raack J.	Terrestrial Planet Cryospheres Posters, Tue, p.m., Town Center Exhibit Area
Radebaugh J. *	Planetary Aeolian Processes, Tue, p.m., Waterway Ballroom 4
Radebaugh J.	Planetary Aeolian Processes Posters, Tue, p.m., Town Center Exhibit Area
Radebaugh J.	Mission Plans and Concepts Posters, Tue, p.m., Town Center Exhibit Area
Radebaugh J.	Satellites and Their Planets Posters, Thu, p.m., Town Center Exhibit Area
Radebaugh J. D.	Several Species of Icy Chunks, Thu, p.m., Waterway Ballroom 5
Radtke K.	Rocks, Life, and Biosignatures, Thu, p.m., Waterway Ballroom 1
Rafkin S. C. R.	Planetary Atmospheres, Wed, p.m., Montgomery Ballroom
Rahman Z.	Nature of the Lunar Regolith, Wed, a.m., Waterway Ballroom 6
Rahman Z.	Origins of Presolar Grains, Wed, p.m., Waterway Ballroom 1
Rahman Z.	Cosmic Dust, Thu, p.m., Waterway Ballroom 1
Rahman Z. U.	Formation of First Solar System Solids Posters, Tue, p.m., Town Center Exhibit Area
Rai N.*	Planetary Differentiation, Mon, a.m., Waterway Ballroom 5
Raiskila S.	Impactite Petrology and Ages Posters, Tue, p.m., Town Center Exhibit Area
Raitala J.	Terrestrial Planet Cryospheres Posters, Tue, p.m., Town Center Exhibit Area
Raitala J.	Mars: Fluvial Geomorphology and Processes, Thu, a.m., Waterway Ballroom 4
Raitala J.	Mars: Sedimentary Rock Record Posters, Thu, p.m., Town Center Exhibit Area
Raith M. M.	Planetary Differentiation, Mon, a.m., Waterway Ballroom 5
Rajasekhar R. P.	Once and Future Moon Posters, Thu, p.m., Town Center Exhibit Area
Rajawat A. S.	A New Moon: Spectral Constraints Posters, Thu, p.m., Town Center Exhibit Area
Ralew S.	Martian Meteorites Posters, Thu, p.m., Town Center Exhibit Area
Rambaux N.	Satellites and Their Planets Posters, Thu, p.m., Town Center Exhibit Area
Ramcharan S.	Stardust Mission Posters, Thu, p.m., Town Center Exhibit Area
Ramesh K. T.	Print Only: Impacts
Ramesh K. T.	Impact Experiments Posters, Tue, p.m., Town Center Exhibit Area
Ramien N.	Stardust Mission to Comet Wild 2, Wed, a.m., Waterway Ballroom 1
Ramírez-Cardona M.	Environments for Life Posters, Thu, p.m., Town Center Exhibit Area
Ramon E. C.	Radionuclides and Early Solar System Chronology, Tue, a.m., Waterway Ballroom 1
Ramon E. C.	Formation of First Solar System Solids Posters, Tue, p.m., Town Center Exhibit Area
Ramos M.	Print Only: Mars
Rampe E. B.	Exploring the Martian Crust Posters, Thu, p.m., Town Center Exhibit Area
Ramsey M. S.	Mars: Sedimentary Rock Record Posters, Thu, p.m., Town Center Exhibit Area
Ramsey M. S.	Igneous and Volcanic Processes Posters, Thu, p.m., Town Center Exhibit Area
Ramstad R.	Planetary Aeolian Processes Posters, Tue, p.m., Town Center Exhibit Area
Ramstad R.	Martian Polar Processes Posters, Tue, p.m., Town Center Exhibit Area
Ranen M. C.	Lunar Origins and Chronology Posters, Tue, p.m., Town Center Exhibit Area
Raney K.	A New Moon: Geologic Processes Posters, Tue, p.m., Town Center Exhibit Area
Raney R. K.	A New Moon: LRO Results, Mon, a.m., Waterway Ballroom 6
Raney R. K.	A New Moon: Geologic Processes Posters, Tue, p.m., Town Center Exhibit Area
Raney R. K.	A New Moon: Lunar Volcanism, Thu, p.m., Waterway Ballroom 6
Raney R. K.	Lunar Cartography, Stereogrammetry, and Imaging Posters, Thu, p.m., Town Center Exhibit Area
Rao M. N.	Martian Meteorites Posters, Thu, p.m., Town Center Exhibit Area
Rask J. C.	Lunar Dust Posters, Thu, p.m., Town Center Exhibit Area
Rask J. C.	E/PO: Environmental Analogs Posters, Thu, p.m., Town Center Exhibit Area
Rasmussen K. R.	Planetary Aeolian Processes Posters, Tue, p.m., Town Center Exhibit Area
Rasmussen K. R.	Planetary Atmospheres Posters, Thu, p.m., Town Center Exhibit Area
Ratcliff J. T.	Lunar Geophysics Posters, Thu, p.m., Town Center Exhibit Area
Raub R.	Data and Image Systems Posters, Tue, p.m., Town Center Exhibit Area
Rauschenbach I.	Spacecraft Instruments Posters, Tue, p.m., Town Center Exhibit Area
Ravine M.	Mission Plans and Concepts Posters, Tue, p.m., Town Center Exhibit Area
Ravine M. A.	A New Moon: LRO Results, Mon, a.m., Waterway Ballroom 6
Ravine M. A.	Print Only: Mars
Rawlings A. R.	Chondrites Posters, Thu, p.m., Town Center Exhibit Area
Raymond C. A. *	Vesta and Dawn, Tue, p.m., Waterway Ballroom 1
Raymond C. A.	Igneous and Volcanic Processes, Thu, a.m., Waterway Ballroom 5
Reach W. T.	Ice and Dust Posters, Thu, p.m., Town Center Exhibit Area
Redding B. L.	Lunar Cartography, Stereogrammetry, and Imaging Posters, Thu, p.m., Town Center Exhibit Area
Reddy K.	Print Only: Impacts
Reddy V. *	Vesta and Dawn, Tue, p.m., Waterway Ballroom 1
Reddy V.	Main Belt Posters, Tue, p.m., Town Center Exhibit Area

Thompson B. J.	A New Moon: Lunar Volcanism, Thu, p.m., Waterway Ballroom 6
Thompson D. R.	Print Only: Mars
Thompson D. R.	Spacecraft Instruments Posters, Tue, p.m., Town Center Exhibit Area
Thompson L. M.	Impact Craters Posters, Tue, p.m., Town Center Exhibit Area
Thompson M.	Lunar Regolith Posters, Thu, p.m., Town Center Exhibit Area
Thompson P.	Spacecraft Instruments Posters, Tue, p.m., Town Center Exhibit Area
Thompson S.	Spacecraft Instruments Posters, Tue, p.m., Town Center Exhibit Area
Thompson T.	A New Moon: LRO Results, Mon, a.m., Waterway Ballroom 6
Thompson T.	A New Moon: Lunar Volcanism, Thu, p.m., Waterway Ballroom 6
Thompson T. W. *	Nature of the Lunar Regolith, Wed, a.m., Waterway Ballroom 6
Thompson T. W.	Lunar Regolith Posters, Thu, p.m., Town Center Exhibit Area
Thomson B.	A New Moon: LCROSS Posters, Tue, p.m., Town Center Exhibit Area
Thomson B. J.	A New Moon: LRO Results, Mon, a.m., Waterway Ballroom 6
Thomson B. J.	A New Moon: Geologic Processes Posters, Tue, p.m., Town Center Exhibit Area
Thomson B. J.	A New Moon: Lunar Volcanism, Thu, p.m., Waterway Ballroom 6
Thomson B. J.	Lunar Cartography, Stereogrammetry, and Imaging Posters, Thu, p.m., Town Center Exhibit Area
Thomson B. J.	Exploring the Martian Crust Posters, Thu, p.m., Town Center Exhibit Area
Thomson B. J.	Mars: Deposition and Erosion, Fri, a.m., Waterway Ballroom 4
Throop H. B.	Satellites and Their Planets Posters, Thu, p.m., Town Center Exhibit Area
Throop H. B. *	Parent Cloud and Solar Nebula, Mon, a.m., Waterway Ballroom 1
Tice M. M.	Water in the Solar System: Primitive Bodies, Mon, p.m., Waterway Ballroom 6
Tikoo S. M. *	Interior of the Moon, Fri, a.m., Waterway Ballroom 6
Timoshenko G. N.	Spacecraft Instruments Posters, Tue, p.m., Town Center Exhibit Area
Tindle A. G.	E/PO: Meteorites Posters, Tue, p.m., Town Center Exhibit Area
Tirsch D.	Planetary Aeolian Processes Posters, Tue, p.m., Town Center Exhibit Area
Tirsch D.	Mars: Fluvial Geomorphology and Processes, Thu, a.m., Waterway Ballroom 4
Titov D.	Spacecraft Instruments Posters, Tue, p.m., Town Center Exhibit Area
Titov D. V.	Venus, Mon, p.m., Waterway Ballroom 5
Titus T. N.	Planetary Aeolian Processes Posters, Tue, p.m., Town Center Exhibit Area
Titus T. N.	Mars Ice and Craters Posters, Tue, p.m., Town Center Exhibit Area
Titus T. N.	Material Analogs Posters, Tue, p.m., Town Center Exhibit Area
Titus T. N.	Mission Plans and Concepts Posters, Tue, p.m., Town Center Exhibit Area
Tobie G.	Impacts Modeling Posters, Tue, p.m., Town Center Exhibit Area
Tobola K.	E/PO: Moon Posters, Tue, p.m., Town Center Exhibit Area
Todd B.	Environmental Analogs Posters, Thu, p.m., Town Center Exhibit Area
Toksöz M. N.	Mercury, Tue, p.m., Montgomery Ballroom
Toksöz M. N.	Mercury Posters, Tue, p.m., Town Center Exhibit Area
Tokunaga A. T.	Characterizing Near-Earth Objects, Thu, p.m., Waterway Ballroom 4
Tomiyama T.	Lunar Origins and Chronology Posters, Tue, p.m., Town Center Exhibit Area
Tomkinson T.	Martian Alteration Processes Posters, Tue, p.m., Town Center Exhibit Area
Tomkinson T.	Spacecraft Instruments Posters, Tue, p.m., Town Center Exhibit Area
Tomkinson T. O. R.	Martian Alteration Processes Posters, Tue, p.m., Town Center Exhibit Area
Tomov B.	Lunar Radiation Posters, Thu, p.m., Town Center Exhibit Area
Tompkins S.	A New Moon: Spectral Constraints, Wed, p.m., Waterway Ballroom 6
Tompkins S.	Large Impact Basins on the Moon, Thu, a.m., Waterway Ballroom 6
Tompkins S.	A New Moon: Spectral Constraints Posters, Thu, p.m., Town Center Exhibit Area
Tompkins S.	Petrologic Characterization of the Moon, Fri, p.m., Waterway Ballroom 6
Tong C. H. *	Impact Models and More, Tue, p.m., Waterway Ballroom 5
Torii M.	Ureilites Posters, Tue, p.m., Town Center Exhibit Area
Törmänen T.	Terrestrial Planet Cryospheres Posters, Tue, p.m., Town Center Exhibit Area
Törmänen T.	Mars: Fluvial Geomorphology and Processes, Thu, a.m., Waterway Ballroom 4
Törmänen T.	Mars: Sedimentary Rock Record Posters, Thu, p.m., Town Center Exhibit Area
Tornabene L.	Planetary Aeolian Processes, Tue, p.m., Waterway Ballroom 4
Tornabene L. L.	A New Moon: Geologic Processes Posters, Tue, p.m., Town Center Exhibit Area
Tornabene L. L.	Martian Alteration Processes Posters, Tue, p.m., Town Center Exhibit Area
Tornabene L. L.	Exploring the Martian Crust, Wed, a.m., Waterway Ballroom 4
Tornabene L. L.	Impacts on the Moon, Mars, and Beyond, Wed, p.m., Waterway Ballroom 5
Tornabene L. L.	Exploring the Martian Crust Posters, Thu, p.m., Town Center Exhibit Area
Tornabene L. L.	Mars Craters Posters, Thu, p.m., Town Center Exhibit Area
Torrence M. H.	A New Moon: LRO Results, Mon, a.m., Waterway Ballroom 6
Torrence M. H.	Mercury, Tue, p.m., Montgomery Ballroom
Torrence M. H.	A New Moon: LCROSS Posters, Tue, p.m., Town Center Exhibit Area
Torrence M. H.	A New Moon: Geologic Processes Posters, Tue, p.m., Town Center Exhibit Area
Torrione P.	Spacecraft Instruments Posters, Tue, p.m., Town Center Exhibit Area
Tosca N. J.	Martian Alteration Processes Posters, Tue, p.m., Town Center Exhibit Area
Tosi F.	Spacecraft Instruments Posters, Tue, p.m., Town Center Exhibit Area
Tosi F.	Several Species of Icy Chunks, Thu, p.m., Waterway Ballroom 5

Tosi F.	Satellites and Their Planets Posters, Thu, p.m., Town Center Exhibit Area
Toucoulou R.	Stardust Mission to Comet Wild 2, Wed, a.m., Waterway Ballroom 1
Towner M.	Planetary Aeolian Processes Posters, Tue, p.m., Town Center Exhibit Area
Towner M. C.	Achondrites Posters, Tue, p.m., Town Center Exhibit Area
Towner M. C.	Mars: Gullies and Slope Streaks Posters, Thu, p.m., Town Center Exhibit Area
Townsend L.	Lunar Radiation Posters, Thu, p.m., Town Center Exhibit Area
Toyoda N.	Solar Wind, Volatile Elements, and Organics Posters, Thu, p.m., Town Center Exhibit Area
Toyota T.	Planetary Atmospheres Posters, Thu, p.m., Town Center Exhibit Area
Trafton L.	Planetary Atmospheres Posters, Thu, p.m., Town Center Exhibit Area
Trafton L. M.	Satellites and Their Planets Posters, Thu, p.m., Town Center Exhibit Area
Trafton L. M.	A New Moon: LCROSS Posters, Tue, p.m., Town Center Exhibit Area
Trafton L. M.	Planetary Atmospheres, Wed, p.m., Montgomery Ballroom
Tragheim D. G.	Mars: Sedimentary Rock Record Posters, Thu, p.m., Town Center Exhibit Area
Trainer M.	Mission Plans and Concepts Posters, Tue, p.m., Town Center Exhibit Area
Tran T.	A New Moon: Lunar Volcanism, Thu, p.m., Waterway Ballroom 6
Tran T.	Lunar Cartography, Stereogrammetry, and Imaging Posters, Thu, p.m., Town Center Exhibit Area
Tran T. N.	Once and Future Moon Posters, Thu, p.m., Town Center Exhibit Area
Tranfield E.	Lunar Dust Posters, Thu, p.m., Town Center Exhibit Area
Trang D.	A New Moon: Geologic Processes Posters, Tue, p.m., Town Center Exhibit Area
Trang D.	BOOM! Posters, Thu, p.m., Town Center Exhibit Area
Trappitsch R.	Cosmic Dust Posters, Thu, p.m., Town Center Exhibit Area
Trauthan F.	Terrestrial Planet Cryospheres, Tue, a.m., Waterway Ballroom 4
Trauthan F.	Mars: Gullies and Slope Streaks Posters, Thu, p.m., Town Center Exhibit Area
Trávnícek P. M.	Mercury Posters, Tue, p.m., Town Center Exhibit Area
Trease B.	Spirit Posters, Thu, p.m., Town Center Exhibit Area
Treiman A.	Venus, Mon, p.m., Waterway Ballroom 5
Treiman A.	Venus Posters, Tue, p.m., Town Center Exhibit Area
Treiman A.	Spacecraft Instruments Posters, Tue, p.m., Town Center Exhibit Area
Treiman A.	Impacts on the Moon, Mars, and Beyond, Wed, p.m., Waterway Ballroom 5
Treiman A. H.	Lunar Meteorites Posters, Tue, p.m., Town Center Exhibit Area
Treiman A. H.	Spacecraft Instruments Posters, Tue, p.m., Town Center Exhibit Area
Treiman A. H.	Igneous and Volcanic Processes, Thu, a.m., Waterway Ballroom 5
Treiman A. H. *	Rocks, Life, and Biosignatures, Thu, p.m., Waterway Ballroom 1
Treiman A. H.	Thermal and Aqueous Processes on Chondrite Parent Bodies, Fri, a.m., Waterway Ballroom 1
Treiman A. H.	Martian Igneous Processes, Fri, a.m., Waterway Ballroom 5
Treiman A. H.	Petrologic Characterization of the Moon, Fri, p.m., Waterway Ballroom 6
Tretyakov V.	Spacecraft Instruments Posters, Tue, p.m., Town Center Exhibit Area
Tretyakov V.	A New Moon: LRO Results, Mon, a.m., Waterway Ballroom 6
Tretyakov V.	A New Moon: Volatile Species Posters, Tue, p.m., Town Center Exhibit Area
Tricarico P.	Small Body Missions Posters, Tue, p.m., Town Center Exhibit Area
Tricarico P.	Igneous and Volcanic Processes, Thu, a.m., Waterway Ballroom 5
Trieloff M.	Ground Truth Galore: Terrestrial Impact Craters, Tue, a.m., Waterway Ballroom 5
Trieloff M.	Impactite Petrology and Ages Posters, Tue, p.m., Town Center Exhibit Area
Trieloff M.	Stardust Mission to Comet Wild 2, Wed, a.m., Waterway Ballroom 1
Trieloff M.	Stardust Mission Posters, Thu, p.m., Town Center Exhibit Area
Trigo-Rodriguez J.	Stardust Mission Posters, Thu, p.m., Town Center Exhibit Area
Trígo-Rodríguez J. M.	Print Only: Small Bodies
Tringe S. G.	Rocks, Life, and Biosignatures, Thu, p.m., Waterway Ballroom 1
Trinkle D.	Planetary Differentiation, Mon, a.m., Waterway Ballroom 5
Tripa C. E.	Solar Wind, Volatile Elements, and Organics, Thu, a.m., Waterway Ballroom 1
Tripa C. E.	Solar Wind, Volatile Elements, and Organics Posters, Thu, p.m., Town Center Exhibit Area
Troadec D.	Stardust Mission to Comet Wild 2, Wed, a.m., Waterway Ballroom 1
Troiano J.	Chondrites Posters, Thu, p.m., Town Center Exhibit Area
Trombka J.	A New Moon: LRO Results, Mon, a.m., Waterway Ballroom 6
Trombka J.	A New Moon: Volatile Species Posters, Tue, p.m., Town Center Exhibit Area
Trombka J.	Spacecraft Instruments Posters, Tue, p.m., Town Center Exhibit Area
Trombka J. I.	A New Moon: Volatile Species Posters, Tue, p.m., Town Center Exhibit Area
Tronnick S.	Rocks, Life, and Biosignatures, Thu, p.m., Waterway Ballroom 1
Trumble M. E.	Igneous and Volcanic Processes, Thu, a.m., Waterway Ballroom 5
Tsang S. W. R.	Print Only: Mars
Tschimmel M.	Lunar Cartography, Stereogrammetry, and Imaging Posters, Thu, p.m., Town Center Exhibit Area
Tsou P.	Stardust Mission to Comet Wild 2, Wed, a.m., Waterway Ballroom 1
Tsou P.	Stardust Mission Posters, Thu, p.m., Town Center Exhibit Area
Tsuboi N.	A New Moon: Spectral Constraints Posters, Thu, p.m., Town Center Exhibit Area
Tsuchiya F.	Spacecraft Instruments Posters, Tue, p.m., Town Center Exhibit Area
Tsuchiyama A.	Stardust Mission to Comet Wild 2, Wed, a.m., Waterway Ballroom 1
Tsuchiyama A.	Solar Wind, Volatile Elements, and Organics Posters, Thu, p.m., Town Center Exhibit Area

Wright I. P.	Print Only: Exobiology
Wright K. W.	Environmental Analogs Posters, Thu, p.m., Town Center Exhibit Area
Wright S. P.	Impact Ejecta Posters, Tue, p.m., Town Center Exhibit Area
Wright S. P.	Impact Craters Posters, Tue, p.m., Town Center Exhibit Area
Wright S. P.	Material Analogs Posters, Tue, p.m., Town Center Exhibit Area
Wu J.	A New Moon: LCROSS, Chandrayaan, Chang'E, Tue, a.m., Waterway Ballroom 6
Wu R.	Mission Plans and Concepts Posters, Tue, p.m., Town Center Exhibit Area
Wu T.	Print Only: Environmental and Material Analogs
Wu Y. Z. *	A New Moon: LCROSS, Chandrayaan, Chang'E, Tue, a.m., Waterway Ballroom 6
Wu Z. H.	Lunar Geophysics Posters, Thu, p.m., Town Center Exhibit Area
Wulf G.	Data and Image Systems Posters, Tue, p.m., Town Center Exhibit Area
Wünnemann K.	Impacts Modeling Posters, Tue, p.m., Town Center Exhibit Area
Wünnemann K.	Impact Models and More, Tue, p.m., Waterway Ballroom 5
Wünnemann K. *	Impact Models and More, Tue, p.m., Waterway Ballroom 5
Wünnemann K.	Impacts Modeling Posters, Tue, p.m., Town Center Exhibit Area
Wurz P.	Mission Plans and Concepts Posters, Tue, p.m., Town Center Exhibit Area
Wyatt M.	A New Moon: Geologic Processes Posters, Tue, p.m., Town Center Exhibit Area
Wyatt M. B.	A New Moon: LRO Results, Mon, a.m., Waterway Ballroom 6
Wyatt M. B.	A New Moon: Spectral Constraints, Wed, p.m., Waterway Ballroom 6
Wyatt M. B.	A New Moon: Spectral Constraints Posters, Thu, p.m., Town Center Exhibit Area
Wyatt M. B.	Exploring the Martian Crust Posters, Thu, p.m., Town Center Exhibit Area
Wyatt M. B.	Environmental Analogs Posters, Thu, p.m., Town Center Exhibit Area
Wyatt M. C.	BOOM! Posters, Thu, p.m., Town Center Exhibit Area
Wye L.	Data and Image Systems Posters, Tue, p.m., Town Center Exhibit Area
Wye L.	Several Species of Icy Chunks, Thu, p.m., Waterway Ballroom 5
Wynne J. J.	Material Analogs Posters, Tue, p.m., Town Center Exhibit Area
Wyrick D. Y.	Planetary Dynamics and Tectonics Posters, Thu, p.m., Town Center Exhibit Area
Xiang S.	Print Only: Moon
Xiang S.	Print Only: Environmental and Material Analogs
Xiao L.	Print Only: Environmental and Material Analogs
Xiao L.	A New Moon: Geologic Processes Posters, Tue, p.m., Town Center Exhibit Area
Xiao L.	A New Moon: Lunar Volcanism, Thu, p.m., Waterway Ballroom 6
Xiao L.	Lunar Cartography, Stereogrammetry, and Imaging Posters, Thu, p.m., Town Center Exhibit Area
Xiao L.	Martian Meteorites Posters, Thu, p.m., Town Center Exhibit Area
Xiao L.	Igneous and Volcanic Processes Posters, Thu, p.m., Town Center Exhibit Area
Xiao X.	Spacecraft Instruments Posters, Tue, p.m., Town Center Exhibit Area
Xiao Z.	A New Moon: Geologic Processes Posters, Tue, p.m., Town Center Exhibit Area
Xiao Z.	Venus Posters, Tue, p.m., Town Center Exhibit Area
Ximenes S. W.	Environmental Analogs Posters, Thu, p.m., Town Center Exhibit Area
Xiong S. Q.	Once and Future Moon Posters, Thu, p.m., Town Center Exhibit Area
Xu A. A.	A New Moon: LCROSS, Chandrayaan, Chang'E, Tue, a.m., Waterway Ballroom 6
Xu W. B.	Igneous and Volcanic Processes Posters, Thu, p.m., Town Center Exhibit Area
Xu Z.	A New Moon: Volatile Species Posters, Tue, p.m., Town Center Exhibit Area
Yabuta H. *	Solar Wind, Volatile Elements, and Organics, Thu, a.m., Waterway Ballroom 1
Yagi M.	Main Belt Posters, Tue, p.m., Town Center Exhibit Area
Yakovlev O. I.	Print Only: Cosmochemical Origins
Yakovlev V.	Mars: Gullies and Slope Streaks Posters, Thu, p.m., Town Center Exhibit Area
Yamada A.	Solar Wind, Volatile Elements, and Organics Posters, Thu, p.m., Town Center Exhibit Area
Yamada I.	Solar Wind, Volatile Elements, and Organics Posters, Thu, p.m., Town Center Exhibit Area
Yamada R.	Once and Future Moon Posters, Thu, p.m., Town Center Exhibit Area
Yamagishi A.	Laboratory Instruments and Samples Posters, Tue, p.m., Town Center Exhibit Area
Yamaguchi A.	Lunar Meteorites Posters, Tue, p.m., Town Center Exhibit Area
Yamaguchi A.	Differentiated Meteorites, Wed, p.m., Waterway Ballroom 4
Yamaguchi A.	Martian Meteorites Posters, Thu, p.m., Town Center Exhibit Area
Yamaguchi A.	Igneous and Volcanic Processes Posters, Thu, p.m., Town Center Exhibit Area
Yamaguchi A.	Petrologic Characterization of the Moon, Fri, p.m., Waterway Ballroom 6
Yamaguchi Y.	A New Moon: Geologic Processes Posters, Tue, p.m., Town Center Exhibit Area
Yamaguchi Y.	Mars: Fluvial Geomorphology and Processes Posters, Thu, p.m., Town Center Exhibit Area
Yamaji A.	A New Moon: Spectral Constraints Posters, Thu, p.m., Town Center Exhibit Area
Yamamoto N.	Lunar Cartography, Stereogrammetry, and Imaging Posters, Thu, p.m., Town Center Exhibit Area
Yamamoto S.	Lunar Petrology and Geochemistry Posters, Tue, p.m., Town Center Exhibit Area
Yamamoto S. *	A New Moon: Spectral Constraints, Wed, p.m., Waterway Ballroom 6
Yamamoto S.	A New Moon: Spectral Constraints Posters, Thu, p.m., Town Center Exhibit Area
Yamamoto S.	Petrologic Characterization of the Moon, Fri, p.m., Waterway Ballroom 6
Yamamoto T.	Parent Cloud and Disk Processes Posters, Tue, p.m., Town Center Exhibit Area
Yamashita N.	Lunar Petrology and Geochemistry Posters, Tue, p.m., Town Center Exhibit Area
Yamashita N.	Large Impact Basins on the Moon, Thu, a.m., Waterway Ballroom 6

Zhao H.	Mission Plans and Concepts Posters, Tue, p.m., Town Center Exhibit Area
Zhao W. J.	Lunar Geophysics Posters, Thu, p.m., Town Center Exhibit Area
Zhao X.	Origins of Presolar Grains, Wed, p.m., Waterway Ballroom 1
Zhao X.	Origins of Presolar Grains Posters, Thu, p.m., Town Center Exhibit Area
Zheng W. M.	Mission Plans and Concepts Posters, Tue, p.m., Town Center Exhibit Area
Zheng Y.	Print Only: Moon
Zhong S. J.	Lunar Origins and Chronology Posters, Tue, p.m., Town Center Exhibit Area
Zhong S. J.	Planetary Dynamics and Tectonics, Wed, a.m., Waterway Ballroom 5
Zhu M. H.*	A New Moon: LCROSS, Chandrayaan, Chang'E, Tue, a.m., Waterway Ballroom 6
Ziegler K. *	Differentiated Meteorites, Wed, p.m., Waterway Ballroom 4
Ziegler K.	Environments for Life Posters, Thu, p.m., Town Center Exhibit Area
Ziethe R.	Mercury Posters, Tue, p.m., Town Center Exhibit Area
Ziffer J.	Characterizing Near-Earth Objects, Thu, p.m., Waterway Ballroom 4
Zila V.	Planetary Differentiation Posters, Tue, p.m., Town Center Exhibit Area
Zimbelman J. R.	Planetary Aeolian Processes Posters, Tue, p.m., Town Center Exhibit Area
Zimbelman J. R.	Igneous and Volcanic Processes, Thu, a.m., Waterway Ballroom 5
Zimbelman J. R. *	Igneous and Volcanic Processes, Thu, a.m., Waterway Ballroom 5
Zimbelman J. R.	Mars: Geologic, Geomorphic, etc., Posters, Thu, p.m., Town Center Exhibit Area
Zindler A.	Lunar Origins and Chronology Posters, Tue, p.m., Town Center Exhibit Area
Zinner E.	Iron and Stony Iron Meteorites Posters, Tue, p.m., Town Center Exhibit Area
Zinner E. *	Origins of Presolar Grains, Wed, p.m., Waterway Ballroom 1
Zinner E.	Origins of Presolar Grains Posters, Thu, p.m., Town Center Exhibit Area
Zinner E.	Formation of Building Blocks Posters, Thu, p.m., Town Center Exhibit Area
Zinner E.	Thermal and Aqueous Processes Posters, Thu, p.m., Town Center Exhibit Area
Zinovev A. V.	Solar Wind, Volatile Elements, and Organics, Thu, a.m., Waterway Ballroom 1
Zinovev A. V.	Solar Wind, Volatile Elements, and Organics Posters, Thu, p.m., Town Center Exhibit Area
Zinzi A.	Main Belt Posters, Tue, p.m., Town Center Exhibit Area
Zinzi A.	Mars Remote Sensing Techniques Posters, Thu, p.m., Town Center Exhibit Area
Zolensky M.	Cosmic Dust Posters, Thu, p.m., Town Center Exhibit Area
Zolensky M.	Ureilitic Asteroids: Almahata Sitta, Tue, p.m., Waterway Ballroom 1
Zolensky M.	Stardust Mission Posters, Thu, p.m., Town Center Exhibit Area
Zolensky M. E.	Ureilitic Asteroids: Almahata Sitta, Tue, p.m., Waterway Ballroom 1
Zolensky M. E.	Ureilites Posters, Tue, p.m., Town Center Exhibit Area
Zolensky M. E.	Stardust Mission to Comet Wild 2, Wed, a.m., Waterway Ballroom 1
Zolensky M. E.	Stardust Mission Posters, Thu, p.m., Town Center Exhibit Area
Zolensky M. E.	Solar Wind, Volatile Elements, and Organics Posters, Thu, p.m., Town Center Exhibit Area
Zolotov M. Yu. *	Igneous and Volcanic Processes, Thu, a.m., Waterway Ballroom 5
Zolotov M. Yu.	Thermal and Aqueous Processes Posters, Thu, p.m., Town Center Exhibit Area
Zuber M.	A New Moon: Geologic Processes Posters, Tue, p.m., Town Center Exhibit Area
Zuber M.	Lunar Cartography, Stereogrammetry, and Imaging Posters, Thu, p.m., Town Center Exhibit Area
Zuber M. T.	Print Only: Moon
Zuber M. T.	Planetary Differentiation, Mon, a.m., Waterway Ballroom 5
Zuber M. T.	A New Moon: LRO Results, Mon, a.m., Waterway Ballroom 6
Zuber M. T.	Venus, Mon, p.m., Waterway Ballroom 5
Zuber M. T.	Mercury, Tue, p.m., Montgomery Ballroom
Zuber M. T. *	Mercury, Tue, p.m., Montgomery Ballroom
Zuber M. T.	A New Moon: LCROSS Posters, Tue, p.m., Town Center Exhibit Area
Zuber M. T.	A New Moon: Geologic Processes Posters, Tue, p.m., Town Center Exhibit Area
Zuber M. T.	Martian Polar Processes Posters, Tue, p.m., Town Center Exhibit Area
Zuber M. T.	Mercury Posters, Tue, p.m., Town Center Exhibit Area
Zuber M. T. *	Large Impact Basins on the Moon, Thu, a.m., Waterway Ballroom 6
Zucker R. V.	Impacts Modeling Posters, Tue, p.m., Town Center Exhibit Area
Zufall A.	E/PO: Mars Remote Sensing Posters, Thu, p.m., Town Center Exhibit Area